Energy, Environment, and Sustainability
Series Editors: Avinash Kumar Agarwal · Ashok Pandey

Rashmi Avinash Agarwal
Avinash Kumar Agarwal
Tarun Gupta
Nikhil Sharma *Editors*

Pollutants from Energy Sources

Characterization and Control

Springer

Energy, Environment, and Sustainability

This books series publishes cutting edge monographs and professional books focused on all aspects of energy and environmental sustainability, especially as it relates to energy concerns. The Series is published in partnership with the International Society for Energy, Environment, and Sustainability. The books in these series are editor or authored by top researchers and professional across the globe. The series aims at publishing state-of-the-art research and development in areas including, but not limited to:

- Renewable Energy
- Alternative Fuels
- Engines and Locomotives
- Combustion and Propulsion
- Fossil Fuels
- Carbon Capture
- Control and Automation for Energy
- Environmental Pollution
- Waste Management
- Transportation Sustainability

More information about this series at http://www.springer.com/series/15901

Rashmi Avinash Agarwal
Avinash Kumar Agarwal
Tarun Gupta · Nikhil Sharma
Editors

Pollutants from Energy Sources

Characterization and Control

Springer

Editors
Rashmi Avinash Agarwal
Department of Civil Engineering
Indian Institute of Technology Kanpur
Kanpur, Uttar Pradesh, India

Tarun Gupta
Department of Civil Engineering
Indian Institute of Technology Kanpur
Kanpur, Uttar Pradesh, India

Avinash Kumar Agarwal
Department of Mechanical Engineering
Indian Institute of Technology Kanpur
Kanpur, Uttar Pradesh, India

Nikhil Sharma
Department of Mechanical Engineering
Indian Institute of Technology Kanpur
Kanpur, Uttar Pradesh, India

ISSN 2522-8366 ISSN 2522-8374 (electronic)
Energy, Environment, and Sustainability
ISBN 978-981-13-3280-7 ISBN 978-981-13-3281-4 (eBook)
https://doi.org/10.1007/978-981-13-3281-4

Library of Congress Control Number: 2018961692

This Springer imprint is published by the registered company Springer Nature Singapore Pte Ltd.
The registered company address is: 152 Beach Road, #21-01/04 Gateway East, Singapore 189721, Singapore

Preface

Energy demand has been rising remarkably due to increasing population and urbanization. Global economy and society are significantly dependent on the energy availability because it touches every facet of human life and activities. Transportation and power generation are two major examples. Without the transportation by millions of personalized and mass transport vehicles and availability of 24×7 power, human civilization would not have reached contemporary living standards.

The International Society for Energy, Environment and Sustainability (ISEES) was founded at Indian Institute of Technology Kanpur (IIT Kanpur), India in January 2014 with an aim to spread knowledge/awareness and catalyse research activities in the fields of Energy, Environment, Sustainability and Combustion. The Society's goal is to contribute to the development of clean, affordable and secure energy resources and a sustainable environment for the society and to spread knowledge in the above-mentioned areas and create awareness about the environmental challenges, which the world is facing today. The unique way adopted by the society was to break the conventional silos of specialications (Engineering, science, environment, agriculture, biotechnology, materials, fuels etc.) to tackle the problems related to enegy, environment and sustainability in a holistic manner. This is quite evident by the participation of experts from all fields to resolve these issues. The ISEES is involved in various activities such as conducting workshops, seminars, conferences, etc. in the domains of its interests. The society also recognizes the outstanding works done by the young scientists and engineers for their contributions in these fields by conferring them awards under various categories.

Second International Conference on 'Sustainable Energy and Environmental Challenges' (SEEC-2018) was organized under the auspices of ISEES from December 31st 2017–January 3rd, 2018 at J N Tata Auditorium, Indian Institute of Science Bangalore. This conference provided a platform for discussions between eminent scientists and engineers from various countries including India, USA, South Korea, Norway, Finland, Malaysia, Austria, Saudi Arabia and Australia. In this conference, eminent speakers from all over the world presented their views related to different aspects of energy, combustion, emissions and alternative energy

resource for sustainable development and cleaner environment. The conference presented 5 high voltage plenary talks from globally renowned experts on topical themes namely "Is It Really the End of Combustion Engines and Petroleum?" by Prof. Gautam Kalghatgi, Saudi Aramco; "Energy Sustainability in India: Challenges and Opportunities", by Prof. Baldev Raj, NIAS Bangalore; "Methanol Economy: An Option for Sustainable Energy and Environmental Challenges", by Dr. Vijay Kumar Saraswat, Hon. Member (S&T) NITI Ayog, Government of India; "Suprcirtical Carbon Dioxide Brayton Cycle for Power Generation" by Prof. Pradip Dutta, IISc Bangalore and "Role of Nuclear Fusion for Environmental Sustainability of Energy in Future" by Prof. J. S. Rao, Altair Engineering.

The conference included 27 technical sessions on topics related to energy and environmental sustainability including five plenary talks, 40 keynote talks, and 18 invited talks from prominent scientists, in addition to 142 contributed talks, and 74 poster presentation by students and researchers. The technical sessions in the conference included Advances in IC Engines: SI Engines, Solar Energy: Storage, Fundamentals of Combustion, Environmental Protection and Sustainability, Environmental Biotechnology, Coal and Biomass Combustion/Gasification, Air Pollution and Control, Biomass to Fuels/Chemicals: Clean Fuels, Advances in I.C. Engines: CI Engines, Solar Energy: Performance, Biomass to Fuels/Chemicals: Production, Advances in I.C. Engines: Fuels, Energy Sustainability, Environmental Biotechnology, Atomization and Sprays, Combustion/Gas Turbines/Fluid Flow/Sprays, Biomass to Fuels/Chemicals, Advances in I.C. Engines: New Concepts, Energy Sustainability, Waste-to-Wealth, Conventional and Alternate Fuels, Solar Energy, Waste Water Remediation and Air Pollution. One of the highlights of the conference was the Rapid Fire Poster Sessions in (i) Energy Engineering, (ii) Environment and Sustainability, and (III) Biotechnology, where more than 75 students participated with great enthusiasm and won many prizes in a fiercely competitive environment. 200+ participants and speakers attended this four days conference, which also hosting Dr. Vijay Kumar Saraswat, Hon. Member (S&T) NITI Ayog, Government of India as the chief guest for the book release ceremony, where 16 ISEES books published by Springer, under a special dedicated series "Energy, Environment and Sustainability" were released. This was the first time that such significant and high quality outcome has been achieved by any society in India. The conference concluded with a panel discussion on "Challenges, Opportunities & Directions for Future Transportation Systems", where the panelists were Prof. Gautam Kalghatgi, Saudi Aramco; Dr. Ravi Prashanth, Caterpillar Inc.; Dr. Shankar Venugopal, Mahindra and Mahindra; and Dr. Bharat Bhargagava, DG, ONGC Energy Center, and Dr. Umamaheshwar, GE Transportation, Bangalore. The panel discussion was moderated by Prof. Ashok Pandey, Chairman, ISEES. This conference laid out the roadmap for technology development, opportunities and challnges in Energy, Environment and Sustainability domain. All these topic are very relevant for the country and the world in present context. We acknowledge the support received from various funding agencies and organizations for the successful conduct of the Second ISEES conference SEEC-2018, where these books germinated. We would therefore like to acknowledge SERB, Government of

India (Special thanks to Dr. Rajeev Sharma, Secretary); ONGC Energy Center (Special thanks to Dr. Bharat Bhargava), TAFE (Special thanks to Sh. Anadrao Patil), Caterpillar (Special thanks to Dr Ravi Prashanth), Progress Rail, TSI, India (Special thanks to Dr. Deepak Sharma); Tesscorn, India (Special thanks to Sh. Satyanarayana); GAIL, VOLVO, and our publishing partner Springer (Special thanks to Swati Meherishi).

The editors would like to express their sincere gratitude to large number of authors from all over the world for submitting their high quality work in a timely manner and revising it appropriately at a short notice. We would like express our special thanks to Dr. Tapan Kumar Pradhan, Dr. Atul Dhar, Dr. Akhilendra Pratap Singh, Dr. Ludovica Luise, Dr. Joonsik Hwang, Dr. Chetan Patel, Dr. Pravesh Chandra Shukla, Dr. Sundeep Singh, Dr. Rohit Singla, Dr. Rajesh Prasad, Dr. Vikram Kumar, Dr. Dev Prakash Satsangi, Dr. Anoop Kumar Shukla, Mr. Maneesh Kumar, Mr. Neeraj Sharma, Mr. Sunil Kumar, Mr. Yeshudas Jiotode, Mr. Pawan Kumar, who reviewed various chapters of this book and provided very valuable suggestions to the authors to improve their manuscript.

The book covers different aspects of Energy consumption, environmental pollution and progress of a country is dependent on such aspects. This book is relevant for engineers, agriculturists, environmentalists, ecologists, governmental individuals, policy makers involved in area of pollutants from energy sources, environmental safety, and health issues. The book language is easy to understand, comprehensive in diagnostic techniques and may continue to serve well to students working in the field of energy and sustainability. The effective utilization of high-grade energy through thermochemical conversion of different wastes is discussed in this book. The methods and techniques to extract energy from e-wastes and biomass and their optimization can surely support the energy sector and satisfy a part of energy demand.

Kanpur, India

Rashmi Avinash Agarwal
Avinash Kumar Agarwal
Tarun Gupta
Nikhil Sharma

Contents

Editors and Contributors

About the Editors

Dr. Rashmi Avinash Agarwal is a senior researcher at IIT Kanpur. She completed her doctoral degree in Inorganic Chemistry from IIT Kanpur in 2014. She completed her M.Sc. in Organic Chemistry from Rajasthan University, Jaipur in 2002 and B.Sc. in Chemistry, from Kanoria College, Rajasthan University, Jaipur in 2000. She has expertise in coordination chemistry, coordination polymers, organic synthesis, inorganic synthesis, crystal structure determination, supramolecular chemistry, porous materials, topology, florescence, SC (single crystal)-to-SC transformation, synthesis of nano-particles. Dr. Rashmi A. Agarwal has published over 20 research papers in leading international journals.

Avinash Kumar Agarwal is a Professor in the Department of Mechanical Engineering in Indian Institute of Technology Kanpur. His areas of interest are IC engines, combustion, alternative fuels, conventional fuels, optical diagnostics, laser ignition, HCCI, emission and particulate control, and large bore engines. He has published 24 books and 230+ international journal and conference papers. Professor Agarwal is a Fellow of SAE (2012), ASME (2013), ISEES (2015) and INAE (2015). He received several awards such as Prestigious Shanti Swarup Bhatnagar Award—2016 in Engineering Sciences, Rajib Goyal

prize—2015, NASI-Reliance Industries Platinum Jubilee Award—2012; INAE Silver Jubilee Young Engineer Award—2012; SAE International's Ralph R. Teetor Educational Award—2008; INSA Young Scientist Award—2007; UICT Young Scientist Award—2007; INAE Young Engineer Award—2005.

Dr. Tarun Gupta Professor and PK Kelkar Research Fellow at the Department of Civil Engineering, IIT Kanpur, India. He holds a Doctor of Science (2004) in Environmental Health, Harvard University (USA) and Master of Technology (2000), Environmental Science and Engineering, Indian Institute of Technology Bombay (9-month research stay at the TU Dresden, Germany). He has published more than 95 articles in ISI indexed journals, 4 book chapters, and filed 4 Indian patents. A submicron aerosol sampler designed, developed and evaluated at the IIT Kanpur has since been commercialized by Envirotech (Delhi). He has developed several low-flow-rate and high-flow-rate impaction-based samplers and a non-selective membrane-based diffusion denuder. He is a member of INYAS (2016), PK Kelkar Research Fellowship (2015), NASI Scopus Young Scientist (2015), INSA Young Scientist (2011), INAE Young Engineer (2009), and IEI Young Engineer (2008).

Nikhil Sharma is a scientist in the Engine Research Laboratory in IIT Kanpur, India. He received his M.Tech. in Mechanical Engineering from NIT Hamirpur, India in 2012. and his Ph.D. from IIT Kanpur, in 2017. He was an assistant professor at Amity University's Department of Mechanical and Automation Engineering, Noida. His areas of research include alternative fuels for IC engines (biodiesel, alcohols), emission control and particulate characterisation.

Contributors

Avinash Kumar Agarwal Engine Research Laboratory, Department of Mechanical Engineering, Indian Institute of Technology Kanpur, Kanpur, India

Rashmi Avinash Agarwal Department of Civil Engineering, Indian Institute of Technology Kanpur, Kanpur, India

Ahfaz Ahmed Clean Combustion Research Center, King Abdullah University of Science and Technology, Thuwal, Saudi Arabia

Awad B. S. Alquaity Institute for Combustion Technology, RWTH Aachen University, Aachen, Germany

R. Anand Department of Mechanical Engineering, National Institute of Technology, Tiruchirappalli, Tamil Nadu, India

Spyros Andronopoulos NCSR Demokritos, Institute of Nuclear and Radiological Sciences and Technology, Energy and Safety, Attiki, Greece

B. Aravind Combustion Research Laboratory, Department of Aerospace Engineering, Indian Institute of Technology Bombay, Mumbai, India

D. Babu Department of Mechanical Engineering, National Institute of Technology, Tiruchirappalli, Tamil Nadu, India

Monoj Bardalai Department of Mechanical Engineering, Tezpur University, Sonitpur, Assam, India

D. K. Chandraker Reactor Design and Development Group, Bhabha Atomic Research Centre, Mumbai, Maharashtra, India

Biplab Das Department of Mechanical Engineering, Tezpur University, Sonitpur, Assam, India

Rajiv Ganguly Department of Civil Engineering, Jaypee University of Information Technology, Waknaghat, Solan, Himachal Pradesh, India

Sneha Gautam Department of Environmental Science and Engineering, Marwadi University, Rajkot, Gujarat, India

A. R. K. Gollakota Department of Safety, Health and Environmental Engineering, National Yunlin University of Science and Technology, Douliu, Yunlin, Taiwan, ROC

Abhishek Gupta Department of Desalination and Water Treatment, Zuckerberg Institute for Water Research, Ben-Gurion University of the Negev, Beersheba, Israel; Department of Desalination and Water Treatment, The Jacob Blaustein Institutes for Desert Research, Ben-Gurion University of the Negev, Beersheba, Israel

Ashok Kumar Gupta Department of Civil Engineering, Jaypee University of Information Technology, Waknaghat, Solan, Himachal Pradesh, India

Tarun Gupta Department of Civil Engineering, Indian Institute of Technology Kanpur, Kanpur, India

B. R. Gurjar Department of Civil Engineering, IIT Roorkee, Roorkee, Uttarakhand, India

Radek Hofman University of Vienna, Vienna, Austria

Ievgen Ievdin Ukrainian Center of Environmental and Water Projects, Kiev, Ukraine; BfS—Federal Office for Radiation Protection, Oberschleissheim, Germany

Tamour Javed Fuel Technology Division, Research and Development Center, Saudi Aramco, Dhahran, Saudi Arabia

Bengt Johansson Clean Combustion Research Center, King Abdullah University of Science and Technology, Thuwal, Saudi Arabia

Ivan Kovalets Institute of Mathematical Machines and Systems Problems NAS of Ukraine, Kiev, Ukraine; Ukrainian Center of Environmental and Water Projects, Kiev, Ukraine

Sudarshan Kumar Combustion Research Laboratory, Department of Aerospace Engineering, Indian Institute of Technology Bombay, Mumbai, India

L. A. Kumaraswamidhas Indian Institute of Technology (ISM), Dhanbad, India

D. K. Mahanta Department of Mechanical Engineering, Tezpur University, Sonitpur, Assam, India

R. Muthu Dinesh Kumar Department of Mechanical Engineering, National Institute of Technology, Tiruchirappalli, Tamil Nadu, India

Debajyoti Paul Department of Earth Sciences, Indian Institute of Technology Kanpur, Kanpur, India

Swatantra Pratap Singh Department of Desalination and Water Treatment, Zuckerberg Institute for Water Research, Ben-Gurion University of the Negev, Beersheba, Israel

Oleksandr Pylypenko Institute of Mathematical Machines and Systems Problems NAS of Ukraine, Kiev, Ukraine; Ukrainian Center of Environmental and Water Projects, Kiev, Ukraine

Pradhi Rajeev Department of Civil Engineering, Indian Institute of Technology Kanpur, Kanpur, India

Vallinayagam Raman Clean Combustion Research Center, King Abdullah University of Science and Technology, Thuwal, Saudi Arabia

A. Santhoshkumar Department of Mechanical Engineering, National Institute of Technology, Tiruchirappalli, Tamil Nadu, India

Petra Seibert University of Vienna, Vienna, Austria

Anchal Sharma Department of Civil Engineering, Jaypee University of Information Technology, Waknaghat, Solan, Himachal Pradesh, India

Deepika Sharma Department of Civil Engineering, Jaypee University of Information Technology, Waknaghat, Solan, Himachal Pradesh, India

Nikhil Sharma Engine Research Laboratory, Department of Mechanical Engineering, Indian Institute of Technology Kanpur, Kanpur, India

Amritanshu Shriwastav Centre for Environmental Science and Engineering, IIT Bombay, Mumbai, India

Chi-Min Shu Department of Safety, Health and Environmental Engineering, National Yunlin University of Science and Technology, Douliu, Yunlin, Taiwan, ROC

Gyanesh Kumar Singh Department of Civil Engineering, Indian Institute of Technology Kanpur, Kanpur, India

Nitin Kumar Singh Department of Environmental Science and Engineering, Marwadi University, Rajkot, Gujarat, India

Alok Sinha Department of Environmental Science and Engineering, Indian Institute of Technology (ISM), Dhanbad, India

S. L. Sinha Mechanical Engineering Department, Malla Reddy Engineering College (Autonomous), Secunderabad, Telangana, India

Abhrajyoti Tarafdar Division of Environmental Science and Ecological Engineering, Korea University, Seoul, Republic of Korea

Vinoth Thangarasu Department of Mechanical Engineering, National Institute of Technology, Tiruchirappalli, Tamil Nadu, India

R. K. Upadhyay Indian Institute of Technology Kanpur, Kanpur, India; Indian Institute of Technology (ISM), Dhanbad, India

Shashi Kant Verma Mechanical Engineering Department, Malla Reddy Engineering College (Autonomous), Secunderabad, Telangana, India

Manish Yadav Environment Department, Central Mine Planning and Design Institute Limited, Bhubaneswar, India

Part I
General

Chapter 1
Introduction to Pollutants from Energy Sources: Characterization and Control

Rashmi Avinash Agarwal, Avinash Kumar Agarwal, Tarun Gupta and Nikhil Sharma

Abstract Energy consumption, environmental pollution, and progress of a country are interconnected. This topic is relevant for engineers, agricultural scientists, environmentalists, ecologists, governmental agencies, and policy makers involved in the area of pollutants from energy sources, environmental safety, and health issues. The topic is easy to understand, comprehensively covered and would continue to serve the researchers/students working in the field of energy and sustainability. The effective utilization of high-grade energy through thermochemical conversion of different wastes is discussed in this book. The methods and techniques to extract energy from e-waste, and biomass and their optimization can support the energy sector and satisfy a fraction of energy demand. With this thought, the book is divided into five sections namely (i) General, (ii) Pollutants from Coal, (iii) Pollutants from Nuclear Energy, (iv) MSW and Disposal, and (v) Coatings.

Keywords Coal · Nuclear energy · MSW · Pollutants · Control

1.1 Introduction

Automobiles account for large part of greenhouse gas (GHG) emissions globally, which are highly legislated. The first part of this book comprises of general introduction, in two chapters. Chapter 1 is the introduction to the book and Chap. 2 introduces the combustion based transportation in a carbon-constrained world. This chapter gives a holistic overview of the current and prospective regulations targeted

R. A. Agarwal · T. Gupta
Department of Civil Engineering, Indian Institute of Technology Kanpur, Kanpur 208016, India

A. K. Agarwal (✉) · N. Sharma
Engine Research Laboratory, Department of Mechanical Engineering, Indian Institute of Technology Kanpur, Kanpur 208016, India
e-mail: akag@iitk.ac.in

R. A. Agarwal et al. (eds.), *Pollutants from Energy Sources*, Energy, Environment, and Sustainability,
https://doi.org/10.1007/978-981-13-3281-4_1

at curbing transport origin CO_2 emissions and pollution. This chapter presents the prospective regulatory framework for road transport, and marine and aviation sectors, aimed at curbing the CO_2 emissions.

The second part of the book is specific to coal-based energy generation and comprises of pollutants from coal power plants, and includes six chapters. Chapter 3 of this part discusses the measurement and control of pollutants from coal-based power plants. This chapter includes an overview of various emitted pollutants from various types of power plants, their measurement and control techniques, both past and present, using various approaches. Various opportunities in the power sector, along with key challenges and issues related to climate change mitigation in this sector are discussed. Most of the electricity demand in India is primarily met by coal-fired power plants and the resulting pollution is the main cause of concern affecting ambient air quality, especially in urban areas. In this context, Chap. 4 in this part covers aerosols generated by coal-fired power plants and their associated environmental impacts. At the point where coal burns, chemical and physical changes take place, and numerous harmful pollutants are formed and emitted. Highlighting this fact, Chap. 5 of this part covers polycyclic aromatic hydrocarbons (PAHs) generated by coal-fired thermal power plants. This chapter discusses their formation mechanism, characterization, and profiling. Combustion of pulverized coal to produce electricity in the thermal power plants results in large quantities of residual ash generation, with varying properties. Ash (Bottom ash and Fly ash) are post-combustion particulate residue. Chapter 6 of this part is related to strategies for collection, treatment, and recycling of fly ash from thermal power plants. This chapter covers a wide spectrum of information on strategies for collection, treatment, and recycling of fly ash from thermal power plants. At present, private sector firms in India are only allowed to mine coal for their own use (captive mining) in cement, steel, power, and aluminum plants. Coal India Ltd. (CIL) is the sole commercial miner in India with 80% market share and it is the world's largest coal producer. Chapter 7 of this part is related to commercial coal mining in India, which is opened for the private sector. In a major "reform" in the coal sector since its nationalization in 1973, the government on 20th February 2018 allowed private companies to mine coal for commercial use, ending the monopoly of state-owned CIL. Chapter 8 of this part covers the development of small-scale thermoelectric power generators using different micro-combustor configurations for stand-alone power applications. Few highly efficient micro-combustors suitable for thermos-electric power generation have been fabricated and evaluated. A detailed experimental investigation on the thermal performance of micro-combustors and thermoelectric generators integrated with the bare surface of the combustor along with the cooling jackets for the power generation is included in this chapter.

Atomic energy is important for clean-air and carbon-free electricity generation. It does not produce GHG emissions or other air pollutants. The third part of this book comprises of pollutants emanating from nuclear energy, in two chapters. Chapter 9 in this part is related to sources of nuclear pollutants and their controls. Nuclear pollution is harmful for human health hence it is quite essential to take all necessary steps for its prevention. This chapter gives an overview of various undesirable

radioactive materials or substances, which affect the atmosphere and their control methods, both past and present, using different approaches. Chapter 10 in this part is related to advanced source inversion module of the EU nuclear emergency response system (RODOS). In this chapter, authors describe the development of the source inversion algorithm, in which measurements of gamma dose rate and other quantities taken at a wide range of distances from the nuclear power plant (from ~1–1000 km) are used to establish time-dependent source rates of different nuclides at unknown heights.

Waste disposal is a major problem in most countries. The fourth part of this book comprises of municipal solid waste (MSW) and its disposal, in five chapters. Chapter 11 of this part is related to the effective utilization of high-grade energy through thermochemical conversion of different waste streams. Waste-to-energy conversion will be catering the future energy demand as well as resolving the pollution issue. This work mainly involves extensive study of pyrolysis and gasification of biomass, and hazardous e-waste into useful energy and its impact on the environment. Chapter 12 of this part is related to matrix method for evaluation of existing solid waste management processes in the city of Jalandhar, Punjab, India. This chapter highlights the existing status of MSW management practices in Jalandhar, considering a dumpsite of Wariana and Suchipind villages and suggests remedial measures for the major problems faced by the existing system of MSW management. Coal-based fly ash is a significant threat across the globe, and there is rapid advancement in technology to control the fly ash and utilize it for various economic activities. Chapter 13 of this part is related to turning fly ash into zeolite for effective waste management The toxic nature of this atmospheric pollutant obtained by burning coal posed a serious threat to mankind. Authors covered a broad spectrum of information pertained to the synthesis of zeolite from fly ash so that the reader can understand its utilization aspects. Chapter 14 of this part covers production and characterization of teak tree saw-dust and rice-husk biochar: Authors explained about the production of biochar from teak tree saw-dust (TTSD) and rice-husk (RH) and their characterization. The biochars were produced from TTSD and RH at pyrolysis temperature of 450 °C with the heating rate of 15 °C/min in a fixed bed reactor. Open dumping of MSW causes environmental degradation including air, soil, and groundwater pollution, leading to an adverse impact on public health. In this context, Chap. 15 of this part is related to the parametric evaluation of leachate generated from a non-engineered landfill site and its contamination potential of the surrounding soil and water bodies. This study provides the physico-chemical characterization of groundwater, leachate, and surface water being affected by the percolation of leachate into aquifers in the study region of Solan, Himachal Pradesh, India.

The fifth part of this book comprises of Chap. 16 related to coatings. This chapter is related to sustainable coating design and role of liquid-mediated contact, wherein the development of new technological innovations needs more reliable and cost-effective materials.

Overall, this book covers a wide range of topics related to pollutants from energy sources and will be of interest to researchers in the field. Specific topics covered in this book include:

1. Introduction to pollutants from energy sources and their control
2. Combustion-based transportation in a carbon-constrained world
3. A Review on pollutants from coal-based power sector: Measurements and control
4. Aerosols generated from coal-fired power plants and associated environmental impacts
5. Polycyclic aromatic hydrocarbons (PAHs) pollution generated from coal-fired thermal power plants: formation mechanism, characterization, and profiling
6. Strategies for collection, treatment, and recycling of fly ash from thermal power plants
7. Commercial coal mining in India opened for the private sector: A boon or inutile
8. Development of small scale thermoelectric power generators using different micro-combustor configurations for stand-alone power applications
9. Sources of nuclear pollutants and their controls
10. Advanced method for source term estimation in the EU nuclear emergency response system RODOS
11. Effective utilization high-grade energy through thermochemical conversion of different wastes
12. Matrix method for evaluation of existing solid waste management processes in Jalandhar city, Punjab, India
13. Turning coal fly ash into zeolite for effective waste management
14. Production and characterization of teak tree saw-dust, and rice-husk biochar
15. Parametric evaluation of leachate generated from a non-engineered landfill site and its contamination potential of surrounding soil and water bodies.
16. Sustainable coating design and role of liquid-mediated contact.

Chapter 2
Combustion-Based Transportation in a Carbon-Constrained World—A Review

Tamour Javed, Ahfaz Ahmed, Vallinayagam Raman, Awad B. S. Alquaity and Bengt Johansson

Abstract The transportation sector accounts for around a quarter of global CO_2 emissions and is powered predominantly by fossil-derived fuels. The regulatory framework is evolving globally to more stringent requirements for fuel efficiency and CO_2 emissions, forcing the OEMs to adopt advanced powertrain technologies. Such changes are more evident in the light-duty road transportation sector compared to the heavy-duty road, marine and air transportation sectors. Here, a holistic review of the current and prospective regulations targeted at curbing transportation-based CO_2 emissions is presented. For road transport, these include various government- and state-level policy initiatives such as the Corporate Average Fuel Economy (CAFE) and CO_2 emission standards and the zero emission mandates. For marine and aviation sectors, these include the International Maritime Organization (IMO) and the International Civil Aviation Organization (ICAO) regulations and aspirations targeted at reducing the CO_2 footprint. The compliance options for these regulations are evaluated using a combination of fuels, engines, and hybridization in each transportation sector. Furthermore, a brief overview of how OEMs are working toward achieving these targets is presented. An overview of several advanced spark and compression ignition engine technologies with the potential to improve the fuel economy and CO_2 emissions is presented. Finally, an overview of major disruptions that are changing the road-based transportation is presented and a balanced life cycle based policy approach is advocated.

T. Javed (✉)
Fuel Technology Division, Research and Development Center, Saudi Aramco, Dhahran, Saudi Arabia
e-mail: tamour.javed@aramco.com

A. Ahmed · V. Raman · B. Johansson
Clean Combustion Research Center, King Abdullah University of Science and Technology, Thuwal, Saudi Arabia

A. B. S. Alquaity
Institute for Combustion Technology, RWTH Aachen University, 52056 Aachen, Germany

R. A. Agarwal et al. (eds.), *Pollutants from Energy Sources*, Energy, Environment, and Sustainability,
https://doi.org/10.1007/978-981-13-3281-4_2

Keywords Transport · Climate change · Fuel economy · CO_2 Regulations · ZEV · Aviation · Marine · LCA

2.1 Introduction

2.1.1 History

Combustion of fuels has been a dominant source of energy for mankind since ages. In primitive times, wood was the major fuel used for heating, lighting, and cooking purposes. As mankind's understanding of their surroundings improved, the focus shifted to an improved version of fuels such as coal, marking the beginnings of the fossil fuel era (Morris 2015). Coal-offered significant advantages over wood such as higher energy density, better flammability, etc., making it a fuel of choice for heating, lighting, and even powering mobility. Locomotives with coal-powered steam engines were introduced in the eighteenth century and became popular (McNeil 2002). Arguably, a paradigm shift in mobility came along when Nikolaus Otto patented his 4-stroke engine in 1876 along with Gottlieb Daimler and Wilhelm Maybach, which used one of the light fractions from crude oil distillation as fuel (Morris 2015). Henry Ford eventually reinforced the significance of this discovery in 1908 when he introduced the first mass-produced affordable vehicle, Model-T. This innovation, along with other similar developments in the European markets, revolutionized the personal mobility sector leading to its wide acceptance among common people. Despite enabling freedom of movement for the mass population, the early vehicles were riddled with issues such as poor fuel efficiency, low power density, and were very high on carbon emissions. These shortcomings became more evident (De Groot 1996; Tushman 1997; Kline and Rosenberg 2009) when the World Wars broke out in Europe and to support the war effort, fuel efficient and high powered vehicles were needed. One inhibitor in improving the fuel efficiency of these engines was their low compression ratio, which was limited by engine knock (Seyferth 2003). Fuels at that time had lower octane numbers because of limited advancement in refinery processes (Splitter et al. 2016) such as catalytic reforming, cracking, etc. Amid attempts on engine and fuel improvement in the 1920s, a young engineer Thomas Midgley and his associates came up with the suggestion of blending small quantities of Tetra Ethyl Lead (TEL) to the gasoline to increase its knock resistance and hence allowing engines to deliver higher power and better efficiency in the process. However, due to health and environmental impacts of TEL, it was phased out in the 1970s around major parts of the world, thereby affecting the automotive efficiency adversely (Splitter et al. 2016). Soon after, automotive manufacturers started using electronic fuel injection system and engine management software, which revived engines' performance to TEL levels.

The foci of the automotive industry till this point were to improve fuel efficiency and power density while the emissions were of little concern.

The obliviousness toward increasing pollutant emissions from vehicles led to the constitution of California Air Resources Board (CARB) in California (United States) in 1967 (Hanemann 2008). This board established regulations on vehicular emissions paving the way for Environmental Protection Agency (EPA) in the US and EU emission standards in the Europe and subsequently around the world. These regulatory bodies acted primarily to address the poor air quality in the developed parts of the world. However, in the same context, another significant event took place in 1966. World Meteorological Organization (WMO) (a body within United Nations) published a report (Mitchell et al. 1966) on climate change which referred to human activity as a predominant reason causing the alteration of natural course of Earth's climate regulating processes. These findings were later followed by the commencement of the United Nations Climate Change Conferences under the United Nations Framework Convention on Climate Change (UNFCC 1992). The main goal of the UNFCC is to "stabilize greenhouse gas concentrations in the atmosphere at a level that would prevent dangerous anthropogenic interference with the climate system."

Since then, two meetings of UNFCC have had a significant impact in shaping global climate change policies. In 1997, during Kyoto summit, it was decided that the participating states will strive to reduce greenhouse gas emissions based on the scientific consensus that global warming is occurring and it is extremely likely due to anthropogenic CO_2 emissions. During the second meeting in Paris, an agreement to keep the increase in global average temperature to well below 2 °C above pre-industrial levels was reached (UNFCC 2015); in addition to the consensus to limit the increase to 1.5 °C to substantially mitigate the risks associated with climate change.

2.1.2 Overview

The agreements ratified at these meetings were executed in different versions across major parts of the world with a unified goal to cut down on greenhouse gases promoting climate change. These agreements, however, also led to an increased attention on the emissions from the combustion engines, since automotive sector accounts for around 25% of carbon emissions. To address these implicit demands placed on automotive industries, many new technologies came to forefront including advanced gasoline and diesel technologies. Although these engine technologies are significantly fuel efficient than conventional engines and facilitate tremendous control of emissions with high power density, major economies around the world still felt the need to take more aggressive steps toward curbing the carbon emissions from the vehicular operation. It eventually led to various announcements during 2016–2018 by many countries including the United Kingdom, China, India, parts of Europe etc. to move away from new sales of passenger vehicles powered by

pure internal combustion engine in 2030–2040 timeframe. However, the nature of technology to replace internal combustion engines on such a large scale is still under debate. In the most likely scenario, it seems that the combustion engines will stay for longer than hyped in the popular media, especially in the heavy-duty road transport, marine and aviation sectors; however, to address the stricter regulations, combustion engines must reinvent themselves.

In this chapter, first, the regulatory framework around the world and their potential directions in response to climate change, including road transport, marine, and aviation sectors are discussed. In Sects. 2.3 and 2.4, the focus is shifted to fuel and engine technologies in various transportation sectors including their historic trends and current efforts to address the market demands and legislations. Further, a brief review of sustainability efforts by major automakers, in the road transport sector, will be provided. Finally, major trends of disruptions in the transportation sector, using examples of important disruption agents, are discussed. In the end, a holistic overview of the entire chapter is presented.

2.2 The Regulatory Framework

2.2.1 Fuel Economy and CO_2 Emission Standards for Road Transport

As a response to climate change, increasing fuel import bills, energy security, and wider impacts of transportation sector on the environment, the regulatory framework across the world to improve the fuel economy and reduce the CO_2 emissions has evolved over the past 50 years and has become quite stringent. Figure 2.1 shows the improvements in CO_2 emissions and fuel economy over the years for passenger cars and light trucks (including pickup trucks, minivans, and SUVs) in the US market. Between 2004 and 2016, the CO_2 emissions and fuel economy have improved by 22 and 28%, respectively (EPA 2017). The benefits of such

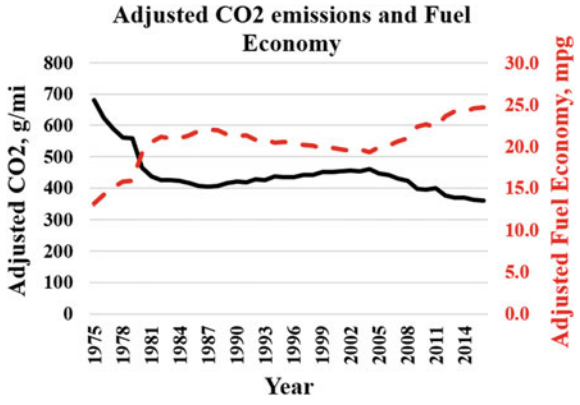

Fig. 2.1 Historic CO_2 emissions reduction and fuel economy improvement in the US for passenger cars and light trucks (EPA 2017)

regulations are further amplified in the passenger cars sector where adjusted fuel economy has reached a historic high of around 29.1 mpg in 2017. Such improvements are consistent in the rest of the world as well and EU reported a CO_2 reduction of 16% in the 2010–2015 period (EU 2018).

As seen in the figure above, the regulatory framework has evolved significantly over the past decade. Just over a decade ago, only the US, Japan, South Korea, and China had enforced regulations for the CO_2 emissions and fuel economy (Yang and Bandivadekar 2017), while the EU and Canada had expressed their aspirations for such regulations. However, in 2017, such regulations are commonplace and enforced in 80% of the light-duty vehicle market. These standards are too detailed to be summarized here, and only a brief overview of these standards is presented. Table 2.1 shows the fuel economy and CO_2 emissions of passenger cars and light trucks in the US (Transport Dept 2012), the EU (Regulation (EU) No 333 2014; Regulation (EU) No 253 2014), China and India (Yang and Bandivadekar 2017). In the US, National Highway Traffic Safety Administration (NHTSA) sets the fleet regulations called the Corporate Average Fuel Economy (CAFE) standards since 1975, and Environmental Protection Agency (EPA) sets the CO_2 standards since 2007, both standards are harmonized since 2010 for the cars and light-duty trucks of the model year 2012 and beyond. The EU legislation sets EU-wide CO_2 emission targets for new cars and commercial vehicles (vans) sold in the EU market. Similar

Table 2.1 Fuel economy and CO_2 emissions of passenger cars and light trucks in the US (Transport Dept 2012), the EU (Regulation (EU) No 333 2014; Regulation (EU) No 253 2014), China (Yang and Bandivadekar 2017) and India (Yang and Bandivadekar 2017)

Country/region	Category	Fuel economy and CO_2 emissions (in year)
US	Cars	36.2 mpg and 225 gCO_2/mi (2016)
		55.3 mpg and 143 gCO_2/mi (2025)
	Light trucks	28.8 mpg and 298 gCO_2/mi (2016)
		39.3 mpg and 204 gCO_2/mi (2025)
EU	Cars	130 gCO_2/km (2015)
		95 gCO_2/km (2021)
		30% CO_2 reduction compared to 2021 (2030)
	Vans	175 gCO_2/km (2017)
		147 gCO_2/km (2020)
		30% CO_2 reduction compared to 2021 (2030)
China	Cars	6.9 L/100 km (2015)
		5 L/100 km (2020)
	Light trucks	6.9 L/100 km (2020)
		–
India	Cars	130 gCO_2/km (2017)
		113 gCO_2/km (2022)
	Light trucks	–
		–

government bodies set the fuel economy and/or CO_2 emissions standards in China, India, and in rest of the world. However, there are some differences in the interpretation of these regulations. First, vehicles are categorized differently in different regions; the maximum Gross Vehicle Weight (GVW) for passenger cars and light-duty trucks in the US is 3856 kg, whereas that in the EU, China, and India is 3500 kg (Yang and Bandivadekar 2017). Also, the test cycles used for reporting and certifying these regulations are different. The US regulators use US combined cycle, while the EU, China, and India use New European Driving Cycle (NEDC). EU plans to shift to a worldwide harmonized Light vehicle Test Procedure (WLTP) in the future (Yang and Bandivadekar 2017). Therefore, direct comparison of these standards across various regions should be reported cautiously. However, across the globe, such standards are becoming ever stringent and the CO_2 emissions in most regions are expected to reduce by around 50% by 2025 compared to baseline years (baseline year is different for different regions, see Table 2.1) (Yang and Bandivadekar 2017). Hence, it could be stated that such regulations are successful in reducing the global warming impact of the transportation sector and also bear financial benefits to the consumers and governments.

The fuel economy and CO_2 emission standards for the Heavy-Duty Vehicles (HDVs) are still evolving compared to Light-Duty Vehicles (LDVs). The EU only recently (COM//284 (EU) 2018) presented proposals for regulating HDV CO_2 emissions. The EU proposals calls for 15 and 30% reduction in CO_2 emissions, compared to 2019 levels, by 2025 and 2030, respectively, whereas 2030 reduction targets are subjected to review in 2022. Moreover, the EU proposals target only large lorries to start with and plan to widen the regulatory coverage to other HDV's post 2022. In 2016, the US EPA and NHTSA jointly announced the fuel economy and CO_2 emissions phase-II standards for medium- and heavy-duty vehicles through the model year 2027 (Transport Dept 2016). These standards are performance-based and are expected to further improve fuel savings by 25% compared to terminal phase-I respective category baseline. They rely on available and futuristic technological improvements to achieve the targets with a neutral attitude toward different technologies. In China, the stage-II and stage-III standards for HDV fuel consumption are expected to improve the fuel economy by 15% compared to 2015 levels by 2021. Fuel consumption standards for HDVs are also planned to be regulated in phases in India starting in 2018 (phase-I effective from 2018, phase-II effective from 2021) (Garg and Sharpe 2017). It is expected that the coverage of fuel economy and CO_2 emissions standards will continue to grow across the world and these standards will continue to evolve towards stricter targets.

2.2.2 The Zero-Emission Mandates

Several regulatory bodies, at the country/region and state level, have started enforcing regulations that require automakers to directly invest in zero-emissions vehicles (Battery Electric Vehicles (BEVs), Fuel Cell Vehicles (FCVs)). In 2016, the US state of California issued the Zero-Emissions Vehicle (ZEV) mandate for passenger cars, light-duty trucks, and medium-duty vehicles (CARB 2016). The ZEV mandate since then has been adopted by nine other US states including Connecticut, Maine, Maryland, Massachusetts, New Jersey, New York, Oregon, Rhode Island, and Vermont. At the core of this mandate, the automakers are required to produce a certain percentage of their vehicles conforming to ZEV standards. This mandate assigns credit based on the zero emitting drive range, e.g., pure ZEVs, i.e., BEVs and FCVs, depending on their driving range. Although the credits for non-ZEVs are lower compared to pure ZEVs, Plug-in Hybrid Vehicles (PHEVs), conventional hybrid vehicles (HEVs), and clean gasoline vehicles qualify for such credits. The mandate allocates "ZEV credits" to the automakers for each vehicle sold and the automakers are required to maintain a certain percentage of ZEV credits of total sales credits year through 2025 (see Table 2.2). For example, an automaker with average sales of 100,000 vehicles between 2014–2016 will require to earn 4500 ZEV credits in 2018 (required ZEV credits in 2018 are 4.5%), this does not directly translate into 4500 ZEVs sold as minimum ZEV floor for 2018 is 2.5%. The manufacturers are allowed to carry over excess credits in a year to subsequent year and can also trade a certain percentage of their credits with other automakers. China introduced a similar mandate in 2017 called the New Energy Vehicle (NEV) mandate (Cui 2018). The NEV mandate calls for each automaker to have a minimum of 10% NEV credits in 2019 and 12% in 2020. The NEV mandate in China also allows the automakers to use their surplus NEV credits for Corporate Average Fuel Consumption (CAFC) compliance, credits trade and credits carry over to next year. The EU has introduced the super-credits system (Regulation (EU) No 333/ 2014) for Low CO_2 Emitting Vehicles (LEVs) (below 50 gCO_2/km) vehicles, and plans to incentivize automakers who surpass their share of ZEVs and LEVs (15% in 2025 and 30% in 2030) with less

Table 2.2 ZEV credit requirement for the automakers selling vehicles in California and nine other US states (CARB 2016)

Model year	ZEV credit requirement (%)	Minimum ZEV credits (%)
2018	4.5	2
2019	7	4
2020	9.5	6
2021	12	8
2022	14.5	10
2023	17	12
2024	19.5	14
2025 and beyond	22	16

stringent CO2 targets. Additionally, EU renewable energy directive II (EU-RED II) (COM//0767 final//0382 (COD) 2016), proposes to make it mandatory for the fuel suppliers to include at least 10% renewables by energy in their fuel blends by 2030, where to qualify as renewable, the fuel must provide 70% CO_2 savings compared to fossil fuels in 2021. In short, many regions across the world are expected to adopt similar aggressive mandates for promoting zero-emissions vehicles in the passenger car sector; however, even in presence of such stringent regulations, based on regulators own estimates, the light-duty fleet will still be a mix of ZEV and non-ZEV vehicles by 2050. In reality, the transition toward complete ZEV vehicles will be slow spanning several decades.

2.2.3 Regulatory Framework for Aviation Sector

Aviation sector accounted for around 11% of oil share in transportation in 2014 and is the fastest growing oil-based transportation sector in terms of energy consumption (IEA 2017). Due to the global nature of aviation business, the civil aviation sector is regulated globally by UN-chartered International Civil Aviation Organization (ICAO). The ICAO during its 39th general assembly in 2016 has introduced a strategy to reduce CO_2 emissions from the aviation sector (ICAO Resolution 2016). The Carbon Offsetting and Reduction Scheme for International Aviation (CORSIA) proposed in these resolutions call for adopting offset mechanisms to curb CO_2 emissions in the aviation sector. As a part of this mechanism, all aviation operators that emit more than 10,000 tons of CO_2 per year must report their CO_2 emissions from January 1, 2019 for recording average emissions in the 2019–2020 period. The CORSIA mechanism is expected to ensure carbon neutral growth of aviation sector from 2021 by offsetting any CO_2 emissions above the 2020 average baseline. The CORSIA mechanism will be rolled out in phases with the pilot phase from 2021 to 2023 and the first phase from 2024 to 2026, both of which are voluntary. The second phase of this mechanism targets 2027–2035 period where all states with international aviation activities in Revenue Tonne Kilometers (RTKs) in the year 2018 above 0.5% of total RTKs or whose cumulative share in the list of States from the highest to the lowest amount of RTKs reaches 90% of total RTKs must participate. Participation in the second phase is voluntary for the Least Developed Countries (LDCs), Small Island Developing States (SIDS), and Landlocked Developing Countries (LLDCs). There are many ways proposed to offset the CO_2 emissions from aviation using CORSIA which includes financing afforestation, wind energy, clean cookstove, methane capture, and other emissions-reducing or avoidance projects. Additionally, technological, operational, and infrastructure measures are proposed for CO_2 reduction in the aviation sector, however, the aviation sector is set to rely heavily on the CORSIA mechanism and hence is expected to be powered by oil-based jet fuels as the primary energy source. Moreover, the NO_x, SO_x, soot emissions, and the noise pollution are receiving increased attention and are expected to be more regulated in future.

2.2.4 Regulatory Framework for Marine Sector

Marine industry accounted for around 10% of oil share in transportation in 2014 and this share is expected to rise to 16% by 2050 (IEA 2017). The United Nation's chartered International Maritime Organization (IMO) regulates marine transportation globally. Heavy Fuel Oil (HFO), also known as the bunker fuel, intermediate fuel oil, residual fuel oil, is the primary fuel used in the marine sector. The IMO has imposed Sulphur cap on the HFO limiting the Sulphur content to 0.5% m/m (MARPOL Annex VI), which is a sharp decline from the current Sulphur limits of 3.5% m/m. The new Sulphur regulation will come into effect on January 1, 2020. The Sulphur levels in the HFO for vessels operating in the Emission-Controlled Areas (ECAs), the Baltic Sea area, the North Sea area, the North American area (covering designated coastal areas off the United States and Canada), and the United States Caribbean Sea area (around Puerto Rico and the United States Virgin Islands), are further lower at 0.1% m/m. Therefore, in ECAs, most vessels are already operating on more expensive distillate fuels, which have lower Sulphur content. These regulations apply to both main and auxiliary engines and also to any boilers onboard. Sulphur levels in various fuel oils and commonly used distillates are shown in Table 2.3.

The MARPOL Annex VI also regulates the NO_x emissions for seagoing vessels. The NO_x emission levels are set for ships according to engine maximum operating speed levels and are different for old (Tier I, ships in service before January 1, 2000) and new (Tier II, ships constructed after January 1, 2011) vessels, and the vessels operating in NO_x-ECAs (Tier III, ships constructed after January 1, 2016) (see Fig. 2.2).

More recently, IMO has in principle agreed on the initial strategy to reduce the CO_2 footprint of the marine sector by 50% compared to 2008 levels by 2050. This CO_2 reduction is expected to take into account all facets of the marine sector including technological, operational, and fuel/energy source measures update (ITF 2018). The plans may also include market-based offsetting mechanisms for trading CO_2 credits. The IMO plans to revise the agreement by 2023, based on fourth and fifth round of IMO greenhouse gas studies from 2019 to 2022, which would be carried out before drafting any regulations.

Table 2.3 Sulphur content in commonly used fuel oil grades

Common name	ISO name	Typical composition	Typical Sulphur content (%)
Marine Gas Oil (MGO)	DMA	100% distillate	0.1–1.5
Marine Distillate Oil (MDO)	DMB	Distillate with traces of residual oil	0.3–2
Intermediate Fuel Oil 180 (IFO 180)	RME	10% distillate 90% residual oil	2.0–3.5
Intermediate Fuel Oil 380 (IFO 380)	RMG	99% residual oil	3.5

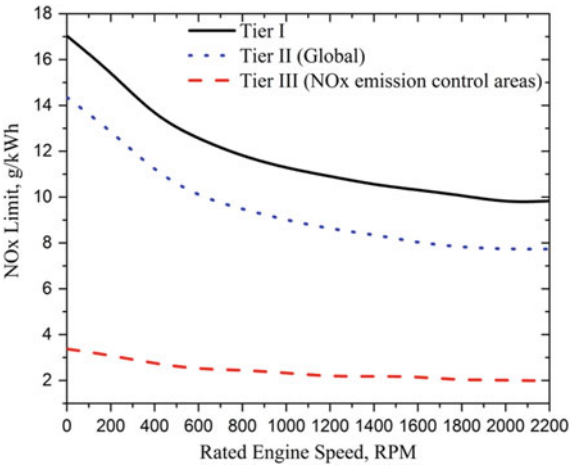

Fig. 2.2 NO_x limit for different tiers as a function of engine speed (McGill and Winther 2013)

2.3 Developments in Transportation Sectors to Meet CO_2 Emission Challenges

2.3.1 Recent Developments in Light-Duty Sector

There are several ways to meet future emission targets in the light-duty sector (Elgowainy et al. 2018). CO_2 emissions can be mitigated by increasing fuel efficiency through advanced gasoline and diesel powertrains, hybridization of ICE and battery, using fuels with low *C*/*H* ratio, using electric and fuel cell vehicles, etc. Among the various options available, the majority of the mainstream automotive manufacturers are choosing the hybridization and electrification route to achieve the futuristic emission goals (Hebert 2017). Although Battery Electric Vehicles (BEVs) do not pollute at the point of use, the pollution caused during electricity generation and in the production and recycling processes of the batteries is often neglected. Since the current regulatory framework for CO_2 emissions of light-duty vehicles is based on the tank-to-wheel emissions (Thiel et al. 2014), BEVs tend to get an unfair advantage over ICE-driven vehicles. In countries or regions where the electricity generation is predominantly based on fossil fuels, especially coal, BEVs can lead to more GHG emissions as compared to the fossil-fuel-driven vehicles (Huo et al. 2015; Faria et al. 2013; Manzetti and van der Spoel 2015). Additionally, a life cycle inventory of BEVs shows increased risk of human toxicity, eutrophication, and metal depletion compared to conventional fossil-fuel-driven vehicles (Hawkins et al. 2013). A more practical issue is the relatively limited driving range, long charging times, short life of battery pack, and lack of charging infrastructure for mainstream BEVs. Improvements in these aspects are an absolute necessity for the widespread adoption of electric vehicles. Therefore, BEVs require more eco-friendly, low-cost, and high energy density batteries to occupy a significant share of the total vehicle fleet. However, despite their current limitations,

automotive manufacturers continue to invest in BEVs relying on future potential for improvement in batteries. Additionally, BEVs help the automotive manufacturers in meeting the fleet-averaged CO_2 emission regulations as they are considered as "Zero-Emissions Vehicles" under the current regulatory framework.

A more viable and practical option is to hybridize ICEs for improved fuel efficiency and reduced CO_2 emissions (Elgowainy et al. 2018). Different hybrid options may be suitable for a different class of vehicles within the light-duty sector and hence diversified options are expected moving forward. Series, parallel, and mix hybrid are the various options available currently and each has their own advantages and challenges. Series-hybrid vehicles offer a promising solution of increasing the fuel efficiency in urban driving conditions by allowing the engine to operate under its optimum condition. In such a scheme, ICE will continue to be the primary energy source for the vehicle.

Other options for reducing CO_2 emissions include using fuels with lower carbon to hydrogen ratio. In this case, CNG-driven vehicles become promising due to reduced CO_2 emissions by virtue of their low *C*/*H* ratio (Hesterberg et al. 2008). Long-term options include the use of Fuel Cell Vehicles (FCVs) powered by hydrogen or other fuels. Although FCVs have long been touted as the next transportation solution, their market uptake has been slow and they continue to be part of a niche market. However, some of the mainstream vehicle manufacturers are focusing again on fuel cell vehicles and have invested heavily in their research and development (Toyota 2018). The future of hydrogen produced from fossil sources using carbon capture and renewable hydrogen as a fuel, along with fast refueling and long driving range, makes it an attractive and eco-friendly solution. However, the high cost of fuel cell stack and the lack of hydrogen refueling infrastructure are significant bottlenecks currently. Economies of scale are expected to reduce the price of FCVs, however, this is a typical chicken and egg problem. Following Tesla's lead, Toyota has also shared patents related to various aspects of FCV development to accelerate the growth in this segment (Toyota 2018). Additionally, three major Japanese automakers namely Toyota, Honda, and Nissan are cooperating to jointly accelerate the introduction of a hydrogen fueling network by supporting the operation cost and their development.

All the aforementioned medium to long-term options require the development of new fueling infrastructure and/or vehicle modifications and are, therefore, time-consuming and costly to implement. To summarize, there are multiple promising options to achieve future emission targets. However, a holistic cradle to grave analysis needs to be conducted to select an appropriate solution on a case-by-case basis rather than implementing a solution, which merely shifts the burden from one life cycle to another.

2.3.2 Recent Developments in Heavy-Duty Sector

Despite the availability of transportation modes such as rail and shipping, freight and non-urban public transportation will continue to rely on heavy-duty vehicles such as trucks and buses. It is, therefore, vital that the heavy-duty segment should also be equipped with alternative or advanced combustion engine powertrains to contain the increasing carbon emissions. In heavy-duty segment, there are two major changes, i.e., advancement of the combustion powertrain and electrification. In the rest of this section, both of these worldwide trends have been discussed with regards to the heavy-duty segment.

Most of the commercial vehicles around the world use diesel engine as a propulsion system for long-haul road freight truck. To reduce emissions from diesel engine, the thermal efficiency needs to be improved. Initially, when the diesel engine was invented in the 1880s, its efficiency was around 26% and due to continuous improvement in fuel injection systems, engine and piston designs, modern engines exhibit 43–44% thermal efficiency, and it is set to reach 50% by 2030 (Lutsey 2018). The US Department of Energy's Super Truck program is one among various initiatives toward improving the overall performance of heavy-duty segment. The first phase of the Super Truck program was started in 2009 and Cummins, Volvo Group, Daimler Trucks, and Peterbilt were tasked with improving the overall freight efficiency by 50%, quantified in ton-miles per gallon, and engine's brake thermal efficiency by 50%. Super Truck-I (Delgado and Lutsey 2014) program was successful in achieving its goals and the industrial partners even exceeded their commitments (Koeberlein 2014; Stanton 2010; Gibble 2013). The improvements made during the program not only involved powertrain components but also advanced several vehicle components including aerodynamics, transmissions, chassis, air-conditioning, tires, and auxiliaries. As a result, many significant efficiency improvement technologies were developed and are in the process of commercialization, which will further help vehicle manufacturers around the world. To further improve the heavy-duty segment, Super Truck-II (Gilroy 2016; Mulero 2016) was launched in 2016 and brings onboard teams from industry and national labs to research, develop, and demonstrate greater improvement in vehicle freight efficiency thereby cutting down significantly on CO_2 emissions.

EU has taken a less involved approach to improvising the efficiency of heavy-duty vehicles as compared to the US. The EU plans to regulate CO_2 emissions and the targets have been announced in 2018. AEA-Ricardo (AEA-Ricardo 2011) and TIAX (TIAX 2011) reports described extensive research effort by major heavy-duty manufacturers such as Daimler (Daimler 2017), Scania (Scania 2017) and Volvo for increasing diesel engine's efficiency. Major initiatives include improving the combustion system via higher pressure fuel injection systems, reducing engine friction, waste-heat recovery turbo-compounding, and other improvements in the engine such as friction reduction in other parts of the powertrain, redesigning of accessories, etc. These measures are taken continuously to reduce vehicle CO_2 emissions in addition

to other developments such as aerodynamics, the increment of bio-component into the fuel blends and hybridization of drivetrains.

2.3.3 Recent Developments in Marine Sector

There are several proposed compliance options to meet the upcoming IMO regulations and aspirations. As far as the availability of 0.5% m/m Low Sulphur Fuel Oil (LSFO) to meet the IMO Sulphur cap is concerned, there have been conflicting reports on the availability of such fuel. A study (Delft 2016) on the availability of compliant LSFO by the IMO chartered CE-Delft reported that all refineries have the capability to supply sufficient quantities of marine fuels with a Sulphur content of 0.50% m/m or less and with a Sulphur content of 0.10% m/m or less to meet demand for these products, while also meeting demand for non-marine fuels. On the other hand, Ensys and Navigistics supplemental marine fuel availability study (Ensys and Navigistics 2016) presented to IMO suggests that the global refining industry will lack sufficient capacity to fully respond to the IMO Sulphur cap resulting in the price increase of not only fuel oil but also distillates and sweeter (low Sulphur) crudes. It is expected that the traditional fuels compliance option will be a mix of distillates (MGO/MDO), LSFO, and their blends; based on the compliance option used, the price for IMO-compliant marine fuels would be significantly more than HFO causing an increase in freight tariffs and will eventually result in some degree of stress on world economy. LNG is proposed as an important alternative option to HFO and LSFO in the marine sector. It offers several advantages; using a gas (LNG)-only engine can reduce the SO_x and soot emissions by almost 100% without further need of after-treatment with manageable NO_x emissions. The CO_2 saving potential of LNG compared to HFO is high (5–30%) but methane slip issues currently reduce the total CO_2 savings (0–20%). Depending on the location, LNG is also price competitive to distillates (MGO/MDO) compliance option with a discount of around $5/MMBtu (OIES 2018a). However, there is a severe infrastructure development barrier that the LNG markets need to overcome for any meaningful marine market penetration and LNG share in marine sector is expected to be around 5% by 2025 (WoodMackenzie 2018).

The other compliance option to meet IMO Sulphur cap is to use scrubber technology for exhaust after-treatment of SO_x emissions. One of the challenges in the uptake of the scrubber technology is the complexity associated with the shipping business. Typically, three to four parties are involved in the entire chain of the shipping business, a shipbuilder who manufactures the ships based on the order by shipowner, the shipowner either directly leases the ships-to-ship charterer or through a middle company to ship charterers who operates the ship. The problem with installing scrubbers is that the ship owners have no incentive to take their ships out of service in the shipyards and also charterers do not see value in paying more up front to the ship owners to make use of low priced HFO which in the long run is a cheaper compliance option. Due to these reasons, scrubber technology is expected to have a limited uptake of around 10–20% by 2020.

Table 2.4 Estimated life cycle CO_2 emissions reduction and current supply and uptake availability of alternative and renewable fuels (adopted from ITF 2018)

Alternative and renewable fuels	CO_2 emissions reduction (%)	Current supply and uptake potential (% of total marine energy)
Advanced biofuels	25–100	0
LNG	0–20	1–2
Hydrogen	0–100	0
Ammonia	0–100	0
Methanol	25–100	0

Several alternative and renewable fuel options are receiving increased attention in the marine sector to meet the upcoming SO_x, NO_x, and CO_2 emissions regulations and aspirations. These include advanced biofuels, LNG, Hydrogen, Ammonia, and Methanol. These options intrinsically produce negligible (well below the 0.5% Sulphur cap) SO_x emissions, manageable NO_x emissions that could be treated using conventional selective catalytic reduction (SCR)-based exhaust after-treatment, and based on the process used for production, can be fully CO_2 neutral. Table 2.4 shows some estimates on CO_2 savings and current supply and uptake potentials of these options for the marine sector. It can be seen from Table 2.4 that although the potential CO_2 savings could be quite significant, depending on the synthesis process of these fuels, the current supply and uptake potential of most of these options, apart from LNG, is quite limited. It is expected that the marine sector will continue to be dominated by oil-based residual and distillate fuels.

Furthermore, various technological and operational measures have been proposed to improve the overall energy efficiency of the marine sector (ITF 2018). The traditional energy efficiency criteria for the new ships is the so-called Energy Efficiency Design Index (EEDI), which measures the CO_2 emissions of the ships and is expected to reduce the CO_2 footprint by 30% by 2030. Other proposed technological measures that are expected to improve the energy efficiency of the ships include using lighter materials to reduce the weight of the ship, slender design for improved hydrodynamics, friction reduction using specialized hull coatings and air lubrication, and incorporating ways to recover waste heat. Operational measures for improving the energy efficiency of the shipping industry include reducing ship speed, increasing ship size, improving the ship–port interface, and providing onshore power at the port.

2.3.4 Recent Developments in Aviation Sector

As explained earlier, the aviation sector is set to rely greatly on the CORSIA mechanism for carbon-neutral growth from 2020. As such, it is expected that oil-based jet fuels will continue to power the aviation sector. The approved Sustainable Aviation Fuels (SAFs) under ASTM D7566, the standard for

Table 2.5 A summary of regulations to curb CO_2 emissions and evolution of technology in various transportation sectors on 1–5 scale

	Light-duty sector	Heavy-duty sector	Marine sector	Aviation sector
Regulations	5	4	1	3
Evolution of technology	5	3	2	2

specifications for aviation turbine fuel containing synthesized hydrocarbons, include Fischer-Tropsch hydro processed synthesized paraffinic kerosene (FT-SPK), synthesized paraffinic kerosene produced from hydro processed esters and fatty acids (HEFA-SPK), synthesized iso-paraffins produced from hydro processed fermented sugars (SIPS-HFS), synthesized kerosene with aromatics derived by alkylation of light aromatics from non-petroleum sources (SPK/A), and alcohol to jet synthetic paraffinic kerosene (ATJ-SPK). These SAFs are expected to be blended in a certain ratio (10–50%) with typical aviation jet kerosene fuels; as such, there are many questions and barriers that need to be overcome by SAFs to have any meaningful market share; there are concerns on the environmental benefits of these fuels (well to wings life cycle footprint), and on the cost and availability of these SAFs.

Overall, it is the light-duty road transportation sector where the regulations are stringent and to meet these regulations most of the innovation in engine/fuel technology is witnessed. Heavy-duty road transportation sector has also seen a surge in legislation for regulating emissions and pollutants and is closely following light-duty segment's lead. The reason for relatively strict regulations for light- and heavy-duty segment stems from the fact that these vehicles have higher visibility in urban and rural spaces where they are often used for transporting people and goods. Additionally, the rapid evolution of technology to meet the regulations has led to tighter regulations in these segments. The regulations in Aviation or Marine sector are still evolving, but several recent developments highlighted in this chapter indicate that tighter legislation will soon be in place. A tabular comparison is presented in Table 2.5 to further summarize the state of regulations and their implementation in various mobility segments on the scale of 1–5 with 5 being highest.

2.4 Technology Trends of Internal Combustion Engines Toward High Efficiency

For the light-duty (LD) passenger transport applications, spark-ignited (SI) engines are mainstream, except Europe, and there is a lot of scope for improvements. The gaseous emissions such as hydrocarbon (HC), carbon monoxide (CO), and nitrogen

oxide (NO_x) are treated by three-way catalytic converter with emissions levels being already very low. Therefore, all research directions with SI engines are geared toward the improvement of engine efficiency based on several strategies. The commercial transport applications such as heavy-duty truck, and marine sector rely on compression ignition (CI) engines. CI engine is more efficient than SI engines; however, the emissions of NO_x and soot are higher, and diesel after-treatment is quite expensive. The best possible way to mitigate these emissions would be through in-cylinder phenomenon to achieve low-temperature combustion (LTC) without compromising the efficiency. The other goals pertaining to CI engine research are to maximize the engine efficiency by analyzing the thermodynamic cycles and to develop a fuel-flexible hardware. The trends and recent developments in this context are explained in the following sections.

2.4.1 High-Efficiency SI Engine Research

Ever since the advent of the combustion engine, the thermal efficiency of the ICE has continuously improved. The evolution of efficiency over the past few centuries is depicted in Fig. 2.3. The significant breakthrough came in 1876 from Nikolaus August Otto, who pioneered the invention of an engine that is commonly referred to as a gasoline engine. With the advancement in fuel supply system from the conventional carburetor to port fuel injection (PFI) system, the efficiency improved to 35%. Subsequently, the transition from the PFI system to Gasoline Direction Injection (GDI) system is marked as one of the technological milestones towards higher efficiency in SI engine development (Zhao et al. 1999). The direct injection of fuel into the cylinder with the GDI system reduces the global equivalence ratio, and the cooling effect also adds to improvement in efficiency. In the wake of various engine development strategies, the current efficiency of the SI engine has increased to 42%. Researchers are still in the race to achieve better thermal

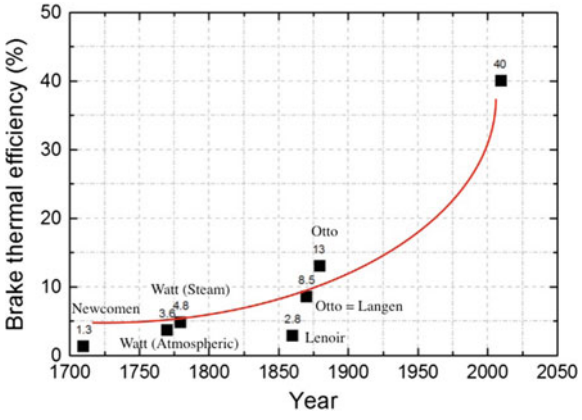

Fig. 2.3 Historical evolution of energy efficiency of a Spark-Ignited (SI) engines

efficiency and the key technology enablers are (1) Engine downsizing (2) Lean burn technology with dilution tolerance, and (3) Government-level initiatives such as the Co-Optima Program.

2.4.1.1 Engine Downsizing

Increasing the compression ratio of the SI engine and diluted combustion are important pathways to improve the efficiency of the engine. However, attaining a maximum compression ratio is limited by engine knock and dilution decreases the burnt rate of combustion. Engine downsizing is an effective approach to improve the efficiency that directly relates to the reduction of carbon footprint (Turner et al. 2014). Despite the smaller displacement volume of the engine, the power output is higher as more air is inducted to burn the fuel through boosting. Reducing the pumping, frictional and heat losses reduce the fuel consumption with the reduced engine out emissions (Avola et al. 2015). The pressure/temperature history of these modern engines are far away from the RON/MON conditions in that the octane rating scale is no longer agreeable. These engines depend on a factor "*k*", which is a constant in the octane index formulation (OI = RON – $k * S$). The factor "*k*" is negative for highly boosted downsized engines when knock limited and requires fuels with higher octane sensitivity (Avola et al. 2015). Variable Geometry Turbine (VGT) is a technological advancement in the development of turbocharged engines that allows for a fast transient response to synergize appropriately with the engine (Tang 2016). Currently, Mazda, Ford and Chevrolet, BMW, Mercedes-Benz, and Volkswagen Auto Group have adopted downsized GDI engine with turbocharger technology. The maximum efficiency of the reported commercial engine is 35% and efforts are being taken to further increase the efficiency. This advanced powertrain coupled with hybrid technology is beneficial and Toyota Prius plug-in hybrid electric vehicle showed a brake efficiency of 42%. Dilution through Exhaust Gas Recirculation (EGR) is an effective approach in a turbocharged GDI engine. Diluted combustion relates to stoichiometric operation in boosted downsized gasoline engines and offers greater potential to reduce fuel consumption (Wei et al. 2012). Cooled EGR reduces the engine knock, minimizes pumping losses and avoids the enrichment zones to improve fuel economy. However, the development of flame kernel under heavily diluted condition is difficult and high spark discharge system is recommended. Honda R&D recently demonstrated 45% efficiency using 35% EGR at an engine speed of 2000 rpm with an optimized combustion chamber design (Ikeya et al. 2015). In order to overcome the dilution tolerance and support auto-ignition; higher spark energy of 450 mJ is used. A 3% increase in efficiency when compared to the existing commercial vehicle is a promising improvement.

2.4.1.2 Lean Burn Technology

Lean combustion in SI engines improves the fuel economy and reduces the global CO_2 emissions (Tully 2002; Ayala and Heywood 2007). Moving from stoichiometric to lean mixture increases the specific heat ratio and reduces the pumping losses, which increases the thermal efficiency. However, the disadvantage of this technology is the incompatibility of the catalytic converter at lean conditions. Catalytic converter is effective only at stoichiometric ($ø = 1$) condition and, therefore, the use of lean technology leads to increased HC and CO emissions. The main problem with the lean combustion technology is the inadequacy of the ignition energy supplied from the spark plug. As the mixture is lean, the ignition energy is increased to improve the combustion stability and tolerate the dilution level (Shah et al. 2012; Toulson et al. 2010). Thus, development and characterization of the ignition system for lean-burn SI engines are crucial.

In a measure to adopt lean combustion technology in modern gasoline engines, Turbulent Jet Ignition (TJI) through pre-chamber combustion system was proposed (Alvarez et al. 2017). While the spark energy is not sufficient to burn the lean mixture in a gasoline engine, Turbulent Jet Ignition (TJI) is favorable to support lean combustion. The pre-chamber system is incorporated in place of a spark plug in the cylinder head. Initially, the TJI concept was applied for operation of natural gas in an SI engine to improve the efficiency (Attard et al. 2012a). Currently, gasoline only system substitutes the use of natural gas with improved durability (Attard et al. 2012b). According to the pre-chamber concept that functions with gasoline alone, a small quantity of liquid fuel is injected in the pre-chamber. In the main combustion chamber, fuel is directly injected early in the cycle so that a lean mixture is formed. Given the volume of pre-chamber is only 3% of the main combustion chamber, a rich mixture is burnt in the pre-chamber to create a stratified charge. The more active radicals of the burnt mixture in the pre-chamber pervade as turbulent jets into the main combustion chamber and create multiple ignition sites. This turbulent jet has more active energy compared to the spark energy and increases the mass burnt rate. The increased flame propagation extends the knock limit that helps to improve the efficiency. MAHLE powertrain showed an ultra-lean homogeneous combustion ($\lambda \sim 1.6$) with an efficiency of 42.8% based on a new design of pre-chamber system in a gasoline engine (Bunce and Blaxill 2016). Since knock is limited, the compression ratio of the engine can be increased (hardware upgrade) to further increase the efficiency up to 45%. Based on pre-chamber jet ignition system, HONDA (i-CVCC) demonstrated an efficiency of 47.2%. These technologies would be commercialized in the near future so that the benchmark to compete with would be a higher efficiency of around 48–50%.

2.4.1.3 Government Level Initiatives (Co-optima Program)

The Co-Optima Program aims to introduce clean, efficient, and high-performance engine by establishing synergy between fuel and engine technologies (U.S. DOE

2016). The Co-Optima approach helps to identify a new blend-stock that can be blended with gasoline to improve the performance of the vehicle and reduce the emissions. The selection of blend-stock from domestic resources delineates to cellulosic biomass, renewable, nonfood, and surplus resources. The blend-stock is evaluated based on the fuel properties and design parameters that maximize the efficiency of the engine through mitigation of knock. Research Octane Number (RON), octane sensitivity (S = RON − MON), and heat of vaporization are the important properties that improve knock resistance of modern SI engines. For achieving these favorable properties, the chemical families identified are alcohols, ketones, furans, alkenes, and aromatics. The blend-stock produced from any of these families when blended with gasoline improves efficiency. Before blending, the compatibility of these blend-stocks on engine infrastructure is screened. Furthermore, system-level analysis of these blend-stocks with respect to economic, technological, market, and environmental factors is performed. The gasoline blended with the blend-stock when operated in a boosted SI engine results in a highly efficient co-optimized fuel/engine system. The Co-Optima researchers demonstrated a direct correlation between knock performance and Octane Index (OI), which is a crucial derived property (OI = RON – k * S). While Low-Speed Pre-Ignition (LSPI) limits the engine efficiency, measures to identify and prevent pre-ignition occurrence for various gasoline blends under boosted conditions are essential. Computational analysis based on numerical algorithms and validated engine models provide insights into the development of the engine, which cannot be operated in a laboratory scale due to practical limitations. The co-optimized engine operated under multi-mode combustion concept is the next step to further increase the efficiency. Overall, fuel properties and advanced combustion concepts help to improve engine efficiency, and programs like Co-Optima could facilitate the identification of an optimum fuel-engine combination.

2.4.2 High-Efficiency CI Engine Research

Diffusion-controlled spray combustion leads to the formation of increased NO_x and soot emissions in a CI engine. Today's commercial medium and heavy-duty fleets adopt the Mixing-Controlled Compression Ignition (MCCI) concept for gaining higher efficiency but require effective emission control technologies. The diesel after-treatment utilizes Selective Catalytic Reduction (SCR) and particulate filter to reduce the NO_x and particulate matter emissions, whereas HC and CO emissions are treated by Diesel Oxidation Catalyst (DOC) (Johnson 2010). These after-treatment devices are much more complex and expensive when compared to the three-way catalytic converter in SI engines. High-pressure Common Rail fuel Direct Injection (CRDI) system is a pioneering technology to improve the fuel atomization and air/fuel mixing. However, the advancement from mechanical injection to CRDI system could not mitigate the deleterious emissions of NO_x and PM. Measures to overcome the NO_x/soot tradeoff have been up-taken over several decades and paved the way

to the development of new combustion concepts. Instead of after-treatment technique, advanced combustion concepts such as Homogenized Charge Compression Ignition (HCCI) and Partially Premixed Combustion (PPC) are proposed for simultaneous reduction of NO_x and soot emissions (Zheng 2009; Noehre et al. 2006). Furthermore, these combustion strategies also improve the efficiency due to low-temperature combustion (minimized heat loss), which mitigates the CO_2 emission. Besides new combustion concepts, the thermodynamic cycle analysis to realize higher efficiency has been investigated and researched. The eight-stroke engine is the latest technology that improves the thermodynamic process to reduce the heat losses and allows for efficiency improvements. These renewed combustion concepts that aim to achieve 60% efficiency are current research initiatives pertaining to CI engine technology.

2.4.2.1 High-Efficiency Combustion Concepts

Few in-cylinder combustion strategies proposed to mitigate NO_x and soot emissions without compromising engine efficiency are HCCI, PPC, and Reactivity-Controlled Compression Ignition (RCCI) (Sarangi 2012). These Low-Temperature Combustion (LTC) concepts reduce the local flame temperature and equivalence ratio in such a way that NO_x and soot formation are reduced simultaneously. When the Start of Injection (SOI) is advanced from late to early fuel injection timings, combustion drifts from CI toward HCCI condition (Vallinayagam et al. 2017). In HCCI mode, fuel and air are completely premixed during the significant delay period and combustion is controlled by mixture chemical kinetics. Given that the controllability of combustion is a problem at high load with HCCI due to rapid pressure rise rate; studies on PPC emerged that effectively controls combustion due to increased combustion stratification (Najafabadi 2017). While combustion phasing is sensitive to SOI in CI combustion, it is dependent on intake air temperature for HCCI combustion. PPC is intermediate between HCCI and CI combustion in that the fuel injection is crucial for controlling the combustion phasing. In 2001, Nissan Motor Company investigated diesel PPC through modulated kinetics combustion concept (Kimura et al. 2001). Based on EGR, the required ignition delay was created at various loading conditions. Due to low temperature and premixed combustion, a simultaneous reduction in NO_x and soot emission was achieved. The high load diesel operation demanded 70% EGR, which deteriorated the combustion process. Given that diesel PPC was not advantageous at all the operating ranges, gasoline PPC was introduced in 2006 (Kalghatgi et al. 2006). When fuels with resistance to auto-ignition are used in CI engines, they create an adequate delay period for premixing; this decreases the in-cylinder temperature to suppress NO_x formation, while local fuel to air equivalence ratio is decreased to reduce soot emission. Gasoline PPC is also described as Gasoline Compression Ignition (GCI), which has grabbed more attention in the past decade and most of the engine manufacturers are in the endeavor to commercialize the first GCI engine.

Ignition assistance is required to support the auto-ignition and maintain combustion stability when using high RON gasoline fuels in a Compression Ignition (CI) engine. However, high RON fuels prove difficult to auto-ignite at low load condition, as the available boost is limited (Manente et al. 2009). In the current scenario, low-load GCI is a big challenge and efforts are being made to improve the combustion stability. Selection of low RON gasoline could avert this problem and RON 70 gasoline is an ideal candidate for GCI investigation (Solaka et al. 2012). Naphtha (a low octane gasoline fuel with RON ∼ 60–70) has been tested as a suitable fuel for GCI engines (Alabbad et al. 2018; Leermakers et al. 2013) due to its suitable fuel properties such as its optimal reactivity to ignite under compression, low well-to-tank carbon footprint due to reduced refinery processing and higher H/C ratio (due to paraffinic composition) ascertaining lower tank-to-wheel carbon emissions. Furthermore, based on its boiling point (BP), naphtha can be categorized as light (BP = 75 °C) or heavy (BP = 175 °C). Since it is a less-processed fuel, less refining energy is required thereby reducing production costs; it is also less intensive in terms of reduced well-to-tank CO_2 emission. The vehicular demonstration of naphtha in a PPC engine demonstrated improved fuel economy and better combustion stability at low load condition (Chang et al. 2013). Thus, low-load operation of GCI is possible without any auto-ignition problems using low RON gasoline or naphtha. However, the low RON gasoline fuels are not commercially available and adaption of these fuels could be a choice in the future. At present, high RON gasoline is being used commercially and strategies to overcome auto-ignition problems and enable low load and idle operation are essential. In this respect, Delphi is involved in the development of Gasoline Direct injection Compression Ignition (GDCI) engine using US market gasoline (Sellnau et al. 2014, 2016). The fuel injection strategy was optimized in such a way to achieve PPC at very low fuel injection pressure, typical of GDI engines. Delphi electrical cam phaser's actuated the exhaust valve train to enable secondary valve lift, recuperating heat from hot exhaust gases to support auto-ignition at low loads. Retaining the residuals helps to reduce the oxygen flow rate and local flame temperature with increased heat capacity. The longer ignition delay also influences the local fuel to air equivalence ratio. As such, both NO_x and soot emissions are simultaneously reduced. Measures to control the combustion by spark assistance provided a better solution (Manofsky et al. 2011). Spark-assisted GCI is the evolving technology toward the extension of low load limit until now (2018). A recent innovative combustion concept called Spark-Assisted Compression Ignition (SACI) of gasoline was introduced by MAZDA (2018). With Mazda's Skyactive-X is ready for launch on 2019, it is touted as the world's first commercial gasoline engine running on compression ignition mode.

The pictorial layout in Fig. 2.4 elucidates the different high-efficiency combustion concepts that have been identified thus far.

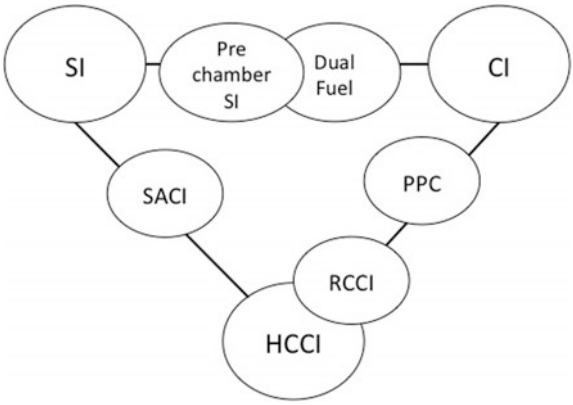

Fig. 2.4 Advanced high-efficiency combustion concepts for ICE

2.4.3 Eight-Stroke Engine Concept (High-Pressure Combustion)

Eight-stroke concept is a staged engine concept and is an alternative step to achieve up to 60% engine efficiency (Lam et al. 2015). Staged or complex engines have been around for over a century. Most powertrains are staged engines with a rotary compressor and expander before and after the piston machine. The reason to assess replacing these rotary units with piston machines is the greater efficiency of piston machines at volumes that are typical of light- and heavy-duty engines. The challenge to attain maximal efficiency from this architecture requires a thorough understanding of inherent loss mechanisms. The 1D modeling of such complex devices provides us a design tool to evaluate the performance of such a device with various design features such as staging ratios, insulation, modifications to air path, and combustion concepts (Shankar et al. 2017, 2018). The development of any high-efficiency system must also consider the boundary conditions for an effective after-treatment system, which is also evaluated using 1D gas exchange models. The concept is a bit down the road from being fully realized as only a demonstrably superior efficiency compared to present architectures could convince manufacturers to adopt this technology.

2.5 Disruptions in Transportation Sector and Policy Implications

Transportation sector is going through a major disruption phase and personal mobility is on the cusp of change from what we have known for the past 50 years or so, and such disruptions are most evident in the LDV road transportation sector. Electrification and hybridization are important disruption agents (OIES 2018b). In recent years, several new technologies have featured in the otherwise ICE-dominated

LDV road transport sector. These include HEVs, PHEVs, BEVs, and FCVs. Of these technologies, HEVs and PHEVs, depending on the mode of operation (e.g., charge sustaining versus charge depleting modes in PHEV), still rely heavily on ICE as primary energy source in the vehicle, and only the BEVs, typically of limited driving range, are powered by fully electrified powertrains; nonetheless, it has to be acknowledged that pure ICE vehicle models, without any hybridization or electrification, may well be phased out from the LDV sector in the next 15–20 years time frame. In much of the popular media, such disruptions, in one form or the other, are readily linked to an eventual demise of oil-based ICE-powered vehicles. Such a hype should be evaluated cautiously as the technologies go through many hype and disappointment cycles before they make a major impact in the market or die down (Melton et al. 2016). Kalghatgi in his recent work tried to answer some of the hype associated with this notion in his paper titled "Is it really the end of internal combustion engines and petroleum in transport?" (Kalghatgi 2018). He argues that, for LDVs, available battery capacity will have to increase by several hundred-fold, perhaps by several thousand-fold, for complete electrification. This will have serious economic, social, environmental, and political impacts and, as such, is highly unlikely in near future. In addition, the requirements for complete electrification of HDVs are even more stringent (Kalghatgi 2018; Sripad and Viswanathan 2017), and are so extreme for marine and aviation, that proposing such electrified solutions for them, even in the presence of current media hype, should be backed up by thorough, unbiased and scientific analyses of which nothing could be found in literature. Hence, unless renewable electricity becomes abundantly available and price competitive, the massive infrastructure requirements for electrification are dealt with, and the battery capacities and costs dramatically improve to meet the transportation needs, transportation sector is expected to be powered by oil-based solutions, in one form or another, particularly for HDVs, marine, and aviation, for the foreseeable future. Hybridization of ICE vehicles is the most probable way forward for improving the efficiency and environmental footprint of ICE-only vehicles, and the transition of transportation, even for LDVs, to complete electrification will be evolutionary and not disruptive spanning several decades.

The other disruptive agents in the transportation sector, again primarily in the LDV sector, are the emergence of shared mobility and autonomous vehicles (OIES 2018b). The Ubers, the Lyfts, the Careems, etc., model of transportation as a service has certainly received widespread acceptance since such a model allows the consumers to have a ride ready whenever and wherever they want without worrying too much about the problems (parking, refueling, service, maintenance, insurance, etc.) associated with the transportation ownership model. The advent of shared mobility model and the autonomous vehicles also combine well with each other and it is expected that in future, especially in big metropolises, these two disruptive agents will steadily overtake the transportation ownership model. The cost of such rides per kilometer are expected to come down; and although the transportation as a service model and autonomous vehicles will improve the traffic congestion and problem related to ever-increasing cars, the total number of kilometers are expected

to be increased because of the ease of use offered by such models (OIES 2018b). The profit margin and continuous vehicle availability are expected to be among major considerations of the vehicle/fleet operators under transportation as a service model, again, complete electrification of the LDV fleet in such a model could only be realized if the electric cars become price competitive and the charging times and the mileage of BEVs significantly improve. Fleet operators will also closely monitor all of these parameters for the scenarios where the government provided subsidies for electric vehicles and battery charging dry out.

In addition to the disruptions discussed above, some countries have announced their aspirations to ban ICE-only vehicles. Such aspirations are meant to curb the pollutants related to local air quality, the NO_x, SO_x, CO, HCs and soot emissions, and the climate change. The governments of UK, France, China, India, Germany, along with city administrators of major metropolises including Paris, Barcelona, Madrid, have expressed aspirations to ban ICE only vehicles in 2030–2040 time-frame. Most of these aspirations are announced in the popular media without formal government-level proposals or regulations drafted thus far. Implicit in these news is the fact that most of these countries, although aspire to ban ICE-only vehicle, will still continue to use combustion engine hybridized in one form or another as a primary energy source for the vehicles. It is beyond question that transportation must do more to improve its environmental footprint. However, it is equally important that the governments and regulators, instead of picking the winners, take a balanced and informed approach while formulating policies and regulations for the transportation sector. Life Cycle Analysis (LCA)-based policies and decision-making (Abdul-Manan 2018) should be adopted to arrive at scientifically backed policies and practical solutions to improve the environmental impact of the transportation sector. All the technological options should be properly evaluated utilizing LCA-based methodologies to arrive at a sustainable transportation model for the future. Policy makers and regulators must avoid simple burden shifting as such short-sighted approaches may alleviate the pollution concerns in the cities but may not overcome the climate change concerns globally.

2.6 Conclusions

The mobility of man and goods accounts for around a quarter of greenhouse gas emissions globally and, therefore, naturally attracts the most stringent regulations for emissions and fuel efficiency. Here, current and prospective regulatory framework for road, marine, and aviation transport sectors, aimed at curbing the CO_2 emissions from the transportation is presented. It is shown that the fuel economy and CO_2 emission targets are becoming stricter across the various transportation sectors. For light-duty sector, such regulations are even more stringent and the recent introduction of zero-emission mandates is forcing the OEMs to invest more in hybridization and electrification. The available compliance options for various transport sectors are also discussed. Holistically speaking, the fossil fuel powered

combustion engines/turbines are expected to continue powering the transport sector for decades to come. The passenger transport sector is expected to have a slow transition, spanning several decades, towards electrification. Several advanced engine technologies, with the potential to improve fuel economy and CO_2 emissions, including highly boosted and downsized SI engine concepts, pre-chamber SI engine concept, 8-stroke and GCI/PPC CI concepts are briefly discussed. Various disruption agents are presented, especially in the light-duty sector, and it is expected that the personal mobility models may change in the near future. Finally, it is argued that a LCA-based policy must be adopted for proposing any future regulations for the transport sector.

References

Abdul-Manan AF (2018) On the appropriate use of life-cycle thinking for evidence-based sustainable transport policy. Environ Sci Policy Sustain Dev 60:18–25

AEA-Ricardo (2011) Reduction and testing of greenhouse gas emissions from heavy duty vehicles-LOT 2. Development and testing of a certification procedure for CO_2 emissions and fuel consumption of HDV, report by AEA and RIcardo

Alabbad M, Issayev G, Badra J, Voice AK, Giri BR, Djebbi K, Ahmed A, Sarathy SM, Farooq A (2018) Autoignition of straight-run naphtha: a promising fuel for advanced compression ignition engines. Combust Flame 189:337–346

Alvarez CEC, Couto GE, Roso VR, Thiriet AB, Valle RM (2017) A review of prechamber ignition systems as lean combustion technology for SI engines. Appl Therm Eng

Attard WP, Toulson E, Huisjen A, Chen X, Zhu G (2012a) Spark Ignition and pre-chamber turbulent jet ignition combustion visualization. SAE Technical Papers

Attard WP, Blaxill H, Anderson EK, Litke P (2012b) Knock limit extension with a gasoline fueled pre-chamber jet igniter in a modern vehicle powertrain. SAE Int J Engines 5(3):1201–1215

Avola C, Copeland T, Duda R, Burke S, Akehurst CB (2015) Review of turbocharger mapping and 1D modeling inaccuracies with specific focus on two-stag systems. SAE Technical Paper Report No 0148–7191

Ayala FA, Heywood JB (2007) Lean SI engines: the role of combustion variability in defining lean limits. SAE Technical Papers

Bunce M, Blaxill H (2016) Sub-200 g/kWh BSFC on a light duty gasoline engine. SAE Technical Paper

CARB (2016) Zero-emission vehicle standards for 2018 and subsequent model year passenger cars, light-duty trucks, and medium-duty vehicles, California Air Resource Board

Chang J, Kalghatgi G, Amer A, Adomeit P, Rohs H (2013) vehicle demonstration of naphtha fuel achieving both high efficiency and drivability with EURO6 engine-out NOx emission. SAE Int J Engines 6(1):101–119

COM//0767 final//0382 (COD) (2016) Proposal for a directive of the European parliament and of the council on the promotion of the use of energy from renewable sources (recast), COM//0767 final//0382 (COD)

COM//284 (EU) (2015) Proposal for a regulation setting CO_2 emission performance standards for new heavy-duty vehicles

Cui H (2018) China's new energy vehicle mandate policy (Final Rule). Policy update. ICCT report

Daimler (2017) Diamler Sustainability focus report, Diamler 2017

De Groot GJ (1996) Blighty: British society in the era of the great war. Addison-Wesley Longman

Delft (2016) Assessment of fuel oil availability, Final report, CE Delft, July 2016

Delgado O, Lutsey N (2014) The U.S. SuperTruck program: expediting development of advanced HDV efficiency technologies
Elgowainy A, Han J, Ward J, Joseck F, Gohlke D, Lindauer A, Ramsden T, Biddy M, Alexander M, Barnhart S, Sutherland I, Verduzco L, Wallington TJ (2018) Current and future united states light-duty vehicle pathways: cradle-to-grave lifecycle greenhouse gas emissions and economic assessment. Environ Sci Technol 52(4):2392–2399
EnSys and Navigistics (2016) Supplemental marine fuel availability study to the IMO, EnSys and Navigistics, July 2016
EPA (2017) Carbon dioxide emissions and fuel economy trends report, US EPA 2017
EU (2018) Monitoring of CO_2 emissions from passenger cars—Regulation (EC) No 443/2009
Faria P, Marques P, Moura F, Freire J, Delgado AT, de Almeida R (2013) Impact of the electricity mix and use profile in the life-cycle assessment of electric vehicles. Renew Sustain Energy Rev 24:271–287
Garg M, Sharpe B (2017) Fuel consumption standards for heavy-duty vehicles in India, ICCT report
Gibble K (2013) Scattering of cold-atom coherences by hot atoms: frequency shifts from background-gas collisions. Phys Rev Lett 110(18):180802
Gilroy RW (2016) SuperTruck II aims to more than double freight efficiency of Class 8s
Hanemann M (2008) California's new greenhouse gas laws. Rev Environ Econ Policy 2(1):114–129
Hawkins TR, Singh B, Majeau Bettez G, Strømman AH (2013) Comparative environmental life cycle assessment of conventional and electric vehicles. J Ind Ecol 17(1):53–64
Hebert A (2017) Developing future light-duty vehicle regulations in California, CARB 2017
Hesterberg TW, Lapin CA, Bunn WB (2008) A comparison of emissions from vehicles fueled with diesel or compressed natural gas. Environ Sci Technol 42(17):6437–6445
Huo H, Cai H, Zhang Q, Liu F, He K (2015) Life-cycle assessment of greenhouse gas and air emissions of electric vehicles: a comparison between China and the U.S. Atmos Environ 108:107–116
ICAO Resolution A39-2 (2016) Consolidated statement of continuing ICAO policies and practices related to environmental protection—climate change and global market-based measure (MBM) scheme, 39th ICAO Assembly
IEA (2017) Energy technology perspectives. http://www.iea.org/etp/explore/
Ikeya K, Takazawa M, Yamada T, Park S, Tagishi R (2015) Thermal efficiency enhancement of a gasoline engine. SAE Int J Engines 8
ITF (2018) Decarbonizing maritime transport: pathways to zero-carbon shipping by 2035. OECDs International Transport Forum (ITF)
Johnson TV (2010) Review of diesel emissions and control. SAE Int J Fuels Lubr 3:16–29
Kalghatgi G (2018) Is it really the end of internal combustion engines and petroleum in transport? Appl Energy 225:965–974
Kalghatgi GT, Risberg P, Ångström HE (2006) Advantages of fuels with high resistance to auto-ignition in late-injection, low-temperature, compression ignition combustion. SAE Technical Paper
Kimura K, Tsukahara K, Usui T, Okuda J, Kitamura Y, Kosuge M, Sano T, Tohyama S, Yamanaka O, Yoshii Y, Umemura S (2001) Low-dose tissue plasminogen activator followed by planned rescue angioplasty reduces time to reperfusion for acute myocardial infarction treated at community hospitals. Jpn Circ J 65(10):901–906
Kline SJ, Rosenberg N (2009) An overview of innovation, Studies on Science and the Innovation Process, pp. 173–203 (2009)
Koeberlein D (2014) Technology and system level demonstration of highly efficient and Class 8 trucks, Cummins Super Truck Program
Lam N, Tuner M, Tunestal P, Andersson A, Lundgren S (2015) Double compression expansion engine concepts: a path to high efficiency. SAE Int J Engines 8
Leermakers CAJ, Bakker PC, Somers LMT, Goey L, Johansson BH (2013) Butanol-diesel blends for partially premixed combustion. SAE Int J Fuels Lubr 6(1):217–229

Lutsey N (2018) The ever-improving efficiency of the diesel engine, ICCT report
Manente V, Johansson B, Tunestal P, Cannella W (2009) Effects of different type of gasoline fuels on heavy duty partially premixed combustion. SAE Int J Engines 2(2):71–88
Manofsky L, Vavra J, Assanis DN, Babajimopoulos A (2011) Bridging the gap between HCCI and SI: spark-assisted compression ignition. SAE Technical Paper
Manzetti S, van der Spoel D (2015) Impact of sludge deposition on biodiversity. Ecotoxicology 24 (9):1799–1814
MAZDA (2018) Next-generation Skyactive-X gasoline engine. MAZDA
McGill WR, Winther K (2013) Alternative fuels for marine applications, from the motor fuels implementing agreement. A report from the IEA advanced motor fuels
McNeil I (2002) An encyclopedia of the history of technology, Routledge Companion Encyclopedias
Melton N, Axsen J, Sperling D (2016) Moving beyond alternative fuel hype to decarbonize transportation. Nat Energy 1(3)
Mitchell J Jr, Dzerdzeevskii B, Flohn H, Hofmeyr W, Lamb H, Rao K, Wallen C, Mitchell Wallen J (1966) Climate change. World Meteorological Organisation Technical note
Morris I (2015) The unexpected origin of human values. New Sci 226(3017):28–31
Mulero E (2016) DOE debuts 2nd phase of SuperTruck; pledges $80 million to efficiency effort. American Trucking Associations. ISSN: 0041–1558
Najafabadi MI (2017) Optical study of stratification for partially premixed combustion, PhD thesis, Technische Universiteit Eindhoven 2017
Noehre C, Andersson M, Johansson B, Hultqvist A (2006) Characterization of partially premixed combustion. SAE Technical Paper
OIES (2018a) A review of demand prospects for LNG as a marine transport fuel, The Oxford Institue for Energy Studies
OIES (2018b) Disruptive change in transport sector. The Oxford Institute for Energy Studies
Regulation (EU) No 253 (2014) European Parliament and of the Council amending Regulation (EU) No 510/ to define the modalities for reaching the target to reduce CO_2 emissions from new light commercial vehicles (2014)
Regulation (EU) No 333 (2014) European Parliament and of the Council of 11 March 2014 amending Regulation (EC) No 443/2009 to define the modalities for reaching the 2020 target to reduce CO_2 emissions from new passenger cars
Sarangi A (2012) Diesel low temperature combustion: an experimental study. Loughboro University
Scania (2017) Scania sustainability report, Scania 2017
Sellnau M, Foster M, Hoyer K, Moore W, Sinnamon J (2014) Development of a gasoline direct injection compression ignition (GDCI) Engine. SAE Int J Engines 7(2):835–851
Sellnau M, Foster W, Moore J, Sinnamon K, Hoyer W, Klemm M (2016) Second generation GDCI multi-cylinder engine for high fuel efficiency and US tier 3 emissions. SAE Int J Engines 9:1002–1020
Seyferth D (2003) The rise and fall of tetraethyllead. 1. Discovery and slow development in european universities, 1853–1920. Organometallics 23(5):2346–2357
Shah A, Tunestal P, Johansson B (2012) Investigation of performance and emission characteristics of a heavy duty natural gas engine operated with pre-chamber spark plug and dilution with excess air and EGR. SAE Int J Engines 5(4):1790–1801
Shankar VSB, Lam N, Andersson A, Johansson B (2017) Optimum heat release rates for a double compression expansion (DCEE) engine. SAE Technical Paper
Shankar B, Shankar V, Johansson B, Andersson A (2018) Double compression expansion engine: a parametric study on a high-efficiency engine concept. SAE Technical Paper Series
Solaka SA, Boshamer SE, Parworth CL, Heard GL, Setser DW, Holmes BE (2012) Isomerisation of CF2ClCH2Cl and CFCl2CH2F by interchange of Cl and F atoms with analysis of the unimolecular reactions of both molecules. Chemphyschem Eur J Chem Phys Phys Chem 13 (3):869–878

Splitter DA, Pawlowski A, Wagner R (2016) A historical analysis of the co-evolution of gasoline octane number and spark-ignition engines. Front Mech Eng 1
Sripad S, Viswanathan V (2017) Performance metrics required of next-generation batteries to make a practical electric semi truck. ACS Lett 2:1669–1673
Stanton D (2010) High efficient clean combustion for SuperTruck. DEER 2010
Tang H (2016) Application of variable geometry turbine on gasoline engines and the optimisation of transient behaviours
Thiel C, Schmidt J, Zyl AV, Schmid E (2014) Cost and well-to-wheel implications of the vehicle fleet CO_2 emission regulation in the European Union. Transp Res Part A 63(4):25–42
TIAX (2011) European union greenhouse gas reduction potential for heavy-duty vehicles, prepared by TIAX for ICCT
Toulson E, Schock HJ, Attard WP (2010) A review of pre-chamber initiated jet ignition combustion systems. SAE Technical Paper
Toyota (2018) New vehicle zero CO_2 emissions challenge, Toyota Environmental report 2018
Transport Dept (2012) 2017–2025 model year light-duty vehicle greenhouse gas emissions and corporate average fuel economy standards, US Department of Transport
Transport Dept (2016) Greenhouse gas emissions and fuel efficiency standards for medium- and heavy-duty engines and vehicles—phase 2, US Department of Transport
Tully L (2002) A universal view of data. Interview by Anne Zender. J AHIMA 73(10):92
Turner JWG, Popplewell A, Richardson S, Lewis AGJ, Akehurst S (2014) Ultra boost for economy: realizing a 60% downsized engine concept. SAE Int J Engines 7:387–417
Tushman ML (1997) Winning through innovation. Strat Leadship 25(4):14–19
UNFCC (1992) United Nations framework convention on climate change. United Nations New York
UNFCC (2015) United nations framework convention on climate change, Paris, France
U.S. DOE (2016) Co-optimization of fuels & engines, US Department of Energy 2016
Vallinayagam R, Vedharaj S, An Y, Dawood A, Najafabadi MI, Somers B, Johansson B (2017) Combustion stratification for naphtha from CI combustion to PPC. SAE Technical Paper
Wei H, Zhu T, Shu G, Tan L, Wang Y (2012) Gasoline engine exhaust gas recirculation—a review. Appl Energy 99(2):534–544
WoodMackenzie (2018) IMO 2020 updated analysis of the marine fuel sulphur changes. https://www.woodmac.com/reports/refining-and-oil-products-imo-2020-updated-analysis-of-the-marine-fuel-sulphur-changes-18902
Yang Z, Bandivadekar A (2017) Light-duty vehicle greenhouse gas and fuel economy standards. ICCT report
Yao Z, Zheng HML (2009) Progress and recent trends in homogeneous charge compression ignition (HCCI) engines. Prog Energy Combust Sci 35:398–437
Zhao F, Lai MC, Harrington DL (1999) Automotive spark-ignited direct-injection gasoline engines. Prog Energy Combust Sci 25:437–562

Part II
Pollutants from Coal

Chapter 3
A Review on Pollutants from Coal Based Power Sector

Shashi Kant Verma, S. L. Sinha and D. K. Chandraker

Abstract Pollutants management techniques in thermal power station could be a key issue to contemplate once analyzing environmental deterioration. The release of harmful pollutants from warm power plants into water bodies as well as our surrounding atmosphere would bring about unsafe effects on the environmental life. This chapter gives an overview of various types of emitted pollutants from various fuel base based power plant and their measurement and control techniques, both past and present using various approaches. Various opportunities in power sector along with key challenges and issues related to climate change mitigation in the power sector would be discussed. In this chapter, some of the good correlation with their conclude remarks have been discussed. Stack Height for Small Boilers with emission limits as suggested by Central Pollution Control Board have also been discussed. Different theories and application for measurements and control of such hazards pollutants such as CO_2, SO_2, NO_2 and mercury have been presented. This chapter will include the some of the new emerging areas for thermal pollution control. The undesirable outputs of various fuel base thermal power plants not only affect the environmental laws but also have negative impacts on the water quality and ecological life. At the end, some of the good models with solutions and recommendations will be presented.

Keywords Thermal pollution · CO_2 · SO_2 · NO_2 · PM · Control techniques

S. K. Verma (✉) · S. L. Sinha
Mechanical Engineering Department, Malla Reddy Engineering College (Autonomous), Maisammaguda, Dhulapally, 500100 Secunderabad, Telangana, India
e-mail: mailme.shashi09@gmail.com

S. L. Sinha
e-mail: slsinha.mech@nitrr.ac.in

D. K. Chandraker
Reactor Design and Development Group, Bhabha Atomic Research Centre, Hall-7, Trombay, Mumbai 400085, Maharashtra, India
e-mail: dineshkc@barc.gov.in

R. A. Agarwal et al. (eds.), *Pollutants from Energy Sources*,
Energy, Environment, and Sustainability,
https://doi.org/10.1007/978-981-13-3281-4_3

3.1 Introduction

Power is the most fundamental needs in the everyday existence of each one in this dynamic world. As the world population increases, the demands of electricity have also being increased. Due to this, the difference between energy source and demand is forever present and it requires primary concern. At the same time, pollutants from the various thermal power plants increase. To defeat the situation of the distinction between the supply and demand, the effectiveness of the current power plants should be taken care and furthermore the newly power plants should be built up with the supercritical innovation. This increases the global temperature of the world. The substance that unconstructively affects the atmosphere, animals as well as human being, due to emission into the environment is called pollution. The air/water temperature rises so that it becomes unsafe to human being and other organisms. Table 3.1 shows the different pollutants from thermal power plants and

Table 3.1 Different thermal pollutants and their effects

S. No.		Types of pollutants	Effects
1.	Particulate types	Suspended particulate matter/dust	Depends on specific composition, reduces sunlight and visibility, increases corrosion, pneumoconiosis, asthma, cancer, and other lung diseases
2.		Fly ash	Settles down on vegetation, houses. Adds to the suspended participate matter (SPM) in the air. Leachates contain harmful material
3.	Gaseous pollutants	Carbon compound (CO and CO_2)	Respiratory problems, Green house effect
4.		Sulphur compounds (SO_2 and H_2S)	Respiratory problems in humans, Loss of chlorophyll in plants (chlorosis), acid rain
5.		SPM (Suspended particulate matter) (Any solid and liquid) particles suspended in the air, (flush, dust, lead)	Poor visibility, breathing problems, Lead interferes with the development of red blood diseases and cancer, Smog (smoke and fog) formation leads to poor visibility and aggravates asthma in patients
6.	Primary pollutants	NO_x	Lung irritation (e.g. inflammation, respiratory cell damage, premature ageing) Increased susceptibility to respiratory infection, Respiratory and cardiac diseases, Asthma attacks

their effects. There are different sources of thermal pollution like Petroleum refiners, Thermal power station, and Nuclear power plants. Over the last few years the energy part/area has come up against new challenges about the reduction of its effect on the surrounding conditions or on the health of the Earth. The higher types of amphibian life require oxygen for survival. The high temperature diminishes the grouping of oxygen in water. Thus, it is critical to weaken the warm fixation into water bodies and limit it into little territories to keep up the suitable furthest reaches of oxygen required for the oceanic life. Because of global atmosphere commitments, there may be a need to restrict the measure of unmitigated CO_2 outflows being radiated into the climate. Alleviation of such discharges at coal terminated power plants offers an effortlessly controllable method for lessening such outflows.

Wang et al. (2018) used Life cycle carbon emission modelling for coal-fired power plant in Chinese case. They analyse the carbon emissions from coal mining, processing and transport to coal-fired plant with the help of life cycle accounting model. They concluded that the availability and quality of data play a major role in Life Cycle Assessment (LCA) for developing the models.

3.2 Insight from Previous Study

Hassim et al. (2014) have studied Polychlorinated dibenzo-p-dioxins (PCDDs) and polychlorinated dibenzofurans (PCDFs) emissions measured from a coal-fired power plant. They established emission factors for each combustion condition using the following Eq. (3.1), modified from U. S. EPA (1997):

$$\text{Emission factor} = \frac{\text{Pollutant concentation}\left(\frac{\text{ng}}{\text{N m}^3}\right) \times \text{Flue gas flow rate}\left(\frac{\text{N m}^3}{\text{h}}\right)}{\text{Coal feeding rate}\left(\frac{\text{kg}}{\text{h}}\right)} \tag{3.1}$$

The emission factors range from 0.08 to 0.11 ngI–TEQ/kg, which is depends on country. Hassim et al. (2014) also summarized the emission factors for different country i.e. in Taiwan for coal-fired power plant this value is 0.133, in Poland for Coal-fired circulating fluidized bed (CFB) (7.51–46.4). They concluded that due to the high combustion efficiency, most probably the emissions of PCDD/Fs were low. Figure 3.1 shows the schematic block diagram of thermal power plant.

Kadali et al. (2017) used optimum thermal generation schedule using new fangled grey wolves optimization (GWO) technique for emission operation. The emission objective function defined as follows:

$$\text{Minimize } E\left(P_{\text{gi}}\right) = \sum_{i=1}^{N} \alpha_i + \beta_i P_{\text{gi}} + \gamma_i P_{\text{gi}}^2 \tag{3.2}$$

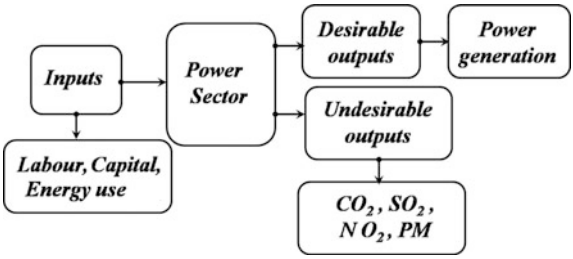

Fig. 3.1 Schematic diagram of thermal power plant

Equation (3.2) expresses the emission release (ER) incurs during generation which is estimated as the sum of quadratic function of real power generation. Where E denotes the total emission release (kg/h), P_{gi} is lower limits of ith unit generation, α_i, β_i and γ_i are express the emission coefficients of the ith unit. They concluded that the numerical results would be helpful for authoritarian bodies as the cleanliness environment to the society.

Fu et al. (2014) used Linear Programming (LP) algorithm for determination of the cost of achieving emission reductions with the help of Multi-pollutant emission model.

They assuming that if there are N power plants and M types of control technologies for pollutant j, the mathematical formulation for emission control can be written as:

$$R_{j,k} = E_{j,k}\left(1 - \sum_{i=1}^{M}\left(EFF_{i,j}X_{i,k}\right)\right) \tag{3.3}$$

Equation (3.3) shows the remaining emission of pollutant (j) after installing control technology (i) at power plant (k).The original emission of pollutant (j) at power plant (k) is expressed by $E_{j,k}$ ton. Where $EFF_{i,j}$ denotes the removal rate of control technology for pollutant in terms of percentage and $X_{i,k}$ (set of integers 0 and 1) express the degree to which the control technology is useful to reduce the emission from power plant. They found that LNB (Low-NO_x Burners) reduced the NO_x emission by 64.7% on the selected region as compared to combination of Selective Catalytic Reduction (SCR) and LNB. They also discuss the application of control technologies for different thermal pollutants in the selected region for the base year (2010).

Mao et al. (2014) defined an air pollutant equivalence (AP_{eq}) indicator by combines all the pollutants (i.e., SO_2, NO_x, and CO_2) as one in the study. The reductions on SO_2, NO_x, and CO_2 for a specific technology have been represented by S, N and C with their weight factor α, β, and γ respectively.

The air pollutant equivalence (AP_{eq}) indicator is defined mathematically as follows by Eq. (3.4).

$$AP_{\text{eq}} = \alpha S + \beta N + \gamma C \tag{3.4}$$

where

$$0 \leq \alpha \leq 1$$
$$0 \leq \beta \leq 1$$
$$0 \leq \gamma \leq 1$$
$$\alpha + \beta + \gamma = 1$$

As per the requirement other pollutants such as particulate matter and mercury can be consider into the equation as shown in Eq. (3.4). The higher weight pollutants reflect the higher pollutant priority according to pollution prevention scheme. They concluded that the multi-pollutant reduction co-control routes are always better to single-pollutant reduction routes.

Duan et al. (2017) defined Mercury Emission Factor (MEF) by Eq. (3.5) for comparing the mercury emissions in different power plants or at different loads (100, 85, 68% output). They used different types of coal and test has been conducted in a 350 MW pulverized coal combustion power plant. They utilized different types of thermal pollutant control devices such as Selective Catalytic Reduction (SCR), Electrostatic Precipitator and Fabric Filter (ESP + FF), and Wet Flue Gas Desulfurization (WFGD).

$$\text{MEF} = \frac{\text{Ultimate mercury emitted to the atmosphere}}{\text{Heat value coming from the feeding coal}} \tag{3.5}$$

They concluded that the elemental mercury (Hg^0) taken a huge proportion (70.3–74.8%) in the stack. The calculated MEF was 0.92–1.17 g/10^{12}J, which is lower than the average value of both Chinese and US power plants.

Wang et al. (2017) established a high-resolution inventory of thermal pollutants from coal-fired power plants by using two unit-level approaches. The annual emissions of each species have been calculated by using Eqs. (3.6) and (3.7) as follows:

$$Q_i = \sum_{j=1}^{m} M_j \times GF_{i,j} \times \frac{(1 - \eta_{i,j})}{1000} \tag{3.6}$$

$$Q_i = \sum_{j=1}^{m} M_j \times \frac{EF_{i,j}}{1000} \tag{3.7}$$

where, Q_i denotes the annual emission of the species i (ton).The annual amount of coal consumption is expressed by M in ton and GF express the generation factor in g/kg of coal. η is the overall decontamination efficiency. Equation (3.6) can only be applicable, if generation factor and the overall decontamination efficiency are known. Otherwise, select Eq. (3.7). Subscript i, j and superscript m represent the

emission species, individual unit and unit number, respectively. They found that coal quality play a major role for emission of SO_2 and PM, respectively. They have been discussed various types of decontamination technologies along with their corresponded removal efficiencies and applied percentages for different pollutants. For SO_2 the used decontamination methods are Wet Flue Gas Desulphurization (Wet FGD), Dry/semi-dry FGD, 0 Desulfurization during combustion with average decontamination efficiency (75%) along with average applied percentage (13.3%). For NO_x the used decontamination methods are Low Nitrogen Burners (LNB), Selective Catalytic Reduction (SCR), Selective Non-Catalytic Reduction (SNCR), combined SCR-SNCR and ammonia desulphurization with average decontamination efficiency (39.6%) along with average applied percentage (37.56%). Similarly for fine particulate matter ($PM_{2.5}$) and inhalable particulate matter (PM_{10}), the used decontamination methods are ESP, high effective ESP, Fabric filters, ESP combined with fabric filters, Wet scrubbers, Cyclones machinery and ESP combined with wet-FGD with average decontamination efficiency (89.3%) along with average applied percentage (14.13%).

3.3 Continuous Emission Monitoring System

Continuous Emission Monitoring System (CEMS) involves analysers and related things for estimation of SO_x, NO_x, CO_2, Mercury and Particulate emission supervision for chimney emission monitoring. Vent gas analyzers should be accommodated stack consistent outflow checking framework (CEMS). The stack emission observing framework includes SO_x, NO_x, CO_2, stack gas flow and mercury analyzer. All flue gas analyzers at stack should be situated at a height or according to contamination control board standards and might be open for repairs and maintenance work. Figure 3.2 shows the schematic of continuous emission monitoring system.

3.4 Stack Height for Small Boilers with Emission Limits (Central Pollution Control Board)

A stack is a type of chimney or similar structure through which combustion product gases called flue gases are exhausted to the outside air.

The stack or chimney takes part in a significant role for the abatement and control of such air contamination emissions. Stacks are used to diminish the ground level concentration of a pollutant by emitting the process gas at immense height at which the scattering of pollutants over a greater area reduces their concentrations in ambient air to retain the air quality in fulfilment with different regulatory limits.

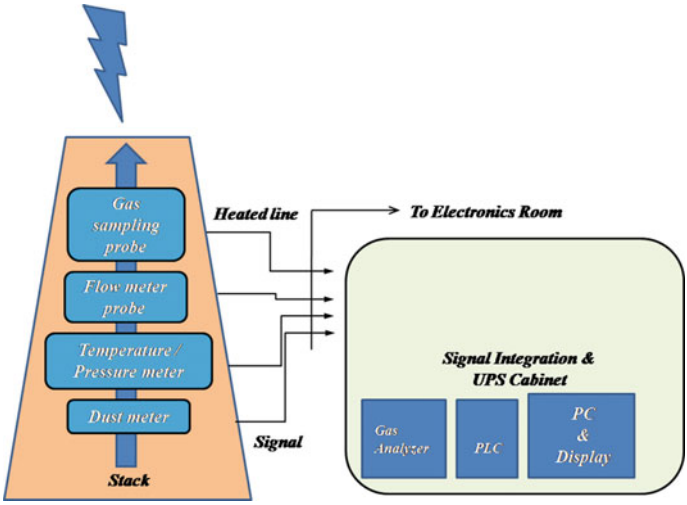

Fig. 3.2 Schematic of continuous emission monitoring system

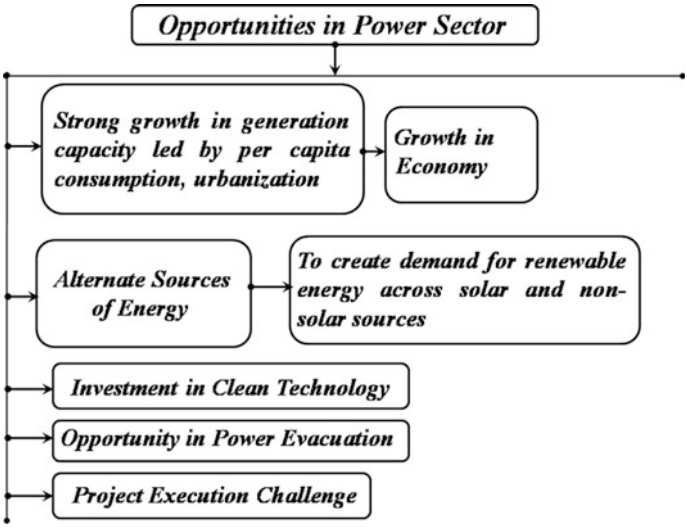

Fig. 3.3 Opportunities in power sector

For a thermal power plant fitted with Flue Gas Desulphurisation (FGD), the required size of the stack is administered by quantum of SO_2 being transmitted from the chimney. Figure 3.3 shows the different opportunities in power sector.

For 100 MW power generation capacity, the stack height (H) is calculated based on following equation as given below:

Table 3.2 Emission limit for small boilers

S. No.	Steam generation capacity (tph)	Pollutant	Emission limit (mg/Nm^3)
1	Less than 2	Particulate matter	1200[a]
2	2 to less than 10	Particulate matter	800[a]
3	10 to less than 15	Particulate matter	600[a]
4	15 and above	Particulate matter	150[b]

[a] To meet the individual norms, cyclone/multi-cyclone is suggested as control equipment with the boiler

[b] To meet the individual norms, bag filter/ESP is suggested as control equipment with the boiler

$$H = 6.902(Q \times 0.277)^{0.555} \quad \text{or} \quad 100\ \text{m whichever is high} \tag{3.8}$$

For less than 100 MW power generation capacity, the stack height is calculated based on following equation as given below:

$$H = 6.902(Q \times 0.277)^{0.555} \quad \text{or} \quad 30\ \text{m whichever is high} \tag{3.9}$$

where Q is the emission rate of SO_2 in kg/h and H is the physical stack height in m. The SO_2 emission depends upon the size and number of units associated to a chimney (CEA 2017). Table 3.2 shows the emission limit for small boilers according to central pollution control board.

3.5 Guidelines for Pollution Prevention in Small Boilers (Central Pollution Control Board)

Figure 3.4 shows the key challenges in power sector. Figure 3.5 shows the issues related to climate change mitigation in the power sector.

3.6 Control Techniques for Different Pollutants

The thermal power plants generated pollutants such as carbon monoxide, nitrogen oxides, sulphur dioxide, thermal radiation, particulate matters, noise and vibration, which deteriorate the atmosphere. Figure 3.6 shows the pollutant emission, as discussed by Hogetsu (2005). Some of the micro-pollutants like Cl_2, Cu, Cr, Pb, and F which cause a severe risk to the environment.

These toxins, if not checked and controlled, change the photosynthesis procedure of plants which diminish the significant supplement in plant, lessen soil ripeness, dis-structure the dirt strata, and encourages offices erosion and assault man

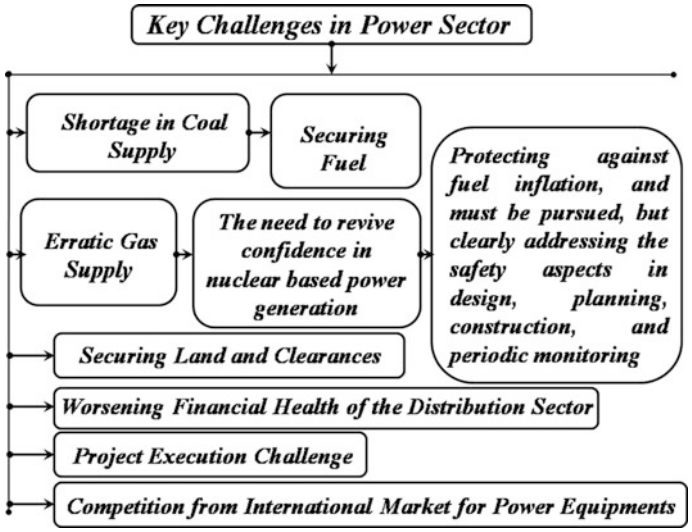

Fig. 3.4 Different key challenges in power sector

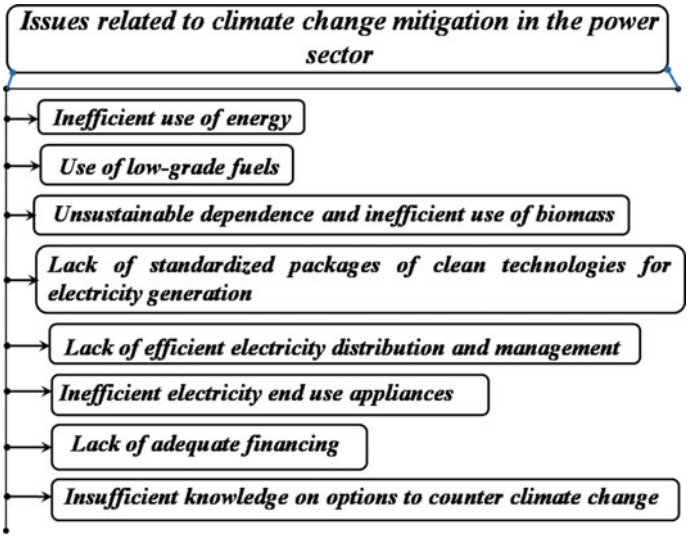

Fig. 3.5 Issues related to climate change mitigation in the power sector

and creature specifically. Electrostatic precipitators, Low NO_x burners, Flue gas stack and Dry ash extraction are the devices or technique used for air pollution controls.

Some control methods as observed were set up to diminish these poisons. Figure 3.7 shows the pollutants and pollution control in coal fire power plant.

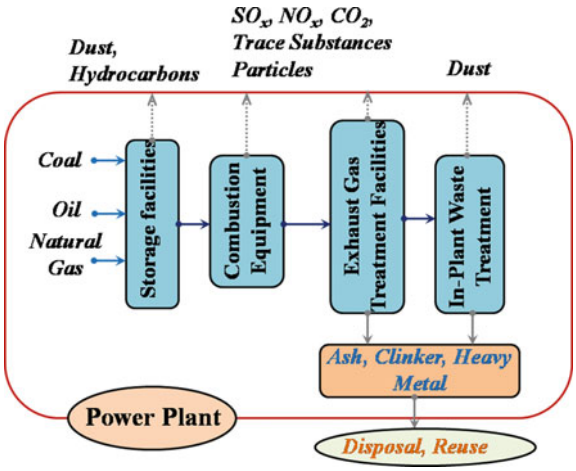

Fig. 3.6 Pollutant emission, Hogetsu (2005)

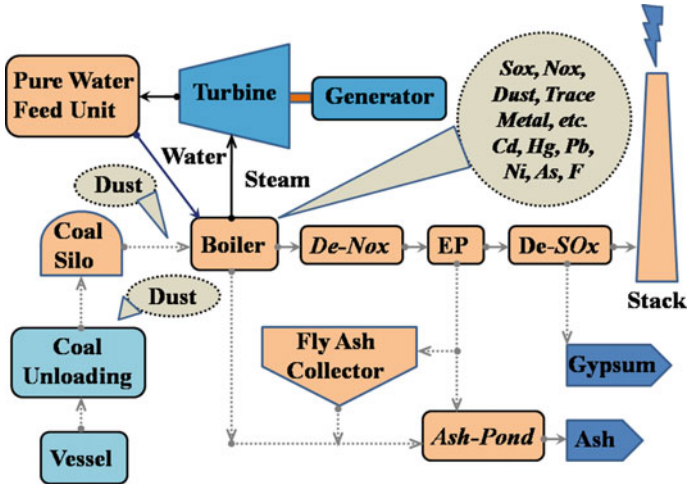

Fig. 3.7 Pollutants and pollution control in coal fire power plant, Hogetsu (2005)

Figure 3.8 shows the pollutants and pollution control in oil fire power plant. The amount of emitted dust is very less in the case of oil fired power plant as compared to coal-fired power plant. Figure 3.9 shows the pollutants and pollution control in gas fire power plant.

Figure 3.10 shows the way to modify the existing power plant for low carbon emission. NO_x is the dominated pollutant in gas-fired power plants, following which nickel and cadmium are emitted from oil-fired power plants. Fig. 3.11 shows the prevention and control of thermal pollution. Figure 3.12 shows the NO_x control system.

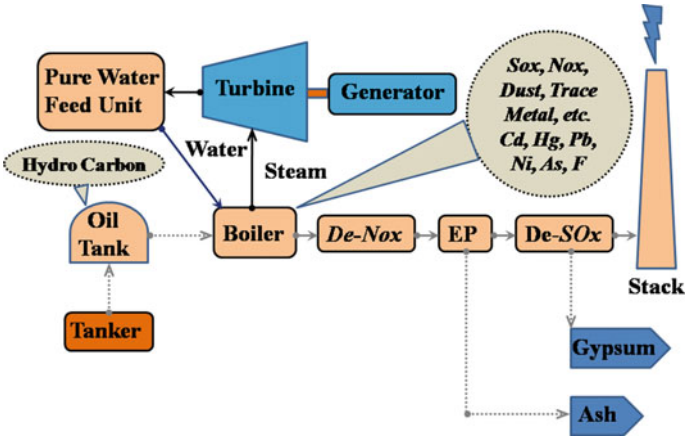

Fig. 3.8 Pollutants and pollution control in oil fire power plant, Hogetsu (2005)

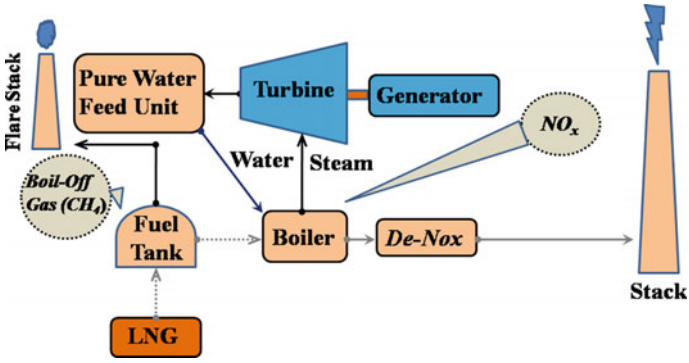

Fig. 3.9 Pollutants and pollution control in gas fire power plant, Hogetsu (2005)

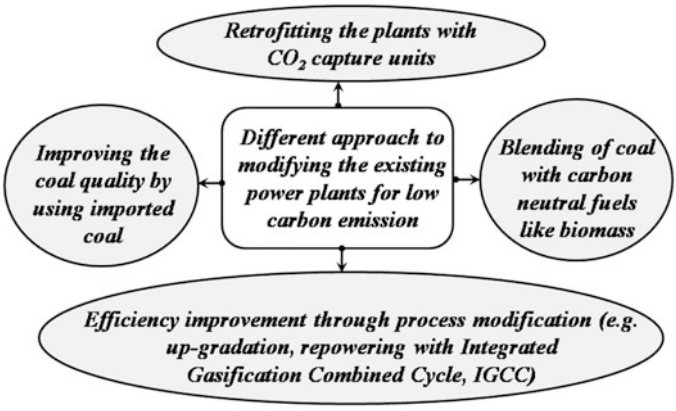

Fig. 3.10 Way to modify the existing power plant for low carbon emission, Singh and Rao (2016)

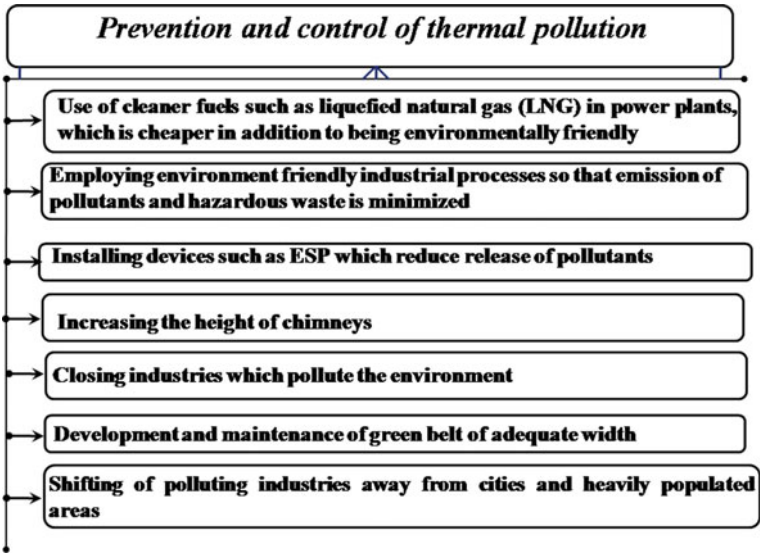

Fig. 3.11 Prevention and control of thermal pollution

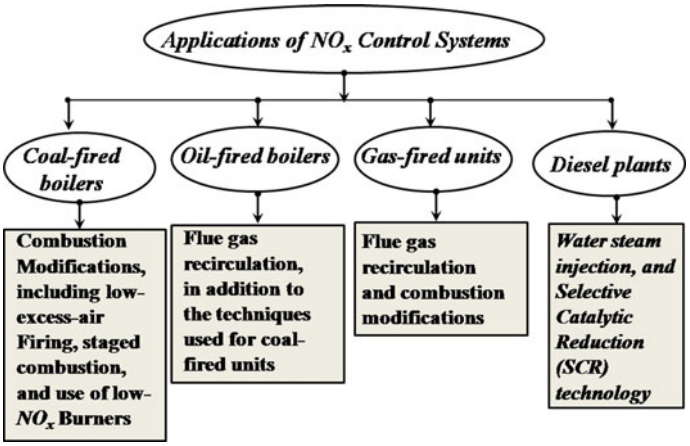

Fig. 3.12 NO_x control system

3.7 Recommendations

The "Emerging pollutants" (EPs) and "emerging contaminants" (ECs) utilized reciprocally that are not usually checked in the earth be that as it may, which can possibly enter the earth and cause known or suspected unfavourable biological and human health effect. Figure 3.13 shows the control devices for mercury emissions.

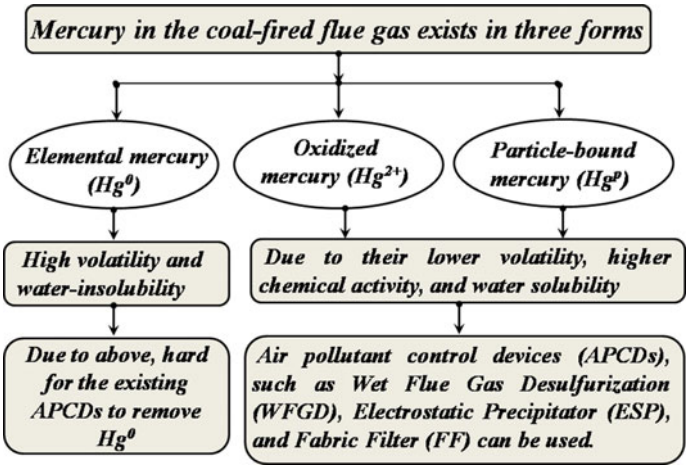

Fig. 3.13 Emission of mercury and their control devices

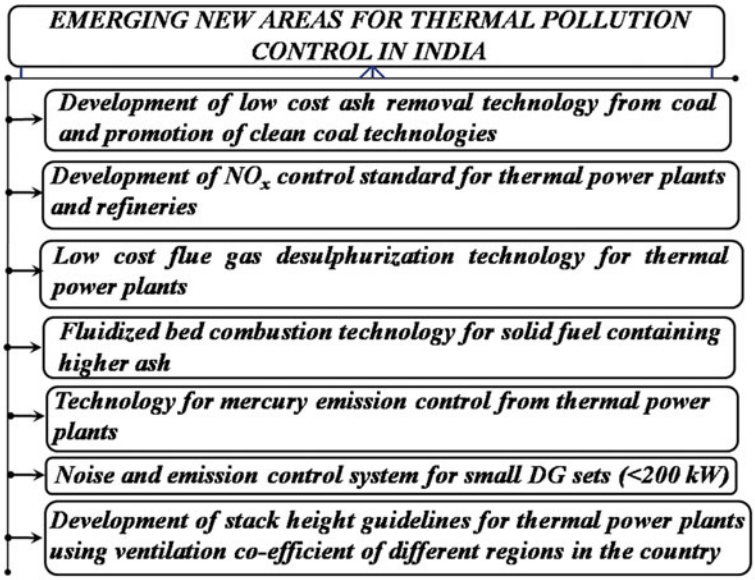

Fig. 3.14 Emerging new areas for thermal pollution controls

Different types of model have been suggested by the investigators and it has been found that the high power generation demand could be achieved by applying different control techniques with a lesser amount of emission of pollutant into our surroundings. Some researcher suggest flue gas desulfurization (FGD) technique for the reduced of emission of PCDD/Fs. Figure 3.14 shows the Emerging new areas

for thermal pollution controls. The emission of NO_x can be reduced by the use of low-NO_x burners and low nitrogen fuels (natural gas). The overall removal efficiency of mercury can be increased by the installation of a Wet Electrostatic Precipitator (WESP) in the coal-fired power plants. The measurement of annual emissions of each species with the help of unit-level approaches could offer scientific sustain for strategy makers to extend valuable emission control programs.

3.8 Conclusion

A few nations and even individual states and regions require restricts on releases that prompt warm contamination of getting waters. Direction may adopt altogether for different strategies; in a few laws, a best practice is required, for example, the utilization of cooling lakes or cooling towers for waste warm release. Specialists need to create associations with other segments to recognize and execute need intercessions for pollution control. Advances to decrease air contamination at the source are settled and ought to be utilized as a part of all new mechanical improvement. Retrofitting of existing power plants is additionally advantageous. The ideology and practices of sustainable improvement, united with local research, will help contain or eliminate health risks resulting from thermal pollution. Universal joint effort including both legislative and non-governmental associations can guide this highly interdisciplinary and intersectional area of disease control.

3.9 Emerging New Areas

Further research should be based on improving the control of carbon emission along with eco-friendly fuels. So that it can minimize the Green House Gasses (GHG) into the atmosphere. Some of the technological substitutions like hydro, nuclear and wind energies are significant way to minimize GHG. A comprehensive coal emission boundary should be clearly defined for the controls of direct emissions of CO_2, CH_4 etc. prior to use in coal-fired plant. These boundaries include coal mining, processing, transportation and fugitive emissions. Further Research needs to be focused on Gangue utilization (Wang et al. 2018) which has a great significance for saving energy and reducing environmental pollution.

References

Hogetsu A (2005) Air pollution control technology in thermal power plant. Overseas Environmental Cooperation Center, Japan

Kadali KS, Rajaji L, Moorthy V, Viswanatharao J (2017) Economic generation schedule on thermal power system considering emission using grey wolves optimization. Energy Proc 117:509–518

Mao XQ, Zeng A, Hu T, Xing YK, Zhou J, Liu ZY (2014) Co-control of local air pollutants and CO_2 from the Chinese coal-fired power industry. J Clean Prod 67:220–227

Mokhtar Mutahharah M, Taib RM, Hassim MH (2014) Measurement of PCDD/Fs emissions from a coal-fired power plant in Malaysia and establishment of emission factors. Atmos Pollut Res 5:388–397

Singh U, Rao AB (2016) Techno-economic assessment of carbon mitigation options for existing coal-fired power plants in India. Energy Proc 90:326–335

Siwal PD (2017) Standard technical specification for Retrofit of wet limestone based flue gas desulphurisation (FGD) system in a typical 2×500 MW thermal power plant. Central Electricity Authority New Delhi

Sun J, Schreifels J, Wang J, Fu JS, Wang S (2014) Cost estimate of multi-pollutant abatement from the power sector in the Yangtze river delta region of China. Energy Policy 69:478–488

U.S. EPA (U.S. Environmental Protection Agency) (1997) Procedures for preparing emission factors documents. U.S. Environmental Protection Agency, Research Triangle Park, NC 27711

Wang N, Ren Y, Zhu T, Meng F, Wen Z, Liu G (2018) Life cycle carbon emission modelling of coal-fired power: Chinese case. DOI:10.1016/j.energy.2018.08.054

Xu Y, Hu J, Ying Q, Hao H, Wang D, Zhang H (2017) Current and future emissions of primary pollutants from coal-fired powerplants in Shaanxi, China. Sci Total Environ 595:505–514

Zhao S, Duan Y, Chen L, Li Y, Yao T, Liu S, Liu M, Lu J (2017) Study on emission of hazardous trace elements in a 350 MW coal-fired power plant. Part 1. Mercury, Environ Pollut 229:863–870

Chapter 4
Atmospheric Emissions from Thermal (Coal-Fired) Power Plants and Associated Environmental Impacts

Gyanesh Kumar Singh, Pradhi Rajeev, Debajyoti Paul and Tarun Gupta

Abstract Power plants, which are major point source of air pollutants, contribute significantly to the overall ambient air particulate matter (PM) loading. Due to low grade of coal utilized in the power plants, emitted gases and PM affect the environment as well as public health. Gaseous as well as particulate emissions from power plants depend on types of coal and combustion conditions. Coal is subjected to various processes from arrival up to the combustion in a power plant. Particle size distribution and composition of PM emitted by coal combustion sources vary according to various formation and transformation processes to which they are subjected during their lifetime such as grade of coal, pulverization, and storage and combustion conditions including type of boiler, etc. Gaseous emissions in large amount from stack of power plants include gases such as sulfur dioxide, carbon monoxide, oxides of nitrogen, carbon dioxide, and volatile organic compounds. Respirable particulate matter is also emitted at a large scale in the form of fly ash, bottom ash, and flue gas. Toxicity associated with suspended PM can deteriorate human health by penetrating and affecting human respiratory system. Apart from this, these emissions can alter the atmospheric radiation balance by inducing climate forcing, and provide excess condensation nuclei for fog and cloud formation, thereby significantly altering the regional level weather conditions and patterns. Advanced techniques to track the precursors of PM such as stable isotope analysis and metal identification along with various modeling methods can be used quite effectively for understanding the sources and health hazards related to power plants. These mechanisms can be understood by making use of a tracer (such as stable isotope ratios, for example, $\delta^{13}C$ or elemental ratios), which can track down the PM formation processes either in the stack exiting flue gases or further downstream from the source. Emissions from coal-fired power plants also contain certain toxic trace metals, which can severely affect the health of general public.

G. K. Singh (✉) · P. Rajeev · T. Gupta
Department of Civil Engineering, Indian Institute of Technology Kanpur, Kanpur, India
e-mail: gyanesh@iitk.ac.in

D. Paul
Department of Earth Sciences, Indian Institute of Technology Kanpur, Kanpur, India

R. A. Agarwal et al. (eds.), *Pollutants from Energy Sources*,
Energy, Environment, and Sustainability,
https://doi.org/10.1007/978-981-13-3281-4_4

Keywords Coal · Power plants · Toxicity · Particulate matter Emissions

4.1 Introduction

Most of the electricity demand in India is primarily met by coal-fired power plants and the resulting pollution is a severe cause of concern with respect to ambient air quality. One of the major fossil fuels used for electric power generation worldwide is coal, which satisfies nearly 40% of the electricity demand (Energy Information Administration, EIA 2013). In India during 1990s, electric power generation from thermal power plants was estimated to have contributed about 96% of total carbon dioxide (CO_2) emissions (ALGAS 1998), while it was reported ~62% in 1994 (NATCOM 2004) and 69% in 2007 of the total CO_2-equivalent emissions from energy sector (INCCA 2010; Mittal et al. 2012).

Coal is a heterogeneous, complex, and variable substance that contains mineral inclusions in addition to the fossilized carbonaceous material (Flagan and Seinfeld 2012). Coal is generally classified based on percentage of carbon content, its calorific value, and sulfur content. General classification of Indian coals is presented in Table 4.1. The composition of coal is normally reported in terms of proximate analysis (fixed carbon, volatile matter, moisture, and ash, all in weight %) and ultimate analysis (elemental composition of carbon, hydrogen, nitrogen, oxygen, and sulfur, all in weight %) (Francis 1961; Whitehurst et al. 1980; Bustin et al. 1993).

Since coal-fired power plants (Fig. 4.1) are the cheapest source for producing per kWh of electricity, therefore, there is an expansion in construction of such power plants. Most of the coal consumption occurs in countries such as India, China, and US, which own nearly half of the worldwide coal reserves (Conti et al. 2016). Environment and human health are at risk owing to the emissions caused by thermal (coal-fired) power generation. In addition to CO_2 emissions, the pollutants that are released from combustion of coal include particulate matter (PM), sulfur dioxide (SO_2), carbon monoxide (CO), nitrogen oxides (NO_x), volatile organic compounds (VOCs), and various trace metals such as mercury, arsenic, cadmium, selenium, etc. Emission of large amounts of CO_2 can affect the global atmospheric radiative balance and in turn leads to global warming and associated climatic changes. SO_2 emitted is a precursor of acid rain and secondary fine PM, whereas NO_x can significantly affect the tropospheric ozone chemistry. Previous studies have shown that submicron particles from coal combustion can be formed through vaporization, condensation, and nucleation. On the other hand, larger sized particles can be formed from fragmentation and coagulation (Ninomiya et al. 2004). PM emissions from coal-based power plants are high in countries such as India and China due to the low thermal efficiency of boiler and usage of lower grade coal resulting in severe air pollution.

Table 4.1 General classification of Indian coals (IS: 770-1794) (Classification and Codification of Indian Coals and Lignites 1977)

Type	Name	Symbol	Volatile matter % at 900 ± 15 °C (Unit coal basis)	Gross calorific value (kcal/kg)	Chief uses
Anthracite	Anthracite	A_1	3–10	8330–8670	Gasification, producers, domestic, where intense heating is not required
	Semi-anthracite	A_2	10–15	8440–8780	
Bituminous	Low-volatile (caking)	B_1	15–20	8670–8890	Carbonization for the production of metallurgical coke
	Medium-volatile (caking)	B_2	20–32	8440–8780	
	High-volatile (caking)	B_3	Over 32	8280–8610	Coking coals, gasification
	High-volatile (semi-caking)	B_4	Over 32	8000–8440	Log-flame heating
	High-volatile (noncaking)	B_5	Over 32	7500–8060	Steam raising, gasification, long flame heating
Sub-bituminous	Noncaking	B_6	Over 32	6940–7500	Steam raising, gasification
Lignites or brown coal	Normal lignite	L_1	45–55	6110–6940	Steam raising, briquetting
	Canneloid	L_2	55–65	6940–7500	

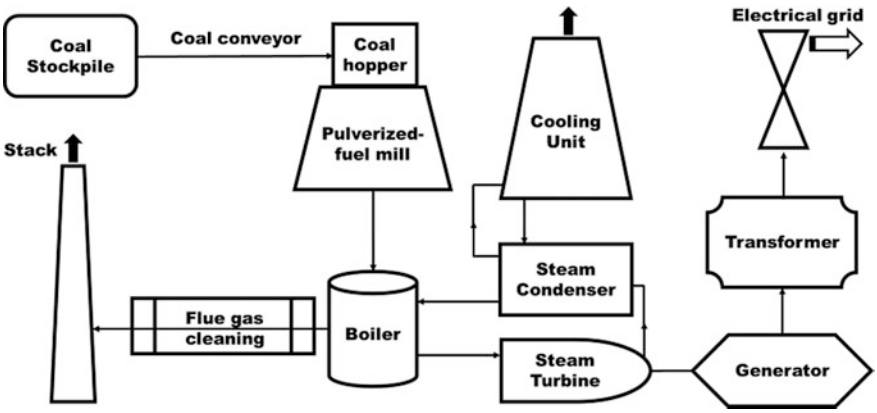

Fig. 4.1 Flowchart of a typical thermal power plant (inspired by Davis 2000; Buhre et al. 2005; Chawla et al. 2011; Park et al. 2018)

Since finer fractions of atmospheric PM including emissions from thermal power plants have longer residence time in the ambient atmosphere, therefore, they can cause respiratory problems to population residing even far off from such sources as they can penetrate deeper into the lungs. Adverse health effects can be caused by the toxic elements that are released from coal combustion such as copper (Cu), cadmium (Cd), arsenic (As), cobalt (Co), chromium (Cr), manganese (Mn), selenium (Se), lead (Pb), iron (Fe), mercury (Hg), nickel (Ni), vanadium (V), and zinc (Zn) in particle or gaseous form (Linak et al. 2000; Lighty et al. 2000; Huggins et al. 2004; Reddy et al. 2005; Cordoba et al. 2012). Significant amount of mercury (Hg) is emitted from coal combustion, which is toxic and hazardous and it can enter into the food chain causing fatal diseases. Apart from the chemical constituents, PM_{10} (particles having aerodynamic diameter ≤ 10 μm) and $PM_{2.5}$ (particles having aerodynamic diameter ≤ 2.5 μm) also possess a critical health hazard as they are inhalable and can deeply penetrate into the lungs causing respiratory illness and cardiovascular diseases (Pope et al. 1995). Interdependence of PM with mortality and daily morbidity has been reported by previous studies due to deteriorating heart and lung functions (Dockery et al. 1993; Pope et al. 1995, 2004; Jerret et al. 2005). Fly ash and coal dust in millions of tons are emitted annually during coal combustion that results in the formation of PM, which also possess a life expectancy risk (Chen et al. 2004; Clancy et al. 2002; Pope et al. 2009). During high exposure events, co-pollutants (gaseous) also have an effect on the cardiopulmonary system (Chen et al. 2005; Samoli et al. 2006; Ackermann-Liebrich et al. 2007; Arif and Shah 2007). In post-combustion phase, PM toxicity is increased due to the presence of polycyclic aromatic hydrocarbons (PAHs) and metal content (Bostrom et al. 2002). Health effects due to primary particle emissions from coal, which has been widely studied by many researchers, and additionally a study titled "Toxicological Evaluation of Realistic Emission Source Aerosols" (TERESA) reported adverse effects due to exposure, created under various simulated atmospheric conditions, from secondary emissions of coal combustion (Ruiz et al. 2007a; Diaz et al. 2011; Lemos et al. 2011; Wellenius et al. 2011; Godleski et al. 2011). Various control strategies have been successfully applied over the years in past to limit emissions but still coal combustion is relatively important source of some trace elements, especially mercury (Sloss 2002). Present pollution control equipment for power plant emissions is effective in reducing major trace element emissions but fail to capture more volatile trace elements (Sloss 2002). Policymakers need to consider the environmental degradation potential of coal-based power plants and policy frameworks should be formed to control these emissions. Presently, the methods and technology to reduce the emissions include electrostatic precipitators (ESP), flue gas desulfurization, dry sorbent injection (DSI), fabric filters, selective catalytic reduction (SCR) methods, and mercury control methods (MCM) (Baig and Yousaf 2017). Also, efforts should be made to reduce the dependence on coal-based power plants for electricity generation and use of renewable sources should be promoted. With the increase in the environmental degradation, power plants will face more stringent governmental pollution norms in the near future. National and international regulations should be improved to control trace element emissions and avoid uncertain risks.

In this chapter, we have discussed the processes occurring in power plants which are responsible for large-scale emissions that elevate the gaseous and particulate matter concentrations in the atmosphere. The types of coal used in power plants, their characteristics, conditioning and pulverization, role of boilers, and subsequent by-products formed (fly ash) during the combustion process have been presented. Control measures are adopted for the reduction of emissions like installation of electrostatic precipitators, and stack sampling required to govern the total contribution to air pollutants has also been discussed. The chapter also highlights the characteristics of the gaseous and particulate matter from coal-based power plants and their impact on the atmospheric processes and human health. Eventually, the estimation of emissions from this particular source into the atmosphere has been discussed as it is crucial for understanding the contribution from this particular source to atmospheric loading and to undertake preventive actions. The detailed information included can help the policymakers to take suitable preventive measures to control the global atmospheric impacts and health risk.

4.2 Processes in Power Plants

4.2.1 Conditioning and Pulverization of Coal in Power Plant

Due to limited capacity of combustion, conventional fuel firing methods (e.g., stoke firing) do not respond to fluctuations in the loads. Also, these are unsuitable for large-scale electricity generation because of difficulties in managing and removing large amounts of ash. Hence, the pulverized fuel system was adopted for large capacity power plants using lower grade fuel because of enhancement in thermal efficiency and control. Before combustion in the boiler, coal passes through different phases, which include receipt, storage, and feeding coal to boiler to release energy. In this regard, coal is first prepared for firing by pulverizing it into granular size. Raw coal is transported to a thermal power plant via different transport mechanisms and is first crushed into a smaller size by a crusher. Coal is then crushed to a fine particle form in a coal mill by application of force by hammering or by mutual effect of shearing and compressive forces. Coal from coal stock equipment is transferred to coal pulverizer (grinder) and then fed in the form of fluidized bed into a combustion chamber with the aid of hot air current.

At the power plants, large lumps of coal having a size range between 2 and 50 mm are usually available. In a thermal power plant, purpose of pulverizer is basically to crush and break down bigger coal lumps into fine particles to increase the surface area which facilitates efficient combustion of coal. For coal combustion, it is a fundamental requirement that all carbon particles get enough air to burn. Conversion into fine particle form is carried out before it is taken to boiler for combustion. If pulverization is not done, incomplete burning of coal will take place

resulting in wastage of fuel. Therefore, size of powdered coal governs the efficiency of pulverized fuel firing system. Boiler responds to load variations more promptly after pulverization. A vertical roller mill (as a grinder) is commonly used for pulverization and drying of coal. The components of mill include a bowl type plate and various rollers. Application of steady pressure is employed onto the plate with rollers and pulverization of coal is achieved by rotation of plate.

The advantage of pulverization lies in the fact that greater surface area of coal per unit mass reduces excess air required for complete combustion. Also, constant steam pressure is maintained under different load variations in pulverized coal-fired boilers through automatic control. Large variety and lower grade coals can be combusted with ease after pulverization. The requirement of furnace volume is decreased in case of pulverized boilers as the burners producing turbulence in furnace enable complete combustion with lower residence time. The unburnt carbon particles, which get emitted with ash in older combustion boilers are reduced drastically as the overall surface area gets increased.

4.2.2 Boiler

The objective of a boiler is the conversion of chemical energy of fuel into internal energy (steam) for driving turbines to generate power. A boiler includes a furnace in which fuel is burnt, surface-transmitted heat from combustion and space is utilized for steam formation and collection in a typical steam power plant (Fig. 4.2). Boiler drum receives water from boiler feed pump. In the pulverized coal furnaces, the pulverized coal from mill having, typically, 40–80 μm mass median diameter is transported into furnace with primary (carrier) air. Coal particles are then heated up to temperatures in surplus of 1500 K through conduction and radiation from hot gases (Flagan and Seinfeld 2012). Depending on ash removal technique, pulverized coal furnaces can be divided into two types: dry or wet bottom. In slag tap or wet-bottom furnaces, low or moderate ash fusion temperature coal is used. Subsequently, draining of molten ash is carried out from the bottom of the furnace. Coal with high ash fusion temperatures is fired in dry-bottom furnaces with dry ash extraction technique. Depending on the firing position of the burners, pulverized coal furnaces are classified into single (rear or front) wall, tangential, vertical, and horizontally opposed or arch fired (Davis and Buonicore 2000).

4.2.3 Fly Ash

The fine residue that is released from combustion of pulverized coal and carried from the combustion chamber by exhaust gases is referred to as fly ash. It is primarily a by-product of coal-based electric power generation plants. It is present in PM in size ranging from 0.01 to 100 μm (Davison et al. 1974). The typical

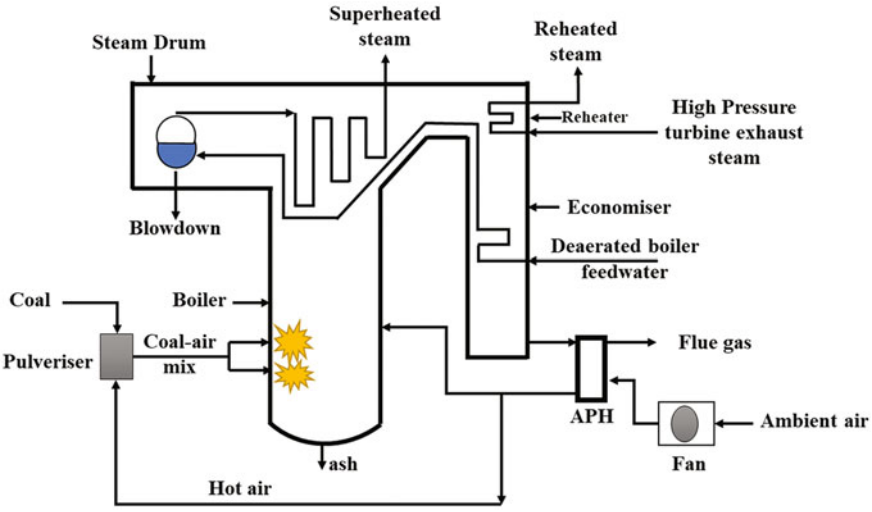

Fig. 4.2 Boiler schematic (inspired by Elshafei et al. 2014; Fan et al. 2016)

characteristics (i.e., physical, chemical, and mineralogical) depend on the category of coal, handling approaches, control devices for emission, and combustion conditions. Finely distributed components of ash reach the particle surface due to burning out of carbon matter around the mineral components.

Silica (SiO_2), magnetite (Fe_2O_3), and alumina (Al_2O_3) dominate the fly ash (Table 4.2), which also comprises of oxides, carbonates, silicates, sulfates, and hydroxides of a variety of elements which includes Mg, P, Ca, etc. Also, variable levels of heavy metals including Pb, Ba, Cu, B, As, Cd, Zn, Cr, Ni, Ag, Mo, Hg, Co, Se, and Sb are present in fly ash depending on the type of coal and conditions of combustion (Xiang et al. 2012). Previous study by Bhangare et al. (2011) reported toxic heavy metal concentrations for fly ash samples which were collected from various thermal plants having capacities varying between 90 and 3000 MW in India (Table 4.3).

Other pollutants such as polycyclic aromatic hydrocarbons (PAHs) and polychlorinated biphenyls (PCB) are also formed during combustion and adsorbed to fly ash. These organic pollutants are mutagenic and carcinogenic. Total PAHs and PCBs reported by a previous study in India in fly ash samples ranged from 43.6 to 936.1 ng/g and 7.3 to 178.7 ng/g, respectively, with concentration of benzo (a) pyrene which is also the most potent carcinogenic PAH, ranging from 0.8 to 18.1 ng/g (Sahu et al. 2009).

Table 4.2 Fly ash chemical composition of various coal types (Ahmaruzzaman 2010)

Components (wt%)	Lignite	Sub-bituminous	Bituminous
SiO_2	15–45	40–60	20–60
Fe_2O_3	4–15	4–10	10–40
Al_2O_3	10–25	20–30	5–35
CaO	15–40	5–30	1–12
MgO	3–10	1–6	0–5
Na_2O	0–6	0–2	0–4
SO_3	0–10	0–2	0–4
K_2O	0–4	0–4	0–3

Table 4.3 Heavy metal concentrations in fly ash samples (Bhangare et al. 2011)

Sample	Cd	Pb	Hg	As
Fly ash (μg/g)	0.6–0.93	7.6–35.3	0.51–2.13	0.19–0.35

4.2.4 Electrostatic Precipitator (ESP)

For removal of particulates from boiler-emitted flue gas, electrostatic precipitators are utilized extensively in thermal or steam power plants. It is a device that uses the induced electrostatic charge force for removal of particles flowing through a gaseous stream (e.g., air) and onto collector plates. Electrical charge is provided to particles by directing them to a corona, which is an area where flow of gaseous ions occurs (EPA/452/B-02-001). Then, electric field forces the charged particles to get deposited onto the walls. This electric field is provided from electrodes, which are maintained in the central flow lane at a very high voltage.

The power requirement of ESP is low, and it can work at high temperature and pressures due to which ESP is the preferred method for collection of small particles at a higher efficiency. ESP offers very low resistance to flow of gases through them and achieve extremely high efficiencies for removing fine particles (Mudakavi 2010). Dust particles which are deposited onto the plates are removed by shaking the plates through cams driven by external means and are collected in dust hoppers from where they are removed.

Small particles like smoke, fly ash, and mist can be effectively removed through ESP, which has a wide dust removal size range. Particles below 10 microns cannot be removed through mechanical separators or wet scrubbers (sufficient water required) but can be removed by ESP very effectively. ESP has low operation and maintenance cost and can handle large volumes of high-temperature gas. The ESPs can be configured in various ways such as (a) flat-plate precipitator, (b) plate-wire precipitator, (c) two-stage precipitator, (d) wet precipitator, and (e) tubular precipitator.

4.2.5 Sampling from Stack

Particulate concentration is derived from isokinetic sampling of a particular amount of gas from the flue gases and separation of particles from gas. Particulate matter from stationary sources is withdrawn and collected onto a filter (preferably glass fiber) (USEPA). The kinetic energy of the steam of gas in the stack should be similar to the kinetic energy of gas stream in sampling nozzle. Filter paper (thimble) is used to collect particulates down to 3 µm with stack temperature between 0 and 600 °C at particulate sampling range of 10–60 LPM. Gaseous sampling is conducted at a flow rate of 1–2 LPM on a set of impingers containing selective reagents (CPCB). Sample recovery and procedure for sampling can be adapted from central pollution control board (CPCB) or USEPA air programs chapter. For determination of particulate emissions from stationary sources, specifications of various equipment are presented in Table 4.4.

4.3 Emissions and Their Characteristics

4.3.1 Characteristics of Gaseous Emissions

Gondwana coal, which is used in the Indian subcontinent, has high ash content (35–50%), low sulfur content (0.2–0.7%), high moisture content (4–20%), and low calorific value (averaging 2500–5000 kcal/kg) (Mittal et al. 2012). Thermal power plant's operational efficiency is affected by high ash content and low calorific value resulting in enhanced emissions per kWh of produced energy. Indian power plants use ~1.5 times higher coal amount to generate 1 kWh than that in USA (Chikkatur 2008). In India, between 2004 and 2011, the mean thermal efficiency of the coal-fired power plants was reported to be varying in the range of 32–33% (Central Electricity Authority, CEA, 2012), while a relatively high efficiency (above 35%) is attained for the power plants located in China (Seligsohn et al. 2009). Coal-fired power plant emissions contribute a major fraction in deteriorating air quality, which in turn is responsible for risks associated with human health and climate change. The estimate of emissions and their analysis lead toward implementation of pollution control regulations which includes flue gas desulfurization, constraining of emission standards for all criteria pollutants, and improved protocols for environmental impact assessments. Enormous amounts of carbon dioxide (665 million tons), sulfur dioxides (2100 ktons), nitrogen oxides (2000 ktons), carbon monoxide (1100 ktons), and volatile organic compounds (100 ktons) were emitted from various plants in India, which consumed 503 million tons of coal in 2010–2011 (Guttikunda and Jawahar 2014).

Figure 4.3 shows emission of SO_2, NO_x, CO, VOC, and CO_2 in tons per MW of power generated in various states of India. Delhi, Madhya Pradesh, Chhattisgarh, and Uttar Pradesh show the highest emission of these gases per MW of energy

Table 4.4 Specifications for the ascertainment of particulate emissions from immobile sources

S. No.	Equipment	Specifications
1	Probe nozzle	Stainless steel or glass with sharp, tapered leading edge. For isokinetic sampling range of sizes of nozzle should be available, e.g., 0.32–1.27 cm. If large volume sampling trains are utilized then the inner diameter of nozzles in increasing order of 0.16 cm should be used and calibrated
2	Probe liner	Quartz or borosilicate glass tubing. Heating system must be capable of maintaining a gas temperature of 120 ± 14 °C at the end of sampling during exit
3	Pitot tube	Type S and should be connected to probe to permit constant monitoring of velocity of stack gas
4	Differential pressure gauge	Inclined manometer or comparable device should be used
5	Filter holder	Borosilicate glass along with a silicone rubber gasket and a glass frit filter support
6	Filter heating system	A heating system which must be capable of sustaining a gas temperature of 120 ± 14 °C. Temperature in the vicinity of filter holder shall be monitored and regulated throughout sampling, and therefore temperature gauge efficient of measuring temperature to within 3 °C shall be fitted
7	Condenser	Series-connected four impingers with no leak ground glass fittings or similar non-contaminated fittings should be used
8	Metering system	Leak-free pump, vacuum gauge, the dry gas meter having a capacity of measuring volume within 2%, thermometers able to measure temperature within 3 °C shall be connected
9	Barometer	Barometer with a capacity of measuring pressure within 2.5 mm Hg

Adapted from method 5 PART 60—Standards of performance for new stationary sources, National Archives and Records Administration, Washington, DC. (USEPA 2002)

generation. However, the highest power generation units are used in Maharashtra, Gujarat, Uttar Pradesh, West Bengal, Andhra Pradesh, Chhattisgarh, and Orissa. Thus, these states contribute the maximum loading of SO_2, NO_x, CO, VOC, and CO2 to the regional air quality. At Delhi, it has been reported that 55% SO_2, 7% NO_x, 31% CO, and 13% VOC of total respective gaseous emissions arise from coal-based power plants (Guttikunda and Goel 2013). There is no legal mandatory emission standard imposed for the emission of these gases in India. SO_2 contribution to the ambient air is highest from coal-based power plant emissions as it depends on the sulfur content of coal used in these power plants. However, Indian coal's sulfur content (0.6%) is low compared to United States (1.0–1.8%) and Chinese coals (0.5–1.0%) (Guttikunda and Jawahar 2014; Reddy and Venkataraman 2002). SO_2 gases undergo physicochemical transformation to form secondary sulfates. Secondary sulfate and nitrate formation constitute about 30–40% of $PM_{2.5}$ concentration. By installation of flue gas desulfurization unit, these secondary products can be eliminated from the particulate matter loading. Thus, it

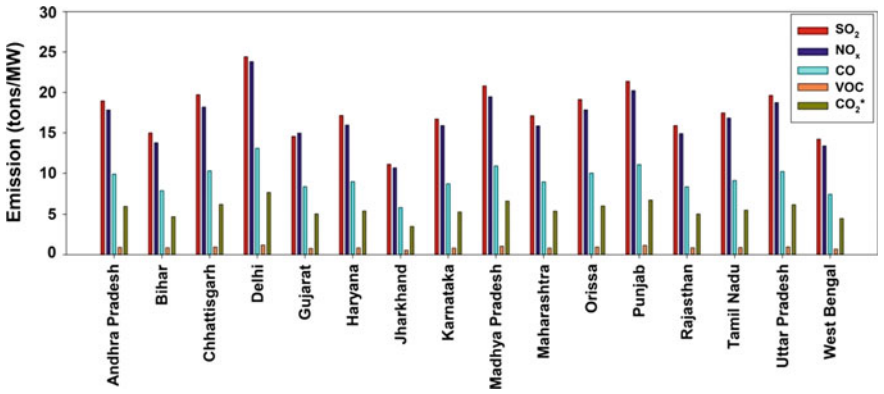

Fig. 4.3 Emission of various gases in tons/MW of power generated in different states of India. * CO_2 is generated in kilotons/MW of power generated (Guttikunda and Jawahar 2014)

has been mandated to install systems of flue gas desulfurization for the various plants operating in India, which can results in 30–40% reduction in $PM_{2.5}$ concentrations.

4.3.2 Characteristics of PM Emissions

Particulate matter composition and its concentration levels are highly dependent upon the power plant processing (combustion process and boiler operation) and properties of coal (Davis 2000). The complication in ash derived from combustion of Indian coal is the presence of high silica and alumina content since it enhances the resistivity of ash and thus decreases the removal efficiency of electrostatic precipitators (ESPs). Thus, as a preventive measure, utilization of coal with low ash content has been directed by the government for various areas according to their land use pattern. Out of 503 million tons of coal consumption in various plants (121 GW capacity) in 2010–2011, 580 ktons of particulates with a diameter less than 2.5 μm ($PM_{2.5}$) were estimated to be generated (Guttikunda and Jawahar 2014).

Figure 4.4 shows emission of particulate matter ($PM_{2.5}$ and PM_{10}) in tons/MW of power generated in different states of India. The $PM_{2.5}$ and PM_{10} levels have been observed to be highest in Delhi, Madhya Pradesh, Uttar Pradesh, and Punjab. The weighted concentration of 3.6 mg/m^3 (normalized by population) is attributed to emission from coal-fired power plants. Weighted mean of plant-wise $PM_{2.5}$ emitted from coal-based power generation units is ~8.1 (1.1–19.0) g/kg of coal consumed (Reddy and Venkataraman 2002). A study at Delhi reported that coal-based power plants contribute ~16% $PM_{2.5}$ and ~15% PM_{10} of the total emission of $PM_{2.5}$ and PM_{10}, respectively (Guttikunda and Goel 2013). The particle

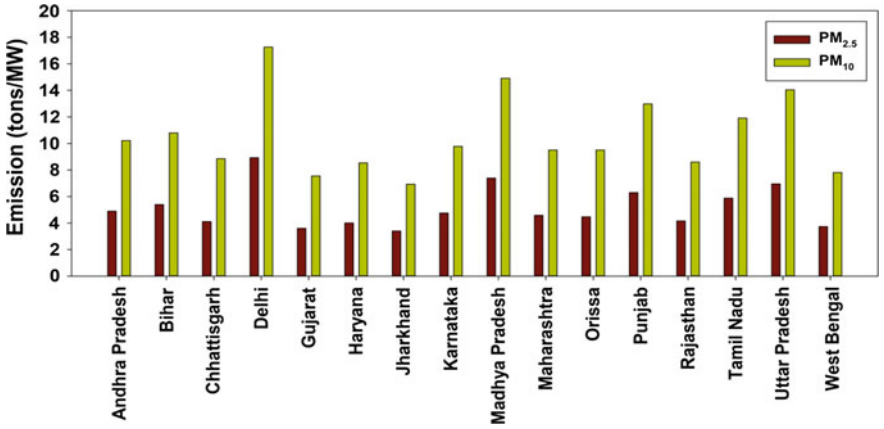

Fig. 4.4 Emission of particulate matter ($PM_{2.5}$ and PM_{10}) in tons/MW of power generated in different states of India (Guttikunda and Jawahar 2014)

size distribution is generally bimodal with one peak in the range of 0.5–0.8 μm (submicron range) and the other in 5–10 μm range (coarser) for coal-fired power plant emissions (Ehrlich et al. 2007).

The black carbon and organic matter emitted from per kg coal consumption in power plants are ~0.077 (0.01–0.18) g and 0.33 (0.044–0.77) g (plant-wise weighted average), respectively (Reddy and Venkataraman 2002). Elevated heavy metal concentrations such as As, Pb, Cd, Cu, Hg, and Zn have been observed in particles present in flue gas (Finkelman 2007). Reddy et al. (2005) reported various chemical constituents present in bottom ash, fly ash, and flue gas from power plant located in western India and estimated Zn (1–7%), Cu (2–7%), Mn (5–8%), Co (7–10%), Cd (12–18%), Se (60–70%), Hg (70–80%), and traces of As, Fe, Pb, and Cr in the flue gas. The heavy metal concentration in the fly ash, bottom ash, flue gas, and particle associated to the gas phase is given in Table 4.5.

A study by Rey et al. (2003) suggests that Mn and U are generally found in bottom ash while Pb, As, Se, Cd, B, Sb, and Zn are concentrated in fly ash based on partitioning behavior of different elements during coal combustion. However, Hg being more volatile than other metals is generally found in the gas phase, thus coal combustion is a prominent source of mercury in the environment.

A study from Finland reports that particulate matter concentration in flue gas can be reduced by 97% by the installation of desulfurization plant (DSP) which includes baghouse filters and flue gas desulfurization unit (FGD). However, although the trace metals can be removed proficiently, input of some ionic compounds may rise in the FGD process (Saarnio et al. 2014).

In a study, where aged particles emitted from coal-fired power plants have been considered, reported that organic carbon and particulate sulfate (H_2SO_4 + neutralized sulfate) with added secondary organic aerosols form the major fraction of aged

Table 4.5 Typical concentrations of heavy metal in coal and its combustion product emitted into the environment (Reddy et al. 2005)

Elements	Fly ash (mg/kg)	Bottom ash (mg/kg)	Flue gas (μg/Nm^3)	Particle associated to gas phase (μg/Nm^3)
As	172.3	9.8	19.5	62.5
Cd	1.57	2.58	1.2	0.62
Co	0.31	0.24	0.08	0.29
Cr	13.4	10.5	0.75	1.8
Cu	328.4	389.4	6.7	16.7
Fe	54,326.5	64,325.5	16.8	230
Hg	0.29	–	22.3	0.42
Mn	4.5	3.5	0.98	3.4
Ni	73.9	69.8	3.8	1.9
Pb	266.1	325.6	1.3	0.89
Se	32.4	8.9	51.8	0.78
Zn	465	514	19	28

particles (Kang et al. 2011). In addition to this, the mass concentration is mainly dependent on SO_2/NO_x ratio, which depends on coal composition and emission controls.

Dispersal of emissions from stacks of power plant is highly subjected to the meteorological conditions as during the onset of southwest monsoons (May–September) pollutants are transported upwards toward north, whereas northeast monsoons (October–November) cause inland wider dispersion of emissions. Strong winds and higher mixing heights during spring season (March–April) lead to the upliftment of pollutants to higher altitudes in troposphere causing diminished ground concentrations. Secondary aerosol concentration (mainly sulfates and nitrates) increases during summer months due to the enhancement in photo-oxidization process. Guttikunda and Jawahar (2014) reported that secondary aerosol contribution to be between 30 and 40%, mostly in the form of aerosol sulfate (gas-particle conversion). Several researchers have compared wet and dry scavenging of such aerosol from the atmosphere (Rajeev et al. 2016, 2018).

4.4 Atmospheric and Health Impacts Due to Stack Emissions

4.4.1 Atmospheric Impacts

Large amount of gaseous and particulate emissions from coal-fired power plants has different environmental impacts associated with them. High concentration of greenhouse gases (such as CO_2) is emitted from coal-fired power plants. It had been

seen that there is an increase in the global level of CO_2 thus causing enhanced global warming and ocean acidification. Black carbon is also responsible for global warming (second after CO_2 emissions) as it absorbs the solar radiation. Black carbon concentration in the ambient PM is enhanced due to contribution from power plants as discussed in previous section. Apart from absorption properties, black carbon can be transported over long distances and mixing with other pollutants can result in the formation of atmospheric brown clouds (Ramanathan and Carmichael 2008). Coal-fired power plants are the major source of SO_2 emissions leading to elevated secondary sulfate concentrations. Increase in sulfate concentration in the atmosphere leads to increment in the acidity in precipitation which can cause acid rain. The various organic compounds emitted in the atmosphere from coal-fired power plants can be easily mixed in the presence of metals, which acts as catalyst for various chemical processes, forming compounds that can affect the radiation balance of the atmosphere, enhance cloud condensation nuclei formation and human health.

4.4.2 Health Impacts

The emissions from various thermal plants in India caused nearly 80,000–115,000 premature deaths along with 20.0 million asthma cases due to $PM_{2.5}$ exposure (Guttikunda and Jawahar 2014). The health risk of pollutants emitted from coal-based power plant, including $PM_{2.5}$, gases (O_3, NO_x, SO_2, and CO), benzene, benzo(a)pyrene, and 1,3-butadiene, includes various diseases like respiratory problems, congestive heart problem, cerebrovascular, asthma, myocardial infarction, angina pectoris, hypertension, sleep disturbance, and cancer.

The estimated total premature mortality and child mortality (under 5 years) are 80,000–115,000 and 10,000, respectively, in a year from coal-fired power plants (Guttikunda and Jawahar 2014). The other health risks like respiratory symptoms, chronic bronchitis, chest discomfort, and asthma attacks are estimated to be 625, 0.17, 8.4, and 20.9 million, respectively for 1 year. The emergency room visits and restricted activity days are estimated to be 0.9 and 160 million, respectively, for a year.

According to this data (Table 4.6), Zone 5 and 6 is the largest energy generation units, and the mortality rate is also highest in this region. However, in Kutch, the generation units have a high consumption of coal as well as emissions also but still the mortality rate is lowest. This can be attributed to the effect of coastal conditions which enables higher dispersion of pollutants, thus lowering the exposure concentrations of pollutants. The high percentage of toxic heavy metals emitted from coal-based power plants tends to increase the health risk to the exposed population. The toxic metals like Ni, Cr, Cd, and Hg are listed as a carcinogenic pollutant by US EPA. The trace amounts of these metals in the particulate matter enters the human body through either ingestion, inhalation, or even dermal contact causes different diseases. The typical concentrations of these toxic metals have been

Table 4.6 Estimated premature mortality for different regions in India (Guttikunda and Jawahar 2014)

Zone No.	Regions	Units	Installed capacity (MW)	Estimated premature mortality within the region
1.	Delhi–Haryana	8	8080	6400–8800
2.	Kutch (Gujarat)	5	9900	100–120
3.	Western Maharashtra	3	2780	1700–2400
4.	Eastern Maharashtra and Northern Andhra Pradesh	10	14,800	1100–1500
5.	Madhya Pradesh–Chhattisgarh–Jharkhand–Orissa	21	29,900	7900–11,000
6.	West Bengal–Jharkhand–Bihar	19	17,100	10,700–14,900
7.	Eastern Andhra Pradesh	2	3000	1100–1500

indicated in Table 4.5. According to some toxicological studies, transition metals present in fly ash from coal power plants (like iron) cause adverse health effects. Mercury though emitted in very less amount can cause severe health damage as it can be converted to toxic methyl mercury which can be easily deposited in terrestrial and aquatic environments. Apart from this, the large amount of volatile organic compounds (VOCs) leads to the formation of secondary organic aerosols, resulting in the production of reactive species which induces adverse health effects (Chen and Hopke 2009).

Numerous studies have reported about the toxicological effects of emissions from coal-based power plants (Ruiz et al. 2007b; Diaz et al. 2011; Godleski et al. 2011; Lemos et al. 2011 in TERESA—Toxicological Evaluation of Realistic Emissions of Source Aerosols) for assessing health impacts of coal combustion emissions. Laboratory rats have been examined to study breathing pattern and pulmonary function, blood cytology, bronchoalveolar lavage, in vivo oxidative stress, and histopathology. However, insignificant variation in the results has been observed between exposed (to the stack emission) rats and control (exposed to filtered air) ones (Rohr et al. 2011).

4.5 Estimation of Power Plant Contribution in Ambient PM

Particulate matter is classified in certain size classes such as ultrafine particles (aerodynamic diameter < 0.1 μ), $PM_{2.5}$, PM_{10}, and total suspended particulates (TSP) (Fang et al. 2003). The classification of fine and coarse particles based on size is important as they have a distinct composition, sources, formation mechanism,

temporal and spatial variability, and health effects. PM can be emitted from naturally occurring sources such as forest fires, dust storms, volcanoes and sea spray, and also from anthropogenic (human-induced) activities such as biomass burning, vehicular exhaust, industrial emissions, and land use. Out of those, chief anthropogenic combustion sources involve residential fuel for cooking and heating, industrial manufacturing plants, open biomass burning, fossil-fuel-based power plants, and vehicular engines (Gupta and Agarwal 2010). By formation mechanism, ambient PM can be divided into two categories, namely, primary and secondary aerosols. Particles which are emitted immediately into the atmosphere from natural or anthropogenic sources are called primary aerosols, whereas particles which are formed by chemical transformation of gaseous pollutants like NO_x, SO_2, NH_3, and volatile organic compounds (VOCs) are called secondary aerosols.

Receptor-based source apportionment techniques can be used to determine the sources of both primary as well as secondary aerosols. Distinct emission sources have characteristic chemical profiles of pollution which are used for the apportionment purpose. The chemical constitution of ambient PM in terms of contribution of various sources can be understood by source apportionment. Ambient samples can be amassed in the regions of interest and then analyzed for chemical composition. Source sampling can also be done to determine their chemical profile. Further, receptor modeling techniques can be utilized to ascertain the relative contributions of various sources to the ambient PM.

PM from the urban centers around the world exhibit similar major components but in distinct proportions depending on the sampling location (Harrison and Yin 2000). These major components comprise elemental carbon (EC), organic carbon (OC), sulfate (SO_4^{2-}), nitrate (NO_3^-), ammonium (NH_4^+), chloride (Cl^-), crustal materials (including metals), and biological materials (pollens, spores, bacteria, etc.). Energy production facilities such as power plants, incineration of waste, and residential combustion are the most significant stationary sources of combustion. Chemical profile data of ambient aerosols and sources such as ions, metal concentration, OC, EC, and stable isotope ratios ($\delta^{13}C$ and $\delta^{15}N$) are used for true source identification and ultimately source apportionment. The chemical profile varies from region to region and also varies according to the type of dominant sources. For example, $\delta^{13}C$ value for gaseous combustibles varies between −28.1 and −39.7‰, for liquid fuels (diesel and fuel oil) between −26.4 and −28.6‰, and for coal between −22.9 and −24.9‰ (Widory 2006). These values depend on the physical state of the samples. Combustion processes and the type of fuel burnt govern the physical and chemical characteristics of the PM released from these sources. The unique elemental profiles of various sources which contribute to airborne PM are recognized through various models. Various source apportionment models have been used widely for determining sources of ambient PM that include multiple linear regression (MLR), principal component analysis (PCA), chemical mass balance (CMB), factor analysis (FA), and positive matrix factorization (PMF). Previous PMF studies by Rajput et al. (2016) and Rai et al. (2016) apportioned the sources contributing to PM_1 at an urban location in Indo-Gangetic plain (Kanpur) and ascertained the contribution from coal combustion to be 6.5% during massive

loading. Rai et al. (2016) also employed wind speed and direction information to identify the sources of coal combustion as brick kiln cluster and a thermal power plant near the receptor site. Similar study at a wider scale can be conducted in the future to present comprehensive emission inventory due to this source.

4.6 Conclusion

This chapter discusses different processes from coal treatment in power plant to the emission by-products that elevate the atmospheric pollutant concentration in the atmosphere. Also, it presents an overview of power plant functioning and different manufacturing steps at which we can take preventive measures to control these emissions. Enormous amount of gaseous and particulate matter is being emitted from power plants which consists of high elemental carbon, sulfate, and toxic metals that have adverse impact on atmosphere as well as human health. Therefore, it is essential to estimate the contribution of power plants in ambient air pollution through advanced techniques and modeling to curb the menace of atmospheric pollutants.

References

Ackermann-Liebrich U, Dietrich DF, Gemperli A, Liu LS, Schindler C, Gaspoz J et al (2007) Long-term effect of NO_2 exposure on heart rate variability: results of the SAPALDIA study. Epidemiology 18(5):S134–S135

Ahmaruzzaman M (2010) A review on the utilization of fly ash. Prog Energy Combust Sci 36 (3):327–363

ALGAS (Asian Least-cost Greenhouse Gas Abatement Strategy—India), Asian Development Bank, Manila, Philippines (1998)

Arif A, Shah S (2007) Association between personal exposure to volatile organic compounds and asthma among US adult population. Int Arch Occup Environ Health 80(8):711–719

Bhangare RC, Ajmal PY, Sahu SK, Pandit GG, Puranik VD (2011) Distribution of trace elements in coal and combustion residues from five thermal power plants in India. Int J Coal Geol 86 (4):349–356

Boström CE, Gerde P, Hanberg A, Jernström B, Johansson C, Kyrklund T, Rannug A, Törnqvist M, Victorin K, Westerholm R (2002) Cancer risk assessment, indicators, and guidelines for polycyclic aromatic hydrocarbons in the ambient air. Environ Health Perspect 110(Suppl 3):451

Buhre BJP, Elliott LK, Sheng CD, Gupta RP, Wall TF (2005) Oxy-fuel combustion technology for coal-fired power generation. Prog Energy Combust Sci 31(4):283–307

Bustin RM, Mastalerz M, Wilks KR (1993) Direct determination of carbon, oxygen and nitrogen content in coal using the electron microprobe. Fuel 72:181–186

Chawla V, Chawla A, Puri D, Prakash S, Gurbuxani PG, Sidhu BS (2011) Hot corrosion & erosion problems in coal based power plants in India and possible solutions—a review. J Miner Mater Charact Eng 10(4):367–385

Chen X, Hopke PK (2009) Secondary organic aerosol from α-pinene ozonolysis in dynamic chamber system. Indoor Air 19(4):335–345

Chen Y, Shah N, Huggins FE, Huffman GP, Linak WP, Miller CA (2004) Investigation of primary fine particulate matter from coal combustion by computer-controlled scanning electron microscopy. Fuel Process Technol 85(6–7):743–761

Chen LH, Knutsen SF, Shavlik D, Beeson WL, Petersen F, Ghamsary M, Abbey D (2005) The association between fatal coronary heart disease and ambient particulate air pollution: are females at greater risk? Environ Heal Perspect 113(12):1723–1729

Chikkatur AP (2008) A resource and technology assessment of coal utilization in India. Pew Center on Global Climate Change, Arlington, VA (United States)

Clancy L, Goodman P, Sinclair H, Dockery DW (2002) Effect of air-pollution control on death rates in Dublin, Ireland: an intervention study. The lancet 360(9341):1210–1214

Classification and Codification of Indian Coals and Lignites, 770, Indian Standards Institution, New Delhi (1977)

Conti J, Holtberg P, Diefenderfer J, LaRose A, Turnure JT, Westfall L (2016) International energy outlook 2016 with projections to 2040 (No. DOE/EIA-0484 (2016)). USDOE Energy Information Administration (EIA), Washington, DC (United States). Office of Energy Analysis

Córdoba P, Ochoa-Gonzalez R, Font O, Izquierdo M, Querol X, Leiva C, López-Antón MA, Díaz-Somoano M, Martinez-Tarazona MR, Fernandez C, Tomás A (2012) Partitioning of trace inorganic elements in a coal-fired power plant equipped with a wet flue gas desulphurisation system. Fuel 92(1):145–157

Davis WT (2000) Air pollution engineering manual, 2nd edn. Air and Waste Management Association, Wiley, New York

Davis WT, Buonicore AJ (eds) (2000) Air pollution engineering manual. Wiley, New York, pp 117–135

Davison RL, Natusch DF, Wallace JR, Evans Jr CA (1974) Trace elements in fly ash. Dependence of concentration on particle size. Environ Sci Technol 8(13):1107–1113

Diaz EA, Lemos M, Coull B, Long MS, Rohr AC, Ruiz P, Gupta T, Kang CM, Godleski JJ (2011) Toxicological evaluation of realistic emission source aerosols (TERESA)—power plant studies: assessment of breathing pattern. Inhal Toxicol 23(sup2):42–59

Dockery D, Pope A, Xu X, Spengler J, Ware J, Fay M, Ferris B, Speizer F (1993) An association between air pollution and mortality in six U.S. cities. N Eng J Med 329(24):1753–1759

Ehrlich C, Noll G, Kalkoff WD, Baumbach G, Dreiseidler A (2007) PM10, PM2. 5 and PM1. 0—emissions from industrial plants—results from measurement programmes in Germany. Atmos Environ 41(29):6236–6254

Eia U (2013) Annual energy outlook 2013. US Energy Information Administration, Washington, DC, pp 60–62

Elshafei M, Habib MA, Al-Zaharnah I, Nemitallah MA (2014) Boilers optimal control for maximum load change rate. J Energy Res Technol 136(3):031301

Fan B, Hao H, Guo A, Yang R (2016) Fabrication and evaluation of an attapulgite membrane as the filter for recycling blowdown water from industrial boilers. J Water Reuse Desalin, p. jwrd2016148

Fang GC, Chang CN, Chu CC, Wu YS, Fu PPC, Yang IL, Chen MH (2003) Characterization of particulate, metallic elements of TSP, PM2. 5 and PM2. 5-10 aerosols at a farm sampling site in Taiwan, Taichung. Sci Total Environ 308(1–3):157–166

Finkelman RB (2007) Health impacts of coal: facts and fallacies. AMBIO J Hum Environ 36 (1):103–106

Flagan RC, Seinfeld JH (2012) Fundamentals of air pollution engineering. Courier Corporation

Francis W (1961) Coal: its formation and composition. E. Arnold

Godleski JJ, Diaz EA, Lemos M, Long M, Ruiz P, Gupta T, Kang CM, Coull B (2011) Toxicological Evaluation of Realistic Emission Source Aerosols (TERESA)-power plant studies: assessment of cellular responses. Inhal Toxicol 23(sup2):60–74

Gupta T, Agarwal AK (2010) Toxicology of combustion products. Handbook of combustion: Online, pp 357–376

Guttikunda SK, Goel R (2013) Health impacts of particulate pollution in a megacity—Delhi, India. Environ Dev 6:8–20

Guttikunda SK, Jawahar P (2014) Atmospheric emissions and pollution from the coal-fired thermal power plants in India. Atmos Environ 92:449–460

Harrison RM, Yin J (2000) Particulate matter in the atmosphere: which particle properties are important for its effects on health? Sci Total Environ 249(1–3):85–101

Indian Network for Climate Change Assessment (INCCA), India: Greenhouse Gas Emissions 2007, Ministry of Environment & Forests, India, 2010

Jerrett M, Burnett R, Ma R, Pope C, Krewski D, Newbold K, Thurston G, Shi Y, Finkelstein N, Calle E (2005) Spatial analysis of air pollution and mortality in Los Angeles. Epidemiology 16 (6):727–736

Kang CM, Gupta T, Ruiz PA, Wolfson JM, Ferguson ST, Lawrence JE, Rohr AC, Godleski J, Koutrakis P (2011) Aged particles derived from emissions of coal-fired power plants: The TERESA field results. Inhal Toxicol 23(sup2):11–30

Lemos M, Diaz EA, Gupta T, Kang CM, Ruiz P, Coull BA, Godleski JJ, Gonzalez-Flecha B (2011) Cardiac and pulmonary oxidative stress in rats exposed to realistic emissions of source aerosols. Inhal Toxicol 23(sup2):75–83

Lighty JS, Veranth JM, Sarofim AF (2000) Combustion aerosols: factors governing their size and composition and implications to human health. J Air Waste Manag Assoc 50(9):1565–1618

Linak WP, Miller CA, Wendt JO (2000) Comparison of particle size distributions and elemental partitioning from the combustion of pulverized coal and residual fuel oil. J Air Waste Manag Assoc 50(8):1532–1544

Mittal ML, Sharma C, Singh R (2012 Aug) Estimates of emissions from coal fired thermal power plants in India. In: 2012 international emission inventory conference, pp 13–16

Mudakavi JR (2010) Principles and practices of air pollution control and analysis. IK International Pvt Ltd

NATCOM (2004) India's initial national communication (NATCOM) to the United Nations framework convention on climate change. Ministry of Environment and Forests, Government of India

Ninomiya Y, Zhang L, Sato A, Dong Z (2004) Influence of coal particle size on particulate matter emission and its chemical species produced during coal combustion. Fuel Process Technol 85 (8–10):1065–1088

Otero-Rey JR, López-Vilariño JM, Moreda-Piñeiro J, Alonso-Rodríguez E, Muniategui-Lorenzo S, López-Mahía P, Prada-Rodríguez D (2003) As, Hg, and Se flue gas sampling in a coal-fired power plant and their fate during coal combustion. Environ Sci Technol 37(22):5262–5267

Park SH, Kim JY, Yoon MK, Rhim DR, Yeom CS (2018) Thermodynamic and economic investigation of coal-fired power plant combined with various supercritical CO_2 Brayton power cycle. Appl Therm Eng 130:611–623

Pope C 3rd, Thun M, Namboodiri M, Dockery D, Evans J, Speizer F, Heath C Jr (1995) Particulate air pollution as a predictor of mortality in a prospective study of U.S. adults. Am J Respir Crit Care Med 151(3):669–674

Pope C, Burnett R, Thurston G, Thun M, Calle E, Krewski D, Godleski J (2004) Cardiovascular mortality and long-term exposure to particulate air pollution: epidemiological evidence of general pathophysiological pathways of disease. Circulation 109:71–77

Pope CA III, Ezzati M, Dockery DW (2009) Fine-particulate air pollution and life expectancy in the United States. N Engl J Med 360(4):376–386

Rai P, Chakraborty A, Mandariya AK, Gupta T (2016) Composition and source apportionment of PM1 at urban site Kanpur in India using PMF coupled with CBPF. Atmos Res 178–179:506–520

Rajeev P, Rajput P, Gupta T (2016) Chemical characteristics of aerosol and rain water during an El Nino and PDO influenced Indian summer monsoon. Atmos Environ 145:192–200

Rajeev P, Rajput P, Singh AK, Gupta T (2018) Study of temporal variability and mass closure of $PM_{2.5}$ and its chemical constituents during weak south-west monsoon. Atmos Pollut Res

Rajput P, Mandaria A, Kachawa L, Singh DK, Singh AK, Gupta T (2016) Chemical characterisation and source apportionment of PM1 during massive loading at an urban

location in Indo-Gangetic Plain: impact of local sources and long-range transport. Tellus B Chem Phys Meteorol 68(1):30659

Ramanathan V, Carmichael G (2008) Global and regional climate changes due to black carbon. Nat Geosci 1:221–227

Reddy MS, Venkataraman C (2002) Inventory of aerosol and sulphur dioxide emissions from India: I—Fossil fuel combustion. Atmos Environ 36(4):677–697

Reddy MS, Basha S, Joshi HV, Jha B (2005) Evaluation of the emission characteristics of trace metals from coal and fuel oil fired power plants and their fate during combustion. J Hazard Mater 123(1–3):242–249

Ruiz PA, Lawrence JE, Wolfson JM, Ferguson ST, Gupta T, Kang CM, Koutrakis P (2007a) Development and evaluation of a photochemical chamber to examine the toxicity of coal-fired power plant emissions. Inhal Toxicol 19:597–606.

Ruiz PA, Gupta T, Kang CM, Lawrence JE, Ferguson ST, Wolfson JM, Rohr AC, Koutrakis P (2007b) Development of an exposure system for the toxicological evaluation of particles derived from coal-fired power plants. Inhal Toxicol 19(8):607–619

Rohr AC, Koutrakis P, Godleski J (2011) Toxicological evaluation of realistic emissions of source aerosols (TERESA): application to power plant-derived PM2. 5. Electric Power Research Institute, Incorporated

Saarnio K, Frey A, Niemi JV, Timonen H, Rönkkö T, Karjalainen P, Vestenius M, Teinilä K, Pirjola L, Niemelä V, Keskinen J (2014) Chemical composition and size of particles in emissions of a coal-fired power plant with flue gas desulfurization. J Aerosol Sci 73:14–26

Sahu SK, Bhangare RC, Ajmal PY, Sharma S, Pandit GG, Puranik VD (2009) Characterization and quantification of persistent organic pollutants in fly ash from coal fueled thermal power stations in India. Microchem J 92(1):92–96

Samoli E, Aga E, Touloumi G, Nisiotis K, Forsberg B, Lefranc A, Pekkanen J, Wojtyniak B, Schindler C, Niciu E, Brunstein R, DodičFikfak M, Schwartz J, Katsouyanni K (2006) Short-term effects of nitrogen dioxide on mortality: an analysis within the APHEA project. Eur Respir J 27(6):1129–1138

Seligsohn D, Heilmayr R, Tan X, Weischer L (2009) WRI policy brief. China, the United States, and the climate change challenge

Shahzad Baig K, Yousaf M (2017) Coal fired power plants: emission problems and controlling techniques. J Earth Sci Clim Change 8(404):2

Sloss LL (2002) Trace elements—controlling emissions from coal com bustion. Int J Environ Pollut 17:110–125

USEPA E (2002) Air pollution control cost manual. EPA/452/B-02-001

Wellenius GA, Diaz EA, Gupta T, Ruiz PA, Long M, Kang CM, Coull BA, Godleski JJ (2011) Electrocardiographic and respiratory responses to coal-fired power plant emissions in a rat model of acute myocardial infarction: results from the toxicological evaluation of realistic emissions of source aerosols study. Inhal Toxicol 23(sup2):84–94

Whitehurst DD, Mitchell TO, Farcasiu M (1980) Coal liquefaction: the chemistry and technology of thermal processes. Academic Press Inc, New York

Widory D (2006) Combustibles, fuels and their combustion products: A view through carbon isotopes. Combust Theor Model 10(5):831–841

Xiang W, Han B, Zhou D, Nzihou A (2012) Physicochemical properties and heavy metals leachability of fly ash from coal-fired power plant. Int J Min Sci Technol 22(3):405–409

Chapter 5
Polycyclic Aromatic Hydrocarbons (PAHs) Pollution Generated from Coal-Fired Thermal Power Plants: Formation Mechanism, Characterization, and Profiling

Abhrajyoti Tarafdar and Alok Sinha

Abstract Coal can turn out to be more vital as an energy source in the present century, and coal includes substantial amounts of organic and inorganic matter. At the point when coal burns, chemical and physical transformations take place, and numerous harmful mixes are shaped and excreted. The combustion of pulverized coal to produce electrical energy in thermal power plants results in large quantities of coal ash with varying properties. Coal ashes (Bottom ash and Fly ash) are post-combustion particulate residue. It contains various inorganic and organic compounds and some of which have already been identified as pollutants like mercury and polycyclic aromatic hydrocarbons (PAHs). Environmental contamination by PAHs has become one of the major concern across the globe. Huge amount of coal ash is being dumped at deposition sites nearby the power plant, which can contaminate the soil by its comparatively high PAH contains. PAHs contain reactive metabolites like epoxides and dihydrodiols which have the potential to bind with proteins and DNA, resulting in tumors and cancer via biochemical disruption and cell damage. The organic structure of coal generally composed of two complementary parts. The major component consists of ether or thioether linked insoluble and macromolecular networks of fused aromatic and hydroaromatic moiety. The recessive component is soluble in organic solvents. This molecular state involves aliphatic hydrocarbons, PAH, hydroxylated PAH, and heterocyclic compounds. Incomplete coal combustion is regarded as an important factor leading to the formation of PAHs. It is recommended that the development mechanisms of PAHs will be an undeniably imperative point for specialists to

A. Tarafdar
Division of Environmental Science and Ecological Engineering, Korea University, Seoul, Republic of Korea

A. Sinha (✉)
Department of Environmental Science and Engineering, Indian Institute of Technology (ISM), Dhanbad 826004, India
e-mail: aloksinha11@yahoo.com; alok@iitism.ac.in

R. A. Agarwal et al. (eds.), *Pollutants from Energy Sources*, Energy, Environment, and Sustainability,
https://doi.org/10.1007/978-981-13-3281-4_5

discover techniques for controlling emanations amid coal ignition. In the current chapter, formation mechanism of coal and hydrocarbons, uses of coal, generation of PAHs during coal combustion, and harmful effects of PAHs to environment and human are discussed. Towards the end, recent findings on the characterization and PAHs profiling in coal ash have been described.

Keywords PAHs · Coal · Thermal power plants · Coal ash · Coal pollution

Abbreviation

PAHs	Polycyclic aromatic hydrocarbons
pPAHs	Parent polycyclic aromatic hydrocarbons
NPAHs	Nitrated derivatives of PAHs
CPAH	Carcinogenic polycyclic aromatic hydrocarbons
Flu	Fluorene
Phen	Phenanthrene
Anth	Anthracene
Flan	Fluoranthen
Pyr	Pyrene
BaA	Benz[a]anthracene
Chry	Chrysene
BbF	Benzo[b]fluoranthene
BkF	Benzo[k]fluoranthene
BaP	Benzo[a]pyrene
DBA	Dibenzo(a,h)anthracene
IP	Indeno(1,2,3-Cd) pyrene
BgP	Benzo(g,h,i)perylene
CFPPs	Coal-fired power plants
FBC	Fluidized bed combustor

5.1 Introduction

Environmental contamination by polycyclic aromatic hydrocarbons (PAHs) have become one of the major concerns across the globe. PAHs are a group of semi-volatile chemical compounds consisting of two to six condensed aromatic rings (Ye et al. 2011). These are persistent in nature and consist of hundreds of chemically related compounds of various structures and toxicity. They are freed into nature because of the fragmented burning of organic matter in vehicle deplete, coal ignition, petrochemical businesses, unplanned spills amid the transportation of oil, cremation control plant wastes, and so on (Li et al. 1995; Wheatley and Sadhra 2004; Choi and Spengler 2014). The International Agency for Research on Cancer enlisted some PAHs as potential human carcinogens (IARC 2010) and USEPA has considered 16 PAHs as priority pollutants (Yuan et al. 2000; Martorell et al. 2010).

PAHs contains responsive metabolites like epoxides and dihydrodiols which can possibly tie with proteins and DNA, coming about tumors and cancer by means of biochemical disturbance and cell modification (Kim et al. 2013).

The burning of pulverized coal to create electrical vitality in thermal power plants brings about expansive amounts of coal ash with varying properties (Ruwei et al. 2013). Parent polycyclic aromatic hydrocarbons (pPAHs) and their nitrated derivatives (NPAHs) can be emitted directly through combustion, or can be formed in the atmosphere as a result of the oxidation of pPAHs by oxidants (e.g., O_3, NO_x and OH radicals) (Wang et al. 2016; Li et al. 2018). The average emission amount of PAHs for coal-fired power plants (CFPPs) are 1016.60 g/day and 371,073.60 g/year (Wang et al. 2018). Coal ashes (Bottom ash and Fly ash) are post-combustion particulate residue. It contains various inorganic and organic compounds and some of which have already been identified as pollutants like mercury and PAHs (Zou et al. 2003; Barst et al. 2017). Enormous measure of coal ash remains are being dumped at immediate locales adjacent to the power plant, which can taint the soil by its comparatively high PAH contains. Again, as per some past examines, the measure of human introduction to PAHs through soil is higher than by means of air or water (Menzie et al. 1992). Under extreme pressure and heat, plant materials like cellulose, lignin, stem, roots, etc. transformed into coal. Inadequate coal ignition is viewed as an essential factor prompting the development of PAHs (Laflamme and Hites 1978). It is prescribed that the formation pathways of PAHs will be a certainly basic point for researchers to find methods for controlling radiations in the midst of coal combustion.

The present chapter manages the arrangement procedure of PAHs from coal-fired thermal plants and the strategies, reports of characterization, and profiling of the same.

5.2 Formation Mechanism of Coal and Hydrocarbons

The procedure that makes coal differ marginally in various territories relying upon the plants and conditions that are available, yet the general procedure is similar. There are two fundamental stages in coal development: peatification and coalification. Bacterial action is the fundamental procedure that makes the peat amid peatification. Expanding temperature and weight from burial are the principal factors in coalification. There are four phases in coal development: peat, lignite, bituminous, and anthracite. The stage relies on the conditions to which the plant remains are subjected after they were buried—the more prominent the weight and heat, the higher the rank of coal (Fig. 5.1).

Plant matter in mires and wetlands, for example, ferns, bushes, vines, trees, and algae bites the dust and gathers on earth surface. At first, the organic matter is decayed by microbes, yielding CO_2 and CH_4. The plant matter winds up and covered and never comes in contact of air again. Anaerobic microscopic organisms at that point begin to decay the material. Burial and accumulation can happen for several thousands of years, creating a few meters of in part decayed plant matter known as peat. When this peat is profoundly covered, water and different other

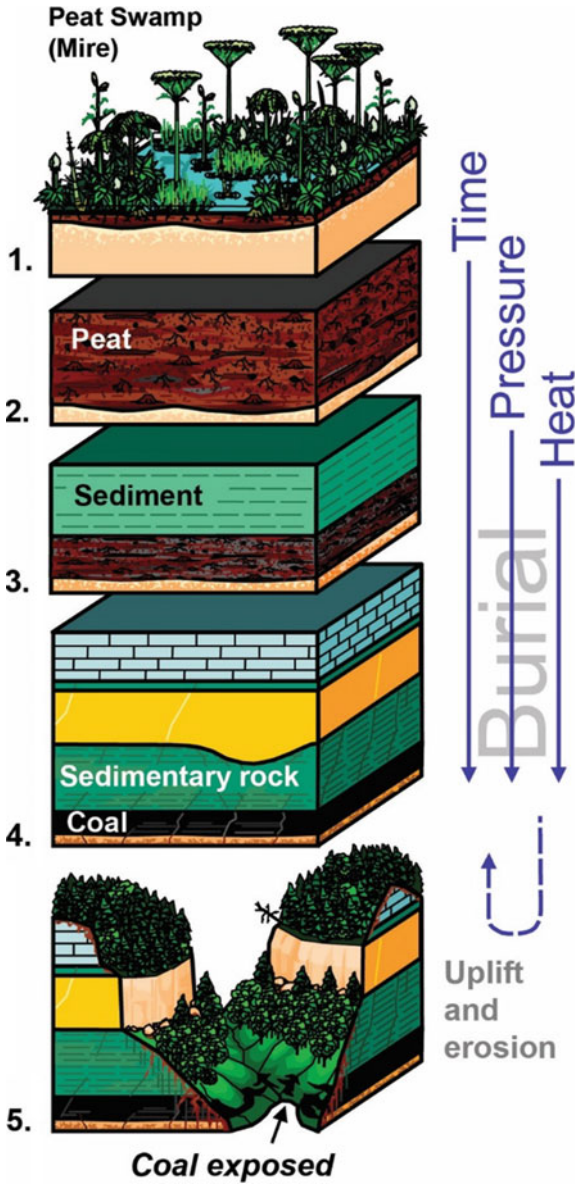

Fig. 5.1 Steps of coal formation. Adapted with permission from Stephen Greb, Kentucky Geological Survey, University of Kentucky

compound mixes are squeezed out from the expanding pressure, reduces its volume (called compaction) and the least quality of coal, lignite, starts to form. Heating prompts hydrocarbon complexes (mixes made out of hydrogen, carbon, and oxygen) in the peat to separate and modify in an assortment of routes bringing about coal. Proceeded with entombment more profound into the earth likewise opens the material to higher temperatures. By and large, warm in the earth rises one degree

Fahrenheit for each 70–100 ft of profundity. A heating amid burial can likewise happen through association with hydrothermal liquids, or through contact transformative metamorphism.

Proceeded with internment, bringing about expanding pressure and temperatures causes this low-quality lignite coal to be changed into higher quality "dark or black coals". Initially, lignite moves toward becoming subbituminous coal, then to bituminous coal and lastly the most astounding quality anthracite coal. As these changes happen, the measure of water and different mixes in the coal diminishes and the coal turns out to be denser. Alongside this, comes a higher carbon concentration.

In short, according to Kentucky Geological Survey, "Coal is formed from the physical and chemical alteration of peat. Peat is composed of plant materials that accumulate in wetlands (bogs and fens), which break down through the process of peatification. If peats are buried, then the peats can be altered into different ranks of coal through the process of coalification."

Again, coal is formed from plant materials, for example, cellulose, lignin, pitches, spores, leaves, stems, and roots under serious heat and pressure. The organic matter of coal is by and large viewed as being made out of two reciprocal structures (Chen et al. 2005). The transcendent segment is a macromolecular, insoluble, three-dimensional framework made out of merged aromatic and hydroaromatic units related by ether or thioether linkages and short alkyl spans. The second structure is a molecular period of complexes that are regularly dissolvable in organic solvents. This molecular stage contains moving dispersals of aliphatic hydrocarbons, polycyclic aromatic and hydroaromatic hydrocarbons, hydroxylated polycyclic aromatic and heterocyclic complexes.

PAHs are compounds developed of benzene rings that take after sections of single layers of graphite. They have planar structures and a wide assortment of shapes and sizes. The predominant part of coal is by all accounts made out of a three-dimensional system of dense aromatic and hydroaromatic units associated by weaker bonds. The extent of conjugated aromatic rings, per structural unit, inside the framework decides the aromaticity and increments with expanding coalification, at last bringing about graphite. Dehydroxylation, demethylation, and condensation reactions create a relative increment in carbon joined with an abatement in oxygen and hydrogen as it is recommended in the van-Krevelen-chart (Fig. 5.2).

Aromatic structures are regularly connected by ether or methylene bridges. Aliphatic side chains comprise fundamentally of methyl, and less of ethyl, propyl or butyl functional groups. The normal number of aromatic rings per auxiliary unit in most coals is 3–5 (Stout and Emsbo-Mattingly 2008) with some individual units containing up to 10 rings. An ordinary hard coal is portrayed by 2–6 PAH connected by methylene bridges with furthermore bound aliphatic side chains and phenol functional groups. With expanding rank, aromatic units increase from 3 to 4 dense rings at low rank to around 30 combined rings in anthracite. Simultaneously, the lengths of side chains diminish.

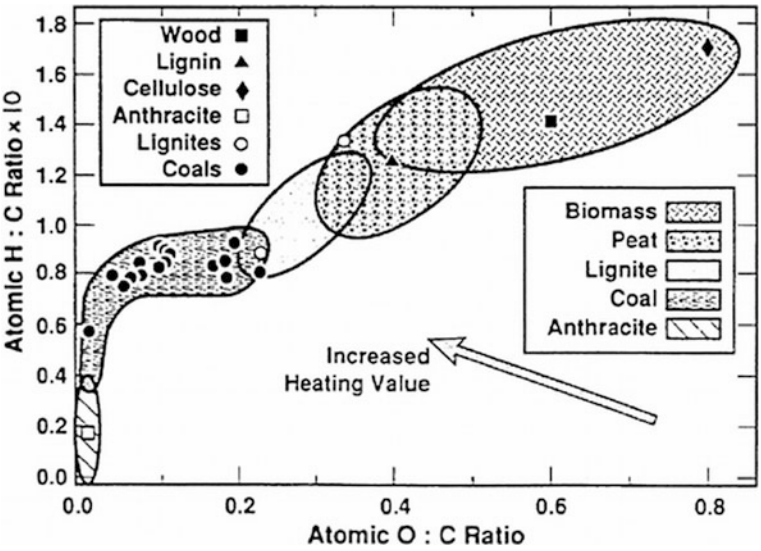

Fig. 5.2 van Krevelen diagram. Adapted from van Krevelen (1993)

5.3 Uses of Coal

Coal has numerous essential uses around the world. The most noteworthy employments of coal are in production of electricity, steel creation, cement producing, and as a fossil fuel. Diverse kinds of coal have distinctive employments,

- *Steam coal*—otherwise called thermal coal—is fundamentally utilized as a part of the production of power.
- *Coking coal*—otherwise called metallurgical coal—is fundamentally utilized as a part of steel generation.

Other imperative clients of coal incorporate alumina refineries, paper producers, and the chemical and pharmaceutical enterprises. A few chemical items can be created from the by-products of coal. Filtered coal tar is utilized as a part of the production of synthetic compounds, for example, creosote oil, naphthalene, phenol, and benzene. Ammonia gas recouped from coke broilers is utilized to produce ammonia salts, nitric acid, and horticultural composts. A large number of various items have coal or coal by-products as parts: cleanser, aspirins, solvents, colors, plastics and filaments, for example, rayon and nylon.

Coal is additionally a basic fixing in the creation of master items:

- *Activated carbon*—utilized as a part of filters for water and air decontamination and in kidney dialysis machines.
- *Carbon fiber*—a great degree solid however lightweight fortification material utilized as a part of development, trailblazing bicycles and tennis rackets.

- *Silicon metal*—used to create silicones and silanes, which are thusly used to influence greases, to water repellents, resins, beautifiers, hair shampoos, and toothpaste.

The prerequisite of electric power cannot be overstressed; society requires electricity for their regular day to day existences, which incorporates viewpoints, for example, well-being and the arrangement of safe drinking water and in addition, industrial production. As a portion of the thousand years, advancement objectives are met by the Government, for example, lightening poverty, the interest for electricity will increment. Coal assumes an essential part in electricity generation worldwide and coal-terminated power plants as of now fuel 37% of worldwide power (Table 5.1). In a few nations, coal powers a higher level of power and that may proceed past 2030; the utilization of coal for power may even ascent to 44% around the world.

Steam coal, otherwise called thermal coal, is utilized as a part of energy stations to produce electricity. Coal is first processed to a fine powder, which expands the surface territory and enables it to burn more rapidly. In these pulverized coal combustion (PCC) frameworks, the powdered coal is blown into the ignition assembly of a boiler where it is combusted at high temperature. The hot gases and heat energy delivered changes over water—in tubes covering the evaporator—into steam.

The high force steam is passed into a turbine containing countless propeller-like sharp edges. The steam pushes these sharp edges causing the turbine shaft to turn at quick. A generator is mounted toward one side of the turbine shaft and comprises of deliberately twisted wire loops. Power is created when these are quickly rotated in a strong magnetic field. In the wake of going through the turbine, the steam is consolidated and come back to the evaporator to be heated by and by.

The power produced is changed into the higher voltages (up to 400,000 V) utilized for financial, effective transmission by means of electrical cable grids. When it nears the purpose of utilization, for example, our homes, the power is changed down to the more secure 100–250 voltage systems utilized as a part of the local market.

Georgia Power's Plant Scherer is one of the biggest coal-terminated thermo-electric power-creation stations in the United States. It is a 3520,000-kW coal-terminated station that gives power to Georgia. As this figure appears, it consumes coal to deliver heat that transforms water into steam, which at that point turns turbines in a generator (Fig. 5.3).

Table 5.1 Percentage of coal usage[a] in electricity generation worldwide

South Africa 93%	Poland 92%
P.R. China 79%	Australia 77%
Kazakhstan 70%	India 69%
Israel 63%	Czech Republic 60%
Morocco 55%	Greece 52%
USA 49%	Germany 46%

[a]Adapted from www.worldcoal.org

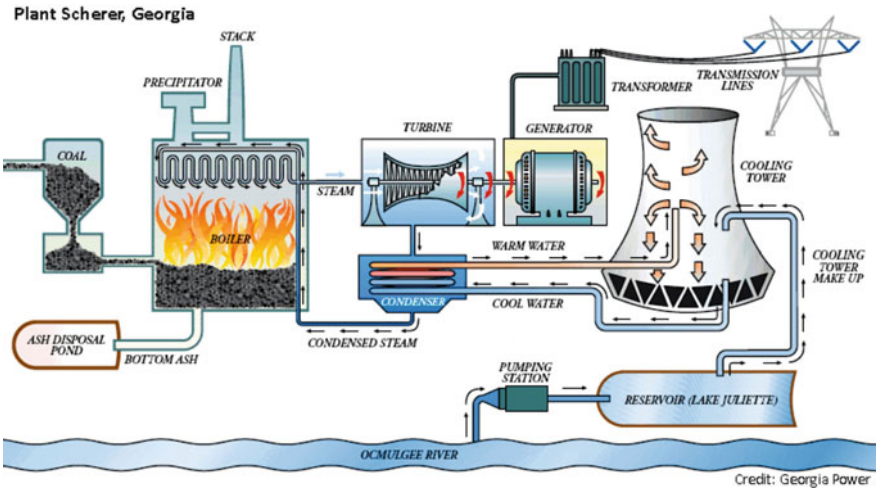

Fig. 5.3 Schematic diagram of an ideal coal-fired thermal power plant. Adapted from https://water.usgs.gov/edu/

Coal that has been ground into a fine powder by a pulverizer is blown into a furnace-like gadget, called a boiler, and ignited. The heat created changes over water, which goes through a progression of channels in the boiler, to steam. The high-pressure steam turns the cutting edges of a turbine, which is associated by a shaft to a generator. The generator twists and delivers power.

In the chart, we can perceive how the fundamental utilization of water is to cool the condenser units, which gets the consolidated steam that was utilized to turn the turbines. The hot, consolidated steam water is gone through channels that are cooled by the cooler water. The condensed water is hence cooled and after that recycled back through the coal-terminated boiler to again swing to steam and power the turbines. This is the closed-cycle circle some portion of the framework and it reuses the water ceaselessly.

In the open-circle cycle, which is the other part of the water utilization cycle of the plant, huge amount of water is taken from a water body and is pumped to the condensers. This cooler water encompasses the pipes containing the hot consolidated steam and consequently is warmed up a considerable measure.

5.4 Generation of PAHs During Coal Combustion

Amid coal burning PAH development and outflow components can be classified into two procedures: pyrolysis and pyrosynthesis. On coal heating, the organic compounds are incompletely cracked to littler and unstable fragments (pyrolysis). These fragments, predominantly exceptionally receptive free radicals with a short

normal lifetime, prompt steadier PAH development through recombination responses (pyrosynthesis). In this way, BaP and different PAHs are framed through pyrolysis of methane, acetylene, butadiene, and different other compounds. PAH development in burning resembles a cascade mechanism in which PAH are developed through little radicals to which radicals are included, shaping compounds of higher molecular weight, soot, and fullerenes (Mastral et al. 2000).

While utilizing the coal, e.g., warming or burning, coal structures experience major physical and synthetic changes and discharge unstable organic mixes. Weaker bonds in aliphatic extensions and rings separate first, then aromatic structures, resulting in more aromatic hydrocarbons in the items. These fractions experience cyclization responses prompting polycyclic aggravates that can exist in vaporous and in solid stages, contingent upon the encompassing temperature and their molecular volume. They can exist in the gas stage (<3-ring PAHs), in the solid stage (>6-ring PAHs), or in the two stages (4- and 5-ring PAHs), depending upon their molecular mass. A portion of the organic compounds might be radiated as unburnt material, in this manner turning into a wellspring of organic outflows.

Recent studies have proposed union components of PAH from C_2 species to benzo[u]pyrene, however, comparative pathways could prompt a large portion of the known PAH created in coal ignition and organized by the USEPA as priority contaminations as a result of their cancer-causing and mutagenic impacts (Baek et al. 1991). The least complex and earliest PAH framed can, depending on the flue gas conditions, facilitate pyrolytic responses to frame bigger, exceedingly dense PAH by intermolecular reactions, for example, buildup and cyclization (as stated earlier). In this manner, the PAH can exist in the gas exhausted or be upheld on particulate matter, or even produce particulate matter, contingent upon their association (Mastral et al. 1996).

5.5 Why and How PAHs Are Harmful to Environment and Human?

Environmental Protection Agency of United States defines the term PAH as, "*Short for polycyclic aromatic hydrocarbons, PAHs describe chemicals that are often found together in groups of two or more. PAHs are found naturally in the environment but they can also be man-made. In their purest form, PAHs are solid and range in appearance from colorless to white or pale yellow-green. PAHs are created when products like coal, oil, gas, and garbage are burned but the burning process is not complete.*" (USEPA 2008).

In another words, polycyclic aromatic hydrocarbons (PAHs) are the complex of ecologically persevering organic substance mixes containing at least two combined aromatic rings in linear, angular, or cluster plan, containing just carbon and hydrogen (Gurjeet et al. 2014).

Table 5.2 Evaluations of genotoxicity and carcinogenicity of 16 USEPA PAH priority pollutants. Adapted from Larsen (2013)

Common name	Genotoxicity	Carcinogenicity
Naphthalene	Not genotoxic	Questionable
Acenaphthene	Inadequate data	Questionable
Acenaphthylene	Inadequate data	Inadequate studies
Fluorene	Inadequate data	Negative
Anthracene	Limited evidence	Positive
Phenanthrene	Equivocal	Questionable
Fluoranthene	Equivocal	Positive?
Pyrene	Not genotoxic	Questionable
Benzo(a)anthracene	Genotoxic	Positive
Chrysene	Genotoxic	Positive
Benzo(b)fluoranthene	Limited evidence	Negative?
Benzo(k)fluoranthene	Genotoxic	Positive
Benzo(a)pyrene	Genotoxic	Positive
Dibenzo(a,h)anthracene	Genotoxic	Positive
Benzo(g,h,i)perylene	Genotoxic	Negative?
Ideno(1,2,3-c,d)pyrene	Genotoxic	Positive

Various PAH, including coal tars and different complex blends containing PAH from ignition outflows, have indicated cancer-causing nature in trial animals and genotoxicity/mutagenicity in vitro and in vivo (IARC 2010). The differing potential for toxicity, carcinogenicity, and mutagenicity of PAHs can be attributed to the differences in chemical structure and molecular size. Generally, LMW PAHs are acutely toxic and as the number of aromatic rings and the molecular size increases, there is a shift towards chronic toxicity including carcinogenesis (Miller and Miller 1981). In general, within this group of PAH, the confirmation of genotoxicity indicates significant covering with cancer-causing nature, in concurrence with the mechanistic connection between DNA adducts development, mutation, and malignancy result following PAH introduction. Table 5.2 lists the carcinogenic and genotoxic properties of the 16 USEPA PAH priority pollutants.

In humans, PAHs have the potential to be absorbed through the skin, pulmonary tract or the gastrointestinal tract (IPCS 2001). The skin carcinogenicity of a number of PAH after dermal application to sensitive strains of mice is well established (Siddens et al. 2012). In some studies, PAHs were tested alone, but in most of the studies, PAHs were tested as initiators of skin cancer together with tumor promoters. Following absorption through any of these routes, lipophilic PAHs are widely distributed throughout the internal organs but are predominantly present in those that are lipid rich. A number of PAHs including chrysene, benzo(a)pyrene, and fluoranthene give rise to metabolites that form DNA adducts in animals (Muñoz and Albores 2010). PAH structure has a role in the toxigenic potential of the

molecule. In fact, the shape of the PAH molecule as an indicator of acceptable targets for cytochrome enzymes is thought to be the best predictor of PAH carcinogenicity (Klopman et al. 1999). Overwhelming DNA adducts of PAH can instigate frameshift mutations, deletions, S-phase arrest, strand breakage, and distinctive chromosomal modifications, all progressions, which might be of significance in oncogenesis (Larsen 2013). The pathway of mutagenicity of PAH has principally been considered utilizing benzo[a]pyrene and benzo[a]pyrene-7,8-diol-9,10-epoxide (BaPDE) as model complexes. The mutational range incited by BaPDE in vitro and in vivo demonstrates a predominance of base-pair substitutions (G > T transversions). Tests in rats directed benzo[a]pyrene by the oral, dermal, or intratracheal courses, demonstrate that adduct advancement happens at both the site of contact and fundamentally PAH metabolism in the body generally leads to detoxification involving the conversion of parent compounds to phenols, diols, and tetrols via epoxide intermediates (Abdel-Shafy and Mansour 2016).

Two mechanisms are responsible for the damage and toxicity caused by PAHs. The first is the association or reaction of the PAH parent compound with lipids in cell membranes or other cellular components. Collaborations amongst PAHs and the cell membrane can influence the penetrability of the membrane and in addition alter transport into and out of the cell (Knutzen 1995). The second mechanism is the reaction of PAH metabolites with nucleic acids and proteins. The most important step of primary PAH metabolism is epoxidation and subsequent diol formation. Epoxide compounds with mutagenic and carcinogenic properties were formed as a result of PAHs' metabolism in human body and there are case reports of lung, skin, intestinal, pancreas, and liver cancers (Tarafdar and Sinha 2017). The typical destinations of attack on nucleic acid bases are the extranuclear amino groups of guanine and adenine. Albeit a significant number of the PAH-deoxyribonucleoside adducts framed in human cells and tissues have not been completely described, the accessible proof from bronchial epithelium, colon, skin, and cultured mammary cells recommends adducts shaped are fundamentally the same as those from relating rat tissues. The significant adduct is framed on the N2 position of guanine (SCF 2002). Several studies indicate that the number of adducts formed is related to the degree of PAH exposure (Godschalk et al. 1998; Juhasz and Naidu 2000). Most PAHs are oxidized to form phenols and dihydrodiols via monooxygenase enzymes associated with cytochrome P-450, but a small proportion will be further epoxidized to reactive intermediates (diol epoxides) that result in carcinogenic activity in mammalian cells (Klopman et al. 1999). These activities take place predominantly within the microsomes of the endoplasmic reticulum and in nuclear membranes.

Apart from genotoxic and mutagenic effects, PAHs also is known to have teratogenicity effects. Embryotoxic impacts of PAHs have been portrayed in test animals exposed to PAH, for example, benzo(a)anthracene, benzo(a)pyrene, and naphthalene. Research facility examines directed on mice have shown that the ingestion of elevated amounts of benzo(a)pyrene amid pregnancy brought about birth abandons and diminished body weight in the posterity (Kristensen et al. 1995). It is not known whether these impacts can happen in people. In any case, it was

accounted for and shown that exposure to PAH contamination amid pregnancy is identified with unfavorable birth results including low birth weight, unexpected labor, and heart deformities (Perera et al. 2005).

5.6 Characterization and PAHs Profiling in Coal Ash

Amid coal use forms, for example, coal burning and pyrolysis, PAHs discharged might be isolated into two classes as indicated by their generation pathways: one pathway is derived from complex chemical responses and the other is from free PAHs exchanged from the pristine coal.

Williams and Taylor (1993) presumed that the outcomes are of enthusiasm for the illustration of PAH development forms and for the justification of the pervasive arrangement of a particular arrangement of PAHs amid combustion.

Mastral et al. (1995) considered the system of PAH arrangement and demonstrated that, despite the fact that the individual PAH sum found in atmospheric fluidized bed combustion (AFBC) as a component of the ignition temperature takes after an irregular circulation, the aggregate of PAH keeps up a pattern.

The coal structure impacts the nature and measure of the PAH discharges, however in a yet obscure manner. It may be the case that in deficient burning, because of the breakdown of the macromolecular system of the coal a few compounds present as bigger molecules of this complex network are discharged totally unblemished. At the same time, little molecules from the subatomic coal segment or potentially from the breakdown of the extensive aromatic structures may recombine by the expansion of little ring frameworks to create bigger PAH atoms through condensation reactions, which can be radiated to the environment. At long last, cyclization responses of carbon chains and ensuing ring expansion may bring about the creation of PAHs. All these pathways of PAH emanation are probably going to happen all the while, inferable from the low selectivity at high temperatures and to the considerable complexity of the natural coal structure. The rate of each will rely upon the productivity and states of ignition and on the nature of the coal.

Acevedo et al. (1996) reasoned that the perplexing hydrocarbons do not need to fundamentally break into little sections previously performing recombination forms. Mixes with a few rings can experience fractional cracking taken after by dehydrogenation of the primary radicals.

Two fundamental elements influencing the PAH discharges from coal fluidized bed combustor (FBC) are the conditions under which the burning is completed and the pyrolytic responses between the radicals transmitted and framed at the highest point of the ignition reactor. While the previous is appeared to have a lower impact, the last has significantly more prominent pertinence. Cyclization, interconversion, affiliation, and different procedures between radicals imply that while the measure of each PAH produced is variable, the aggregate sum of the PAH transmitted takes after a particular pattern with the burning temperature. In every one of the

examinations, the measure of PAH transmitted in the gas stage was higher than that bolstered on particulate matter (Mastral et al. 1996).

Important factors in PAHs emission are operating parameters of the plant, reflected in oxygen excess and unburnt matter in ashes. This parameter signifies the combustion efficiency. Coal type is also a considerable parameter for PAHs generation from burning of coal. But this parameter has enough influence only when operating conditions are not optimal (Revuelta et al. 1999).

Emanations of PAHs in the flue gas from the ignition of coals were estimated amid 1000 h combustion runs utilizing the 0.1 MW heat-input (MWth) bench-scale fluidized bed combustor (FBC) (Liu et al. 2000). The outcomes showed that the discharges of PAHs in a FBC framework are basically reliant on the ignition temperature and overabundance air proportion. The infusion of secondary air with high speed in the freeboard adequately decreases PAH discharges. The expansion of additional limestone can advance the generation of PAHs in the FBC framework. Chlorine in the coal can prompt expansive benzene ring PAH development amid ignition. The aggregate PAH discharge increments with an expansion in the sulfur substance of coal. Incomplete combustion outcomes in PAHs with at least 4 benzene rings. High effectiveness ignition brings about PAHs with two and 3 benzene rings.

A study on Greek lignite-fired power plants reveals a turn around the relationship of concentration with particle size for all PAHs, especially the heavier compounds (Arditsoglou et al. 2004). The percent mass of all components and PAH species in the suspendable part (−63 mm) was in the vicinity of 25 and 30%. In every single fly ash, the PAH blend was ruled by 4-ring species (48–62%) trailed by 3-ring mixes (38–41%), while the cancer-causing 5- and 6-ring PAHs were less plenteous (2–11%). Fly ash remains PAH concentrations were found to associate emphatically with the groupings of certain follow components either decidedly (e.g. Ba) or adversely (Mg, Cr, V, U) in this manner proposing that some lignite components may advance or forestall PAH arrangement amid burning.

The fly ashes remains created from five thermal power stations from various parts of India were examined in an investigation with respect to the elaboration of conveyance types of persistent organic pollutants (POPs) for example, PAHs (Sahu et al. 2009). Lower molecular weight PAHs were observed to be prevalent in fly ash samples. The convergence of Benzo(a)Pyrene which is the most strong cancer-causing PAH fluctuated between 0.82 and 18.14 ng/g with a mean amount of 9.02 ng/g.

The conditions in which lignite frames, generally are the reason for the arrangement of bigger PAH particles (up to 5-ring atoms). Convergences of naphthalene in lignite are roughly 5 times smaller than 3-ring molecules, around 28 times smaller than centralizations of 4-ring particles, and just about 79 times smaller than groupings of 5-ring PAH particles according to a study on coal-powered power plant in Belgrade (Pergal et al. 2013). The ignition procedure lessens the aggregate PAH concentration in burning side effects in contrast with coal yet, and in addition, changes the appropriation among the PAH particles. Amid the burning of coal, overwhelmingly PAHs with 2 aromatic rings are shaped yet a portion of the

compounds with a higher number of rings likewise exist. Naphthalene, acenaphthylene, acenaphthene, fluorene, phenanthrene, anthracene, fluoranthene, pyrene, chrysene, benzo(a)anthracene, benzo(a)pyrene, dibenzo(a,h)anthracene, and benzo (g,h,i)perylene are framed, in any event at a few temperatures, amid ignition, while benzo(b)fluoranthene, benzo(k)fluoranthene, and indeno(1,2,3-c,d)pyrene were not shaped at all and, in this manner, cannot be presented to the conditions display in the region of the plant and risk environment. Benzo(g,h,i)perylene is the main PAH molecule that is turned out to be available in bigger fixations in fiery debris tests than in the lignite. With the expansion of the lignite ignition temperature the amount of PAHs in burning side effects increments from 930 to 973.5 °C, while with the further increment of the temperature, it becomes consistent.

Another study on CFPP Bottom Ash and Fly Ash from Huainan, China uncovers fly ashes were ruled by medium molecular weight PAHs and low molecular weight PAHs, while bottom ash debris were inexhaustible in 5- and 6-ring PAH species (Ruwei et al. 2013). The CPAHs levels of a few ashes, particularly bottom ashes, were more prominent than the points of confinement controlled by a few nations, demonstrating that this kind of coal ignition product requires unique treatment before landfill. PAH levels and patterns in fly ash were clearly influenced by particle size, and total organic content had a nearer relationship with PAH content than particle size measure in bottom and fly ash, which might be expected to unburned carbon existing in bottom ash.

Li et al. (2014) also state similar findings as PAHs with 3 and 4 rings were the command species in all the fly ash from Anhui, China. The sum low subatomic weight PAHs with 2, 3, and 4 rings was conversely associated with the particle sizes of the fly ash.

Coal being heterogeneous, periodical assessment of conceivably lethal components and PAHs in the dirt, water, air, and farming productions in the region of the power plant is suggested by an Indian study (Verma et al. 2015). The aggregate PAHs content was significantly higher in coal (4542 μg/kg) than fly ash (32.40 μg/kg) and bottom ash remains (10.10 μg/kg). High molecular weight PAHs were overwhelming in coal and fly ash remains, low molecular weight PAHs in bottom ash. The cancer-causing PAHs were higher in coal (3623 μg/kg) trailed by fly ash debris (25.10 μg/kg) and bottom ash (0.90 μg/kg). All the cancer-causing PAHs (BaA, Chy, BbF, BkF, BaP, DahA, and InP) were distinguished to be prevailing in coal; while fly ash has BbF, BkF, and BaP; and bottom ash debris has BbF and BkF.

A large-scale study on 18 CFPPs from China deals with the BaP-based toxic equivalency (BaPeq) of coal fly ashes (Li et al. 2016). PAH profiles for 16 CFPPs with individual block power capacity as 600 MW (IBPC-600) were altogether not quite the same as other industrial stacks in light of higher coefficients of uniqueness. The BaPeq concentration and BaP-based equal carcinogenic potency (BaPE) for 16 CFPPs with IBPC-600 were 0.83 and 0.57 ng/g, much lower than relating 20.50 and 15.40 ng/g for 2 CFPPs with IBPC-200/300. No distinction existed for Σ_{86}PCBs between CPFFs with IBPC-600 and -200/300, which extended from 9.60 to 32.10 ng/g. Higher mean cancer-causing PAH concentrations for 2 CFPPs with IBPC-200/300 and PCBs-TEQ concentration for 18 CFPPs showed the use of coal

Table 5.3 Comparative view of PAH contents in coal ash in literature

Country	Type	Reference	No. of PAHs	Total CPAH (µg/g)	Total PAH (µg/g)
USA	Fly ash	Liu et al. (2000)	11	7.60–57.99	77.12–694.5
Greece	Fly ash	Arditsoglou et al. (2004)	13	2–11% of total PAH content	0.065–1.983
India	Fly ash	Sahu et al. (2009)	14	0.01–0.16	0.04–0.94
China	Fly ash (PM10 fraction)	Kong et al. (2011)	17	140.33–3345.46	290.20–7055.72
China	Fly ash certified reference material	Masala et al. (2012)	15	13.09 (mean)	22.08 (mean)
China	Fly ash	Ruwei et al. (2013)	16	0.26–0.87	0.93–2.08
China	Bottom ash	Ruwei et al. (2013)	16	1.76–3.76	2.73–5.32
China	Fly ash	Li et al. (2014)	16	0.17–0.32	3.47–4.8

fly ashes as soil amendment ought to be restricted. The PAH concentrations for 18 CFPPs were all around associated with the total organic carbon (TOC) values, while PCB concentrations demonstrated not this pattern, showed the diverse arrangement pathways amongst PCBs and PAHs.

By and large, the portions of pPAH and NPAH in various size-isolated particulate matters were affected by boiler kinds and working conditions. Individual PAHs demonstrated significantly unique improvement/dividing practices between PM2.5–10, PM1–2.5 and PM1. Low molecular weight PAHs were moderately simpler to equilibrate amongst fine and bulk particles, while heavier species were more related to littler particles due to their slower volatilization/sorption procedures (Wang et al. 2016).

A table of PAH contents in coal ashes from some previous studies has been constructed hereby (Table 5.3).

5.7 Conclusions

Coal may turn out to be more imperative as a power source in the twenty-first century, and coal has huge amounts of natural organic matter. When coal ignites, chemical and physical transformation happen, and numerous poisonous complexes are shaped and radiated. Amid coal usage forms, for example, combustion and pyrolysis, PAHs discharged might be separated into two classes as indicated by their generation mechanisms: one mechanism is generated from complex chemical responses and the other is from free PAHs exchanged from the pristine coal. The

development and outflow of PAHs is a complex physico-chemical process that has received impressive consideration lately. It is proposed that the development pathway of PAHs will be an undeniably imperative point for analysts to find techniques for controlling outflows amid coal ignition. Polycyclic aromatic hydrocarbons (PAHs) are amid those pollutants generated and are taken as to posture potential health dangers, since some PAHs are known cancer-causing agents. LMW PAHs are acutely toxic and as the number of aromatic rings and the molecular size increases, there is a shift towards chronic toxicity including carcinogenesis. Human body metabolizes PAHs to epoxide compounds with mutagenic and carcinogenic properties which can result in lung, skin, intestinal, pancreas, and liver cancers. In addition to genotoxic and mutagenic effect, PAH exposure can cause teratogenic effects too. Fly ashes have more medium and low molecular weight PAHs, while bottom ash debris was inexhaustible in cancer-causing 5- and 6-ring PAH species which may be attributed to unburnt carbon in bottom ash.

References

Abdel-Shafy HI, Mansour MSM (2016) A review on polycyclic aromatic hydrocarbons: source, environmental impact, effect on human health and remediation. Egypt J Pet 25(1):107–123

Acevedo S EG, Antonieta MR, Luis BG (1996) The PMO method for analysis of structural features of polycyclic aromatic hydrocarbons relevant to asphaltenes. Fuel 75(9):1139–1144

Arditsoglou A, Petaloti C, Terzi E, Sofoniou M, Samara C (2004) Size distribution of trace elements and polycyclic aromatic hydrocarbons in fly ashes generated in Greek lignite-fired power plants. Sci Total Environ 323(1–3):153–167

Baek SO, Field RA, Goldstone ME, Kirk PW, Lester JN, Perry R (1991) A review of atmospheric polycyclic aromatic hydrocarbons: sources, fate and behavior. Water Air Soil Pollut 60(3–4):279–300

Barst BD, Ahad JME, Rose NL, Jautzy JJ, Drevnick PE, Gammon PR, Sanei H, Savard MM (2017) Lake-sediment record of PAH, mercury, and fly-ash particle deposition near coal-fired power plants in Central Alberta, Canada. Environ Pollut 231:644–653

Chen Y, Sheng G, Bi X, Feng Y, Mai B, Fu J (2005) Emission factors for carbonaceous particles and polycyclic aromatic hydrocarbons from residential coal combustion in China. Environ Sci Technol 39(6):1861–1867

Choi H, Spengler J (2014) Source attribution of personal exposure to airborne polycyclic aromatic hydrocarbon mixture using concurrent personal, indoor, and outdoor measurements. Environ Int 63:173–181

Godschalk RWL, Maas LM, Van Zandwijk N, Van 'T Veer LJ, Breedijk A, Borm PJA, Verhaert J, Kleinjans JCS, Van Schooten FJ (1998) Differences in aromatic-DNA adduct levels between alveolar macrophages and subpopulations of white blood cells from smokers. Carcinogenesis 19(5):819–825

Gurjeet P, Kothiyal NC, Kumar V (2014) Bioremediation of some polycyclic aromatic hydrocarbons (PAH) from soil using *Sphingobium indicum*, *Sphingobium japonicum* and *Stenotrophomonas maltophilia* bacterial strains under aerobic conditions. J Environ Res Dev 8 (3):395–405

IARC (2010) IARC monographs on the evaluation of carcinogenic risks to humans: some non-heterocyclic polycyclic aromatic hydrocarbons and some related exposures. IARC Monogr Eval Carcinog Risks Humans 92:1–868

IPCS (2001) Environmental health criteria for arsenic and arsenic compounds. Geneva
Juhasz AL, Naidu R (2000) Bioremediation of high molecular weight polycyclic aromatic hydrocarbons: a review of the microbial degradation of benzo[a]pyrene. Int Biodeterior Biodegradation 45(1–2):57–88
Kim K-H, Jahan SA, Kabir E, Brown RJC (2013) A review of airborne polycyclic aromatic hydrocarbons (PAHs) and their human health effects. Environ Int 60:71–80
Klopman G, Tu M, Fan BT (1999) META 4. Prediction of the metabolism of polycyclic aromatic hydrocarbons. Theor Chem Acc Theory Comput Model (Theor Chim Acta) 102(1–6):33–38
Knutzen J (1995) Effects on marine organisms from polycyclic aromatic hydrocarbons (PAH) and other constituents of waste water from aluminium smelters with examples from Norway. Sci Total Environ 163(1–3):107–122
Kong S, Shi J, Lu B, Qiu W, Zhang B, Peng Y, Zhang B, Bai Z (2011) Characterization of PAHs within PM10 fraction for ashes from coke production, iron smelt, heating station and power plant stacks in Liaoning Province, China. Atmos Environ 45(23):3777–3785
Kristensen P, Eilertsen E, Einarsdottir E, Haugen A, Skaug V, Ovreba S (1995) Fertility in mice after prenatal exposure to benzo[a]pyrene and inorganic lead. Environ Health Perspect 103 (6):588–590
Laflamme RE, Hites RA (1978) The global distribution of polycyclic aromatic hydrocarbons in recent sediments. Geochim Cosmochim Acta 42(3):289–303
Larsen JC (2013) Polyaromatic Hydrocarbons (PAH). Evaluation of health hazards and estimation of a quality criterion in soil
Li C-T, Lee W-J, Mi H-H, Su C-C (1995) PAH emission from the incineration of waste oily sludge and PE plastic mixtures. Sci Total Environ 170(3):171–183
Li H, Liu G, Cao Y (2014a) Content and distribution of trace elements and polycyclic aromatic hydrocarbons in fly ash from a coal-fired CHP plant. Aerosol Air Qual. Res. 14(4):1179–1188
Li Z, Ma Z, van der Kuijp TJ, Yuan Z, Huang L (2014b) A review of soil heavy metal pollution from mines in China: pollution and health risk assessment. Sci Total Environ 468–469:843–853
Li Z, Chen L, Liu S, Ma H, Wang L, An C, Zhang R (2016) Characterization of PAHs and PCBs in fly ashes of eighteen coal-fired power plants. Aerosol Air Qual Res 16(12):3175–3186
Li X, Li J, Wu D, Lu S, Zhou C, Qi Z, Li M, Yan J (2018) Removal effect of the low-low temperature electrostatic precipitator on polycyclic aromatic hydrocarbons. Chemosphere 211:44–49
Liu K, Xie WEI, Riley JT, Zhao Z-B, Pan W-P, Riley JT (2000) Investigation of polycyclic aromatic hydrocarbons in fly ash from fluidized bed combustion systems. Environ Sci Technol 34(11):2273–2279
Martorell I, Perello G, Marti-Cid R, Castell V, Llobet JM, Domingo JL (2010) Polycyclic aromatic hydrocarbons (PAH) in foods and estimated PAH intake by the population of Catalonia, Spain: temporal trend. Environ Int 36(5):424–432
Masala S, Bergvall C, Westerholm R (2012) Determination of benzo[a]pyrene and dibenzopyrenes in a Chinese coal fly ash certified reference material. Sci Total Environ 432:97–102
Mastral AM, Callen M, Mayoral C, Galban J (1995) Polycyclic aromatic hydrocarbon emissions from fluidized-bed combustion of coal. Fuel 74(12):1762–1766
Mastral AM, Callén M, Murillo R (1996) Assessment of PAH emissions as a function of coal combustion variables. Fuel 75(13):1533–1536
Mastral AM, Mastral AM, Callén MS, Callén MS (2000) A review on polycyclic aromatic hydrocarbon (PAH) emissions from energy generation. Environ Sci Technol 34(15):3051–3057
Menzie CA, Potocki BB, Santodonato J (1992) Ambient concentrations and exposure to carcinogenic PAHs in the environment. Environ Sci Technol 26(7):1278–1284
Miller EC, Miller JA (1981) Searches for ultimate chemical carcinogens and their reactions with cellular macromolecules. Cancer 47(10):2327–2345
Muñoz B, Albores A (2010 Aug) DNA damage caused by polycyclic aromatic hydrocarbons : mechanisms and markers. Intech Online, pp 124–145

Perera F, Tang D, Whyatt R, Lederman SA (2005 Mar) DNA damage from polycyclic aromatic hydrocarbons measured by benzo [a] pyrene-DNA adducts in mothers and newborns from Northern Manhattan, The World Trade Center Area, Poland and China. Cancer Epidemiol Biomarkers Prev 14

Pergal MM, Tešić ŽL, Popović AR (2013) Polycyclic aromatic hydrocarbons: Temperature driven formation and behavior during coal combustion in a coal-fired power plant. Energy Fuels 27 (10):6273–6278

Revuelta CC, de la Fuente Santiago E, Vázquez JAR (1999) Characterization of polycyclic aromatic hydrocarbons in emissions from coal-fired power plants: the influence of operation parameters. Environ Technol 20(1):61–68

Ruwei W, Jiamei Z, Jingjing L, Liu G (2013) Levels and patterns of polycyclic aromatic hydrocarbons in coal-fired power plant bottom ash and fly ash from Huainan, China. Arch Environ Contam Toxicol 65(2):193–202

Sahu SK, Bhangare RC, Ajmal PY, Sharma S, Pandit GG, Puranik VD (2009) Characterization and quantification of persistent organic pollutants in fly ash from coal fueled thermal power stations in India. Microchem J 92(1):92–96

SCF (2002) Polycyclic aromatic hydrocarbons—occurrence in foods, dietary exposure and health effects. Brussels, Belgium

Siddens LK, Larkin A, Krueger SK, Bradfield CA, Waters KM, Tilton SC, Pereira CB, Löhr CV, Volker AM, Phillips DH, Williams DE, Baird WM (2012 Nov) Polycyclic aromatic hydrocarbons as skin carcinogens: comparison of benzo[a]pyrene, dibenzo[def,p]chrysene and three environmental mixtures in the FVB/N mouse. Toxicol Appl Pharmacol 76:377–386

Stout SA, Emsbo-Mattingly SD (2008) Concentration and character of PAHs and other hydrocarbons in coals of varying rank—implications for environmental studies of soils and sediments containing particulate coal. Org Geochem 39(7):801–819

Tarafdar A, Sinha A (2017) Estimation of decrease in cancer risk by biodegradation of PAHs content from an urban traffic soil. Environ Sci Pollut Res 24(11):10373–10380

USEPA (2008) Polycyclic aromatic hydrocarbons (PAHs). Washington, DC

Van Krevelen DW (1993) Coal. 3rd Edition, Elsevier Science Publishers, Amsterdam

Verma SK, Masto RE, Gautam S, Choudhury DP, Ram LC, Maiti SK, Maity S (2015) Investigations on PAHs and trace elements in coal and its combustion residues from a power plant. Fuel 162:138–147

Wang R, Yousaf B, Sun R, Zhang H, Zhang J, Liu G (2016) Emission characterization and δ13C values of parent PAHs and nitro-PAHs in size-segregated particulate matters from coal-fired power plants. J Hazard Mater 318:487–496

Wang R, Liu G, Sun R, Yousaf B, Wang J, Liu R, Zhang H (2018) Emission characteristics for gaseous- and size-segregated particulate PAHs in coal combustion flue gas from circulating fluidized bed (CFB) boiler. Environ Pollut 238:581–589

Wheatley AD, Sadhra S (2004) Polycyclic aromatic hydrocarbons in solid residues from waste incineration. Chemosphere 55(5):743–749

Williams PT, Taylor DT (1993) Aromatization of tyre pyrolysis oil to yield polycyclic aromatic hydrocarbons. Fuel 72(11):1469–1474

Ye J-S, Yin H, Qiang J, Peng H, Qin H-M, Zhang N, He B-Y (2011) Biodegradation of anthracene by *Aspergillus fumigatus*. J Hazard Mater 185(1):174–181

Yuan S, Wei S, Chang B (2000) Biodegradation of polycyclic aromatic hydrocarbons by a mixed culture. Chemosphere 41(9):1463–1468

Zou D, Liu K, Pan WP, Riley JT, Xu Y (2003) Rapid analysis of PAHs in fly ash using thermal desorption and fast GC-TOF-MS. J Chromatogr Sci 41(5):245–250

Chapter 6
Strategies for Collection, Treatment, and Recycling of Fly Ash from Thermal Power Plants

Swatantra Pratap Singh, Amritanshu Shriwastav and Abhishek Gupta

Abstract Coal-based thermal power plants cater to a larger fraction of power generation and supply in developing countries including India. However, after electrostatic precipitation of finer ash particles from flue gases, a huge amount of fly ash is produced in these plants as a solid waste. The fly ash consists of silica, alumina, oxides of iron, calcium, magnesium, heavy metals, and organic compounds. The disposal of fly ash in conventional ash ponds and landfills may further cause soil and groundwater pollution and requires proper management. This chapter provides a detailed review about the pollutions caused by the fly ash as well as current strategies for their collection, treatment, and recycling. Different strategies of recycling and reuse are reviewed and discussed including applications for construction materials and in pollution abatement, thus acting as a useful resource rather than a waste product.

Keywords Fly ash · Thermal power plant · Heavy metals
Soil and water pollution · Recycling

S. Pratap Singh (✉) · A. Gupta
Department of Desalination and Water Treatment, Zuckerberg Institute for Water Research, Ben-Gurion University of the Negev, Sede-Boqer Campus, Beersheba 84990, Israel
e-mail: swatantr@post.bgu.ac.il

S. Pratap Singh · A. Gupta
Department of Desalination and Water Treatment, The Jacob Blaustein Institutes for Desert Research, Ben-Gurion University of the Negev, Sede-Boqer Campus, Beersheba 84990, Israel

A. Shriwastav (✉)
Centre for Environmental Science and Engineering, IIT Bombay, Mumbai 400076, India
e-mail: amritan@iitb.ac.in

R. A. Agarwal et al. (eds.), *Pollutants from Energy Sources*, Energy, Environment, and Sustainability,
https://doi.org/10.1007/978-981-13-3281-4_6

6.1 Introduction

Thermal power plants have been historically instrumental for power generation in majority of countries, including India, and still contribute significantly toward their economic growth. In India, these plants contribute toward more than 50% of the electricity generation. Also, a very significant portion of this (>80%) is achieved with coal-based thermal power plants, where the pulverized coal is burnt, and the energy generated through this combustion is finally converted to electricity (GoI 2018). In this combustion process, different inorganic minerals present in the coal (e.g., clay, shale, quartz, feldspar, etc.) melt and fuse together. Some of these fused minerals get suspended with combustion gases, and after cooling, solidify into particles (Scheme 6.1). These suspended particles in the exhaust gases are collectively called as fly ash (Ondova et al. 2012) and form a significant portion of the waste material from such power plants. For example, in India, 40% of the coal used in thermal power plants is converted to fly ash (Pandey et al. 2011).

The generated fly ash is a heterogeneous mixture of minerals with wide variation in physical and chemical properties that depend on the type of coal and production process among other factors. The size of fly ash particles varies from 10^{-8} to 10^{-4} m, with different colors, ranging from gray to black depending on the fraction of unburnt carbon present. Also, many of these minerals do not get time to recrystallize during the cooling process, and hence fly ash contains a significant portion of amorphous materials. Fe_2O_3, SiO_2, Al_2O_3, and CaO are some typical constituents in fly ash (Shehata et al. 1999).

Due to their diverse characteristics and compositions, a proper management of fly ash is challenging. Further, due to the presence of trace elements, heavy metals (Chaudhary and Banerjee 2007), and toxic organic compounds (Ribeiro et al. 2014), a direct disposal of this fly ash into different environmental matrices, viz. water, air, and land, in an unscientific manner, creates numerous environmental issues. Following sections discuss various environmental concerns with disposal of fly ash and the means for proper collection and treatment. Further, various applications toward sustainable management of fly ash are also discussed.

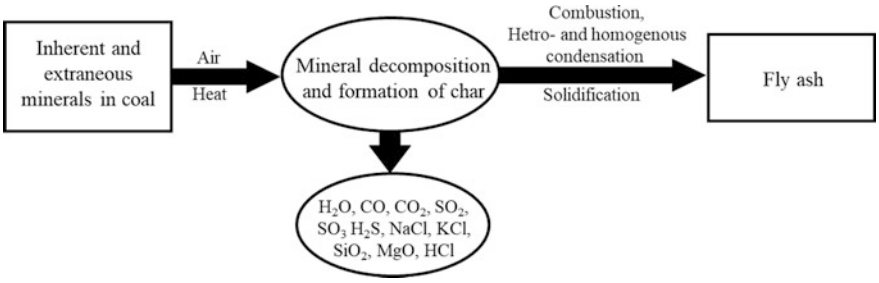

Scheme 6.1 Schematic of the coal fly ash formation mechanism from pulverized fuel combustion

6.2 Fly Ash as an Environmental Pollutant

In addition to various pollutant gases, viz. SO_x and NO_x, fly ash forms a major part of the exhaust gases from coal-based thermal power plants and if not managed properly may result in significant environmental pollution (He et al. 2012). This is due to the presence of various heavy metals, e.g., As, Ba, Cr, Se, Hg, etc., and adsorbed or deposited organic compounds (e.g., PAHs) on particle surfaces (Chaudhary and Banerjee 2007; Ribeiro et al. 2014).

Inhalation is the most direct and important route of exposure to fly ash in humans since a significant portion of particulate matter ($PM_{2.5}$ and PM_{10}) in the atmosphere is contributed from coal fly ash (Kim et al. 2015). Further, such particulate matters have well-recognized health hazards including respiratory and cardiovascular diseases as well as premature mortality (Kim et al. 2015; Davidson et al. 2005). Coal fly ash, in particular, poses a significant health risk due to the very heterogeneous composition and presence of multiple heavy metals and toxic compounds. Sufficient data is now available which links the health risks to the communities living in the vicinity of coal thermal power plants to the inhalation exposure to the coal fly ash being emitted into the atmosphere.

The emitted fly ash further contaminates the receiving land and water bodies. For example, a significant accumulation of heavy metals, viz. As, Cd, Cr, Ba, Hg, etc., in the soil was directly linked to the fly ash deposition from coal power plant in Santaldih, West Bengal, India (George et al. 2015). Once enriched in the soil, multiple exposure pathways (viz. ingestion, inhalation, dermal contact, and consumption of contaminated vegetation, etc.) exist. In addition, the enrichment of these toxic elements in topsoil further deteriorates the soil quality. Leaching and runoff with rainwater is also a serious concern, and can potentially contaminate the surface and groundwater depending on the site geology and prevalent redox conditions (Spadoni et al. 2014).

6.3 Collection and Disposal of Fly Ash

A proper collection and disposal system of fly ash is important to effectively address the associated environmental concerns. The collection of fly ash from flue gases is normally done using electrostatic precipitators (ESP) and fabric filters (baghouses) (Al-Hamouz 2014). ESPs are installed near the chimney, where fly ash particles are charged at high voltage and then collected through electrostatic attraction at oppositely charged electrodes. The separated particles are then scraped from the electrode and collected in hoppers at the bottom (Scheme 6.2).

The collected fly ash is then transported to disposal sites either in a wet slurry or dry form. A high concentration slurry disposal (HCSD) system is generally adopted (Chandel et al. 2009) in which collected fly ash is fed to the mixing tank after conditioning. A uniform slurry of this conditioned ash is made by adding required

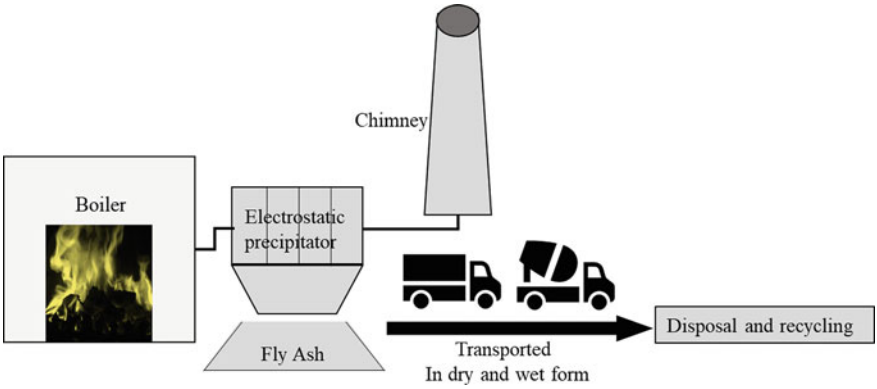

Scheme 6.2 Scheme of fly ash production in a conventional thermoelectric power plant

amount of water to achieve the desired characteristics. Ash concentration is maintained at 60% or above (w/w) in this high concentration slurry. Afterward, the uniform slurry is transferred through high concentration slurry disposal (HCSD) pump up to the ash dyke through seamless pipelines, where it is disposed on a slope. The disposed slurry spreads over a substantial area and solidifies.

A recent trend in power plants is to collect the fly ash in dry form and utilize it in various applications as raw material. Dry fly ash from ESPs and baghouses is collected in ash vessels. A free flow of dry ash in ash vessels is maintained using electric heaters. The heaters maintain the temperature well above the ash fusion temperature to prevent the formation of clusters of ash and ensure smooth functioning of the conveying system. The ash is further transported to fly ash silos with the help of compressed air. The moisture from the compressed air is removed using an adsorbent air dryer or refrigeration air dryer. Finally, the ash is transported into sealed vessel trucks.

6.4 Treatment

The combustion of coal during the power generation results in the heavy metal and organic micropollutants release with fly ash. This fly ash should go through treatment before landfilling or recycling (Eleonora and Margarida 2016). Some of the treatment methods are discussed below in detail.

6.4.1 Washing Process

Washing with water leads to removal of soluble salts. Further, the resulted solution could be evaporated to produce salt (Francois and Criado 2007; Chimenos et al. 2005; Nzihou and Sharrock 2002). The washing with water released heavy metals (e.g., Pb and Zn) along with the soluble salts. Wang et al. have shown the release of ~1% of Pb and other heavy metals with water, whereas another study by Weibel et al. have shown enhanced metal removal with acid water (Wang et al. 2009; Weibel et al. 2018). The metals in the fly ash also could be immobilized by chemical additives, such as soluble phosphates, which react with metals and form insoluble metal complexes (Uchida et al. 1996).

6.4.2 Leaching

Leaching process could be used to extract the metal ions from fly ash. Addition of chemical agents promotes faster leaching of heavy metals from the fly ash. Sabbas et al. presented the effect of pH on leaching (Sabbas et al. 2003) and showed that pH is strongly affecting the leaching process. Three main leaching behaviors have been shown in the literature: (1) cation-forming species and non-amphoteric metal ions (e.g., Cd); (2) amphoteric metals (including Al, Pb, and Zn) increase solubility under both strong acidic and strong alkaline conditions; and (3) oxyanion-forming metals (e.g., As, Cr, Mo, V, B, and Sb) decrease solubility in alkaline ranges (pH > 10) (Sabbas et al. 2003; Van der Bruggen and Vandecasteele 2003).

6.4.3 Electrochemical Processes

The main advantage of electrochemical processes is no requirement of additional chemicals. Temperature, current density, mixing conditions, the distance between the electrodes, and the pH of the solution were identified as main parameters which affect the electrochemical treatment process. Pedersen et al. showed an electrochemical treatment process named as electrodialytic remediation, which could be effectively used for the remediation of heavy metals and chlorides from fly ashes. It has been introduced as a new possible extraction method (Pedersen et al. 2005, 2003).

6.4.4 Thermal Treatment

This technique could be used for eliminating heavy metals through evaporation processes where the temperature was raised (less than melting point). This technique also allows recycling of the metals at the same time of evaporation. Jakob et al. examined the evaporation of heavy metals at 1000–1100 °C temperature. The Pb, Cd, and Cu have shown ~98% evaporation efficiencies, and the evaporated amounts and evaporation rates were strongly influenced by chlorides (Jakob et al. 1995). Stucki and Jakob showed that under reduced condition addition of chlorine gas can evaporate ~99% of the metals present in fly ash (evaporated as metal chlorides), and they can be collected separately as heavy metal condensates (Jakob et al. 1996).

6.4.5 Solidification

Solidification treatments are among the most widespread processes used for waste incineration remainders (Tang et al. 2016; Diaz-Loya et al. 2012). The principal purpose of solidification is to immobilize hazardous components in the fly ash. The binder materials (e.g., Portland cement) used for solidification not only hardens the hazardous waste by chemical means but also immobilize it by making stable complexes. These complexes are solids and either non-hazardous or less hazardous than the original waste by encapsulating the pollutants which leads to low permeability.

6.4.6 Chemical Stabilization

Chemical stabilization involves chemical precipitation of heavy metals into insoluble composites or heavy metal complex with various mineral species or chemical agents. The main chemical agents used for stabilization include sulfides (Katsuura et al. 1996), soluble phosphates (Nzihou and Sharrock 2002; Derie 1996; Eighmy et al. 1997), ferrous iron sulfate (Lundtorp et al. 2002), and carbonates (Ecke et al. 2003). Chemical stabilization leads to the substantial decrease in trace metal elements (Sabbas et al. 2003; Bayuseno and Schmahl 2011; Cornelis et al. 2008).

6.5 Recycling of Fly Ash: Applications

Fly ash collected from different parts of power plants has different properties and could be used for various applications, which are discussed below in detail.

ESP ash/chimney ash/dry fly ash: It is best suited for manufacturing of cement and other construction materials. In cement, fly ash could be used as cementitious materials (Lee et al. 1999). The other construction materials can also be made, e.g., fly ash bricks (without clay), blocks, pavers, sheets for roofing, tiles, etc (Mandal and Mandal 1996; Shanthakumar et al. 2008).
Bottom ash: Due to the coarse size of bottom ash, it is suitable for geotechnical applications, e.g., landfilling, construction of barriers, road and flyover bridges, etc (Chang and Wey 2006). Bottom ash could be also used as a substitute for the sand in mortar and concrete after the removal of organic carbon (Chindaprasirt et al. 2009).
Pond ash: Pond ash has a medium grain size, which is mainly the mixture of ESP and bottom ash. Agriculture, wasteland development, and forestry are the best suited for pond ash applications, and it can also be used for geotechnical applications. Protocols have been established to construct bricks with pond ash and clay mixture. Another important utilization of pond ash is in the manufacturing of clay bricks. It has been shown that 30–80% of clay can be mixed with pond ash and will result to improve quality, which reduces the breakage during transportation. This ash is also suitable for ceramic products (Chang and Wey 2006; Ghosh 2009; Kumar Bera et al. 2007). Fly ash could be effectively used as construction materials as discussed below.

6.5.1 Constructive Materials

Fly ash has been highly used as a supplementary cementitious material (SCM) in the construction of Portland cement. Fly ash use as a SCM in concrete has been started in last century (Thomas 2007; Newman 1979), especially after the pioneering research conducted by Davis et al. at the University of California, Berkeley in 1937 (Dreher et al. 1997; Chindaprasirt et al. 2008; Thomas et al. 2002). In the last 50 years, fly ash use in concrete grows dramatically. In 2005, ~15 million tons of fly ash was used in concrete, concrete products, and grouts in the USA alone (Edil et al. 2006). There are many drawbacks such as slower strength gain, higher salt scaling, and benefits such as high strength gain, reduced heat of hydration, and denser concrete with smooth surfaces for fly ash as construction materials.

At present, more than 50% of the concrete has fly ash in the USA. The dosages varied with the quality of the fly ash (15–40%) in the concrete. There are mainly two types of fly ashes used in the concrete which are Class C and Class F fly ash. Both types of fly ashes react with concrete in similar ways except that of Class C that has enough lime to undergo self-cementing. The chemical composition of Class C, Class F, and Portland cement chemical is shown in Table 6.1.

Lightweight construction products from fly ash have many advantages such as low costs of shipping as compared to the non-light weight product. The reduced

Table 6.1 A brief description of the chemical composition of fly ash and Portland cement (American Coal Ash Association 2003)

Compounds	Fly ash Class F	Fly ash Class C	Portland cement
SiO_2	55	40	23
Al_2O_3	26	17	4
Fe_2O_3	7	6	2
CaO (Lime)	9	24	64
MgO	2	5	2
SO_3	1	3	2

cost is visible for bricks as fly ash bricks weigh one-third of the conventional clay-fired bricks (Sharma and Dhir 2015) leading to reduced shipping costs (Rajgor et al. 2013). The fly ash bricks may appear expensive than conventional products but the final financial benefit should be evaluated in terms of its increased physical properties, chemical properties, and environmental benefits. Bricks from fly ash and clay mixture are more porous than fly ash bricks, and results in high strength than fly ash bricks. Fly ash brick manufacturing units could be set up near thermal power stations to make it cost-effective. These manufacturing units can get free fly ash from the power plants. Nowadays, there is good demand for fly ash bricks. The awareness among the people is required for better results along with government support. This technology is eco-friendly as it reduces solid waste and dust in the environment as well as the cost is quite comparable to conventional bricks. Fly ash could be also used for the construction of roads. The fly ash could be used in the earthen core which prevents the heavy metal leaching as fly ash reacts with cement and reduces any leaching effect. Hence, chances of pollution due to the use of fly ash in roads are negligible.

6.6 Pollution Abatements by Fly Ash

Fly ash could be used as an effective absorbent for the abatement of pollutants, e.g., SO_x, NO_x, metals, and other pollutants.

6.6.1 Adsorbents for Flue Gas

Generally, SO_x emission is controlled by installing wet-type limestone scrubbers and as a result of it, high desulfurization efficiency and easy operation can be achieved. But this process has high water consumption resulting in wastewater generation which needs further treatment, whereas dry-type flue gas desulphurization (FGD) has advantages as no wastewater is generated in this process but it

requires large amount of adsorbent. Fly ash could be effectively used for dry-type FGD as it is available in large amount. Similar to SO_x, NO_x could be effectively removed using fly ash. NO_x adsorption into fly ash depends on the carbon content and specific surface area. The unburnt carbon in the fly ash contributes maximum in the specific surface area, which could be further activated through gasification for the higher adsorption. For better activation of fly ashes, minerals should be removed before the activation of fly ashes to avoid interference.

6.6.2 *Adsorption of Various Types of Heavy Metals and Fluorides on Fly Ash*

Researchers have shown the potential of fly ash for heavy metal removal (Bhattacharya et al. 2008; Gupta et al. 1998, 2011; Yadava et al. 1987). The most studied metals are Hg, Cr, Ni, Pb, As, Cu, and Cd. Enhanced mercury adsorption was reported after oxidizing the unburnt carbon in the fly ash at 400 °C (Li and Maroto-Valer 2012). This confirmed the important role of oxygen-containing functional groups in the adsorption process. In another study, Masaki et al., have shown the effect of calcium chloride and activated carbon concentration with synthetic fly ash on the adsorption of mercury, and best result was obtained for 5–7% in synthetic fly ash with 1% calcium chloride (Takaoka et al. 2000). There are many studies for removal of Cr(VI) and Cr(III) using fly ash as adsorbent and established the effect of fly ash dosages, contact time, and pH on the removal of chromium (Bhattacharya et al. 2008; Gupta et al. 1998; Gupta et al. 2011). Pandey et al., have used fly ash and wollastonite (1:1) mixture for the removal of chromium (Panday et al. 1984). Bayat et al., have shown higher adsorption capacity for Cd(II) as compared to Cr(VI) in a mixture with fly ash and crystalline CaO in fly ash significantly affect the adsorption of Cr(VI) and Cd(II) (Bayat 2002). Chromium and nickel were effectively removed by low-cost adsorbent made from raw bagasse and fly ash (Rao et al. 2002). The metal adsorption by fly ash was strongly dependent on the experimental system, and physical and chemical characteristics of the adsorbent and adsorbate (Babel and Kurniawan 2003).

Several studies have been reported for the removal of fluoride from waters using fly ash (Chaturvedi et al. 1990; Nemade et al. 2002). Chaturvedi et al. showed the effect of different concentrations, contact times, temperatures, and pH of the solution on the removal of fluoride from contaminated water (Chaturvedi et al. 1990; Nemade et al. 2002). A column study has shown complete removal of fluoride in 120 h for low concentration of fluoride and in 168 h with the high concentration of fluoride (Nemade et al. 2002; Tor et al. 2009).

6.7 Summary and Future Prospects

This chapter reviewed various strategies for collection, treatment, and recycling of fly ash from coal-based thermal power plants. The requirement of proper ash management system is also identified to address the related environmental concerns with ash disposal. Certain applications where fly ash is utilized as a resource are also discussed. Fly ash has shown potential to be used as construction material as well as an adsorbent for pollution abatement. However, majority of the studies are conducted at lab scale and limited information is available for their large-scale application.

Based on the review of the literature, the following future research directions are identified:

- Industrial scale applications of fly ash for pollution abatement have been not established till date, so there is an urgent need to scale up the fly ash application. In general, fly ash has low adsorption capacity and need modification to enhance the adsorption capacity and mass production should reduce the cost effectively.
- Similarly, for construction purposes, there is a need for well-established protocols for effective use of different types of fly ashes.
- There are many other products where fly ash could be used as initial raw materials such as geopolymers, mullite, and quartz–cristobalite–tridymite. Such novel applications at large scale need to be further investigated for proper utilization of fly ash.
- Full-scale application of fly ash to enrich agriculture soil is needed.
- Life cycle assessment and environmental impact assessment are required for different fly ash products to assess long-term benefits and disadvantages.

References

Al-Hamouz Z (2014) Numerical and experimental evaluation of fly ash collection efficiency in electrostatic precipitators. Energy Convers Manag 79:487–497

American Coal Ash Association (2003) Fly ash facts for highway engineers, 1–74

Babel S, Kurniawan TA (2003) Low-cost adsorbents for heavy metals uptake from contaminated water: a review. J Hazard Mater 97(1–3):219–243

Bayat B (2002) Comparative study of adsorption properties of Turkish fly ashes: II. The case of chromium (VI) and cadmium (II). J Hazard Mater 95(3):275–290

Bayuseno AP, Schmahl WW (2011) Characterization of MSWI fly ash through mineralogy and water extraction. Resour Conserv Recycl 55(5):524–534

Bhattacharya A, Naiya T, Mandal S, Das S (2008) Adsorption, kinetics and equilibrium studies on removal of Cr (VI) from aqueous solutions using different low-cost adsorbents. Chem Eng J 137(3):529–541

Chandel S, Seshadri V, Singh SN (2009) Effect of additive on pressure drop and rheological characteristics of fly ash slurry at high concentration. Part Sci Technol 27:271–284

Chang F-Y, Wey M-Y (2006) Comparison of the characteristics of bottom and fly ashes generated from various incineration processes. J Hazard Mater 138(3):594–603

Chaturvedi A, Yadava K, Pathak K, Singh V (1990) Defluoridation of water by adsorption on fly ash. Water Air Soil Pollut 49(1–2):51–61

Chaudhary S, Banerjee DK (2007) Speciation of some heavy metals in coal fly ash. Chem Speciat Bioavailab 19(3):95–102

Chimenos J, Fernández A, Cervantes A, Miralles L, Fernández M, Espiell F (2005) Optimizing the APC residue washing process to minimize the release of chloride and heavy metals. Waste Manag 25(7):686–693

Chindaprasirt P, Rukzon S, Sirivivatnanon V (2008) Resistance to chloride penetration of blended Portland cement mortar containing palm oil fuel ash, rice husk ash and fly ash. Constr Build Mater 22(5):932–938

Chindaprasirt P, Jaturapitakkul C, Chalee W, Rattanasak U (2009) Comparative study on the characteristics of fly ash and bottom ash geopolymers. Waste Manag 29(2):539–543

Cornelis G, Johnson CA, Van Gerven T, Vandecasteele C (2008) Leaching mechanisms of oxyanionic metalloid and metal species in alkaline solid wastes: a review. Appl Geochem 23 (5):955–976

Davidson CI, Phalen RF, Solomon PA (2005) Airborne particulate matter and human health: a review. Aerosol Sci Technol 39(8):737–749

Derie R (1996) A new way to stabilize fly ash from municipal incinerators. Waste Manag 16 (8):711–716

Diaz-Loya EI, Allouche EN, Eklund S, Joshi AR, Kupwade-Patil K (2012) Toxicity mitigation and solidification of municipal solid waste incinerator fly ash using alkaline activated coal ash. Waste Manag 32(8):1521–1527

Dreher KL, Jaskot RH, Lehmann JR, Richards JH, Ghio JKMAJ, Costa DL (1997) Soluble transition metals mediate residual oil fly ash induced acute lung injury. J Toxicol Environ Health Part A 50(3):285–305

Ecke H, Menad N, Lagerkvist A (2003) Carbonation of municipal solid waste incineration fly ash and the impact on metal mobility. J Environ Eng 129(5):435–440

Edil TB, Acosta HA, Benson CH (2006) Stabilizing soft fine-grained soils with fly ash. J Mater Civ Eng 18(2):283–294

Eighmy TT, Crannell BS, Butler LG, Cartledge FK, Emery EF, Oblas D, Krzanowski JE, Eusden JD, Shaw EL, Francis CA (1997) Heavy metal stabilization in municipal solid waste combustion dry scrubber residue using soluble phosphate. Environ Sci Technol 31(11): 3330–3338

Eleonora L, Margarida J (2016) Chemical stabilization of municipal solid waste incineration fly ash without any commercial chemicals: first pilot-plant scaling up. ACS Sustain Chem

Francois D, Criado C (2007) Monitoring of leachate at a test road using treated fly ash from municipal solid waste incinerator. J Hazard Mater 139(3):543–549

George J, Masto RE, Ram LC, Das TB, Rout TK, Mohan M (2015) Human exposure risks for metals in soil near a coal-fired power-generating plant. Arch Environ Contam Toxicol 68 (3):451–461

Ghosh A (2009) Compaction characteristics and bearing ratio of pond ash stabilized with lime and phosphogypsum. J Mater Civ Eng 22(4):343–351

GoI (2018) Annual report 2017–18, pp 1–276. Ministry of Power, Government of India

Gupta VK, Mohan D, Sharma S, Park KT (1998) Removal of chromium (VI) from electroplating industry wastewater using bagasse fly ash—a sugar industry waste material. Environmentalist 19(2):129–136

Gupta V, Agarwal S, Saleh TA (2011) Chromium removal by combining the magnetic properties of iron oxide with adsorption properties of carbon nanotubes. Water Res 45(6):2207–2212

He Y, Luo Q, Hu H (2012) Situation analysis and countermeasures of China's fly ash pollution prevention and control. Procedia Environ Sci 16:690–696

Jakob A, Stucki S, Kuhn P (1995) Evaporation of heavy metals during the heat treatment of municipal solid waste incinerator fly ash. Environ Sci Technol 29(9):2429–2436
Jakob A, Stucki S, Struis RPWJ (1996) Complete heavy metal removal from fly ash by heat treatment: influence of chlorides on evaporation rates. Environ Sci Technol 30(11):3275–3283
Katsuura H, Inoue T, Hiraoka M, Sakai S (1996) Full-scale plant study on fly ash treatment by the acid extraction process. Waste Manag 16(5–6):491–499
Kim K-H, Kabir E, Kabir S (2015) A review on the human health impact of airborne particulate matter. Environ Int 74:136–143
Kumar Bera A, Ghosh A, Ghosh A (2007) Compaction characteristics of pond ash. J Mater Civ Eng 19(4):349–357
Lee SH, Sakai E, Daimon M, Bang WK (1999) Characterization of fly ash directly collected from electrostatic precipitator. Cem Concr Res 29(11):1791–1797
Li J, Maroto-Valer MM (2012) Computational and experimental studies of mercury adsorption on unburned carbon present in fly ash. Carbon 50(5):1913–1924
Lundtorp K, Jensen DL, Christensen TH (2002) Stabilization of APC residues from waste incineration with ferrous sulfate on a semi-industrial scale. J Air Waste Manag Assoc 52 (6):722–731
Mandal PK, Mandal TK (1996) Electrostatic precipitator performance in Indian pulverized coal based thermal power stations: problems and solutions. Water Energy Res Dig 19(4):31–40
Nemade P, Rao AV, Alappat B (2002) Removal of fluorides from water using low cost adsorbents. Water Sci Technol Water Supply 2(1):311–317
Newman JR (1979) Effects of industrial air pollution on wildlife. Biol Cons 15(3):181–190
Nzihou A, Sharrock P (2002) Calcium phosphate stabilization of fly ash with chloride extraction. Waste Manag 22(2):235–239
Ondova M, Stevulova N, Estokova A (2012) The study of the properties of fly ash based concrete composites with various chemical admixtures. Procedia Eng 42:1863–1872
Panday K, Prasad G, Singh V (1984) Removal of Cr (V1) from aqueous solutions by adsorption on fly ash-wollastonite. J Chem Technol Biotechnol 34(7):367–374
Pandey VC, Singh JS, Singh RP, Singh N, Yunus M (2011) Arsenic hazards in coal fly ash and its fate in Indian scenario. Resour Conserv Recycl 55(9):819–835
Pedersen AJ, Ottosen LM, Villumsen A (2003) Electrodialytic removal of heavy metals from different fly ashes: influence of heavy metal speciation in the ashes. J Hazard Mater 100 (1–3):65–78
Pedersen AJ, Kristensen IV, Ottosen LM, Ribeiro AB, Villumsen A (2005) Electrodialytic remediation of CCA-treated waste wood in pilot scale. Eng Geol 77(3–4):331–338
Rajgor MB, Makwana AH, Pitroda J (2013) Automation in clay and thermal industry waste products. Int J Eng Trends Technol 4(7):2870–2877
Rao M, Parwate A, Bhole A (2002) Removal of Cr^{6+} and Ni^{2+} from aqueous solution using bagasse and fly ash. Waste Manag 22(7):821–830
Ribeiro J, Silva TF, Mendonça Filho JG, Flores D (2014) Fly ash from coal combustion—an environmental source of organic compounds. Appl Geochem 44:103–110
Sabbas T, Polettini A, Pomi R, Astrup T, Hjelmar O, Mostbauer P, Cappai G, Magel G, Salhofer S, Speiser C (2003) Management of municipal solid waste incineration residues. Waste Manag 23(1):61–88
Shanthakumar S, Singh D, Phadke R (2008) Influence of flue gas conditioning on fly ash characteristics. Fuel 87(15–16):3216–3222
Sharma S, Dhir AG (2015) Assessment of the use of steel slag and/or air pollution control devices dust in the manufacturing of fly ash bricks/blocks
Shehata MH, Thomas MDA, Bleszynski RF (1999) The effects of fly ash composition on the chemistry of pore solution in hydrated cement pastes. Cem Concr Res 29(12):1915–1920
Spadoni M, Voltaggio M, Sacchi E, Sanam R, Pujari PR, Padmakar C, Labhasetwar PK, Wate SR (2014) Impact of the disposal and re-use of fly ash on water quality: the case of the Koradi and Khaperkheda thermal power plants (Maharashtra, India). Sci Total Environ 479–480:159–170

Takaoka M, Takeda N, Fujiwara T (2000) Experimental studies on the removal mechanism of mercury vapor by synthetic fly ash. J Jpn Soc Atmos Environ (Taiki Kankyo Gakkaishi) 35 (1):51–62

Tang Q, Liu Y, Gu F, Zhou T (2016) Solidification/stabilization of fly ash from a municipal solid waste incineration facility using Portland cement. Adv Mater Sci Eng

Thomas M (2007) Optimizing the use of fly ash in concrete, vol 5420. Portland Cement Association Skokie, IL

Thomas M, Hopkins D, Girn G, Munro R, Muhl E (2002) The use of high-volume fly ash in concrete. In: Proceedings, 7th international gypsum and fly ash science and technology conference, Toronto

Tor A, Danaoglu N, Arslan G, Cengeloglu Y (2009) Removal of fluoride from water by using granular red mud: batch and column studies. J Hazard Mater 164(1):271–278

Uchida T, Itoh I, Harada K (1996) Immobilization of heavy metals contained in incinerator fly ash by application of soluble phosphate—treatment and disposal cost reduction by combined use of "High Specific Surface Area Lime". Waste Manag 16(5–6):475–481

Van der Bruggen B, Vandecasteele C (2003) Removal of pollutants from surface water and groundwater by nanofiltration: overview of possible applications in the drinking water industry. Environ Pollut 122(3):435–445

Wang Q, Yang J, Wang Q, Wu T (2009) Effects of water-washing pretreatment on bioleaching of heavy metals from municipal solid waste incinerator fly ash. J Hazard Mater 162(2–3):812–818

Weibel G, Eggenberger U, Kulik DA, Hummel W, Schlumberger S, Klink W, Fisch M, Mäder UK (2018) Extraction of heavy metals from MSWI fly ash using hydrochloric acid and sodium chloride solution. Waste Manag

Yadava K, Tyagi B, Panday K, Singh V (1987) Fly ash for the treatment of Cd (II) rich effluents. Environ Technol 8(1–12):225–234

Chapter 7
Commercial Coal Mining in India Opened for Private Sector: A Boon or Inutile

Manish Yadav, Nitin Kumar Singh and Sneha Gautam

Abstract At present, private sector firms in India are only allowed to mine coal for its own use (captive mining) in cement, steel, power, and aluminum plants, etc. Coal India Ltd. (CIL) is the sole commercial miner in India with 80% market share and the world's largest coal producer by production. In a major "reform" in the coal sector since its nationalization in 1973, the government on February 20th, 2018 allowed private companies to mine the fossil fuel for commercial use, ending the monopoly of state-owned CIL. With this latest development, decision-makers expect private players to bring in competition along with private investment, technology adoption, and international best practices. However, with this decision, still there may be some key questions associated with proposed mining approach such as, is land acquisition being easy for private players, whether private players will do rehabilitation and resettlement as per government norms, will the firms be sensitive toward the environmental degradation caused by mining, was this decision needed because CIL was not able to cater current demand of coal. Therefore, in this chapter, the impact of private mining is discussed and presented along with its economic, environmental, and social viability.

Keywords Captive coal block · Commercial coal mining · Coal India Limited

M. Yadav
Environment Department, Central Mine Planning and Design Institute Limited, Bhubaneswar, India

N. K. Singh (✉) · S. Gautam
Department of Environmental Science and Engineering, Marwadi University, Rajkot 360003, Gujarat, India
e-mail: nitinkumar.singh@marwadieducation.edu.in

R. A. Agarwal et al. (eds.), *Pollutants from Energy Sources*,
Energy, Environment, and Sustainability,
https://doi.org/10.1007/978-981-13-3281-4_7

7.1 Introduction

7.1.1 History

India was involved in commercial coal mining since 1774 by M/s John Sumner and Suetonius Grant Heatly of East India Company. The first coalfield was Raniganj coalfield in the bank of river Damodar. The production growth was very static in those days. The introduction of steam engines in 1853 gave a drastic boom to the demand of coal. The average production raised to 1 Mty (million tons per year) and by the end of 1900, India started producing 6.12 Mty. The pace of coal production again boosted during the first world war but again got dull in the 1930s. Before the independence of the country, the production level reached to 30 Mty. Till 1980, the coal production was around 100 Mty, which was drastically doubled by 1990 and crossed 200 Mty, and by the end of 2010, the production of coal reached around the 550 Mty.

After independence, during the introduction of first five-year development program, the leader and planners felt the need of increasing the coal production efficiently by the introduction of new technology. The Government of India now decided to form National Coal Development Corporation (NCDC), a government of India undertaking in 1956. Another coal company Singareni Collieries Company Limited (SCCL), which was already operating since 1945 was given control to the Government of Andhra Pradesh (Coal India Limited 2018; Lahiri-Dutt 2016).

7.1.2 Nationalizations of Coal Mines

The unscientific mining practices and substandard living condition of labors involved in coal mining industry becomes the matter of concern for the government of India. Taking all these matters into account, the government of India decided to take a revolutionary step to nationalize the private coal sectors.

As per the government's national energy policy, the nationalization of coal mine took place in two stages in the 1970s. In the first stage, The Coking Coal Mines (Emergency Provisions) act 1971 was formed by Government of India (GoI) on October 16, 1971, which states that the captive mines of IISCO (The Indian Iron & Steel Company), TISCO (Tata Iron and Steel Company Limited), and DVC (Damodar Valley Corporation), the GoI took over the management of all 226 coking coal mines and nationalized them on May 1, 1972. The company under central government was formed that is known as Bharat Coking Coal Limited. In second the stage, the Government of India announced the Coal Mines (Taking over of Management) Ordinance 1973 on January 31, 1973, which empowers the central government to take control over all 711 noncoking coal mines. In the next phase of nationalization, these mines were nationalized with effect from May 1, 1973 and a public sector company named Coal Mines Authority Limited (CMAL) was formed

to manage these noncoking mines (Coal India Limited 2018; Singh and Kalirajan 2003). A formal holding company in the form of Coal India Limited (CIL) was formed in November 1975 to manage both the companies.

Now, again the union cabinet of India on February 20, 2018 decided to open up the coal sector to commercial mining by private entities. It is a revolutionary move that puts an end to its own Coal India Limited (CIL) monopoly and removing one of the last vestiges of the licence-quota raj of the 1970s.

7.1.3 Existing Scenario for Private Companies

In the present scenario, the government has a monopoly over the coal production that accounts for more than 90% through state-owned mines. In 1993, the policy of captive mining was introduced. The introduction of this policy opened the door for the private investment in the coal sector. Though the performance of captive block was not promising as the production from all these captive blocks were 32.54 Mt in 2016–17. So far, the private companies are allowed to do coal mining for their captive use. Captive coal mining means that the coal mined could be used only in the said industry for which the allocation/auction of the block has been done. It cannot be used for any other purposes. Any surplus coal would have to be sold to Coal India at the notified price. A captive coal block is not allowed to sell its produce in the open market and all of that must go to the end-use industry for which it is approved.

7.2 The Proposed Policy

Under this new reform, the coal blocks will be allocated on the basis of price per ton of coal offered to the state government and there shall be no restriction on the sale and/or utilization of coal from the coal mine to power plants, steel mills, and other users (Goyal 2018). The move is also seen as lowering prices and imports while introducing better technology, apart from saving on foreign exchange and improving energy security. The policy is expected to usher in competition in coal supply, reduce coal imports, and help stressed power plants to attempt a turnaround through better fuel management. The move will also increase supply in the market and help achieve the target of producing a billion ton of coal by 2022. However, it is still unsure about the pros and cons of this policy. In this chapter, benefits and drawback are presented of coal sector privatization in terms of short term and long-term impacts (Yilmaz 2015).

7.2.1 Need and Impact of New Policy

7.2.1.1 Need for Privatization

The rising demand in the power sector resulted in an increase in coal-based power capacity, in the draft national energy policy by the NITI Ayog (think tank of India) stated that coal-based power generation capacity of 125 GW in 2012 is likely to go up to more than 330–441 GW by 2040 (192 GW in FY 2017). This huge demand in near future requires sustainable exploitation of our available resources. As per the assessment of NITI Ayog the production level requires to be more than 1.3 billion tons per year (Draft Energy Policy 2017).

The shortage in coal supply can lead to the pressure on import of coal. Imported coal is generally more expensive than the locally mined coal and as the Coal India cannot meet the expected demand, and imports are expected to rise. The linkages are pending to the power sector by 600 GW for which more than one-billion-ton production is required. This is about three times India's current installed coal-based power capacity. Now, the question arises that how will India meet the target of huge coal demand. This gives rise to the need for privatization in the coal sector to cater to the need of power in coming future (Modak et al. 2017).

7.2.1.2 Impact of Privatization

In the current scenario, if we see then that huge gap between demand and supply can be met through the import of coal only. The government also has not formed any policy regarding the import of coal. The stakeholders mainly related to power sectors and their financers also never make their business plan based on the import of coal. They always believed on the huge availability of domestic coal which was never promised.

As discussed above, the cost of imported coal is much higher compared to domestic coal. The reason for this, in India 90% coal is extracted from surface mining (open cast mining) and world's average production through surface mining is 40%. China is doing their 90% coal production through underground mining. The cost of surface mining is one-fourth of underground mining. But due to surface mining, the heavy environmental degradation takes place and most of the coal blocks that are given to private players are open cast projects.

The government's intensions behind this policy is that the private players will bring the competition and price will lower down. However, this does not imply that state-owned Coal India limited is not capable of meeting the expectation of government. It is also important to look that on what stake private players are reducing the price. They will make a profit by giving lower wages to labors as mining is a labor-intensive sector and a lot of miners are involved in the production of coal. In the state-owned company, average wages are more than 40,000 per month, on a other hand, private players give them 10,000–12,000 per month. That comes from strong representation from the union side. With such heavy labor-oriented industry, their wages cost around 50% of the coal in pit head.

7.2.1.3 Where Coal India Is Lagging

The biggest hurdle for the state-owned Coal India to meet the given target is environmental and forestry clearances. Out of all total mines, around 66 projects are short of environmental clearances and 132 projects are short of forestry clearance from the state. Apart from environmental and forestry clearances, the second biggest reason is an investment in R&D sector. The company is not investing much in the R&D sector for the implementation of new technology. The biggest reserve of cash is taken up by the government in form of a dividend. Inspite of these dividends, if government push to Coal India to invest in R&D for better technology and sustainable growth then much of the environmental issues will be sorted out by giving a scientific solution.

7.2.2 SWOT (Strength Weakness Opportunity Threat) Analysis

The SWOT analysis of coal would help visualize the relative strength and weakness of the scenario of commercial coal mine sector along with the opportunities and challenges that lie ahead. Based on the analysis of exogenous and endogenous forces, following SWOT has been derived which is shown in Fig. 7.1. Strengths and weaknesses are endogenous whereas threats and opportunities are exogenous in nature.

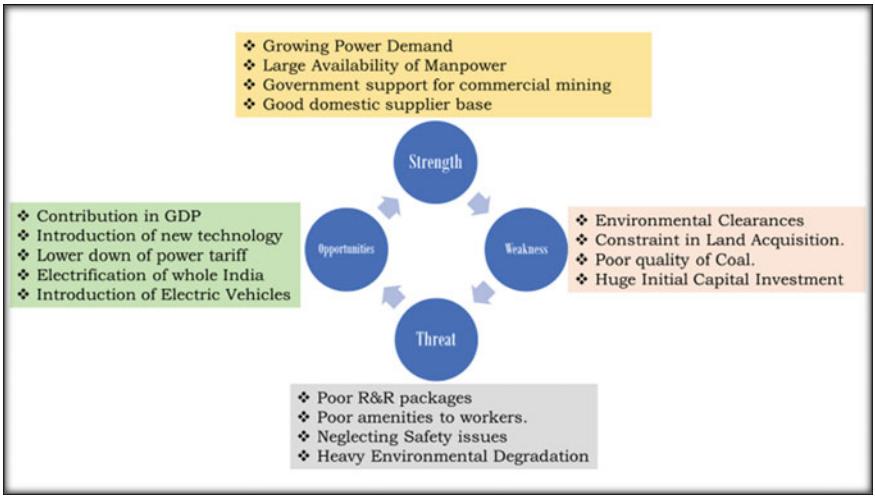

Fig. 7.1 SWOT analysis of commercial mining in India

7.2.3 Advantages Proposed and/or Suggested Benefits of the Policy

- To bring efficiency into the coal sector by moving from an era of monopoly to competition.
- To increase the energy security of the country as 70% of the country's electricity is generated from thermal power plants.
- To ensure assured coal supply, accountable allocation of coal, and affordable coal as well as power prices for consumers.
- To give the highest priority to transparency, ease of doing business, and ensure that natural resources are used for national development.
- To allow the use of the best possible technology in the sector, drive investments, and create direct and indirect employment in coal-bearing areas.
- To collect revenue from private commercial mining to help to the coal-bearing States, this approach shall incentivize them with increased revenues which can be utilized for the growth and development of backward areas and their inhabitants including tribals, especially in the eastern parts of the country.
- Opening up the sector will also lead to energy security through assured coal supply, accountable allocation, and affordability.
- Opening up of commercial coal mining marketing will speed up the opening of new mines and create direct and indirect jobs.

7.3 Challenges to Private Coal Companies

7.3.1 Land Acquisition

It is not the first time where private coal companies are doing mining. Many private companies have got the coal blocks for their captive use but still many mines have not started till now. The big challenge to them is land acquisition. The land acquisition can only be done under Coal Bearing (Areas Acquisition and Development) (CBA) Act 1957 or Land acquisition act 2013. Although the mining land is acquired through CBA act 1957, it is mandated that compensation and rehabilitation should be provided under the new Land Acquisition, Rehabilitation and Resettlement Act, 2013(LARR). The CBA Act 1957 is applicable only for the government companies. Under this act and its different notification, government can take the land under which coal is present. It is strictly limited to the coal-bearing areas. Other than coal-bearing areas, land acquisition is done under Land Acquisition, Rehabilitation and Resettlement act, 2013.

The CBA act 1957 is a strong act for the acquisition of land under coal-bearing area and the government has the power to take that land easily under CBA act 1957 but now new LARR act, 2013 is a strong act for the people who are losing their land. This act empowers to the land loser. The private companies have to acquire

their land under LARR act, 2013, which is again a very tedious job for the private player as in case of LARR act, 2013 consent of 80% people is required. The compensation is also very high in this case (Lahiri-Dutt et al. 2012).

The state-owned company Coal India Limited has a monopoly in the coal sector in India. The company provides good R&R packages to landowners whose land falls under coal-bearing areas. The company has got different R&R schemes and give options to landowners to choose which R&R package they want. Landowner can opt either respective state government's R&R package or Coal India's own R&R package or CIL's subsidiary's own R&R package. Generally, people choose subsidiary's R&R package because these packages are designed taking into account of the local people's interest. Coal India Limited or its subsidiary, in its R&R package, provides a job in Coal India Limited as per the norms.

The troublesome for private companies arises here. It has been seen that generally private companies or any other public sector unit (PSU's) provides the R&R package of respective state government or company's own R&R. In case of own R&R package, they provide an extra package to attract the local people. In spite of all, none of the companies provides the job against the land. The coal block which is allocated to these private companies or other PSUs are near to the CIL coal blocks. People residing nearby start comparing and questioning that if Coal India can provide a job then why not them. In spite of providing jobs by private firms against the land, people do not have much faith in private jobs. Moreover, usually people have more inclination towards government mining firms such as Coal India Limited, as compared to any other private firm. Even for the Coal India Limited to provide a job against land is not very profitable but for short term, they are succeeding in achieving their goal.

7.3.2 Coal Demand Growth in Power Sector

In India, the quality of coal is not very good and it is generally of power grade. The major consumer of our coal is the power sector. As India, after Paris summit (COP21 commitments) working hard to shift from nonrenewable source of power generation to renewable source of power generation. It can be seen that due to competition and government policy the per unit charge of power generation through solar power plants are less or equivalent to coal-driven power plants. So, the future of coal is not very much in our country. Before any private company would make a huge investment, they will take into account if they earn profit for long-term, which may come to stake as policy changes.

7.3.3 *Adverse Geology Can Constrain the Competitiveness of Future Coal Production*

Most of these blocks left for the auctions are difficult ones—in that they are either in densely populated areas or have difficult terrain. Some have coal seams buried deep underground. The stripping ratio in India is worsening leading to increased cost of production. On the other hand, the grade of coal is also worsening. Therefore, with increasing cost of production and lowering of grade, the competitiveness of coal would get increasingly constrained. This does not take into account the increase in capital cost due to revised land acquisition policy and overall inflation. Compared to alternative sources, particularly solar, coal could be increasingly disadvantaged. Cost of operations on these blocks are likely to be high.

To overcome all these constraints, it is necessary to bring down the following points into the consideration:

- Prepare the roadmap regarding the future of coal in India, so that participation from private player is boosted.
- The coal block opened for the auction of private players should be competitive for them based on stripping ratio, coal reserve, and forest cover.
- The single window system should be developed for the statutory clearances. The ease of doing business should be there which must be regulated by the ministry of coal.
- During land acquisition, local administration should come up with the proponent to deal with local situation.

7.4 Environment and Forest Clearances

It is the irony of coal that it is present in abundance where forest is there. In India, the open cast projects are only profitable and productive. For the extraction of coal in open cast projects, heavy degradation of forest and land occurs which affects socioeconomic structure of society residing nearby area. Other than that air pollution, fall of water table in nearby areas are also big challenges. MoEF&CC (Ministry of Environment & Forest and Climate Change) is regulatory body to monitor all these things. As discussed above, the biggest hurdle for the state-owned Coal India Limited was environmental and forestry clearances and the same will be applied to private players also. The time required for environmental and forestry clearances are very high. Minimum of 1 year will be required to get the environmental clearance from MoEF&CC and that too if everything is in order. If some poor technology or any poor environment management is sought by the experts of MoEF&CC, then that can go long for an indefinite time until and unless proper environmental management plan is not promised from the proponent. Similar to the environment clearance, forest clearance is another time-consuming process. It takes

several years to get the forest clearance. Huge investment is required for the getting a coal block. The biggest challenge to private players are with such huge investment still it is very uncertain that when will mine come in operation phase due to this stringent law and regulation.

7.4.1 Environmental Norm's Violation

Although the private mining companies are supposed to strictly follow the all environmental norms but previous experiences of privatization of others sectors are such that there are always remain some flaws in the process of performing their activities. Therefore, the government needs to take care of all previous policies and experiences related to the similar type of activities. It is important to mention here that new/private firms must go through strict screening round for final selection. Bidding the highest price for per ton of coal should not be the only criteria for the selection.

7.4.2 Threat Due to Privatization of Coal Sector

7.4.2.1 Environmental Threats

The private companies must be under severe surveillance of MoEF&CC or SPCB (State Pollution Control Board) or CPCB (Central Pollution Control Board) for the betterment of environment otherwise it will lead to questions that are these private companies as much as responsible and sensitive toward environmental parameters? Do they take care of everything that comes under rules and regulation and making a profit will not be the only motive for them? From the past, it has been seen many times that private players have the main motive of making money and making a profit is their main objective. With respect to them, PSUs are more responsible and sensitive for the environmental issues. Like in Coal India Limited, a dedicated subsidiary CMPDIL (Central Mine Planning and Design Institute Limited) is working for environmental issues with coal mining. They have a dedicated department for the proper monitoring of air pollution, water pollution and water table monitoring and providing environmental management plan related to any issues. It cannot be said that PSU's or Coal India Limited, all along have adopted the best practices but at least they have got a system which is evolved and inherited from past long experiences.

7.4.2.2 Socioeconomic Issues

The biggest socioeconomic issues are associated with the privatization is following labor laws. As the mining is labor-intensive industry, so the involvement of labors is very high in the production of coal. There will always be a chance that the shift hours are long and wages are very small compared to the hazardous nature of work or compared to the wages in PSUs. The need for nationalization in 1973 was due to the ill-treatment of labors by the mine owners. So in this case also strong monitoring should be done for labor law department for the better status of labors in the mining industry.

7.5 Conclusions

Considering the huge coal demand (>1.3 billion tons per year) in near future as well as the sustainable exploitation of our available resources, the union cabinet of India on February 20, 2018 decided to open up the coal sector for commercial mining by private entities. Under this new reform, the coal blocks will be allocated on the basis of price per ton of coal offered to the state government. Furthermore, there shall be no restriction on sale and/or utilization of coal from the coal mine to power plants, steel mills, and other potential users. The proposed policy will not only meet the country's coal demand but also lower down the production cost of coal due to competitiveness. In spite of these expected benefits, it will not be much easy for private investment in the coal sector. The biggest hurdle for private players includes land acquisition, future coal demand, as the country is shifting from conventional to renewable sources of energy so the demand for coal may be decreased in the future. Another major barrier is to get environmental and forest clearances which is very time taking process. The greatest risk associated with this policy is that private players may tend to overshadow environmental regulations and other ethical concerns of labor laws, just for their economic growth.

References

Coal India Limited. https://coal.nic.in/ (site accessed on 20 June, 2018)

Draft Energy Policy, Niti Ayog, Government of India, 2017

Goyal Y (2018) The coal mine Mafia of India: a mirror of corporate power. Am J Econ Sociol 77 (2):541–574

Lahiri-Dutt K (2016) The diverse worlds of coal in India: energising the nation, energising livelihoods. Energy Policy 99:203–213

Lahiri-Dutt K, Krishnan R, Ahmad N (2012) Land acquisition and dispossession: private coal companies in Jharkhand. Econ Polit Wkly, 39–45

Modak M, Pathak K, Ghosh KK (2017) Performance evaluation of outsourcing decision using a BSC and fuzzy AHP approach: A case of the Indian coal mining organization. Resour Policy 52:181–191

Singh K, Kalirajan K (2003) A decade of economic reforms in India: the mining sector. Resour Policy 29(3–4):139–151

Yilmaz F (2015) The relationship between privatization and occupational safety in coal industry in Turkey; a statistical review of coal mine accidents. J Sci Res Rep 5(4):265–274

Chapter 8
Development of Small-Scale Thermoelectric Power Generators Using Different Micro-combustor Configurations for Standalone Power Applications

B. Aravind and Sudarshan Kumar

Abstract In the present study, few highly efficient micro-combustors suitable for thermoelectric power generation are fabricated. The micro-combustors consist of multiple backward facing steps and a heat recirculating cup for proper flame stabilisation. A detailed experimental investigation on the thermal performance of the micro-combustors was carried out initially and thermoelectric generators were integrated to the bare surfaces of the combustor along with the cooling jackets for the power generation. The power output of 3.89 W with a conversion efficiency of 4.03%, the power output of 3.2 W with a conversion efficiency of 3.39% and power output of 4.5 W with a conversion efficiency of 4.66% are achieved for planar, triangular, and dual micro-combustor based power generators respectively. These results represent an improvement in portable-scale electrical power production from hydrocarbon fuels state of the art. Moreover, the power characteristics ensure the use of a proposed small-scale power generator for various aerospace and defence applications as a portable power source.

Keywords Thermoelectric generator · Micro-combustor · Flame stability Conversion efficiency

8.1 Introduction

Over the years, researchers have aimed at miniaturising combustion-based devices, especially those that are devoid of moving parts for the purpose of small-scale propulsion systems and use in MEMS (Ju and Maruta 2011). Chemical batteries,

B. Aravind (✉) · S. Kumar
Combustion Research Laboratory, Department of Aerospace Engineering,
Indian Institute of Technology Bombay, Mumbai, India
e-mail: aravindbpillai69@gmail.com

R. A. Agarwal et al. (eds.), *Pollutants from Energy Sources*,
Energy, Environment, and Sustainability,
https://doi.org/10.1007/978-981-13-3281-4_8

being at the peak of their evolution, are still unable to meet the high power density requirements pertaining to such applications (Chou et al. 2011). As power requirements, both total and specific, of electronic devices keep on increasing, this gap in performance will inevitably widen. Hydrocarbon fuels in general have an energy density two orders of magnitude higher than conventional fuel cells (Maruta 2011). Therefore, innovate methods to use combustion as a source for electricity for such applications have been in the frontlines for years now. Energy densities of the fuel and energy conversion systems need to be investigated to increase the operational life span of a power device (Fernandez-Pello 2002). The basic concept is to utilise the high specific energy of fuel in a combustor to produce power. Liquid hydrocarbon fuels have very high energy density of approximately 45 MJ/kg and are easily transportable and quite safe (Aravind et al. 2018). The top batteries currently available (lithium-ion) have energy densities of approximately 0.6 MJ/kg (Aravind et al. 2018; Walther and Ahn 2011). Hence, a small-scale combustor even with a 10% overall conversion efficiency will be six times better than a comparable lithium-ion battery (Table 8.1). Park et al. (2012) have prototyped a micro-photovoltaic based power generator that can deliver power output of 2.35 W with an overall conversion efficiency of 2.12% at the optimum conditions. They used a single backward facing step combustor along with propane as fuel. Lee et al. (2013) have adopted the similar combustor configuration and investigated with different fuels. The power output of 4.4, 5.2 W with an overall conversion efficiency of 2.3 and 2.1% is achieved for propane–air mixtures and $NH_3 + H_2$–air mixtures respectively. Li et al. (2009) developed a TPV-based power generator using a micro-combustor having a volume of ~ 5 cm^3. They harvested an electric power output of 8.3 W with an overall conversion efficiency of 1.47% using liquid *n*-heptane and pentane as fuels. Merotto et al. (2016) integrated a catalytic combustor with a TEG and produced a conversion efficiency of 2.85% with an electric power output of 9.86 W. Shimokuri et al. (2017) prototyped a mesoscale vortex combustor coupled with TE modules. Their result shows that the heat transfer was improved significantly due to the vortex flow and produced a power output of 18.1 W with a conversion efficiency of 3%. Yoshida et al. (2006) fabricated a silicon-coated catalytic combustor and harvested an electric power output of 184 mW with 2.8% conversion efficiency by integrating it with TE modules. Qiu and Hayden (2012) prototyped a power generation system by integrating thermophoto voltaic cell and thermoelectric modules together. The result suggests that power output can be enhanced by using TPV-TEG than the TPV or TEG alone. Yadav et al. (2015) used a backward facing three-step combustor with a heat recirculation cup for source for heat. Their result indicates that the conversion efficiency is improved from 1.2% (single module) to 2.56% for two modules and 4.6% for four module arrangements using the same combustor. Aravind et al. (2018) prototyped a high power density (12 mW/mm^3) thermoelectric-based power generator using stepped micro-combustor. They achieved 3.89 W of electric power with a conversion efficiency of 4.03% at an equivalence ratio of 0.9. Several efforts, both experimental and numerical, were made towards the flame stabilisation techniques in small-scale combustors through heat and flow recirculation or

employing catalyst (Hardesty and Weinberg 1973; Ronney 2003; Khandelwal and Kumar 2010; Zhou et al. 2009). The excess enthalpy concept has been a widely used technique for flame stabilisation in small-scale combustors. Swiss roll combustors were one of the widely used combustor (Kim et al. 2005, 2007; Chen and Buckmaster 2004) where the unburned fuel–air mixture is preheated through the enthalpy of exhaust gas recirculated. This results in enhanced flame temperature and improved flame stability limits compared to the standard operating conditions. Yang et al. (2002, 2014) and Khandelwal et al. (2013) have performed a detailed investigation on flame stabilisation in micro-scale with backward facing step micro-combustor configurations. The flame stability limits can be significantly improved with the help of backward facing step as it induces small eddies near the step and enhance mixing of combustion products with the charge due to the formation of a recirculation zone. It is also shown by Khandelwal et al. (2013), Sahota et al. (2011), and Taywade et al. (2013) that wide flame stability limit can be achieved by incorporating more number of steps. They have done an investigation to comprehend the influence of various parameters such as inlet velocity, equivalence ratio, etc., on flame stability limits and wall temperature profiles in multiple-stepped combustors. Aravind et al. (2016) and Singh et al. (2015, 2017) conducted a detailed numerical studies to understand the transient behaviour of flame in micro- and stepped tubes. They studied the effect of convective heat loss on flame propagation velocity and flame angle for various operating conditions (Table 8.1).

In the present study, a detailed experimental investigation on thermal performance and flame stability of number of backward facing stepped micro-combustor configurations are carried out. Then a prototype of small-scale power generation by integrating the micro-combustors with thermoelectric modules along with the cooling jackets has been developed. The aim of the present study is to develop an

Table 8.1 Comparison of the energy density of different power sources

Source	Energy density [MJ/kg]
Lead acid batteries	0.17
Nickel cadmium batteries	0.288
Lithium-ion batteries	0.36–0.875
Lithium batteries (non-rechargeable)	1.8
Methanol combustion	19.7
Ethanol combustion	26.4
Gasoline combustion	44.4
Kerosene combustion	46
Liquefied petroleum gas combustion	46.4
Diesel combustion	48
Methane combustion	55.5
Hydrogen combustion	142

efficient power generator with a high power density for various remote, standalone military, and aerospace applications.

8.2 Working Principle of Micro-thermoelectric Power Generators

Thermoelectric power generators (TEGs) are the solid-state devices which convert temperature difference into electric potential based on Seebeck effect. A thermo-electrical generator essentially consists of a high temperature heating source (combustor), low temperature heat sink (cooling jacket), and thermoelectric device (usually semiconductor material) as shown in Fig. 8.1. Temperature difference between the heat source and sink induces a current that flows through the load resistance connected across the TEG. Thermoelectric generators are categorised as a direct conversion device as it does not have any intermediate part for energy conversion as the micro-turbine has. The power characteristics of the thermoelectric device can be enhanced by increasing either the temperature difference (increasing hot side temperature or decreasing cold side temperature) or by connecting several TEGs in series or parallel. This device can be considered as a DC power source for charging low-power electronic devices and the voltage can be step up or down using a DC–DC convertor. However, the usage of TEGs is limited due to its low conversion efficiency. Performance of the modules can be improved by adopting semiconductor materials having high figure of merit.

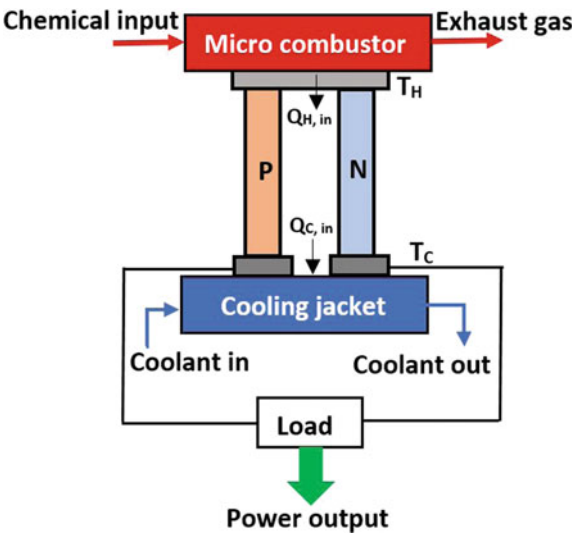

Fig. 8.1 Schematic of working principle of typical combustion-based thermoelectric power generators

8.3 Development of Micro-combustors

Micro-combustors are the crucial parts of any thermoelectric power generators. The major challenge in micro-combustion is thermal and chemical management. As the combustor size decreases the surface to volume ratio increases and hence heat losses also increases. This leads to thermal quenching which is caused by rapid heat loss to the walls of the combustor and thus the quenching of flame. Due to strong flame-wall thermal coupling, the wall temperature increases as the size of combustor decreases and heat loss increase (Fernandez-Pello 2002). In addition, as the result of shortening the length of the combustor, the diffusion time scale and the formation time scale of the chemical radicals will become comparable and result a strong radical quenching and the flame quenching (Ju and Maruta 2011; Maruta 2011). In micro-scale combustion, thermal quenching and radical quenching are two key phenomena that can be considered for the flame stabilisation. Thermal quenching is predominant at low wall temperature whereas radical quenching occurs at high wall temperature and it affects the flame propagation. For combustion to happen in a small-scale combustors, the residence time of the reactants must be larger than the chemical time for the combustion. However, higher heat losses lower the inner wall temperature which increases chemical time (slow the chemical Kinetics) (Lee and Kwon 2002). Hence, chemical time increases and residence time decreases with the decrease in the characteristic length of the combustor. Thus, less residence time results in incomplete combustion and poor efficiency. Chemical time can be decreased by preheating the reactants and using a highly energetic fuel. Flame stability is also very important for micro-combustion. Basically, there are two types of instability mechanism: hydrodynamic instability and diffusion thermal stability (Maruta et al. 2005). Hydrodynamic disturbances include the viscous effect, boundary layer effect, velocity profile changes, etc. Numerous researchers reported that flame dynamics in micro-channels are highly sensitive to these effects. Because the long wavelength hydrodynamics instability is suppressed in mesoscale combustion, thermal diffusion plays a dominant role. The term "Long wavelength hydrodynamic instability" refers to the hydrodynamic disturbances with high intensity. The effect of hydrodynamics is feeble in the present study as the flow is in laminar nature. In the present study, few backward-facing three-step micro-combustor with a heating cup configurations have been adopted. The multiple backward facing steps induce local flow recirculation and heating cup provides heat recirculation there by providing wide flame stabilisation limits.

8.3.1 Micro-combustor with Separate Heat Recirculation Cup

Three backward-facing steps with gradually increasing diameter from 2 to 6 mm is fabricated using stainless steel. The micro-combustor dimension is similar to the

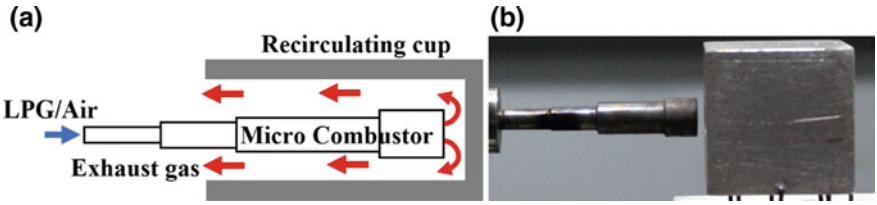

Fig. 8.2 **a** Schematic **b** real image of micro combustor with single pass heat recirculation cup

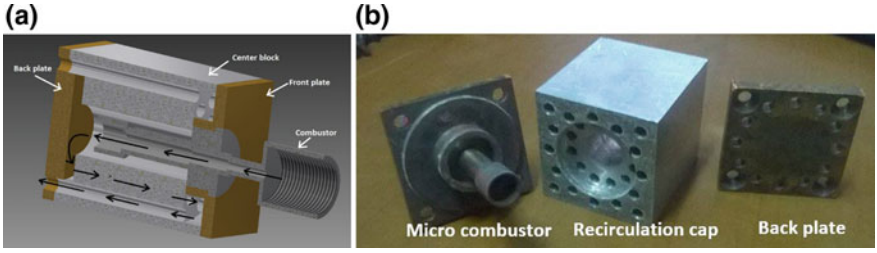

Fig. 8.3 **a** Schematic **b** real image of the micro combustor with multipass heat recirculation cup

earlier works of author's research group (Yadav et al. 2015; Khandelwal and Kumar 2010; Khandelwal et al. 2013; Aravind and Kumar 2016). A heating cup of a rectangular block of 32 mm × 12 mm size, made up aluminium having 11 mm diameter hole is used. The heating cup is placed at the exit of the combustor in such way that 2 mm recirculation gap is maintained between in the combustor exit and the inside surface of the heating cup as shown in Fig. 8.2a. On the other hand, two-pass heating cup is fabricated to enhance the heat transfer by improving the residence time of the exhaust gas. Two-pass heating cup is a square block of 32 mm × 32 mm size and 12, 3 mm holes were drilled on front and back sides of the heating cup to achieve multiple pass as shown in Fig. 8.3. Taywade et al. (2013) have studied the geometrical effects of heating cup on wall temperature in detail. It was found that an optimum size of heating cup configuration bears maximum temperature. The local recirculation near each step helps to increase the residence time of the reactants to achieve stable flame in the micro-combustor. Further, a two-pass heating cup also considered which would significantly enhance the residence time of the exhaust gas and expected to improve the thermal characteristics over the single pass combustors. For all the combustor configurations, inlet velocity is calculated based on 2 mm diameter, which is the inlet side of the micro-combustors. Inlet velocity is obtained from the total flow rate divided by the cross-sectional area of 2 mm at channel inlet and mixture density. The volume flow rate of fuel and air is individually calculated based on the required equivalence ratio and flow through respective mass flow controllers. For dual micro-combustor, the total mixture is equally divided into two combustors through the two 2 mm inlets of the dual combustor.

8.3.2 *Integrated Micro-combustor-Heat Recirculation Cup Configurations*

This section details different integrated type micro-combustors based on backward-facing step concept. Planar and triangular micro-combustors consist of a single, three-stepped micro-combustor and a provision for exhaust gas feedback. Triangular micro-combustor has lower thermal characteristics compared to the single combustor due to the increased heat loss. Further, in the dual combustor configuration, authors have incorporated two micro-combustors to increase the intensity of combustion for enhancing the thermal performance. The detailed analysis has been discussed in the following subsections.

Figure 8.4a shows the schematic view of planar micro-combustor used in the present work. Three cylindrical backward-facing step micro-combustor with dimensions similar to the authors previous works (Khandelwal et al. 2013; Taywade et al. 2013; Anil et al. 2011) is fabricated inside a rectangular heating medium of 32 × 32 × 10 mm^3 overall size. The dimensions of the heating medium are chosen similar to the size of the modules for proper integration. The steps provided in the micro-combustor induce local flow recirculation and there by enhances the flame stability limit (Khandelwal et al. 2010). In addition, backward-facing step, two 4 mm diameter holes are provided. Further, a triangular-shaped micro-combustor has been fabricated to accommodate three modules to understand the effect of number modules on power generation for a fixed thermal input (Fig. 8.4b). In addition to that, a dual combustor is fabricated with two parallel three-stepped micro-combustors to increase the intensity of heating by multiple combustion zones as shown in Fig. 8.5. A dual combustor consists of two similar multiple-step combustors placed in between the two recirculation holes. Total mixture velocity is calculated corresponding to the 2 mm inlet diameter. The total mixture is equally divided through the two inlets. It is found that dual combustor offers high surface temperature compared to the single combustor configuration.

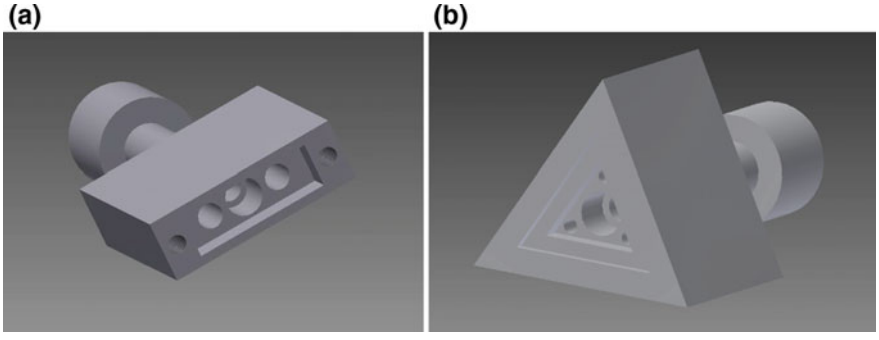

Fig. 8.4 Schematic of integrated **a** planar **b** triangular micro combustor configurations (without recirculation cap view)

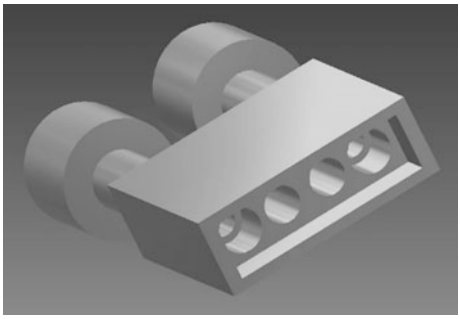

Fig. 8.5 Schematic of dual combustor configuration (without recirculation cap view)

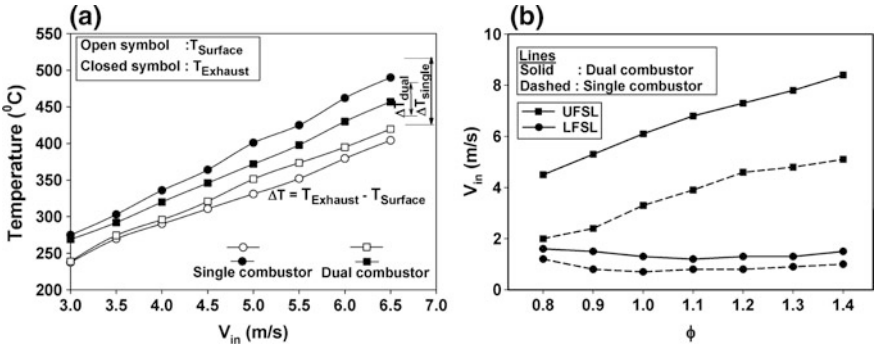

Fig. 8.6 Comparison of **a** thermal performance and **b** stability limit of the single with dual micro combustor

It can be seen from Fig. 8.6b that the average surface temperature reaches around 400 °C for a 6 m/s mixture velocity. However, the surface temperature drops significantly to allowable operating limits of the TEGs (<250 °C) while mounting the modules to the micro-combustor. There is a notable rise in the heat transfer from the exhaust gas to the combustor for the dual combustor configuration when compared to single micro-combustor ($\Delta T_{\text{dual}} < \Delta T_{\text{single}}$). This is because of the increased flame–wall interaction and better heat recirculation. Comprehensively, around 15 °C rise is observed for a dual combustor configuration compared to a single combustor configuration. Detailed investigation on the flame stability of single and dual combustor has been performed. A significant improvement in the upper flame stability limit (UFSL) has been observed for dual micro-combustor compared to the single combustor as shown in Fig. 8.6b. This might be due to the better preheating of the incoming mixture via the increased intensity of combustion of the dual micro-combustor. However, lower flame stability limit (LFSL) is found to lower slightly due to the splitting of mixture velocity at the two inlets.

8.4 Integration of Thermoelectric Modules

8.4.1 Selection of Thermoelectric Modules

Four thermoelectric generators namely TEG1-127-30-30T250HP from Nippon Pvt. limited India, HZ-2 from Hi-z Technology USA, SP1848 and TES 12704 have been tested to select the suitable thermoelectric generator for the present study. Open circuit voltage and power output characteristics are compared for different heat inputs as shown in Fig. 8.7. It is observed that Nippon TEGs are offering better performance as compared to other modules for all the mixture velocities investigated. For instance, TEG1-127-30-30T250HP, HZ-2, SP1848, and TES 12704 was able to achieve a power output of 0.82, 0.53, 0.38, and 0.21 W respectively at ~67 W of chemical input. Therefore, Nippon modules have been taken for the present study due to its better performance characteristics than the other modules. Detailed specification of Nippon module used in the present study has been tabulated in Table 8.2. However, the three material properties are difficult to attain as the manufacture's proprietary. In general, the manufactures provide the four measured maximum parameters which include electrical output characteristics corresponding to several temperature differences, thermal and contact resistance, etc. Therefore, an attempt has been made to deduce the three material properties of Nippon modules from the four manufacture's maximum parameters (Eqs. 1–9). It is of interest to find the three material properties from any four maximum parameters specified by the manufacturer. Therefore, parameters such as V_{max}, W_{max}, I_{max}, and η_{mp} are chosen for the present study. W_{max} is chosen instead of V_{max} due to its practical relevance. The calculated effective material properties here can be approximated as the real material properties that can be used for calculating the various performance indicators of the TEGs such as figure of merit, material index, etc., which is of great interest for the material researchers this field.

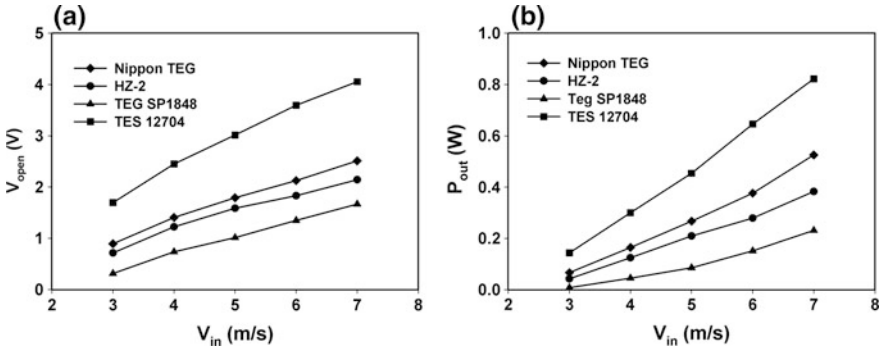

Fig. 8.7 Variation of **a** open circuit voltage and **b** power output for different thermoelectric generators

Table 8.2 Specification of Nippon TEG used in the present study

TEG1-127-30-30T250HP	
Maximum power (P_{max})	4.6 W
Maximum current (I_{max})	1 A
Maximum voltage (V_{open})	9.6 V
Load voltage (V_L)	4.8 V
Hot side temperature (T_H)	523 K
Cold side temperature (T_C)	303 K
Maximum power efficiency (η_{mp})	6%
Internal resistance (nR)	5 Ω
Number of thermocouples (n)	127
Area of thermoelectric element (A)	1.69 mm^2
Length of thermoelectric element (L)	1.4 mm

$$\text{Resistivity}\,(\rho^*) = \frac{4\left(\frac{A}{L}\right)W_{max}}{nI_{max}^2} = 1.75 \times 10^{-4}\,\Omega\,\text{m} \tag{1}$$

$$\text{Seebeck coefficient}\,(S^*) = \frac{4W_{max}}{nI(T_H - T_C)} = 6.59 \times 10^{-3}\,\text{V/K} \tag{2}$$

$$\text{Effective figure of merit}\,(Z^*) = \frac{\frac{4}{T_C}\frac{T_C}{T_H}}{\eta_c\left(\frac{1}{\eta_{mp}} - \frac{1}{2}\right) - 2} = 1.467 \times 10^{-3}\,\text{K}^{-1} \tag{3}$$

$$\text{where } \eta_c = \left(1 - \frac{T_C}{T_H}\right)$$

$$K^* = \frac{S^{*^2}}{\rho^* Z^*} = 1.69\,\text{W/mK} \tag{4}$$

$$Z^* T_C = 0.44 \tag{5}$$

$$Z^* T_H = 0.77 \tag{6}$$

$$Z^* \bar{T} = 0.605 \tag{7}$$

$$\text{Maximum conversion efficiency}\,(\eta_{max}) = \left(1 - \frac{T_C}{T_H}\right)\frac{\sqrt{1+ZT}-1}{\sqrt{1+ZT} - \frac{T_C}{T_H}} = 6.1\% \tag{8}$$

$$\text{Heat absorbed at hot junction}\,(Q_H) = \frac{W_{max}}{\eta_{max}} = 75.65\,\text{W} \tag{9}$$

The various performance parameters of the TEG are normalised by its maximum values for the better understanding. It can be seen from the following equations

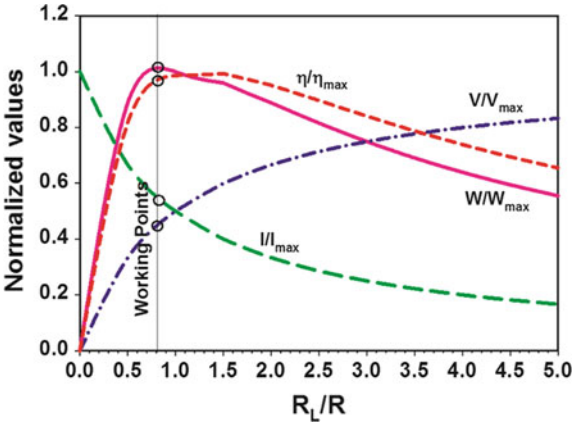

Fig. 8.8 Normalized parameters of Nippon TEG

(Eqs. 10–13) that, power, current, and the voltage are only the function of R_L/R and the efficiency is a function of three parameters T_C/T_H, R_L/R, and ZT_C. Though the internal resistance of the TEG is specified as 5 Ω in the specification (Table 8.2), the maximum power is observed at load resistance of 4 Ω during the experimental trials. Therefore, the normalised parameters of the experiments are calculated by taking $R_L/R = 0.8$ and $ZT_C = 0.44$. It is evident from Fig. 8.8 that, the working points are very close to the maximum power and efficiency points which ensures the optimum operating condition of the system.

$$\frac{W}{W_{\max}} = \frac{4\frac{R_L}{R}}{\left(\frac{R_L}{R}+1\right)^2} = 0.99 \tag{10}$$

$$\frac{I}{I_{\max}} = \frac{1}{\frac{R_L}{R}+1} = 0.56 \tag{11}$$

$$\frac{V}{V_{\max}} = \frac{\frac{R_L}{R}}{\frac{R_L}{R}+1} = 0.44 \tag{12}$$

$$\frac{\eta}{\eta_{\max}} = \frac{\left(\frac{R_L}{R}\right)\left[\sqrt{1+\frac{ZT_C}{2}\left(1+\left(\frac{T_C}{T_H}\right)^{-1}\right)}-\frac{T_C}{T_H}\right]}{\left[\left(\frac{R_L}{R}+1\right)-\frac{1}{2}\left(1-\frac{T_C}{T_H}\right)+\frac{\left(\frac{R_L}{R}+1\right)^2\frac{T_C}{T_H}}{ZT_C}\right]\left(\sqrt{1+\frac{ZT_C}{2}\left(1+\left(\frac{T_C}{T_H}\right)^{-1}\right)}-1\right)} \tag{13}$$

8.4.2 Power Generation Using Micro-combustor with a Separate Heating Cup

A three-stepped micro-combustor made up of stainless steel and two different heating cups (HC) of single and multiple pass configurations have been considered as a heating source for thermoelectric power generation. Geometrical details of both the micro-combustors have been detailed in the previous section. Two thermoelectric generators and four thermoelectric generators are attached on the bare surfaces of single and multi-pass heating cups respectively along with the water cooling jackets. It can be seen from Fig. 8.9a that the single pass configuration produces much higher power output compared to the multipass configuration irrespective of its better thermal performance. This might be due to lower hot side temperature of multipass configuration as it is mounted by four TEGs and cooling jackets. The hot side temperature is inversely proportional to the number of modules mounted as it absorbs significant amount of heat from the hot surface. The lower power output of the multipass power generator has an adverse influence in its conversion efficiency as shown in Fig. 8.9b. A conversion efficiency of 1.8 and 1.1% are achieved for single and multi-pass heating cup power generators respectively.

8.4.3 Power Generation Using Integrated Micro-combustor Configuration

8.4.3.1 Single Micro-combustor Configurations

Since the separate micro-combustor-heating cup configuration provides comparatively lower power output and conversion efficiency, a couple of integrated micro-combustors to incorporate two and three thermoelectric generators (planar

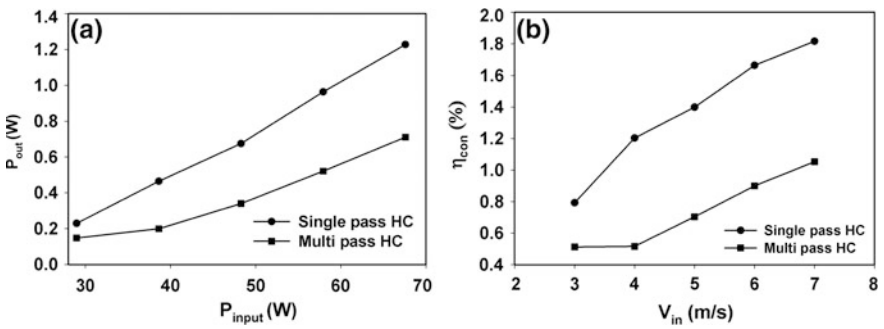

Fig. 8.9 Variation of **a** power output and **b** conversion efficiency for single pass and dual pass micro combustors

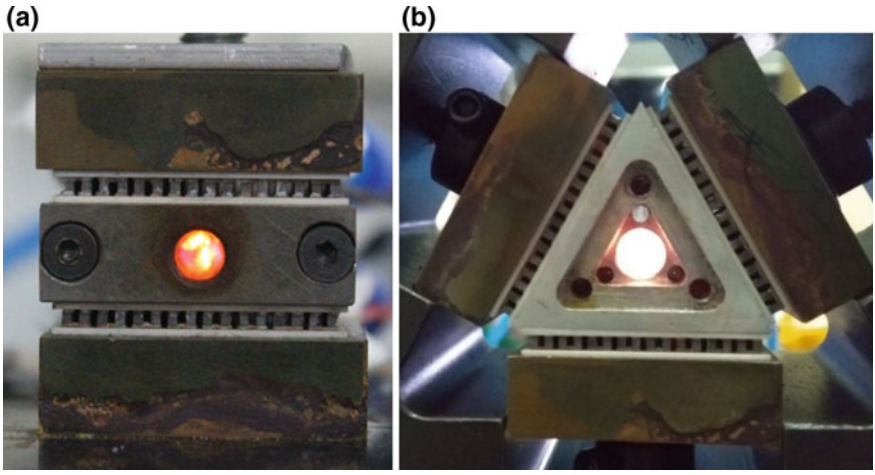

Fig. 8.10 Real photography of **a** planar and **b** triangular micro combustor based power generators

and triangular micro-combustor respectively) have been fabricated using aluminium owing to its high thermal conductivity and light weight. Geometrical details of the combustor have been detailed in the previous sections. Figure 8.10 shows the real photographs of flame stabilisation in the planar and triangular micro-combustors. A ceramic wool of 2 mm thickness has been introduced at the third step to further enhance the upper flame stability limit.

The average surface temperature is measured for both planar and triangular combustor to understand its thermal performance. It is observed that 15–20% reduction in the surface temperature of the triangular combustor than the planar combustor due to the increased heat loss. Both the micro-combustors were able to achieve uniform surface temperature and more than 400 °C temperature even with 60 W of thermal input. However, surface temperature was found to drop significantly with application of modules due to large convective loss as shown in Fig. 8.11. None of the combustor was able to reach the allowable limit of thermoelectric generator even at the higher thermal inputs. Maximum hot side temperature of 158 and 190 °C are achieved for the planar and triangular micro-combustor. Reduction in the hot side temperature of triangular combustor would be perhaps due to the higher convective heat loss due to the three thermoelectric generators. It is also found that all the three TEGs of triangular combustor produces almost equal output voltage due to the uniform and equal surface temperature in the three faces as shown in Fig. 8.11b.

Further, the power output and conversion efficiency have been calculated for planar and triangular combustor as shown in Fig. 8.12. The conversion efficiency is calculated by the ratio of the sum of individual power output of modules to the fuel input. Planar micro-combustor offers better power characteristics compared to the triangular micro-combustor due to its improved thermal performance. A power output of 3.8 W with conversion efficiency of 4.03% and power output of 3.2 W

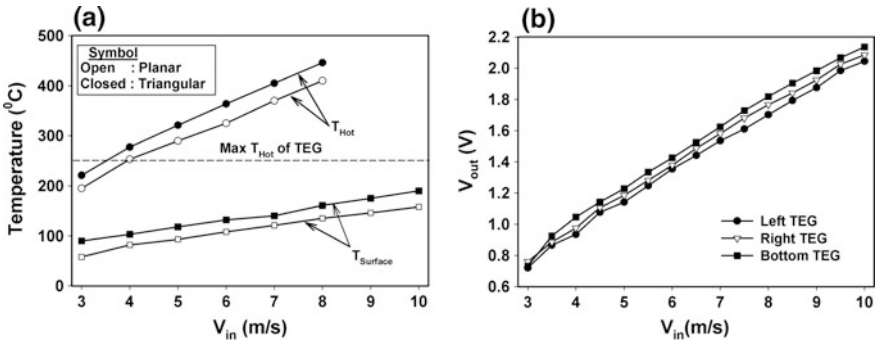

Fig. 8.11 **a** Temperature comparison of the planar and triangular combustor. **b** Variation of the output voltage of triangular combustor

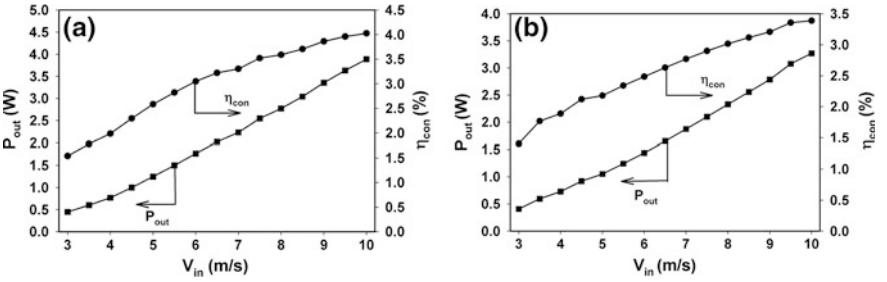

Fig. 8.12 Output power and efficiency variation with inlet velocity for **a** planar combustor **b** triangular combustor

with a conversion efficiency of 3.39% is achieved for planar and triangular micro-combustor respectively at 10 m/s mixture velocity and ϕ = 0.9 (Fig. 8.13).

Additionally, to study the electrical behaviour of the system, TEGs are electrically connected in series and parallel at optimum operating condition. Various electric parameters are noted in each electric conditions at a fixed operating condition of 10 m/s and $\phi = 0.9$ (Fig. 8.13). It is found that, maximum power is observed at load resistance of 4, 8 and 2 Ω load resistances for individual, series and parallel connections respectively. Maximum power is obtained for individual connection whereas maximum output voltage and current are obtained at series and parallel connections respectively.

8.4.3.2 Dual Micro-combustor

A real photograph of flame stabilisation in dual microcombustor based power generator is shown in Fig. 8.14. The system comprises of two Nippon TEGs mounted on either side of the microcombustor along with water cooling jackets.

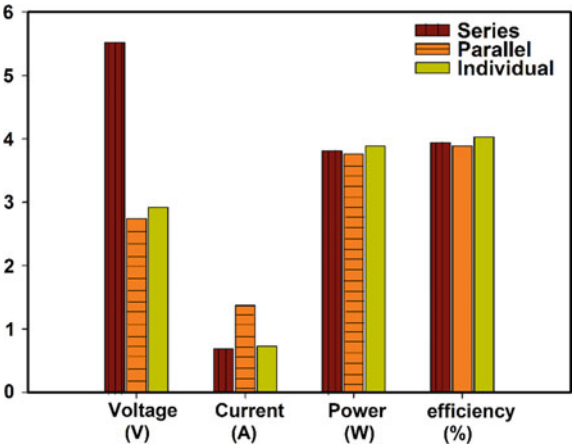

Fig. 8.13 Effect of different electric connections on output characteristics of planar combustor at 10 m/s and $\phi = 0.9$

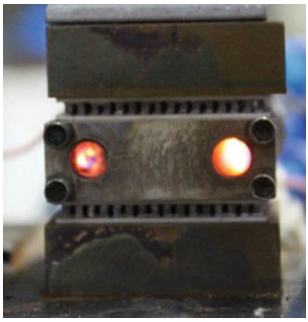

Fig. 8.14 Direct photography of dual combustor based micro power generator

A thorough investigation on the thermal and performance of the dual combustor based power generation system has been carried out. It is found that the hot side temperature of the module increases with thermal input for both with and without module case. Although the surface temperature of the dual micro-combustor has been increased beyond 400 °C even at 6.0 m/s inlet velocity, the hot side temperature is dropped significantly (∼210 °C at 10 m/s) with the application of the modules as shown in Fig. 8.15a.

Figure 8.15b shows variation of performance and thermal characteristics of the power generator with operating time at 6 m/s and $\phi = 1.0$. Combustion has been ignited using a butane torch at the ignition port. The ignition port is closed once a stable flame is obtained ($t = 0$ min), and hot side temperature increases to 150 °C within 6 min of operation. A steady hot side temperature is achieved from 6 min to the fuel supply ceases. Operational time of 25 min has been shown in Fig. 8.15b. Due to the high specific heat capacity of the water, cold side temperature was found to be nearly constant about 35 °C throughout the operation. The experimental result indicates that the proposed prototype is able to produce steady electric output from 6 min of operational time which ensures the practicality of the system. The dual

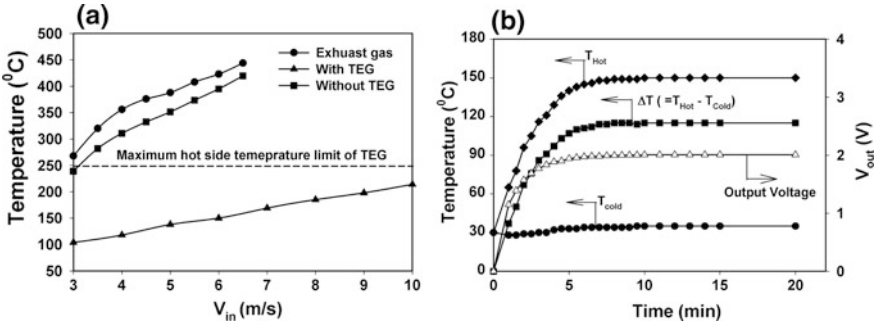

Fig. 8.15 **a** Variation of temperature with total mixture velocity for with and without TEG cases. **b** Temporal variation of temperatures and output voltage for 6 m/s at $\phi = 1.0$

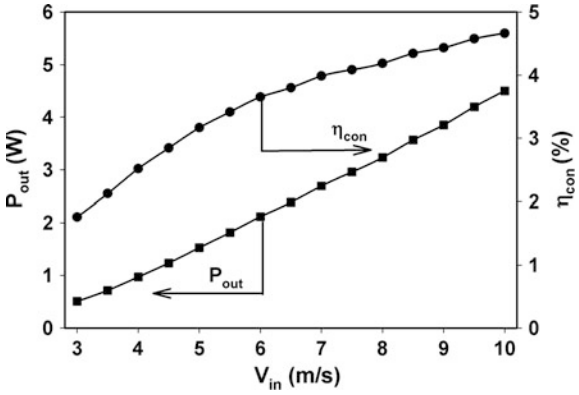

Fig. 8.16 Variation of output power and conversion efficiency with total mixture velocity at $\phi = 0.9$

Table 8.3 Summary of micro power generators investigated in the present study

Sl. No.	Combustor-heating cup type	Configuration	No. of modules	P_{out} (W)	η_{con} (%)	Remarks
1	Separate	Single pass	2	2.01	2.0	Poor heat transfer due to lack of flame-surface contact
2		Multipass	4	1.53	1.58	
3	Integrated	Planar	2	3.89	4.03	Better thermal performance due to direct flame-surface contact
4		Triangular	3	3.20	3.39	
5		Dual	2	4.50	4.66	Combustion intensity is enhanced by multiple combustion zones

combustor based power generator was able to harvest an electric power of 4.5 W with conversion efficiency of 4.66% using ~96 W of input power as shown in Fig. 8.16. The various power generators investigated in the presented study has been summarised in Table 8.3.

8.5 Conclusion

Thermoelectric power generation using various combustor configurations has been reported in the present study. Two types of heat recirculating three-stepped micro-combustors, one is having separate micro-combustor and heating cup and the second type is having integrated micro-combustor and heating cup were fabricated. Detailed investigations on the thermal characteristics of both the combustor types were analysed. It is found that the integrated combustor design offers higher surface temperature than the separate combustor design due to the direct combustor wall–flame interactions, indeed it reflects in the improvement in power generation. Single pass and multipass heating cup designs are tested in the separate combustor configuration. Even though there is a slight improvement in the thermal performance of the multipass heating cup due to the large residence time of the exhaust gas, power output was found to be less. This might be due to the higher number of modules mounted in the multipass heating cup power generator. Further, three different integrated configurations namely planar, triangular, and dual micro-combustor were analysed. The dual combustor offers highest power characteristics due to the multiple combustion zones. The power output of 3.89 W with a conversion efficiency of 4.03%, the power output of 3.2 W with a conversion efficiency of 3.39% and power output of 4.5 W with a conversion efficiency of 4.66% are achieved for planar, triangular, and dual micro-combustor respectively. The high-efficient power generators prototyped in the present study can be easily brought to the product level for various small-scale standalone power applications.

References

Anil AD, Bhupendra K, Sudarshan K (2011) Flame stabilization studies in a three backward facing step configuration based microcombustor with premixed methane-air mixtures

Aravind B, Kumar S (2016) Parametric studies on thermo-electric power generation using micro combustor. In: Techno-societal 2016, international conference on advanced technologies for societal applications. Springer

Aravind B, Velamati RK, Singh AP, Yoon Y, Minaev S, Kumar S (2016) Investigations on flame dynamics of premixed H_2–air mixtures in microscale tubes. RSC Adv 6(55):50358–50367

Aravind B, Khandelwal B, Kumar S (2018a) Experimental investigations on a new high intensity dual microcombustor based thermoelectric micropower generator. Appl Energy 228:1173–1181

Aravind B, Raghuram GK, Kishore VR, Kumar S (2018b) Compact design of planar stepped micro combustor for portable thermoelectric power generation. Energy Convers Manag 156:224–234

Chen M, Buckmaster J (2004) Modelling of combustion and heat transfer in Swiss roll micro-scale combustors. Combust Theor Model 8(4):701–720

Chou S, Yang W, Chua K, Li J, Zhang K (2011) Development of micro power generators—a review. Appl Energy 88(1):1–16

Fernandez-Pello AC (2002) Micropower generation using combustion: issues and approaches. Proc Combust Inst 29(1):883–899

Hardesty D, Weinberg F (1973) Burners producing large excess enthalpies. Combust Sci Technol 8(5–6):201–214

Ju Y, Maruta K (2011) Microscale combustion: technology development and fundamental research. Prog Energy Combust Sci 37(6):669–715

Khandelwal B, Kumar S (2010) Experimental investigations on flame stabilization behavior in a diverging micro channel with premixed methane–air mixtures. Appl Therm Eng 30(17–18):2718–2723

Khandelwal B, Sahota GPS, Kumar S (2010) Investigations into the flame stability limits in a backward step micro scale combustor with premixed methane–air mixtures. J Micromech Microeng 20(9):095030

Khandelwal B, Deshpande AA, Kumar S (2013) Experimental studies on flame stabilization in a three step rearward facing configuration based micro channel combustor. Appl Therm Eng 58 (1–2):363–368

Kim NI, Kato S, Kataoka T, Yokomori T, Maruyama S, Fujimori T, Maruta K (2005) Flame stabilization and emission of small Swiss-roll combustors as heaters. Combust Flame 141 (3):229–240

Kim NI, Aizumi S, Yokomori T, Kato S, Fujimori T, Maruta K (2007) Development and scale effects of small Swiss-roll combustors. Proc Combust Inst 31(2):3243–3250

Lee DH, Kwon S (2002) Heat transfer and quenching analysis of combustion in a micro combustion vessel. J Micromech Microeng 12(5):670

Lee S, Um D, Kwon O (2013) Performance of a micro-thermophotovoltaic power system using an ammonia-hydrogen blend-fueled micro-emitter. Int J Hydrogen Energy 38(22):9330–9342

Li YH, Lien YS, Chao YC, Dunn-Rankin D (2009) Performance of a mesoscale liquid fuel-film combustion-driven TPV power system. Prog Photovoltaics Res Appl 17(5):327–336

Maruta K (2011) Micro and mesoscale combustion. Proc Combust Inst 33(1):125–150

Maruta K, Kataoka T, Kim NI, Minaev S, Fursenko R (2005) Characteristics of combustion in a narrow channel with a temperature gradient. Proc Combust Inst 30(2):2429–2436

Merotto L, Fanciulli C, Dondè R, De Iuliis S (2016) Study of a thermoelectric generator based on a catalytic premixed meso-scale combustor. Appl Energy 162:346–353

Park J, Lee S, Wu H, Kwon O (2012) Thermophotovoltaic power conversion from a heat-recirculating micro-emitter. Int J Heat Mass Transf 55(17–18):4878–4885

Qiu K, Hayden A (2012) Development of a novel cascading TPV and TE power generation system. Appl Energy 91(1):304–308

Ronney PD (2003) Analysis of non-adiabatic heat-recirculating combustors. Combust Flame 135 (4):421–439

Sahota GPS, Khandelwal B, Kumar S (2011) Experimental investigations on a new active swirl based microcombustor for an integrated micro-reformer system. Energy Convers Manag 52 (10):3206–3213

Shimokuri D, Taomoto Y, Matsumoto R (2017) Development of a powerful miniature power system with a meso-scale vortex combustor. Proc Combust Inst 36(3):4253–4260

Singh AP, RatnaKishore V, Minaev S, Kumar S (2015) Numerical investigations of unsteady flame propagation in stepped microtubes. RSC Adv 5(122):100879–100890

Singh AP, Kishore V, Yoon Y, Minaev S, Kumar S (2017) Effect of wall thermal boundary conditions on flame dynamics of CH_4-air and H_2-air mixtures in straight microtubes. Combust Sci Technol 189(1):150–168

Taywade UW, Deshpande AA, Kumar S (2013) Thermal performance of a micro combustor with heat recirculation. Fuel Process Technol 109:179–188

Walther DC, Ahn J (2011) Advances and challenges in the development of power-generation systems at small scales. Prog Energy Combust Sci 37(5):583–610

Yadav S, Yamasani P, Kumar S (2015) Experimental studies on a micro power generator using thermo-electric modules mounted on a micro-combustor. Energy Convers Manag 99:1–7

Yang W, Chou S, Shu C, Li Z, Xue H (2002) Combustion in micro-cylindrical combustors with and without a backward facing step. Appl Therm Eng 22(16):1777–1787

Yang W, Chua K, Pan J, Jiang D, An H (2014) Development of micro-thermophotovoltaic power generator with heat recuperation. Energy Convers Manag 78:81–87

Yoshida K, Tanaka S, Tomonari S, Satoh D, Esashi M (2006) High-energy density miniature thermoelectric generator using catalytic combustion. J. Microelectromech Syst 15(1):195–203

Zhou J, Wang Y, Yang W, Liu J, Wang Z, Cen K (2009) Combustion of hydrogen–air in catalytic micro-combustors made of different material. Int J Hydrogen Energy 34(8):3535–3545

Part III
Pollutants from Nuclear Energy

Chapter 9
Sources of Nuclear Pollutants and Their Controls

Shashi Kant Verma

Abstract Atomic energy is basis of clean-air and carbon free electricity. It does not produce greenhouse gases or air pollutants. Nuclear pollution is very harmful for human health and thus it is very essential to take important steps for its prevention. Reprocessing is one alternative solution but it may also source of other pollution problems by risking contaminating in the surroundings. The storage facilities should be highly secure with regularly checks and updates about present situation of feasibility. During the operation of atomic power plants, groundwater contamination (Tritium) occurs which is a slightly radioactive type of hydrogen. The process of mining uranium and spent fuel rod which is still radioactive affects the atmosphere. The radioactive material release due to nuclear accidents is one of the slightest possible and most relating to atmospheric issue. This chapter will give planners and administrators of atomic offices in which ventilation and air-cleaning frameworks are utilized with the components which must be considered to make safe working conditions inside the nuclear facilities and without dirtying the air or nature to an unsafe level. This chapter gives an overview of various types of undesirable's materials or substances which affect the atmosphere and their control methods, both past and present using different approach. At the end, some of the grey areas with solutions and recommendations will be presented.

Keywords Atmospheric pollution hazard · Groundwater contamination
Spent fuel rod

S. K. Verma (✉)
Mechanical Engineering Department, Malla Reddy Engineering College (Autonomous), Maisammaguda, Dhulapally, Secunderabad 500100, Telangana, India
e-mail: mailme.shashi09@gmail.com

R. A. Agarwal et al. (eds.), *Pollutants from Energy Sources*,
Energy, Environment, and Sustainability,
https://doi.org/10.1007/978-981-13-3281-4_9

9.1 Introduction

In numerous nations atomic power plants are an imperative piece of the national vitality framework. Atomic power is economically aggressive and naturally spotless contrasted with most different types of energy utilized as a part of power creation. It provides data on strategies and techniques which can be connected to control of typical radioactive discharges from nuclear power plants, research reactors, critical assemblies and other test facilities. The air pollution problems are common for not only in all types of reactor such as research and power reactors but also in radioisotope and research laboratories. The ventilation and air-cleaning systems play a very important role in universal design of every nuclear facility. The radioactive contamination of the air in working areas can be prevented by a well designed ventilation system. The internal radioactive contamination can be avoided by cleaning of exhaust air in a well designed ventilation system. When designing the ventilation system, it should be kept in mind that the radiation dose rates do not exceed the established international standards. This could be done by monitoring in ducts as well as environment. Nuclear power plants create huge amount of the extremely radioactive spent nuclear fuel on a universal scale. Figure 9.1 shows the classification of radioactive contaminants. Nuclear power plants have produced very low greenhouse gas emission as compared to other renewable energy sources.

Figure 9.2 shows the different sources of radioactive effluents within a NPP. Tritium is responsible for ground water contamination, which is a mildly radioactive type of hydrogen. Ecological Assessment Laboratories (EAL) is very helpful for monitoring the atmosphere at each of the NPP sites. Figure 9.3 shows the role of ecological assessment laboratories. Figure 9.4 shows the ecological impact due to NPP. Chemical reprocessing plants and waste disposal system work as a supporting facilities in NPP.

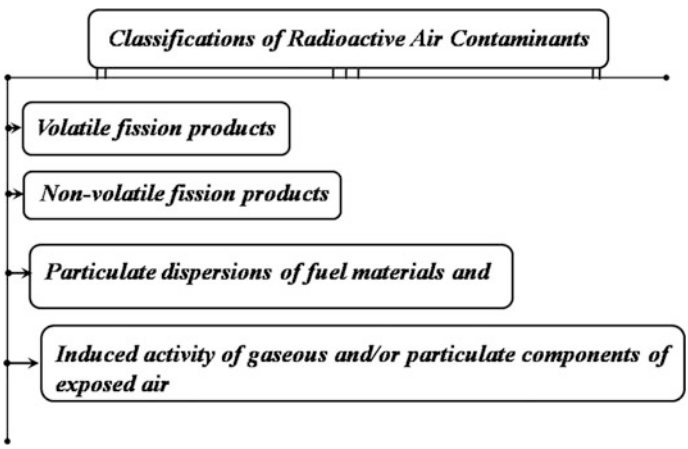

Fig. 9.1 Classification of radioactive contaminants

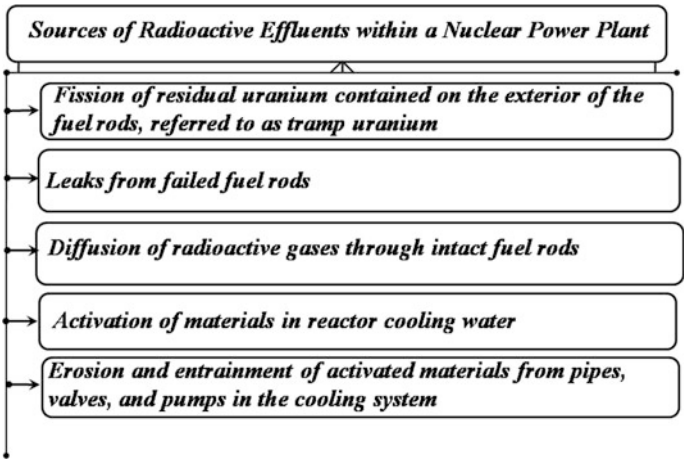

Fig. 9.2 Sources of radioactive effluents within a NPP

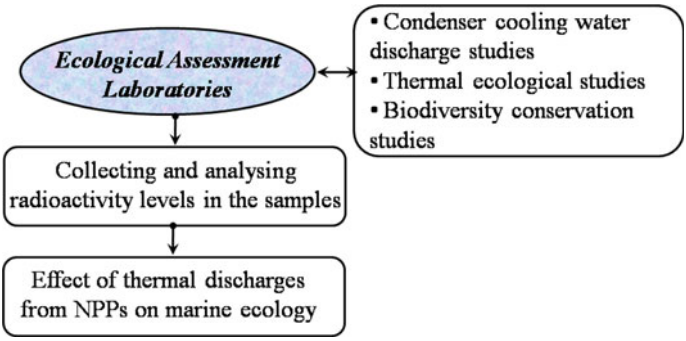

Fig. 9.3 Role of ecological assessment laboratories

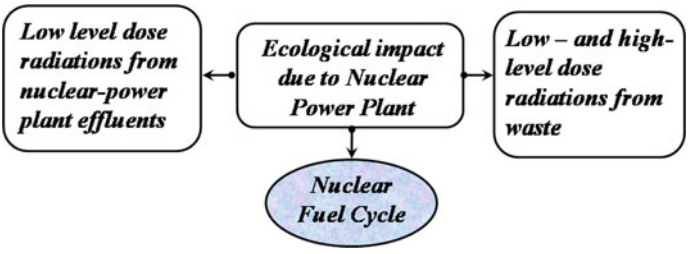

Fig. 9.4 Ecological impact due to NPP

In a chemical reprocessing plant, strong fuel components are broken up and prepared to isolate the un-fissioned uranium from the fission items.

The accessibility, fulfilment, and nature of data on vaporous and fluid radioactive discharges and direct radiation presented from nuclear facilities required to assess dosages for an ecological examination. A nuclear fuel cycle is combination of different stages (uranium recovery, conversion, enrichment, deconversion, fuel fabrication and reprocessing of high level waste) through which extract energy from heavy atoms. Each stage of the nuclear fuel cycle or nuclear fuel chain produces radioactive substances which finally affect the atmosphere. Low-level radioactive waste includes infected hand tools, investigated apparatus from laboratories where radioactive resources are used. High-level wastes are extremely radioactive and it is mostly used nuclear fuel. It requires vigilant supervision over the very long term because it contains long-lived radioactivity and create large amount of heat.

Choi et al. (2017) studied different types of geological disposal systems for spent fuels. They concluded that geological disposal systems are good for long-term supervision of spent fuel from nuclear power plants.

Hamling and Jenkins (2012) analyzed different disposal technique for the gaseous effluents from Nuclear Power Plants. They suggest two different philosophies which are applied to the disposal of radioactive wastes.

Kim et al. (2017) recommend silo farm for efficient removal of very low level decommissioning waste with less reliance on the site situation. They used different arrangement/Shape of silo for his analysis. They calculated decommissioning waste generation from small NPPs by using Eq. (9.1) which is given below:

$$\text{Waste Generation} = \text{WA}_{\text{ref}} \times \left(\frac{c_i}{c_{\text{ref}}}\right)^{0.6} \tag{9.1}$$

where c_i express the target NPP capacity and WA_{ref} is reference amount which was 19,000 drums. c_{ref} denotes the reference NPP capacity which was 1000 MWe in his analysis. They found that the proposed method (silo farm) shows big difference between the options like one-piece disposal, cutting, or melting. For the one-piece volume reduction, the rectangular silos are more efficient than a cylindrical silo because it contains more number of containers (or drums) in each silo along with site area is also significantly decreased (Kim et al. 2017).

9.2 Ventilation and Air-Cleaning Systems

The ventilation and air-cleaning system play an important role for protection of control room employees against radiation. The assessment of a control room outline, particularly its crisis ventilation framework, concerning radiation security principally comprises of deciding the radiation measurements to control room work force under industrial accident conditions. The main functions of ventilation

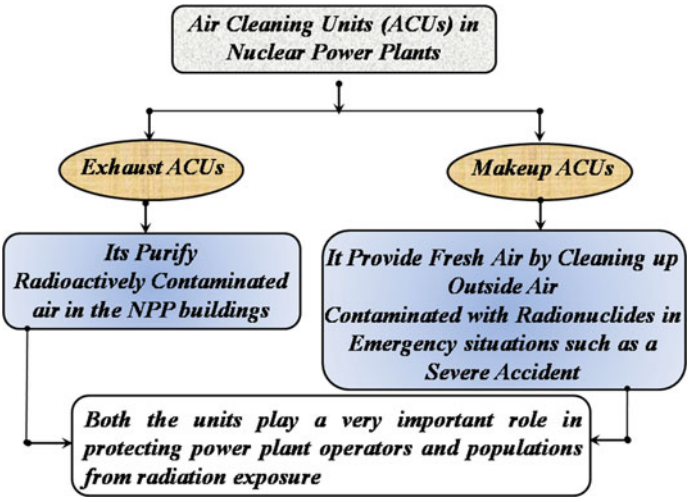

Fig. 9.5 ACUs in NPP

systems are to keep the designed pressure ratios and flow directions and to maintain temperatures below design limits. The ventilation system should also fulfil the other requirements such as heating, cooling, and dust control which is necessary for the comfort of the operators. The effect of radioactive effluent on human resources can be avoided by using healthy intended ventilation system and by using protective devices such as fume-hoods and glove-boxes or respiratory equipment. Figure 9.5 shows the ACUs in NPP.

The expulsion of particulate radioactive material from depletes air or gas is the important characteristic of every single nuclear facilities. The ventilation framework is the vital means for both keeping the spread of radioactivity inside and outside a building and for providing a secure effective atmosphere (IAEA 1991).

9.3 Basic Flow Sheet for Ventilation Design

There are all in all two fundamental ways to deal with outline of a ventilation framework. First one is that the stream of air from the cleanest zones to those zones where air tainting is available or can be relied upon to be available. In this manner, air will ordinarily spill out of hallways and workplaces to general research centre regions, to rage cabinets, hoods and glove boxes or to exceptionally dynamic cells and thereupon out to climate, more often than not through a channel framework. Second ways is arrangement of discrete ventilation frameworks for territories with various levels of pollution. Ductwork is an extremely vital part of exhaust ventilation systems. Ductwork should be design in such a way that it should be avoiding

gathering of radioactive dust within the ducts as discussed in IAEA (1966). In order to fulfil this requirement, it should be avoid sharp bends in construction.

Accessibility, fulfillment, and nature of data on gaseous and liquid radioactive discharges and direct radiation introduction from atomic facilities required to assess measurements for an epidemiologic investigation. The radioactive dust can be decreased or even wiped out by little changes in process tasks or dealing with systems. It is regularly more suitable as regards hazards and economics to offer exhaust filtration at the source of the infected exhaust air rather than immediately former to final exhaust (IAEA 1966). Inspection and cleaning ports in the ductwork can be done without spreading radioactivity to the environment.

9.4 Methods of Removing Vapours and Gases

Apart from aerosols, the air in the atomic power plants may be infected by radioactive gases. The vapours and gases such as noble gases, tritium, iodine and its volatile compounds, formed due to molecular dispersions. Figure 9.6 shows the air cleaning facilities in NPP. The nuclear fission reaction and neutron activation of different substances generates radioactive vaporous and gaseous products. It is troublesome and regularly innovatively difficult to evacuate minute amounts of radioactive vapours and gases from the air of the fumes ventilation. Adsorption and chemisorptions, absorption and retention in storage until the isotope has substantially decayed are the basic methods which can be used for treatment of effluent air containing gaseous radioactive products (IAEA 1966).

The use of High-Efficiency Particulate Filter (HEPA filter) and granular activated carbon filters are shown in figure. Figure 9.7 shows the ecological impact due to process of mining of uranium. Uranium mining and processing affect surface water quality and air quality. The process of mining of uranium creates ecological impact such as carbon emissions, run-off and equipment rehabilitation. Traces of

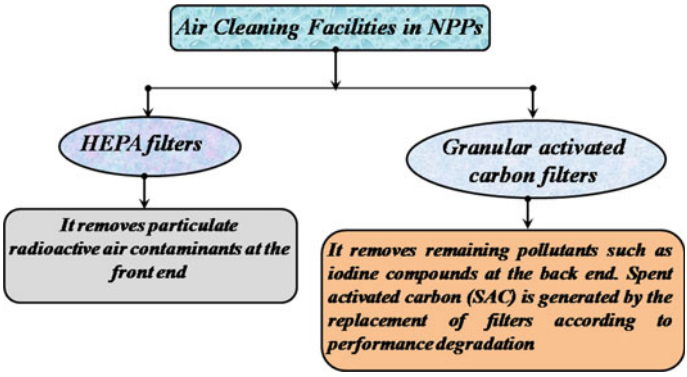

Fig. 9.6 Air cleaning facilities in NPP

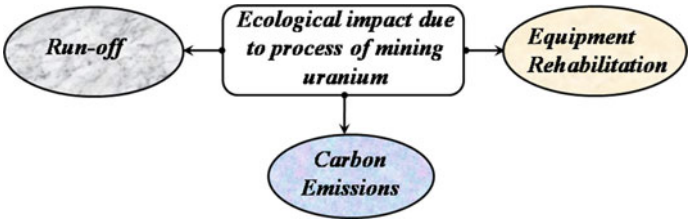

Fig. 9.7 Ecological impact due to process of mining of uranium

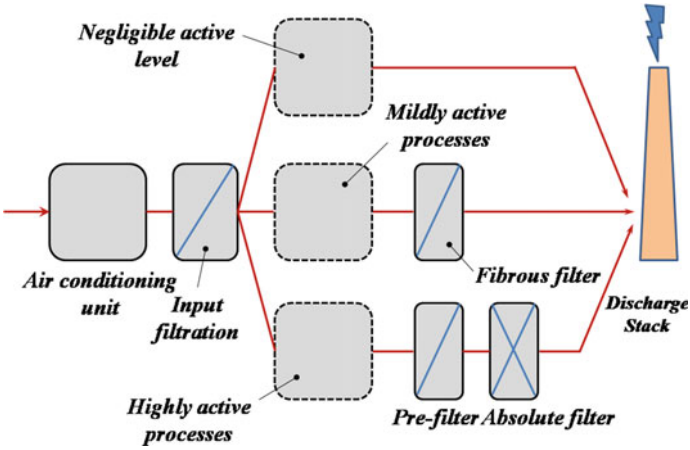

Fig. 9.8 Basic flow sheet for ventilation design (IAEA 1966)

radium and additional metals produce due to run-off of mining uranium which could be harmful to ecological system. The process of mining and milling uranium creates thousand tons of carbon dioxide depending on the rating of the uranium ore.

The negligible active level is nothing but the low magnitude of dust concentration work room as shown in Fig. 9.8. In work-rooms where there is no requirement for respirators or breathing mechanical assembly, the air does not typically need to be filtered before discharge into the climate IAEA (1966). Particular dust enclosures are supplied with confined pre-filters to diminish the dust concentration to a level appropriate for the high-efficiency filters.

9.5 New Developments

The innovative work mirrors the way that the atomic industry and utilities take awesome care in a protected and monetary administration of radioactive waste at atomic power plants, and that changes in existing innovation are foreseen.

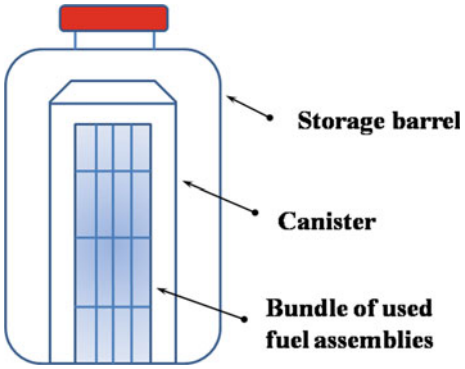

Fig. 9.9 Dry canister storage systems for spent nuclear fuel (Swift 2017)

A progressing push to redesign innovation to limit radioactive release is additionally going on. Swift (2017) discussed about the Dry Storage Systems for Spent Nuclear Fuel (DSSSNF). In this system a certified canister which is used for storage and transportation of spent nuclear fuel. Figure 9.9 shows the dry canister storage systems for spent nuclear fuel (Swift 2017).

9.6 Conclusion

The critical component of the social view of the atomic power industry and its genuine impact on the indigenous habitat is guaranteeing safe transfer of the atomic waste in the way that it secures the earth against unsafe defilement. Even though atomic power plants don't deliver CO_2 or other ozone depleting substances, every year they create a large number of huge amounts of the profoundly radioactive spent atomic fuel on a worldwide scale. Air contamination issues related with atomic power plants could emerge from pollution of the natural environment with these radioactive materials in the event that they are not controlled. In perspective of the qualities and capability of the radioactivity as a natural contaminant and an organic risk, especially for those isotopes with long viable life, the sheltered dealing with and extreme transfer of squanders from the atomic power establishments are fundamental and critical parts of their designs and operations. For developing any nuclear power programme, the waste generation, land and water uses remain a key challenge, which affect our ecosystem. Such issues are perceived with worries that development and task of Nuclear Power Plants (NPPs) must be explored to decrease, limit, or wipe out potential effects. In choosing the suitable reactor innovation, a newcomer nation should choose criteria for reactor plan assessment (Musyoka and Field 2018). Another key challenge associated with improved understanding of the uncertainties in the dose received by humans from internal emitting radionuclides.

The mix of a few scientific procedures radiometric and mass spectrometric enables an extensive variety of radioisotopes to be identified in various sorts of tests, i.e. soil, silt, waters, and in addition squander materials at a low level of fixation. The checking of the earth can subsequently be performed by utilizing these most exceptional instrumental strategies allowing quick disclosure of atomic mischance's and of the scattering of radioactivity into the biosphere.

References

Choi H-J, Lee JY, Choi J (2013) Development of geological disposal systems for spent fuels and high-level radioactive wastes in Korea. Nuclear Eng Technol 45(1)

Hamling BH, Jenkins GF (2012) Disposal of gaseous effluents from nuclear power plants. J Air Pollut Control Assoc 7(4):256–261. https://doi.org/10.1080/00966665.1958.10467812

Kim C-L, Choi Y-J, Lee S-C (2017) Proposal for effective disposal options of very low level decommissioning waste. Prog Nuclear Energy 94:36–45

Musyoka D, Field RM (2018) Review of the environmental oversight framework in Kenya, in light of a nuclear power programme. Prog Nuclear Energy 108:89–98

Safety series no. 17 (1966) Techniques for controlling air pollution from the operation of nuclear facilities. International Atomic Energy Agency Vienna

Swift P (2017) Recent developments in disposal of high-level radioactive waste and spent nuclear fuel. In: Interagency steering committee on performance and risk assessment community of practice, Annual technical exchange meeting Albuquerque NM, Sandia National Laboratories

Technical reports series no. 325 (1991) Particulate filtration in nuclear facilities. International Atomic Energy Agency Vienna

Chapter 10
Advanced Source Inversion Module of the JRODOS System

Ivan Kovalets, Spyros Andronopoulos, Radek Hofman, Petra Seibert, Ievgen Ievdin and Oleksandr Pylypenko

Abstract The development of the source inversion algorithm is described which allows for estimation of the release rates of multiple nuclides and source height with the use of gamma dose rate (GDR) measurements. The method is applicable for the dispersion problems of different spatial scales: from $\sim$1 to $\sim$1000 km. The variational formulation of source inversion problem is used in which unknown release rates of different nuclides are adjusted to minimize the difference of calculated values and measurements. The sensitivities of calculated results with respect to release rates of different radionuclides are calculated with the aid of atmospheric transport model DIPCOT and the source receptor matrix (SRM) is thus constructed. The source inversion problem is regularized using prior (first guess) estimation of release rates. The method is proposed to account for the restrictions on the ratios of the release rates of different radionuclides in formulation of source inversion problem which allows for the assessment of the nuclide composition in radioactive release. The above restrictions are evaluated using the first guess source term. Parameterizations for the regularization parameters of source inversion problem which include root mean squared errors of measurents, first guess release rates, calculated values etc., are developed. The method was successfully tested using

I. Kovalets (✉) · O. Pylypenko
Institute of Mathematical Machines and Systems Problems NAS of Ukraine, Kiev, prosp. Glushkova, 42, Kiev 03187, Ukraine
e-mail: ivkov084@gmail.com

I. Kovalets · I. Ievdin · O. Pylypenko
Ukrainian Center of Environmental and Water Projects, Kiev, prosp. Glushkova, 42, Kiev 03187, Ukraine

S. Andronopoulos
NCSR Demokritos, Institute of Nuclear and Radiological Sciences and Technology, Energy and Safety, Aghia Paraskevi, Attiki, Greece

R. Hofman · P. Seibert
University of Vienna, Althanstr. 14, 1090 Vienna, Austria

I. Ievdin
BfS—Federal Office for Radiation Protection, Ingolstaedter Landstr. 1, 85764 Oberschleissheim, Germany

R. A. Agarwal et al. (eds.), *Pollutants from Energy Sources*,
Energy, Environment, and Sustainability,
https://doi.org/10.1007/978-981-13-3281-4_10

artificial measurements precalculated for the conditions of the ETEX experiment. Pilot implementation of the developed algorithm in the European nuclear emergency response system JRODOS is described.

Keywords Inverse problem · Source term estimation · Radioactive release RODOS

10.1 Introduction

After the accidents at nuclear power plants (NPPs) in Chernobyl and Fukushima a great effort has been spent for the development of algorithms capable of calculation of the source terms following the accident. These algorithms could be subdivided in two broad categories. The algorithms in the first category could be called 'bottom-up' (or process-based) because information concerning technical details of the accident and models of the physical processes in the reactor are used to assess the release rates. Excellent example of the source terms calculated in this way is the library of source terms described by Landman (2007). The difficulty in application of the 'bottom-up' algorithms arises from the very high uncertainty by a factor of 10–100 of their results even when exact information of technical details of the accident is available (US NRC 1990).

The algorithms in the second category could be classified as 'top-down' (or measurement-based) since release rates are evaluated by altering the solution of atmospheric transport model to measuremed values. These 'top-down' algorithms are frequently called also the 'source inversion' algorithms since the described problem is a particular example of the inverse problem occurring in many scientific and practical applications (Tarantola 2005). The drawback of the 'top-down' approach is that the inverse problem is frequently ill-conditioned, i.e., the solution is non-unique (or unstable) unless the problem is properly regularized with the aid of first guess estimations of the release rates which in turn are usually obtainted by using 'bottom-up' approaches.

In present work inverse modeling is employed and the source inversion is treated as a variational data assimilation problem with use of so-called source-receptor matrices (SRMs). The source receptor matrix characterizes sensitivity of calculated values (air concentrations, deposition, gamma dose rates) at points of measurements to values of nuclides emission rates. In present work SRM is calculated in a forward run of atmospheric dispersion model DIPCOT following the approach described by Tsiouri et al. (2012). The above approach was modified to take into account influence of deposition on gamma doses.

SRM concept can be applied both to scenarios where the source location is known or not. Scenarios where the source location is known (a nuclear facility) are considered. The estimated parameters are: (a) isotopic composition of the release,

(b) time-dependent emission rates and (c) effective height of the release. Generally, besides the source term, many other inputs to the dispersion models can be estimated. It is assumed that these inputs—including meteorological fields—are good enough to produce useful results.

This concept was successfully applied in the field of radiation protection (Davoine et al. 2007; Winiarek et al. 2011; Stohl et al. 2012; Saunier et al. 2013). However as a consequence of the described difficulties in achieving of robust solution of the inverse problems the source-inversion algorithms are usually not included in automated real-time decision support systems like JRODOS which are usually used in emergency phase of the accident. A strongly simplified form of source inversion method was developed for operational application in the context of the Comprehensive Nuclear Ban Treaty (Wotawa et al. 2003). In the work of Winiarek et al. (2011), automated algorithms were developed for nearly real-time evaluation of radioactive releases using concentration measurements. However GDRs measurements are much more widely available than concentrations and GDR measurements are routinely collected by every nuclear power plant. The problem of source term estimation based on GDR measurements is especially complex because the nuclide composition of release is poorly known in advance. In a work of Saunier et al. (2013) it was proposed to use information regarding possible ranges of ratios of released inventories of different nuclides to solve the problem of source inversion in case of multiple nuclides using GDR measurements and variational data assimilation method. In the work by Zhang et al. (2017) the Ensemble Kalman Filter was used for the same purpose. In frame of the EU FP7 PREPARE project (Raskob et al. 2016) the automated source inversion algorithm was developed in which GDR measurements collected at different distances from the source could be used to evaluate release rate, source height and nuclide composition of the release. The brief summary of the developed algorithm in frame of the PREPARE project was previously published in short communication by Kovalets et al. (2016). Recently the algorithm was integrated in the EU decision support system in case of nuclear emergencies JRODOS (Ievdin et al. 2010). The present work presents the algorithm and results of its testing in technical detail.

The novelty of present work consists in creation of the algorithm for the identification of the unknown time dependent release rate and nuclide composition following radiological accident using GDR measurements. In this algorithm all regularization parameters are constructed on the basis of the first guess source term provided by user with the aid of empirical parameterizations. The algorithm is implemented in automated Source Inversion Module of the JRODOS nuclear emergency response system and hopefully will become available to the users of the system.

10.2 Source Inversion Method

10.2.1 Source Term Estimation as an Inverse Problem

Consider at first the most general statement of the inverse problem following Tarantola (2005). The observations are combined in a vector $\bar{y} \in R^{N_o}$, where N_o is total number of measurements (in general different than the number of monitoring stations). The model parameters to be found in process of the solution of the inverse problem (such as time distributed source rate and other) are combined in a vector $\bar{x}$ (sometimes called "control vector"), while other parameters which are considered known are combined in vector $\bar{i}$. The model can be understood as—generally non-linear—operator $g(.)$ transforming sources to measurements: $\bar{y} \approx g(\bar{x})$ (approximate equality means that model is imperfect). Denote the conditional distribution function of the observations with given parameter vectors as $P(\bar{y}|\bar{x}, \bar{i})$. Prior information about vector $\bar{x}$ is described by the conditional distribution function $P(\bar{x}|\bar{i})$. Then the inverse problem could be posed as the problem of finding posterior distribution function $P(\bar{x}|\bar{y}, \bar{i})$ of the vector $\bar{x}$ with given vectors $\bar{y}$ and $\bar{i}$. The famous Bayes formula is used: $P(\bar{x}|\bar{y}, \bar{i}) \propto P(\bar{y}|\bar{x}, \bar{i})P(\bar{x}|\bar{i})$.

The important particular case is when distribution functions are Gaussian. Let also the covariance matrix of the distribution be diagonal. Then the distribution functions have the following form:

$$P(\bar{y}|\bar{x}, \bar{i}) \propto \exp\left[-\sum_l \frac{(y_l - g_l(\bar{x}))^2}{\sigma_{O,l}^2 + \sigma_{M,l}^2}\right] \tag{10.1}$$

$$P(\bar{x}|\bar{i}) \propto \exp\left[-\sum_l \frac{(x_l - x_l^B)^2}{\sigma_{B,l}^2}\right] \tag{10.2}$$

Here $\sigma_{B,l}$ is standard deviation of the prior (also called 'background' or 'first guess') estimate of the lth component of the vector $\bar{x}$; $\sigma_{M,l}$ is the rms of model error (provided that correct values of $\bar{x}$ are known) and $\sigma_{O,l}$ is the rms error of observations. Then posterior distribution function is of the form:

$$P(\bar{x}|\bar{y}, \bar{i}) \propto \exp\left[-\left\{\sum_l \frac{(y_l - g_l(\bar{x}))^2}{\sigma_{O,l}^2 + \sigma_{M,l}^2} + \sum_l \frac{(x_l - x_l^B)^2}{\sigma_{B,l}^2}\right\}\right] = \exp(-J). \tag{10.3}$$

Thus maximum of probability distribution function (10.3) coincides with the minimum of function J:

$$J(\bar{x}) = \sum_l \frac{(y_l - g_l(\bar{x}))^2}{\sigma_{O,l}^2 + \sigma_{M,l}^2} + \sum_l \frac{(x_l - x_l^B)^2}{\sigma_{B,l}^2} = (\bar{y} - g(\bar{x}))^{\mathrm{T}} \underline{\underline{R}}^{-1} (\bar{y} - g(\bar{x})) + (\bar{x} - \bar{x}^B)^{\mathrm{T}} \underline{\underline{B}}^{-1} (\bar{x} - \bar{x}^B). \tag{10.4}$$

Here $\underline{\underline{R}}$ and $\underline{\underline{B}}$ are error covariance matrices (diagonal in the present case) representing combined model and measurement errors and first guess errors, respectively: $r_{ll} = \sigma_R^2 = \sigma_{O,l}^2 + \sigma_{M,l}^2$, $b_{ll} = \sigma_{B,l}^2$.

Thus minimization of function (10.4) yields the solution of inverse problem $\bar{x}^S$:

$$\bar{x}^S = \arg\min_{\bar{x}}(J(\bar{x})). \tag{10.5}$$

Below control vector consists (unless noted otherwise) of time distributed emission rates: $\bar{x} = (q_1(t_1), q_2(t_1), \ldots, q_{N_{\mathrm{nu}}}(t_1), \ldots, q_{N_{\mathrm{nu}}}(t_{N_{\mathrm{s}}}))$, where $q_i(t_m)$ is release rate of ith nuclide at time step m, N_{nu} and N_{s} are number of nuclides and of time steps (onto which source function is split) respectively. In this case relationship $g(\bar{x})$ is linear and it is represented with matrix (sometimes called source-receptor matrix SRM): $g(\bar{x}) = \underline{\underline{G}}\bar{x}$, where the elements of SRM are then defined as $g_{ij} = \partial y_j / \partial x_i$.

The linear case is applicable to passive tracers and substances which do not undergo nonlinear chemical transformation and substances with a prescribed decay or growth rate, e.g. radionuclides (Seibert et al. 2002). In this case, the minimization problem (10.5) is a linear regression problem of minimizing the cost function

$$J(\bar{x}) = (\bar{y} - \underline{\underline{G}}\bar{x})^{\mathrm{T}} \underline{\underline{R}}^{-1} (\bar{y} - \underline{\underline{G}}\bar{x}) + (\bar{x} - \bar{x}^B)^{\mathrm{T}} \underline{\underline{B}}^{-1} (\bar{x} - \bar{x}^B) = J_1 + J_2 \tag{10.6}$$

Note that second term J_2 ensures strict convexity of the cost function (10.6) and thus uniqueness of the solution of minimization problem. Therefore, this term 'regularizes' the solution of (10.5). Without regularization the problem may be ill-conditioned, i.e. the solution is non-unique or unstable with respect to small changes in the parameters of the problem or with respect to numerical errors.

10.2.2 Nuclide Composition and Augmented Minimization Problem

The most common quantities used in the inversion of sources of radioactivity emitted into the atmosphere are the atmospheric activity concentration, the surface contamination (deposition) and the GDR from the cloud and deposited activity. Activity concentration and deposition measurements provide nuclide-specific data which can be used for estimation of isotopic composition of the release. In a few countries, concentration measurements of radioactivity are routinely available and

are used for source estimation (Winiarek et al. 2011). Many NPPs have the possibility to perform concentration measurements on an irregular basis, for instance, by using mobile laboratories in the case of a hypothetical release and measuring daily (or sub-daily) averaged concentrations of aerosols and nuclides of the iodine group. A significant obstacle in using these data in real-time applications is their poor time resolution, where sampling times are hours or even days long. Nevertheless, these data were successfully used for source inversion of the Fukushima disaster by Stohl et al. (2012), in tandem with the Lagrangian atmospheric transport model FLEXPART (Stohl et al. 2005).

Receptors measuring GDR are the most widespread observation system. Unless devices for in situ spectrometry are used, these data provide only bulk measurements of gamma dose from cloud and deposition with no information on isotopic composition of the release. However, these data provide real-time information on plume passage with high temporal resolution and networks of these receptors are present around every nuclear installation or even country-wide and are relatively dense.

For source term estimation using GDR measurements with the present method, at least approximate knowledge of nuclide ratios is assumed. Following Hofman et al. (2015) the method based on minimization of the cost function (10.6) is modified in a way that it can be used for inversion of a source term with multiple nuclides using bulk GDR measurements. Nuclide ratios enter the problem in the form of additional linear equations, where the deviations from prescribed ratios are weighted by factors. The error variance of these deviations allows to control how strictly the prescribed ratios are fulfilled.

Firstly, let us illustrate the method with a simple case—a release of Xe-133, I-131 and Cs-137. If release rates for the respective radionuclides are denoted with x_1, x_2 and x_3, the nuclide ratios are formulated as follows (constants are assumed for the sake of the example here): $x_1 = 10x_2$, $x_1 = 2x_3$. This can be re-written as

$$\begin{aligned} x_1 - 10x_2 &= 0 \\ x_1 - 2x_3 &= 0. \end{aligned} \tag{10.7}$$

The above equations are used to augment our cost function. It then reads as follows:

$$J(\bar{x}) = (\tilde{y} - \underline{\underline{\tilde{G}}}\bar{x})^{\mathrm{T}} \underline{\underline{\tilde{R}}}^{-1} (\tilde{y} - \underline{\underline{\tilde{G}}}\bar{x}) + (\bar{x} - \bar{x}^B)^{\mathrm{T}} \underline{\underline{B}}^{-1} (\bar{x} - \bar{x}^B) = J_1 + J_2. \tag{10.8}$$

Here $\tilde{y}$ and $\underline{\underline{\tilde{G}}}\bar{x}$ are augmented in a way that Eqs. (10.7) added to $\tilde{y} - \underline{\underline{\tilde{G}}}\bar{x}$:

$$\begin{bmatrix} y_1 \\ \vdots \\ y_m \\ 0 \\ 0 \end{bmatrix} - \begin{bmatrix} g_{11} & g_{12} & g_{13} \\ \vdots & \vdots & \vdots \\ g_{1m} & g_{2m} & g_{3m} \\ 1 & -10 & \\ 1 & & -2 \end{bmatrix} \begin{bmatrix} x_1 \\ x_2 \\ x_3 \end{bmatrix}. \tag{10.9}$$

Correspondingly, the observation error covariance matrix $\underline{\underline{R}}^{-1}$ is augmented by inversions of variances of ratio conditions deviations:

$$\underline{\underline{\tilde{R}}}^{-1} = \begin{bmatrix} \sigma_{y_1}^{-2} & & & & \\ & \ddots & & & \\ & & \sigma_{y_m}^{-2} & & \\ & & & \sigma_I^{-2} & \\ & & & & \sigma_{Cs}^{-2} \end{bmatrix}. \tag{10.10}$$

Coefficients σ_{I}^2, σ_{Cs}^2 determine how large variances are allowed for errors in (10.7): $\sigma_{\mathrm{I}}^2 = E\left((x_1 - 10x_2)^2\right)$, $\sigma_{Cs}^2 = E\left((x_1 - 2x_3)^2\right)$, and symbol E stands for the expected value. Thus besides the ratios of nuclide release rates the augmented algorithm requires the specification of their error variances as well. These inputs will be discussed below in Sect. 10.2.4.

Extension of the definition of the above augmented matrices to a general case when there is total number of N_{nu} nuclides and the source function is discretized with the total number of N_{s} time steps is straightforward. Obviously it is not necessary to use ratios of release rates of different nuclides to release rate of only the first nuclide. On the contrary, as it will be demonstrated below in Sect. 10.2.4, if the 1st nuclide is noble gas, the range of uncertainties for the ratios $a_{i,m} = x_{(m-1)N_{\mathrm{nu}}+i}/x_{(m-1)N_{\mathrm{nu}}+1}$ (here m stands for time index) will be too large for all indices i which do not correspond to noble gas. Therefore the following function is defined:

$$J(i) = \{j \in (1, \ldots, N_{\mathrm{nu}}), j \neq i\}. \tag{10.11}$$

Equation (10.11) sets correspondence between nuclide number i and nuclide number j with respect to which ratio of release rates $a_{i,m} = x_{(m-1)N_{\mathrm{nu}}+i}/x_{(m-1)N_{\mathrm{nu}}+J(i)}$ is calculated. Obviously, for each time step there could be set $N_{\mathrm{nu}} - 1$ nuclide ratios. The specific form of $J(i)$ implemented for usage in the JRODOS system will be described below in Sect. 10.2.4.

10.2.3 Source-Receptor Matrix

In this work the aim is to estimate the release rate for each of multiple simultaneously released radionuclides significantly contributing to the GDRs measured at receptors. Although the source location is well known in our scenario, all possible release intervals $s: 1 \le s \le N_s$ of all nuclides $i: 1 \le i \le N_{nu}$ must be treated as separate sources in order to achieve this. Under this assumption, each elements g_{lk} of the SRM matrix $\underline{\underline{G}}$ represents the contribution of a source $k = (s-1) \cdot N_{nu} + i$ releasing a particular nuclide i at a given time interval s to total GDR measurement l sampled in a particular time-space point (interval). In the case when also the effective height of the release is to be estimated, sources index i in $\bar{x}$ and $\underline{\underline{G}}$ will also have to iterate over vertical release intervals.

Here the algorithm of SRM calculation implemented in Lagrangian puff model DIPCOT of JRODOS is presented. In contrast to Lagrangian particle model, in Lagrangian puff models puffs are characterized by their finite size (as in Gaussian puff models) but, as in Lagrangian models, turbulent mixing is taken into account by adding in the right part of the equation of puff's movement the wind fluctuations in addition to Reynolds-averaged wind field. This approach leads to significant reduction in computational time in the Lagrangian puff model as compared to Lagrangian particle model. This approach had been studied theoretically by De Haan and Rotach (1998) and widely applied practically. In particular, the Lagrangian puff version of DIPCOT has been extensively validated over numerous wind tunnel and field experiments [see the results referenced in Andronopoulos et al. (2009, 2010) and Davakis et al. (2007)].

Although DIPCOT atmospheric dispersion model does not take into account such processes as resuspension of radionuclides, diffusion in soil, and wash-out, it is likely that those processes are more important in the long term (months and years after the accident), while in emergency phase and for time scales of the few days after the release which correspond to the spatial scale of the dispersion problem up to $\sim$1000 km the above processes are of minor importance.

In the next three sections elements of SRM are derived at first for the simplified case of single point source with the number of release intervals coinciding with the number of puffs $N_s = N_p$. Extension of the presented relationships for the case of multiple sources is straightforward. Extensions of SRM relationships for the case of release intervals of realistically large duration are discussed in Sect. 10.2.3.

10.2.3.1 SRM Calculation in Case of Concentration Measurements

In all kinds of puff models concentration at a given point (x, y, z) and time t is calculated using the relationship (single nuclide is considered for simplicity):

$$C(x,y,z,t) = \frac{1}{(2\pi)^{3/2}} \sum_{p=1}^{N_p} \frac{M_p}{\sigma_{xp}\sigma_{yp}\sigma_{zp}} \exp\left[-\frac{1}{2}\frac{(x_p - x)^2}{\sigma_{xp}^2}\right] \exp\left[-\frac{1}{2}\frac{(y_p - y)^2}{\sigma_{yp}^2}\right]$$
$$\left\{\exp\left[-\frac{1}{2}\frac{(z_p - z)^2}{\sigma_{zp}^2}\right] + \exp\left[-\frac{1}{2}\frac{(z_p + z - 2z_g)^2}{\sigma_{zp}^2}\right]\right\},$$
$$M_p = q_p \tau \gamma(t,\tau,p) \times \Upsilon(t,\lambda,\ldots). \tag{10.12}$$

Here τ is time interval between appearance of successive puffs, N_p is the number of puffs, (x_p, y_p, z_p)—coordinates of puff's centre, (σ_{xp}, σ_{yp}, σ_{zp})—dispersions of matter distribution in a puff (calculated using different parameterizations), z_g—height of ground surface above sea level, M_p inventory of a puff (total amount of radioactivity in Bq), q_p—source rate corresponding to appearance of pth puff, function $\gamma(t,\tau,p) = \mathrm{sgn}(t - p\cdot\tau)$ excludes influence of puffs appeared after time t. Term $\Upsilon(t,\lambda,\ldots)$ in generalized form takes into account radioactive decay, dry and wet deposition. For instance in the case of noble gases, when deposition is absent, $\Upsilon(t,\lambda,\ldots) = \exp(-\lambda(t-(p-1)\tau))$, and λ is the radioactive decay constant.

In Eq. (10.12) full reflection of the plume at the ground surface is assumed. Variations of Eq. (10.12) are possible to take into account reflection from the upper lid of the mixing layer, multiple nuclides with transformations described by matrix, etc. However in all cases it is possible to derive analytical relationships for the elements of source-receptor matrix.

Say, if relationship (10.12) is used, then for the case of instantaneous concentration at a spatial point $\bar{r}_j$ at particular time t^k, the elements of source-receptor matrix are calculated using the formula: $g^{(c)}_{l,(p-1)\cdot N_{nu}+i} = g^{(c)}\left(\bar{r}_j, t^k, p, i\right)$. Here index l corresponds to the number of measurements (according to their storage in vector $\bar{y}$), $g^{(c)}(\bar{r}_j, t^k, p, i) = \partial C(\bar{r}_j, t^k)/\partial q_{p,i}$ obtained from formula (10.12) is the sensitivity of model-calculated concentration with respect to inventory of ith radionuclide in puff p, $g^{(c)}_{l,(p-1)\cdot N_\mathrm{nu}+i}$ is the corresponding element of matrix $\underline{\underline{G}}$.

10.2.3.2 SRM Calculation in Case of Deposition Measurements

Dry deposition C_d of the nuclide i in a given spatial point j characterized by the position vector $\bar{r}_j$ is calculated using the equation:

$$\frac{\mathrm{d}C_{d,i}(t,\bar{r}_j)}{\mathrm{d}t} = F_\mathrm{d}(t,\bar{r}_j)C_a(t,\bar{r}_j) - \lambda_i C_\mathrm{d}(t,\bar{r}_j). \tag{10.13}$$

Here the first term in the r.h.s. described deposition flux, which is proportional to ground-level concentration C_a in the point of interest; proportionality coefficient F_d

depends on land use, friction velocity, etc. The second term describes radioactive decay of the deposited radioactivity.

Provided that initial deposition is zero the solution of the above equation depends on time in a following way:

$$C_{\mathrm{d},\mathrm{i}}(t,\bar{r}_j) = \int_0^t F_{\mathrm{d}}(\tau,\bar{r}_j)C_a(\tau,\bar{r}_j)\exp(-\lambda_i(t-\tau))\mathrm{d}\tau. \tag{10.14}$$

In model run the above integral is approximated by sum which is calculated in a time loop:

$$C^n_{\mathrm{d},i}(t^k,\bar{r}_j) = \sum_{n=0}^{k} F_{\mathrm{d}}(n\cdot\mathrm{d}\tau,\bar{r}_j)C^n_a(n\cdot\mathrm{d}\tau,\bar{r}_j)\exp(-\lambda_i(t^k-n\cdot\mathrm{d}\tau))\mathrm{d}\tau. \tag{10.15}$$

Calculation of sum in r.h.s. of the above equation is performed in a time loop (index n). Let lth element y_l of measurement vector $\bar{y}$ is deposition at point $\bar{r}_j$ and at time t_k. Using the above formula the elements of the lth row of SRM corresponding to deposition measurements are calculated using the formula:

$$\begin{aligned} g^{(\mathrm{dep})}_{l,(p-1)\cdot N_{nu}+i} &= g^{(\mathrm{dep})}(\bar{r}_j,t^k,p,i) \\ &= \sum_{n=0}^{k} F_{\mathrm{d}}(n\cdot\mathrm{d}\tau,\bar{r}_j)g^c(\bar{r}_j,t^n,p,i)(n\cdot\mathrm{d}\tau,\bar{r}_j)\exp(-\lambda_i(t^k-n\cdot\mathrm{d}\tau))\mathrm{d}\tau. \end{aligned} \tag{10.16}$$

Here the same as above $g^{(\mathrm{dep})}(.)$ and $g^{(\mathrm{dep})}_{*,*}$ are sensitivity function of model-calculated deposition with respect to inventory of ith radionuclide in puff p and the corresponding element of SRM. Thus in a time loop the elements of SRM corresponding to deposition measurements are updated using relationships for $g^{(c)}$ according to formula (10.16). It should be noted that change of deposition due to vertical diffusion in soil, wash-out, resuspension, etc. is not taken into account in DIPCOT and hence not accounted for in SRM calculation.

10.2.3.3 SRM Calculation in Case of GDR Measurements

Ambient gamma radiation is created by airborne radionuclides and by deposition. GDR created by deposition is calculated in DIPCOT in a given point using the assumption of infinite homogeneous deposition. The resulting GDR value linearly depends on depositions of radionuclides at a given location.

There are different methods of calculating GDR from cloud using puff data. The methods range by the level of complexity from simplified method of infinite cloud

approximation to comprehensive 3D integration. The method of intermediate level of complexity recently implemented in DIPCOT (Andronopoulos and Bartzis 2010) closely approximates full 3D integral while retaining computational efficiency. However for all kind of methods of GDR calculation the resulting values are linear combination of concentration fields and hence puff inventories.

Therefore in simplest case of infinite cloud approximation elements $g^{(gdr)}$ of source-receptor matrix corresponding to GDR measurements are calculated as linear combination of $g^{(\mathrm{dep})}$ and $g^{(c)}$:

$$g^{(gdr)}_{l,(p-1)\cdot N_{nu}+i} = \beta_c \cdot g^{(c)}(\bar{r}_j, t^n, p, i) + \beta_d \cdot g^{(\mathrm{dep})}(\bar{r}_j, t^n, p, i). \tag{10.17}$$

In the case of more complex method of calculation of GDR from the cloud, the second term in the above equation is preserved, while the first term is calculated using the relationships presented by Tsiouri et al. (2012).

10.2.3.4 Reduction of Control Vector

In the case of the Lagrangian puff model, the elements of source-receptor matrix are stochastic variables and this creates difficulties in direct usage of that matrix in the solution of the inverse problem. This difficulty can be overcome by the simple approach used by Tsiouri et al. (2012). Assume that during some interval Δt the source rate could be considered constant. This is a common assumption in all existing accidental scenarios. For instance, in all of the scenarios existing in JRODOS (Landman 2007) the value of Δt is in the range $10^3 - 10^4$ s. At the same time, the time interval between appearance of successive puffs in Lagrangian model is typically much shorter $\tau \approx 0.1-10$ s. Thus practically $\Delta t/\tau = \Pi \gg 1$.

Then the release period can be divided in N_s time intervals of size Δt with Π puffs in each time interval, so that total number of puffs is $N_\mathrm{P} = \Pi \cdot N_\mathrm{s}$. Even when $\Delta t = 10$ minutes, the value of Π will be large (taking into account the above estimates for τ). In each interval m $(1 \le m \le N_\mathrm{s})$ the release rate can be considered equal to q_m; the values of q_m constitute the reduced control vector $\bar{x}$ of size N_s.

In the 'reduced' (and regularized) minimization problem the cost function is minimized with respect to the reduced control vector $\bar{x}$. Elements of source-receptor matrix $\underline{\underline{G}}$ corresponding to reduced minimization problem are obtained by summing elements of source receptor matrix (let's denote it here g^{full}) corresponding to 'full' minimization problem (i.e. in which control vector consist of individual inventories of each puff):

$$g_{l,m} = \sum_{p=1}^{\Pi} g^{\mathrm{full}}_{l,((m-1)\Pi+p)}, \quad \forall l, m : 1 \le l \le N_o, 1 \le m \le N_\mathrm{s}. \tag{10.18}$$

According to Central Limit Theorem statistically stable values of $g_{l,m}$ are obtained when Π are large enough.

The described regularization procedure has been previously implemented within the DIPCOT model (Tsiouri et al. 2012) and tested against field measurements of GDRs. The case of only one nuclide and GDR only from cloud has been considered in those works.

10.2.4 Parameters of the Minimization Problem

10.2.4.1 First Guess Estimation of Source Term and Its Error Variances

As it was mentioned in previous sections, the usage of the prior information about the source term via the second term in the r.h.s. of Eq. (10.6) regularizes the solution of minimization problem. This form of regularization is useful when a first guess of emissions of particular nuclides exists (e.g. from accident-based analysis like MELCOR calculations (https://melcor.sandia.gov). The task of assignment of the first guess estimation of the source term is to be carried out by the user of the JRODOS system prior to running source inversion algorithm. The library of existing in JRODOS pre-defined source terms (Landman 2007) could assist in this task. The JRODOS system allows user extending this library by importing source term created by user into JRODOS database (Ievdin et al. 2015).

Once the first guess source term is provided, the error variances of this prior source term estimation are to be estimated. For the real-time applicability of the method robust simplifications are frequently applied, usually assuming error variance to be certain fraction of some norm of the source function, such as average or maximum value of the source function through the release interval (Tsiouri et al. 2012; Winiarek et al. 2011). In the present work, the same simplification is used: magnitude of error variance $\sigma_{B,i}$ of first guess source rate for the ith nuclide $\bar{x}_i^B$ is set equal to a certain fraction of its maximum value during the release period:

$$\sigma_{B,i} = \alpha_B \left\| \bar{x}_i^B \right\| = \alpha_B \max_m (x_{i,m}^B). \tag{10.19}$$

The particular value for α_B to be used by default in operational applications of the method could be assessed from the fact that the first guess estimations of the source term are usually characterized by very high uncertainty by a factor of 10–100 (US NRC 1990). If, for instance, there is a constant release of a single nuclide with the release rate estimated as q_B and true release rate is expected to be found within the interval $(0.1q_B, 10q_B)$; this situation yields the estimate: $\sigma_B \approx 5q_B$. Thus the value of $\alpha_B = 5$ could be proposed to be used by default in emergency situations when first guess source term are characterized by high levels of uncertainty.

Note, that the example described above corresponds to the skewed probability distribution of the first guess estimation, while the Bayesian formulation (10.1–10.3) leading to cost function (10.6) assumed Gaussian distributions. Resolving of such controversy requires a change in the cost function as shown in work of Bocquet (2008), and could be subject for future research.

10.2.4.2 Error Variances of Observed and Model-Calculated Values

Let's consider rms errors of observations $\bar{\sigma}_{\mathrm{O}}$ and of model $\bar{\sigma}_{\mathrm{M}}$. For implementation of source inversion algorithms in a real-time emergency response system like JRODOS some automatic procedure should exist for their assignment. Recall that observations and model errors enter the cost function (10.6) through the covariance matrix $\underline{\underline{R}}$ having diagonal elements $r_{ll} = \sigma_R^2 = \sigma_{O,l}^2 + \sigma_{M,l}^2$. Let's consider at first the error of observations. It consists of the instrumental error σ_{d} of the measurement device and an additional error which is introduced by the existence of a background field φ of the measured quantity (e.g. background GDR). The user may wish to discard measurements which are close to the average value of the background field φ_0, therefore the error variance of observations is set to

$$\sigma_o = \alpha_\varphi \varphi_0 + \sigma_{\mathrm{d}}. \tag{10.20}$$

Here the value of α_φ depends on type of measurements and magnitude of natural perturbations of background field. For instance, in Ukraine the background GDR is about $\varphi_0 = 10^{-4}$ mSv/h, while the lowest GDR levels which can be used for alarm are considered between $1.5\varphi_0$ to $3\varphi_0$. Therefore the default value for $\alpha_\varphi = 2$ could be proposed for GDR measurements. In general the measurements which are close to background value contain also some useful information, especially in complex release and atmospheric transport patterns therefore by adjusting α_φ the user can control the degree to which such measurements are taken into account.

One possible choice of the value for observational error σ_{d} is to set it proportional to the measured value

$$\sigma_{d,i} = c_1 y_i + c_0, \tag{10.21}$$

where the constant of proportionality, c_1, is specified, e.g., by the manufacturer of a measuring device or by an expert estimate (Seibert et al. 2011; Tsiouri et al. 2011); c_0 can represent a "background value", a minimum measurable value. For the robust usage of source inversion method the information about the values of c_1, c_0 should ideally be present in JRODOS measurement database for each measurement station. However presently such data are absent in JRODOS database. Therefore the default value $c_0 = 2 \times 10^{-5}$ mSv/h is assumed for GDR measurements, typically characterizing such measurements used at Ukrainian NPPs. The value of c_1 is not taken into account in calculating σ_{d} since as far as for model error σ_{M} its

proportionality to measurement values is also assumed below; the value of c_2 could be implicitly taken into account in calculating σ_M.

The estimation of model error σ_M is problematic. It can be, for example, be estimated using statistics of an ensemble of different dispersion models or one model with different inputs for a given source vector $\bar{x}$. Real-time application of such method is difficult. Therefore, in the present work the simple assumption is used:

$$\sigma_{m,i} = \alpha_m y_i. \tag{10.22}$$

The value of α_m could be estimated from the following considerations. Recall that the physical meaning of σ_m is the error of model provided that exact values for the control vector (source term) are known. Therefore in σ_m errors of different parameters that are known approximately but do not enter control vector (meteorology, parameters of turbulent mixing parameterizations, etc.) are implicitly taken into account.

In numerous validation studies of atmospheric dispersion models, a commonly used statistics for measuring model performance against measurements is the normalized mean squared error: $\mathrm{NMSE} = \left\langle (y_m - y_o)^2 \right\rangle / \langle y_m \rangle \langle y_o \rangle = \sigma_m^2 / \langle y_m \rangle \langle y_o \rangle$. The values of NMSE in different studies range from 0.5 to 10 and more. As it could be seen from the above relationship the following approximation for α_m could be proposed: $\alpha_m \approx \sqrt{\mathrm{NMSE}}$. The default value $\alpha_m = 1$ is proposed.

10.2.4.3 Ratios of Release Rates for Different Nuclides and Corresponding Error Variances

The modified formulation of the minimization problem was described in Sect. 10.2.2, which is used to take into account information regarding ratios of source rates of different nuclides consisting of release composition. Nuclides are subdivided into groups, and release ratios are calculated for different nuclides within each group with respect to the 'reference' nuclide representing each group. Additionally, ratios of release rates between 'reference' nuclides are calculated (Fig. 10.1). By default 3 groups of nuclides are used: Noble gases, Iodine and Aerosols.

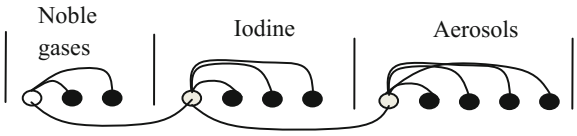

Fig. 10.1 Scheme of calculating ratios between nuclides: vertical lines denote groups of nuclides; empty circle—representative nuclide within group; curved lines connect nuclides for which ratios of release rates are calculated

Now let's consider the issue of how ratios of source rates of different nuclides are calculated. Such ratios are calculated using first guess estimation of source term. Using the notation introduced in Sect. 10.2.2, relationships for ratios (which are generally time dependent) could be rewritten as: $a_{i,m} = x^B_{(m-1)N_{\text{nu}}+i} / x^B_{(m-1)N_{\text{nu}}+J(i)}$. The relationship *J(i)* was introduced in (10.11).

In reality release ratios are time dependent. For instance, in many source term scenarios noble gases are emitted at first, while aerosols are released later. The corresponding time dependence of release ratios could be theoretically evaluated from first guess source term. However in practical situations when exact start time of emissions is not known it is not reasonable to use time dependent prior release ratios assessed from first guess source term since time dependence of true release ratios depends on start time of emission. Therefore at first *time integrated* ratios of the release rates of different nuclides are calculated from the first guess source term:

$$a_i = \sum_{m=1}^{N_s} \left(x^B_{(m-1)N_{\text{nu}}+i} / x^B_{(m-1)N_{\text{nu}}+J(i)} \right). \tag{10.23}$$

For those time steps at which the denominator in (10.23) is zero, the corresponding ratio is set to a large value ($a_{\text{inf}} = 10^5$). However, if in the first-guess source term nuclides are present for which the total released inventory through the whole release period is zero, such nuclides are excluded from the minimization problem and the source term for such nuclides is not analyzed. Elements of the solution vector for such nuclides remain zero. Therefore, the denominator in (10.23) is always greater than zero.

Then, as described above, the matrix $\underline{\underline{G}}$ and the observation vector $\bar{y}$ are augmented with elements corresponding to relationships:

$$x_{(m-1)N_{\text{nu}}+i} - a_i x_{(m-1)N_{\text{nu}}+J(i)} = 0. \tag{10.24}$$

Of course, the solution of augmented minimization problem (10.8) satisfies relationships (10.24) only approximately and corresponding error variances

$$\tilde{\sigma}^2_{R,i} = \mathrm{E}\left(\left(x_{(m-1)N_{\text{nu}}+i} - a_i x_{(m-1)N_{\text{nu}}+J(i)} \right)^2 \right), \tag{10.25}$$

are to be estimated and used in the augmented matrix $\underline{\underline{\tilde{R}}}$ which was introduced above. In the minimization process, $\tilde{\sigma}_R$ are used as measures of allowable deviations of the r.h.s. of Eq. (10.24) from zero.

Let's consider the issue of $\tilde{\sigma}_R$ estimation. Consider for simplicity the case of two nuclides with corresponding estimated (analysed) release rates q_1, q_2 considered as random variables and ratio of release rates a: $q_2 - a \cdot q_1 = 0$. Let the random variable $a = a_0 + \delta a$ have the expected value $E(a) = a_0$ and variance $E\left((a-a_0)^2\right) = \sigma_a$. Then consider the random variable ξ: $\xi = q_2 - a_0 q_1 = q_2 - (a - \delta a) q_1 = \delta a \cdot q_1$.

It is clear that the expected value of ξ: $E(\xi) = 0$, while variance of ξ: $E(\xi^2) = \sigma_a \cdot \sigma_{q_1}$. The well-known theorem about the expected value and variance of the product of uncorrelated random variables is used in the above considerations. Of course, the variance of the analysed source rate σ_{q_1} is not known, but it can be approximated with the corresponding variance of first guess estimation: $\sigma_{q_1} \approx \sigma_{B,1}$. The above considerations are easily extended yielding the relationship:

$$\tilde{\sigma}_{R,i} = \sigma_{a,i} \cdot \sigma_{B,J(i)}, \tag{10.26}$$

where $\sigma_{B,J(i)}$ are estimated using (10.19).

The values of $\sigma_{a,i}$ could be pre-calculated in advance on the basis of several source terms generated for a given accident scenario using process-based tools for source term estimation such as MELCOR (https://melcor.sandia.gov) and/or using expert estimations. However, if such pre-calculated values of $\sigma_{a,i}$ are not available, JRODOS is to be able to provide automatic assessment of those parameters. For this purpose, expert estimations for the bounds of possible ratios of inventories released for different nuclides for the case of the Fukushima accident presented by Saunier et al. (2013) as:

$$0.6 \le \frac{x_{132\mathrm{Te}}(t)}{x_{134\mathrm{Cs}}(t)} \le 16; \quad 2 \le \frac{x_{131\mathrm{I}}(t)}{x_{134\mathrm{Cs}}(t)} \le 100; \quad 0.1 \le \frac{x_{133\mathrm{Xe}}(t)}{x_{134\mathrm{Cs}}(t)} \le 10^4, \tag{10.27}$$

were compared to bounds for release ratios obtained on the basis of literature review by Kovalets et al. (2014):

$$5 \le \frac{x_{132\mathrm{Te}}(t)}{x_{134\mathrm{Cs}}(t)} \le 150; \quad 6 \le \frac{x_{131\mathrm{I}}(t)}{x_{134\mathrm{Cs}}(t)} \le 130; \quad 0 \le \frac{x_{133\mathrm{Xe}}(t)}{x_{134\mathrm{Cs}}(t)} \le 5 \times 10^4. \tag{10.28}$$

From the above data it could be concluded that in all cases the ratio between upper (a_U) and bottom (a_B) bounds of release ratios: $\omega = a_U/a_B$ varies from $\omega = 20$ to $\omega = 50$ between non-noble gas nuclides and $\omega \ge 10^5$ for the ratios of release rates of noble gas/to non-noble gas nuclide.

Let us assume that for the case of non-noble gas nuclides a is Gaussian-distributed with the expected value a_0 and hence $a_U \approx a_0 + 2\sigma_a$, $a_B \approx a_0 - 2\sigma_a$ (known property of Gaussian distribution is that with 95% probability the value of a is found in the interval $(a_0 - 2\sigma_a, a_0 + 2\sigma_a)$). Let us assume $\sigma_a = \alpha_a \cdot a_0$ and substitute this into the above definition of ω: $\omega = a_U/a_B = (a_0 + 2\alpha_a \cdot a_0)/(a_0 - 2\alpha_a \cdot a_0)$. Then the value of $\alpha_a = 0.5$ fits well the above range of $\omega = 20{-}50$.

In case when a is the ratio of release rates of noble gas to non-noble gas nuclides, it spans a too large range of values and it is most likely that its probability distribution is skewed (non-Gaussian). Analogous situation was considered above for the case of error variance of first guess estimation and in the same way the value of $\alpha_a = 5$ could be reasonably used to define $\sigma_a = \alpha_a \cdot a_0$ in such a case.

Since first guess source terms are usually time dependent, instead of using the above parameterizations for σ_a, it can be defined alternatively from the first guess source term:

$$\sigma_{a,i}^{(1)} = \sqrt{\frac{1}{N_s}\sum_{m=1}^{N_s}\left(\left(x^B_{(m-1)N_{nu}+i}/x^B_{(m-1)N_{nu}+J(i)}\right) - a_i\right)^2}, \tag{10.29}$$

where a_i was defined by (10.23).

Both methods are combined for calculating σ_a by choosing the maximum out of the two values obtained using each method:

$$\begin{aligned} \sigma_{a,i} &= \max\left(\sigma_{a,i}^{(1)}, \sigma_{a,i}^{(2)}\right) \\ \sigma_{a,i}^{(2)} &= \alpha_a \cdot a_i, \end{aligned} \tag{10.30}$$

where in (10.30) $\alpha_a = 0.5$ is the default value used for ratios between release rates of non-noble gas nuclides (aerosols, iodine) or between noble gas nuclides (e.g. ratios of release rates of Xe-133 to Kr-85), while $\alpha_a = 5$ is the default value used for ratios of release rates of non-noble gas nuclide to noble-gas nuclide (e.g. Cs-137 to Xe-133). Note that according to Fig. 10.1 the ratio of the last type appears only once out of total number of $N_{nu} - 1$ ratios which are used if release consists of N_{nu} nuclides.

10.2.5 Release Height Estimation

A possibility to establish release height which was used in many works is to consider a vertically distributed release e.g. Talerko (2005), Stohl et al. (2012). In this case, the control vector $\bar{x}$ again consists only of source rates of different puffs. But contrary to the point release considered above, in the case of a vertically distributed release, puffs are released at different heights. Then the minimization problem is again linear regression and the source-receptor matrix could be established during a single forward run of the model. The release height could be defined as the centre mass of the plume:

$$z_R = (1/H_{max}) \int_0^{H_{max}} q(z)dz, \tag{10.31}$$

where $q(z)$ is the source rate vertically distributed from the ground level to maximum height H_{max}.

Further simplification of the source inversion problem with respect to release height estimation is achieved by subdividing the vertical interval of possible release height into subintervals such that in each subinterval the release is distributed

uniformly. This approach has been utilized by Stohl et al. (2012) in which the release following the Fukushima accident has been distributed over three layers: the lower 50 m, between 50 and 300 m and between 300 and 1000 m. In Saunier et al. (2013), also for the Fukushima accident, the release rate has been uniformly distributed over the lowest 160 m.

The calculation of the source-receptor function corresponding to a vertically distributed release has been implemented in the standalone DIPCOT code and the solution of the corresponding minimization problem is presented in the next section. However, in operational practice of the real-time system this approach may be too expensive in terms of computational requirements, since it requires dealing with much more particles in a single run as compared to one with a source at single fixed height.

Therefore, in the JRODOS system, a simplified approach of a release at a fixed height is implemented; the user can do separate inversions for each possible release height, and compare the associated cost function value and/or other obtained statistics of model-measurements comparisons, such as *NMSE*. The result with the lowest value of the selected criteria (e.g. cost function value) would correspond to the best height among the assumptions.

10.2.6 Minimization Method

Minimization of the cost function (10.8) could be performed by using a direct method that solves the system of linear equations resulting from equating the derivative of the cost function J with respect to $\bar{x}$ to zero e.g. Tarantola (2005). This method was applied at first stages of model testing (Sect. 10.4.2), however, its drawback is that it can potentially yield in unphysical negative values.

Therefore another method was chosen to be used by default: nonnegative least squares (Lawson and Hanson 1974). Implementation of this method (NNLS subroutine) was extracted from freeware Netlib library (http://www.netlib.org). Before applying the linear regression solver, the cost function (10.8) to be minimized was brought to the standard form which is used by linear regression solvers:

$$J = J_1 + J_2 = \left\| \underline{\underline{\hat{G}}} \bar{x} - \hat{y} \right\|_2. \tag{10.32}$$

This is possible since all covariance matrices entering the cost function (10.8) are assumed to be diagonal and therefore matrix $\underline{\underline{\hat{G}}}$ and vector $\hat{y}$ in (10.32) can be calculated using the previous definitions as:

$$\underline{\underline{\hat{G}}} = \begin{pmatrix} \underline{\underline{\tilde{R}}}^{-1/2} \cdot \underline{\underline{\tilde{G}}} \\ \underline{\underline{B}}^{-1/2} \end{pmatrix}, \quad \hat{y} = \begin{pmatrix} \bar{y} \\ \underline{\underline{B}}^{-1/2} \cdot \bar{x}^B \end{pmatrix}. \tag{10.33}$$

It was checked that the results of the NNLS method were identical to the results of the direct method when the last didn't yield negative results.

10.3 Integration of the Source Inversion Module in the JRODOS System

10.3.1 Implementation of the Source Inversion Module (SIM)

10.3.1.1 SIM Structure

The source inversion module was initially developed and implemented in Fortran90 within the standalone version of Lagrangian dispersion model DIPCOT. After this initial implementation adaptation of the developed code for the work within the JRODOS system was performed as described above and specific details of this integration are described in this section. First the important details of SIM implementation are described.

The implemented source inversion module could be logically subdivided into four main submodules:

- Steering submodule which initializes input data, allocates memory for necessary arrays. In the standalone version data are initialized by reading files. In the integrated version, this submodule communicates with the JRODOS system and receives input data from databases. Then it consequently calls other submodules and gets output data from them;
- Submodule of SRM calculation based on a modification of the DIPCOT atmospheric dispersion model (Andronopoulos et al. 2009, 2010);
- The task of the data processing submodule is to pre-calculate all parameters of minimization problem, described in Sect. 10.2.4, such as error variances, ratios of release rates of different nuclides, initialize corresponding matrices and vectors;
- The minimization submodule which prepares matrices and vectors in a form suitable for further usage in minimization procedure. In particular, the 'design' matrix (which is SRM complemented to include first guess estimation of source term) is prepared and passed to the linear regression solver.

The key variables used in each submodule are stored in Fortran modules of the implemented SIM code.

10.3.1.2 Workflow of Main Computational Blocks

The preparation of the source term estimation consists of two main stages: (1) computation of the source-receptor matrix and (2) preparation of the regularization parameters and minimization. The flowchart of the source-receptor matrix calculation is presented in Fig. 10.2.

The workflow is very similar to the forward model run with the following two main differences: (a) gradients of deposition with respect to puff's inventories are

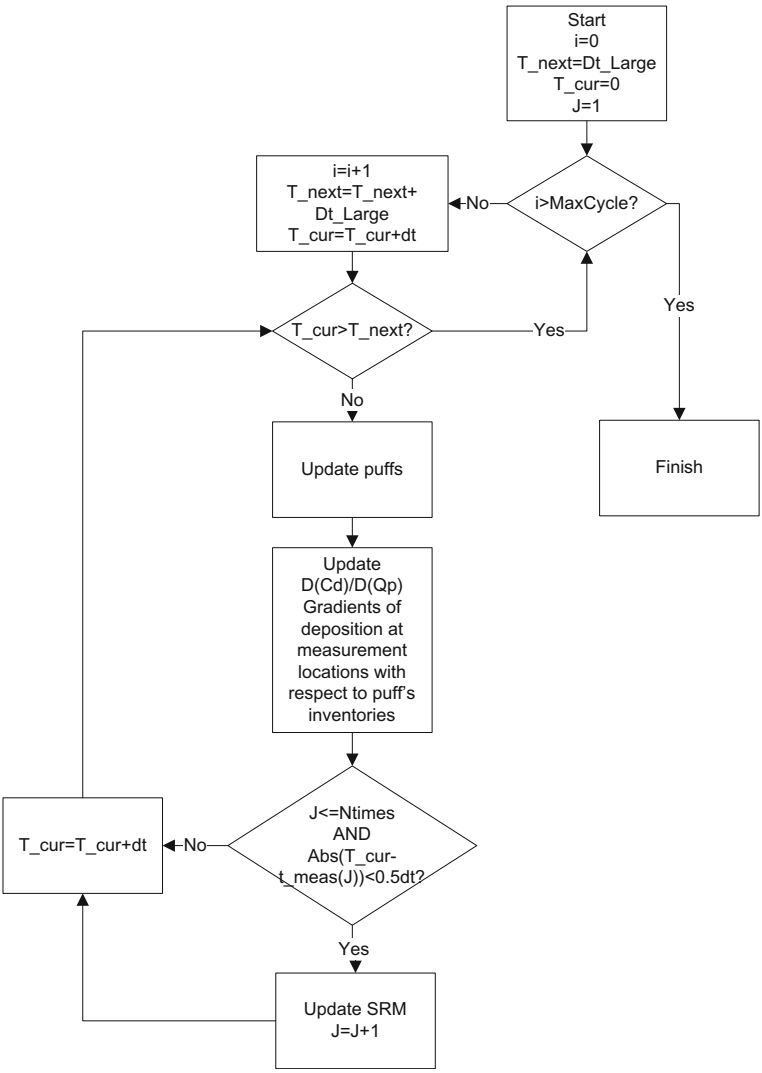

Fig. 10.2 Flowchart of SRM calculation

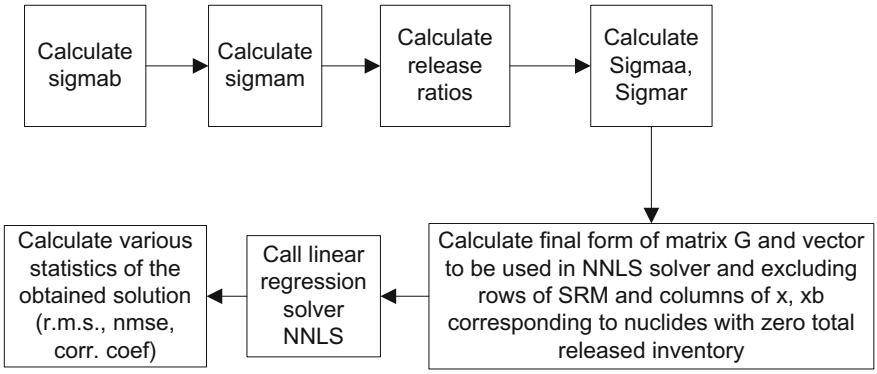

Fig. 10.3 Flowchart of data preprocessing and minimization procedure

updated at every time step by updating the sum according to (10.16); (b) when model time fits next measurement time to be processed, rows of the source receptor matrix corresponding to measurements at a given time are calculated. As it is clear from this description measurements should be sorted by time.

After the SRM has been calculated and before the minimization procedure is called, various regularization parameters entering the minimization problem (10.8) are calculated, including ratios of nuclide rates and their variances, etc. (Fig. 10.3). Then according to (10.33), matrices and vectors are brought into the form suitable for usage in the linear regression solver, and at this stage those rows of SRM and of solution and first guess vectors which correspond to nuclides with zero total released inventory in the first guess estimation are excluded. The linear regression solver (cf. Sect. 10.2.6) is called afterwards and when the solution has been obtained, various statistical measures related to the difference of simulated results against measurements are calculated, including the final value of the cost function, r.m.s. deviation, and NMSE (Fig. 10.3).

10.3.2 SIM Integration in JRODOS

10.3.2.1 SIM Operation Within the JRODOS

The flowchart of full SIM operation within the JRODOS is shown in Fig. 10.4. The workflow of SIM calculation was described above while other steps of SIM operation within the JRODOS include initialization with user-defined parameters and data from system databases and saving output results in project database. Most of the computational time during a full cycle of source term estimation is spent on SRM calculation; therefore it is reasonable to give users the possibility after completion of the first SIM run to repeat the minimization part with changed values of regularization parameters when other parameters of the problem were not

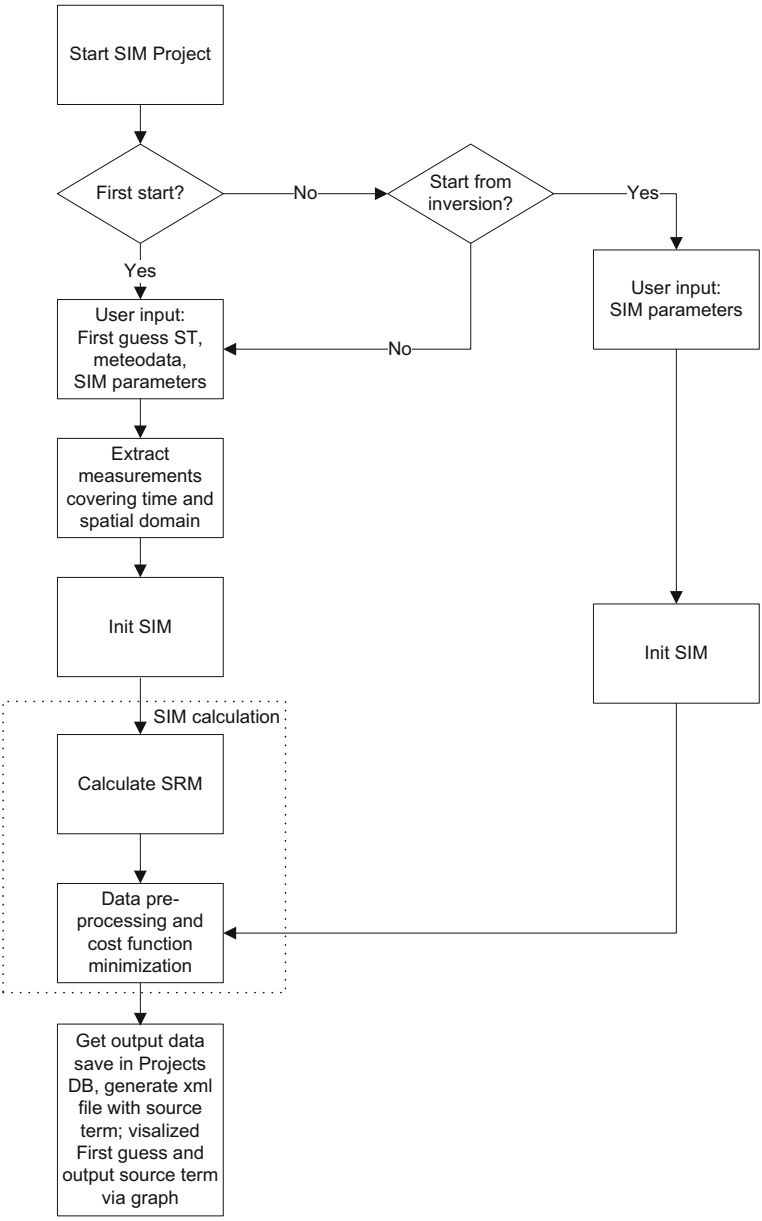

Fig. 10.4 Flowchart of SIM operation within the JRODOS system

changed (i.e. no new measurements, no change in start and end times of first guess source term, same meteorology, etc.). This part of workflow is also shown in Fig. 10.4.

The input data include:

- Steering parameter (start_from_inversion)
- Set of variables describing measurement data, with the measurement values sorted by increasing time of measurements
- Set of variables describing first guess source term, including start and end time of release, released inventories per time step
- Time resolution of analyzed source term
- End time of simulation
- Set of regularization parameters
- Other parameters: the same as for normal LSMC run: meteorology, etc.

Output data include:

- Analyzed source term, presented also in form suitable for usage in normal LSMC run (xml file)
- Statistical indicators of quality of solution in tabular form
- SRM and corresponding measurement data and first guess, available for export to binary files for the users who may wish to try their own minimization algorithms.

10.3.2.2 User Interfaces

To run the source inversion module, the user has to start the project of the corresponding type (Fig. 10.5, Project tree). Entering of basic data necessary to run SIM is very similar to input data of the JRODOS Local-Scale Model Chain (LSMC), therefore the existing user interface of LSMC called RoLite and described in Ievdin et al. (2015) was modified accordingly (Fig. 10.6).

As in the case of LSMC, the first guess source term could be input in different forms: time dependent release (in Bq) for different nuclides, or release for groups of nuclides (Bq), or released fractions of reactor inventory. Existing JRODOS software components convert the input source term data in whatever form into release rates for different nuclides, and this is used as first guess source term in SIM. Therefore there were no changes in UI input window for setting the source term (except that the corresponding tab in RoLite was renamed to 'First guess source term').

Meteorological data for running SIM can be input by the user or obtained from NWP models. The parameter timestep in Fig. 10.6 is used as time resolution of source term analysis when running SIM. The duration of the analysis is to be selected by the user, and only measurements falling into the selected time interval will be extracted for usage in source inversion procedure. Note that only measurements of those providers which were registered for a given site using standard tools existing in JRODOS will be used in the source inversion procedure.

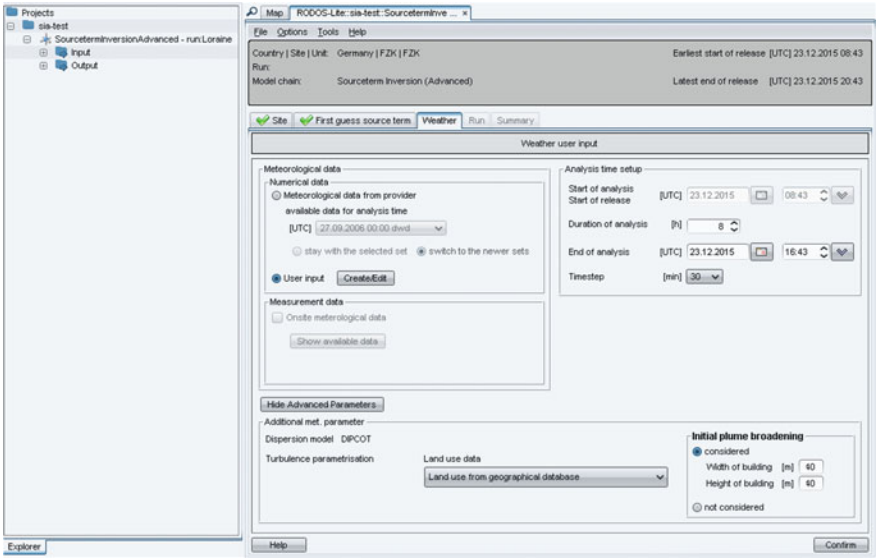

Fig. 10.5 Setting SIM calculation through the modified RoLite interface of the JRODOS system

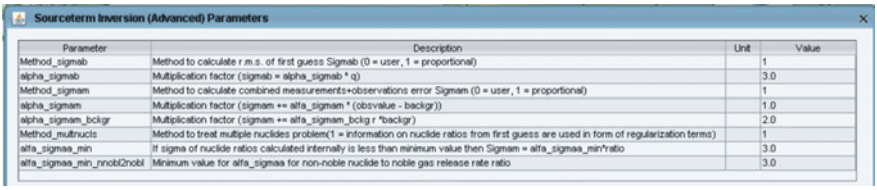

Parameter	Description	Unit	Value
Method_sigmab	Method to calculate r.m.s. of first guess Sigmab (0 = user, 1 = proportional)		1
alpha_sigmab	Multiplication factor (sigmab = alpha_sigmab * q)		3.0
Method_sigmam	Method to calculate combined measurements+observations error Sigmam (0 = user, 1 = proportional)		1
alpha_sigmam	Multiplication factor (sigmam += alfa_sigmam * (obsvalue - backgr))		1.0
alpha_sigmam_bckgr	Multiplication factor (sigmam += alfa_sigmam_bckg r *backgr)		2.0
Method_multnucls	Method to treat multiple nuclides problem(1 = information on nuclide ratios from first guess are used in form of regularization terms)		1
alfa_sigmaa_min	If sigma of nuclide ratios calculated internally is less than minimum value then Sigmam = alfa_sigmaa_min*ratio		3.0
alfa_sigmaa_min_nnobl2nobl	Minimum value for alfa_sigmaa for non-noble nuclide to noble gas release rate ratio		3.0

Fig. 10.6 Selection of SIM parameters for calculation of regularization parameters through menu 'Model parameters' of the JRODOS system

Figure 10.6 shows menu 'Model parameters' for parameters $\alpha_B, \alpha_m, \alpha_r, \alpha_a$ which are described in Sect. 10.2.4 above. The parameters Method_* also shown in model parameters window are set to 1 and presently cannot be changed. This means that error variances described above are calculated with the entered values for $\alpha_B, \alpha_m, \alpha_r, \alpha_a$ using relationships described in Sect. 10.2.4. Other options (methods) for calculation of error variances could be implemented in the future.

Figures 10.7 and 10.8 show output results of the source inversion module indicated in Project Tree. The output results include the source term prepared in the xml file which could be then imported to standard a LSMC Project (Fig. 10.7). Statistical indicators of quality of the achieved solution are presented in the form of a table (Fig. 10.8) and include the norm of residual $\|\bar{r}\|_2 = \|Gx - y\|_2$ before and after minimization and the final achieved value of the cost function. The norm of the measurement vector $\bar{y}$ is also displayed since the relative value of $\|\bar{r}\|_2 / \|\bar{y}\|_2$ may be of interest.

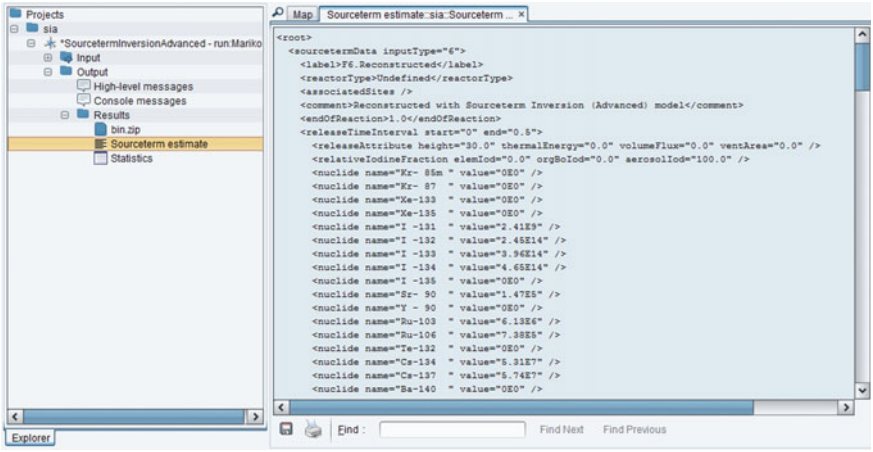

Fig. 10.7 Output results of SIM in Project Tree (left) and estimated source term in xml format ready for export to LSMC (right)

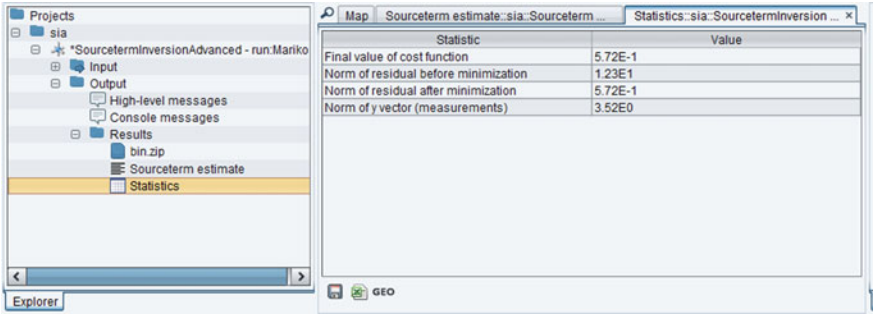

Fig. 10.8 Statistical indicators of quality of solution of source inversion problem

10.4 Results of Calculations

10.4.1 Description of the Test Cases

The developed source inversion method was applied for the meteorological and geographical conditions of the European Tracer Experiment ETEX (Gryning et al. 1998). The computational domain, topography etc. is shown in Fig. 10.9. Artificially generated measurements were used for testing the source inversion method, i.e. values of GDR calculated by DIPCOT using the true source term in the points of locations of sensors (Fig. 10.9) with 10 min time resolution.

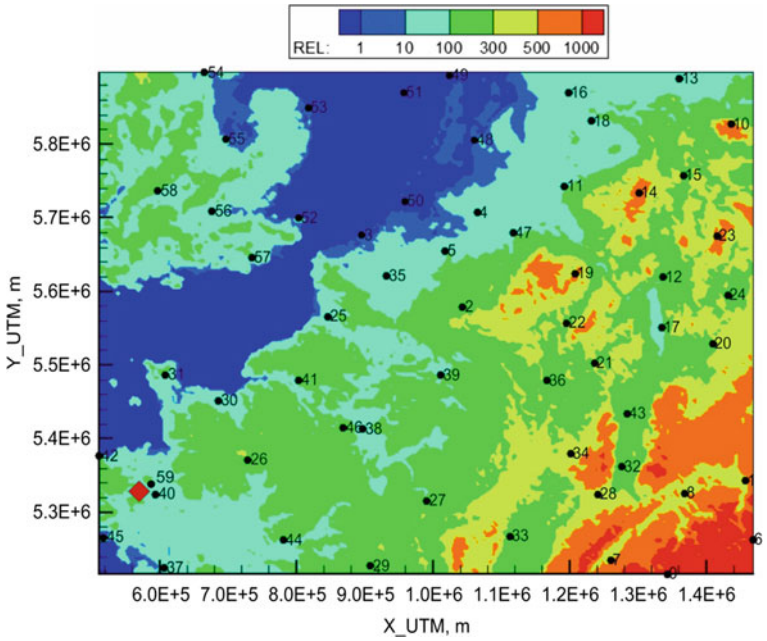

Fig. 10.9 Topography and locations of sensors and source in the computational domain

Two source terms were used for testing:

1. Source term 1. Simplified source term with constant release rate during 12 h of three radionuclides with total released activities 1.0E+18 Bq of Xe-133, 1.0E +17 Bq of I-131 and 5.0E+17 Bq of Cs-137, source height is 8 m.
2. Source term 2. Hypothetical release of 21 nuclides (Rb-88, Sr-89, Sr-90, Sr-91, Ru-103, Ru-105, Ru-106, Te-131 m, Te-132, I-131, I-132, I-133, I-134, I-135, Cs-134, Cs-136, Cs-137, Kr-87, Kr-88, Xe-133, Xe-135). There were two phases in the release period, having durations of 0.5 and 4 h (source term Muehleberg-1 from flexRISK study, http://flexrisk.boku.ac.at/). Release rates varied from 0 to 1E+12 Bq/s. During the first phase of release 100% of the inventory of noble gases and 90% of aerosols and iodine was emitted. During next phase of release emission rate was constant (Fig. 10.10). It was a vertically distributed release, described by 10 vertical levels within the layer 0–100 m with a Gaussian profile of release rate (height of maximum release rate at 50 m).

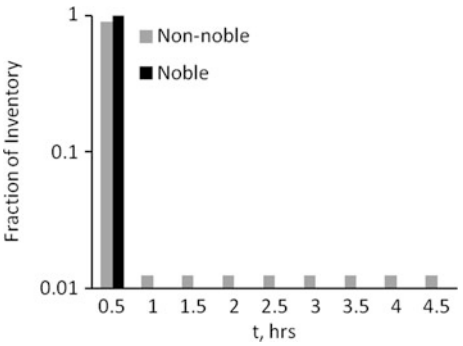

Fig. 10.10 Emitted fraction of inventory at different phases of release: noble gases and aerosols + iodine (denoted as 'non-noble')

10.4.2 Testing of Source-Receptor Matrix

Figure 10.11 demonstrates the correctness of the implementation of the source receptor matrix. Results calculated in forward run excellently agree with the results obtained by multiplication of the SRM with the vector of true source rates. Note that as it is evident from the Fig. 10.11, the influence of deposition on GDR is correctly accounted for in SRM calculation: GDR does not diminish to zero after plume passage but remains nearly constant due to radiation created by deposition of long-lived racionuclides.

Table 10.1 presents a quantitative comparison of measurements generated in forward run and of respective values calculated using the SRM. More specifically, the norm of residuals $\|Gx - y\|_2$ and the norm of the 'measurement' vector $\|y\|_2$ calculated using SRM and 'measurements' computed in the same model run (Run 0) and with 'measurements' computed in a different run (Run 1) are presented. Excellent results for Run 0 are evident in case of both source terms, while results of SRM as compared to results of independent forward run are not so good but still acceptable. This difference is caused by the stochastic nature of the Lagrangian

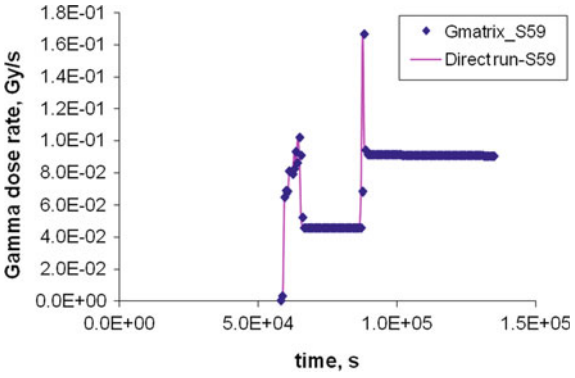

Fig. 10.11 Time series of GDR at sensor No. 59 (most close to point of release) calculated with forward model (line) and reconstructed using the source-receptor matrix (signs) for the case of Source term 1

Table 10.1 Norm of residual $\|Gx - y\|_2$ and norm of 'measurement' vector $\|y\|_2$ calculated using SRM and 'measurements' computed in the same model run (Run 0) and with 'measurements' computed in different run (Run 1)

Source term	Run	Norm of residual (normr)	Norm of y (normy)	Normr/normy
1	0	2.8E−06	0.36	7.8E−06
1	1	0.012	0.36	3.3E−02
2	0	5.1E−07	3.9E−02	1.3E−05
2	1	2.0E−03	3.9E−02	5.2E−02

model and thus even after application of the regularization procedure (control vector reduction) described in Sect. 10.2.3, the SRM is not identical to independently calculated results of the forward model.

10.4.3 Results of Source Inversion with Adjusted Regularization Parameters

In this section the results obtained with predefined and/or adjusted values of error variances are presented.

10.4.3.1 Source Term 1

In the first experiment, it is assumed as prior knowledge that the release is constant both in time and vertically. The SRM and the vector of samples y were calculated in different runs of DIPCOT. Because DIPCOT is stochastic model, the results obtained in different runs are somewhat different. The release can be fully described by three numbers (dim $\boldsymbol{x} = 3$), representing releases of the three nuclides, and the augmented cost function is identical to that in Sect. 10.2.2. The matrix $\underline{\underline{G}}_1 \in R^{N_o \times 3}$ was calculated from $\underline{\underline{G}} \in R^{N_o \times 12}$ by aggregating corresponding columns.

The comparison of the true and estimated emissions using different methods is presented in Table 10.2:

Table 10.2 True and estimated release rates

	True release, Bq/s	Estimated release rates (Bq/s)		
		A1	A2	A3
Xe-133	2.32E+13	−5.24E+11	1.80E+13	2.28E+13
I-131	2.32E+12	8.53E+12	4.44E+12	2.28E+12
Cs-137	1.16E+13	6.67E+12	1.03E+13	1.14E+13

- (A1) pure linear regression, no weighting, no regularization ($J_2 = 0$ in Eq. (10.6); at this stage direct solver of linear regression problem was used which could yield negative values
- (A2) minimization of cost function (10.6) without nuclide ratios, and
- (A3) minimization of (10.8). Release ratios used in A3 are the precise nuclide ratios of the true source term.

In the second experiment, the assumption of the homogeneity of the release is dropped and released activities in all 12 time slots are estimated. This means that we estimate release rates in 12 independent phases for three nuclides—dim **x** = 36 (it might be interesting to examine influences of prescribing some continuity between the ratios in neighbouring phases). Analogously to case A1 presented above, in case of solving linear regression without any weighting or regularization the result is quite poor. When the same as in case A2 presented above the inversion method is applied based on the cost function (10.6) without any conditions on nuclide ratios, a more reasonable result is obtained. But estimated emissions again do not resemble the true release as shown in the upper Fig. 10.12.

For taking into account nuclide ratios the matrices $\bar{y}, \underline{\underline{G}}$ must be augmented by 24 rows and $\underline{\underline{R}}$—with 24 rows and columns (12 for I-131 ratios and 12 for Cs-137 ratios). In this setup, the influence of variances of nuclide ratios on the performance of the estimations is examined. If the first guess ratios for I-131 and Cs-137 are distorted by factors 100 and 0.01, respectively, as compared to the true ratios, and if higher augmented variances are used ($\sigma_R = 1E15$), the result is shown in bottom Fig. 10.12. Release rates of Xe-133 and Cs-137 were estimated more or less precisely, rates of I-131 fluctuate around the true value.

10.4.3.2 Source Term 2

A time interval of 0.5 h was selected for calculations of SRM. Vertically, the release is distributed over 10 point sources uniformly distributed from 0 to 100 m. In the vertical, the profile is not homogeneous, emitted activity has a Gaussian distribution with the mode at 50 m. SRM is computed in a way that the actual release is preceded and followed by a 2-h period with zero emissions. This practically means that the release is splitted on 4 phases with a total number of 17 time intervals. The dimension of the source vector is 21 nuclides × 10 levels × 17 time intervals = 3570. There are 12,744 10-min GDR measurements from 59 receptors. As before, there are two runs of DIPCOT, one for $\underline{\underline{G}}_1 \in R^{12,744 \times 3570}$ and one (independent run)—for $\bar{y}$. As it was shown in Table 10.1, the results between different runs of the stochastic model (mentioned as Run 0 and Run 1 in Table 10.1) are not much different, but it is not an identical twin experiment.

Since there are zero emissions of noble gases in the second phase, a minimum emission $x_{\min} = 1.0\text{E} + 3\,\text{Bq/s}$ is defined in order to prevent numerical problems.

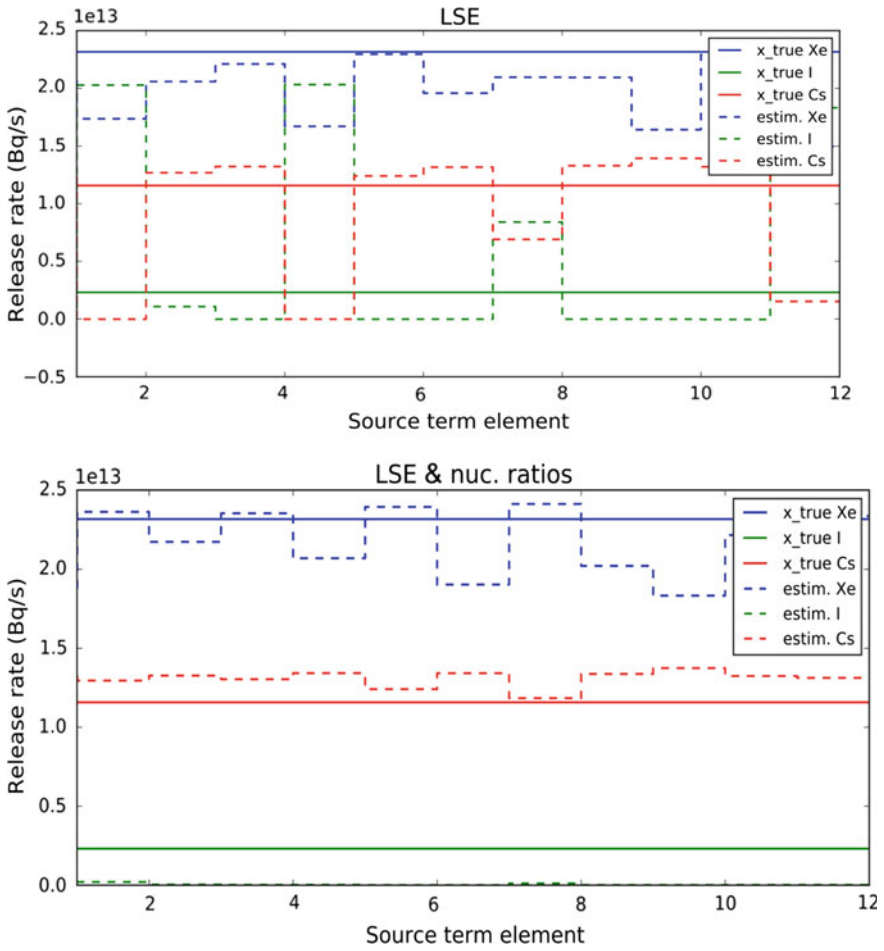

Fig. 10.12 Results of solving the source inversion problem in case of source term No. 1, (upper)—without additional conditions for nuclide ratios; (bottom)—with using conditions for nuclide ratios as described in text

This minimum value is used for calculation of ratios etc. In all cases, the observation error is set to $\bar{\sigma}_{\mathrm{m}} = 0.1 \cdot \bar{y} + 10^{-6}$.

At this stage each time slot is not treated separately, but columns of SRM are aggregated in a way that emissions of each nuclide at each vertical source for the whole phase are estimated. Thus, the dimension of the source vector is 21 nuclides $\times$ 4 phases $\times$ 10 levels = 840. As first guess, all values are assumed to be zero $x_B = 0$. Its standard deviation is set to be 1.0E12 for the releases in the second phase (the first release phase) and 1.0E9 otherwise.

At first, different values of the uncertainty $\tilde{\sigma}_R$ are specified in the augmentations of $\underline{\underline{R}}$ for each phase. The following results shown in Figs. 10.13 and 10.14 were

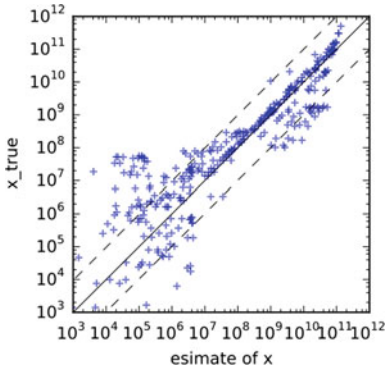

Fig. 10.13 Estimated versus true release rates (Bq/s) obtained with assumption of four phases and variable variances of nuclide ratios for each phase (see text)

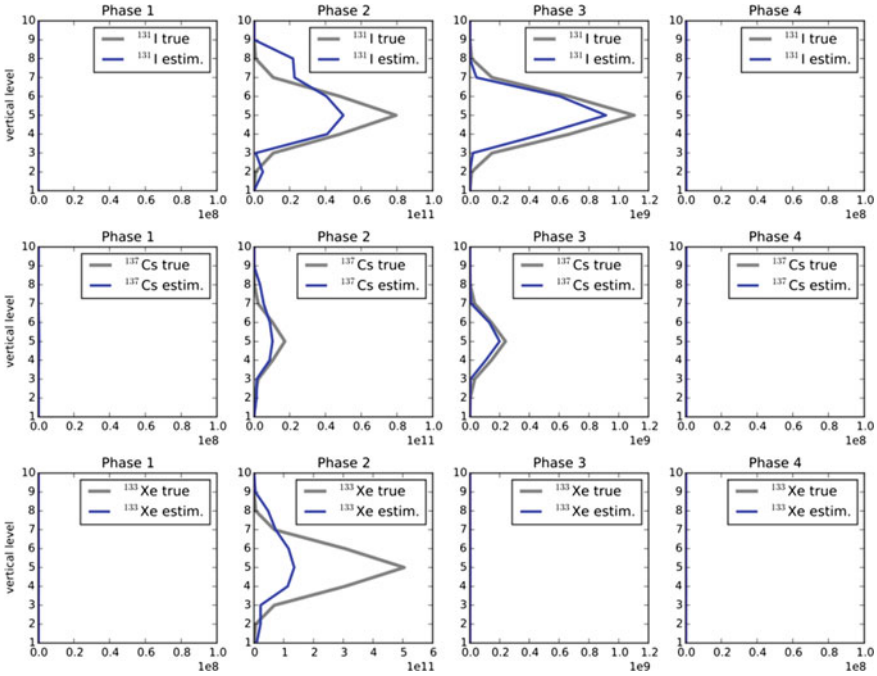

Fig. 10.14 Estimated and true profiles of release rate (Bq/s) at different vertical levels for selected nuclides with assumption of four phases and variable variances of nuclide ratios for each phase (see text)

obtained with variances of nuclide ratios equal to 1.0E1, 1.0E10, 1.0E8, 1.0E1, respectively, for the different phases. The low values for the first and last phases mean that nuclide ratios in these 'no-release' phases are imposed strictly. The results obtained without any additional information about timing of the release will be presented in the next section.

The higher emissions were estimated correctly. Underestimation of lower emissions is caused by big differences in emission of respective vertical sources even in one phase. Such big differences cannot be parameterized by a single number neither in first guess error nor in nuclide ratio variance. However, the results obtained are still acceptable and resolve the most important features of the release (timing and magnitude of higher emissions).

10.4.4 Results with Automatically Calculated Error Variances

In the previous section, results of testing the source inversion algorithm with arbitrarily adjusted values of the regularization parameters were presented. In operational practice of SIM usage within the JRODOS, regularization parameters are to be pre-calculated using the approach presented in Sect. 10.2.4. Therefore, here results of testing with automatically calculated values of regularization parameters are presented.

The same source term 2 as described in Sect. 10.4.1 was used but a point release was assumed with the release height equal to 50 m. In the tests presented, two different first guess source functions were used. Both source functions were created by shifting true source function backward in time by 2 h and then: increasing (Case A) and decreasing (Case B) true source function values by the factor of 10. Thus, the first guess release started immediately with the beginning of the simulations while true release started 2 h later. The source term was estimated with the time resolution equal to 0.5 h. The first guess source term was provided with the same time resolution.

The results of source inversion are presented in Fig. 10.15. Results are shown for selected nuclides Kr-87, Cs-137 and I-131, representative of each of the three groups (noble gases, iodine and aerosols). As it is seen from the results presented in those figures, the time of maximum emission is accurately evaluated by the algorithm. If the first guess source function is too low (Case B), the reconstructed source term is strongly underestimated for noble gas Kr-87. This is a consequence of lower values of root mean squared errors of the first guess release rates which according to (10.19) are proportional to the prior estimations of the release rates. In contrast the Case B yields overestimation of release rate of Kr-87. Emission rates of Cs-137 obtained in both cases A and B are almost identical and underestimated by the factor of about 2. Emission rate of I-131 is excellently identified in Case A while in Case B it is underestimated by the factor of 3.

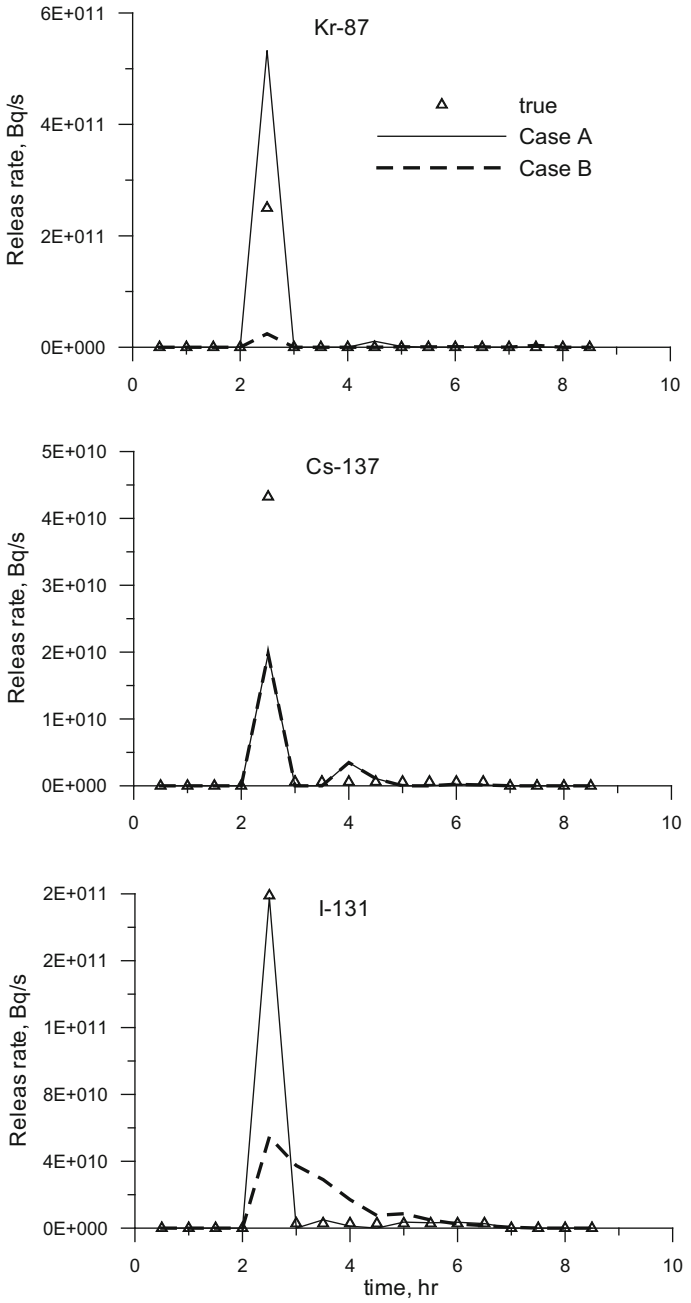

Fig. 10.15 True (triangles) and calculated release rates for Kr-87, Cs-137, and I-131 in the cases A (solid line) and B (dashed line) as described in text

Table 10.3 Mean absolute error and mean relative bias of the first guess and estimated emission rates

Case	MAE	MRB
First guess-A	10.8	9.0
First guess-B	1.1	−0.9
Source inversion-A	0.49	−0.24
Source inversion-B	0.96	−0.76

Table 10.3 presents statistical indicators of the accuracy of the evaluated source rates calculated over all 21 nuclides and over all time periods in cases A and B. The mean relative absolute error MAE $= \langle |x_{sol} - x_{true}| \rangle / \langle x_{true} \rangle$ and mean relative bias MRB $= \langle x_{sol} - x_{true} \rangle / \langle x_{true} \rangle$ are presented. According to the definition of MAE when first guess release rate is by the order of magnitude greater than true release rate this leads to large values of MAE (in Case A presented in Table 10.3 MAE of first guess equals 9). When first guess release rate is much less than the true value this leads to the value of MAE asymptotically reaching MAE = 1 when first guess release rate reaches zero. This explains why for the Case B MAE of first guess equals 1.1.

In Case A errors of the first guess source rate are reduced very significantly in result of source inversion procedure. It is interesting to note that errors in estimated source term (MAE = 0.49, MRB = −0.24) are similar to errors obtained by Tsiouri et al. (2012) for the case of source inversion of release rate using GDR measurements in case of a single nuclide. In results of Tsiouri et al. (2012) MAE varied from 0.39 to 0.71 and MRB from −0.27 to −0.9. Since present case of release of multiple nuclides is much more complex than the case of a single nuclide it could be concluded that the level of improvement achieved in Case A is very good.

In Case B the level of improvement is essentially worse as compared to Case A and it is marginal as compared to initial errors of first guess source term. This is due to mentioned above effect of reduced variances of first guess source term estimation which according to Eq. (10.19) are proportional to first guess source rate itself. In result the solution is too strongly forced to first guess estimation. Therefore in setting first guess source term for usage in JRODOS SIM it is advised to use conservative estimates.

Table 10.4 presents results of source height estimation. The source height in the run with the minimum obtained value of the cost function is considered to be the result of source inversion. The Case A of first guess source term is used. As in Table 10.1, two runs were performed: with using measurements calculated in the same run in which SRM was calculated (Run 0); and with using measurements calculated independently (Run 1). In both cases, the algorithm is able to estimate the source height, but in the case of Run 1 the cost function minimum is not as distinct as in the case of Run 0. If the model error would increase even more, this minimum will be further smoothed and might even disappear. Therefore, further testing of this algorithm will require use of real measurements.

Table 10.4 Dependence of the resultant cost function value on the release height for the case of using measurements from the same run in which SRM was calculated (Run0) and from an independent model run (Run1)

Release height, m	$Jmin^{1/2}$ (Run 1)	$Jmin^{1/2}$ (Run 0)
10	0.0066	0.0060
25	0.0061	0.0065
50	**0.0020**	**0.0004**
75	0.0030	0.0020
100	0.0033	0.0070
150	0.0120	0.0120
200	0.0120	0.0160

Figures in bold denote the minimum value achieved and the corresponding estimated release height. The first guess source term correspond to the Case A

10.5 Conclusions

In this work the development of a source inversion algorithm is described which allows to evaluate time-dependent release rates of different radionuclides and source height with the aid of GDR measurements collected at different distances from the source: from ~ 1 to ~ 1000 km. The automated version of the algorithm was developed which could be used in real-time. The algorithm was integrated in the Source Inversion Module of the European nuclear decision support system JRODOS.

A variational approach for the problem of source inversion was used. The source-receptor matrix is calculated with the aid of the atmospheric transport model DIPCOT.

To estimate release rates of different radionuclides from GDR measurements, in formulation of source inversion problem the SRM and measurement vector are augmented with additional linear relationships describing ratios of release rates of different radionuclides. The possible ranges for the respective ratios are calculated from the first guess source term provided by user.

Parameterizations for the regularization parameters of source inversion problem which include root mean squared errors of measurents, first guess release rates, calculated values etc., are developed.

Testing of the proposed method using the artificial measurements precalculated for the conditions of ETEX experiment had shown that in all cases the error of the evaluated release rates are less than the errors of the respective first guess. The level of improvement was better when first guess release rates were greater than the true values. Therefore in setting first guess source term for usage in JRODOS SIM it is advised to use conservative estimates.

It is also recommended to use the developed SIM together with the meteorological data assimilation tools previously implemented in the JRODOS system

(Kovalets et al. 2004; Davakis et al. 2007; Andronopoulos et al. 2016). Further testing of the algorithm is planned to be performed using real data from field experiments and/or real-case accident scenarios.

Acknowledgements The presented research was supported with the EURATOM grant No.323287. I. Kovalets was also supported with the grant of the President of Ukrane No. Ф78/40053.

References

Andronopoulos S, Davakis E, Bartzis JG (2009) RODOS-DIPCOT model description and evaluation. Report RODOS(RA2)-TN(09)01. Available at: https://www.researchgate.net/publication/228862960_RODOS-DIPCOT_Model_Description_and_Evaluation, last accessed 2018/06/01

Andronopoulos S, Bartzis JG (2010) Gamma radiation dose calculation method for Lagrangian-puff atmospheric dispersion models used in real-time emergency response systems. J Radiol Prot 30(4):747–759. https://doi.org/10.1088/0952-4746/30/4/008

Andronopoulos S, Davakis E, Bartzis JG, Kovalets IV (2010) RODOS meteorological pre-processor and atmospheric dispersion model DIPCOT: a model suite for radionuclides dispersion in complex terrain. Radioprotection 45(5):S77–S84. https://doi.org/10.1051/radiopro/2010017

Andronopoulos S, Ievdin I, Kovalets I, Anulich S, Trybushnyi D (2016) New functionalities developed in the NERIS-TP project regarding meteorological data used by Decision Support Systems. Radioprotection 51(HS1):S13–S16. https://doi.org/10.1051/radiopro/2016004

Bocquet M (2008) Inverse modelling of atmospheric tracers: non-Gaussian methods and second-order sensitivity analysis. Nonlinear Process Geophys 15:127–143. https://doi.org/10.5194/npg-15-127-2008

Davakis E, Andronopoulos S, Kovalets I, Gounaris N, Bartzis JG, Nychas SG (2007) Data assimilation in meteorological preprocessors: effects on atmospheric dispersion simulations. Atmos Environ 41(14):2917–2932. https://doi.org/10.1016/j.atmosenv.2006.12.031

Davoine X, Bocquet M (2007) Inverse modeling-based reconstruction of the Chernobyl source term available for long term transport. Atmos Chem Phys 7:1549–1564. https://doi.org/10.5194/acp-7-1549-2007

De Haan P, Rotach MW (1998) A novel approach to atmospheric dispersion modelling: the puff-particle model. Q J R Meteorol Soc 124:2771–2792. https://doi.org/10.1002/qj.49712455212

Gryning SE, Batchvarova E, Schneiter D et al (1998) Meteorological conditions at the release site during the two tracer experiments. Atmos Environ 32(24):4213–4137. https://doi.org/10.1016/s1352-2310(98)00191-5

Hofman R, Seibert P, Kovalets I, Andronopoulos S (2015) Analytical source term optimization for radioactive releases with approximate knowledge of nuclide ratios. In: EGU general assembly 2015 conference abstracts, vol 17, EGU2015-3033

Ievdin Y, Trybushny D, Zheleznyak M, Raskob W (2010) RODOS re-engineering: aims and implementation details. Radioprotection 45(5):S181–S190. https://doi.org/10.1051/radiopro/2010024

Ievdin I, Trybushnyi D, Landman C (2015) JRODOS user guide, version 3.21. Karlsruhe Institute of Technology

Kovalets I, Andronopoulos S, Bartzis J, Gounaris N, Kushchan A (2004) Introduction of data assimilation procedures in the meteorological pre-processor of atmospheric dispersion models

used in emergency response systems. Atmos Environ 38(3):457–467. https://doi.org/10.1016/j.atmosenv.2003.09.068

Kovalets I, Hofman R, Seibert P, Andronopoulos S (2014) Dispersion modelling and 1st-guess source term uncertainties. Report of the EU FP7 PREPARE project PREPARE(WP4)-(14)-05. https://doi.org/10.13140/rg.2.2.16116.86403

Kovalets I, Andronopoulos S, Hofman R, Seibert P, Ievdin I (2016) Advanced method for source term estimation and status of its integration in JRODOS. Radioprotection 51(HS2):S121–S124. https://doi.org/10.1051/radiopro/2016046

Landman C (2007) Scenario data sets and scenarios for RODOS PV6 final. Report RODOS(RA7)-TN(04)-02. Germany Karlsruhe: Karlsruhe Institute of Technology. Available at: https://resy5.iket.kit.edu/RODOS/Documents/Public/Handbook/Volume2/3_3_scenariodata.pdf, last accessed 2018/06/01

Lawson CL, Hanson RJ (1974) Solving least squares problems. Prentice-Hall, Inc., Englewood Cliffs, New Jersey

Raskob W, Schneider T, Gering F, Charron S, Zheleznyak M, Andronopoulos S, Heriard-Dubreuil G, Camps J (2016) Innovative integrative tools and platforms. Key results of the PREPARE European Project. Radioprotection 51(HS2), S59-S61. doi:https://doi.org/10.1051/radiopro/2016032

Saunier O, Mathieu A, Didier D, Tombette M, Quélo D, Winiarek V, Bocquet M (2013) An inverse modeling method to assess the source term of the Fukushima nuclear power plant accident using gamma dose rate observations. Atmos Chem Phys 13:11403–11421. https://doi.org/10.5194/acp-13-11403-2013

Seibert P, Frank A, Kromp-Kolb H (2002) Inverse modelling of atmospheric trace substances on the regional scale with Lagrangian models. In: Proceedings of the EUROTRAC-2 symposium. Garmisch-Partenkirchen, Germany, pp 11–15

Seibert P, Kristiansen NI, Richter A, Eckhardt S, Prata AJ, Stohl A (2011) Uncertainties in the inverse modelling of sulphur dioxide eruption profiles. Geomat Nat Hazards Risk 2(3):201–216. https://doi.org/10.1080/19475705.2011.590533

Stohl A, Forster C, Frank A, Seibert P, Wotawa G (2005) Technical note: the Lagrangian particle dispersion model FLEXPART version 6.2. Atmos Chem Phys 5:2461–2474. https://doi.org/10.5194/acp-5-2461-2005

Stohl A, Seibert P, Wotawa G, Arnold D, Bukhart JF, Eckhardt S, Tapia C, Vargas A, Yasunari TJ (2012) Xenon-133 and caesium-137 releases into the atmosphere from the Fukushima Dai-ichi nuclear power plant: determination of the source term, atmospheric dispersion, and deposition. Atmos Chem Phys 12:2313–2343. https://doi.org/10.5194/acp-12-2313-2012

Talerko N (2005) Reconstruction of ^{131}I radioactive contamination in Ukraine caused by the Chernobyl accident using atmospheric transport modeling. J Environ Radioact 84(3):343–362. https://doi.org/10.1016/j.jenvrad.2005.04.005

Tarantola A (2005) Inverse problem theory and methods for model parameter estimation. SIAM Publishers, USA, Philadelphia. https://doi.org/10.1137/1.9780898717921

Tsiouri V, Kovalets I, Andronopoulos S, Bartzis J (2011) Development and first tests of a data assimilation algorithm in a Lagrangian puff atmospheric dispersion model. Int J Environ Pollut 44(1–4):147–155. https://doi.org/10.1504/IJEP.2011.038413

Tsiouri V, Kovalets I, Andronopoulos S, Bartzis JG (2012) Source function estimation with data assimilation of gamma dose measurements in Lagrangian atmospheric dispersion model DIPCOT. Radiat Prot Dosimetry 148(1):34–44. https://doi.org/10.1093/rpd/ncq592

US NRC (1990) Analysis of CDF from internal events: expert judgment. US NRC Report NUREG/CR-4550, vol 2. Available online: https://www.nrc.gov/docs/ML0634/ML063460465.pdf, last accessed 2018/06/01

Winiarek V, Vira J, Bocquet M, Sofiev M, Saunier O (2011) Towards the operational estimation of a radiological plume using data assimilation after a radiological accidental atmospheric release. Atmos Environ 45(17):2944–2955. https://doi.org/10.1016/j.atmosenv.2010.12.025

Wotawa G, DeGeer L-E, Denier P, Kalinowski M, Toivonen H, D'Amours R, Desiato F, Issartel J-P, Langer M, Seibert P et al (2003) Atmospheric transport modelling in support of CTBT verification overview and basic concepts. Atmos Environ 37(18):2529–2537. https://doi.org/10.1016/S1352-2310(03)00154-7

Zhang X, Raskob W, Landman C, Trybushnyi D, Li Y (2017) Sequential multi-nuclide emission rate estimation method based on gamma dose rate measurement for nuclear emergency management. J Hazard Mater 325(5):288–300. https://doi.org/10.1016/j.jhazmat.2016.10.072

Part IV
MSW and Disposal

Chapter 11
Effective Utilization of High-Grade Energy Through Thermochemical Conversion of Different Wastes

A. Santhoshkumar, R. Muthu Dinesh Kumar, D. Babu, Vinoth Thangarasu and R. Anand

Abstract Waste disposal is a major problem in most of the countries. Thus, waste to energy conversion will fulfill the future energy demand as well as resolve the pollution issues. This work mainly involved in the extensive study on pyrolysis and gasification of biomass and hazardous e-waste into useful energy and its impact on the environment. Microwave-assisted pyrolysis (MAP) technique has attracted the research society because of its energy efficient process and more viable route for converting the waste into potential products. Similarly, this chapter provides the assessment of biomass and e-waste volarization route to produce syngas using different gasification strategies. In addition, this study focused on the pyrolysis and gasification parameters like temperature, equivalence ratio, and particle size, which influence the product yield and emission formation. In general, pyrolysis and gasification of biomass and e-waste produce the volatile products, and it leaves the solid residue like char and ash. As an implementation, this study explained the conversion of waste residue from pyrolysis and gasification into useful products like activated carbon, silicon carbide, and zeolite, which can be used as the catalyst in microwave process and some other applications. At the end, the study covers the utilization of pyrolysis fuel and syngas in compression ignition engines with advanced technologies like CRDI and dual fuel strategies. CRDI and dual fuel mode combustion are the appropriate methods to reduce the engine emissions and enhance the engine efficiency.

Keywords Biomass · E-waste · Microwave-assisted pyrolysis
Gasification · Syngas · Engine

A. Santhoshkumar · R. Muthu Dinesh Kumar · D. Babu
V. Thangarasu · R. Anand (✉)
Department of Mechanical Engineering, National Institute of Technology, Tiruchirappalli 620015 Tamil Nadu, India
e-mail: anandachu@nitt.edu

R. A. Agarwal et al. (eds.), *Pollutants from Energy Sources*,
Energy, Environment, and Sustainability,
https://doi.org/10.1007/978-981-13-3281-4_11

Nomenclature

ABS	Acrylonitrile–butadiene–styrene
ASTM	American Society for Testing and Materials (ASTM)
BFRs	Brominated flame retardants
CAG	Comptroller and Auditor General of India
CFC	Chlorofluorocarbon
COHb	Carboxyhemoglobin
CPV	Concentrator photovoltaics
CRDI	Common rail direct injection
CRTs	Cathode ray tube
CSP	Concentrated solar power
DME	Direct methyl ether
DSC	Differential scanning calorimetry
EDX	Energy dispersive X-ray analysis
ER	Equivalence ratio
FPSPS	Free-pressureless spark sintering technique
FTIR	Fourier-transform infrared spectroscopy
GC	Gas chromatography
HCBs	Hexa-chlorobenzenes
HDPE	High-density polyethylene
HIPS	High impact polystyrene
HPLC	High-performance liquid chromatography
MAOS	Microwave-assisted organic synthesis
MAP	Microwave-assisted pyrolysis
MB	Methylene blue
MSW	Municipal solid waste
MWS	Maxwell–Wagner–Sillars
NMFs	Nonmetallic fractions
NMR	Nuclear magnetic resonance spectroscopy
OECD	Organisation for economic cooperation and development
PAH	Polycyclic aromatic hydrocarbons
PBDD/Fs	Polybrominated dibenzo-p-dioxins and dibenzofurans
PCDD/Fs	Polychlorinated dibenzo-p-dioxins and dibenzofurans
POPs	Persistent organic pollutants
PP	Polypropylene
PS	Polystyrene
PVC	Polyvinyl chloride
SiC	Silicon carbide
TBBPA	Tetrabromobisphenol
TGA	Thermogravimetric analysis
WCO	Waste cooking oil

WEEE	Waste electrical and electronic equipment
WPCBs or WCB	Waste printed circuit boards
XRF	X-ray fluorescence

11.1 Introduction

Biomass is one of the major renewable energy sources which fulfill about 14% of the energy requirement. In case of rural areas, up to 90% of energy demand is fulfilled by biomass. In the year of 2050, most of the peoples in the world are predicted to live in the developing countries, and biomass is expected to remain a major source of energy contribution to the large populations (Balat and Ayar 2005). To recover energy from the biomass and recently plastic waste, gasification technology is focused as a sustainable waste management technique; hence, it will be able to reduce the toxicity of waste, the burden on landfills, and also the environmental hazards (Seltenrich 2016). Plastic waste management is increasing day by day, so it must be urgently addressed. Low degradability of plastic waste causes enormous problem in marine environments (Andrady 2015). Likewise, in Europe over the last decade recycled plastic contribute energy sector have increased from 55% and also dumping of waste plastics reduced by nearly 40% (Hestin et al. 2017). Plastic polymers are extensively used in the current world such as in automobiles, packing, agriculture, electronics, building materials, and so forth. This massive consumption was promoted to the production of an increased amount of e-waste, especially in more developed countries. Industrialization and population growth increasing the energy demand, petroleum products consumption, and disposal of e-waste were described in energy demand and scenario. E-waste is defined as discarded waste electronic and electrical equipment during the manufacturing and repairing process. The e-waste is mostly collected from household and business equipment with circuitry or electrical components. The e-waste contains plastics, different metals like copper, tin, lead, cadmium, beryllium, mercury, and flame retardant additives like bromine, chlorine, fluorine, and iodine that affect the landfill and ecological system. Thermochemical conversion processes are the best alternative to meet the energy requirements by converting wastes into most valuable products (Joshi et al. 2016).

The e-waste contains lots of different constituents and elements, creating an intricate heterogeneous waste containing plastics, metals, and ceramics. Conventional procedures of recycling e-waste (i.e., separating, shredding, and sorting) generates a residual material that still contains valuable metals, they often turn out to be landfills (Lee et al. 2007; Cui and Forssberg 2003). Recycling of e-waste also causes environmental problems pertaining to the presence of various halogenated and nonhalogenated flame retardants (Schlummer et al. 2005). The flame retardant is used for preventing the flame propagation on the plastic materials. The halogenated flame retardant infers to a chemical mixture which contains

halogen atoms (bromine, fluorine, chlorine, and iodine), and they are not electrolytic in nature. Nonhalogenated flame retardants like phosphorus, phosphate, and nitrogen are widely used in plastics. These halogenated and nonhalogenated components pollute the environment during the direct combustion of plastics. Moreover, polymers have been identified in e-waste such as high impact polystyrene, acrylonitrile butadiene styrene, polystyrene, polyvinyl chloride, polycarbonate, and polypropylene (Alston et al. 2011). The pyrolysis process can probably be utilized to convert plastics into diesel-like fuel or other more valuable products (Anuar Sharuddin et al. 2016) and surely be considered as an important process of restoring and reuse of the polymeric content of the e-waste (Muhammad et al. 2015; Martinho et al. 2012; Al-Salem et al. 2009). In the realm of pyrolysis, microwave-assisted pyrolysis is an efficient process which gives some advantages over conventional pyrolysis process—e.g., it offers a volumetric heating that improves heating efficiencies (Appleton et al. 2005). Two different types of microwave absorbers (i.e., "C" based, "Fe" based) were used to study the microwave-assisted pyrolysis of e-waste and different experimental setups used to increase the quality and quantity of liquid fraction and to reduce the solid residue (Rosi et al. 2018).

In traditional pyrolysis technique, the heating mechanism is less efficient and slower as it is based on conduction and convection. Energy efficient volumetric heating can be attained in microwave pyrolysis due to the diffuse character of the electromagnetic field; it heats all the substances uniformly (Domínguez et al. 2007). In the realm of pyrolysis, the microwave-assisted pyrolysis (MAP) is an efficient process which gives some advantages over conventional pyrolysis process offers volumetric heating that improves heating efficiencies (Jones et al. 2002). According to Paradela et al. (2009), e-waste plastics were mixed with pine biomass with the purpose of maximizing liquid yields by studying the experimental conditions. The primary intention behind the co-pyrolysis is to improve pyrolysis oil liquid fraction and its properties (i.e., a mixture of varieties of plastics and pine residue).

Microwave heating had intensive functions in food, ceramic, and chemical processes industries in recent days. Microwave heating is resulting from the conversion of magnetic attraction energy to thermal power, and additionally, the effectiveness of the conversion depends upon the nonconductor nature of substances. In many cases, the energy consumption in microwave-assisted heating could be a smaller quantity than that of other heating processes and so the handling time is shorter (Rattanadecho et al. 2007). Compared to conventional heating, microwave-assisted heating is having many advantages like faster heating rate and faster rate of reaction. Municipal solid waste is used in pyrolysis process, and different susceptors have used for increasing the efficiency of microwave pyrolysis process. For municipal solid waste activated carbon, solid beads, fly ash, aluminum are the suitable susceptors (Suriapparao and Vinu 2015). Several types of research were described by Wang et al. (2014) the use of pyrolysis oil in internal combustion engines for a better replacement of the diesel fuel. For efficient utilization of energy, it is essential to consider the quality and quantity of energy.

Conversion of waste plastics into value-added products using gasification in the bubbling fluidized reactor produces syngas which mainly consists of H_2, CO, CO_2, CH_4, and N_2. The generated syngas can be converted to fuels like methanol and dimethyl ether (Sansaniwal et al. 2017). An astounding favorable position of gasification contrasted with pyrolysis is the more noteworthy adaptability to together valorise plastics of various syntheses or blends or plastics blended with different feedstocks. Therefore, composition and application depend on several factors such as gasifying agent, catalyst, bed material, and reactor configuration. Syngas produced from gasification of plastics have an average heating value in the range of 6–8 MJ/m^3 (Sancho et al. 2008; Arena and Di Gregorio 2014; Arena et al. 2010; Xiao et al. 2007).

An exhaustive literature search is already done, and further study is needed throughout the full project tenure to get updated with current research in the proposed area. Conventional procedures of recycling e-waste will generate a residual material that still contains valuable residues; they often turn out to landfill. Polymers have been identified in e-waste residues such as high impact polystyrene, acrylonitrile butadiene styrene, polystyrene, polyvinyl chloride, polycarbonate, and polypropylene. Current investigation work shows that the thermal conversion process called pyrolysis is an effective way to recover energy from the e-waste. However, the pyrolysis oil can be replaced as diesel fuel was addressed and its application for use in a diesel engine. The performance and combustion characteristics of the CI engine with pyrolysis oil as fuel was comparable to the standard diesel fuel. Several types of research described the use of pyrolysis oil in internal combustion engines for a better replacement of the diesel fuel. Among various possible technological developments, a common rail direct injection (CRDI) system has to lead the technological revival. CRDI systems have been observed to significantly reduce specific fuel consumption and soot emissions as compared to conventional diesel operation, however, with a tendency of increased NO_x formation (Roy et al. 2014).

11.2 Environmental Impact of Waste Disposal and Energy Conversion

11.2.1 Global Energy Status and Scenario

World energy demand has been increased due to the rise in population and technological advancement. Approximately, 80% of the energy demand could be fulfilled by the fossil fuels. More utilization of fossil fuel coupled with a steady rise in energy demand and an increase in carbon dioxide (CO_2) and carbon monoxide (CO) emissions are becoming the real threat for the ecosystem. The CO_2 and CO emissions are the main contributor to the environmental pollution and global warming (Anand 2017). Depletion of fossil fuels and environmental threat have

spurred research interest in alternative renewable energy sources. The alternative renewable sources are solar energy, wind energy, tidal energy, geothermal energy, and hydropower energy (Zhang et al. 2003). According to the energy survey, the world energy demand could be fulfilled by 77.9% of fossil fuel and remaining renewable energy sources. The energy production in terms of percentage is oil—35%, coal—29%, natural gas—24%, nuclear energy—5%, and hydropower—6% remaining solar and other sources (Lin et al. 2011). The world population will increase from 74 billion to 92 billion in 2040 according to the energy outlook 2018 survey. Global energy demand will increase by about 25% from 2016 to 2040 for non-OECD countries. Due to the rise in population, the electricity demand will be rise by 60% from 2016 to 2040 (Administration, U.S.E.I 2018).

Solar energy is a promising and freely available renewable energy source to manage the energy crisis. It is superior to the other sources in terms of availability, accessibility, cost-effectiveness, capacity, and efficiency (Kannan and Vakeesan 2016). According to the international energy scenario, 40,000–60,000 MW decentralized rooftop solar PV could be installed in India by 2022 (Shrimali and Rohra 2012). Solar, nuclear energy, and conservation of energy will be meeting the Indian energy demand over the next 20 years (Parikh and Parikh 2011). Estimated CAG of Indian energy demand could be pegged around 3.1% from 2009 to 2035 (International Energy Agency 2012). Indian government is imposing the policy and takes the initiative for the implementation of solar power technology like CSP and CPV. It is solving the energy problem like deficit, energy inequity, and energy security as observed by Sharma et al. (2012). As per the NISEM scenario, the total estimated solar power generation in India is 749 GWP, and its target is 100 GWP solar power in India by 2022 (National Institute of Solar Energy 2014). The estimated annual solar power generation could be 459,900 Million units, and the theoretical annual power generation is 918,573 Million units. By 2030, 12,875 MW wind power may be achieved in India (Singh 2018).

As per the Ministry of Statistic and Programme Implementation, the total estimated wind power generation in India is about 102,772 MW but present wind energy power generation is 23,439 MW. The wind power production is depending on site, wind profile, and master height (Ministry of Statistics and Programme Implementation 2015). Estimated small hydropower generation in India is 19,749 MW, and present installed capacity of the small hydropower in India is 3800 MW by 2014 (Ministry of Statistics and Programme Implementation 2015). Estimated biomass and cogeneration power generation in India is about 17,538 MW and present capacity of biomass electricity generation is 4013 MW in India. The total expected power generation from renewable energy sources in India is about 725,660 Million units and theoretical power generation from renewable sources in India approximately about 13, 13,604 Million units (Ministry of Statistics and Programme Implementation 2015).

11.2.2 Environmental Impact of Waste Disposal

Increase in electronic waste is concern over across the world. Each year globally about 300 million tons of e-waste is produced, and about 10% only recycled. In the world, India is the 5th major producer of e-waste. Roughly each year India is dumping 18.5 lakh metric tons of e-waste, which includes 12% of telecom equipment and 70% of computer devices of the total e-waste, and 18% of mobile e-waste (Mundada et al. 2004). In recent days, electrical and electronic wastes are drastically increased due to population and industrialization. The e-waste is recycled through incineration or pyrolysis process, and non-recycled e-waste is landfilled. E-waste contains lots of heavy metals, brominated flame retardant, and other toxic and hazardous substance. Landfilled causes environmental pollution (Wang and Xu 2014a). The presence of halogenated and nonhalogenated flame retardants in electrical and electronic waste causes environmental pollution and burning gases harmful to human health as noticed by Weber et al. (Weber and Kuch 2003). WEEE is recycled through melting, regeneration, and crushing. The MNFs, WPCBs have hazardous ingredient, which causes environmental pollution, and e-waste contains acrylonitrile butadiene styrene, polystyrene, and polyvinyl chloride (Guo et al. 2009).

Disposal of municipal solid waste (MSW) is one of the major issues not only in India but also in the whole world. The higher rate of population growth, global urbanization, degree of industrialization, and public habits increased the productivity of municipal solid waste (Pandey et al. 2016). According to the life cycle analysis, collection of MSW, storage of MSW, transportation of MSW, Processing of MSW is too difficult. MSW is the potential source for the power generation; it consists of food, paper, wood waste, clothes, rubber, plastics, and daily discharge materials. 90% of MSW is not disposed of properly or mannerly, it is simply dumped in open spaces, which causes environmental hazards, and it is created problem to the public health (Klein 2002). In USA, 90–95% of MSW is converted into useful energy. According to the survey, 3.98 million tons of MSW is recyclable, 3.32 million tons of MSW is landfilled, and 0.60 million tons of MSW is incinerable. According to the World Bank survey, the solid waste increases from 1.3 billion tons to 2.5 billion tons by 2025. In India, 0.1 million tons of MSW/day per capita is produced (Akolkar 2005).

Last few decades, the plastics usage has been drastically increased due to its better characteristics. In total, WEEE waste consists of about 30% of plastic due to its numerous behavior like lightweight and noncorrosive in nature. More landfilling of plastic waste reduced the area and polluted the environment and affected the human health. Especially, BFRs affected the nervous and reproductive systems of mammal (Stegeman et al. 1993). Syamsiro et al. (2014a) synthesized the pyrolysis oil from MSW using Y-zeolite and normal zeolite as catalyst. MSW collected from last disposal place in Indonesia. The results revealed that HDPE waste produced maximum liquid fraction. Presence of catalyst in the reaction reduces the liquid fraction, whereas gases fraction slightly increased as compared to non-catalytic process. MSW-based pyrolysis oil has better calorific value compared to low-grade oil and biomass feedstock.

11.2.3 Importance of Waste to Energy Conversion

In the modern world, due to population and technological advancement, more quantity of waste is produced. The different wastes such as cooking waste, municipal solid waste, plastic waste, automobile waste, electronic or e-waste, and agricultural waste were discarded in the landfill directly. Many researchers have been working on waste to energy conversion technique to meet the world energy demand by utilizing the energy from wastage (Pandey et al. 2016). The most important waste to energy conversion techniques are physical method, thermal conversion method, biological method, and chemical method. In the physical method, the solid waste is converted into pellet, wood chips, and wood briquettes, respectively. Thermal conversion method is classified into three types such as direct combustion, pyrolysis, thermal gasification, and plasma arc gasification. The biological method consists of fermentation and anaerobic digestion. In the chemical method, waste material is converted into useful energy through transesterification and esterification process (Mohn et al. 2008).

The solid waste undergoes combustion or incineration process produces heat energy which can be utilized for the conversion of water to steam. It is used in power generation through the gas turbine (Suksankraisorn et al. 2004). Pyrolysis process is also known as dry distillation or thermal cracking. In the pyrolysis process, the solid wastes are heated with the absence of oxygen. The output of the pyrolysis process is methane, hydrogen, hydrocarbon, charcoal, vinyl chloride and cock, liquid fuel, and solid residue (Liamsanguan and Gheewala 2008). Thermal gasification is the process of converting waste into energy by heating the solid waste at above 700 °C with the presence of limited oxygen. The gasification process outputs are carbon monoxide, hydrogen, and carbon dioxide gases, and they are used in power generation (Management of Solid Waste in Indian Cities 2005). The biological methods are fermentation and anaerobic digestion. Fermentation is the metabolic process which converts sugar into useful product such as acid, gases, and alcohol in the presence of yeast and bacteria. The output gases from the fermentation are used in power generation. Anaerobic digestion is the process of converting biodegradable waste into useful energy. It produced methane and carbon dioxide gases (Boundy 2011).

11.2.3.1 Chemical Method in Waste to Energy Conversion

Waste cooking oil (WCO) is generated from various places such as restaurant and domestic; it is about approximately 10 million tons produced from USA every year, 4.5 million tons from China, 0.7–10 million tons produced from Middle East European countries, India—0.6 million, Malaysia—0.5 million, Japan—0.57 million, Ireland—0.15 million, and Canada—0.12 million per year, respectively (Gui et al. 2008; Kulkarni and Dalai 2006). A large amount of waste cooking oil is dumped by fast food shops and restaurants across the world resulting in

environmental hazards. As the oil is dumped into the water sources, oil layers get formed on the water surface; thus, it prevents the exchange of oxygen across the water surface. The ineffective way of disposing the WCO results in obstruction of drainage pipes which causes soil and water pollution (Babu and Anand 2017). Thus, it is essential to properly recover and reuse the waste cooking oil. When the waste cooking oil is reused, it gets oxidized and produces toxic contents, which leads to health problem in human being (Babu and Anand 2017).

Transesterification is the process of converting waste cooking oil (triglycerides) into biodiesel (methyl ester). Waste cooking oil-based biodiesel could be one of the promising alternative fuels for diesel engines. Maximum biodiesel yield of 97.4% was obtained from sunflower based waste cooking oil using sodium methoxide as a catalyst under molar ratio of 1:6, temperature of 55 °C, 150 min of time, catalyst concentration of 1.5 wt% and 975 rpm of stirrer speed as noticed by Babu and Anand (Babu and Anand 2017). Biodiesel was synthesized from waste cooking oil using KBr impregnated CaO catalyst. The optimum yield of 83.3% was obtained at 1.8 h of reaction time, molar ratio of 1:12, temperature of 50 °C, and catalyst amount of 3 wt% (Mahesh et al. 2015). The optimum biodiesel yield of 97% was obtained from palm oil-based waste cooking oil using KOH catalyst under temperature of 45 °C, reaction time of 3.5 h, stirrer speed of 200 rpm, and molar ratio of 0.4:1 (Kannan and Anand 2012).

11.2.3.2 Pyrolysis Technique in Waste to Energy Conversion

Pyrolysis is the process of converting waste to energy through heating the solid waste with the absence of oxygen. The products are liquid oil, gaseous fuel, and solid char. The product yield is varied based on the operating parameters as noticed by Demirbas (2004a). Microwave pyrolysis is the effective method compared to the conventional heating method in the pyrolysis process. In traditional pyrolysis technique, the heating mechanism is less efficient and slower as it is based on conduction and convection whereas, in microwave pyrolysis due to the diffusion characteristics of the electromagnetic field, heat dissipated throughout the area (Rosi et al. 2018). Thus, microwave pyrolysis provides equal distribution of heat and efficient heat transfer. It only heats the dipole material. So, the hotness was created in the mark substantial and the efficiency of the process is higher than conventional heating (Lam et al. 2010). Microwave pyrolysis technique is one of the best methods in waste to energy conversion technique when compared to conventional pyrolysis process. It converts the e-waste into diesel-like fuel for diesel engines as renewable energy source (Andersson et al. 2012).

Demirbas (2008) extracted the diesel-like fuel from waste engine oil by pyrolysis process. Pyrolysis process converts industrial or solid waste into quality and more desirable product. The maximum yield of 41.8% was obtained at 620 K used alumina-based catalyst. The octane number of the waste engine oil is greater than the gasoline fuel. Flash point is lower than the gasoline fuel. Sharma et al. (2014) examined the liquid hydrogen mixture produced from waste plastic grocery bags

through the pyrolysis process. The product consists of paraffinic hydrogen (96.8%), olefinic hydrogen (2.6%), and aromatic hydrogen (0.6%), respectively. The pyrolysis oil boiling point range is 290–340 °C, the heating value is 46.18 MJ/kg, and it is more than conventional diesel fuel. The experimental studies concluded that pyrolysis blended diesel is suitable for conventional diesel engines. Kalargaris et al. (2017) studied that waste plastic can be a renewable energy as it has higher heating value. It can be converted to useful oil by pyrolysis process and utilized in an internal combustion engine to create mechanical power and heat. The oil is produced by fast pyrolysis method, and the properties of this oil are similar to the diesel oil. Pyrolysis oil derived from plastic was used as an additive to diesel and operated on advanced injection timing in diesel engine resulted in the brake thermal efficiency and emissions all are improved.

11.3 Thermochemical Conversion of Wastes and Its Pollution Formation

11.3.1 Impact of E-waste and Biomass Incineration

The consumption of plastic has been increasing quickly in the last few years due to its lightweight, their capability to be easily formed, and noncorrosive behavior. These excellent properties are replacing the importance of the metals and wood. The global yearly consumption of plastics in the 1950s has been amplified about 20 times to nearly 100 million tons from 5 million tons (Syamsiro et al. 2014b). The e-waste contains lots of different constituents and elements, creating an intricate heterogeneous waste containing plastics, metals, and ceramics. Conventional recycling of e-waste (i.e., separating, shredding, and sorting) generates a residual material that still contains valuable metals, which often turns into a landfill Cui and Forssberg (2003). Different types of plastics were found in the examined electronic equipment rendering to Wang and Xu (2014b) as reported that the dominant polymers contained were high impact polystyrene (HIPS), polypropylene (PP), polycarbonate blends (PC/ABS), polystyrene (PS), and acrylonitrile–butadiene–styrene (ABS). With regard to large refrigeration and air conditioning appliances, cathode ray tube televisions and monitors had the minimum numbers of various polymers, with up to about 11 different types, while printers, typewriter equipment, and central processing units have 14 different polymers according to Vilaplana and Karlsson (2008). In the small electronic equipment case, Dimitrakakis et al. (2009) found the number reached 20 different types. Moreover, metals, color additives, and halogenated flame retardants were also found in electrical and electronic equipment.

Besides with this unusual kind of materials, the various additives (i.e., inorganic and organic) are as well added to polymeric plastics, which are often harmful substances, can change the properties of the material such as melting point, color,

density, and flammability, for legal, cost and/or design purposes. These artificial additives may be dyes (e.g., Cd, ZnO, TiO_2, Fe_2O_3, Cr_2O_3), halogenated flame retardants (often chlorinated/brominated organic compounds added with Sb_2O_3 or polychlorinated biphenyls), and several plasticizers or stabilizers (e.g., compounds of Cd, Ba, Pb, Zn, and Sn, or polychlorinated biphenyls) (Erickson and Kaley 2011). Incineration and gasification will result in emissions of hydrocarbons, brominated dioxins, heavy metals, and polyromantic hydrocarbons. Widmer et al. (2005) said that recycling of e-waste also causes environmental problems about the presence of various nonhalogenated and halogenated flame retardants. Yang et al. (2013) investigated that dehalogenation has become an essential topic in the recycling of e-waste plastics using pyrolysis. E-Waste plastics have been a significant ecological problem because these polymers usually comprise of toxic brominated/chlorinated flame retardants which might cause severe ecological contamination, specifically the formation of hazardous substances like polybrominated dibenzodioxins/furans. According to Rahaman et al. (2001), burning of e-waste plastics will result in emissions of hydrocarbons, brominated dioxins, and heavy metals.

Furthermore, heavy metals such as lead, copper, and mercury present in the e-waste lead to pollute the environment and ecological system and cause the serious health hazards to humans. Most of electrical and electronics devices contain hazards elements such as lead, brominated flame retardants (BFRs), polyvinyl chloride (PVC), cadmium, chromium, mercury, and beryllium. The significant quantity of lead is found in cathode ray tube which is commonly used in computer monitor, and television screens use CRTs. Continuing usage of these materials may affect the human organ systems like nervous and endocrine systems, bones, reproductive, and kidney. Moreover, among these, few of them are highly carcinogenic. Improper disposal of e-waste along with domestic waste (landfilled instead of recycling/incinerated) without any control will pollute the soil, air, and water and create the long-lasting effect on the environment (Needhidasan et al. 2014).

At the point when biomass is burned, their harmful constituents are freed into breathable air discharges and the dangerous fiery remains debase groundwater. The dumping of incomplete incineration ash on landfills is riskier due to the presence of poisonous content. The water is used to filter this unwanted content. Incinerator clinker has been advanced for such applications as fixings in bond, fill for recovering mines, compost, charcoal, mechanical tile, and street base. These are riskier than landfilling, bringing sullying nearer to where they can hurt individuals (Saidur et al. 2011) incineration is a waste treatment process that includes the ignition of natural substances contained in biomass materials. High-temperature waste treatment and incineration are called thermal treatment. Incineration of biomass materials converts into ash, flue gas, and heat. The flue gas carries the solid form of ash which is an inorganic component of the biomass. Before they are exhausted to the atmosphere flue gas must be cleaned. In some cases, electric power is generated by using the heat generated in the incineration of biomass (Fytili and Zabaniotou 2008). Incineration with vitality recuperation is one of a few waste to vitality (WtE) advances, for example, gasification, pyrolysis, and anaerobic processing.

Working principle of incineration and gasification remains the same. The main product from the gasification is the combustible gases (Fytili and Zabaniotou 2008). So, the best alternative is to convert the waste into the most valuable products with the help of thermal conversion processes such as pyrolysis and gasification.

11.3.2 Pyrolysis of E-waste and Biomass

Advanced technologies of thermochemical processes cover a widespread of modern innovations and produce either petrochemical feedstock or fuels. Recent days, thermolysis or pyrolysis (thermal cracking) is gaining renewed attention, like the fact that the added value of petroleum fuels and its valuable potential products from e-waste plastics and biomass.

11.3.2.1 Conventional Pyrolysis Techniques

Investigation on pyrolysis process has been developed by means of numerous kinds of conventional heating mechanism. The conventional heating mechanism is tubular or fixed bed reactors melting containers, blast ovens, and electric and gas heaters. In this mechanism, thermal energy is supplied externally and heats all the substances inside the reactors. In this circumstance, heating is not entirely directed to the substantial and these outcomes in lowering the efficiency of the process (Lam and Chase 2012). So, these processes are used for the pilot production. Current pyrolysis technique has numerous advantages over incineration and steam reforming technique and shows high potential in the field of waste energy recovery. However, there are so many challenges associated with pyrolysis techniques. Engine oil with less thermal conductivity range from 0.15 to 0.30 W/mK requires more processing time for pyrolysis to occur. In electric pyrolysis, the external source is applied which heats up all the substance including the chambers; this results in overall energy losses and formation of toxic compounds (PAH) (Domeño and Nerín 2003) and char (Ramasamy and T-Raissi 2007), which results in coking and fouling of the system. Besides, in conventional way, pyrolysis process distributes the heat in an uneven way, which led to poor control over heating process, and final pyrolysis process depends on the actual process condition applied on the waste materials (Lázaro et al. 2000).

11.3.2.2 Microwave Pyrolysis

Pyrolysis occurring in the absence of oxygen is thermal decomposition procedure to extract liquid oil, gaseous fuel, and solid char (Demirbas 2004b). The yields of these three products vary according to the variation of operation parameter (Bridgwater et al. 1999). There are various methods available for heating the

wastes. Among them, conventional heating and microwave heating are conducted. Real-world wastes can be treated very efficiently in microwave pyrolysis as compared to the conventional pyrolysis. In traditional pyrolysis technique, the heating mechanism is less efficient and slower as it is based on conduction and convection whereas, in microwave pyrolysis due to the diffuse character of the electromagnetic field, it heats all the substances equally. Thus, microwave pyrolysis provides equal distribution of heat and efficient heat transfer and heating methods can be controlled easily. It only heats the dipole material. So, the hotness was created in the mark substantial and the efficiency of the process is higher than conventional heating (Lam and Chase 2012).

Minkova et al. (2001) observed that microwave assisted pyrolysis offers an alternative view in the heating of the molecule where the electromagnetic field infiltrates and strongly collaborates with the dipoles arrangement. Because of the high preference of water atoms with microwaves, humidity content inside a particular biomass molecule is focused explicitly by accidental microwaves. Microwaves evaporate humidity in the deepness of the molecule, before volatilizing natural substance. The mist produced is quickly discharged into the surrounding zone, clearing volatiles, as well as making special diverts in the carbonaceous strong that expansion its absorbency. Thus, supports the arrival of volatiles at small temperatures, and consequently, its response with the mist delivered which primes to partial oxidation and creation of perpetual gases (CH_4, CO_2, H_2, CO).

Microwave pyrolysis has the advantages in the recycling treatment of different wastes, and some of the characteristics of the process include an increase in the chemical reactivity, high-temperature capabilities, in situ treatment of wastes, fast heating, waste volume reduction, etc. Handling of domestic and hazardous industrial waste and nuclear waste can be done by microwave heating. Microwave technology can be applied for control of CFC, methane, and greenhouse gases via microwave catalysis reactions. Wastes which cannot be burned such as concrete, ash, etc., that mostly contain dialectic material can be melted by microwave irradiation (Fernandez et al. 2011). The heat is making its way from the outer most layer to the innermost layer in conventional heating. The microwave heating is not the same as conventional heating. It is basically conversion of energy, not a heat transfer. Microwave can penetrate materials and deposit energy. In microwave heating, electromagnetic energy is transferred to thermal energy. So, the heat generation is done for the whole volume of the material. Microwave heating recognizes the heterogeneous reactions, and conventional heating helps in homogeneous reactions (Zhang and Hayward 2006).

It is observed by Menéndez et al. (2002), Domínguez et al. (2007) that microwave pyrolysis is used to obtain greater gas yield and lesser carbonaceous residue. That demonstrates the efficiency of microwaves in heterogeneous processes. At the higher temperatures, the heating method has the least differences. So, in the case of microwave heating, at lower temperature also, the efficiency is higher (Dominguez et al. 2008). Microwave heating has higher heating rates because no time is wasted in heating the surrounding area. The rate of heating influences devolatilization

(high heating rate improves devolatilization), the residence time of volatile (higher the rate, shorter the time). High heating rate gives high liquid yield and deposition of refractory material is reduced on the inner surface (Allan et al. 1980). If a material has a significant moisture content, microwave pyrolysis shows a unique pattern in the heating process of particle. Water molecules have good harmony with microwaves. The steam generated, by the vaporization of moisture in the core of the particle, is swiftly exited into the adjacent area. It not only sweeps vaporescent but also makes favorable channels in the solid which increases the permeability that favors the liberation of vaporescent at low temperatures (Minkova et al. 2001).

11.3.2.3 Challenges of Energy Recovery from the Pyrolysis

Biological, thermal, and other treatments are the promising technologies widely used to convert and recover energy from waste materials. Carbonization, pyrolysis, and gasification are called as thermal treatment process except for incineration process (Mohan et al. 2006). Majority of biomass energy is produced from green wastes (64%) and solid waste (24%), and remaining are agricultural waste and landfill gases (Demirbas 2000). Important chemical properties for waste treatment include elemental analysis, pyrolysis product, higher heating value, heat of pyrolysis, and heating values of char and volatiles. Some of the properties vary with species concentration, growth, and combustion environment. High moisture content in the biomass affects the pyrolysis process and the end product of pyrolysis. The calorific value of the bio-oil is greatly influenced by the moisture content of the biomass feedstock. In general, moisture content below 15% is processed in the pyrolysis process (Jahirul et al. 2012). Hence, drying process is carried out before pyrolysis. In contrast, high temperature in the drying process results in thermal oxidative reactions. Thermal stability of biomass was affected due to oxidative reaction which results in lower heating value and lower flame temperature (Dobele et al. 2007). Green waste decomposition can be characterized by particle size, specific gravity, ash content, element content (C, H, O, and N), structural content (cellulose, hemicellulose, and lignin), and extractive content. Char is formed due to the presence of inorganic compounds (Environmental Protection Agency 2007). Heat content in green waste is greatly influenced by the presence of organic compounds. Extractive content increases the higher heating values of the wood fuels.

Microwave pyrolysis produces more H_2 and CO compared to conventional pyrolysis process which is called as syngas (Huang et al. 2008). Polycyclic aromatic hydrocarbon produced also less in the microwave pyrolysis. The yield of pyrolysis oil and syngas is 8.52 and 73.26 wt%, respectively, which are higher than that of the conventional pyrolysis process. Simpler constituents are produced in the bio-oil from microwave. The syngas and methane gas produced in microwave pyrolysis are 65.2 and 22.41 and 30% higher heating values than pyrolytic gas from conventional method (Shi et al. 2014). There is a relationship between microwave power and calorific value on the solid residue. Caloric values of solid residues ranged from 18.51 to 19.66 MJ/kg are recorded when microwave power was 200–350 rpm,

which is higher than that of rice straw (15.26 MJ/kg). Calorific value of the residue decreased from 17.44-16.78MJ/kg during microwave pyrolysis process with the power of 400-500 W due to the removal of volatile content. Microwave power is high some of the fixed carbon can be pyrolysis and microwave upgraded pyrolysis has demonstrated its potential as an elective strategy for biomass transformation (Huang et al. 2008).

11.3.2.4 Effect of Pyrolysis and Its Pollution Formation

Numerous amounts of studies were carried out to study the thermal decomposition of e-waste plastics printed circuit board and analyze the product obtained, but few of them reported the toxicity of the gaseous product evolved during the process. There could be a chance of brominated substances and furnace or other by-products containing TBBPA emission during the combustion and pyrolysis process. More attention required for pyrolysis of hazardous emission (EPA 2008). Limited research works have been carried out on PBDD/Fs (brominated dioxins and furans) emission during the combustion and pyrolysis of hazardous wastes (Ortuño et al. 2014; Duan et al. 2011). Further research work is necessary to find the influence of metals and brominated components in the emission of halogenated pollution in the e-waste plastics pyrolysis and combustion.

At elevated temperature, the gaseous product can be varied greatly, which contains methane, ethylene, benzene, toluene, acetylene, carbon oxides, and other hydrocarbons. However, ploy cyclic aromatic hydrocarbons (PAHs) were also formed at elevated temperature in the pyrolysis, and it was represented by non-desired pollution. The higher PAH pollutants formed for the different hazardous wastes above 850 °C of the pyrolytic temperature (Conesa et al. 2009). A relatively higher naphthalene yield or emission factor can be noticed at the same temperature. Nevertheless, no research work has investigated the formation of pollutant emissions resulting from the thermal treatment of substances combining biomass and metal-free wastes. Only limited work has analyzed the pollution formation of biomass and other kinds of municipal solid waste during the pyrolysis process (Soler et al. 2018). Maasikmets et al. (2016) reported that the combustion of municipal solid waste results in high emission of PCDD/Fs and hexachlorobenzenes (HCBs). Edo et al. (2017) assessed torrefaction of municipal solid waste combined with wood pellets and waste wood emits the PCDD/Fs. Lundin et al. (2013) studied the organic pollutants (POPs) emissions formation and reduction of persistent during the biomass combustion with waste products from paper industry and pulps. The total yield of chlorinated benzene for WCB sample is varied from 0.01 to 17 mg/kg, however for NMF-WCB sample, the mono-, di- and trichlorobenzene is varied from 0.42 to 34 mg/kg.

11.3.3 Thermochemical Reactors for Gasification of E-waste and Biomass

Presently fossil fuels in power industries, as well as automobile industries, are used widely but at a cost of damaging the environment by adding more and more deposited carbon into the atmosphere. Biomass gasification has the potential to convert renewable biomass solid waste into combustible gases which can be used to power those industries. Many countries including India are trying to combine the use of surplus biomass in power industries and started integrated gasification combined cycle method.

The technologies associated with plastic gasification are essentially those already established for the gasification of other feedstock, such as the coal and biomass. However, the plastic characteristics include: high volatility, sticky behaviour, low thermal conductivity and tar formation are the major challenges in the conventional gasification techniques (Lopez et al. 2018). Gasifier design for handling plastics should has the following features: (i) high heat transfer rate for plastic depolymerization, (ii) operating conditions that are controlled in a better way, and (iii) appropriate retention time for cracking of tar (Lopez et al. 2018). The main biomass gasification technologies are updraft, downdraft, cross-draft, fixed bed, and fluidized reactors (Sansaniwal et al. 2017). Gasification of plastic is very difficult in updraft and downdraft gasifiers. fluidized beds have special features and therefore widely used in gasification of plastic (Wilk and Hofbauer 2013). Gasifier reactors are used to generate heat from the thermochemical reactions to produce the mixture of combustible gases for power generation. Gasifiers are mainly classified based on bed and flow. On the basis of bed, they are classified as fixed and fluidized bed. Whereas on the basis of flow, they are classified as updraft, downdraft, and cross-draft flow gasifier. For example, the fixed bed reactors are used with downdraft gasifier.

Fixed bed gasifier

The usage of fixed bed gasifier in plastic gasification processes is associated mainly in their design, operation and limited investment cost, poor heat transfer, limited gas to solid contact, continuous operation. These are challenges which are to be rectified for implementing the process (Friengfung et al. 2014). Very few studies have been carried out in the fixed bed gasifier with the co-processing of plastic waste with biomass (Straka and Bičáková 2014). Burra and Gupta (2018) examined gasification of biomass with plastics wastes. Polycarbonate, polyethylene terephthalate, polypropylene, and pine wood are gasified in their study and found that co-gasification led to enhance H_2 production up to three times the individual gasification with no loss of carbon conversion. Ahmed et al. (2011) investigated coprocessing of mixture of wood chips and polyethylene feedstocks in a fixed bed reactor at 900 °C. Moreover, they studied the synergistic on hydrogen yield and gasification efficiency of biomass and plastic wastes. The optimum plastic content in the feed was evaluated as 60 and 80% only.

Parparita et al. (2015) investigated polypropylene and biomass waste composites in a dual-fixed bed reactor in the ratio of 0.5 each with steam as a gasifying medium in the temperature range of 700–850 °C with iron cerium iv oxide (Fe–CeO_2) as a catalyst. 2.55 m^3/kg of gas yield is reported with gas composition (% vol.). Gas composition is hydrogen—40, carbon monoxide—5, carbon dioxide—16, methane—6, and with the heating value of 35.5 MJ/m^3. Ponzio et al. (2006) investigated updraft fixed bed gasifiers (60 kg/h) using biomass (0.45) and waste polyolefin (0.55) with air as a gasifying medium operated in the temperature range of 800–930 °C with ER of 0.19–0.24. The gas yield of 2.6–3.4 m^3/kg was reported with gas composition (% vol.) of H_2: 10–15, CO: 15–14, CO_2: 8, CH_4: 6–5, tar content reported to be high in the range 11.2–22 g/m^3. He et al. (2009) examined the waste polyethylene in a fixed bed reactor (0.3 kg/h) using nickel aluminum oxide as a catalyst (Ni/γ-Al_2O_3) with a standard pressure of 1.33 operated in the temperature range of 700–900 °C. The gas yield is varied from 1.22 to 2.04 m^3/kg and is reported with gas composition (% vol.) H_2: 17–37, CO: 20–27, CO_2: 35–21, CH_4: 21–10 and higher tar content of 13–106 g/m^3. The lower heating value reported in the range is 11.3–12.45 MJ/m^3. Moreover, compared to fixed bed, research activities in plastic gasification are usually carried out in the fluidized bed gasifier reactor (Hackett et al. 2012).

11.3.3.1 Updraft Gasifier

In updraft gasifiers, steam, oxygen, and air may be used as a gasifying agent; it is introduced at the bottom of the reactor for the interrelation with the biomass feedstock which is fed in the top of the reactor. The reaction bed is supported with metallic grate that is provided in the bottom of the reactor as shown in Fig. 11.1. The producer gas is drawn at the upper side with high calorific value (Pereira et al. 2012). The particle size used in these gasifier ranges from 2 to 50 mm. The operating pressure is in the range of 0.15–2.45 MPa and retention time is 15–30 min (Malik and Mohapatra 2013; Mondal et al. 2011). To avoid overheating inside the reactor and also to get quality end product, evaporation of steam is carried out into the combustion zone. This type of gasifiers has the highest thermal efficiency due to the passage of hot gases through the reactor, which leaves the gasifier unit at low temperature (Anis and Zainal 2011). Due to an elevated temperature which is achieved in the bottom of the reactor, low ash content is produced nearly equal to ash discharge point (Mandl et al. 2011). The high tar content is produced from the gasifier and is not suitable for engine applications (Brachi et al. 2014). Gunarathne et al. (2014) experimented with a pilot scale updraft gasifier using biomass pellet as feedstock and produced high syngas with a heating value of 7.3–10.6 MJ/N m^3. A countercurrent gasifier has four distinctly defined zones starting from bottom partial oxidation zone at the bottom then reduction zone followed by pyrolysis then at the top is drying zones, studied by Huang et al. (2017). The combustible gases produced in the reduction zone leave the gasifier as a mixture of gases with the volatiles produced in the pyrolysis zone and steam in the

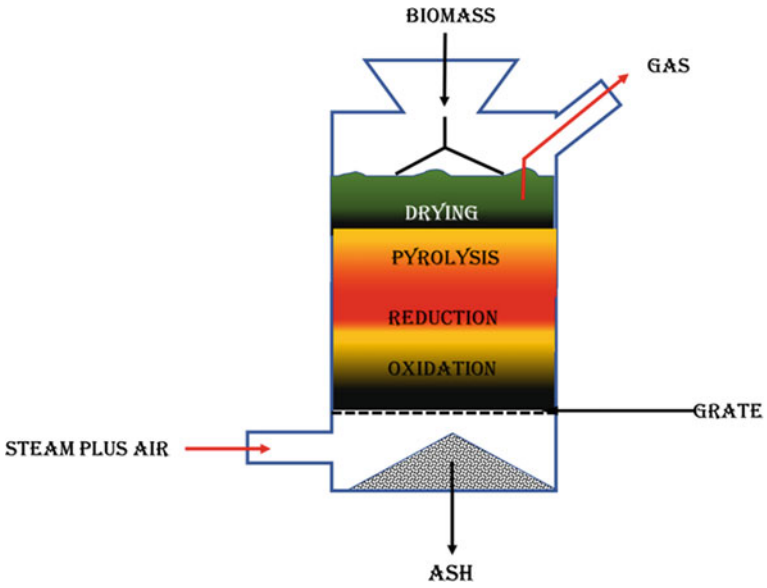

Fig. 11.1 Schematic view of updraft gasifier

drying zone. The producer gas produced in updraft gasifier is rich in hydrocarbons and has a higher heating value which makes it more suitable for heating applications, for example, in industrial furnaces but for generating electricity the producer gas needs to be thoroughly cleaned. The advantage of updraft gasifier is ease of construction and high thermal efficiency. The sensible heat is recovered by direct heat exchange with help of entering biomass feed, which is then dried and preheated, and undergoes pyrolysis before entering gasification. The excess amount of tar presence in raw gas is the disadvantage of updraft gas producer. Therefore, substantial cleanup is necessary for the fuel gas if further processing is to be carried out (Samiran et al. 2016)

11.3.3.2 Downdraft Gasifier

In downdraft gasifiers, biomass feedstock material is passed from the top whereas air is passed downward and producer gas leaves from the bottom of the gasifier. Because air is passed in the same direction as that of biomass feedstock, it is also called cocurrent gasifier. There are four zones, namely, drying, pyrolysis, oxidation, and reduction as shown in Fig. 11.2. Oxidation zone is below the pyrolysis zone and reduction zone is below the oxidation zone, as studied by Khosasaeng et al. (2017). A clean mixture of combustible gases in the exit stream is obtained. Its main advantage is that the produces gas is produced with low tar content formed during devolatilization of the material which is thermally cracked (Buragohain et al. 2010).

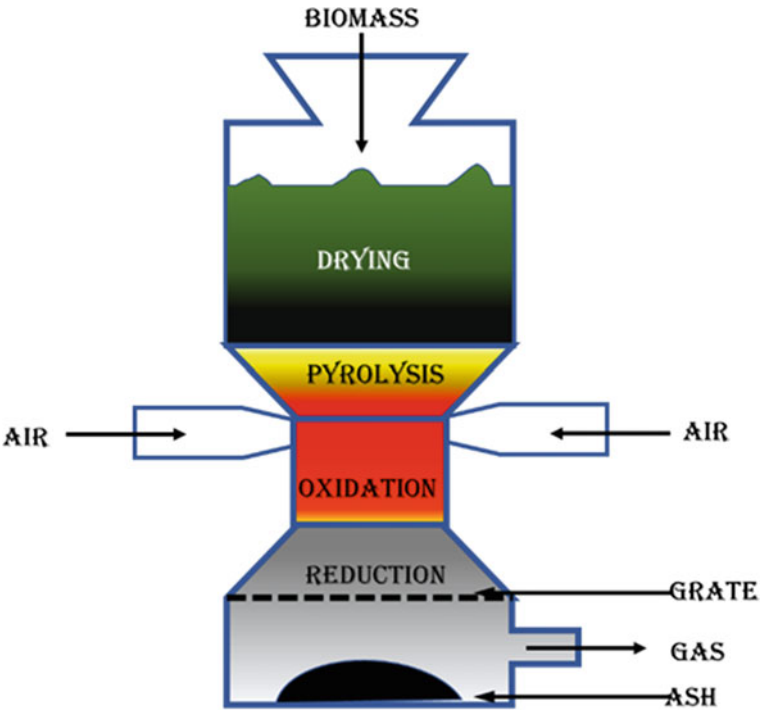

Fig. 11.2 Schematic view of downdraft gasifier

Lower tar content is suitable for gas engines and turbines (Hebden and Stroud 1982). The position of the oxidation zone is thus a critical parameter in the design of downdraft gasifier. The feedstock requirement for gasifier reactor is associated with the size of the throat. The particle size of the feedstock ranges in 1–30 cm (Couto et al. 2013). The downdraft gasifier is not appropriate for large-scale plants because of the throat size limitation for the scale-up process (Martínez et al. 2012). The feedstock material used for downdraft gasifier should have low moisture content up to 30% and low ash content of less than 1% weight (Boateng and Mtui 2012). The downdraft gasifiers are suitable for the conversion of biomass to high volatile fuel for the generation of power (Prasad et al. 2014). The elevated temperature at the exit of the gasifier in the downdraft gasifier enables low tar content of about less than 0.5 g/m^3 (Olgun et al. 2011). This lower tar content makes it advantageous for electricity production by using internal combustion engine (Martínez et al. 2012). Oxidation zone with high temperature results in melting of some ash constituents (Di Blasi and Branca 2013). Syngas is produced in the downdraft gasification in the range of 4–5 MJ/N m^3 with residence time of around 900–1800 s with carbon conversion efficiency of around 93–96% (Huang et al. 2017; Siedlecki et al. 2011).

11.3.3.3 Cross-Draft Gasifier

Cross-draft gasifier has some advantage over updraft and downdraft gasifier, but they are not of superlative type. It is one of the simplest types of gasifier where biomass fuel enters from the top of the reactor followed by drying, pyrolysis, oxidation, and reduction zones. Air may be used as gasifying medium enters through sides rather than from top or bottom as shown in Fig. 11.3. Less ash content is produced in the gasifier and has a separate ash pin, reduction zone hence reduces the biomass fuel used for operation (Srivastav 2013). The advantage of the cross-draft gasifier is a fast response to load, flexible gas production. They are unable to handle high tar content and small particle size biomass material. The carbon dioxide reduction is also poor in the cross-draft gasifiers (Anil 1986).

Fluidized bed

In fluidized bed gasifiers, the biomass feedstock is brought into an inert bed of sand, char, etc., or other fluidized bed. The biomass feedstock is fed into this fluidized bed depending upon the density and size of the biomass feedstock. Biomass feedstock is fed in two ways: one way is above the bed and other is directly into the bed depending upon how it is affected by the bed velocities, as suggested by Warnecke (2000). The process is normally carried out at a maintained temperature of bed media between 550 and 1000 °C. When the biomass feedstock is kept under such temperature conditions, the reactions in the drying zone and pyrolysis zone start and proceed rapidly, producing the gaseous components of the biomass feedstock at relatively low temperatures. The char which is remained after

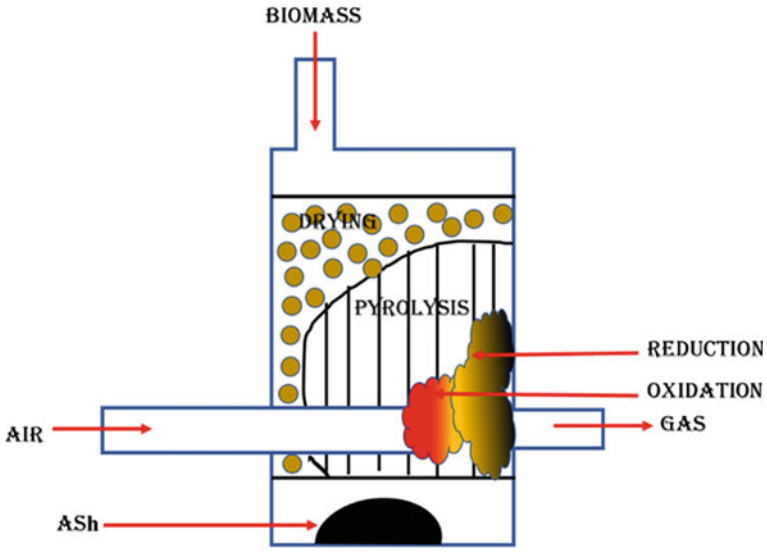

Fig. 11.3 Schematic view of cross-draft gasifier

pyrolysis zone is oxidized within the bed to produce the heat energy for other zones to continue the process like drying and devolatilization reactions.

Suda et al. (2010) suggested that the mechanism of fluidized bed gasifier is actually a hotbed made of sand particles which are continuously agitated by air that helps in producing more heat. The nozzles are located at the bottom of the bed for air distribution. fluidized bed gasifiers are having advantage on fixed bed gasifier because they produce more heat in short time with a uniform high-temperature bed of 800–1000 °C due to the abrasion phenomenon between sand particles and biomass. Generally, two kinds of fluidized beds have been utilized as a part of gasification specifically, bubbling fluidized beds and circulating fluidized bed (Molino et al. 2016). Plastic gasification generally preferred for bubbling fluidized bed. Even though, circulating fluidized beds have special features such as high yield and low tar content (McKendry 2002). Plastic gasification generally preferred for bubbling fluidized bed. The primary points of interest of bubbling fluidized reactor deal with high heat and mass transfer rate, better gas–solid contact, excellent control of temperature, and flexibility. This reactor is always operated with air as a gasifying agent when co-gasification carried out with biomass or coal (Martínez-Lera et al. 2013). Arena et al. (2010) investigated bubbling fluidized bed with a capacity of 100 kg/h using polyethylene as feedstock in sand bed material. The equivalence ratio of 0.2–0.31 and operating temperature of 845–897 is maintained which produced a gas yield of 3–4.3 m^3/kg with gas composition (% vol.) of H_2: 9.1–9.5, CO: 2.8–2.2, CO_2: 9.1–10.4, and CH_4: 10.4–7.1. Tar content of 81–160 g/m^3 is recorded with lower heating value of 6.3–7.9 MJ/m^3.

11.3.3.4 Challenges of Energy Recovery from Gasification

Although there is various technology available in the world to recover energy from waste matter, gasification has been developed as a capable method to establish ecological waste management scheme that will able reduce pollution in the environment and maximize the energy recovery from waste materials. The co-gasification of coal, plastics, and biomass has been recently focused in an effort to generate high calorific syngas from gasification technology. Kannan et al. (2013) investigated co-gasification blends of polyethylene and polyethylene terephthalate. Better cold gas efficiency and heating value have been produced from steam as a medium compared to polyethylene gasification with steam and air as a medium. By varying the blend ratio of feedstock material, it is likely to envisage quality of the syngas thus according to the application feedstock material is selected. Blending polyethylene and polyethylene terephthalate showed the optimistic effect on heating value and producer gas yield. The H_2/CO molar ratio is a key parameter for using producer gas in several applications through proper selection of biomass feedstock and an oxidizing agent.

The integration of small-scale downdraft gasification system with internal combustion engines produces electricity and heat from the biomass waste. The biomass feedstock material used for the gasification is pellets of redwood having a lower heating value of 17 MJ/kg. The experimental result showed a maximum yield

of syngas of 33.6 N m^3/h has been reported in the gasifier. The maximum exergy and energy analysis of the integrated system have been found to be 15 and 32% from the thermodynamic analysis. Moreover, gasification system creates a bottom ash in a considerable amount that may be harmful to the atmosphere and safety issues if appropriate perseverance is not made. Along these lines, this work additionally centered around the reutilization of ash keeping in mind the end goal to diminish the earth and wellbeing concerns related with its transfer, making the general procedure all the more ecologically inviting. From elemental analysis, gasification with redwood pellets showed a considerable silica amount, influencing it to end up a profoundly potential hotspot for combining compound containing silica gel. The aluminum silicate compound of zeolite is formed from the hydrothermal reaction of bottom ash which can be effectively used as an adsorbent material.

Synthesis of zeolite using hydrothermal method is used in zeolite synthesis, and this method is used in the collection of ash from the redwood pellets gasification. 5 g of ash mixed in the ratio of 2:1 with 10 g of anhydrous NaOH and grounded into a fine powder with the help of mortar and pestle. The dry mixture is taken in an alumina crucible and placed in a tubular furnace at a temperature lying between 400 and 650 °C for 1 h and 30 min. The resultant mixture is once again grounded to a fine powder before mixing with a little amount of $NaAlO_2$ and 90 ml of deionized water and stirring is done at an rpm of 500 (Hong et al. 2017). The resultant slurry mixture is then transferred to an autoclave which is made up of Teflon-lined stainless steel and kept in an oven at a temperature lying between 100 and 160 °C for a specified reaction time. After that, the reactor is allowed to cool sufficiently for a certain time in order to handle the slurry safely, and finally, it is to be filtered with vacuum unit and washing is done until pH of 7 or 8 is reached. The drying of the final product is carried out in an oven at a temperature of 100 °C overnight (Maneerung et al. 2018).

In order to evaluate the adsorption capabilities of prepared zeolites, a cationic dye which consists of an aqueous solution of methylene blue (MB) is used to perform the adsorption experiments. The batch type of adsorption experiments performed with original bottom ash and zeolite by using 25 mg of sample and 100 ml of a solution which consists of 60 mg of methylene blue. The continuous stirring of adsorption mixture was done at 300 rpm over a specific time period. From that point onward, a gathering of the supernatant was carried out at certain time interim and the color grouping remained was then analyzed by using UV-visible spectrophotometer (wavelength close to 664 nm). The direct relationship between methylene blue fixation and absorbance unit was built up utilizing standard arrangements arranged by the various weakening of the first methylene blue arrangement. The rate expulsion of color and the particular adsorption capacity, qt (mg/g) were then ascertained utilizing the accompanying condition (Molina and Poole 2004).

11.3.3.5 Influence of Gasification and Its Pollution Formation

Gasification facilities share the natural issues as like those related with mass consume incinerators, including water contamination, air contamination, transfer of slag, and other side effects (Lata et al. 2006). Gasification process includes tremendous measures of water for cooling purposes and furthermore incorporates well-being, security, and scent issues. The last major natural effect of biomass vitality might be that of loss of biodiversity. Tar is the major problem associated with the biomass gasification process (Balat et al. 2009). During gasification, tars, antacid mixes, incandescent light, and overwhelming metals are discharged and can cause ecological and operational inconveniences (Arena et al. 2009). Asadullah (2014) reported that biomass gasification technology generates diverse kind of ecological effect and perils, for example, harmful, fire, blast, and natural dangers.

Air pollution
Biomass ash, dust, fly ash/char, and gaseous emission are released into surroundings as air pollutants during biomass gasification that leads to unpleasantly influence both condition and human well-being. The producer gas leaving the reactor will enter into an air pollution control (APC) system for post process gas cleaning. The wet scrubber system has successively achieved low emission standards during biomass gasification system (Bridgwater 1995).

Dust
Dust will be generated during feedstock preparation, handling, storage, and fly ash removal (Gunarathne et al. 2014). The treatment of strong materials is an infamous wellspring of airborne particles, particularly when the solids are dry and friable. A few kinds of gasifiers may deliver hot particles as a result of glitch or hardware issues. These may touch off combustible materials and cause a fire (Technical report Central Pollution Control Board 2008). Lata et al. (2006) announced that residue can cause lung harm, aggravation of skin and eyes and may frame hazardous blend with air. The gasifier should not create in excess of 2–6 g/m^3 of residue (Deutsche Gesellshaft fur Sonnenenergie et al. 2005). Di Blasi et al. (1999) reported that the use of non-woody biomass in gasification results in high measure of sulfur, chlorine, and cinder, in contrast to gasification of woody biomass. Sulfur and chlorine have the few negative effects on condition (Sutton et al. 2001). Nitrogen and sulfur are available in a significant number of the results and the comparing oxides are created amid burning of the fuel gas; these oxides (NO_x and SO_x) can have a negative ecological effect.

Carbon monoxide poisoning
Carbon monoxide is a major constituent of producer gas and is the most widely recognized reason for gas harming. It is predominantly poisonous due to the

absence of color or smell. Carboxyhemoglobin (COHb) framed as 80–90% of consumed CO ties with hemoglobin, which is a particular biomarker of presentation in blood. Hemoglobin partiality for CO is 200–250 times that for oxygen. Epidemiological and clinical information show that CO from smoking and word related exposures ecological may provide for cardiovascular mortality and myocardial localized necrosis (Mishra et al. 2015).

Health and environmental effects associated with selected aromatic hydrocarbons (tar)
Output put gas from biomass gasification process is cleaned by water scrubbing. The developed organic compounds enter the cooling stream with flue gas dust particles. The disposal and treatment of this waste through gasification are tedious process due to the presence of toxic compounds. It will affect human health and the environment. The maize cops are used as feedstock in downdraft biomass gasification process and the condensates were collected and cooled by producer gas and it was kept in cooler at about 2 °C for 24 h before analyzing with gas chromatographer. The chemical compositions of producer gas are 1,3 + 1,4-dimethyl benzene, naphthalene, toluene, benzene, ethylbenzene, and 1,2-dimethyl benzene. Among these, naphthalene and xylene concentration were found higher than permissible exposure limit (PEL), which are hazards to both human health and surroundings, but the concentration of benzene, toluene, and ethylbenzene was below the permissible limits (Menya et al. 2014).

11.4 Factors Affecting Thermochemical Conversion Process

11.4.1 Factors Affecting Microwave Pyrolysis

The pyrolysis yield was varied depends on temperature, heating rate, residence time, and the addition of microwave absorber on the pyrolysis process. The following sections explain the individual factors and its effect on the pyrolysis process.

11.4.1.1 Influence of Temperature on Pyrolysis Yield

Miandad et al. (2016) stated that pyrolysis of polystyrene waste at 400 °C for 75 min of reaction time yields 8, 16, and 76% of gas, char, and liquid oil by mass, respectively. Increasing the pyrolysis temperature to 450 °C increases the gas and liquid yield to 13 and 80.8% by mass, respectively, but decreases the char yield to 6.2% by mass. The optimum temperature and response time was found to be 450 °C and 75 min. higher temperature exhibits the formation of gaseous product due to secondary cracking and higher kinetic energy.

In the polyethylene pyrolysis, there was no wax produced above 600 °C related to the lower temperatures shown by Williams and Williams (1997). Lighter components were produced by breaking down the massive wax. The amount of gas increases with increase in the temperature. A wide variety of smaller organic molecules were generated due to high temperature which increases the gas formation as the molecules break down and secondary reaction (Miandad et al. 2016). The amount of oil and wax decreases with an increase in pyrolysis temperature. The Increase in temperature above 800 °C promotes the secondary chemical reactions in the pyrolysis process which influence the formation of smaller chain hydrocarbons and hydrogen. The hydrogen and smaller chain hydrocarbons contain higher energy content (Calorific value) compared to longer chain hydrocarbons. Singh and Ruj (2016) also observed the same results where high temperatures result in the high formation of gas with an increased amount of smaller chain hydrocarbon compounds in the products. Adrados et al. (2012) found that the cracking reduces because of the residence time deficiency on increasing the temperature in the compounds and reactor as well as aromatic compounds in the form of wax having large molecular chains were obtained in oil product.

11.4.1.2 Effects of Heating Rate on Pyrolysis Yield

The microwave heating and conventional heating are distinguished based on differential heating rates of the material being heated. Microwave heating shows a higher heating rate because microwave energy is transferred directly to the material by means of molecular interaction with the electromagnetic field, which does not waste time for heating the environment. Therefore, significant time and energy savings are achieved in microwave pyrolysis. High heating rates improve the devolatilization of material which decreases the conversion time. The residence time of volatiles is regulated by heating rate also. The shorter residence time, the faster the volatiles, and the higher heating rate reaches to the regions of external cold results in bringing down the activity of vapor phase products belongs to secondary reactions which gives high liquid yields and decreased deposition on the char's internal surface of the refractory condensable material (Dobele et al. 2007).

Slow pyrolysis process can be described with parametric conditions such as 400 °C of temperature and heating rate of (0.1–1 °C/s) with residence time of more than 30 min. The composition of slow pyrolysis product is found as 35% biochar (solid), 30% bio-oil (liquid), and 35% syngas (Marcilla et al. 2013). Demirbas and Arin (2002) stated that flash pyrolysis has the fast heating rates with the temperatures of (400–600 °C). Vapor retentions times are typically under 2 s. Compared to slow pyrolysis, extensively less tar and gas are delivered. The circumstances under which the fast pyrolysis happens to result in the generation of low water and char content bio-oil, with the expanded energy esteem. Rapid cooling of the pyrolysis vapors provides the pyrolysis oil. Compare to conventional electrical pyrolysis, microwave

pyrolysis has higher heating rate, efficiency and provides uniform volumetric heating of the substances. The microwave-assisted pyrolysis increases the gas production and decreases the char formation due to hot spot formations (Appleton et al. 2005).

11.4.1.3 Effects of Microwave Absorber on Pyrolysis

The pyrolysis process products can be altered or tailored by incorporating receptors in the material. Dielectric properties of product determine the heating mechanism of the process, so it must be considered, because all these factors play a role in interaction with volatiles (Dominguez et al. 2008). A spent catalyst can change over waste oil into diesel oil. Lesmana and Wu (2015) reported the pyrolysis of waste oils within sight of a spent impetus, and also the recovery properties of the spent impetus, for example, the sort of recovery (in situ and ex situ) and time and temperature for spent impetus recovery. The yield of pyrolysis oil was higher than 60% when waste oil was pyrolyzed at 370 °C.

The addition of proper susceptors in microwave method can increase the yield value of the liquid oil. Previous experiments conducted on pyrolysis of waste engine oil as observed by Tripathi et al. (2015) examined that yield of saturated hydrocarbons is 40, 55, and 50%, respectively, at the temperatures of 300, 400, and 500 °C, and also reveal that aromatic benzene derivatives are high content at the higher and lower temperatures and chain length decreases as temperatures increase. This shows the temperature at which the work should be carried on. It clearly shows that the temperature must be around 400 for maximum output of saturated hydrocarbons. Domínguez et al. (2006) study the effects of char and graphite on pyrolysis oil yield. It observed that the maximum yield was obtained in char as a receptor in microwave pyrolysis method as compared to graphite receptor. Moreover, it was noticed that graphite cracking the aliphatic chains and converted into lighter species. The rate of reaction depends upon the size and shape of the mesh (Hussain et al. 2010). On the other hand, Wan et al. (2009) studied the effect of different catalysts on microwave pyrolysis, corn stover, and aspen wood used as a feedstock in microwave pyrolysis. It was found that the catalysts to speed up the heating participate in the so-called in situ upgrading of pyrolytic vapors.

11.4.2 Factors Affecting Gasification

11.4.2.1 Effects of Equivalence Ratio on Syngas

The comparability proportion is the actual proportion of air to biomass, as for the stoichiometric requirements of biomass gasification (Mevissen et al. 2009). Narváez et al. (1996) reported that CO and H_2 divisions in syngas upgraded when equivalence ratio (ER) esteems were diminished. However, the yield of vaporous items will diminish as well when the ER is lessened underneath the limit, which is the

commencement of pyrolysis. Higher ER brings about the lower yield of CO and H_2, with an expansion in CO_2, which in turn diminishes the warmth substance of the Syngas. By differentiating, higher ER enhances the breaking of tar because of higher O_2 accessibility for unpredictable species to respond with. Be that as it may, an inconsequential impact of ER was found on nitrogenous items, amid gasification. Zhou et al. (2000) revealed a small increment in smelling salts (NH_3) yield at a temperature of 800 °C, utilization of sawdust as the feedstock material when the ER was increased from 0.25 to 0.37. Gasification is ruled by the pyrolysis process having comparability proportion lower than 0.2 and ruled by ignition with identicalness proportion higher than 0.4.

11.4.2.2 Effects of Biomass Size and Moisture Content

In fixed bed gasifiers, there is a constraint in measure related to the biomass (Kaupp and Goss 1981). For case, positive properties of maker gas are accomplished at the feedstock size of 1–2 cm amid peach pruning gasification (Yin et al. 2012). Hydrogen (H_2) and carbon dioxide (CO_2) substance expanded with the reduction in the size of peach pruning. There is a perception that little size biomass fundamentally builds the vitality proficiency of gasification process (Alauddin et al. 2010). The small size biomass yields more producer gas as compared with bigger size biomass for specific gasification time. Warmth exchange region increments with molecule estimate lessening, in this way upgrades unstable, discharged amid pyrolysis process (Hernández et al. 2010). There may be a chance of high weight drop issue in the gasification of little size biomass and in addition high residue content in producer gas. The issue of inadmissible develop gasification bed in the reduction zone additionally emerge with little size and low-thickness biomass (Biagini et al. 2015). Homogeneity of biomass measure likewise influences the execution of gasifier. The proficiency of gasifier increments as expanding the level of homogeneity of biomass estimate (Belonio 2005).

In most fuels, there is little selection in wet content since it is decided by the fuels type, its origin, and treatment. It is fascinating to use fuel with low wet content as a result of heat loss thanks to its evaporation before the chemical change is appreciable and also the heat budget of the chemical change which impedes the reaction. For example, for fuel at the temperature of 250 °C and the exit temperature of raw gas from gasifier at 3000 °C, 2875 kJ/kg of heat is required for heating and evaporating the wetness. Besides, impairing of the heat budget of the gasifier, high wetness content conjointly develops a load on filtering and cooling the instruments with the increment in the pressure drop across these units owing to compressing liquid. Biomass with over 30% dampness content decreases calorific estimation of producer gas because of the inefficient process of pyrolysis during biomass gasification (Lata et al. 2006). Nature of producer gas in term of quality of heating value can be influenced by the dampness content of biomass. Biomass with high dampness content yields producer gas with low calorific value or heating values (Warnecke 2000). Warmth required for finishing pyrolysis process is

deficient in light of the fact that more warmth is consumed by feedstock for driving off dampness amid drying process. The maker gas from rice husk with dampness content of 15% has higher CO and H_2 rate than the maker gas from rice husk with the dampness of 30% (Mevissen et al. 2009).

11.4.2.3 Effects of Gasification Temperature

The temperature of gasification temperature can be influenced by proportionality proportion. The gasification temperature can be influenced by proportionality proportion. Increase in temperature increases the proportion of proportionality due to the upgrade of the combustion procedure in the oxidation zone (Guo et al. 2014). The elevated temperature in gasifier is advanced tar splitting and improved endothermic singe gasification rate, which helps in yielding producer gas with enhanced warming quality (Liu et al. 2012). The levels of ignitable gas are CO and H_2 increments with expanding gasification temperature (Wang et al. 2015). By and large, not surprisingly, the oxidation zone has the most elevated temperature among different zones, while the temperatures everything being equal amid gasification. The wavering happens because of the automatic nature of downdraft gasifiers (Balu and Chung 2012). For normally suctioned gasifier, air flow rate to the oxidation zone varies amid gasification which is relied upon bed porosity and suction fan limit. The variety of air flow rate modifies warm discharged amid oxidation process, therefore, gasification temperature swayed.

Temperature plays an important role in operating parameters, which puts an effect on the composition of gases and conversion of carbon throughout the gasification and oxidation reactions. Heating value, gas yield, the efficiency of cold gas, and finally yield of char and tar in the process of gasification are influenced by the temperature. This effect relies on the thermodynamic behavior associated with the reactions and the balance between exothermic and endothermic reactions (Lata et al. 2006; Belonio 2005; Basu 2010; Wood and Branch 1986). There is a restriction to how high the temperature for the gasification process can go up to (tolerable level) due to its impact upon (1) the unstable issue content in fuels; (2) materials of development utilized as a part of the gasifier; (3) the creation of undesired-capable gases, for example, NO_x; and (4) its impact on the fiery debris combination (Warnecke 2000; Paethanom et al. 2012; Kim et al. 2014). High gasifier working temperature has been accounted for reasonable high biomass carbon change which eventually lessens the tar substance and delivers more flammable gases (Paethanom et al. 2012). Hydrogen focus has been seen to be expanded at first and after that steadily diminished with the expansion in the temperature.

11.4.2.4 Effects of Biomass Consumption Rate

The rate of biomass utilization is influenced via air stream rate and estimation of biomass. The utilization rate of biomass is corresponding to air current rate and

conversely corresponding to the biomass measure (Tinaut et al. 2008). As the flow rate of air increments, accessibility of oxygen expands which enhances the rate of oxidation. This implies biomass utilization rate heightens with expanding air flow rate. The littler size of biomass upgrades the process of oxidation because of bigger add up to response zone per unit volume of biomass.

11.5 Synthesis of Microwave Absorber from Waste Residues

11.5.1 Microwave Heating of the Carbon-Based Material

Based on the existing studies, the microwave heating of carbon-supported materials may be categorized into two classes named as solution heating and stable solid heating. The section of microwave absorber determines the type of heating required. Solution heating is characterized by means of microwave-assisted organic synthesis (MAOS), and the opposite is stable solid heating, where the key objectives are stable carbons and metals. Solution and stable heating fluctuate to a great extent due to the additional reactions that take place during the heating process. Microwave heating is especially associated with the dipole rotation of polar solvent molecules. Conversely, freely rotatable dipoles are not available in carbon-rich solids. Therefore, the movement of electrons generates heat either through Joule heating within the grain or arc generation at segment boundary barriers (Kim et al. 2014).

Microwave heating involves with dipolar polarization and ionic conduction of the microwave absorbing material. Water and major solvents like dimethylformamide and ethanol tetrahydrofuran have dipole substance in nature (Kim et al. 2014). The dipoles are rotating when the microwave is applied, and the rotation will delay to the modification of electrical field which is the reason for heat dissipation due to friction. Further, the solution is additionally heated by ions exist in the ionic conduction phenomenon. In the case of solids supported by carbon does not contain free rotary dipoles, so that microwave heating cannot be explained beyond the limit due to the interaction between microwaves and electrons is critical. The Maxwell–Wagner–Sillars polarization [MWS] called surface polarization is the main cause of solid heating supported by carbon. Moreover, semiconductivity function is obtained in the carbon-supported solids due to delocalized pi electrons inside the graphitic vicinity (Wallace 1947; Ganguli and Krishnan 1941). Thus, carbon-supported solids heated by Joule heating play important role in the microwave phenomena. In these cases, in contrast to solution heating, microwave heating could be very effective and selective due to the fact the target material entirely absorbs the microwave power.

Conducting materials, for example, metals with redirect microwaves and results that unable to execute the conversion of microwave vitality to heat (Clark et al. 2000). There may be a variation in the response of bulk metals and metal

nanoparticles to microwaves. In the microwave process, the skin depth can be a quantity of the depth of microwave penetration during which the incident radiation decreases to 36.8% of its incentive from the surface (Metaxas and Meredith 1983). If the skin depth value of a material is less than its thickness that begins the microwave heating on its surface. Particle size observation studies depicted that skin depth value of bulk materials is within the order of microns (Mishra et al. 2006). However, micro- and nanometal powders well interact with microwaves pores since the pores and skin depth of the metals will increase with a decrease in its particle size (Gupta and Eugene 2011). The heating of bulk metals with the aid of microwaves is not an easy task, and it is likely to heat nanosize metal powders.

In the heat transfer concerns, the microwave is an attractive susceptor. The literature study illustrated that SiC susceptor provides the heat to the core metal through the conduction and radiation (Janney et al. 1992). It denotes that effective utilization of microwave absorber which results in lower heating potency. The effectiveness may be further enhanced by a selection of suitable microwave vessels. Especially the vessel materials itself has a tendency to convert the microwave into heat means, the vessel plays a vital role in hybrid microwave heating. Heating materials comprise of polar molecules are used for microwave heating which promotes higher heat transfer characteristics with cost economic. In addition to this, the materials with a high dielectric loss factor may be applicable to various processes in view of microwave heating. Among the existing absorber, carbons are excellent microwave absorbers which would be created or changed by microwave heating. Furthermore, carbon materials have a potential capability to convert microwave strength into heat, and so it would also act as a microwave receptor to indirectly heat the material which is transparent to microwaves. In continuation with this, carbon materials could be used as microwave receptors in different process applications such as pyrolysis of organic wastes, soil remediation, catalytic heterogeneous reactions, and biomass. The dielectric loss tangent of different carbons is greater than the loss factor of distilled water (distilled water tan $\delta = 0.118$ GHz and 298 K) and it is lesser than coal (Menéndez et al. 2010).

Among the different carbon-based materials, graphite is a strongly suggested microwave absorbing substance that can withstand higher temperatures and also gives off higher heating rates. Graphite with carbon substances are evident to produce a microplasma but at the same time as they are heated in presence of microwaves (Menéndez et al. 2010). The microplasma has generated while adding carbon-based material like graphite. During this process, the small dimension (10–1000 μm) plasma was generated because several electrons might jump out of the material because of their higher kinetic energy. The ionization of the atmosphere due to the arcing that visualizes the spark output for a short time and a small spatial region. However, during this process, few more electrons may come out from the core materials. This is due to driving force existed in the electrons caused by higher kinetic energy. If it is continuous, ionizing the electrons which are the so-called micro-plasma, they exist for a short period of time. This could be visualized by sparks or arc formation existed during the process (Menéndez et al. 2010, 2011), although graphite or other carbon items were used for supporting the microwave

pyrolysis (Menéndez et al. 2004; Domínguez et al. 2005). Considering the microplasma, it has a behavior of arc formation during the pyrolysis which could adversely affect the equipment. In order to avoid this circumstance, it is advisable to use the graphite with other substances to enhance the heating effectiveness without arc formation. However, graphite mixed with different materials, which requires an in-depth examination throughout the microwave heating. A high-grade graphite powder combined with either microwave absorbing material or non-microwave absorbing material can be used for creating the crucibles. This would increase the heating value of microwave heating. Several studies reported about microwave engrossing materials named as char or graphite to SiC that increase the conversion efficiency of microwave to heat (Revesz et al. 2002). The alumina or zirconia can be combined with silicon carbide for executing microwave heating at different temperature (Vandervoort et al. 2007; Fall and Shulman 2003). However, there is no report existing for investigating the microwave heating of mixtures including graphite.

11.5.2 Synthesis of Carbon-Based Material from Ash and Char

Carbides are widely known for its stability in thermochemical process with high wear resistance and hardness among the all other modern ceramics (Martínez et al. 2006; Sun and Gong 2001). The silicon carbide (SiC), non-oxide ceramics can be formed as whiskers or fibers by different thermal processes (Martínez et al. 2006; Silva and figueiredo 2001). The two primary methods followed in this process to make silica carbide are (i) mixing silica and carbon at 1300–1500 °C inert atmosphere (Martínez et al. 2006; Freitas et al. 2004) and (ii) mixing of carbon and silica at 1300–1550 °C in the chlorhydric atmosphere (Martínez et al. 2006). Another way widely known is thermal decomposition (pyrolysis) in a controlled atmosphere of rice husk (RH), comprises above 90% of silica. The fine SiC whisker or elements forms in length between 10 and 80 μm and diameter between 0.5 and 1 μm can be obtained from this process (Kirk-Othmer 1996; Gorthy and Mukunda Pudukottah 2004). Vapor–liquid–solid (VLS) process was also used to produce the SiC whiskers in the presence of transition metals such as Fe, Co, and Ni as catalysts. In this process, the vapor is transported to the liquid catalyst as precursors which is positioned at the tip of the whiskers, the integration of the component into the precipitation of the solid crystal and liquid at the solid–liquid interface. The existence of liquid catalyst discriminates this process from other whiskers growth process. The SiC whiskers are commonly in cubic structure which is mounting in $\langle 1 \times 1 \times 1 \rangle$ direction (Li et al. 2016).

The SiC is prepared by temporarily bonding a stoichiometric mixture of micronized (<20 μm) metallic silicon and carbon. The temporary binders such as polyvinyl alcohol, methyl cellulose, sodium silicate, polyethylene glycol, and the

SiO_2 sol can be used for bonding silicon and carbon. The SiC precursor is formed into green bodies by using common technologies such as pelletizing, extrusion, and granulation. For the production of open cell foams or 3D structures using existing methods such as pelletisation, extrusion and granulation (Sehwartzwalder and Somers 1963; Studart et al. 2006). In this process, the slurry is synthesized by using the similar raw material, but a significant quantity of temporary binders and rheological additives has used to attain the essential viscosity and thixotropy for the slurry. The outcome structure is then dried out at atmospheric temperature and subsequently undergoes thermal treatment at atmospheric pressure under inert condition in a furnace up to 1360 °C. Continuous heat treatment of 1 hour is essential for the preparation of self-adhesive porous SiC. The temperature should be maintained below the melting point of 1400 °C for SiC during heat treatment process. The high carbon yield resin converted into amorphous carbon in the pyrolyzed condition, which combines and bind the silicon and carbon particles together (Duong-Viet et al. 2016).

SiO is formed above 1000 °C when the metallic silicon may react with remaining traces of oxygen. The SiO gas further reacts with the carbon structure forms into SiC and CO according to Eq. 3, further the CO is reacted with metallic silicon forms into SiO and SiC according to Eq. 4.

$$SiO_{(g)} + 2C_{(s)} \rightarrow SiC_{(s)} + CO_{(g)} \quad (1)$$

$$CO_{(g)} + 2Si_{(s)} \rightarrow SiO_{(g)} + SiC_{(s)} \quad (2)$$

The oxidative treatment carried out for SiC for 2 h in air at 800 °C to remove the unreacted carbon residue in their matrix (Duong-Viet et al. 2016). The activation carbon obtained from rice husk can be activated with chemical or physical methods. The chemical impregnation of rice husk ash with KOH or NaOH at 650–850 °C results in activation with extremely high surface area (Brunauer–Emmett–Teller (BET) 1413–3014 m^2/g) (Guo et al. 2002). The increase pore size in rice husk and removed the silica by using of KOH or NaOH. Similarly, activation carbon is also synthesized from tire-derived char (TC) by using the following method. In this process, a preliminary assay is performed to determine which environment, alkaline or acidic, is better to reduce the Zn content of the tire-derived char. Then the tire-derived char samples were subjected to demineralization by following methods (López et al. 2013).

- 1 M ($(NH_4)H(CO_3)$ $(NH_4)CO_2NH_2$)) ammonium carbonate solution with a concentration of 25 or 50 g/L, and a TC concentration of 12.5 or 25 g/L.
- Char concentration of 20 or 25 g/L and 1 M or 2 M solution of H_2SO_4.
- 1 or 2 M HCl, with a char concentration of 20 g/L.
- A mixture of concentrated commercial HNO_3 (69% HNO_3) plus 1 M H_2SO_4, and a TC concentration of 20 g/L.
- A mixture of commercial concentrated HNO_3 and water, and a TC concentration of 20 g/L.

20–25 g of TC is mixed in a demineralizing solution for 2 h by using stirrer at room temperature. The pretreatment of 20 g TC for 24 h in 16 ml of HNO_3 is involved in HNO_3/H_2SO_4 treatment. finally, the mixture of one litre of 1 M H_2SO_4 is added and the mixture is shaken for 2 h. The pretreatment of 20 g of TC with 16 ml of HNO_3 (Panreac, 65% pure; density 1.41 g/mL) for 24 h is involved in demineralization process by HNO_3/H_2O. The mixture is shaken for 2 h by adding 1 l of distilled water. Zn content is reduced significantly in the TC sample, which is corresponded to the one prepared by HNO_3/H2O demineralization treatment (DTC-NW). It was stimulated by KOH chemical treatment (López et al. 2013).

Agricultural waste or residues contains organic compounds from organic sources such as rice straw, sugar cane, coconut shell, bagasse, and others (Sudiana et al. 2017). Rice husk is one of the alternative material which can be potentially used in microwave absorber fabrication. The production of AC-SiC nanowire from agricultural waste is through a novel free-pressureless spark sintering technique (FPSPS) which is manifested below. In this process, one gram of Si powder is mixed with 20 ml of ethanol and exposed for a time of 3 min to 20 kHz ultrasonic frequency. The obtained liquid solution is mixed with already available biomass and is stirred or distributed by using mechanical means. Then vacuum drying is used to dry the sample and silicon-treated stalk samples will be added to graphite. Then FPSPS processing is carried out by heating as well as cooling at a specific rate of 20, 50 and 100 °C. In the vacuum dryer, it is held at 1300, 1500 and 1600 °C and the applied pressure will be around 5 MPa (Bradbury and Olevsky 2010).

11.5.3 Dielectric Properties of Carbon-Based Materials

The Magnetic and Electric field components are perpendicular to each other in all electromagnetic waves and microwaves. Materials can be classified according to the component of the electric field interaction with the microwave field in three ways: i) Microwave-transparent insulators that pass through the medium without losses, (ii) conductors-reflect micro-waves cannot penetrate and (iii) absorptions. Microwave heating is also referred to as dielectric heating because dielectrics are the materials which absorb microwave radiation (Thostenson and Chou 1999). These include dipole orientation, atomic polarization, electronic polarization, ionic conduction, and interfacial or Maxwell–Wagner polarization mechanisms. The transfer of electromagnetic energy to thermal energy occurs only in dipole and Maxwell–Wagner polarizations at microwave frequencies (Mijović and Wijaya 1990). The Maxwell–Wagner polarization exhibits on the boundary of two dissimilar dielectric materials or freely movable charged particles such as π-electrons in the solid carbon material (Zlotorzynski 1995).

The accumulation of the charge, at the material interface, is produced and the energy is dissipated in the form of heat. This is due to the so-called Maxwell–Wagner effect, i.e., when the charged particles cannot couple to the changes of phase in electric field. The communication of microwaves with metal powder or

metals might be further contributed to the energy absorption effect (Marken et al. 2006). In the irradiated sample, the polarization occurs when the effective current is out of range with reference to the applied field by a difference (termed δ). This difference describes the loss factor or dissipation factor, or the dielectric loss tangent represented by tan δ. The study of dielectric parameters is most essential in order to select optimal condition in designing microwave absorber which influences the absorption through heat dissipation. Magnetic parameters such as permeability and magnetic loss influences absorption. Hence, the material is described only the mixed dielectric material of carbon and resin, and the function of magnetic loss and permeability in microwave absorption will not be discussed (Meredith 1998).

Permittivity

The relation between the dielectric material capacitance and the microwave propagation is described by the permittivity of a substance. The mathematical representation of both real and imaginary part in a material and the quantity of electrostatic energy stored in a unit volume for a given applied field are determined by the real permittivity "ε", also known as dielectric constant. The permittivity of imaginary part is represented by ε'' in mathematical equation. The energy loss is described by the lag in the polarization upon wave propagation as it passes through a dielectric material. The ratio of natural permittivity of the material, ε, to permittivity of free space ε_0 is the relative permittivity of a material, ε_r (Yusof 2004).

$$\varepsilon_r = \frac{\varepsilon}{\varepsilon_0} \tag{3}$$

The most common formula for complex permittivity of a substance is written as

$$\varepsilon_r = \varepsilon_r' - j\varepsilon_r'' \tag{4}$$

Loss Tangent, tan δ.

The dissipation of power or energy from the incident waves are represented by loss or tan δ. The loss factor is a most important parameter in microwave absorption, which converts incoming microwave energy into heat. The conductivity and permittivity of the material influences the overall losses based on dissipation as noticed by Neelakanta and Park (Neelakanta 1995). In general, an efficient absorber material would have a considerable amount of loss factor. The ratio of the loss aspect to stored component of absorptive material is termed as dissipative factor or the loss tangent, and it is commonly expressed as (Vinoy and Jha 1995)

$$\tan\delta = \frac{\sigma + \omega\varepsilon''}{\omega\varepsilon'} \tag{5}$$

Especially with pure dielectric where losses are very low, the influence of conductivity inside losses is considered zero. A dielectric with small loss is considered to have $\sigma \ll \omega\varepsilon''$ with $\sigma \approx$ zero. Therefore, for pure dielectric:

$$\tan\delta = \frac{\omega\varepsilon''}{\omega\varepsilon'} \tag{6}$$

$$\tan\delta = \frac{\varepsilon''}{\varepsilon'} \tag{7}$$

It has reverse properties with $\sigma = \infty$ and $\sigma \gg \omega\varepsilon''$ in the case of conductor. The loss tangent for conductor is then:

$$\tan\delta = \frac{\sigma}{\omega\varepsilon'} \tag{8}$$

The reflection loss (RL) in dB unit could evaluate the microwave absorbing potential; if the RL values of an absorber are lower than 10 dB (90% absorption), the absorber works properly in the microwave field. Due to the low complex permittivity, the microwave absorbing properties are poor which cannot disperse electromagnetic energy efficiently (Ding et al. 2012).

11.5.4 Factors Influencing Dielectric Properties

Dielectric properties of the materials may be affected by some of the parameters such as temperature, frequency, moisture content, and density as in the circumstance of wet materials like biomass (Nelson and Trabelsi 2012).

Frequency
Dielectric constant and loss factor of material are momentously varying with frequency, but low-loss and transparent materials are exceptions (Nelson and Trabelsi 2012). The relationship between the frequency and dielectric properties depends on the loss mechanism(s), involved. Debye equation is the predominantly used one which relates the polar materials permittivity and frequency (Metaxas and Meredith 1983).

$$\varepsilon = \varepsilon_\infty + \frac{\varepsilon_s - \varepsilon_\infty}{1 + j\omega\tau} \tag{9}$$

where ε_s and ε_∞ are the dielectric constants at d.c (static) and high frequency, respectively, and τ represents the relaxation time in seconds.

Relaxation time can be defined as when the applied field is removed, the time needed for the dipole to return to a random alignment (Nelson and Trabelsi 2012). Intermolecular forces are substantially associated with relaxation time, and these are

affected by temperature (Gabriel et al. 1998). At higher frequency, the dielectric constant starts to drop due to that the molecules are not able to rotate with significant amount before the field is reversed. At very low and very high frequencies the loss factor tends to zero. Dielectric properties of heterogeneous materials are complex in nature due to the involvement of more than one loss mechanism at the same time. The conductive and dipolar losses are the dominant factor at lower and higher frequencies, respectively (Adam 2017).

Temperature and moisture content

Studying the influence of temperature on dielectric properties is essential because the temperature is changing under electromagnetic heating. Molecules mobility and their intermolecular forces are adversely affected by temperature. Energy storage and dissipation of molecules are affected by temperature (Nelson and Trabelsi 2012; Gabriel et al. 1998). Applied frequency and loss mechanism involved are the factors which affect the influence of temperature on the dielectric property (Nelson and Trabelsi 2012). Polarization losses are exhibited by polar materials; relaxation time increases with decreasing in temperature. Intermolecular forces between molecules get weaken and rotation ability of molecules increases with increase in temperature (Adam 2017). Dielectric properties of biomass generally depend on the water content. Hence, at low-temperature dielectric properties of biomass can be understood by studying the temperature effects on polar materials dielectric properties. Moreover, free water is not only responsible for biomass water content. Compared free water, the bound water has less polarization ability which in turn lower dielectric constant and loss factor due to restricted movement (Metaxas and Meredith 1983; Bergo et al. 2012).

The physical structure and chemical composition of biomass are significant changes which start with drying to char formation during the pyrolysis process. In this, the physical structure and chemical composition of raw biomass are entirely different from final one. These changes adversely influence the dielectric properties of biomass. Effect of pyrolysis temperature on loss tangent of wood mass at 2.45 GHz microwave oven was investigated by Robinson et al. (2015). They reported that increasing the temperature up to 120 °C, a significant drop in loss tangent was observed which is due to evaporation of moisture content. When the temperature is raised above 200 °C a second reduction was observed followed by meager loss materials get evaporated between 250 and 480 °C. After that rapid increment of loss tangent was observed at above 500 °C due to good microwave absorptivity of char which was formed by carbonization of biomass (Adam 2017).

Density

The packing density of granular and pulverized solids are greatly affected their dielectric properties and also increases the permittivity. This is because of less void fraction and permittivity than solid fraction in the mixture at higher packing density, which results in increases in the overall permittivity of the mixture. Different forms of biomass such as sawdust, chips, shavings, logs, and pellets. The density of

biomass is varying with their size and shape. Also, dimensions of the feedstock for processing are decided based on factors such as the form at which the material feedstock is available, processing requirements, and the economic considerations (Nelson and Trabelsi 2012; Adam 2017; Nelson 2005).

11.5.5 Microwave Enhancement of Carbon Catalyst Reaction

Carbon-supported substances are activated carbon, carbon fiber, and others that contain a specific segment of graphitic which can be expanded by raising the temperature of heat treatment process (Kim et al. 2014; Marsh and Rodríguez-Reinoso 2006). In this manner, microwave heating of different carbon-supported materials is also described. Activated carbon, char, and biomass are for the most part frequently connected with absorbents during the microwave heating. Reclamation of NO_x-saturated activated carbon and char was extensively stated in the 1990s (Cha and Kong 1995; Kong and Cha 1996). Restored activated carbon and char in the microwave heating efficiently provide sufficient energy for several cycles. Guo and Du (2012) stated within a minute regeneration of NO*x*-saturated char was done while the input power was over 300 W. Additionally, Menéndez et al. (1999a, b) suggested refurbishment of a simple property of activated carbon by using getting rid of oxygenated functionalities. The carbon and oxygen substance of oxidized activated carbon were enhanced from 84.50 to 97.82% and 14.98 to 1.56%, respectively, after exposure to 1.5 min of microwave irradiation. Temperature over 900 °C was attained approximately in a minute when the activated carbon was irradiated by 1000 W due to high carbon content. In conventional heating, 900 °C was attained at 3 h. Organic chemicals, dye, and SO_2 were removed in microwave radiation with the use of activated carbon (Hua-Shan and Chih-Ju 1999; Liu et al. 2004). The use of activated carbon increases the regeneration efficiency after repeated cycle (Ania et al. 2004), porous structure preservability (Ania et al. 2007) and improve the representative strengths included with the short time required (Zhang et al. 2007). Recently, activated carbon conversion from biomass was reported with the aid of microwave heating (Yagmur et al. 2008; Li et al. 2008). Carrott et al. (2001) mentioned the elemental composition of activated carbon fibers differed due to rapid heating over 800 °C/min, and improvement in the carbon content was noticed. Li et al. (2009) used carbon fiber as a microwave absorber for the remediation of crude oil contaminated soil.

Microwave pyrolysis was conducted continuously over a long duration; the carbonaceous char was trapped within the reactor. Increasing amount of char in the reactor will influence the pyrolysis yield and products. The volatile material present in the char during microwave pyrolysis of waste engine oil could act as a catalyst and microwave absorbent and improve the heating rate. Also, promote the heterogeneous reaction in the pyrolysis gases evolved from the pyrolysis process,

leading to different composition in the oil yield observed in the process. This work also suggested inorganic metal containing char can potentially use as a catalyst for thermal cracking (Domínguez et al. 2006; Lam et al. 2015). The presence of Fe, Ni in the char improves the catalytic effect of heterogeneous reaction like methane decomposition reaction will be reported by different studies (Muradov et al. 2005; Avdeeva et al. 2002). In addition, the valuable gases H_2 and syngas were produced in microwave pyrolysis of sewage sludge and coffee hulls in presence of char catalyst (Domínguez et al. 2007, 2008; Menéndez et al. 2007).

The high carbon and relatively low volatile content were reported in pyrolysis of waste oil at 550 °C. XRF analysis discovered that metal oxides including mainly of CaO, Fe_2O_3, Al_2O_3, ZnO, SiO_2, MgO, and NiO are present in the metallic char. The energy-dispersive X-ray spectroscopy for the metallic char revealed the existence of metalloid (Si), metals (Mg, Cu, Al, Fe, Ca, Pb, Ni, Zn), nonmetals (C, P, O, S), and halogen (Cl). Metal elements like Al, Cu, Fe, Mg, and Ni were already reported in many studies for their catalytic effect in the pyrolysis process (Muradov et al. 2005; Avdeeva et al. 2002). The metallic char added to the pyrolysis reactor led to the hot spot formation in the pyrolysis of waste engine oil promote the heterogeneous reaction in between the waste engine oil and metallic char to produce higher yield of CO and H_2 and lesser yields of CH_4 and CO_2 and. Also, the formation of lower chain hydrocarbons in both pyrolysis fuel (i.e., C_5–C_{10} hydrocarbons) and non-condensable gases was reported. Moreover, the metals get converted into metal oxides and absorb the sulfur existing in the oil.

The microwave absorber (silicon carbide, magnetite, and manganese dioxide) and microwave non-absorbing powders (alumina, titanium, and zirconia) along with graphite powder are investigated and compared with pure materials. The graphite–silicon carbide was found to have better microwave heating characters than other combinations. The weight ratio of 1:1 (graphite powder to microwave absorber) has chosen for their work. Similarly, graphite–magnetite combination showed superior heating rate pure iron oxides. The average rise in temperature of 60 °C/min attained while using a pure iron oxide (Fe_3O_4). Cheng et al. (2002) reported Fe_3O_4 heated in both E and H fields. Most of the iron oxides such as FeO and Fe_2O_3 are heated in E field. On further addition of graphite with Fe_3O_4, the heating rate of the substance becomes stronger and formation of microplasmic impacts the graphite. Fe_3O_4 converted into FeO during microwave heating of graphite–Fe_3O_4 composite and graphite and Fe could be consumed. The FeO is the poor microwave absorber and affects the heating rate subsequently, due to the fact that it cannot be used as crucible material. On the other hand, the mixture provided uniform heating and did not go through any massive change in the weight and chemical composition during the process. Also, the same results were obtained when SiC–graphite mixture reused repeatedly, hence its dielectric properties of this mixture unchanged. Weight ratio ranging among 40–50% exhibits the higher heating rate of the mixture. SEM and XRD analysis confirmed that graphite and SiC chemical response does not change during the process. Hence, SiC with graphite aggregate is more suitable for making microwave crucible and susceptors (Chandrasekaran et al. 2013).

11.5.6 Regeneration of Carbon Material

Activated carbon (AC) is a naturally synthesized material obtained by calcination of biomass and extensively used as a catalyst support and adsorbent due to its huge surface area per unit mass and great adsorbing ability (Thomas and George 2015). Generally, AC materials are directly burned to produce steam or thrown as wastes which will initiate the secondary pollute formation. Instead of utilizing AC in incineration or throwing as waste it can be regenerated, by doing so the adsorbing ability of AC can be reactivated and substantially secondary pollution formation also minimized. The regeneration of AC can be achieved through oxidization, thermal, microwave, and biological regeneration methods. Among these methods, the biological and oxidization way of regeneration are more time-consuming and economically not suitable (Sabio et al. 2004). However, microwave irradiation is an efficient regeneration method, but it is not widely used due to its limited application. Thermal regeneration is the well-known and popularized method used in AC regeneration (Dehdashti et al. 2011). In this, the process is carried out in a muffle furnace. The optimum regeneration temperature and time were found by conducting a series of experiments which involve:

- Drying at around 105 °C,
- Pyrolysis under N_2 atmosphere, and
- Gasification of residual organics by an oxidizing gas, such as steam or carbon dioxide (Guo and Du 2012; San Miguel et al. 2001).

The AC is obtained by carbonization of biomass materials under an N_2 atmosphere at 800 °C. The carbonization process evaporates the moisture content and decomposes and eliminates the low volatile matters which are adsorbed on the carbon surface (San Miguel et al. 2001). The final AC contains carbonized char in the carbon pores which is strongly linked with AC structure. Generally, steam or CO_2 or mixed of both is used as a mildly oxidizing agent in the process of controlled gasification of carbon at 800 °C (San Miguel et al. 2001). Water vapor can be used to eliminate the carbonated carbon, at elevated temperature. The remaining carbonated carbon will be oxidized by reacting with water vapor. Finally, the obtained AC has its original adsorption capacity and carbon pore structure. Compared to steam generation, all the phenolic compounds cannot be eliminated by pyrolyzing at 700–900 °C which will result in AC with the lower surface area per unit mass. It can be concluded that steam generation is the effective and cost-effective method to produce AC with the large surface area and high porosity (Cheng et al. 2007).

11.6 Characterization of Alternate Fuels Derived from Thermochemical Conversion

11.6.1 Physical Properties

11.6.1.1 Density

The density is defined as the mass per unit volume. In order to measure the weight of the sample, the electronic weighing machine is employed having an accuracy of ±0.1 g. First, the sample whose density has to be measured is taken in 50 mL of volume. Then the sample quantity weight is measured in the electronic weighing machine, and then again, the process is repeated for 40, 30 mL volume of sample fuel. This is done to ensure that the value is very accurate.

11.6.1.2 Viscosity

Brookfield viscometer DV3T model was used to calculate the kinematic viscosity of different liquid fuels. Viscosity is defined as the resistance offered by one layer to another while in motion. This property was measured as per the ASTM D445 standard. 16 mL of liquid fuel was poured into a spindle and cylindrical cup type arrangement and was subjected to continuous shear stress. The temperature of 40 °C should be maintained according to ASTM standard which is taken care by the water bath arrangement. The value of the viscosity was directly given on the screen display.

11.6.1.3 flash and fire Point

To find the flash and fire point of different liquid fuels, the open cup Cleveland apparatus is used. ASTM D93 standards have used for conducting the experiment. A practical detonation source will cause the vapor of the trial to burn at a flash point. The flash point is determined by warming an example of the fuel in a container and passing the flame over the surface of the sample. If the temperature is at or above the flash point, the vapor will ignite and an easily detachable flash can be observed. The flash produced need not sustain for a long time. Whereas, fire point is the minimum temperature at which vapor of the fuel steadily burns at least for five seconds once ignited.

11.6.1.4 Cloud and Pour Point

The apparatus as per ASTM D97 and ASTM D2500 standards were used for the tests. Pour point is a minimum temperature below which a liquid loses its flow characteristics. Cloud point is the lowest temperature at which the first crystal formation starts. A freezer which can cool below 0 °C is used, where the

temperature is decreased in steps of 3 °C, till a cloud or haze or wax crystal is formed at the bottom of the test tube containing fuel. The temperature at which the cloud forms is called cloud point. After cloud point, the temperature is reduced in steps of 1 °C till the temperature at which the fuel stops moving when the test tube is tilted. This temperature is the pour point.

11.6.1.5 Acid Value

Acid value is defined as 1 mg of potassium hydroxide (KOH) which is required to neutralize 1 g of chemical substance; it measured the carboxylic acid group in the chemical component. In acid value testing, two solutions have to prepare like burette solution and beaker solution. In beaker solution, taking 1:3 ratio of diethyl ether and ethanol and adding lesser than 1 g of testing fuel along with two drops of phenolphthalein color indicator. In burette solution, 0.1 N of KOH solutions dissolved in deionized water. The burette solution is titrated with beaker solution. The standard methods are available to determine the acid value such as ASTM D974, ASTM D664, and European Standard EN 14104. The acid value is the parameter in which found the free fatty acid of raw oil as well as biodiesel. This parameter directly affects the biodiesel property like viscosity, density, calorific value, and cetane number, and also affects the engine emission, performance, and combustion characteristics. Fatty acid causes dehydration or peroxide in biodiesel, because normally biodiesel contains more unsaturated contents. So, it easily reacts with oxygen and makes sledge, fatty acid and corrodes the engine components.

11.6.2 Ultimate Analysis and Proximate Analysis

Elemental composition of fuel is determined by ultimate analysis. The ultimate analysis is one of the vital components when considering biomass powers properties. It evaluates the level of N, S and to think about the natural effect of biomass. Also, it helps to estimate the percentage of C, H, O and heating value of the biomass fuels (Sheet 2008). Table 11.1 shows the ultimate analysis of different types of biomass. The ultimate analysis shows the contents of the organic constituents along with ash and moisture. It provides a convenient and uniform system for comparing and evaluating the fuels. The ultimate analysis gives the chemical composition of the biomass fuels (Kirubakaran et al. 2009). The accompanying ASTM norms are accessible for assurance of ultimate analysis of biomass fuels (Basu and Basu 2010).

Carbon, hydrogen	E-777 for refuse-derived fuels (RDF)
Nitrogen	E-778 for RDF
Sulfur	E-775 for RDF
Moisture	E-871 for wood fuels
Ash	D-1102 for wood fuels

Table 11.1 Ultimate analysis of different types of biomass types (wt% dry basis) (Demirbas 2004b; Haykiri-Açma 2003)

S. No.	Biomass	C	H	O	N	S
1	Lignite	65.20	4.50	17.50	1.3	4.1
2	Spruce wood	51.40	6.10	41.20	0.3	0.0
3	Hazelnut shell	50.80	5.60	41.10	1.0	0.0
4	Corncob	49.00	5.40	44.20	0.4	0.0
5	Corn stover	49.40	5.60	42.50	0.6	0.1
6	Tobacco stack	49.30	5.60	42.80	0.7	0.0
7	Tobacco leaf	41.20	4.90	33.90	0.9	0.0
8	Almond shell	47.90	6.00	41.70	1.1	0.06
9	Saw dust	53.60	6.6	35.50	1.5	0.1
10	Rice husk	46.90	5.20	37.80	0.1	0.04

Proximate analysis

The fundamental characteristics of any fuel are determined by proximate and ultimate analyses. The proximate analysis shows the quantity of combustible constituents and noncombustible constituents. It also provides the basis for estimating its commercial value. The proximate analysis examination is critical to contemplate the burning marvel of biomass (Kirubakaran et al. 2009). For example, Ash remains substance in biomass fills can cause start and ignition issues. It also gives as the gross composition of biomass and also easy to measure. For wood fuels, we can use standard E_870-06. Separate ASTM standards are applicable for the determination of the individual component of biomass.

Volatile matter	E_*&@ for wood fuels
Ash	D-1102 for wood fuels
Moisture	E-871 for wood fuels
fixed carbon	Determined by difference

Fixed carbon content is different from ultimate analysis carbon. In proximate analysis it is referred to us char yield does not include carbon in the volatile matter. Proximate analyses of various samples are mentioned in Table 11.2 (Jenkins et al. 1998).

Table 11.2 Proximate analysis of different types of biomass types (wt% dry basis) (Jenkins et al. 1998)

S. No	Biomass	Fixed carbon	Volatile matter	Ash
1	Alfalfa stems	15.81	78.92	05.27
2	Wheat straw	17.71	75.27	07.02
3	Rice hulls	16.22	63.52	20.26
4	Rice straw	15.86	65.47	18.67
5	Switch grass	14.34	76.69	08.97
6	Sugar cane bagasse	11.95	85.61	02.44
7	Willow wood	16.07	82.22	01.71
8	Hybrid poplar	12.49	84.81	02.70
9	Almond shells	20.71	76.00	03.29
10	Almond hulls	20.07	73.80	06.13

11.6.3 Thermogravimetric Analysis

Thermogravimetric analysis (TGA) is a technique which is used in the thermal analysis to study and observe the various chemical and physical changes through the changes in the weight of the materials with temperature and time. This analysis has been used widely during the pyrolysis process to study the biomass decomposition and its constituents (Collard and Blin 2014). Thermogravimetric analysis can also be used to carry out proximate analysis of several types of biomass matters which include determining the volatile matter, ash content, fixed carbon, and the presence of moisture (García et al. 2013). As per the earlier study, the enthalpy for pyrolysis process can be said as the minimum energy which is required to carry out pyrolysis. It can be stated as the sum of the energy which is required for heating the biomass matter up to the reaction temperature in pyrolysis which is necessary to drive the reaction in pyrolysis process. Differential scanning calorimetry (DSC) is used for determining the enthalpy for pyrolysis. The measurements were carried out in an SDT apparatus which is a combination of DSC-TGA device that measures the change in weight and heat flow as the functions of temperature. Before performing the analysis, drying of the samples was carried out in an electric oven at a temperature of 105 °C for 1 h.

The purpose of drying was the prediction of accurate enthalpy values for the pyrolysis process independent of the moisture content. On a dry basis, enthalpy for the pyrolysis process is generally reported because of the variation of moisture content when it goes for processing. Generally, the moisture content of the feedstock would be around 6–12% on dry basis. The moisture content can be found without drying of the feedstock. The moisture content and enthalpy value deviated more as compared to the experimental value. The deviation of the enthalpy value is due to moisture content available in the feedstock. The enthalpy associated with heating and evaporating the moisture present in the biomass matter can be summed with the enthalpy for pyrolysis. This can be achieved by the calculation latent heat

for evaporation of water and sensible enthalpy for heating the water present in the biomass up to the temperature of 100 °C, after that multiplying the sum by the fraction of water in the biomass matter (Chen et al. 2014; He et al. 2006). The major outputs from the TGA-DSC measurements were the change in weight and heat flow as a function of temperature. The calculation of enthalpy for pyrolysis can be done by integrating the heat flow curve over the temperature range of pyrolysis as mentioned below:

$$Q_{\mathrm{py}} = \int_{T_0}^{T_{\mathrm{py}}} \frac{H(T)}{\mathrm{d}T/\mathrm{d}t}\mathrm{d}T \tag{10}$$

where

Q_{py} is the specific enthalpy for pyrolysis (J/g),
T_{py} and T_0 are the final and starting temperatures, respectively (°C),
H(T) is the specific flow of heat to the sample at temperature T (W/g), and
dT/dt is the constant heating rate.

The heat flow values were also used for the calculation of the specific heat capacity, (T), of the biomass matter as a function of temperature as given below:

$$(T) = \frac{-H(T)}{\mathrm{d}T/\mathrm{d}t} \tag{11}$$

Kinetics is a useful tool for characterization and performance estimation. Thermal analysis such as differential scanning calorimetry and thermogravimetric analysis is used as an effective tool for the kinetic parameters determination. During pyrolysis reactions, the conversion was described by kinetic models. These kinetic models are complex and computationally rigorous, but they are more detailed and accurate. Various kinetic models can be found on pyrolysis of different feeds in the open literature (Sharma and Rajeswara Rao 1999).

Ozawa (1965) mentioned that the variable heating rate methods are also called iso-conversional methods. Moreover, the advantages of these models are that they apply to complex, multi-staged reactions and provide activation energy and pre-exponential factor, excellent reliability, and easy to manually perform. However, isoconversional methods assume reaction order as one and they take lengthy calibrations. Inversely single heating rate methods have simple calibration, the simple rapid experiment is sufficient to study the kinetics, and they provided all the three parameters (i.e., pre-exponential factor, and order of reaction, and activation energy). Moreover, the drawback of the single heating rate models is they have poor reliability, applicable only to nth order reactions. From this, the advantages of both the models are suitable for the computer the pyrolysis kinetic parameters. Rosi et al. (2018) investigated that the styrene polymers such as high impact polystyrene and acrylonitrile butadiene styrene; both of which are significant e-waste components plastics. So, these two plastic types have been employed to investigate the behavior of kinetics.

11.6.4 Chemical Constituent's Analysis

Gas chromatography and mass spectrometry (GC-MS) is a systematic method that conglomerates the structures of gas chromatography and mass spectrometry to recognize different matters inside a test trial. From the GC-MS results, the amount of alkane, alkene, ketone, and cycloalkane can be found. More the alkane means more efficiently the fuel will be ignited as the C–H bond is a single bond. However, more the alkenes mean the fuel will not readily ignite as C–H bond is a double bond. The presence of avoidable elements like alkene, cycloalkane, and ketone which directly affects the properties of the fuels could be quite low. The data obtained from GC-MS can be used to find out the total percentage of carbon number range. The total percentages of different levels of carbon number range will indirectly signify whether the improvement or deterioration in the values of properties such as viscosity and calorific values (Pittman et al. 2012). Additionally, it can identify trace elements in materials that were earlier assumed to have fragmented beyond identification. Like liquid chromatography–mass spectrometry, it permits inquiry and recognition even of small quantities of an element. In recent developments, the multidimensional hyphenated chromatographic methods have improved considerably the value of data collected from every sample. Furthermore, complex samples contain constituents with different characteristics; an individual method cannot offer the full analysis. Therefore, a mixture of analytical methods such as gas, high-pressure liquid, gel permeation chromatography, Fourier-transform infrared spectra, and nuclear magnetic spectroscopy is acquired to evaluate the bio-fuel composition (Ware et al. 2017). Appropriate classification of bio-fuel constituents appraising the analytical approach which applied for their identification tends to their classification in approximately four divisions: (1) the medium polar monomer identifiable by GC, around 40 wt%, (2) polar monomers also identifiable from HPLC (or GC after derivation) in the region of 10–15 wt%, (3) 20–30 wt% of water determined from the Karl-Fischer technique, and (4) oligomeric components, around 20 wt% also observed from HRMS or GPC. Although traditional GC and HPLC have offered certain information on the bio-fuel constituents and still are applied for qualitative and quantitative analysis, the actual elucidation of bio-fuel production has observed using the application of LC or LC GC × GC, combined with mass spectroscopy (Michailof et al. 2016). Atomic absorption spectroscopy (AAS) is a Spectro analytical technique used for the quantifiable determination of the chemical elements present in the sample using the absorption of light (optical radiation). Atomic absorption spectroscopy (AAS) is conducted for diesel, e-waste, and pyrolysis oil to know the percentage amount of other metals such as lead, iron, chlorine, and bromine. AAS analysis for e-waste, waste oil and pyrolysis oil are important to know the kind of harmful halogenated metals present in the feed as well as in the produced pyrolysis oil and further methods of elimination of these metal contents in the pyrolysis oil can be employed. Inductively coupled plasma is a method which is used for detecting the metal and nonmetal content at concentrations as low as one part in 1015. This can be done by

ionizing the sample by inductively coupled plasma. Compared to atomic absorption spectrometry, this test gives more accurate and sensitive value (Oasmaa et al. 1997).

11.6.5 Heating Value

The amount of heat produced on complete combustion of 1 g of fuel is called heating value or calorific value. The product of combustion is cooled to normal condition and water vapor leaves without being condensed is called lower calorific value or net calorific value. Higher heating value (HHV) is the quantity of heat released when unit quantity of fuel is completely burned at atmospheric temperature under stoichiometric conditions; the water vapor produced during combustion is being condensed when reaches to the initial temperature. HHV includes latent heat of evaporation of condensed water vapor. Higher heating value is used in boilers and lower heating value is used in internal combustion engine. Liquid and solid fuel calorific values are measured by bomb calorimeter, and gases fuel calorific value is measured by Junkers gas calorimeter. Chemical composition, moisture content, and molecular structure are the parameters affect the calorific value of the fuels. The waste cooking oil and pyrolysis oil calorific value are measured by using IKA 2000 model bomb calorimeter. A bomb calorimeter is a constant-volume type calorimeter used in computing the heat of burning of a particular response or simply to measure the calorific value of a fuel. Bomb calorimeters are built in such a way that it can withstand the large pressure that produced within the calorimeter due to reaction or burning of fuel. Electrical energy is used to burn the fuel, and as the fuel is burning, it will warm up the nearby air, which enlarges and outflows through a tube that primes the air out of the calorimeter. When the air is evading through the copper tube, it will also warm up the water. The change in temperature of the water permits for computing the calorie content of the fuel.

11.7 Performance, Combustion, and Emission Analysis of Syngas and Pyrolysis Fuel in Dual Fuel CI Engine

11.7.1 Effective Utilization of Pyrolysis Fuel in CI Engine

Kalargaris et al. (2017) studied that pyrolysis fuel derived from waste plastic can be used as the best alternative fuel because of its higher heating value. It can be converted to useful oil by pyrolysis process and utilized in an internal combustion engine to create mechanical power and heat. The oil is produced by fast pyrolysis method, and the properties of this oil are similar to the diesel oil. Pyrolysis oil derived from plastic was used as an additive to diesel and operated on advanced injection timing in diesel engine resulted in the brake thermal efficiency and emissions all are improved. The motor ignition attributes, performance, and exhaust emissions were broke down and related to diesel fuel action. The outcomes

demonstrated that the locomotive could keep running on plastic pyrolysis oil at rated load introducing similar performance to diesel. Mani et al. (2009) studied pyrolysis oil derived from plastic was used as an additive to diesel and operated on advanced injection timing in diesel engine resulted in the brake thermal efficiency and emissions all are improved. The motor ignition attributes, performance, and exhaust emissions were broke down and related to diesel fuel action. Shukla et al. (2016) described the use of plastic pyrolysis oil in internal combustion engines for a better replacement of the diesel fuel.

Researchers started opting for dual fuel strategy to challenge emission problems occurring in conventional diesel engines. The combustion phase and combustion duration will be controlled by reactivity gradient with port injection of a low reactive fuel like CNG combining direct injection of an extremely reactive fuel in cylinder (Wu et al. 2011). Auto-ignition of fuel can be restricted by higher octane number (ON) of the fuel which always indicates a high resistance toward self-ignition. This extends the upper load limit of the dual fuel engine effectively with less EGR operation. It can be concluded that the natural gas with good reserves and high-octane number is the best choice of the port injection fuel (Machrafi et al. 2008). To meet the current environmental legislations, it is highly required to reduce NO_x emissions in the exhaust gas. It is required to obtain energy conservation with low emission and high efficiency. Present developments in the CI engine combustion allow it to use alternative gaseous fuels such as CNG (natural gas), LPG (liquefied petroleum gas), DME (dimethyl ether), and hydrogen which help to resolve the emission problems (Ryu 2013).

The diesel ignited natural gas engine has the maximum explosion pressure lower than that of the original diesel engine. Due to the higher flame propagation speed of gaseous fuel, combustion duration will have decreased in CI engine combustion at rated load. Soot and NO_x emissions are lower when compared with the original diesel engine. Whereas at Low loads, the diesel ignited natural gas engine has higher unburned HC and CO emissions (Papagiannakis and Hountalas 2008). Among different possible technologies in the CI engine combustion, common rail direct injection (CRDI) systems can be lead to the technological revival. Compared to conventional diesel engine operation, CRDI system has been reported to reduce the specific fuel consumption and smoke emission significantly. However, NO_x formation is increased. Dual fuel strategies at rated load will decrease the NO_x formation but it is not suitable for lower load due to higher HC emissions.

11.7.2 Energetic Utilization of Syngas in Dual Fuel Engine

Syngas is produced through the gasification process by partial burning or oxidation of coal and biomass feedstock. It consists of hydrogen and carbon monoxide gases. The composition of gases mainly depends on feedstock particle size, flow rate, moisture content, and reactor, operating condition, catalyst, and residence time as noticed by Shilling and Lee (2003). The drawback of syngas is inferior calorific

value and density. The heating value can be increased by supplying pure oxygen during gasification process; then, the heating value increases by 9–13 MJ/N m^3. The syngas is free from oxides of sulfur, little amount of oxide of nitrogen. It is diatomic molecule, and it is produced from residual oil, natural gas, petrol coke, coal, and biomass. Syngas offer sustainable development in automobile and energy sector as observed by Pradhan et al. (2015).

Mahgoub et al. (2015) investigated the influence of syngas on diesel engine performance and emissions characteristics. The engine was operated at dual fuel mode with different engine speed like 1200, 2000 and 3000 rpm. The experimental results revealed that power output was decreased for syngas fuel due to its lower heating value and density compared to conventional diesel. The syngas will be a promising renewable source of energy for future due to its feedstock availability. It can be used as a substitute fuel in diesel engine under dual fuel mode as noticed by Sahoo et al. (2011). Sahoo et al. (2012) studied the influence of syngas on diesel engine performance, emissions, and combustion characteristics operated at dual fuel mode. The engine test was carried out at different engine load and different syngas composition. The results showed that 100% hydrogen syngas produced a good performance, but nitric oxide emission was increased. 50 and 75% hydrogen syngas showed good engine performance is about 16.1 and 18.3%, respectively. At 25 and 50% CO presence, syngas provides more CO and UBHC emission due to CO fraction in syngas composition.

Power output and engine performance and emissions depend on hydrogen and carbon monoxide percentage in syngas. The higher proportion of hydrogen syngas is emitted more nitric oxide emission compared to carbon monoxide syngas. The faster combustion due to increased hydrogen fraction resulted in more in-cylinder pressure and temperature in cylinder; high adiabatic flame temperature of hydrogen also influenced the formation of nitric oxide emission as observed by Shudo (2008). Azimov et al. (2011) studied the effect of different compositions of syngas and equivalence ratio on diesel engine under dual fuel mode. Hydrogen and carbon monoxide proportion in syngas affect the engine performance and emissions characteristics. The higher percentage of hydrogen in syngas improved the combustion efficiency and reduced the CO and UBHC emissions, whereas nitric oxide was increased due to complete combustion led to higher in-cylinder temperature and pressure. The presence of CO in syngas improved the engine performance up to a certain limit. Higher percentage on CO in syngas reduced the engine performance; similarly, emission of CO and UBHC emissions was increased. The above literature studies clearly stated that 50–75% hydrogen syngas can provide better efficiency under dual fuel mode. Hence, syngas will be a predominant renewable energy source and better substitute fuel for conventional diesel engines.

11.8 Conclusions

The methods and techniques to extract energy from e-wastes and biomass and their optimization can surely support the energy sector and satisfy a part of energy demand. Microwave heating provides more benefits compared to the conventional pyrolysis of e-waste and biomass. The volumetric heat generation and hot spot formation influence the product yield and pyrolysis oil characterization. The higher gaseous product and solid char are obtained in the microwave pyrolysis compared to conventional pyrolysis. The gaseous products evolved in the microwave pyrolysis contain higher H_2 and CO yields. The liquid and gaseous products obtained from the microwave pyrolysis having higher calorific value compared to conventional pyrolysis. The addition of carbon-based material like activated carbon, fly ash, graphite, and SiC in microwave pyrolysis has improved the process efficiency. The higher alkane is formed while using SiC as the microwave absorber. The graphene acts as a good microwave absorber, and it promotes the higher heating rate compared to other microwave absorbers. The higher PAH emission is formed above the pyrolytic temperature 850 °C in microwave pyrolysis. Moreover, the metal content present in the waste promotes the methane reforming reaction in the microwave pyrolysis. Further, metals converted into metal oxides leads to sulfur removal. Chlorinated benzenes and PCDD/Fs were detected during the pyrolysis of organic pollutants combined with wood pellets.

Gasification is one of the major approaches to fabricate syngas consists of higher proportion of H_2 to CO from waste biomass. The content of tar observed in this literature mainly depends on the design of reactor, operating conditions, and characteristics of feedstock. The gasification flexibility method is improved significantly when plastic-like materials are combined with coal or biomass. At lower operating temperature than traditional process, the biomass and e-waste from gasification can fabricate a H_2 gas product free from tars. Hence, the production rate of H_2 will be higher at 30 wt% recorded. From different gasification technologies, the syngas is applied to develop power and also produces bottom ash which consists of a significant quantity of silica. From the hydrothermal reaction, this silica can be developed into zeolite and applied as absorbent material. The utilization of different gaseous fuels such as LPG, CNG, and hydrogen with pyrolysis oil in CI engine decreases the emission to great extent. The common rail direct injection (CRDI) system has certain benefits while comparing with the traditional mechanical injection system. The high-pressure injection system improves the homogeneity and turbulence in the air–fuel mixture to determine the lower emission rate and higher thermal efficiency. The use of syngas in diesel engine (dual fuel medium) will reduce the brake thermal efficiency as compared with conventional fuel (diesel) operation. The incrementing of CO constituents in the gas will reduce the NO_x emission and improves performance due to lower heating. The enhancement of hydrogen in syngas tends to enhance the performance of the engine.

Acknowledgements The authors would like to thank the Department of Science and Technology, New Delhi, India, and the Director, National Institute of Technology, Tiruchirappalli, India for extending the facilities to carry out the research work.

References

Adam MAB (2017) Understanding microwave pyrolysis of biomass materials. Ph.D. thesis, University of Nottingham

Administration, U.S.E.I. (2018) Annual energy outlook. J Phys A Math Theor 44:1–64. DOE/EIA-0383(2017)

Adrados A, de Marco I, Caballero BM, López A, Laresgoiti MF, Torres A (2012) Pyrolysis of plastic packaging waste: a comparison of plastic residuals from material recovery facilities with simulated plastic waste. Waste Manag 32:826–832. https://doi.org/10.1016/j.wasman.2011.06.016

Ahmed II, Nipattummakul N, Gupta AK (2011) Characteristics of syngas from co-gasification of polyethylene and woodchips. Appl Energy 88:165–174. https://doi.org/10.1016/j.apenergy.2010.07.007

Akolkar AB (2005) Status of solid waste management in India, implementation status of municipal solid wastes, management and handling rules 2000. Central Pollution Control Board, New Delhi

Alauddin ZABZ, Lahijani P, Mohammadi M, Mohamed AR (2010) Gasification of lignocellulosic biomass in fluidized beds for renewable energy development: a review. Renew Sustain Energy Rev 14:2852–2862. https://doi.org/10.1016/j.rser.2010.07.026

Allan GG, Krieger BB, Work DW (1980) Dielectric loss microwave degradation of polymers: cellulose. J Appl Polym Sci 25:1839–1859. https://doi.org/10.1002/app.1980.070250904

Al-Salem SM, Lettieri P, Baeyens J (2009) Recycling and recovery routes of plastic solid waste (PSW): a review

Alston SM, Clark AD, Arnold JC, Stein BK (2011) Environmental impact of pyrolysis of mixed WEEE plastics part 1: experimental pyrolysis data. Environ Sci Technol 45:9380–9385. https://doi.org/10.1021/es201664h

Anand R (2017) Simultaneous control of oxides of nitrogen and soot in CRDI diesel engine using split injection and Cool EGR fuelled with waste frying oil biodiesel and its blends. In: Air Pollution and Control, Energy, Environment and Sustainability. Springer, Berlin, pp 11–44

Andersson M, Knutson Wedel M, Forsgren C, Christéen J (2012) Microwave assisted pyrolysis of residual fractions of waste electrical and electronics equipment. Miner Eng 29:105–111. https://doi.org/10.1016/j.mineng.2011.09.005

Andrady AL (2015) Persistence of plastic litter in the oceans. In: Marine anthropogenic litter, pp 29–56 (2015)

Ania CO, Menéndez JA, Parra JB, Pis JJ (2004) Microwave-induced regeneration of activated carbons polluted with phenol. A comparison with conventional thermal regeneration. Carbon 1377–1381

Ania CO, Parra JB, Menéndez JA, Pis JJ (2007) Microwave-assisted regeneration of activated carbons loaded with pharmaceuticals. Water Res 41:3299–3306. https://doi.org/10.1016/j.watres.2007.05.006

Anil K (1986) Rajvanshi: biomass gasification. Alternative energy in agriculture. CRC Press, pp 83–102 (1986)

Anis S, Zainal ZA (2011) Tar reduction in biomass producer gas via mechanical, catalytic and thermal methods: a review

Anuar Sharuddin SD, Abnisa F, Wan Daud WMA, Aroua MK (2016) A review on pyrolysis of plastic wastes

Appleton TJ, Colder RI, Kingman SW, Lowndes IS, Read AG (2005) Microwave technology for energy-efficient processing of waste. Appl Energy 81:85–113. https://doi.org/10.1016/j.apenergy.2004.07.002

Arena U, Di Gregorio F (2014) Energy generation by air gasification of two industrial plastic wastes ina pilot scale fluidized bed reactor. Energy 68:735–743. https://doi.org/10.1016/j.energy.2014.01.084

Arena U, Zaccariello L, Mastellone ML (2009) Tar removal during the fluidized bed gasification of plastic waste. Waste Manag 29:783–791. https://doi.org/10.1016/j.wasman.2008.05.010

Arena U, Zaccariello L, Mastellone ML (2010) Fluidized bed gasification of waste-derived fuels. Waste Manag 30:1212–1219. https://doi.org/10.1016/j.wasman.2010.01.038

Asadullah M (2014) Barriers of commercial power generation using biomass gasification gas: A review. Renew Sustain Energy Rev 29:201–215. https://doi.org/10.1016/j.rser.2013.08.074

Avdeeva LB, Reshetenko TV, Ismagilov ZR, Likholobov VA (2002) Iron-containing catalysts of methane decomposition: accumulation of filamentous carbon. Appl Catal A Gen 228:53–63. https://doi.org/10.1016/s0926-860x(01)00959-0

Azimov U, Tomita E, Kawahara N, Harada Y (2011) Effect of syngas composition on combustion and exhaust emission characteristics in a pilot-ignited dual-fuel engine operated in PREMIER combustion mode. Int J Hydrogen Energy 36:11985–11996. https://doi.org/10.1016/j.ijhydene.2011.04.192

Babu D, Anand R (2017) Effect of biodiesel-diesel-n-pentanol and biodiesel-diesel-n-hexanol blends on diesel engine emission and combustion characteristics. Energy 133:761–776. https://doi.org/10.1016/j.energy.2017.05.103

Balat M, Ayar G (2005) Biomass energy in the world, use of biomass and potential trends. Energy Sour 27:931–940. https://doi.org/10.1080/00908310490449045

Balat M, Balat M, Kirtay E, Balat H (2009) Main routes for the thermo-conversion of biomass into fuels and chemicals. Part 2: Gasification systems. Energy Convers Manag 50:3158–3168. https://doi.org/10.1016/j.enconman.2009.08.013

Balu E, Chung JN (2012) System characteristics and performance evaluation of a trailer-scale downdraft gasifier with different feedstock. Bioresour Technol 108:264–273. https://doi.org/10.1016/j.biortech.2011.12.105

Basu P (2010) Biomass gasification design handbook. In: Biomass gasification and pyrolysis, pp 117–165 (2010)

Basu P, Basu P (2010) Biomass characteristics (Chap. 2). In: Biomass gasification and pyrolysis, pp 27–63

Belonio AT (2005) Rice husk gas stove handbook. Bioenergylists.Org

Bergo P, Moraes ICF, Sobral PJDA (2012) Effects of moisture content on structural and dielectric properties of cassava starch films. Starch/Staerke. https://doi.org/10.1002/star.201200023

Biagini E, Barontini F, Tognotti L (2015) Gasification of agricultural residues in a demonstrative plant: corn cobs. Bioresour Technol 173:110–116. https://doi.org/10.1016/j.biortech.2014.09.086

Boateng AA, Mtui PL (2012) CFD modeling of space-time evolution of fast pyrolysis products in a bench-scale fluidized-bed reactor. Appl Therm Eng 33–34:190–198. https://doi.org/10.1016/j.applthermaleng.2011.09.034

Boundy B (2011) Biomass energy data book, 4 edn. Deparment of Energy, p. 254

Brachi P, Chirone R, Miccio F, Miccio M, Picarelli A, Ruoppolo G (2014) Fluidized bed co-gasification of biomass and polymeric wastes for a flexible end-use of the syngas: focus on bio-methanol. Fuel 128:88–98. https://doi.org/10.1016/j.fuel.2014.02.070

Bradbury WL, Olevsky EA (2010) Production of SiC–C composites by free-pressureless spark plasma sintering (FPSPS). Scr Mater 63:77–80. https://doi.org/10.1016/j.scriptamat.2010.03.009

Bridgwater AV (1995) The technical and economic feasibility of biomass gasification for power generation. Fuel 74:631–653. https://doi.org/10.1016/0016-2361(95)00001-l

Bridgwater AV, Meier D, Radlein D (1999) An overview of fast pyrolysis of biomass. Org Geochem 30:1479–1493. https://doi.org/10.1016/s0146-6380(99)00120-5

Buragohain B, Mahanta P, Moholkar VS (2010) Biomass gasification for decentralized power generation: the Indian perspective

Burra KG, Gupta AK (2018) Synergistic effects in steam gasification of combined biomass and plastic waste mixtures. Appl Energy 211:230–236. https://doi.org/10.1016/j.apenergy.2017.10.130

Carrott PJ, Nabais JM, Ribeiro Carrott MM, Menéndez J (2001) Thermal treatments of activated carbon fibres using a microwave furnace. Microporous Mesoporous Mater 47:243–252. https://doi.org/10.1016/s1387-1811(01)00384-5

Cha CY, Kong Y (1995) Enhancement of NO_x adsorption capacity and rate of char by microwaves. Carbon 33:1141–1146. https://doi.org/10.1016/0008-6223(95)00066-m

Chandrasekaran S, Basak T, Srinivasan R (2013) Microwave heating characteristics of graphite based powder mixtures. Int Commun Heat Mass Transf 48:22–27. https://doi.org/10.1016/j.icheatmasstransfer.2013.09.008

Chen Q, Yang R, Zhao B, Li Y, Wang S, Wu H, Zhuo Y, Chen C (2014) Investigation of heat of biomass pyrolysis and secondary reactions by simultaneous thermogravimetry and differential scanning calorimetry. Fuel 134:467–476. https://doi.org/10.1016/j.fuel.2014.05.092

Cheng J, Roy R, Agrawal D (2002) Radically different effects on materials by separated microwave electric and magnetic fields. Mater Res Innov 5:170–177. https://doi.org/10.1007/s10019-002-8642-6

Cheng MY, Yang SC, Hsieh C Te (2007) Thermal regeneration of activated carbons exhausted with phenol compound. Sep Sci Technol 42:639–652. https://doi.org/10.1080/01496390601070059

Clark DE, Folz DC, West JK (2000) Processing materials with microwave energy. Mater Sci Eng A 287:153–158. https://doi.org/10.1016/s0921-5093(00)00768-1

Collard FX, Blin J (2014) A review on pyrolysis of biomass constituents: mechanisms and composition of the products obtained from the conversion of cellulose, hemicelluloses and lignin. Renew Sustain Energy Rev 38:594–608. https://doi.org/10.1016/j.rser.2014.06.013

Conesa JA, Font R, Fullana A, Martín-Gullón I, Aracil I, Gálvez A, Moltó J, Gómez-Rico MF (2009) Comparison between emissions from the pyrolysis and combustion of different wastes. J Anal Appl Pyrolysis 84:95–102. https://doi.org/10.1016/j.jaap.2008.11.022

Couto N, Rouboa A, Silva V, Monteiro E, Bouziane K (2013) Influence of the biomass gasification processes on the final composition of syngas. In: Energy Procedia, pp 596–606

Cui J, Forssberg E (2003) Mechanical recycling of waste electric and electronic equipment: a review

Dehdashti A, Khavanin A, Rezaee A, Asilian H (2011) Regeneration of granular activated carbon saturated with gaseous toluene by microwave irradiation. Turkish J Eng Environ Sci 35:49–58. https://doi.org/10.3906/muh-1004-13

Demirbas A (2000) Biomass resources for energy and chemical industry. Energy Educ Sci Technol 5:21–45

Demirbas A (2004a) Effects of temperature and particle size on bio-char yield from pyrolysis of agricultural residues. J. Anal. Appl. Pyrolysis 72:243–248. https://doi.org/10.1016/j.jaap.2004.07.003

Demirbas A (2004b) Combustion characteristics of different biomass fuels. Prog Energy Combust Sci 30:219–230. https://doi.org/10.1016/j.pecs.2003.10.004

Demirbas A (2008) Gasoline-like fuel from waste engine oil via catalytic pyrolysis. Energy Sources Part A Recover Util Environ Eff 30:1433–1441. https://doi.org/10.1080/15567030701258469

Demirbaş A, Arin G (2002) An overview of biomass pyrolysis. Energy Sources 24:471–482. https://doi.org/10.1080/00908310252889979

Di Blasi C, Branca C (2013) Modeling a stratified downdraft wood gasifier with primary and secondary air entry. Fuel 104:847–860. https://doi.org/10.1016/j.fuel.2012.10.014

Di Blasi CD, Signorelli G, Portoricco G (1999) Countercurrent fixed-bed gasification of biomass at laboratory scale. Ind Eng Chem Res 38:2571–2581. https://doi.org/10.1021/ie980753i

Dimitrakakis E, Janz A, Bilitewski B, Gidarakos E (2009) Determination of heavy metals and halogens in plastics from electric and electronic waste. Waste Manag 29:2700–2706. https://doi.org/10.1016/j.wasman.2009.05.020

Ding DH, Zhou WC, Luo F, Zhu DM (2012) Influence of pyrolytic carbon coatings on complex permittivity and microwave absorbing properties of Al_2O_3 fiber woven fabrics. Trans Nonferrous Met Soc China (English Ed. 22:354–359. https://doi.org/10.1016/s1003-6326(11)61183-7

Dobele G, Urbanovich I, Volpert A, Kampars V, Samulis E (2007) Fast pyrolysis-effect of wood drying on the yield and properties of bio-oil. BioResources 2:699–706. https://doi.org/10.15376/biores.2.4.698-706

Domeño C, Nerín C (2003) Fate of polyaromatic hydrocarbons in the pyrolysis of industrial waste oils. J Anal Appl Pyrolysis 67:237–246. https://doi.org/10.1016/s0165-2370(02)00064-5

Dominguez A, Fernandez Y, Fidalgo B, Pis JJ, Menendez JA (2008) Bio-syngas production with low concentrations of CO_2 and CH_4 from microwave-induced pyrolysis of wet and dried sewage sludge. Chemosphere 70:397–403. https://doi.org/10.1016/j.chemosphere.2007.06.075

Domínguez A, Menéndez JA, Inguanzo M, Pis JJ (2005) Investigations into the characteristics of oils produced from microwave pyrolysis of sewage sludge. Fuel Process Technol 86:1007–1020. https://doi.org/10.1016/j.fuproc.2004.11.009

Domínguez A, Menéndez JA, Inguanzo M, Pís JJ (2006) Production of bio-fuels by high temperature pyrolysis of sewage sludge using conventional and microwave heating. Bioresour Technol 97:1185–1193. https://doi.org/10.1016/j.biortech.2005.05.011

Domínguez A, Menéndez JA, Fernández Y, Pis JJ, Nabais JMV, Carrott PJM, Carrott MMLR (2007) Conventional and microwave induced pyrolysis of coffee hulls for the production of a hydrogen rich fuel gas. J Anal Appl Pyrolysis 79:128–135. https://doi.org/10.1016/j.jaap.2006.08.003

Duan H, Li J, Liu Y, Yamazaki N, Jiang W (2011) Characterization and inventory of PCDD/Fs and PBDD/Fs emissions from the incineration of waste printed circuit board. Environ Sci Technol 45:6322–6328. https://doi.org/10.1021/es2007403

Duong-Viet C, Ba H, El-Berrichi Z, Nhut JM, Ledoux MJ, Liu Y, Pham-Huu C (2016) Silicon carbide foam as a porous support platform for catalytic applications. New J Chem 40:4285–4299. https://doi.org/10.1039/c5nj02847g

Edo M, Skoglund N, Gao Q, Persson PE, Jansson S (2017) Fate of metals and emissions of organic pollutants from torrefaction of waste wood, MSW, and RDF. Waste Manag 68:646–652. https://doi.org/10.1016/j.wasman.2017.06.017

Environmental Protection Agency (2007) Queensland Government 2002: 'fact sheet—"green waste" to charcoal & energy. Retrieved Oct 2007

EPA (2008) Flame retardants in printed circuit boards. Des Environ 237 (2008). https://doi.org/10.1214/07-ejs057

Erickson MD, Kaley RG (2011) Applications of polychlorinated biphenyls. Environ Sci Pollut Res 18:135–151. https://doi.org/10.1007/s11356-010-0392-1

Fall ML, Shulman HS (2003) Comparison of energy consumption for microwave heating of alumina, zirconia and mixtures. In: 105th Annual Americal Ceramic Society National Convention. Nashville Tennesse, US

Fernandez Yolanda, Ana Arenillas J, Menendez Angel (2011) Microwave heating applied to pyrolysis. Adv Induction Microw Heat Miner Org Mater 31:723–752. https://doi.org/10.5772/13548

Freitas JCC, Moreira JS, Emmerich FG, Bonagamba TJ (2004) Development of Si/C/N/O ceramics from pyrolyzed and heat-treated rice hulls. J Non Cryst Solids 341:77–85. https://doi.org/10.1016/j.jnoncrysol.2004.04.019

Friengfung P, Jamkrajang E, Sunphorka S, Kuchonthara P, Mekasut L (2014) NiO/dolomite catalyzed steam/O_2 gasification of different plastics and their mixtures. Ind Eng Chem Res 53:1909–1915. https://doi.org/10.1021/ie401893s

Deutsche Gesellshaft fur Sonnenenergie, fur Sonnenenergie, D.G., Sonnenenergie, D.G. fur (2005) Planning and installing bioenergy systems: a guide for installers, architects, and engineers

Fytili D, Zabaniotou A (2008) Utilization of sewage sludge in EU application of old and new methods—a review

Gabriel C, Gabriel S, Grant EH, Halstead BSJ, Michael P, Mingos D (1998) Dielectric parameters relevant to microwave dielectric heating. Chem Soc Rev 27:213–223. https://doi.org/10.1039/a827213z

Ganguli N, Krishnan KS (1941) The magnetic and other properties of the free electrons in graphite. Proc R Soc A Math Phys Eng Sci 177:168–182. https://doi.org/10.1098/rspa.1983.0054

García R, Pizarro C, Lavín AG, Bueno JL (2013) Biomass proximate analysis using thermogravimetry. Bioresour Technol 139:1–4. https://doi.org/10.1016/j.biortech.2013.03.197

Gorthy P, Mukunda Pudukottah G (2004) Production of silicon carbide from rice husks. J Am Ceram Soc 82:1393–1400. https://doi.org/10.1111/j.1151-2916.1999.tb01929.x

Gui MM, Lee KT, Bhatia S (2008) Feasibility of edible oil vs. non-edible oil vs. waste edible oil as biodiesel feedstock

Gunarathne DS, Mueller A, Fleck S, Kolb T, Chmielewski JK, Yang W, Blasiak W (2014) Gasification characteristics of steam exploded biomass in an updraft pilot scale gasifier. Energy 71:496–506. https://doi.org/10.1016/j.energy.2014.04.100

Guo Y, Du E (2012) The effects of thermal regeneration conditions and inorganic compounds on the characteristics of activated carbon used in power plant. Energy Procedia 17:444–449. https://doi.org/10.1016/j.egypro.2012.02.118

Guo Y, Yang S, Yu K, Zhao J, Wang Z, Xu H (2002) The preparation and mechanism studies of rice husk based porous carbon. Mater Chem Phys 74:320–323. https://doi.org/10.1016/s0254-0584(01)00473-4

Guo J, Guo J, Xu Z (2009) Recycling of non-metallic fractions from waste printed circuit boards: a review. J Hazard Mater 168(2–3):567–590

Guo F, Dong Y, Dong L, Guo C (2014) Effect of design and operating parameters on the gasification process of biomass in a downdraft fixed bed: an experimental study. Int J Hydrog Energy 5625–5633

Gupta M, Eugene WWL (2011) Microwaves and metals. https://doi.org/10.1002/9780470822746

Hackett GA, Gerdes K, Song X, Chen Y, Shutthanandan V, Engelhard M, Zhu Z, Thevuthasan S, Gemmen R (2012) Performance of solid oxide fuel cells operated with coal syngas provided directly from a gasification process. J Power Sources 214:142–152. https://doi.org/10.1016/j.jpowsour.2012.04.050

Haykiri-Açma H (2003) Combustion characteristics of different biomass materials. Energy Convers Manag 44:155–162. https://doi.org/10.1016/s0196-8904(01)00200-x

He F, Yi W, Bai X (2006) Investigation on caloric requirement of biomass pyrolysis using TG-DSC analyzer. Energy Convers Manag 47:2461–2469. https://doi.org/10.1016/j.enconman.2005.11.011

He M, Xiao B, Hu Z, Liu S, Guo X, Luo S (2009) Syngas production from catalytic gasification of waste polyethylene: Influence of temperature on gas yield and composition. Int J Hydrogen Energy 34:1342–1348. https://doi.org/10.1016/j.ijhydene.2008.12.023

Hebden D, Stroud HJF (1982) Coal gasification processes. In: lliot MA (1982) Book review: chemistry of coal utilization, Second Supplementary Volume. Angew Chemie Int Ed English 21: 710–710 (1982). https://doi.org/10.1002/anie.198207101

Hernández JJ, Aranda-Almansa G, Bula A (2010) Gasification of biomass wastes in an entrained flow gasifier: effect of the particle size and the residence time. Fuel Process Technol 91:681–692. https://doi.org/10.1016/j.fuproc.2010.01.018

Hestin M, Mitsios A, Ait Said S, Fouret F, Berwald A, Senlis V (2017) Deloitte sustainability blueprint for plastics packaging waste: Quality sorting & recycling Final report, pp 1–50

Hong JLX, Maneerung T, Koh SN, Kawi S, Wang C-H (2017) Conversion of coal fly ash into zeolite materials: synthesis and characterizations, process design, and its cost-benefit analysis. Ind Eng Chem Res 56. https://doi.org/10.1021/acs.iecr.7b02885

Huang YF, Kuan WH, Lo SL, Lin CF (2008) Total recovery of resources and energy from rice straw using microwave-induced pyrolysis. Bioresour Technol 99:8252–8258. https://doi.org/10.1016/j.biortech.2008.03.026

Huang S, Wu S, Wu Y, Gao J (2017) Structure characteristics and gasification activity of residual carbon from updraft fixed-bed biomass gasification ash. Energy Convers Manag 136:108–118. https://doi.org/10.1016/j.enconman.2016.12.091

Hua-Shan T, Chih-Ju GJ (1999) Application of granular activated carbon packed-bed reactor in microwave radiation field to treat phenol. Chemosphere 38:2667–2680. https://doi.org/10.1016/s0045-6535(98)00432-9

Hussain Z, Khan KM, Hussain K (2010) Microwave-metal interaction pyrolysis of polystyrene. J Anal Appl Pyrolysis 89:39–43. https://doi.org/10.1016/j.jaap.2010.05.003

International Energy Agency (2012) Understanding energy challenges in India. Policies, Players and Issues. IEEE Ind Appl Mag 17:116

Jahirul M, Rasul M, Chowdhury A, Ashwath N (2012) Biofuels production through biomass pyrolysis—a technological review. Energies 5:4952–5001. https://doi.org/10.3390/en5124952

Janney MA, Calhoun CL, Kimrey HD (1992) Microwave sintering of solid oxide fuel cell materials: I, Zirconia-8 mol% Yttria. J Am Ceram Soc 75:341–346. https://doi.org/10.1111/j.1151-2916.1992.tb08184.x

Jenkins BM, Baxter LL, Miles TR, Miles TR (1998) Combustion properties of biomass. Fuel Process Technol 54:17–46. https://doi.org/10.1016/s0378-3820(97)00059-3

Jones DA, Lelyveld TP, Mavrofidis SD, Kingman SW, Miles NJ (2002) Microwave heating applications in environmental engineering. Resour Conserv Recycl 34:75–90. https://doi.org/10.1016/s0921-3449(01)00088-x

Joshi R, Ahmed S, Ng CA (2016) Status and challenges of municipal solid waste management in India: a review PUBLIC INTEREST STATEMENT. Cogent Environ Sci 2. https://doi.org/10.1080/23311843.2016.1139434

Kalargaris I, Tian G, Gu S (2017) Combustion, performance and emission analysis of a DI diesel engine using plastic pyrolysis oil. Fuel Process Technol 157:108–115. https://doi.org/10.1016/j.fuproc.2016.11.016

Kannan GR, Anand R (2012) Effect of injection pressure and injection timing on DI diesel engine fuelled with biodiesel from waste cooking oil. Biomass Bioenerg 46:343–352. https://doi.org/10.1016/j.biombioe.2012.08.006

Kannan N, Vakeesan D (2016) Solar energy for future world—a review

Kannan P, Al Shoaibi A, Srinivasakannan C (2013) Energy recovery from co-gasification of waste polyethylene and polyethylene terephthalate blends. Comput Fluids 88:38–42. https://doi.org/10.1016/j.compfluid.2013.09.004

Kaupp A, Goss JR (1981) State of the art report for small scale (to 50 kW) gas producer engine systems. A Publication of Deutsches ZEntrum für Entwicklungstechnologien -GATE. 53, p 286 (1981)

Khosasaeng T, Suntivarakorn R (2017) Effect of equivalence ratio on an efficiency of single throat downdraft gasifier using rdf from municipal solid waste. In: Energy Procedia, pp 784–788 (2017)

Kim T, Lee J, Lee K-H (2014) Microwave heating of carbon-based solid materials. Carbon Lett 15:15–24. https://doi.org/10.5714/cl.2014.15.1.015

Kirk-Othmer (1996) Encyclopedia of chemical technology. In: J Am Chem So 540–555 (1996)

Kirubakaran V, Sivaramakrishnan V, Nalini R, Sekar T, Premalatha M, Subramanian P (2009) A review on gasification of biomass

Klein A (2002) Gasification: an alternative process for energy recovery and disposal of municipal solid wastes. http://www.seas.columbia.edu/earth/wtert/sofos/klein_thesis.pdf

Kong Y, Cha CY (1996) Microwave-induced regeneration of NO_x-saturated char. Energy Fuels 10:1245. https://doi.org/10.1021/ef960060j

Kulkarni MG, Dalai AK (2006) Waste cooking oil—an economical source for biodiesel: a review

Lam SS, Chase HA (2012) A review on waste to energy processes using microwave pyrolysis

Lam SS, Russell AD, Chase HA (2010) Pyrolysis using microwave heating: a sustainable process for recycling used car engine oil. In: Industrial and engineering chemistry research, pp 10845–10851

Lam SS, Liew RK, Cheng CK, Chase HA (2015) Catalytic microwave pyrolysis of waste engine oil using metallic pyrolysis char. Appl Catal B Environ 176–177:601–617. https://doi.org/10.1016/j.apcatb.2015.04.014

Lata K, Mande S, Linoj NV, Rajeshwari KV, Sharma DT, Babu L, Kishore VVN (2006) Development of technology for treatment of wastewater generated in biomass gasifier systems. The Energy and Resources Institute

Lázaro MJ, Moliner R, Suelves I, Nerín G, Domeño G (2000) Valuable products from mineral waste oils containing heavy metals. Environ Sci Technol 34:3205–3210. https://doi.org/10.1021/es9905546

Lee J, Song HT, Yoo J-M (2007) Present status of the recycling of waste electrical and electronic equipment in Korea. Resour Conserv Recycl 50:380–397. https://doi.org/10.1016/j.resconrec.2007.01.010

Lesmana D, Wu HS (2015) Pyrolysis of waste oil in the presence of a spent catalyst. J Environ Chem Eng 3:2522–2527. https://doi.org/10.1016/j.jece.2015.09.019

Li W, Zhang L, Peng J, Li N, Zhu X (2008) Preparation of high surface area activated carbons from tobacco stems with K_2CO_3 activation using microwave radiation. Ind Crops Prod 27:341–347. https://doi.org/10.1016/j.indcrop.2007.11.011

Li D, Zhang Y, Quan X, Zhao Y (2009) Microwave thermal remediation of crude oil contaminated soil enhanced by carbon fiber. J Environ Sci 21:1290–1295. https://doi.org/10.1016/s1001-0742(08)62417-1

Li X, Zhang G, Tronstad R, Ostrovski O (2016) Synthesis of SiC whiskers by VLS and VS process. Ceram Int 42:5668–5676. https://doi.org/10.1016/j.ceramint.2015.12.091

Liamsanguan C, Gheewala SH (2008) The holistic impact of integrated solid waste management on greenhouse gas emissions in Phuket. J Clean Prod 16:1865–1871. https://doi.org/10.1016/j.jclepro.2007.12.008

Lin L, Cunshan Z, Vittayapadung S, Xiangqian S, Mingdong D (2011) Opportunities and challenges for biodiesel fuel

Liu X, Quan X, Bo L, Chen S, Zhao Y (2004) Simultaneous pentachlorophenol decomposition and granular activated carbon regeneration assisted by microwave irradiation. Carbon 42:415–422. https://doi.org/10.1016/j.carbon.2003.12.032

Liu H, Hu J, Wang H, Wang C, Li J (2012) Experimental studies of biomass gasification with air. J Nat Gas Chem 21:374–380. https://doi.org/10.1016/s1003-9953(11)60379-4

Lopez G, Artetxe M, Amutio M, Alvarez J, Bilbao J, Olazar M (2018) Recent advances in the gasification of waste plastics. A critical overview

López FA, Centeno TA, Rodríguez O, Alguacil FJ (2013) Preparation and characterization of activated carbon from the char produced in the thermolysis of granulated scrap tyres. J Air Waste Manag Assoc 63:534–544. https://doi.org/10.1080/10962247.2013.763870

Lundin L, Gomez-Rico MF, Forsberg C, Nordenskjöld C, Jansson S (2013) Reduction of PCDD, PCDF and PCB during co-combustion of biomass with waste products from pulp and paper industry. Chemosphere 91:797–801. https://doi.org/10.1016/j.chemosphere.2013.01.090

Maasikmets M, Kupri HL, Teinemaa E, Vainumäe K, Arumäe T, Roots O, Kimmel V (2016) Emissions from burning municipal solid waste and wood in domestic heaters. Atmos Pollut Res 7:438–446. https://doi.org/10.1016/j.apr.2015.10.021

Machrafi H, Cavadias S, Amouroux J (2008) A parametric study on the emissions from an HCCI alternative combustion engine resulting from the auto-ignition of primary reference fuels. Appl Energy 85:755–764. https://doi.org/10.1016/j.apenergy.2008.02.005

Mahesh SE, Ramanathan A, Begum KMMS, Narayanan A (2015) Biodiesel production from waste cooking oil using KBr impregnated CaO as catalyst. Energy Convers Manag 91:442–450. https://doi.org/10.1016/j.enconman.2014.12.031

Mahgoub BKM, Sulaiman SA, Karim ZAA (2015) Performance study of imitated syngas in a dual-fuel compression ignition diesel engine. Int J Automot Mech Eng 11:2282–2293. https://doi.org/10.15282/ijame.11.2015.11.0192

Malik A, Mohapatra SK (2013) Biomass-based gasifiers for internal combustion (IC) engines—a review. Sadhana Acad Proc Eng Sci 38:461–476. https://doi.org/10.1007/s12046-013-0145-1

Management of Solid Waste in Indian Cities (2005) Ministry of Urban Development. Government of India, New Delhi MOUD Report

Mandl C, Obernberger I, Scharler IR (2011) Characterisation of fuel bound nitrogen in the gasification process and the staged combustion of producer gas from the updraft gasification of softwood pellets. Biomass Bioenerg 35:4595–4604. https://doi.org/10.1016/j.biombioe.2011.09.001

Maneerung T, Li X, Li C, Dai Y, Wang C-H (2018) Integrated downdraft gasification with power generation system and gasification bottom ash reutilization for clean waste-to-energy and resource recovery system. J Clean Prod 188:69–79. https://doi.org/10.1016/j.jclepro.2018.03.287

Mani M, Subash C, Nagarajan G (2009) Performance, emission and combustion characteristics of a DI diesel engine using waste plastic oil. Appl Therm Eng 29:2738–2744. https://doi.org/10.1016/j.applthermaleng.2009.01.007

Marcilla A, Catalá L, García-Quesada JC, Valdés FJ, Hernández MR (2013) A review of thermochemical conversion of microalgae. Renew Sustain Energy Rev 27:11–19. https://doi.org/10.1016/j.rser.2013.06.032

Marken F, Sur UK, Coles BA, Compton RG (2006) Focused microwaves in electrochemical processes. In: Electrochimica Acta, pp 2195–2203

Marsh H, Rodríguez-Reinoso F (2006) Activated Carbon

Martínez V, Valencia MF, Cruz J, Mejía JM, Chejne F (2006) Production of β-SiC by pyrolysis of rice husk in gas furnaces. Ceram Int 32:891–897. https://doi.org/10.1016/j.ceramint.2005.07.018

Martínez JD, Mahkamov K, Andrade RV, Silva Lora EE (2012) Syngas production in downdraft biomass gasifiers and its application using internal combustion engines

Martínez-Lera S, Torrico J, Pallarés J, Gil A (2013) Thermal valorization of post-consumer film waste in a bubbling bed gasifier. Waste Manag 33:1640–1647. https://doi.org/10.1016/j.wasman.2013.03.016

Martinho G, Pires A, Saraiva L, Ribeiro R (2012) Composition of plastics from waste electrical and electronic equipment (WEEE) by direct sampling. Waste Manag 32:1213–1217. https://doi.org/10.1016/j.wasman.2012.02.010

McKendry P (2002) Energy production from biomass (part 3): gasification technologies. Bioenergylists, Org

Menéndez JA, Menéndez EM, Iglesias MJ, García A, Pis JJ (1999a) Modification of the surface chemistry of active carbons by means of microwave-induced treatments. Carbon 37:1115–1121. https://doi.org/10.1016/s0008-6223(98)00302-9

Menéndez JA, Menéndez EM, García A, Parra JB, Pis JJ (1999b) Thermal treatment of active carbons: a comparison between microwave and electrical heating. J Microw Power Electromagn Energy 34:137–143. https://doi.org/10.1080/08327823.1999.11688398

Menéndez JA, Inguanzo M, Pis JJ (2002) Microwave-induced pyrolysis of sewage sludge. Water Res 36:3261–3264. https://doi.org/10.1016/s0043-1354(02)00017-9

Menéndez JA, Domínguez A, Inguanzo M, Pis JJ (2004) Microwave pyrolysis of sewage sludge: analysis of the gas fraction. J Anal Appl Pyrolysis 71:657–667. https://doi.org/10.1016/j.jaap.2003.09.003

Menéndez JA, Domínguez A, Fernández Y, Pis JJ (2007) Evidence of self-gasification during the microwave-induced pyrolysis of coffee hulls. Energy Fuels 21:373–378. https://doi.org/10.1021/ef060331i

Menéndez JA, Arenillas A, Fidalgo B, Fernández Y, Zubizarreta L, Calvo EG, Bermúdez JM (2010) Microwave heating processes involving carbon materials. Fuel Process Technol 91(1):1–8

Menéndez JA, Juárez-Pérez EJ, Ruisánchez E, Bermúdez JM, Arenillas A (2011) Ball lightning plasma and plasma arc formation during the microwave heating of carbons. Carbon N. Y. 49:346–349. https://doi.org/10.1016/j.carbon.2010.09.010

Menya E, Olwa J, Hagström P, Okure M (2014) Assessment of pollution levels resulting from biomass gasification. J Environ Chem Eng 2:1228–1235. https://doi.org/10.1016/j.jece.2014.05.013

Meredith RJ (1998) Engineers' handbook of industrial microwave heating. The Institution of Electrical Engineers. 0852969163. London

Metaxas AC, Meredith RJ (1983) Industrial microwave heating. Peter Peregrinus Ltd., UK, pp 97–101

Mevissen N, Schulzke T, Unger CA, Mac An Bhaird S (2009) Thermodynamics of autothermal wood gasification. Environ Prog Sustain Energy 28:347–354. https://doi.org/10.1002/ep.10393

Miandad R, Nizami AS, Rehan M, Barakat MA, Khan MI, Mustafa A, Ismail IMI, Murphy JD (2016) Influence of temperature and reaction time on the conversion of polystyrene waste to pyrolysis liquid oil. Waste Manag 58:250–259. https://doi.org/10.1016/j.wasman.2016.09.023

Michailof CM, Kalogiannis KG, Sfetsas T, Patiaka DT, Lappas AA (2016) Advanced analytical techniques for bio-oil characterization

Mijović J, Wijaya J (1990) Review of cure of polymers and composites by microwave energy. Polym Compos 11:184–191. https://doi.org/10.1002/pc.750110307

Ministry of Statistics and Programme Implementation (2015) Government of India (MOSPI). Energy statistics 2015, New Delhi

Minkova V, Razvigorova M, Bjornbom E, Zanzi R, Budinova T, Petrov N (2001) Effect of water vapour and biomass nature on the yield and quality of the pyrolysis products from biomass. Fuel Process Technol 70:53–61. https://doi.org/10.1016/s0378-3820(00)00153-3

Mishra P, Sethi G, Upadhyaya A (2006) Modeling of microwave heating of particulate metals. Metall Mater Trans B Process Metall Mater Process Sci. 37:839–845. https://doi.org/10.1007/s11663-006-0066-z

Mishra A, Singh R, Mishra P (2015) Effect of biomass gasification on environment. Mesopotamia Environ J 1:39–49

Mohan D, Pittman CU, Steele PH (2006) Pyrolysis of wood/biomass for bio-oil: a critical review

Mohn J, Szidat S, Fellner J, Emmenegger L (2008) Determination of biogenic and fossil CO_2 emitted by waste incineration

Molina A, Poole C (2004) A comparative study using two methods to produce zeolites from fly ash. In: Minerals Engineering, pp 167–173 (2004)

Molino A, Chianese S, Musmarra D (2016) Biomass gasification technology: the state of the art overview

Mondal P, Dang GS, Garg MO (2011) Syngas production through gasification and cleanup for downstream applications—recent developments. Fuel Process Technol 92:1395–1410. https://doi.org/10.1016/j.fuproc.2011.03.021

Muhammad C, Onwudili JA, Williams PT (2015) Catalytic pyrolysis of waste plastic from electrical and electronic equipment. J Anal Appl Pyrolysis 113:332–339. https://doi.org/10.1016/j.jaap.2015.02.016

Mundada MN, Kumar S, Shekdar AV (2004) E-waste: a new challenge for waste management in India. Int J Environ Stud 61:265–279. https://doi.org/10.1080/0020723042000176060

Muradov N, Smith F, T-Raissi A (2005) Catalytic activity of carbons for methane decomposition reaction. Catalysis Today 225–233

Narváez I, Orío A, Aznar MP, Corella J (1996) Biomass gasification with air in an atmospheric bubbling fluidized bed. Effect of six operational variables on the quality of the produced raw gas. Ind Eng Chem Res 35:2110–2120. https://doi.org/10.1021/ie9507540

National Institute of Solar Energy (2014) Ministry of new and renewable energy, Government of India (NISE). State wise Estimation Solar Power Potential 2014, New Delhi

Needhidasan S, Samuel M, Chidambaram R (2014) Electronic waste—an emerging threat to the environment of urban India. J Environ Heal Sci Eng 12:36. https://doi.org/10.1186/2052-336x-12-36

Neelakanta PS (1995) Handbook of electromagnetic materials—monolithic and composite versions and their applications. CRC Press, Florida. pp 491–493 (1995)
Nelson SO (2005) Density-permittivity relationships for powdered and granular materials. IEEE Trans Instrum Meas 54:2033–2040. https://doi.org/10.1109/tim.2005.853346
Nelson SO, Trabelsi S (2012) Factors influencing the dielectric properties of agricultural and food products. J Microw Power Electromagn Energy 46:93–107. https://doi.org/10.1080/08327823.2012.11689828
Oasmaa A, Leppämäki E, Koponen P, Levander J, Tapola E (1997) Physical characterisation of biomass-based pyrolysis liquids application of standard fuel oil analyses. VTT Publications. https://doi.org/10.1016/s0140-6701(98)97220-4
Olgun H, Ozdogan S, Yinesor G (2011) Results with a bench scale downdraft biomass gasifier for agricultural and forestry residues. Biomass Bioenerg 35:572–580. https://doi.org/10.1016/j.biombioe.2010.10.028
Ortuño N, Conesa JA, Moltó J, Font R (2014) Pollutant emissions during pyrolysis and combustion of waste printed circuit boards, before and after metal removal. Sci Total Environ 499:27–35 (2014). https://doi.org/10.1016/j.scitotenv.2014.08.039
Ozawa T (1965) A new method of analyzing thermogravimetric data. Bull Chem Soc Jpn 38:1881–1886. https://doi.org/10.1246/bcsj.38.1881
Paethanom A, Nakahara S, Kobayashi M, Prawisudha P, Yoshikawa K (2012) Performance of tar removal by absorption and adsorption for biomass gasification. Fuel Process Technol 104:144–154. https://doi.org/10.1016/j.fuproc.2012.05.006
Pandey Brijesh Kumar, Vyas Savita, Pandey Mukesh, Gaur Anurag (2016) Municipal solid waste to energy conversion methodology as physical, thermal, and biological methods. Curr Sci Perspect 2:39–44
Papagiannakis R, Hountalas D (2008) Combustion and performance characteristics of a DI diesel engine operating from low to high natural gas supplement ratios at various operating conditions. SAE 776–790. https://doi.org/10.4271/2008-01-1392
Paradela F, Pinto F, Gulyurtlu I, Cabrita I, Lapa N (2009) Study of the co-pyrolysis of biomass and plastic wastes. Clean Technol Environ Policy 11:115–122. https://doi.org/10.1007/s10098-008-0176-1
Parikh J, Parikh K (2011) India's energy needs and low carbon options. Energy 36:3650–3658. https://doi.org/10.1016/j.energy.2011.01.046
Parparita E, Uddin MA, Watanabe T, Kato Y, Yanik J, Vasile C (2015) Gas production by steam gasification of polypropylene/biomass waste composites in a dual-bed reactor. J Mater Cycles Waste Manag 17:756–768. https://doi.org/10.1007/s10163-014-0308-0
Pereira EG, Da Silva JN, De Oliveira JL, MacHado CS (2012) Sustainable energy: a review of gasification technologies
Pittman CU, Mohan D, Eseyin A, Li Q, Ingram L, Hassan EBM, Mitchell B, Guo H, Steele PH (2012) Characterization of bio-oils produced from fast pyrolysis of corn stalks in an auger reactor. Energy Fuels 3816–3825
Ponzio A, Kalisz S, Blasiak W (2006) Effect of operating conditions on tar and gas composition in high temperature air/steam gasification (HTAG) of plastic containing waste. Fuel Process Technol 87:223–233. https://doi.org/10.1016/j.fuproc.2005.08.002
Pradhan A, Baredar P, Kumar Anil (2015) Syngas as an alternative fuel used in internal combustion engines: a review. J Pure Appl Sci Technol 5:51–66
Prasad L, Subbarao PMV, Subrahmanyam JP (2014) Pyrolysis and gasification characteristics of Pongamia residue (de-oiled cake) using thermogravimetry and downdraft gasifier. Appl Therm Eng 63:379–386. https://doi.org/10.1016/j.applthermaleng.2013.11.005
Rahman F, Langford KH, Scrimshaw MD, Lester JN (2001) Polybrominated diphenyl ether (PBDE) flame retardants
Ramasamy KK, T-Raissi A (2007) Hydrogen production from used lubricating oils. Catal Today 129:365–371 (2007). https://doi.org/10.1016/j.cattod.2006.09.037

Rattanadecho P, Suwannapum N, Watanasungsuit A, Duanduen A (2007) Drying of dielectric materials using a continuous microwave belt drier (case study: ceramics and natural rubber). J Manuf Sci Eng 129:157. https://doi.org/10.1115/1.2386166

Revesz RN, Thomas JE, Hargett WP Jr (2002) US Patent No. 6462321B2

Robinson J, Dodds C, Stavrinides A, Kingman S, Katrib J, Wu Z, Medrano J, Overend R (2015) Microwave pyrolysis of biomass: control of process parameters for high pyrolysis oil yields and enhanced oil quality. Energy Fuels 29:1701–1709. https://doi.org/10.1021/ef502403x

Rosi L, Bartoli M, Frediani M (2018) Microwave assisted pyrolysis of halogenated plastics recovered from waste computers. Waste Manag 73:511–522. https://doi.org/10.1016/j.wasman.2017.04.037

Roy S, Banerjee R, Bose PK (2014) Performance and exhaust emissions prediction of a CRDI assisted single cylinder diesel engine coupled with EGR using artificial neural network. Appl Energy 119:330–340. https://doi.org/10.1016/j.apenergy.2014.01.044

Ryu K (2013) Effects of pilot injection timing on the combustion and emissions characteristics in a diesel engine using biodiesel-CNG dual fuel. Appl Energy 111:721–730. https://doi.org/10.1016/j.apenergy.2013.05.046

Sabio E, González E, González JF, González-García CM, Ramiro A, Gañan J (2004) Thermal regeneration of activated carbon saturated with p-nitrophenol. Carbon 42:2285–2293. https://doi.org/10.1016/j.carbon.2004.05.007

Sahoo BB, Saha UK, Sahoo N (2011) Effect of load level on the performance of a dual fuel compression ignition engine operating on syngas fuels with varying H_2/CO content. J Eng Gas Turbines Power 133:122802. https://doi.org/10.1115/1.4003956

Sahoo BB, Sahoo N, Saha UK (2012) Effect of H_2:CO ratio in syngas on the performance of a dual fuel diesel engine operation. Appl Therm Eng 49:139–146. https://doi.org/10.1016/j.applthermaleng.2011.08.021

Saidur R, Abdelaziz EA, Demirbas A, Hossain MS, Mekhilef S (2011) A review on biomass as a fuel for boilers

Samiran NA, Jaafar MNM, Ng JH, Lam SS, Chong CT (2016) Progress in biomass gasification technique—with focus on Malaysian palm biomass for syngas production. Renew Sustain Energy Rev 62:1047–1062. https://doi.org/10.1016/j.rser.2016.04.049

San Miguel G, Lambert SD, Graham NJD (2001) The regeneration of field-spent granular-activated carbons. Water Res 35:2740–2748. https://doi.org/10.1016/s0043-1354(00)00549-2

Sancho JA, Aznar MP, Toledo JM (2008) Catalytic air gasification of plastic waste (polypropylene) in fluidized bed. Part I: Use of in-gasifier bed additives. Ind Eng Chem Res 47:1005–1010. https://doi.org/10.1021/ie071023q

Sansaniwal SK, Pal K, Rosen MA, Tyagi SK (2017) Recent advances in the development of biomass gasification technology: a comprehensive review

Schlummer M, Brandl F, Mäurer A, Van Eldik R (2005) Analysis of flame retardant additives in polymer fractions of waste of electric and electronic equipment (WEEE) by means of HPLC-UV/MS and GPC-HPLC-UV. J Chromatogr A 1064:39–51. https://doi.org/10.1016/j.chroma.2004.12.016

Sehwartzwalder K, Somers AV (1963). US Patent, 309009411963 (1963)

Seltenrich N (2016) Emerging waste-to-energy technologies: solid waste solution or dead end? Environ Health Perspect 124:A106–A111. https://doi.org/10.1289/ehp.124-a106

Sharma A, Rajeswara Rao T (1999) Kinetics of pyrolysis of rice husk. Bioresour Technol 67:53–59. https://doi.org/10.1016/s0960-8524(99)00073-5

Sharma NK, Tiwari PK, Sood YR (2012) Solar energy in India: strategies, policies, perspectives and future potential. Renew Sustain Energy Rev 16:933–941. https://doi.org/10.1016/j.rser.2011.09.014

Sharma BK, Moser BR, Vermillion KE, Doll KM, Rajagopalan N (2014) Production, characterization and fuel properties of alternative diesel fuel from pyrolysis of waste plastic grocery bags. Fuel Process Technol 122:79–90. https://doi.org/10.1016/j.fuproc.2014.01.019

Sheet RF (2008) Characteristics of biomass as a heating fuel. Renewable fact sheet. Renew Energy 1–3

Shi K, Wu T, Yan J, Zhao H, Hall P, Lester E (2014) Microwave enhanced pyrolysis of gumwood. In: Progress in sustainable energy technologies: generating renewable energy, pp 699–708

Shilling NZ, Lee DT (2003) IGCC-Clean power generation alternative for solid fuels. GE Power Systems. Power Generation in Asia, pp 1–9

Shrimali G, Rohra S (2012) India's solar mission: a review

Shudo T (2008) Influence of gas composition on the combustion and efficiency of a homogeneous charge compression ignition engine system fuelled with methanol reformed gases. Int J Engine Res 9:399–408. https://doi.org/10.1243/14680874jer01208

Shukla RS, Divakar Shetty AS, Antony AJ (2016) Performance and emission characteristics of CRDI engine working on plastic oil. Indian J Sci Technol 9. https://doi.org/10.17485/ijst/2016/v9i45/104611

Siedlecki M, de Jong W, Verkooijen AHM (2011) Fluidized bed gasification as a mature and reliable technology for the production of bio-syngas and applied in the production of liquid transportation fuels-a review

Silva PC, Figueiredo JL (2001) Production of SiC and Si_3N_4 whiskers in C + SiO_2 solid mixtures. Mater Chem Phys 72:326–331. https://doi.org/10.1016/s0254-0584(01)00332-7

Singh R (2018) Energy sufficiency aspirations of India and the role of renewable resources: scenarios for future

Singh RK, Ruj B (2016) Time and temperature depended fuel gas generation from pyrolysis of real world municipal plastic waste. Fuel 174:164–171. https://doi.org/10.1016/j.fuel.2016.01.049

Soler A, Conesa JA, Iñiguez ME, Ortuño N (2018) Pollutant formation in the pyrolysis and combustion of materials combining biomass and e-waste. Sci Total Environ 622–623:1258–1264. https://doi.org/10.1016/j.scitotenv.2017.12.068

Srivastav T (2013) Renewable energy (gasification). Adv Electron Electr Eng 3:1243–1250 (2013)

Stegeman MHL, Peijnenburg WJGM, Verboom H (1993) A quantitative structure-activity relationship for the direct photohydrolysis of meta-substituted halobenzene derivatives in water. Chemosphere 26:837–849. https://doi.org/10.1016/0045-6535(93)90359-d

Straka P, Bičáková O (2014) Hydrogen-rich gas as a product of two-stage co-gasification of lignite/waste plastics mixtures. Int J Hydrogen Energy 39:10987–10995. https://doi.org/10.1016/j.ijhydene.2014.05.054

Studart AR, Gonzenbach UT, Tervoort E, Gauckler LJ (2006) Processing routes to macroporous ceramics: a review. J Am Ceram Soc 1771–1789

Suda T, Liu Z, Takafuji M, Narukawa M (2010) Modelling of steam gasifier in dual fluidized bed gasification. Symp A Q J Mod Foreign Lit 1–8 (2010)

Sudiana IN, Mitsudo S, Firihu MZ, Aba L, Ngkoimani LO, Arsana MW, Aripin H (2017) Investigation of silica from rice husk ash wastes as an alternative material for microwave absorbers. In: AIP Conference Proceedings

Suksankraisorn K, Patumsawad S, Vallikul P, Fungtammasan B, Accary A (2004) Co-combustion of municipal solid waste and Thai lignite in a fluidized bed. Energy Convers Manag 45:947–962. https://doi.org/10.1016/s0196-8904(03)00187-0

Sun L, Gong K (2001) Silicon-based materials from rice husks and their applications. Ind Eng Chem Res 40(25):5861–5877. https://doi.org/10.1021/ie010284b

Suriapparao DV, Vinu R (2015) Bio-oil production via catalytic microwave pyrolysis of model municipal solid waste component mixtures. RSC Adv 5:57619–57631. https://doi.org/10.1039/c5ra08666c

Sutton D, Kelleher B, Ross JRH (2001) Review of literature on catalysts for biomass gasification

Syamsiro M, Saptoadi H, Norsujianto T, Noviasri P, Cheng S, Alimuddin Z, Yoshikawa K (2014) Fuel oil production from municipal plastic wastes in sequential pyrolysis and catalytic reforming reactors. In: Energy Procedia, pp 180–188 (2014)

Syamsiro M, Saptoadi H, Norsujianto T, Noviasri P, Cheng S, Alimuddin Z, Yoshikawa K (2014) Fuel oil production from municipal plastic wastes in sequential pyrolysis and catalytic reforming reactors. In: Energy Procedia, pp 180–188

Technical report Central Pollution Control Board (2008) Ministry of Environment and Forestry, Comprehensive industrial documents for producer gas plants and biomass gasifiers

Thomas BN, George SC (2015) Production of activated carbon from natural sources. iMedPub J 1:1–5. https://doi.org/10.1515/chem-2015-0087

Thostenson ET, Chou T-W (1999) Microwave processing: fundamentals and applications. Compos Part A Appl Sci Manuf 30:1055–1071. https://doi.org/10.1016/s1359-835x(99)00020-2

Tinaut FV, Melgar A, Pérez JF, Horrillo A (2008) Effect of biomass particle size and air superficial velocity on the gasification process in a downdraft fixed bed gasifier. an experimental and modelling study. Fuel Process Technol 89:1076–1089. https://doi.org/10.1016/j.fuproc.2008.04.010

Tripathi AK, Ojha DK, Vinu R (2015) Selective production of valuable hydrocarbons from waste motorbike engine oils via catalytic fast pyrolysis using zeolites. J Anal Appl Pyrolysis 114:281–292. https://doi.org/10.1016/j.jaap.2015.06.009

Vandervoort NA, Fall M, Shulman H, Allen S (2007) Improved high temperature susceptors. In: Materials Science and Technology 2007. Conference and Exhibition. Detroit, US

Vilaplana F, Karlsson S (2008) Quality concepts for the improved use of recycled polymeric materials: a review

Vinoy KJ, Jha RM (1995) Trends in radar absorbing materials technology. Sadhana. 20, 815–850. doi:https://doi.org/10.1007/BF02744411

Wallace PR (1947) The band theory of graphite. Phys Rev 71:622–634. https://doi.org/10.1103/physrev.71.622

Wan Y, Liu Y, Lin X, Yang C, Zhang B, Chen P, Lei H, Ruan R (2009) Microwave assisted pyrolysis of corn stover pellets with catalysts for bio-oil production and its component. Nongye Gongcheng Xuebao/Trans Chin Soc Agric Eng 25:190–195 (2009)

Wang R, Xu Z (2014a) Recycling of non-metallic fractions from waste electrical and electronic equipment (WEEE): a review. Waste Manag 34(8):1455–1469

Wang R, Xu Z (2014) Recycling of non-metallic fractions from waste electrical and electronic equipment (WEEE): a review

Wang Y, Sohn MD, Wang Y, Lask KM, Kirchstetter TW, Gadgil AJ (2014) How many replicate tests are needed to test cookstove performance and emissions? Three is not always adequate. Energy Sustain Dev 20:21–29. https://doi.org/10.1016/j.esd.2014.02.002

Wang Z, He T, Qin J, Wu J, Li J, Zi Z, Liu G, Wu J, Sun L (2015) Gasification of biomass with oxygen-enriched air in a pilot scale two-stage gasifier. Fuel 150:386–393. https://doi.org/10.1016/j.fuel.2015.02.056

Ware RL, Rowland SM, Rodgers RP, Marshall AG (2017) Advanced chemical characterization of pyrolysis oils from landfill waste, recycled plastics, and forestry residue. Energy Fuels 31:8210–8216. https://doi.org/10.1021/acs.energyfuels.7b00865

Warnecke R (2000) Gasification of biomass: comparison of fixed bed and fluidized bed gasifier. Biomass Bioenerg 18:489–497. https://doi.org/10.1016/s0961-9534(00)00009-x

Weber R, Kuch B (2003) Relevance of BFRs and thermal conditions on the formation pathways of brominated and brominated-chlorinated dibenzodioxins and dibenzofurans. Environ Int 29 (6):699–710

Widmer R, Oswald-Krapf H, Sinha-Khetriwal D, Schnellmann M. Böni H (2005) Global perspectives on e-waste

Wilk V, Hofbauer H (2013) Conversion of mixed plastic wastes in a dual fluidized bed steam gasifier. Fuel 107:787–799. https://doi.org/10.1016/j.fuel.2013.01.068

Williams EA, Williams PT (1997) The pyrolysis of individual plastics and a plastic mixture in a fixed bed reactor. J Chem Technol Biotechnol 70:9–20. https://doi.org/10.1002/(sici)1097-4660(199709)70:1%3c9:aid-jctb700%3e3.0.co;2-e

Wood M, Branch P (1986) Wood gas as engine fuel. Food and Agriculture Organization of the United Nations, p 133

Wu HW, Wang RH, Ou DJ, Chen YC, Chen TY (2011) Reduction of smoke and nitrogen oxides of a partial HCCI engine using premixed gasoline and ethanol with air. Appl Energy 88:3882–3890. https://doi.org/10.1016/j.apenergy.2011.03.027

Xiao R, Jin B, Zhou H, Zhong Z, Zhang M (2007) Air gasification of polypropylene plastic waste in fluidized bed gasifier. Energy Convers Manag 48:778–786. https://doi.org/10.1016/j.enconman.2006.09.004

Yagmur E, Ozmak M, Aktas Z (2008) A novel method for production of activated carbon from waste tea by chemical activation with microwave energy. Fuel 87:3278–3285. https://doi.org/10.1016/j.fuel.2008.05.005

Yang X, Sun L, Xiang J, Hu S, Su S (2013) Pyrolysis and dehalogenation of plastics from waste electrical and electronic equipment (WEEE): a review. Waste Manag 33:462–473. https://doi.org/10.1016/j.wasman.2012.07.025

Yin R, Liu R, Wu J, Wu X, Sun C, Wu C (2012) Influence of particle size on performance of a pilot-scale fixed-bed gasification system. Bioresour Technol 119:15–21. https://doi.org/10.1016/j.biortech.2012.05.085

Yusof A (2004) The development of microwave absorber from oil palm shell carbon. Univ. Technol. Malaysia, Master Sci. Fac. Mech. Eng. Univ. Technol., p 181

Zhang X, Hayward DO (2006) Applications of microwave dielectric heating in environment-related heterogeneous gas-phase catalytic systems

Zhang Y, Dubé MA, McLean DD, Kates M (2003) Biodiesel production from waste cooking oil: 2. Economic assessment and sensitivity analysis. Bioresour Technol 90:229–240. https://doi.org/10.1016/s0960-8524(03)00150-0

Zhang Z, Shan Y, Wang J, Ling H, Zang S, Gao W, Zhao Z, Zhang H (2007) Investigation on the rapid degradation of congo red catalyzed by activated carbon powder under microwave irradiation. J Hazard Mater 147:325–333. https://doi.org/10.1016/j.jhazmat.2006.12.083

Zhou J, Masutani SM, Ishimura DM, Turn SQ, Kinoshita CM (2000) Release of fuel-bound nitrogen during biomass gasification. Ind Eng Chem Res 39:626–634. https://doi.org/10.1021/ie980318o

Zlotorzynski A (1995) The application of microwave radiation to analytical and environmental chemistry. Crit Rev Anal Chem 25:43–76. https://doi.org/10.1080/10408349508050557

Chapter 12
Matrix Method for Evaluation of Existing Solid Waste Management Processes in Jalandhar City, Punjab, India

Anchal Sharma, Rajiv Ganguly and Ashok Kumar Gupta

Abstract Solid waste management is one of the most serious problems being faced by Indian cities due to increased urbanization and industrialization in India. The present study highlights the existing status of solid waste management practices in Jalandhar city, Punjab, India considering a dumpsite of Wariana village and Suchipind of Jalandhar and suggests remedial measures to the major problems being faced by the existing system of solid waste management. The waste generation of municipal solid waste in Jalandhar city was reported as 400 ton per day. A total of 350 ton of solid waste is disposed of in different disposal sites daily in the city. The per capita waste generation rate in Jalandhar is approximately 0.6 kg/capita/day. The collection efficiency of the municipal solid waste is reported about 70% in the city. The study also summarizes the 'wasteaware' benchmark indicators for the evaluation of the existing scenario of solid waste management in Jalandhar city and matrix method for comparing the overall score of the existing management of municipal solid waste of Jalandhar city with Chandigarh city. The overall score of the analysis of the matrix method for Jalandhar city was reported as 32% and the same for Chandigarh city was 46%. However, the quantification score of Jalandhar city was considerably lower than Chandigarh city. The analysis of matrix method suggested that the management of municipal solid waste in Jalandhar city can be categorized under the category of low index, whereas Chandigarh city was categorized under low–medium index.

Keywords Municipal solid waste · Open dumping · 'Wasteaware' benchmark indicators · Matrix method

A. Sharma · R. Ganguly (✉) · A. K. Gupta
Department of Civil Engineering, Jaypee University of Information Technology, Waknaghat, Solan 173234, Himachal Pradesh, India
e-mail: rajiv.ganguly@juit.ac.in

A. Sharma
e-mail: anchalsharam881@gmail.com

A. K. Gupta
e-mail: ashok.gupta@juit.ac.in

R. A. Agarwal et al. (eds.), *Pollutants from Energy Sources*,
Energy, Environment, and Sustainability,
https://doi.org/10.1007/978-981-13-3281-4_12

12.1 Introduction

Increased urbanization and industrialization has led to severe environmental pollution in the cities due to the drastic increase in the generation of solid waste (Puri et al. 2008; Sethi et al. 2013). Population growth and rising living standards contribute to an increase in the amount and variety of solid waste generated in the countries. In particular, solid waste management has been a pertinent issue for developing countries (Shekdar 2009). The poor waste management practices are primarily due to the lack of authentic data and information to analyse the waste management practices (Chang and Davilla 2007; Hancs et al. 2011; Katiyar et al. 2013). The population of India is reported as 1083 million in 2001 and 1253 million in 2013 (Census report 2011). In general, Indian megacities including [Ahmedabad (6.3 million), Hyderabad (7.7 million), Bengal (8.4 million), Chennai (8.6 million), Kolkata (14.1 million), Delhi (16.3 million) and Greater Mumbai (18.4 million)] having a drastical increase in population as reported by Kumar et al. (2009). The substantial growth in population is the major contributor of solid waste in country (Anand 2005). There is no proper statistics about the nature, volume, collection, transportation and dumping of solid wastes generated in city (Sharholy et al. 2008; Ramachandra 2009). Since there is a lack of proper management of solid wastes, its increased generation coupled with lack of public awareness makes it potentially effective in causing environmental and human health effects. Further, it also reduces the visual aesthetics of the surrounding environment. In India, the existing status of municipal solid waste management is highly unsatisfactory. Currently, about 960 million tonnes of solid waste is being generated annually as by-products during municipal, industrial, mining, agricultural and other processes in India (Pappu et al. 2004). The per capita waste generation is 0.17 kg/capita/day in small towns and 0.62 kg/capita/day in the cities of India (Kumar et al. 2009; Modak et al. 2012). The population growth of major cities in India has been shown in Table 12.1. The statistics of municipal solid waste generated in different states in India has been shown in Table 12.2 and the waste generation rate of major cities in India has been shown in Table 12.3.

Solid waste thus generated in India is not managed properly due to the poor management of municipal corporation of the cities; about 90% of the waste is disposed of as an open dumping in the ground and hence contributes to the

Table 12.1 Population growth of major cities in India (Census 2011)

Sl. No.	City name	Population growth (10^6)
1.	Ahmedabad	6.3
2.	Hyderabad	7.7
3.	Bangalore	8.4
4.	Chennai	8.6
5.	Kolkata	14.1
6.	Delhi	16.3
7.	Mumbai	18.4

Table 12.2 Statistics of municipal solid waste generated in different states in India (CPCB 2015)

Sl. No.	Name of the state/UT	Municipal solid waste MT/day (2009–2012)
1.	Andaman and Nicobar	50
2.	Andhra Pradesh	11,500
3.	Arunachal Pradesh	93.802
4.	Assam	1146.28
5.	Bihar	1670
6.	Chandigarh	380
7.	Chhattisgarh	1167
8.	Daman Diu and Dadra	41
9.	Delhi	7384
10.	Goa	193
11.	Gujarat	7378.775
12.	Haryana	536.85
13.	Himachal Pradesh	304.3
14.	Jammu and Kashmir	1792
15.	Jharkhand	1710
16.	Karnataka	6500
17.	Kerala	8338
18.	Lakshadweep	21
19.	Maharashtra	19.204
20.	Manipur	112.9
21.	Meghalaya	284.6
22.	Mizoram	4742
23.	Madhya Pradesh	4500
24.	Nagaland	187.6
25.	Orissa	2239.2
26.	Puducherry	380
27.	Punjab	2793.5
28.	Rajasthan	5037.3
29.	Sikkim	40
30.	Tamil Nadu	12,504
31.	Tripura	360
32.	Uttar Pradesh	11.585
33.	Uttaranchal	752
34.	West Bengal	12,557
Total		127,485.107

environment pollution. The major problem of ineffective management of solid waste is due to deficit of requisite budgetary provisions for the management of solid waste (Rana et al. 2015).

Table 12.3 Waste generation of major cities in India (CPCB 2015)

Region/city	MSW (TPD)	Compostable (%)	Recyclables (%)	Inerts (%)	Moisture (%)	Cal. value (kcal/kg)
Metros	51,402	50.89	16.28	32.82	46	1523
Other cities	2723	51.91	19.23	28.86	49	2084
East India	380	50.41	21.44	28.15	46	2341
North India	6835	52.38	16.78	30.85	49	1623
South India	2343	53.41	17.02	29.57	51	1827
West India	380	50.41	21.44	28.15	46	2341
Overall Urban India	130,000	51.3	17.48	31.21	47	1751

The present study focuses on the existing solid waste management systems practised in Jalandhar city, Punjab, India. The study also employs the 'Wasteaware Benchmark' techniques and matrix method for grading the efficiency of the existing system. The paper also proposes suitable remedial measures for improving the existing system of municipal solid waste management carried out at these sites.

12.2 Methodology

12.2.1 Site Location

Jalandhar city lies in the coordinates of 31.3260°N and 75.5762°E with a population of 8,73,725 (Census 2011) with an MSW generation of 400 TPD with a collection efficiency of 70% which is openly dumped in land. The location of study area has been shown in Fig. 12.1.

12.2.2 'Wasteaware' Benchmark Indicators

The problem of municipal solid waste management is getting more awful due to diverse factors including poor technical and less financial resources, deficit of enforcement of regulations, lack of coordination between the authorities and scarcity of policies (Kumar et al. 2009).

The major downside of the ineffectual municipal solid waste management system is the absence of relentless data for the designing and interpretation of effective solid waste management system for comparative basis. Integrated solid waste management benchmark indicators are the effective tool to analyse the performance of recycling and municipal solid waste management of the city and municipality. The basic principle of benchmark indicators is to allow the city to determine or

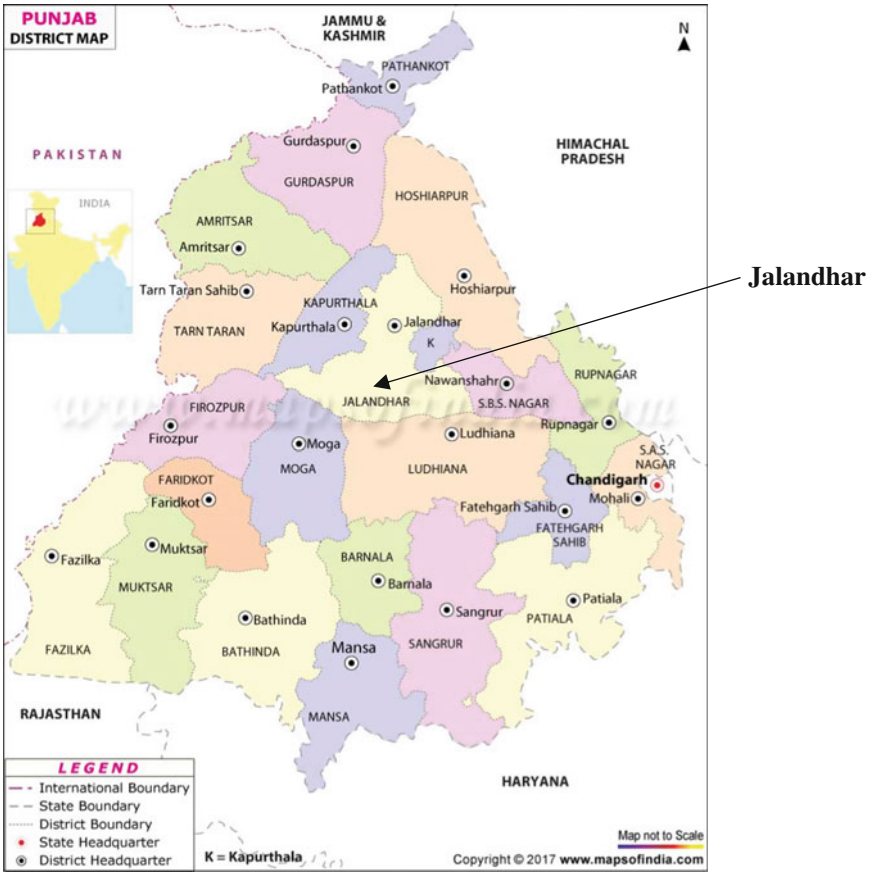

Fig. 12.1 Location of study area in Punjab

judge its performance of waste management services with different cities. Moreover, it also provides information for decision-making on primary issues regarding funds for the improvement of waste management services.

The 'wasteaware' benchmark parameters integrate both qualitative and quantitative indicators (Wilson et al. 2013, 2015) for determining the performance of municipal solid waste management systems practiced in different locations. In the quantitative analysis of waste management, the parameters include public health collection, environmental controlled disposal and resource management—reuse, reduce and recycling and the qualitative indicators consolidates governance parameters like user and provider inclusivity; financial sustainability; and the national policy framework and local institutions (Wilson et al. 2013, 2015).

12.2.3 Matrix Method

The quantification method has been employed for the consideration of existing municipal solid waste management system (Rana et al. 2015). In this context, the 'wasteaware' benchmarks utilized grading system including low (*L*), low/medium (*L*/*M*), medium (*M*), medium/high (*M*/*H*) and high (*H*), a five points classification has been assigned to each of these benchmarks. The above grading systems (*L*, *L*/*M*, *M*, *M*/*H* and *H*) were utilized by assigning each of them a classification point such as ($L = 1$, $L/M = 2$, $M = 3$, $M/H = 4$, $H = 5$). The matrix method has been successfully used to evaluate the functioning of the MSW management in tri-city locations of Chandigarh, Mohali and Panchkula (Rana et al. 2015, 2017) and at selected study locations in Himachal Pradesh (Sharma et al. 2018).

12.3 Results and Discussions

12.3.1 Assessment of Existing Municipal Solid Waste (MSW) Management in Jalandhar City

Generation of MSW Jalandhar city lies in the area of 110 m^2 with a total number of 60 wards as reported by Census (2011). The estimated garbage generation is 400 ton per day in the city and approximately 350 ton of waste is collected and disposed of daily in the dumpsites. The solid waste is generated from residential, commercial, institutional, construction and demolition, industrial, agriculture, etc. and the sources of solid waste are rubbish, garbage, ashes, street waste, bulk waste and hazardous waste (Puri et al. 2008). The area of the city is scattered into three zones including residential zone (85%), industrial zone (10%) and mixed zone (5%). The physical characterization of municipal solid waste has been summarized in Table 12.4.

Table 12.4 Physical characterization of waste (Puri et al. 2008)

Sl. No.	Parameters	Range	Average
1.	Metal (ferrous)	0.00–1.00	0.01
2.	Metal (non-ferrous)	0.00–0.04	0.13
3.	Earth-ware stone	0.50–15.00	5.17
4.	Glass/ceramics	0.00–2.10	0.57
5.	Fine earth	19.92–25.72	24.15
6.	Paper/cardboard	0.2–10.80	3.43
7.	Wooden matter	0.00–0.30	0.09
8.	Rags	0.10–9.80	3.95
9.	Rubber/leather	0.00–4.00	1.31
10.	Plastics	3.20–14.5	7.42
11.	Organic matter	6.90–68.10	44.53

Collection of MSW The type of waste containers and the area of waste storage are mainly based on the frequency and method of solid waste collection (both inorganic and organic waste). It is reported that more than 450 collection bins have been placed roadside in the city and around 60 DP bins of 3.5 m^3 capacities are placed at sensitive littering points. The sweeping frequency of waste has been reported twice in a day under the supervision of ward supervisor. Individual municipal solid waste collectors are also involved and every house is charged a fee of rupee 50 per month for the collection of municipal solid waste. These waste collectors informally separate the waste into biodegradable, paper, rubber, plastics, glass and metals and then, waste is transferred to Sehaj Safai Kendra's (SSKs). The considerable downside of waste management in Jalandhar city is ill-suited collection of municipal solid waste. The solid waste generated in the city is stored in common bins without any prior segregation of waste. There is no provision of separate bins for the dry waste and the wet waste. The rate of waste generation is more and the dustbins for the collection of solid waste are less in number. The insufficient number of dustbins contributes to the littering and spilling of waste and hence contributes to insanitary conditions of the city. It is observed that during the survey of solid waste management plans in the city, there is no provision of daily door-to-door collection of waste. The solid waste is collected from the collection bins from different locations of the city and from the residential and commercial sectors of the city. It is recommended from World Health Organization that the waste is collected through cart pullers and handcarts. The cart pullers used to segregate the paper, plastic, polythene, metal, leather, etc. which is sold to the Kabariwala. In this way, the biodegradable and recycled waste may get separated from inert waste. This collection system is economically viable and also reduces the volume of solid waste in the dumping sites. But in actual practice, the waste is not sorted and segregated in accurate manner and almost all of the biodegradable waste is dumped in open land.

Transportation of MSW There is outrageous need of the expenditure on man-power, vehicles and other resources to improve the efficiency of solid waste management. The conditions of the transportation vehicles depend on the physical layout of the roads, cost of manpower available and maintenance provisions. The vehicles provided by municipal authority for the transportation of waste to the dump sites in Jalandhar includes tippers, loaders, bulldozers, compactor, three wheelers, tractor trolleys, dumper placer hydra cranes, etc. The transportation methodology is divided into three categories in the city including household waste transportation, commercial waste transportation and commercial routes being followed by the workers of municipal corporation of the city. The household waste is collected by waste pickers on rickshaw Rehra's and transported to secondary dumps. Finally, the secondary dumps loaded and transported to Wariana and Suchipind dumpsites. The commercial waste is collected by municipal corporation vehicles such as Tata Ace and Refuse Compactors. The vehicle named Tata Ace

Table 12.5 Number of machineries used for the transportations of municipal solid waste (city profile report of municipal corporation, Jalandhar)

Sl. No.	Name of machinery	Number of machinery
1.	Tippers	20
2.	JC/loaders	09
3.	Bulldozer tracked	02
4.	Three wheelers	27
5.	Tata Ace/Bolero/Ashok Leyland	20
6.	Tractor trolleys including hired	11 + 16 (Hired)
7.	Compactors	03 (Hired)
8.	Dumper placer	09

dumps the commercial waste at secondary collection points and then refuse compactors carry it to dumpsites for disposal. There are five commercial routes for the transportation of waste to the dumping lands. The name of machinery and number of machinery has been shown in Table 12.5.
In this context, it is critically observed from the survey that most of the vehicles are worn out and no maintenances had been carried out of these vehicles since the past years. Apart from this, one of the major drawbacks of transportation system is that waste is transported mostly in open trucks and vehicles which cause littering of waste here and there in the roads and thereby made habitat for mosquitoes (Rana et al. 2015).

Disposal of MSW The daily disposal of municipal solid waste is imperative due to the presence of high organic matter of municipal solid waste that may cause nuisance and unhygienic condition of the surroundings (Kumar et al. 2009). The waste collected from different sources from the Jalandhar city is disposed of in Wariana dumpsite (100 ton of solid waste per day) and in Suchipind dumpsite (250 ton of solid waste per day) that has been used for last 30 years. Presently, all types of solid waste consisting of industrial, biomedical, slaughterhouse and municipal solid waste are dumped on this landfill site. According to the management and handling Rules 2000, only inert waste should be disposed of in the landfills and the remaining waste should be transferred to the processing units. It has been already discussed that the disposal sites are used over 30 years old, and as such, no facility of leachate collection system, liner system and proper gas collection facilities has been constructed. Therefore, it is a threat to the surface and groundwater quality because of the permeation of leachate in the soil. Emission of landfill gases (LFGs) at the dumping site can be clearly observed causing pungent smell and affecting the health of the workers who work in the vicinity of the landfill site. However, no scientific observations for the right quantity of greenhouse gases produced are made to test the concentration of landfill gas (LFGs).

12.3.2 'Wasteaware' Benchmark Indicators

'Wasteaware' benchmark indicator is the index system to evaluate the pollution level by municipal solid waste (Rana et al. 2015). In this context, 'wasteaware' benchmark indicators which include qualitative and quantitative indicators have been addressed in Sect. 2.2 (Wilson et al. 2013, 2015). In this context, the benchmarks for Jalandhar city have been evaluated and are shown in Table 12.5 by adopting the procedure (Wilson et al. 2015). Apart from this, the generated benchmark for Jalandhar city has also been compared with the benchmarks of Chandigarh city. It is observed from Table 12.5 that overall municipal solid waste generated in Jalandhar city is substantially lower than the overall municipal solid waste generated in Chandigarh because of the difference in population of Chandigarh city is more than that of the Jalandhar city. The colour coding in the table indicated that red colour presented for low index, yellow colour for medium index and green colour for high index. In this context, it was observed from the evaluation of 'wasteaware' benchmark parameters that the collection efficiency and waste collection services under the category of qualitative indicators of Jalandhar city lies in low/medium index (*L*/*M*) as compared to Chandigarh city that is having collection efficiency lies in medium/high index (*M*/*H*) (Rana et al. 2015). Apart from this, for the Environmental control and 3R's facilities, both Jalandhar and Chandigarh city were classified under the category of the low index. The 'wasteaware' analysis also reveals that for the qualitative indicators including public health parameters and environmental control measures, Jalandhar city lies in low/medium index (*L*/*M*) and for the same qualitative parameters, Chandigarh city lies in medium index (Rana et al. 2015). The 'Wasteaware' benchmark indicators for Jalandhar city compared with Chandigarh city has been shown in Table 12.6.

Quantification of Indicators Using Matrix Method Matrix method is further used for the quantification of the 'weights' that has been allocated to both quantitative and qualitative parameters of 'wasteaware' benchmarks for Jalandhar and the evaluation comparison with Chandigarh city which has been summarized in Table 12.7 and summary of scores obtained through matrix method has been summarized in Table 12.8.

The overall score of analysis of Matrix method for Jalandhar city was reported 32% and similarly, the score for Chandigarh city was 46%. Hence, it is clearly showed that the quantification score of Jalandhar city was considerably lower than Chandigarh city (Rana et al. 2015). The matrix analysis reported that the management of municipal solid waste generated at study location Jalandhar can be categorized under low index category and the scores of Chandigarh city lies under low–medium index. Further analysis revealed that weightage obtained from quantitative parameters of 'wasteaware' analysis was reported (26%) for Jalandhar city, whereas it was slightly more for Chandigarh city (40%) because it is a planned and designed city and hence it has a marginal advantage in comparison to other Tier-II and Tier-III cities (Rana et al. 2015). Moreover, the score for governance factors of Jalandhar and Chandigarh were reported as 40 and 55% respectively.

Table 12.6 'Wasteaware' benchmark indicators for Jalandhar city

Sr. No.	Category	Indicator	Jalandhar City	Chandigarh City
Background information of the city				
1	Country Income Level	World Bank Indicator Level	Lower-Middle	Lower-Middle
		GNI per Capita	$1,140	$1,140
B2	Population of the City	Total Population of the City	8,73,725	1,055,450
B3	Waste Generation	MSW Generation (tons/year)	127750	135050
W1	Waste per Capita	MSW per capita (Kg per year)	146	128
W2	Waste Composition		3 key fractions – as % wt. of total waste generated	
W2. 1	Organic	Organics (food and green wastes)	44.53%	52%
W2. 2	Paper	Paper	3.43%	6%
W2. 3	Plastic	Plastic	7.42%	7%
1.1	Public health - Waste collection	Waste collection coverage	70% (L/M)	90% (M/H)
1C	-	Quality of waste collection service	70% (L/M)	90% (L/M)
2	Environmental control- waste treatment and disposal	Controlled treatment and disposal	10% (L)	30% (L)

(continued)

Table 12.6 (continued)

2E	-	Degree of environmental protection in waste treatment and disposal	0% (L)		0% (L)	
3	3Rs - reduce, reuse and recycling	Recycling rate	0% (L)		0% (L)	
3R		Quality of 3Rs provision	5% (L)		17% (L)	
6N	Sound institutions, proactive policies	Adequacy of national SWM framework	60% (L/M)		60% (L/M)	
6L	Degree of Institutional coherence		70% (L/M)		75 % (M)	
4U	User inclusivity	User inclusivity	68% (L/M)		75 % (M)	
4P	Provider inclusivity	Degree of provider inclusivity	65% (L/M)		78 % (M)	

12.4 Key Recommendations for Improvement of Municipal Solid Waste Management at the Selected Study Locations

12.4.1 Source Segregation

Source segregation is most important key parameter for the improvement of solid waste management system. Except for inert waste, rest of all the waste including paper, plastic, metal, glass and rubber is recyclable in nature. In this context, proper handling, collection and segregation of waste should be implemented in the city so that dry waste should be recycled properly. It is possible only because of community partnership and public–private ownership for the strategy of municipal solid

Table 12.7 Weightage assignment for evaluation using matrix method

Sl. No.	Category	Indicator	Jalandhar city	Chandigarh city
Quantitative indicators (public health, environmental control, 3R's)				
1.1	Public health	Waste collection coverage	70% (*L*/*M*) (2)	90% (*M*/*H*) (4)
1C	Waste collection	Waste collection services	70% (*L*/*M*) (2)	90% (*M*/*H*) (4)
2	Environment control facilities	Control treatment and disposal	10% (*L*) (1)	30% (*L*) (1)
2E	Waste treatment and disposal	Degree of environmental protection	0% (*L*) (1)	0% (*L*) (1)
3	3R's—reduce, reuse and recycling	Recycling rate	0% (*L*) (1)	0% (*L*) (1)
3R		Quality of 3R's provisions	5% (*L*) (1)	17% (*L*) (1)
Qualitative indicators (governance factors)				
4U	User inclusivity	User inclusivity	*L*/*M* (60%) (2)	*M* (75%) (3)
4P	Provider inclusivity	Provider inclusivity	*L*/*M* (70%) (2)	*M* (78%) (3)
6N	Sound, institutions proactive policies	Adequate national framework	*L*/*M* (60%) (2)	*L*/*M* (60%) (2)
6L	–	Degree of institutional coherence	*L*/*M* (65%) (2)	*M* (75%) (3)

waste management plans. Awareness programmes should be assembled in order to motivate the residents for source segregation of waste and promoted recycling and reuse of segregated waste material. At present, there is no recycling unit situated in Jalandhar city that is unfavourable practise. The public should be encouraged to manage two collection bins for wet, dry and recyclable waste so that the waste must be initially segregated at the household level before reaching to the dumpsites. The municipality should have commenced the provisions of closed-type garbage containers for the collection of waste so that littering and spilling of waste should be avoided.

12.4.2 Provision of Underground Collection Bins

It is critically suggested that the authorities of municipal corporation of the city should have focused on the issue of closed containers and underground bins.

Table 12.8 Summary of scores obtained through matrix method

Sl. No.	Category	Indicator	Jalandhar city	Chandigarh city
Quantitative indicators (public health, environmental control, 3R)				
1.1	Public health—waste collection	Waste collection coverage	2	4
1C		Quality of waste collection service	2	4
2	Environmental control—waste treatment and disposal	Controlled treatment and disposal	1	1
2E		Degree of environment protection in waste treatment and disposal	1	1
3	3R's—reduce, reuse and recycling	Recycling rate	1	1
3R		Quality of 3R's provision	1	1
Total score (quantitative indicators)			08	12
Maximum score			30	30
Weightage (%)			26	40
Qualitative indicators (governance factors)				
4U	User inclusivity	User inclusivity	2	3
4P	Provider inclusivity	provider inclusivity	2	3
6N	Sound institutions proactive policies	Adequacy of national SWM framework	2	2
6L	–	Degree of institutional coherence	2	3
Total score (quantitative indicators)			08	11
Maximum score			20	20
Weightage (%)			40	55
Total score (overall)			08 + 08 = 16	12 + 11 = 23
Total maximum score			30 + 20 = 50	30 + 20 = 50
Overall weightage (%)			32	46

There should be separate collection bins for dry waste (paper, plastic) and wet waste (organic waste). The non-biodegradable and dry waste such as paper, plastic, metal and glass should be recycled and sent to the authorized recyclers for its use in the manufacturing of new materials. The advantage of implementation of such strategy are better environment (no bad odour from smelly dirty bins), secured collection (no overflowing bins or stray animals feeding on waste), increase awareness among citizens, cost saving (no broken and dirty garbage bins) and moreover easy to install, collect and dispose garbage and hence, an effective alternative to present situation.

12.4.3 Composting/Vermicomposting

It is further reported from the literature study of characterization of municipal solid waste in Jalandhar that MSW is rich in organic waste. The past studies of characterization of waste in Jalandhar revealed that most of the waste is biodegradable in nature. In this context, composting and vermicomposting is the best alternative for the decomposition and stabilization of organic fraction of waste. The bio conversion of municipal solid waste into soil enriches the natural fertility of soil. In this context, a composting facility was operated by the M/S Punjab Grow more fertilizers Pvt. Ltd. since 2003 but at present the facility is non-working. (Personal Communication with the Municipal Engineer of Jalandhar). In this context, there is outrageous need of providing adequate training to the operating staff for reanimating of the existing compost plant.

12.4.4 Refused Derived Fuel Plant

Presently, there is no such waste treatment facility of municipal solid waste in Jalandhar city. The installation of RDF plant is one of the feasible alternatives that can be used as a waste processing facility. The literature study on characterization of solid waste in Jalandhar city revealed the composition of paper waste which varied in the range of 3–10%, plastic waste varied in the range of 6–14% and major fraction of organic waste varied in the range of 40–44% and is found suitable for the treatment of solid waste in the city (Puri et al. 2008; Sethi et al. 2013).

12.4.5 Construction of Sanitary Landfill

The survey of the study area revealed that the waste is disposed of in open land in an unscientific manner. The open dumping of waste may cause health hazard issues and having environmental pollution (Puri et al. 2008). In this context, it is strictly suggested to construct engineered landfill system with liner system, leachate collection and removal system, gas collection facility and final cover system. After sorting the biodegradable organic fraction for bioprocessing and recyclable waste to manufacturing units, only the inert material should be disposed of into sanitary landfills. It should be noted that compaction is the mandatory factor while deposition of waste in order to maintain the stability and increase the capacity of closure.

12.5 Conclusion

Solid waste management is the globally concerned occurrence in the present scenario. This paper revealed an expressive image of the present situation in municipal solid waste management under the perspective of the citizens and municipal authorities. There is a dreadful need to educate local authorities and citizens of the city to reinforce environmental sustainability, public health, reduction and segregation at the source, reuse and recycling of waste. Further, it has been observed that the lack of resources including infrastructure, suitable data and planning, financing issues are the major limitations in the municipal solid waste management system. The overall survey showed the per capita waste generation rate in Jalandhar city is 350–400 ton per day with the collection efficiency of 70% that proves ineffectual for the municipal solid waste management system. The paper also focussed on the 'wasteaware' benchmark indicators and the quantification analysis by matrix method system for the study region Jalandhar city and the evaluation comparison with Chandigarh city. The results clearly showed the poor performance of environmental control methods including the collection and treatment of waste, disposal of waste, 3R's facilities, etc. in Jalandhar city. In this context, some of the remedial measures were suggested that must be incorporated by municipal corporations of Jalandhar city for the intensification of solid waste management including sufficient number of collection bins to avoid spilling of waste, facilities of new and advanced machines for segregating and recycling facilities. It is further expected from the study that the adjoining land of 2.25 acres acquired and processes will be started very soon to develop it as sanitary landfill (SLF). Another MSW processing facility will be planned in the city catering to the requirement of 27 cluster urban local bodies (ULBs) including Jalandhar. It is critically observed that there is no such facility of liner system, leachate collection and transfer system, gas monitoring facilities and final cover system for the disposal of solid waste. Open dumping of waste creates annoyance for the health of people as well as aesthetic appearance of the environment. Hence, open dumps should be avoided and waste should be disposed of in sanitary engineered landfill systems.

References

Anand S (2005) Solid waste generation and management in Delhi: a sustainable approach. In Singh J (ed) Environment and development. I.K. Intl Publisher, New Delhi, pp 621–639

Census (2011) Provisional population report, India

Chang NB, Davilla E (2007) Minimax regret optimization analysis for a regional solid waste management system. J Waste Manag 8:820–832

CPCB Central Pollution Control Board, Delhi (2015) Status of solid waste generation, collection, treatment and disposal in metro cities

Hancs A, Novak P, Dvorak M, Habart J, Svehla P (2011) Composition and parameters of household bio-waste in four seasons. J Waste Manag 31:1450–1460

Katiyar RB, Suresh S, Sharma AK (2013) Characterization of municipal solid waste generated by city of Bhopal, India, ICGSEE-2013. Int Conf Glob Scenario Environ Energy 5:623–628

Kumar S, Bhattacharyya JK, Vaidya AN, Chakrabarti T, Devotta S, Akolkar AB (2009) Assessment of the status of municipal solid waste management in metro cities, state capitals, class I cities, and class II towns in India: an insight. J Waste Manag 29:883–895

Modak P, Jiemian Y, Hongyuan Y, Choudhary R (2012) Municipal solid waste management: turning waste into resource. In: Shanghai manual—a guide for sustainable urban development in the 21st century, Shanghai

Pappu A, Saxena M, Asolekar SR (2004) Solid waste generation in India and their recycling potential in building material. Build Environ 42:2311–2320

Puri A, Kumar M, Eonkar J (2008) Solid waste management in Jalandhar city and its impact on community health. J Occup Environ Med 3:76–81

Ramachandra TV (2009) Municipal solid waste management. TERI Press, New Delhi, India

Rana R, Ganguly R, Gupta AK (2015) An assessment of solid waste management in Chandigarh city, India. Electron J Geotech Eng 20:1547–1572

Rana R, Ganguly R, Gupta AK (2017) An assessment of solid waste management in Chandigarh city, India. J Solid Waste Tech Manag 43(4):280–294

Sethi S, Kothiyal NC, Nema AK, Kaushik MK (2013) Characterization of municipal solid waste in Jalandhar city, Punjab, India. J Hazard Toxic Radioact Waste 17:97–106

Sharholy M, Ahmad K, Mahmood G, Trivedi RC (2008) Municipal solid waste management in Indian cities—a review. J Waste Manag 28:459–467

Sharma A, Ganguly R, Gupta AK (2018) Matrix method for evaluation of existing solid waste management system in Himachal Pradesh, India. J Mater Cycles Waste Manag 20(3): 1813–1832

Shekdar A (2009) Sustainable solid waste management: an integrated approach for Asian countries. J Waste Manag 29:1438–1448

Wilson DC, Rodic L, Cowing MJ, Velis CA, Whiteman AD, Scheinberg A, Vilches R, Masterson D, Stretz JZ, Oelz B (2013) Benchmark indicators for integrated & sustainable waste management (ISWM). In: Proceedings of ISWA world congress, International Solid Waste Association, Vienna, Austria

Wilson DC, Rodic L, Cowing MJ, Velis CA, Whiteman AD, Scheinberg A, Vilches R, Masterson D, Stretz JZ, Oelz B (2015) Wasteaware benchmark indicators for integrated sustainable waste management in cities. J Waste Manag 35:329–342

Chapter 13
Turning Coal Fly Ash into Zeolite for Effective Waste Management

A. R. K. Gollakota, Chi-Min Shu and Sneha Gautam

Abstract Despite of technological advancements in energy generation, the augmented usage of electric power, and shortfalls of alternate energy sources forced humankind to rely on coal based electric power. Nevertheless, a low cost and abundant availability, exponentially multiplied the number of coal thermal power plants thereby producing massive volumes of coal fly ash. The toxic nature of these atmospheric pollutant obtained by burning coal posed a serious question to humankind and is considered as the epidemic research area across the globe. Spinning to the other end of the coin, coal fly ash, is a precious waste material with a wide range of applicability, but the refrainment of not being utilized to the fullest extent makes this material underrated. However, the rapid advancement of the technological innovations and the increased efforts and focus toward the CFA utilization breaks the barrier to an extent by developing various applications. Though there is a massive imbalance in the production and the consumption rates, in which the minimum quantity is being utilized, and the rest is directly dumped as a waste material causing substantial contamination to the water bodies and the air. In this regard, the zeolite generation and their application in the acid mine treatment, wastewater treatment technologies could offer some resistance such that, the standards of the consumption rate are enhanced. In lieu of this, the more effective utilization technique followed was synthesizing zeolites from CFA. This, in turn, could be a better solution that serves the dual role of harnessing the environmental contamination and the water bodies that is prominent in the developing nations. The present study refers to the physiochemical properties of CFA, toxic nature of CFA, environmental impact and finally, the surging need to enhance the present and possible futuristic applications especially zeolite. Finally, the advantages and disadvantages of the coal fly ash and its mode of utilization worldwide for future research especially the synthesis of zeolite are considered.

A. R. K. Gollakota (✉) · C.-M. Shu
Department of Safety, Health and Environmental Engineering, National Yunlin University of Science and Technology, Douliu 64002, Yunlin, Taiwan, ROC
e-mail: garkiran@yuntech.edu.tw

S. Gautam
Department of Environmental Science and Engineering, Marwadi University, Rajkot 360003, Gujarat, India

R. A. Agarwal et al. (eds.), *Pollutants from Energy Sources*,
Energy, Environment, and Sustainability,
https://doi.org/10.1007/978-981-13-3281-4_13

Keywords Coal fly ash · Contamination · Acid mine · Zeolite

Abbreviations

Al	Alumina
ASTM	American standard for testing material
Ca	Calcium
CEC	Cation exchange capacity
CFA	Coal fly ash
Fe	Iron
HAP	Hazardous air pollutants
HDTMA	Hexadecyl-trimethyl-ammonium chloride
LCA	Life-cycle assessment
Mg	Magnesium
Na	Sodium
NaOH	Sodium hydroxide
SBU	Secondary building unit
SDMBA	Stearyl-dimethyl-benzyl-ammonium chloride
Si	Silica
ZSM	Zeolite Socony Mobil

13.1 Introduction

Coal fly ash in general is regarded as one of the solid product wastes obtained from the coal-based thermal power plants during the generation of electricity. The expansive utilization of electricity in the modern era, leads to the multiple number of coal-based thermal power plants. Subsequently, the voluminous amount of carbon residues from coal fly ash (CFA) approximately 750 million ton (Heidrich et al. 2013) has been generated annually across the world. Despite the efforts in recycling the waste CFA into useful product lines such as zeolites, cement, binders, soil amendments, road base constructions, sewage treatment, fillers, and fillers in plastic composites, etc., the consumption rate is still below 20%. There is a considerable margin in the balance of CFA generation, and utilization and a majority of the CFA finds no application other than discharging into landfills and ash ponds. Further, the lack of landfill space and escalated disposal costs in the very near future forced the research community to search and develop the new or refine the available technological aspects for the effective utilization.

To date, the commercial grading of the CFA and its effective utilization is still unanswered. Knowing the fact, CFA possesses Si, Al in higher concentrations and traces of Fe, Ca and it could be an excellent resource for the high-value zeolite preparation. From the power generation perspective, CFA is the waste material, and from coal utilization point of view, CFA is a resource not yet utilized to the fullest extent. The dominant CFA production houses across the globe were still looking at

the research community for ways to exploit the CFA. Among, various applications mentioned, synthesizing zeolites from CFA could be the best alternative that caters the dual needs of enhancing CFA usage and economical remedy for the wastewater treatment comprising industrial effluents, acid mine waters, etc. Since, zeolites possess a comprehensive applicability such as ion exchangeable materials, molecular sieves, adsorbents, and catalysts reported by several authors from centuries.

13.1.1 Physical and Chemical Properties of Coal Fly Ash (CFA)

The characterization of CFA relies majorly upon the following factors of chemical composition, trace mineral contents, morphology, and the reactivity. The structural and mineralogical properties of the CFA include generation from the combustion, the macrostructural-level CFA consists of heterogeneous mixtures of different mineral phases. Among the most ones are aluminosilicate glass, mullite, iron oxides, salts, and earth alkali oxides. Further, there are various particle shapes observed at the macrostructural level such as solids, hollow particles (cenospheres), hallow filled with other particles (plerospheres), and porous particles (bloated by gases during combustion). On the other hand, the chemical characteristics of CFA include 85% aluminosilicate, 8% Fe, alkali, and earth metal oxides, 1% sulfates, 5% unburned carbon. And, various applications demand various physicochemical characteristics of the material to up the utility of the CFA. The physical appearance of CFA is amorphous, with predominant spherical shaped fine particles possessing solid and glassy structures. The unburnt residues of coal, i.e., the carbonaceous material of CFA are composed of angular particles. In general, the particle size distribution of the CFA will be less than 0.075 mm. The other physical properties such as the specific gravity, surface area, and the color are 2.1–3.0, 170–1000 m^2/kg, gray to black, and alkaline in nature, respectively.

Nonetheless, the elemental composition of CFA is varied depending on the grade of the coal combusted, and the techniques used to handle and store the same. According to the standards of ASTM C–618 coal fly ash is broadly classified according to the originating source of coal i.e., subbituminous and anthracite leads to “class C”, bituminous and lignite resulting “class F”. The typical compositions of these CFA are Si, Al, Ca, and Mg and the classification of the class of CFA is majorly relied upon these four components. Another factor to identify the class of CFA is the composition of the CFA containing more than 70 wt% of Si + Al + Fe with their respective oxides is considered as Class F and if it is less than 70%, it is classified as Class C. Table 13.1 presents the typical composition of CFA obtained from various grades of coal.

Table 13.1 Chemical composition of CFA from different coal types (Ahmaruzzaman 2010)

S. No.	Component (wt%)	Bituminous	Sub-bituminous	Lignite
1	SiO_2	20–60	40–60	15–45
2	Al_2O_3	5–35	20–30	10–25
3	Fe_2O_3	10–40	4–10	4–15
4	CaO	1–12	5–30	15–40
5	MgO	0–5	1–6	3–10
6	SO_3	0–4	0–2	0–10
7	Na_2O	0–4	0–2	0–6
8	K_2O	0–3	0–4	0–4
9	LOI	0–15	0–3	0–5

13.1.2 Quality of Coal

The quality of the coal is decided upon the gross calorific values of the raw coal. For the Indian scenario, the major classification of the quality is categorized into three classes namely, noncoking coal, coking coal semi coking, and weakly coking coals. It is known that fly ash quality varies with the coal grade, combustion method, and coal geographical origin. Figure 13.1 depicts the various classifications of coal reserves in India. It is clear that the Indian coal reserves solely rely

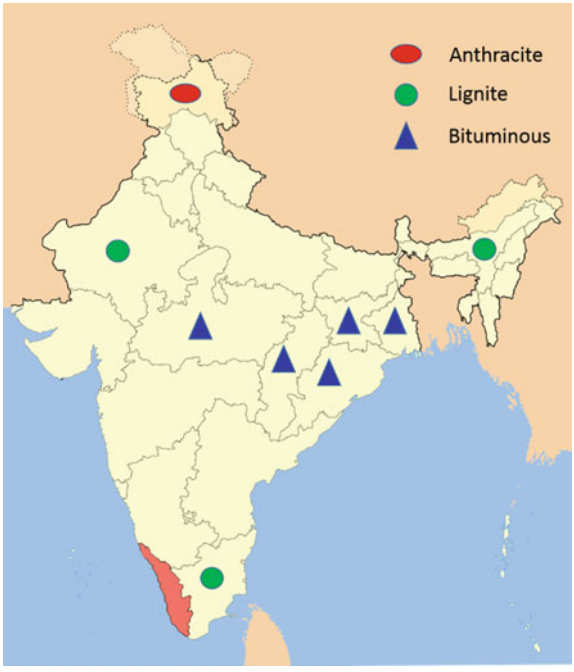

Fig. 13.1 Various grades of coal generated in Indian subcontinent

upon the bituminous coal with major proportion followed by lignite and anthracite. The variations in compositions, especially Si and Al contents alter the nature, properties of products, and zeolites in the present case. The effect of the quality on zeolites was critically altered during the alkali dissolution mechanism. Separate additives need to be imparted during alkali dissolution to separate the active and sufficiently high-active Si and Al species and reduces the morphological benefits of zeolites.

13.1.3 Environment Impact

The surging rate of annual waste generation, i.e., CFA (the prime waste of combustion) across the globe is increased tremendously annoying the industries and challenging the living species with the dangerous health hazards. This has become a challenge to develop a new technology by considering the facts of discharging materials with an anticipated increase of CFA utilization in the future. The most recent environmental regulation on the disposal and the landfill sites shifted the attitudes of social community, industries focusing much on the beneficial recycling of waste, or by-products generated in other words the enhanced synthesis of zeolites. The concept of green revolution also navies the rapid pace of recycled materials in specific zeolites from CFA. Thus, the zeolites from waste CFA contributes to the mitigation of environmental problems such as wastewater purification, heavy metal recovery, acid mine treatments, etc. Table 13.2 summarizes the toxics presence in the CFA obtained from the combustion process and consequent threats possessed.

13.2 Zeolites

The word zeolite is very popular for more than 250 years, and is considered as a new class of crystalline aluminosilicate materials resembling three-dimensional physical structures and characterized by the porous framework (Pfenninger 1999). The context embraced an infinitely stretched group of crystalline Al and Si in their respective anionic network states of $(AlO_4)^{5-}$ and $(SiO_4)^{4-}$ with shared oxygen atoms at the corners and connected to one another (Blissett and Rowson 2012). The structural formulation of a zeolite is as follows.

$$M_xD_y[Alx + 2ySin - (x + 2y)O_2n].H_2O \quad (1)$$

where M denotes "monovalent cation," D denotes "divalent cation," x denotes the monovalent cations, and y denotes divalent cations.

Zeolites are formed naturally according to the demographic and geological orientation including mordenite, clinoptilolite, chabazite, ferrite, etc. (Bandura et al. 2016) alongside the synthetic zeolites (laboratory prepared) namely, Na-X, Na-P,

Table 13.2 Toxic emissions from coal-fired power plants and their impact on human health and the environment (The American Lung Association 2011)

Class of HAPs	Notable HAPs	Impact on human health	Impact on environment
Acid gases	HCl and HF	Skin, eyes, nose, and throat	Acid rains that damage greenery
Dioxins furans	2,3,7,8 Tetrachlorodioxine	Carcinogen: stomach and immune systems; affects endocrine systems	Deposited in rivers, lakes, and oceans, and is taken up by fish and wildlife
Mercury	Methylmercury	Brain, kidney, nervous system, liver, and neurological disorders	Consumed by fish and wildlife
Non-mercury metals	Sb, As, Cd, Cr, Be, Ni, Se, and Mn	Affect lungs, bladder, kidneys, cardiovascular, and respiratory systems	Accumulate in soils and sediments; soluble forms may contaminate water bodies, soil, and sediments
	Lead	Damages nervous system; affects cardiovascular system and kidneys; anemia and orthopedic issues.	Harms plants and wildlife; may adversely affect land and ecosystems
Aromatic hydrocarbons	Anthracene, pyrene fluoranthene, chrysene	Carcinogens: adverse effects on lungs, kidneys, and liver	Exist in vapor and particulate phases
Radioisotopes	Radium	Carcinogens: lung and bone; bronchopneumonia, anemia, and brain abscess	Are deposited in rivers, lakes, and oceans and are taken up by fish and wildlife
	Uranium	Carcinogen: lung and lymphatic system, kidney disease	Is deposited in rivers, lakes, and in oceans and is taken up by fish and wildlife Accumulates in food chain
Volatile compounds	Benzene, xylene	Skin, eyes, throat, nose; breathing; lungs; visual stimulus; impaired memory; liver	Accumulate in soils and sediments

sodalite, etc. The significant difference of naturally formed ones is the existence of impurities, whereas synthetic zeolites prevails the pure forms where they are synthesized under specific controlled operating conditions. Hence, considered as minerals of great importance with a wide range of applicability especially in environmental engineering. At present, zeolite synthesis from coal fly ash is found to be an effective means of utilization comprising 5% of global CFA generation, and scaling up of utilization is still a proactive question.

The vindicated motive for the choice of CFA is due to the existence of Si and Al in higher compositions, a significant constituent for the formation of aluminosilicate. Additionally, the unique structure of zeolites resulting from CFA, due to the ordered system of channels and chambers, governs the properties of CFA-based zeolites. The typical applicability of CFA-based zeolites include ion exchange capacity (Chauhan and Talib 2012), molecular sieving (Breck 1964), and ability to act as a catalyst (Musyoka et al. 2013) renders them mostly in adsorption of metal ions from wastewater treatment (Anbia et al. 2017), acid mine treatment (Font et al. 2009), and leaching studies (Schlumberger et al. 2007).

The conventional method of hydrothermal synthesis is a cost-effective method and requires no additional energy for the zeolite synthesis. Whereas, the other procedures like alkali fusion, microwave assisting reduces the aging or synthesis time significantly, however, additional energy requirements increase the operating cost of the procedure. The resultant quality of the zeolite from either of the process is equal in terms of quality and effectiveness. Thus, in the large scale and commercial production of zeolites, the companies rely and prefer the low-cost method.

13.3 Background

The roots of zeolites dates back to 1751 with the discovery of intriguing crystal structures existed in the nature by a Swedish mineralogist Cronstedt (1751). The scientist made the naming of these typical crystals as zeolites over his observation of the boiling and forming a solid structure resembling a Greek word "zeos" boiling and "lithos" means solid stone. Since then, they emerged as a different group of minerals, abundant in earth crust, or synthesized from various processes. During the early periods of nineteenth century, the process of zeolite synthesis by Barrer (1948) and Milton (1959) converting the known mineral phases under the action of a salt solution at elevated temperatures made an impact on reiterating the possible potentialities of these materials. Following the research of Barrer, Milton proposed a contrary mechanism of zeolite synthesis using alkali metal aluminosilicate gels treated at lower temperature gradients and autogenous pressure conditions. These researchers exposed the potentiality and commercial applicability of zeolites, especially in the field of wastewater treatment. The follow up studies of (Venuto and Habib 1979) lead to hydroxysodalite synthesis with an improved process conditions optimization based on the studies of (Milton 1959) of zeolite Na-P synthesis. Barrer and Denny (1961) pioneered the research on synthesizing zeolites by the replacement technique of altering organic alkyl metal cations with the alkyl ammonium cations. In the follow-up research by Mobil oil, two kinds of zeolites were prepared namely, Zeolite X and ZSM-5 and is used as catalyst in the cracking of petroleum process. Later, Argauer and Landolt (1972) introduced organic cations combining the ZSM-5 significantly improved the structure of the catalyst at the cost of increased Si/Al ratio. Further, Flanigen et al. (1978) prepared the silicate zeolite of higher Si/Al ratio as an alternate to ZSM-5, showed remarkable hydrophobic and

organophilic properties. Nevertheless, introducing CFA as a feedstock by alkaline hydrothermal activation explains the compositional similarities to natural zeolites (Holler and Wirsching 1985). The research findings credited with the first application of alkaline hydrothermal synthesis of zeolites from CFA as a source of Si and Al ions. Other molecular sieves such as the porous aluminophosphates (AlPOs), VPI-5 molecular sieves and their derivatives have been discovered by Flanigen et al. (1986). Following this research, many attempts made over the years to derive zeolites from CFA using one-stage hydrothermal method (Kikuchi 1999). The refrainment of this one-stage hydrolysis lies with the higher reaction temperature of around 200 °C hindering the morphological characteristics such as porosity effecting the formation of NA-X and Na-P (Berkgaut and Singer 1996) and favors the formation of Na-P1, Na-Chabazite, K-Chabazite, Linde F, and other high cation exchange capacity (CEC) zeolites (Querol et al. 2007). A revolutionary attempt of Querol et al. (2001) is to synthesize a variety of zeolites from a single CFA by the combination of the experimental conditions resulting in 13 kinds of zeolites that enlightens the importance of the optimization of critical process parameters. Shigemoto and Hayashi (1993) further introduced pre-fusion at an elevated temperature of above 500 °C with solid alkali prior to hydrothermal synthesis that decomposes the mullite composition of CFA resulting in the formation of high purity zeolites Na-X, P even at high temperatures (Berkgaut and Singer 1996). Proceeding further, Hollman et al. (1999) pioneered the two-stage hydrothermal method in which the first step involves extracting Si and Al using the alkali solution and the second step contains the fine-tuning of Si/Al ratio and performing crystallization stage below 100 °C. The drawbacks of this process arise from the intense usage of water, reagents cost, and long incubation time despite producing high CEC zeolite that has the potential for heavy metal extraction, wastewater treatment. Various studies investigated the optimized water utilization to treat the waste stream of Al industry via two-step method. This result in the higher sources of Al ions mixed with the Si content of CFA in the presence of alkaline solution resulting in high Si yields Otal et al. (2005). So, to surpass the restraints of the aforementioned process, the use of microwave irradiation technique came into existence with the extensive research of Querol et al. (1997) that reduces the synthesis time of zeolites. Later, Park et al. (2000a, b) proposed the most unusual method of zeolitization involving no water content by thermally treating the CFA above 350 °C for extended periods of time up to 3 days in salts/alkaline solutions. Nevertheless, the trails were not successful although eliminating the utilization of water, high temperature, and longer durations along with the low purity CEC zeolites defames the procedure. Furthermore, Kim and Lee (2009) combine the conventional hydrothermal two-step synthesis with the microwave irradiation procedure resulted in the highest purity zeolite crystals of 91%. The authors reported the increment in the dissolution of Si and Al as compared to the conventional heating mechanism. With the progression of technology and time, many new techniques were evolved to synthesize the mechanistic procedures of zeolite synthesis such as fusion extraction, membrane extraction, microwave radiation, etc. But still, the zeolite manufacturers or researchers rely or follow the conventional technique of hydrothermal synthesis

Table 13.3 Evolution of synthetic zeolites (Hamdan 2003)

Late 1940s to early 1950s	Low Si/Al ratio zeolites
Mid to late 1960s	High Si/Al ratio zeolites
Early 1970s	SiO_2 molecular sieves
Late 1970s	$AlPO_4$ molecular sieves
Early 1980s	SAPO and Me APO molecular sieves
Mid 1980s	$AlPO_4$-based molecular sieves
Late 1980s	Metallo-silicates, aluminosilicate
Early 1990s	Mesoporous molecular sieves
Late 1990s	Large-pore zeolites

method due to the reduced complexity and economical. Whereas, the other aforementioned recent techniques involve additional steps prior to the synthesis that increase the capital cost and being the main reason for the limitation or commercialization. Table 13.3 details the evolution of zeolites over the past few decades. Since then, the evolution was majorly toward the advancement of the technologies, optimizing the process parameters solely for diversified applications of zeolites.

13.4 Properties of Zeolite

A detailed analysis on various features of zeolites includes physicochemical–thermal characteristics, exchange capacities, adsorption, geological origins, surface chemistry, pH, crystal structure, framework, and the surface properties which turns the zeolite into various application layers. A brief discussion on each parameter is presented herein.

13.4.1 Physical Properties

The typical physical property that has to be considered for the zeolite is the bulk density and the specific gravity. These two parameters correlate to their porosity and the cation exchange capacity (CEC) (Zeolites 2018; Kumar et al. 2001). Similarly, the most common and the critical feature of the ash-based zeolite is the specific surface area, i.e., dependent on the dissolution of characteristics and the alkaline conditions used (Ma et al. 1998; Singh and Kolay 2002). In line with this, another important physical property of zeolite is the void volume, i.e., again correlated to the CEC of the product and dependent on the specific surface area (Scott et al. 2001). The other crucial physical property is the pore radius (Korkuna et al. 2006) that helps in understanding the adsorption characteristics of zeolite used as an adsorbent. Further, one more significant physical aspect of the zeolite is the particle

size, i.e., ranging between 2 μm and 800 nm. Incidentally, a wide range of particle size and the uniform coefficient are quite commonly associated with the zeolites.

13.4.2 Chemical Properties

The general composition of the zeolite is Al_2O_3, SiO_2, Fe, Ca, MgO, K, etc., within their structure along with the water molecules in the pores (Hollman et al. 1999; Wu et al. 2006). The fundamental research on zeolite suggests that the synthesis ascribes to the Si/Al ratio, i.e., 0.5 (minimum) (Shigemoto and Hayashi 1993). Furthermore, the CEC, adsorption characteristics, pH, and loss of ignition (LOI) are some other critical chemical parameters that influence the zeolite (Park et al. 2000a).

13.4.3 Ion Exchange and Adsorption Properties

During the synthesis of zeolites, they acquire cations such as Na^+, K^+, and NH_4^+ by interaction with the surrounding medium via ion exchange or adsorption (Qiu et al. 2000; Fansuri et al. 2008). These cations are useful in balancing the negative charges developed on the pores of zeolites, i.e., the replacement of Si atoms with Al atoms along with their respective oxides by linkage of the water molecule. The profound researchers over the decades realized that heavy metal cations such as Rb, Cs, Ag, Cd, Pb, Zn, Ba, Sr, Cu, etc. (Inada et al. 2005; Querol et al. 2006) have higher affinity toward the zeolites despite knowing the fact that the selectivity is dependent on the hydrated molecules of cations.

13.4.4 Surface Properties

The organic functionalization of the zeolites bearing negative surface charges of their internal and external surfaces affects the affinity of absorption and classifies the surface properties of the zeolites, i.e., neither hydrophobic nor hydrophilic (Jha and Singh 2011; Mortier 1978). The significance of the external and intrinsic surface properties explains the penetration capacity or absorption capacity of molecules on the surface of the zeolite by the diffusion mechanism. The Si/Al ratio dramatically influences the surface characteristics i.e., the more the Al atoms, the more the electronegativity and leads to the formation of Al-O-Al bonds. Moreover, the Si atoms balances the charges by replacing the Al atoms and forms Si-O-Al bonds, thereby reducing the electronegativity and maintains uniform acid strength (Moreno et al. 2001b). To further enhance the surface properties, the zeolites treated with extended chain surfactants such as hexadecyl-trimethyl-ammonium chloride

(HDTMA), stearyl-dimethyl-benzyl-ammonium chloride (SDMBA), etc. (Jovanovic et al. 2006). This, in turn, modifies the surface properties, i.e., turning the hydrophobic nature to hydrophilic that enhances the adsorption capacity.

13.4.5 The Structural and Morphological Framework

Unlike the natural zeolites, synthetic zeolites possess channeled structures with negatively charged frameworks that enable to have higher anion exchange capacities of the order of 2–5 meq/g. Though, the selectivity and magnitude of these mesoporous materials depend on critical parameters such as the cation size and charge, aperture of pores, concentration, anion species associated with the cation in the solution, the solvent, and the temperature. Generally, there are three classification schemes for zeolite structures among which, two of them were based on crystal structure, and the third one on historical basis (Armbruster and Gunter 2001). In detailed, zeolites on the structural classification with discrete charters receive a three-letter code (Meier et al. 1996) and resembles identical. The method of such classification is particular in cation exchange and synthetic zeolites. Proceeding further, the second classification of zeolites are based on the secondary building units (SBU) defined by Meier (1968). Majority of the zeolites possess tetrahedron-shaped particles as the primary building units, and the SBUs are the geometric arrangements of tetrahedral (Breck 1974). The possible zeolite structures vary according to the secondary building unit (SBU) namely, (a) zeolites of fibrous chains; (b) 4-ring chain single connected; (c) 4-ring chain double connected; (d) the 6-ring, single, or double; (e) the hexagonal sheet; (f) the heulandite unit (Bahruji 2005) that defines the sieving properties. Another significant factor that alters the zeolite framework is the Si/Al ratio. The decrease in the ratio results in hydrophilic and increased values result in hydrophobic (Gualtieri 2006). Another important property of zeolite is acid sites (Brønsted acid and Lewis acid) resulting from the net negative framework charges, which avails them to be used in catalysis (Govind et al. 2002). Table 13.4 presents the classification of zeolites based on the secondary block units and the rig structure.

Table 13.4 Classification of zeolite structure (Breck 1974)

Group	Secondary building unit (SBU)
1	Single 4-ring, S4R
2	Single 6-ring, S6R
3	Double 4-ring, D4R
4	Double 6-ring, D6R
5	Complex 4-1, T_5O_{10} unit
6	Complex 5-1, T_8O_{16} unit
7	Complex 4-4-1, $T_{10}O_{20}$ unit

13.4.6 Overview of Process Parameters

In summary, the process parameters play a crucial role in the synthesis mechanism, and the synthesized zeolites were relatively unstable compared to the other precursors, i.e., aluminosilicate in the presence of water medium due to the larger surface area. Whereas, CFA reacted with the alkali solutions will have a higher affinity toward the K, Ca, and NH4 ions. Further, higher pH is highly unfavorable for the adsorption properties of zeolites. The temperature has a crucial role to play in zeolite synthesis, altering the temperature results in various zeolite types. Thus, every parameter has a role to play in the synthesis process of zeolite.

13.5 Hydrothermal Synthesis

Since the pioneering studies of Barrer (1948) and Milton (1959) on zeolite synthesis, the hydrothermal technique has become the traditional and conventional means from then till date. Hydrothermal synthesis is a chemical reaction that occurs at high temperature, pressure, i.e., (>100 °C, 1 bar) in aqueous solution. The resultant of the hydrothermal synthesis is in the form of crystals and relies majorly on the solubility. The reason for the higher temperatures and pressures in the methodology is to accelerate the rate of reaction among the complexions, intensify the hydrolyzation reaction, significantly affect the redox potential of the reactants, and decreases the dielectric constant values.

The advantages of the hydrothermal method over crystal growth are stable even at the melting point temperatures. The process is likewise for the growth of high-quality crystals with considerable grain size and holding control over the product composition.

13.5.1 Alkaline Conversion of CFA to Zeolite

Among the several available techniques, the zeolite synthesis procedure relies majorly on alkaline hydrothermal treatment due to the simple mechanism and cost-efficient method. The reaction mechanism involves three significant steps that are as follows:

13.5.1.1 Mechanism

a. Dissolution of Al_2O_3 and SiO_2 from CFA using a mineralizing agent. The most commonly used mineralizing agent is the hydroxyl anion (OH^-), which increases the solubility of silicon and aluminum from CFA and effects the formation of silicate and aluminate gel (Elliot 2006).

b. Separation of the aluminosilicate gel from the unreacted CFA, depending on the desired type of zeolite (Panias et al. 2007).
c. Hydrothermal treatment involves the crystal growth stage (Rees et al. 2007).

Figure 13.2 depicts the clear mechanism of the zeolite synthesis from coal fly ash.

Alkali Dissolution

The alkali dissolution stage begins with the reaction of amorphous Si, and Al present in CFA with alkaline solution tends to initiate the hydrolysis mechanism, liberating/separating the Si and Al species into the NaOH solution (Fig 13.3).

Separation

The liberated Si and Al ions are highly active in nature and tend to form readily the new structures such as Si–O–Al–O, exerting the water molecules. In other words,

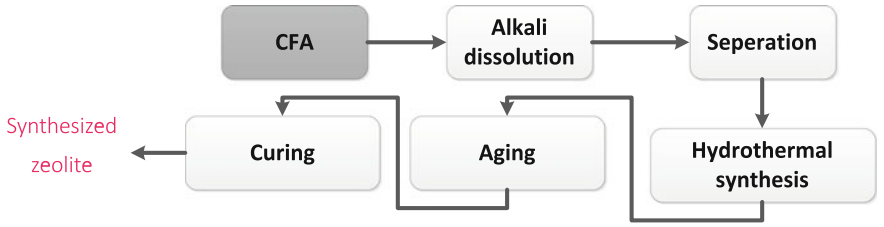

Fig. 13.2 Schematic diagram of conventional hydrothermal method for zeolite synthesis from CFA

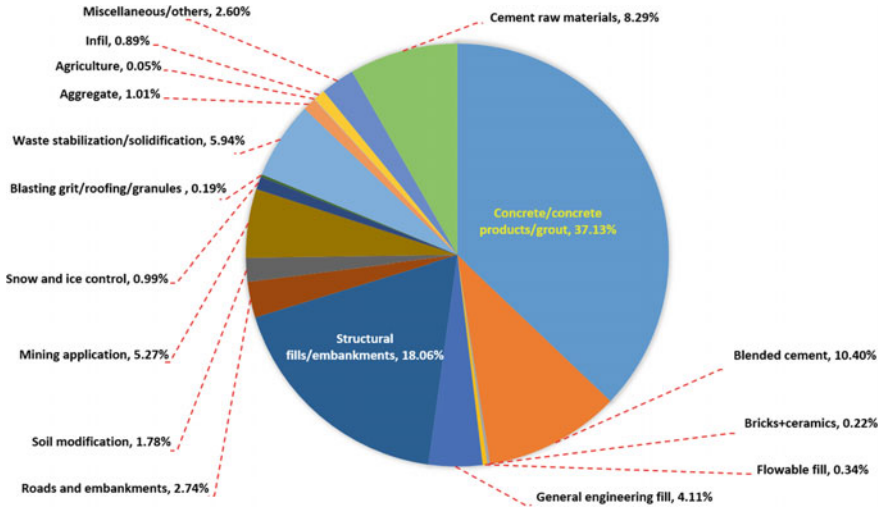

Fig. 13.3 Potential percentage utilization of CFA (ACAA, 2008)

this is the step where the depolymerization reaction occur such that the complex chain of polymers were broken into monomer species mainly Si, Al in the case of CFA.

Hydrothermal Synthesis
Upon different process and operating condition, i.e., controlled temperature, pressure, agitation, pH values, the monomer molecules tends to reorient into new structures of the oligomers, and finally to new polymeric chains or gel form. These newly formed polymer chains resembles in three various forms depending on the ratio of Si/Al, i.e., poly(sialate) –Si–O–Al–O– for Si/Al = 1, poly(sialate–siloxo)–Si–O–Al–O–Si–O– for Si/Al = 2, and poly(sialate–disiloxo) –Si–O–Al–O–Si–O–Si–O– for Si/Al = 3.

Aging
The newly formed slurry referred as a secondary gel, i.e., the zeolite precursor consists of sites for the nucleation and crystal growth. Furthermore, the hydrothermal treatment comprising of elevated temperatures activates the nucleation step, i.e., the assimilation of the aluminosilicate material from the solution phase allows the crystalline growth to desired strength.

Curing
Solidification/curing stage incorporates the formation of agglomeration or continuous gel formation including rearranging and reorganization of aluminosilicate geopolymer in neither amorphous nature nor the crystalline structure.

13.6 Effect of Parameters

13.6.1 Si/al Ratio

CFA serves as the source for the Si and Al required for the zeolite framework. Zeolites is synthesized upon the building blocks of SiO_4 and AlO_4. The rate plays a vital role in determining the type of zeolite based on the structure (Szostak 1989) and may lead to crystallization of secondary phases. Furthermore, Querol et al. (1995) reported that the high Si content of CFA result in high silica zeolite, i.e., more Si–O–Si linkages is formed instead Si–O–Al links, which alters the crystallization mechanism. Further, Szostak (1989) summarized the effects of changing SiO_2/Al_2O_3 ratio on the physical properties as increasing Si/Al ratio increases acid resistance, increases thermal stability, increases hydrophobicity, decreases affinity for polar adsorbents, and decrease cation content. Inversing the relation of Si/Al, i.e., increases the hydrophilicity and increased cation exchange properties.

13.6.2 Alkali Concentration

The alkaline materials act as mineralizing agents that depolymerizes the Si content of CFA and force the reactants into solution (Pfenninger 1999), and the strength of the alkali agent is varied for synthesizing various types of zeolites. The addition of alkali agent in respective concentrations envisages the high crystalline structure (Molina and Poole 2004), assuring the purity of zeolite (Musyoka 2009). The presence of NaOH in the reaction mixture acts as an activator to form soluble silicates of sodium and aluminate salts (Ojha et al. 2004). Further, Na + ions are renowned for its stability under the hydrothermal conditions, which is primarily for the zeolite synthesis. The higher the content of Na, the higher the formation of water-soluble sodium silicates that enhances the yield of zeolites on processing further.

13.6.3 Effect of Synthesis Time

The aging refers to the development of crystal nuclei, and it affects the surface area of the zeolite structure. The synthesis time is another crucial parameter in the process of zeolitization owing to the difficulties associated with the dissolution resulting in the formation of quartz and mullite secondary phases on longer crystallization time (Mainganye 2012). The research of Nagy et al. (1998) explained the essential considerations in preparing pure phase zeolites is the metastability of crystalline phase that can undergo further transformation to form more stable species. This was interpreted as a relative theory of Ostwald's successive transformation, i.e., the initially formed crystalline phase possesses the least stability but with prolonged time forms stable and denser phases Barrer (2007). Besides, protracted aging time of the semisolid material at ambient temperature before crystallization phase may result in the formation of numerous miniature crystal structures (Molina and Poole 2004).

13.6.4 Effect of Temperature

Temperature is an important parameter that influences the crystallization kinetics of zeolite synthesis. Studies of Elliot and Zhang (2005) revealed the relation between the nucleation and the crystal growth as a function of temperature. The increasing temperature leads to enhance the mullite and Si dissolution, compared to Al, which increases the Si/Al ratio, which influences the gel composition and also the morphology and purity of the zeolite crystal. Further, the authors also reported that the higher temperatures favor the formation of P zeolite with narrow porous zeolites (Kotova et al. 2016), and lower temperature favors the formation of faujasite and zeolite A.

13.6.5 Effect of Agitation and Water Utilization

In general, the zeolite synthesis under static conditions is not always desirable, resulting in uneven settling of the synthesis gel and cause the liquid phase to separate from the solid phase of the reaction mixture due to the gravitational forces. Unlike the static conditions, the zeolite synthesis for the commercial aspects to be under agitated conditions. The vitality of the agitation includes the formation of viscous gel from the reaction mixture; and the inadequacy results in the formation of a nonhomogenous pocket of gels with inconsistent composition and the strength of the final product. Moreover, the static conditions require more extended periods for the nucleation and growth. According to the research of Casci (2005), the agitation assists in various stages of the zeolite synthesis such as in the gel formation, proper dissolution of the reagent, maintains the structural gel breakup, crystallization by the balanced transformation of nutrients, and so on. Further, the effect of shear in altering the crystal structure of the zeolites were reported in the significant research studies (Marrot et al. 2001, Weitkamp and Puppe 1999).

Water is a used as a solvating agent, has a greater ability to hydrolyze, enhance the crystal growth by filling the void spaces and stabilizing the zeolite structural framework (Feijen et al. 1994). The ratio of solid to liquid had a significant effect on the zeolite during the hydrothermal treatment that is a direct function of zeolite yield. In general demineralized water is the most widely used in order to elude the complexities related to the mineral deposits of groundwater especially Ca. In general, demineralized water is widely used to avoid the complexities of ions (especially, Ca) prevailed in groundwater sources.

13.7 Applications of Zeolite

Zeolites have discovered far-reaching ecological issues, and increasing new research interests predominantly due to the following properties: adsorption, ion exchange, and catalysis. Noteworthy use of zeolites encompasses petrochemical industries, ion exchange (water purification), gas and solvent separations, agriculture, and mining, etc. Amid, the prime and foremost application of zeolite is water treatment i.e., the separation of toxic metals and minerals obtained from contaminated water sources such as industrial effluents, leachates of mine discharges etc. (Šiška 2005). Zeolites are known for their excellent adsorption capacity, and readily adsorb and treat various effluents that contaminates the groundwater bodies which is an essential application for the present world and could be a dual agent of waste minimization along with useful product generation. The other typical applications of zeolites from coal fly ash comprises of polymer composites, adsorbents, removal of organic and inorganic compounds, catalyst, etc. Table 13.5 presents the major wastewater application of zeolites and the research pertained to it.

Table 13.5 Environmental applications of zeolite in wastewater treatment

Wastewater treatment	References
Ammonia removal	Mercer et al. (1970), Hlavay et al. (1982), Baykal (1998), Langella et al. (2000), Cincotti et al. (2001), Jorgensen and Weatherley (2003), Meininghaus and Prins (2000), Rozic et al. (2000), Marinin and Brown (2000), Saltali et al. (2007)
Heavy metal removal	Kesraoui-Ouki et al. (1994), Mondale et al. (1995), Kesraoui-Ouki and Kavanagh (1997), Moreno et al. (2001a, b), Panayotova (2001), Inglezakis et al. (2001), Inglezakis and Grigoropoulou (2003), Wingenfelder et al. (2005)
Organic compounds removal	García et al. (1993), Li et al. (2000), Schüth et al. (2004), Altare et al. (2007)
Radioactive compounds removal	Dyer and Zubair (1998), Abusafa and Yucel (2002)

From Table 13.5, it is clearly seen that the CFA possess a dangerous threat as it contains the toxic nurtured elements such as Na that could be a beneficial source to soil amelioration, heavy metal recovery that suppresses the global domination on developing nations. Further, organic compounds removal could be a boon for the plant life and finally, the traces of radioactive materials that change the country economy if the process is made feasible especially for the Class C-rich CFA modules.

13.8 Upscaling Zeolite Synthesis from Coal Fly Ash

As can be seen from the literature with respect to zeolite upscale synthesis from coal fly ash, Na-P1 is the primary zeolite focused upon. However, the future scale-up should focus mainly in developing a mechanism by optimization of critical process parameters that could lead to variable zeolites ranging from (Zeolite-X, to sodalite). The recent study of Musyoka and Zeolite (2012) of unique morphology obtained via NaOH of clear fused extract of CFA, a significant breakthrough that upscales zeolite methodology. This enables the maximal structural functions in a confined volume and conferring a high degree of diffusion efficiency (Liu et al. 2013). Another method of hydrodynamic cavitation provided in jet loop reacting system could be a suitable alternative replacing high-temperature fusion process for a large-scale production (Nyale 2014). Further, focusing on the parameters agitation plays a vital role in upscaling zeolite synthesis from CFA. However, the real challenge is determining the impeller type and agitation at industrial scale. In lieu, the recent study of (Wdowin et al. 2014) reported 81% of pure product phase for the zeolites synthesized from CFA. The previously mentioned highpoints present the need for an in-depth analysis on the mechanism of agitation during hydrothermal treatment.

13.9 Conclusions

The anticipated generation of the CFA is increasing in many folds every year, due to the result of global reliance of coal-based power generation. A better knowledge of the production, characterizations, and hazards prone due to CFA will provide a clear insight which serves as the basis for the alternative use of CFA. Besides, CFA is not alone a waste material but also an environmental threat, and its disposal is a monetary risk or liability. This liability could be overturned to a profitable product stream by converting CFA to zeolites. Zeolites have numerous utilizations including sorption, catalysis, particle trade, and numerous utilizations as substitute for making ecologically inviting items. Transformation of CFA into zeolite caters the dual need of producing green advancements, thereby maintaining ecological balance. A profound view of literature suggests that the zeolite synthesis is confined to a limit due to the implementation of conventional hydrothermal synthesis procedures. Moreover, the successful enactments of introducing/enhancing/replacing the conventional method of zeolite synthesis with the modern techniques of microwave assistance, ultra-sonication could improve the commercial and larger scale utilization of CFA. Increasing the utilization would be exceptionally helpful to environment and extremely noteworthy effects towards the accomplishment of greener innovation for the future generations.

References

Abusafa A, Yucel H (2002) Removal of ^{137}Cs from aqueous solutions using different cationic forms of a natural zeolite: clinoptilolite. Sep Purif Technol 28:103–116

Ahmaruzzaman M (2010) A review on the utilization of fly ash. Prog Energy Combust Sci 36:327–363

Altare CR, Bowman RS, Katz LE, Kinney KA, Sullivan EJ (2007) Regeneration and long-term stability of surfactant-modified zeolite for removal of volatile organic compounds from produced water. Microporous Mesoporous Mater 105:305–316

American coal ash association (2008) Production and Use survey reports. CO, USA

Anbia M, Koohsaryan E, Borhani A (2017) Novel hydrothermal synthesis of hierarchically-structured zeolite LTA microspheres. Mater Chem Phys 193:380–390

Argauer RJ, Landolt GR (1972) U.S. Patent No. 3 702 886

Armbruster T, Gunter ME (2001) Crystal structure of natural zeolites. Natural zeolites: occurrence, properties, applications. In: Bish L, Ming DW (eds) Reviews in mineralogy and geochemistry 45. Mineralogical Society of America, Washington, D.C., pp 1–67

Bahruji H (2005) Synthesis of zeolite ferrierite from rice husk ash, characterization and activity towards friedel-crafts acylation for the formation of *p*-methoxypropiophenone. Unpublished Master's thesis. Universiti Teknologi Malaysia, p 124

Bandura L, Panek R, Rotko M, Franus W (2016) Synthetic zeolites from fly ash for an effective trapping of BTX in gas stream. Microporous Mesoporous Mater 223:1–9

Barrer RM (1948) Synthesis and reactions of modernite. J Chem Soc 2158

Barrer RM (2007) Hydrothermal chemistry of zeolites. Academic Press, London

Barrer RM, Denny PJ (1961) Hydrothermal chemistry of the silicates. Part X. A partial study of the field CaO-Al_2O_3-SiO_2-H_2O. J Chem Soc Lond 0:983–1000

Baykal BB (1998) Clinoptilolite and multipurpose filters for upgrading effluent ammonia quality under peak loads. Water Sci Technol 37:235–242
Belviso C, Cavalcante F, Fiore S (2010) Synthesis of zeolite from Italian coal fly ash: differences in crystallization temperature using seawater instead of distilled water. Waste Manage 30:839–847
Berkgaut V, Singer A (1996) High capacity cation exchanger by hydrothermal zeolitization of coal fly ash. Appl Clay Sci 10:369–378
Blissett R, Rowson N (2012) A review of the multi-component utilization of coal fly ash. Fuel 97:1–23
Breck DW (1964) Crystalline zeolite Y. United States Patent, New York, USA, US Patent 3130007
Breck DW (1974) Zeolite molecular sieves: structure, chemistry and use, 1st edn. Wiley, New York, p 313
Casci JL (2005) Zeolite molecular sieves: preparation and scale-up. Microporous Mesoporous Mater 82:217–226
Chauhan YP, Talib M (2012) A novel and green approach of synthesis and characterization of nano-adsorbents (zeolites) from coal fly ash: a review. Sci Rev Chem Commun 2(1):12–19
Cincotti A, Lai N, Orrù R, Cao G (2001) Sardinian natural clinoptilolites for heavy metals and ammonium removal: experimental and modeling. Chem Eng J 84:275–282
Cronstedt A (1751) Observation and description of unknown kind of rock to be named Zeolite. Kungl. Svenska vetenskapsakademiens handlingar 17:120–123
Dyer A, Zubair M (1998) Ion-exchange in chabazite. Microporous Mesoporous Mater 22:135–150
Elliot AD (2006) An investigation into the hydrothermal processing of coal fly ash to produce zeolite for controlled release fertiliser applications. Ph.D. thesis, Curtin University of Technology
Elliot AD, Zhang D (2005) Controlled release zeolite fertilisers: a value added product produced from fly ash. World of Coal Ash (WOCA). Lexington, Kentucky, USA
Eskom (2011) Integrated Report [Internet]. Available from: http://financialre-sults.co.za/2011/eskom_ar2011/. Accessed 17 Feb 2015
Fansuri H, Pritchard D, Zhang D (2008) Manufacture of low-grade zeolites from fly ash for fertilizer applications. QCAT Technology Transfer Centre, Technology Court, Pullenvale Qld 4069, Australia
Feijen EJP, Martens JA, Jacobs PA (1994) Zeolites and their mechanism of synthesis. In: Weitkamp J, Karge, Pfeifer H, Hölderich W (eds) Zeolites and related microporous materials: state of the art. Elsevier, Amsterdam
Flanigen EM, Bennett JM, Crose RW, Cohen JP, Patton RL, Kirchner RM, Smith JV (1978) Silicalite, a new hydrophobic crystalline silica molecular sieve. Nature 271:512–516
Flanigen EM, Lok BM, Patton RL, Wilson ST (1986) Aluminophosphate molecular sieves and the periodic table. Pure Appl Chem 58:1351–1358
Font O, Moreno N, Díez S, Querol X, López-Soler A, Coca P et al (2009) Differential behaviour of combustion and gasification fly ash from Puertollano Power Plants (Spain) for the synthesis of zeolites and silica extraction. J Hazard Mater 166:94–102
García JE, González MM, Notario JS (1993) Phenol adsorption on natural phillipsite. React Polym 21:171–176
Govind N, Andzelm J, Reindel K, Fitzgerald G (2002) Zeolite-catalyzed hydrocarbon formation from methanol: density functional simulations. Int J Mol Sci 3:423–434
Gualtieri M (2006) Synthesis and characterization of zeolite films and membranes. Luleå University of Technology, Ph.D. thesis
Hamdan H (2003) Design and molecular engineering of nanostructured zeolites and mesomorphous materials: advancing through the pores, Penerbit Universiti Teknologi Malaysia
Heidrich C, Feuerborn H, Weir A (2013) Coal combustion products: a global perspective. VGP Power Technol World Coal Ash 12:46–52
Hlavay J, Vigh G, Olaszi V, Inczédy J (1982) Investigations on natural Hungarian zeolite for ammonia removal. Water Res 16:417–420

Holler H, Wirsching U (1985) Zeolite formation from fly ash. Fortschr Miner 63:21–43
Hollman GG, Steenbruggen G, Janssen-Jurkovičová M (1999) A two-step process for the synthesis of zeolites from coal fly ash. Fuel 78:1225–1230
Inada M, Eguchi Y, Enomoto N, Hojo J (2005) Synthesis of zeolite from coal fly ashes with different silica-alumina composition. Fuel 84:299–304
Inglezakis VJ, Grigoropoulou HP (2003) Modeling of ion exchange of Pb^{2+} in fixed beds of clinoptilolite. Microporous Mesoporous Mater 61:273–282
Inglezakis VJ, Hadjiandreou KJ, Loizidou MD, Grigoropolou HP (2001) Pretreatment of natural clinoptilolite in a laboratory scale ion exchange packed bed. Water Res 35:2161–2166
Jha B, Singh DN (2011) A review on synthesis, characterization and industrial application of fly ash zeolites. J Mater Edu 33(1–2):65–132
Jorgensen TC, Weatherley LR (2003) Ammonia removal from wastewaters by ion exchange in the presence of organic contaminants. Water Res 37:1723–1728
Jovanovic V, Dondur V, Damjonovic L, Zakrzewska J, Tomasevic CM (2006) Improved materials for environmental application: surfactant-modified zeolites. Mater Sci Forum 518:223–228
Kesraoui-Ouki S, Kavanagh M (1997) Performance of natural zeolites for the treatment of mixed metal-contaminated effluents. Waste Manag Res 15:383–394
Kesraoui-Ouki S, Cheeseman CR, Perry R (1994) Natural zeolite utilization in pollution control: a review of applications to metals' effluents. J Chem Technol Biotechnol 59:121–126
Kikuchi R (1999) Application of coal ash to environmental improvement. Resour Conserv Recycle 27:333–346
Kim JK, Lee HD (2009) Effects of step change of heating source on synthesis of zeolite 4A from coal fly ash. J Ind Eng Chem 15:736–742
Korkuna O, Leboda R, Skubiszewska ZJ, Vrublevs'ka T, Gun'ko VM, Ryczkowski J (2006) Structural and physicochemical properties of natural zeolites: clinoptilolite and mordenite. Microporous Mesoporous Mater 87:243–254
Kotova OB, Shabalin N, Shuskov DA, Kocheva LS (2016) Hydrothermal synthesis of zeolites from coal fly ash. Adv Appl Ceram 115:152–157
Kumar P, Mal N, Oumi Y, Yamanaa K, Sanoc T (2001) Mesoporous materials prepared using coal fly ash as the silicon and aluminium source. J Mater Chem 11:3285–3290
Langella A, Pansini M, Cappelletti P, De Gennaro B, De Gennaro M, Colella C (2000) NH_4^+, Cu^{2+}, Zn^{2+}, Cd^{2+} and Pb^{2+} exchange for Na^+ in a sedimentary clinoptilolite, North Sardinia, Italy. Microporous Mesoporous Mater 37:337–343
Li Z, Burt T, Bowman RS (2000) Sorption of ionizable organic solutes by surfactant-modified zeolite. Environ Sci Technol 34:3756–3760
Liu B, Chen F, Zheng L, Ge J, Xi H, Qian Y (2013) Synthesis and structural properties of hierarchically structured aluminosilicates with zeolite Y (FAU). RSC Adv 3:15075–15084
Ma W, Brown PW, Komarneni S (1998) Characterization and cation exchange properties of zeolites synthesized from fly ashes. J Mater Res 13(1):3–7
Mainganye D (2012) Synthesis of zeolites from South African coal fly ash: Investigation of scale-up conditions. Ph.D. thesis, Cape Town, University of Technology, Cape Peninsula, South Africa
Marinin DV, Brown GN (2000) Studies of sorbent/ion-exchange materials for the removal of radioactive strontium from liquid radioactive waste and high hardness groundwaters. Waste Manag 20:545–553
Marrot B, Bebon C, Colson D, Klein J (2001) Influence of the shear rate during the synthesis of zeolites. Cryst Res Technol 36:269–281
Meier WM (1968) Zeolite structures. In: Molecular sieves. Society of Chemical Industry, London, pp 10–27
Meier WM, Olson DH, Baerlocher CH (1996) Atlas of zeolite structure types, 4th edn. Elsevier, London
Meininghaus CKW, Prins R (2000) Sorption of volatile organic compounds on hydrophobic zeolites. Microporous Mesoporous Mater 35–36:349–365

Mercer BW, Ames LL, Touhill CJ, Van Slyke WJ, Dean RB (1970) Ammonia removal from secondary effluents by selective ion exchange. J Water Pollut Control Fed 42:95–107
Milton RM (1959) Molecular sieve adsorbents. United States Patent, New York, USA, US Patent 2882244
Molina A, Poole C (2004) A comparative study using two methods to produce zeolites from fly ash. Miner Eng 17:167–173
Mondale KD, Carland RM, Aplan FF (1995) The comparative ion exchange capacities of natural sedimentary and synthetic zeolites. Miner Eng 8:535–548
Moreno N, Querol X, Ayora C, Pereira CF, Janssen-Jurkovičová M (2001a) Utilization of zeolites synthesized from fly ash for the purification of acid mine waters. Environ Sci Technol 35:3526–3534
Moreno N, Querol X, Ayora C, Alastuey A, Fernández-Pereira C, Janssen-Jurkovičová M (2001b) Potential environmental applications of pure zeolitic material synthesized from fly ash. J Environ Eng 127:994–1002
Mortier WJ (1978) Zeolite electronegativity related to physicochemical properties. J Catalysis 55:138–145
Musyoka NM (2009) Hydrothermal synthesis and optimisation of zeolite Na-P1 from South African coal fly ash. M.Sc. thesis, University of the Western Cape
Musyoka NM, Zeolite A (2012) X and Cancrinite from South African coal fly ash: mechanism of crystallization, routes to rapid synthesis and new morphology [thesis]. University of the Western Cape, Cape Town
Musyoka NM, Petrik LF, Fatoba OO, Hums E (2013) Synthesis of zeolites from coal fly ash using mine waters. Miner Eng 53:9–15
Nagy JB, Bodart P, Hannus I, Kiricsi I (1998) Synthesis, characterization and use of zeolitic microporous materials, Szeged, Hungary, Deca Gen Ltd.
Nyale SM (2014) Geopolymers from South African fly ash: synthesis and characteristics.[thesis]. University of the Western Cape, Cape Town
Ojha K, Pradhan NC, Samanta AN (2004) Zeolite from fly ash: synthesis and characterization. Bull Mater Sci 27:555–564
Otal E, Vilches LF, Moreno N, Querol X, Vale J, Fernández-Pereira C (2005) Application of zeolitised coal fly ashes to the depuration of liquid wastes. Fuel 84:1440–1446
Panayotova MI (2001) Kinetics and thermodynamics of copper ions removal from wastewater by use of zeolite. Waste Manag 21:671–676
Panias D, Giannopoulou IP, Perraki T (2007) Effect of synthesis parameters on the mechanical properties of fly ash-based geoploymers. Colloids Surf A: Physicochem Eng Asp 301:246–254
Park M, Choi CL, Lim WT, Kim MC, Choi J, Heo NH (2000a) Molten-salt method for the synthesis of zeolitic materials II. Characterization of zeolitic materials. Microporous Mesoporous Mater. 3:91–98
Park M, Choi CL, Lim WT, Kim MC, Choi J, Heo NH (2000b) Molten-salt method for the synthesis of zeolitic materials I; Zeolite formation in alkaline molten-salt system. Microporous Mesoporous Mater 37:81–89
Pfenninger A (1999) Manufacture and use of zeolites for adsorption process. Mol Sieves 2:164–197
Qiu L, Murashov V, White MA (2000) Zeolite 4A: heat capacity and thermodynamic properties. Solid State Sci 2:841–846
Querol X, Alastuey A, Fernández-Turiel J, López-Soler A (1995) Synthesis of zeolites by alkaline activation of ferro-aluminous fly ash. Fuel 74:1226–1231
Querol X, Alastuey A, López-Soler A, Plana F, Andrés JM, Juan R et al (1997) A fast method for recycling fly ash: microwave-assisted zeolite synthesis. Environ Sci Technol 31:2527–2533
Querol X, Umaña JC, Plana F, Alastuey A, Lopez-Soler A, Medinaceli A et al (2001) Synthesis of zeolites from fly ash at pilot plant scale. Examples of potential applications. Fuel 80:857–865
Querol X, Alastuey A, Moreno N, Alvarez AE, Garcia-Sanchez A, Cam J, Ayora C, Simon M (2006) Immobilization of heavy metals in polluted soils by the addition of zeolitic material synthesized from coal fly ash. Chemosphere 62:171–180

Querol X, Moreno N, Alastuey A, Juan R, Andres JM, Lopez-Soler A, Ayora C, Medinaceli A, Valero A (2007) Synthesis of high ion exchange zeolites from coal fly ash. Geol Acta 5(1):49–57

Rees CA, Provis JL, Lukey GC, Van Deventer JSJ (2007) Attenuated total reflectance fourier transform infrared analysis of fly ash geopolymer gel aging. Langmuir. 23:8170–8179

Rozic M, Cerjan-Stefanovic S, Kurajica S, Vancina V, Hodzic E (2000) Ammoniacal nitrogen removal from water by treatment with clays and zeolites. Water Res 34:3675–3681

Saltali K, Sarı A, Aydın M (2007) Removal of ammonium ion from aqueous solution by natural Turkish (Yıldızeli) zeolite for environmental quality. J Hazard Mater 141:258–263

Schlumberger S, Schuster M, Ringmann S, Koralewska R (2007) Recovery of high purity zinc from filter ash produced during the thermal treatment of waste and inserting of residual materials. Waste Manag Res. 25:547–555

Schüth Ch, Kummer NA, Weidenthaler C, Schad H (2004) Field application of a tailored catalyst for hydrodechlorinating chlorinated hydrocarbon contaminants in groundwater. Appl Catal B: Environ 52:197–203

Scott J, Guang D, Naeramitmarnsuk K, Thabuot M, Amal R (2001) Zeolite synthesis from coal fly ash for the removal of lead ions from aqueous solution. J Chem Technol Biotechnol 77:63–69

Shigemoto N, Hayashi H (1993) Selective formation of Na-X zeolite from coal fly ash by fusion with sodium hydroxide prior to hydrothermal reaction. J Mater Sci 28:4781–4786

Singh DN, Kolay PK (2002) Simulation of ash water interaction and its influence on ash characteristics. Prog Energy Combus Sci 28:267–299

Šiška J (2005) Extraction of heavy metals and ammonium from waters by unsaturated fatty acids and their soaps. Hydrometallurgy 76:155–172

Szostak R (1989) Molecular sieves: principles of synthesis and identification. Blackie Academic and Professional, London

The American Lung Association (2011) Toxic air: the case for cleaning up coal-fired power plants, Chicago, Illinois, USA, p 12

Venuto H, Habib E (1979) Fluid catalytic cracking with zeolite synthesis, pp 156–200

Wdowin M, Franus M, Panek R, Badura L, Franus W (2014) The conversion technology of fly ash into zeolites. Clean Technol Environ Policy 16:1217–1223

Weitkamp J, Puppe L (1999) Catalysis and zeolites: fundamentals and applications. Springer, German

Wingenfelder U, Hansen C, Furrer G, Schulin R (2005) Removal of heavy metals from mine waters by natural zeolites. Environ Sci Technol 39:4606–4613

Wu D, Zhang B, Yan L, Kong H, Wang X (2006) Effect of some additives on synthesis of zeolite from coal fly ash. Inter J Miner Process 80(2–4):266–272

Yao ZT, Xia MS, Ye Y, Zhang L (2009) Synthesis of zeolite Li-ABW from fly ash by fusion method. J Hazard Mater 170:639–644

Zeolites (2018). Chemistry: Foundations and Applications. http://www.encyclopedia.com

Chapter 14
Production and Characterisation of Teak Tree Saw Dust and Rice Husk Biochar

Monoj Bardalai, D. K. Mahanta and Biplab Das

Abstract Biochar is one of the products obtained from biomass pyrolysis and a useful ingredient for agriculture. The present study discusses on the production and characterisation of biochars derived from Teak tree saw dust (TTSD) and Rice husk (RH). The biochars were produced at a pyrolysis temperature 450 °C with the heating rate of 15 °C/min in a fixed bed reactor. Physical, chemical and thermal properties were evaluated in order to compare both the biochars with the help of proximate analysis, ultimate analysis, Thermogravimetric analysis (TGA), X-Ray Diffraction (XRD), Fourier Transform Infrared (FTIR) and Scanning Electron Microscope (SEM). The carbon contents of the biochars ranged from 65.46 to 66.55 wt%, while the oxygen contents were within 30.21 wt%. Both the biochars showed alkalinity behaviour with pH values more than 8 which is similar to many other biochars. The significant degradation was observed on both the biochars after 300 °C and only about 25–40 wt% biochars decomposed till 600 °C. The XRD spectrum identified the possible presence of some elements such as KCl, SiO_2 and $CaCO_3$ on the biochras. In both the biochars, aromatic functional groups were found confirming the aromatic compounds on the biochars. The SEM images showed some flaky fragments and tiny white particles likely to be coalescence of calcium and potassium on TTSD biochar. On the other hand, longitudinal fibrous structures without any pores are observed on RH morphology.

Keywords Biochar · Teak tree · Rice husk · Pyrolysis · Thermogravimetric analysis

M. Bardalai (✉) · D. K. Mahanta · B. Das
Department of Mechanical Engineering, Tezpur University, Napaam, Sonitpur, Assam, India
e-mail: monojb@tezu.ernet.in

R. A. Agarwal et al. (eds.), *Pollutants from Energy Sources*, Energy, Environment, and Sustainability,
https://doi.org/10.1007/978-981-13-3281-4_14

14.1 Introduction

Biomass is a material obtained from any living beings or dead such as woods or animals in the form of waste product. Due to the abundant availability in all the corners of the world, biomass has been considered as the viable source of energy for direct utilisation or converting into some other forms. Moreover, the biomass and some of its derived products can be used as an important tool for soil fertilisation and carbon sequestration. However, there are many challenges while converting the biomass into some other forms (e.g., liquid, gas or solid) in order to obtain better fuel or soil fertilising material. Although many biomass conversion techniques are available in the literature, the pyrolysis and gasification are found to be relatively more flexible and simple (Yanik et al. 2007). Pyrolysis is a process where biomass particles are heated in order to degrade thermally in the temperature range 400–700 °C with presence of no oxygen or limited oxygen. The main products of biomass pyrolysis are liquids, gases and solids (biochar). The liquids and gaseous products can be used as fuel after sufficient upgradation and refinement. The solid product of pyrolysis process known as biochar, contains the required properties which are very useful for improvement of soil quality (Yin et al. 2013; Mukherjee and Lal 2013). Although biomass is primarily pyrolyzed to produce liquid product known as pyrolysis oil, a significant amount of solid product (15–20%) in the form of biochar is also found (Kim et al. 2012). The biochar obtained from biomass can be considered as the carbonaceous residue of pyrolysis, which produces natural fire in limited oxygen (Brown 2009). Biochar has different alternative applications such as fertilization of soil, growth of plants, removal of pollutants such as pesticides, high molecular weight metals and hydrocarbons (Beesley et al. 2011; Cabrera et al. 2011).

The biochar application for improving and sequestration of carbon in soil has been found as the recent topics of interest among the researchers (Pituello et al. 2015). In the solid product of pyrolysis process as found in the form of black carbon is composed by elemental or graphitic and aromatic carbon (Chun et al. 2004). Biochars are highly aromatic and porous with specific surface characteristics, because of which it is considered as a useful tool in agriculture for increasing stability and crop productivity (Jeffery et al. 2011; Sohi et al. 2010). The specific area and micropore volume of biochar are much smaller as compared to the commercially activated carbon, although biochar adsorptivity of organic pollutant and metals with high molecular weight is equal or even more when compared with activated carbon (Chun et al. 2004). Moreover, the extensive literature shows the ability of biochar in restoring decomposed soil, increasing production of crop, CO_2 fixation and decontamination (Tan et al. 2014). In general, the sustainability of biochar in soil is very high as compared to other organic material and thus remain stable for a long period of time (Lehmann 2007; Masiello and Druffel 1998; Pessenda et al. 2001). It was reported that the biochar can reduce the emission of some greenhouse gases such as CH_4 and N_2O from soil of rice paddy field in China (Knoblauch et al. 2011; Liu et al. 2011; Zhang et al. 2010).

The most commonly used reactor types found in the literature in conducting pyrolysis experiment for biochar production include fixed bed, fluidised-bed, ablative, auger, vacuum, rotating cone, pyros, plasma, microwave and solar. The fixed bed reactor is found to be one of the most simplified with high reliability as compared to the others, while the products obtained are quite similar to the other type of reactors (Jahirul et al. 2012; Aysu and Küçük 2014).

The physiochemical characteristics of biochar are influenced by the nature of feedstock and the parameters employed in pyrolysis. The temperature for pyrolysis was found to be the major parameter to influence the biochar yield and its characteristics. It was found that the yield of biochar along with the carbon and some functional groups decreases at high pyrolysis temperature (Yuan et al. 2013; Krull et al. 2009). The temperature affects the pyrolysis mechanism and thus plays an important role on thermal stability, chemical composition, pH and surface morphology of biochar (Al-Wabel et al. 2013).

Wang et al. (2014) performed the characterisation study of biochar derived from rice husk and elm saw dust by fast pyrolysis. They observed some similar and dissimilar properties between the two biochars. Porous biochar and activated carbon was prepared from rice husk and the study revealed the high amount of silica content in the biochar which could be removed by heating at high temperature (Ahiduzzaman and Sadrul Islam 2016). Islam et al. (2017) produced the rice husk biochar in a fixed bed reactor using slow pyrolysis and the various properties were characterised. However, the detail investigation about various properties of the pyrolysed biochar of both RH and TTSD is hardly found in the literature. In the present study, the main objective is to characterise the various physical and chemical properties of the RH and TTSD biochars by comparing with few other previously published biochars, which would be a new addition in the field of biochar characterisation. Rice husk is the protecting cover of the rice grain which is separated at rice mill in order to obtain the rice grain as food. This separated hard cover of the rice grain is known as rich husk and most of the time it is considered as waste material. Teak tree (*Tectona grandis*) is a hard wood belonging to the family of *verbenaceae* and found to be mostly available in the north-eastern region of India along with many other parts of the world. Because of high durability and glaziness, teak wood is mostly consumed in household and furniture making purposes and thus TTSD is found to be easily available in small to large scale saw mill.

14.2 Methods and Materials

14.2.1 Preparation of Feedstock and Production of Biochar

The RH and TTSD were collected from a local rice mill and a sawmill of Assam (India) and further ground in a grinding machine (Make: BAJAJ PLATINI; Model: P x 7 MIXER GRINDER). A mechanical sieve shaker (IKON^{TM} instrument) was

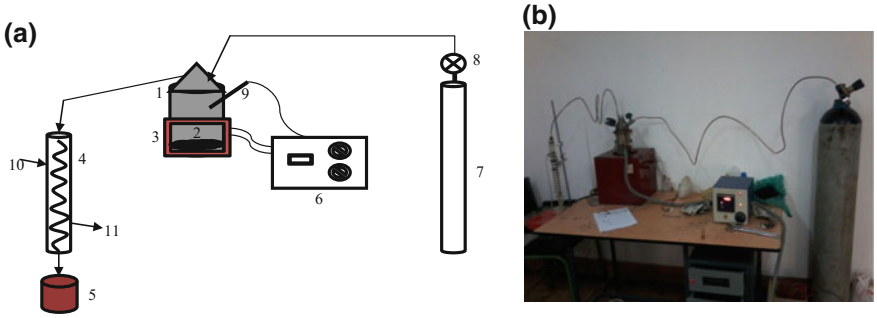

Fig. 14.1 **a** Schematic diagram of pyrolysis setup. 1. Rector, 2. Biochar, 3. Furnace, 4. Condenser, 5. Pyrolysis oil collector, 6. PID controller, 7. N_2 cylinder, 8. Gas flow meter and pressure regulator, 9. Temperature sensor, 10. Cold water inlet, 11. Hot water outlet. **b** Photograph of the setup of pyrolysis plant

used along with the standard test sieve (SETHI, as per IS: 460) to prepare the feedstock particle size in the range of 0.5–1.0 mm. Before conducting the pyrolysis, the biomass samples were dried with the help of an electric heater in order to reduce its moisture contents sufficiently.

The main parts of the pyrolysis setup as shown in Fig. 14.1a, b are fixed bed reactor, a clamp type tubular furnace (2 kW), a glass condenser, a N_2 gas cylinder containing the nitrogen gas of 99.9% purity along with the pressure regulator and gas flow meter and a Proportional Integral and Derivative (PID) temperature controller with a temperature sensor. The reactor is cylindrical in shape with a conical head and made up of stainless steel (Fig. 14.1a, b). The inside and outside diameters of the cylindrical part of the reactor are 88 and 100 mm respectively and total height of the reactor is 250 mm. The biomass is fed into the reactor through a small opening of diameter 27 mm located at the top of the conical part of the reactor. A tubular furnace made of ceramic and stainless steel wraps the reactor with the help of a clamp and two screws covering about three fourth portion of the reactor which helps in providing uniform heating to the biomass particles inside the reactor. The PID controller is connected with the furnace and supply necessary power for required heating and temperature control with the help of temperature sensor which is properly inserted into the reactor.

About 50 g of feedstock was placed in the reactor and the pyrolysis experiment was carried out with the rate of heating 15 °C min^{-1} and it was held at 450 °C for 30 min. Nitrogen was used as a sweeping gas at the flow rate of 25–30 ml min^{-1} to enhance the produced gas coming out from the reactor and to pass through the condenser. The vapour passing through the condenser is collected in the form of liquid by a pyrolysis oil collector (as shown by '5' in Fig. 14.1a). After the completion of pyrolysis, the biochar was collected from the bottom of the reactor as solid residue. In each case, the amount of biochar was found to be about 45 wt%.

14.2.2 Analysis of Physical, Chemical and Morphological Properties

The proximate analysis, elemental analysis, TGA, Differential Thermogravimetric Analysis (DTG), FTIR were conducted as per the methodology explained by Bardalai and Mahanta (2018). For pH measurement, the biochar was properly mixed with deionized water in a ratio of 1:20 (w/v) to prepare a homogeneous suspension and the pH was measured after 1–1.5 h. The XRD analyses of biochars were carried out using an analytical XRD instrument (RIGAKU Mini flex, Japan). The voltage and current of the diffractogram maintained during operation were 30 kV and 15 mA respectively. The range of scanning at the scanning speed 0.05 s^{-1} was 2θ = 10–70°. The analyses of surface morphology of the biochars were performed with the help of a SEM (JEOL, JSM 6390 LV). All the physio-chemical properties of TTSD and RH biochars were measured for three times (range of standard deviation was 0.5–1.5) and the average results are reported in this article.

14.3 Results and Discussion

The results of various analyses performed on TTSD and RH biochars are presented in the following sections with detailed discussion.

14.3.1 Proximate and Ultimate Analysis

The data obtained from proximate and ultimate analysis of TTSD and RH biochars are listed in Table 14.1. The ash content found in the biochar of TTSD was significantly lower than many biochars such as Cattle digestate (CD), Municipal waste (MW), Poultry litter (PL), Sewage sludge (SS) (Pituello et al. 2015) and Palm kernel shell (PKS) (Kong et al. 2013). However, ash content of RH biochar was quite higher than TTSD biochar but similar to many other biochars (see Table 14.1). The biochar with low ash content is more suitable for soil amendment, because the high ash content causes high level of heavy metals contaminant and thus creates soil pollution (Brewer et al. 2009). The low percent of ash in the biochar also results increasing calorific value, since higher ash content leads to dilute the energy content in biochar (Crombie and Mašek 2015). Almost equal amount of volatile matter was found in both TTSD and RH biochars. These values of volatile matter are higher than the biochars of Empty fruit bunches (EFB) and PKS, although they are consistent with many other biochars (Table 14.1). Relatively low volatile matter indicates the presence of lignin content in biochars. Compared with TTSD, RH biochar contained lower fixed carbon, however, it was

quite higher than Coconut shell biochar (CSB-9.52 wt%) and Mesquite wood biochar (MWB-8.9 wt%) as shown in Table 14.1. It was found that the biochars with high fixed carbon is suitable for soil amendment. The moisture contents of both TTSD and RH biochars were quite similar and they ranged within the values of many other biochars. The heating value of TTSD biochar was found to be considerably higher than RH biochar and also some other previously found biochars such as switchgrass, cotton stover etc., while it was slightly higher than Cashew nut shell (CNS: 26.6–28.8 MJ/kg) as seen in Table 14.1.

The carbon contents of the biochars in this study are relatively similar but higher than the biochars produced from some biowastes such as CD (63.2 wt%), MW (29.4 wt%), PL (51.2 wt%) and SS (22.5 wt%) as shown in Table 14.1. However, carbon contents of TTSD and RH biochars were lower when compared with the biochars such as CNS (73.5–79.2 wt%), EFB (67.09–79.04 wt%) and PKS (74.19 wt%) which were produced at about 450 °C (see Table 14.1). The carbon content has the significant contribution to the calorific value of any fuel. Higher is the carbon content, more is the calorific value. Hydrogen is an important element which has significant contribution to the energy value of any substance. In the present study, hydrogen content of TTSD biochar is found to be higher than RH biochar and also EFB (1.50–2.02 wt%) and Bamboo shoot shell (BSS: 3.48 wt%) biochars (Table 14.1). Low oxygen content in biochar indicates the decrease of oxygenated compounds and increase of carbonaceous compounds which occurs during pyrolysis. Low oxygen content also results in increasing calorific value of a substance. The oxygen contents of the biochars in this study range within the values of some previously investigated biochars such as BSS, EFB and Straw pellet (SP). However, very low oxygen content (2.8–9.6 wt%) was observed in SP biochar by varying the operating parameters such as pyrolysis temperature, residence time and carrier gas flow rate (Crombie and Mašek 2015). The atomic ratio H/C of TTSD biochar was slightly higher than the previously reported range while in case of RH biochar, this value was quite consistent with the reported range (Table 14.1). Low H/C ratio indicates the high aromaticity in biochar and high aromatised biochar creates resistance to degradation and becomes intractable, which can be used for carbon sequestration in soil (Yuan et al. 2013; Choudhury et al. 2014). The O/C ratios of TTSD and RH biochars are quite comparable with the previously reported values of some biochars as observed in Table 14.1. On the other hand, the O/C of RH biochar of this study is much lower than the previously studied RH biochar (i.e., 1.31) by other researchers (Wang et al. 2014). The difference of H/C and O/C ratios in different biochars is due to dehydrogenetive polymerisation and dehydrative polycondensation during pyrolysis (De Filippis et al. 2013). In dehydrogenative polymerisation, polymeric compound is produced with less hydrogen or removing hydrogen while in dehydrative polycondensation, high molecular weight compound is formed by dehydration reaction (loss of water molecule) in chemical condensation process.

The pH is an important parameter which determines the alkaline and acidic nature of the biochar. The biochar with high pH value is less acidic and suitable for soil improvement. The pH values of the present biochars (i.e., TTSD and RH) as shown in Table 14.1, are quite comparable with the other biochars as reported by

Table 14.1 Proximate and ultimate analysis of TTSD and RH biochar

Property	TTSD biochar	RH biochar	Other biochars
Ash (dry basis, wt%)	13.65	29.06	0.8–67 (Pituello et al. 2015; Ye et al. 2015; Shariff et al. 2014; Crombie and Mašek 2015; Kong et al. 2013)
Volatile matter (dry basis, wt%)	33.59	32.28	3.3–38.3 (Shariff et al. 2014; Crombie and Mašek 2015; Kong et al. 2013)
Fixed carbon (dry basis, wt%)	52.76	38.66	8.9–63.8 (Brewer et al. 2009; Angalaeeswari and Kamaludeen 2017)
Moisture (wt%)	4.88	4.48	1.07–8.13 (Shariff et al. 2014; Kong et al. 2013)
Calorific value (MJ/kg)	29.04	22.69	13.83–28.80 (Brewer et al. 2009; Moreira et al. 2017)
C (wt%)	66.55	65.46	22.5–79.2 (Pituello et al. 2015; Ye et al. 2015; Shariff et al. 2014; Kong et al. 2013; Moreira et al. 2017)
H (wt%)	4.48	2.94	1.5–3.48 (Ye et al. 2015; Shariff et al. 2014)
N (wt%)	0.5	1.39	1.12–6.83 (Shariff et al. 2014)
O (calculated by difference, wt%)	28.47	30.21	2.8–30.0 (Ye et al. 2015; Shariff et al. 2014; Crombie and Mašek 2015)
H/C (wt%)	0.81	0.54	0.44–0.62 (Ye et al. 2015; Wu et al. 2012)
O/C (wt%)	0.32	0.35	0.23–1.31 (Wang et al. 2014; Ahiduzzaman and Sadrul Islam 2016; Islam et al. 2017; Bardalai and Mahanta 2018; Ye et al. 2015)
pH	8.5	8.3	7.2–10.7 (Pituello et al. 2015; Ye et al. 2015; Kong et al. 2013; Angalaeeswari and Kamaludeen 2017; Park et al. 2014; Bouqbis et al. 2016)

previous researchers. The biochars of both RH and TTSD have considerably higher pH value when compared with the biochars obtained from some biowastes such as SS (7.2) and MW (7.4), while relatively closer to CSB (8.66) and MWB (8.73) (Pituello et al. 2015; Angalaeeswari and Kamaludeen 2017). However, pH values of the biochars in this study are lower than the biochars produced from Argan shells (AS), BSS, PKS and Rice straw (RS) (Ye et al. 2015; Kong et al. 2013; Wu et al. 2012; Park et al. 2014; Bouqbis et al. 2016). Therefore, the acidic soil can be improved by applying the highly alkaline biochar including RH and TTSD.

14.3.2 Theromgravimetric Analysis

TGA and DTG curves of TTSD and RH biochars are shown in Fig. 14.2a and b respectively. In TTSD biochar, only about 3% and in RH biochar about 6% weight loss were observed up to 100 °C (by black dark lines), which were due to evaporation of physiosorbed water. The physically adsorbed water molecules occur due to condensation of vapour at low temperature on biochar surface and involve intermolecular forces (van der walls force) and do not change any electronic pattern of the biochar species. Due to increased temperature on heating, the intermolecular forces breakdown and water molecules evaporate from the surface of the biochar and thus a little amount of weight loss is observed. However, 40% (TTSD biochar) and 25% (RH biochar) weight loss occurred when they were heated till 600 °C (Fig. 14.2a and b). The major weight loss in both the biochars started only after 300 °C indicating the decomposition of undegraded cellulose and lignin content present in the biochars. The highest peak at 356 °C in the DTG profile of TTSD biochar (Fig. 14.2a) represents the decomposition of undegraded form of cellulose. On the other hand, two peaks were found in the DTG profile of RH biochar (Fig. 14.2b) at about 330 and 425 °C respectively revealing residual cellulose and lignin degradation (Ghani et al. 2013). The high lignin contained biochars induce some peculiar fungal flora to grow and enhance the endurance of Fusarium oxysporum cucumerinum (*f.o.c.*) in soil (Adachi et al. 1987).

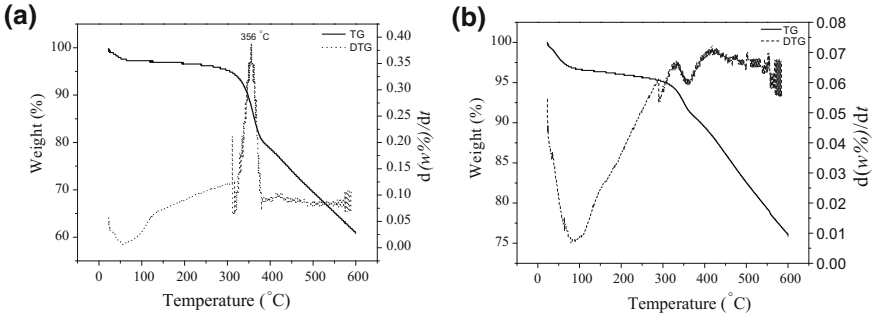

Fig. 14.2 TGA and DTG of **a** TTSD biochar and **b** RH biochar

14.3.3 FTIR Analysis

The Infra-red radiation is absorbed at a definite wavelength or wavenumber or in a region by certain functional groups in the form of peaks or bands. The absorption of Infra-red radiation region is influenced by the vibrational and rotational levels of the atoms. Therefore, by observing the peaks or bands on a FTIR spectrum, the presence of functional groups and the nature of vibration of certain compounds can be identified.

The broad and intense bands at 3411 cm^{-1} in TTSD biochar (Fig. 14.3a) and at ~3435 cm^{-1} in RH biochar (Fig. 14.3b) indicate the presence of –OH group as the result of dehydration of cellulose and hemicellulose components of the biomass samples during pyrolysis. The peaks at ~2921 cm^{-1} (Fig. 14.3a) and 2927 cm^{-1} (Fig. 14.3b) represent the aliphatic compounds in TTSD and RH biochars with C–H stretching or can be attributed to CH_2 or CH_3 deformation (Chen et al. 2011). The C–H stretching vibration bands from 2850 to 2950 cm^{-1}, while C–H bending vibration bands within 1460 and 1350 cm^{-1} in both TTSD and RH biochars are absorbed by the functional groups of alkanes (Ertas and Alma 2010). The aliphatic compounds such as alkanes containing carbon and hydrogen joined by straight or branched chain are non-aromatic hydrocarbon and mostly inflammable. The band between 1648 and 1540 cm^{-1} can be assigned for C=C ring stretching and this indicates the presence of aromatic carbon in the biochars (Abdulrazzaq et al. 2014). Further, bands between 1600 and 1511 cm^{-1} in TTSD biochar (Fig. 14.3a) can be attributed to aromatic skeleton vibrations of lignin (Pituello et al. 2015). Further, the presence of aromatic compounds in the TTSD biochar can again be considered by the aromatic C–C stretching vibration within the range 1450–1550 cm^{-1} as seen in Fig. 14.3a (Das et al. 2004). The aromatic compounds are comparatively less reactive than non-aromatic compounds and thus can be used for improving the stability of the soil. In both biochars (Fig. 14.3a and b), the absorption near 1457 cm^{-1} can be assigned for CH_2 deformation stretching in lignin and xylan (Shi et al. 2012). The band between 1100 and 950 cm^{-1} in RH biochar (Fig. 14.3b)

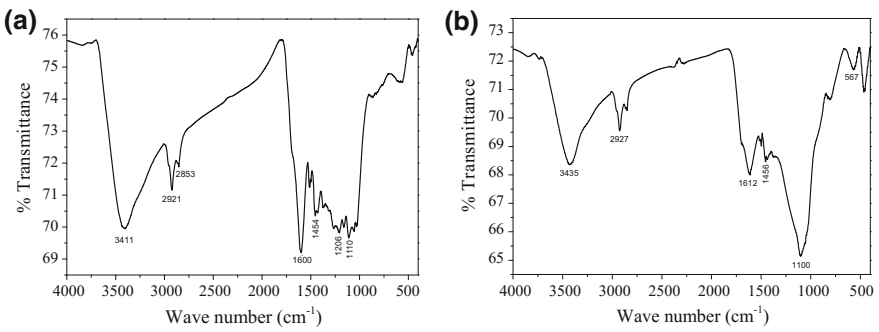

Fig. 14.3 FTIR of **a** TTSD biochar and **b** RH biochar

reveals the presence functional group for compounds like phosphines, phosphine oxides and silicon oxide (Cantrell et al. 2012). Phosphines can be used for fumigation purpose in order to control pests and insects in agriculture. The phosphine oxides are phosphorous-oxygen double bond compounds with alkyl or aryl. These compounds are thermally stable and do not degrade till 450 °C.

14.3.4 XRD Analysis

The XRD spectrum of TTSD biochar is seen in Fig. 14.4a, clearly shows the amorphous behaviour with some local crystallinity. The small sharp peaks at 3.14 and 2.30 Å (Fig. 14.4a) indicate the presence of KCl in the TTSD biochar (Wu et al. 2012). The biochar containing KCl (approximately 50% K) can be used as potassium fertiliser in the soils which cannot supply K at the required amount. Few other peaks at 2.06, 6.0, 5.33, 2.60 Å in TTSD biochar (Fig. 14.4a) are attributed to the localised crystalline structure of cellulose (Abdulrazzaq et al. 2014). Crystalline cellulose can also be indicated with the help of the peaks at 5.8 and 3.89 Å (Fig. 14.4a) (Al-Wabel et al. 2013). The graphite-like structure generally forms on activated carbon; however, the similar structure is observed in TTSD biochar by peaks marked at 3.35 and 2.03 Å (Fig. 14.4a) corresponding to the 2θ values of 26.6 and 44.5° (Azargohar and Dalai 2006). The presence of calcite ($CaCO_3$) in TTSD biochar was identified by the peaks at around 3.03 and 3.04 Å (Al-Wabel et al. 2013; Wu et al. 2012). Microbiologically precipitated calcite has a wide range of applications, such as soil remediation, soil stabilization and concrete repair. The flavour of whewellite in TTSD biochar was revealed by the peaks at *d* spacings of 5.8, 3.63 and 2.35 Å (Al-Wabel et al. 2013).

In XRD spectrum of RH biochar (Fig. 14.4b), many sharp narrow peaks are found to represent the crystallinity of the biochar sample. However, the overall pattern of the diffractogram has shown the amorphous nature. The completely

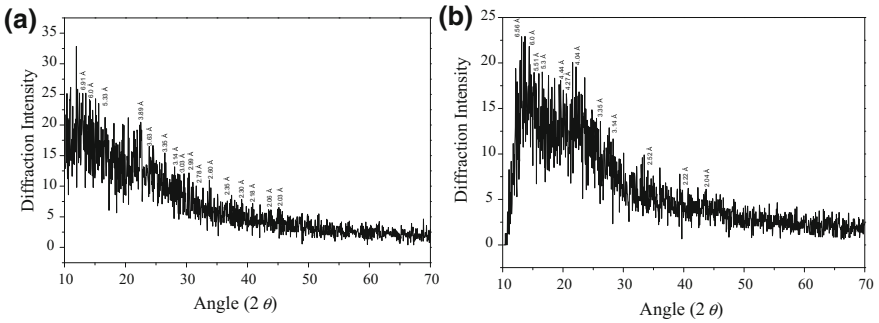

Fig. 14.4 XRD spectrum of **a** TTSD and **b** RH biochar

ordered form of crystallographic planes can be identified in RH biochar (Fig. 14.4b) by the peak spacings at 6.56 and 5.10 Å (Abdulrazzaq et al. 2014). Similar to the TTSD biochar, RH biochar also contains KCl which is detected by the peaks at 3.14 and 2.22 Å (Fig. 14.4b) and consistent with the biochar of another product of rice tree, such as rice straw (Wu et al. 2012). Further, peak spacings at 3.35 and 2.04 Å as seen in Fig. 14.4b (at 2θ value 26.6 and 44.5° respectively) are likely to be due to the existence of graphite like substance in the RH biochar (Azargohar and Dalai 2006). Moreover, the presence of SiO_2 in RH biochar can be identified by the peak spacings of 4.27 and 3.35 Å (Wu et al. 2012). Rice straw and rice husk are some rich sources of silicon and thus derived products of RH such as biochar contains silica. The silica has several usefulness in plant growth, such as strengthening the stalk and stem, toughening and widening the leaves for better capturing of light to enhance photosynthesis. Among all plants, the rice mostly captures the silica from the ground for improvement of the plants.

14.3.5 Morphology Study

SEM can produce the images of very high resolution (up to 1 nm) of any material which provide the sufficient morphological information such as cracks, voids, pores and presence of particles with their sizes on the surfaces. In biochar, the information about the presence or absence of pores and cracks on its surfaces is very important to know about the usefulness in agricultural purposes. Similarly, the presence of particles of different nature on biochar surface also play the significant roles in identifying certain important elements.

The SEM images of TTSD biochar (Fig. 14.5a, b) have shown the flaky fragments at the magnification of ×500. The average size of these flake particles is found to be around 30–40 μm as shown by red marks in Fig. 14.5a. At higher magnification (×2500), few non-uniform distributions of white particles are seen (shown by red circles on Fig. 14.5b) over the fragments. These tiny white particles can be assigned for the coalescence of calcium and potassium, which are likely due to the migration from fuel matrix to the biochar surface (Lee et al. 2010). Disappearance of voids (Fig. 14.5b) on the char particles can be attributed to the melting of certain fuel related compounds. The melting causes the breaking of fibrous cell structure, closes the pores and forms plastic surface.

In SEM micrograph of RH biochar (Fig. 14.5c), some flat materials with fibrillar structure are seen. The longitudinal fibrillar structures (Fig. 14.5d) are observed on the SEM images of RH biochar as it was produced at lower temperature. The presence of these fibrous species on the RH biochar is assumed to be cellulose and degraded crystalline nature. The SEM image at Fig. 14.5d is quite similar with the RH biochar modified by NaOH in the study performed by Chen et al. (2011). This also indicates the softwood material nature of rice husk. Since the RH biochar was produced at low pyrolysis temperature, i.e., ∼450 °C, no significant pore was observed on its surface. In general, the SEM microporosity increases with increase

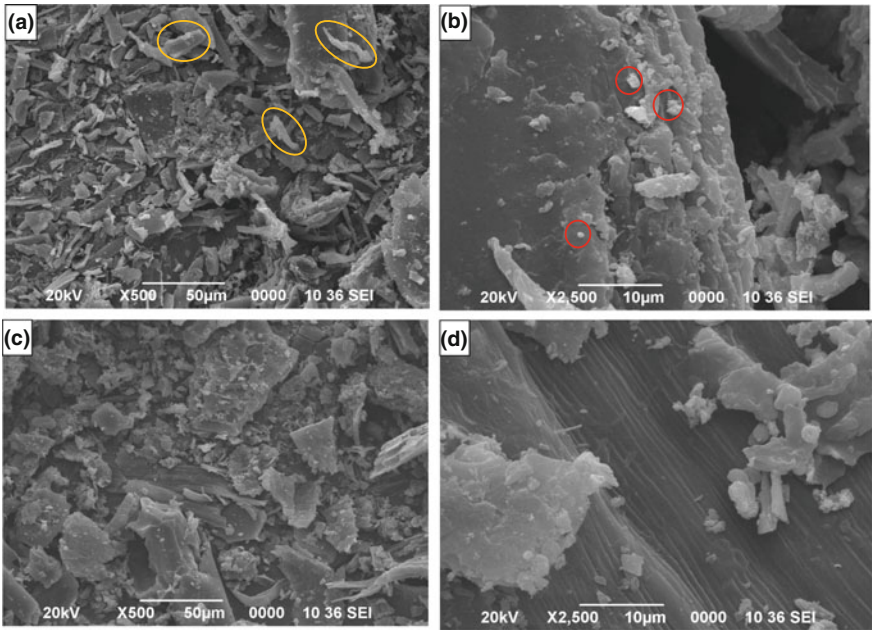

Fig. 14.5 SEM of TTSD biochar (**a** and **b**) and RH biochar (**c** and **d**)

of temperature (Apaydin-Varol et al. 2007). The RH biochar (Fig. 14.5d) shows a mixture of flat surface with some agglomeration likely to be the mixture of crystalline and amorphous carbon over the surface.

14.4 Conclusions

The biochars produced from TTSD and RH by pyrolysis were analysed for various physical and chemical properties and compared with some other biochars. The investigation has shown that ash content of TTSD biochar (13.65 wt%) is quite lower than RH biochar (29.06 wt%) and thus the heating value of TTSD biochar is significantly higher in comparison to RH biochar. Carbon contents of both the biochars (65.46–66.55 wt%) are almost equal and quite higher than the oxygen contents indicating the presence of more carbonaceous compounds in the biochars. The O/C (0.32–0.35) and H/C (0.54–0.81) ratios of the biochars are found within the range of many other biochars indicating high aromaticity and usefulness for C segregating and resisting decomposition in the soil. High pH values (8.3–8.5) of the biochars indicate the alkaline nature and they are consistent with other biochars. TGA analyses show that the degradation of the biochars starts at high temperature (about 300 °C), which indicates the presence of lignin and undegraded cellulose

contents in biocahrs. The FTIR spectra of both the biochars identify the presence of aromatic carbon functional groups by the peaks with C=C stretching vibration. The XRD analyses reveal some local crystalline structure of cellulose on both the biochars. The TTSD biochar was identified for the possible presence of KCl and $CaCO_3$, while SiO_2 and KCl were found to be present on RH biochar by the peaks at the specified *d* spacings. Both the biochars are basically nonporous with some flaky fragments on TTSD biochar while fibrillar structures on RH biochar.

Acknowledgements The authors acknowledge the financial support of Tezpur University in developing the setup of lab scale pyrolysis plant for conducting the experiments of pyrolysis and for providing facilities of various sample analyses.

References

Abdulrazzaq H, Jol H, Husni A, Abu-Bakr R (2014) Characterization and stabilisation of biochars obtained from empty fruit bunch, wood and rice husk. BioResources 9:2888–2898

Adachi K, Kobayashi M, Takahashi E (1987) Effect of the application of lignin and/or chitin to soil inoculated with *Fusarium oxysporum* on the variation of soil microflora and plant growth. Soil Sci Plant Nutr 33:245–259

Ahiduzzaman M, Sadrul Islam AKM (2016) Preparation of biochar and activated carbon from rice husk by leaching ash and chemical activation. Springer Plus 5:1248. https://doi.org/10.1186/s40064-016-2932-8

Al-Wabel MI, Al-Omran A, El-Nagar AH, Nadeem M, Usman ARA (2013) Pyrolysis temperature induced changes in characteristics and chemical composition of biochar produced from conocarpus wastes. Bioresour Technol 131:374–379. https://doi.org/10.1016/j.biortech.2012.12.165

Angalaeeswari K, Kamaludeen SPB (2017) Production and characterization of coconut shell and mesquite wood biochar. Int J Chem Stud 5:442–446

Apaydin-Varol E, Putun E, Putun AE (2007) Slow pyrolysis of pistachio shell. Fuel 86:1892–1899. https://doi.org/10.1016/j.fuel.2006.11.041

Aysu T, Küçük MM (2014) Biomass pyrolysis in a fixed-bed reactor: effects of pyrolysis parameters on product yields and characterization of products. Energy 64:1002–1025. https://doi.org/10.1016/j.energy.2013.11.053

Azargohar R, Dalai AK (2006) Biochar as a precursor of activated carbon. Appl Biochem Biotechnol 131:762–773

Bardalai M, Mahanta DK (2018) Characterisation of pyrolysis oil derived from teak tree saw dust and rice husk. J Eng Sci Technol 13:242–253

Beesley L, Moreno-Jiménez E, Gomez-Eyles JL, Harris E, Robinson B, Sizmur T (2011) A review of biochars' potential role in the remediation, revegetation and restoration of contaminated soils. Environ Pollut 159:3269–3282. https://doi.org/10.1016/j.envpol.2011.07.023

Bouqbis L, Daoud S, Koyro H-W, Kammann CI, Ainlhout LFZ, Harrouni MC (2016) Biochar from argan shells: production and characterization. Int J Recycl Org Waste Agric 5:361–365. https://doi.org/10.1007/s40093-016-0146-2

Brewer CE, Schmidt-Rohr K, Satrio JA, Brown RC (2009) Characterization of biochar from fast pyrolysis and gasification systems. Environ Prog Sustain Energy 28:386–396. https://doi.org/10.1002/ep.10378

Brown R (2009) Biochar production technology. In: Lehman J, Joseph S (eds) Biochar for environmental management: science and technology. Earthscan, London, pp 127–146

Cabrera A, Cox L, Spokas KA, Celis R, Hermosín MC, Cornejo J, Koskinen WC (2011) Comparative sorption and leaching study of the herbicides fluometuron and 4-chloro-2 methylphenoxyacetic acid (MCPA) in a soil amended with biochars and other sorbents. J Agric Food Chem 14:12550–12560. https://doi.org/10.1021/jf202713q

Cantrell KB, Hunt PG, Uchimiya M, Novak JM, Ro KS (2012) Impact of pyrolysis temperature and manure source on physicochemical characteristics of biochar. Bioresour Technol 107:419–428. https://doi.org/10.1016/j.biortech.2011.11.084

Chen Y, Zhu Y, Wang Z, Li Y, Wang L, Ding L, Gao X, Ma Y, Guo Y (2011) Application studies of activated carbon derived from rice husks produced by chemical-thermal process—a review. Adv Colloid Interface Sci 163:39–52. https://doi.org/10.1016/j.cis.2011.01.006

Choudhury ND, Chutia RS, Bhaskar T, Kataki R (2014) Pyrolysis of jute dust: effect of reaction parameters and analysis of products. J Mater Cycles Waste Manage 16:449–459. https://doi.org/10.1007/s10163-014-0268-4

Chun Y, Sheng GY, Chiou CT, Xing BS (2004) Compositions and sorptive properties of crop residue-derived chars. Environ Sci Technol 38:4649–4655. https://pubs.acs.org/doi/pdf/10.1021/es035034w

Crombie K, Mašek O (2015) Pyrolysis biochar system, balance between bioenergy and carbon sequestration. GCB Bioenergy 7:1–13. https://doi.org/10.1111/gcbb.12137

Das P, Sreelatha T, Ganesh A (2004) Bio oil from pyrolysis of cashew nut shell-characterisation and related properties. Biomass Bioenergy 27:265–275. https://doi.org/10.1016/j.biombioe.2003.12.001

De Filippis P, Palma LD, Petrucci E, Scarsella M, Verdone N (2013) Production and characterization of adsorbent materials from sewage sludge by pyrolysis. Chem Eng Trans 32:205–210. https://doi.org/10.3303/CET1332035

Ertas M, Alma MH (2010) Pyrolysis of laurel (*Laurus nobilis* L.) extraction residues in a fixed-bed reactor: characterization of bio-oil and bio-char. J Anal Appl Pyrol 88:22–29. https://doi.org/10.1016/j.jaap.2010.02.006

Ghani WAWAK, Mohd A, da Silva G, Bachmann RT, Taufiq-Yap YH, Rashid U, Muhtaseb AH (2013) Biochar production from waste rubber-wood-sawdust and its potential use in C sequestration: chemical and physical characterization. Ind Crops Prod 44:18–24. https://doi.org/10.1016/j.indcrop.2012.10.017

Islam MN, Ali MH, Ahmed I (2017) Fixed bed pyrolysis of biomass solid waste for biochar. IOP Conf Series: Mater Sci Eng 206:012014. https://doi.org/10.1088/1757-899x/206/1/012014

Jahirul MI, Rasul A, Chowdhury A, Ashwath N (2012) Biofuel production through biomass pyrolysis—a technological review. Energies 5:4952–5001. https://doi.org/10.3390/en5124952

Jeffery S, Verheijen FGA, Velde MVD, Bastos AC (2011) A quantitative review of the effects of biochar application to soils on crop productivity using meta-analysis. Agr Ecosyst Environ 144:175–187. https://doi.org/10.1016/j.agee.2011.08.015

Kim KH, Kim JY, Cho TS, Choi JW (2012) Influence of pyrolysis temperature on physiochemical properties of biochar obtained from the fast pyrolysis of pitch pine (*Pinus rigida*). Bioresour Technol 118:158–162. https://doi.org/10.1016/j.biortech.2012.04.094

Knoblauch C, Maarifat AA, Pfeiffer EM, Haefele SM (2011) Degradability of black carbon and its impact on trace gas fluxes and carbon turnover in paddy soils. Soil Biol Biochem 43:1768–1778. https://doi.org/10.1016/j.soilbio.2010.07.012

Kong SH, Loh SK, Bachmann RT, Choo YM, Salimon J, Rahim SA (2013) Production and physico-chemical characterization of biochar from palm kernel shell. AIP Conf Proc 1571:749–752. https://doi.org/10.1063/1.4858744

Krull ES, Baldock JA, Skjemstad JD, Smernik RS (2009) Characteristics of biochar: organo-chemical properties. In: Lehman J, Joseph S (eds) Biochar for environmental management: science and technology. Earthsan, London, pp 53–66

Lee JW, Kidder M, Evans BR, Paik S, Buchanan AC III, Garten CT, Brown RC (2010) Characterization of biochars produced from cornstovers for soil amendment. Environ Sci Technol 44:7970–7974

Lehmann J (2007) Bio-energy in the black. Front Ecol Environ 5:381–387. https://doi.org/10.1890/1540-9295(2007)5%5b381:BITB%5d2.0.CO;2

Liu Y, Yang M, Wu Y, Wang H, Chen Y, Wu W (2011) Reducing CH_4 and CO_2 emissions from waterlogged paddy soil with biochar. J Soils Sediments 11:930–939. https://doi.org/10.1007/s11368-011-0376-x

Masiello CA, Druffel ERM (1998) Black carbon in deep-sea sediments. Science 280:1911–1913. https://doi.org/10.1126/science.280.5371.1911

Moreira R, Orsini RdR, Vaz JM, Penteado JC, Spinace´ EV (2017) Production of biochar, bio-oil and synthesis gas from cashew nut shell by slow pyrolysis. Waste Biomass Valorization 8:217–224. https://doi.org/10.1007/s12649-016-9569-2

Mukherjee A, Lal R (2013) Biochar impacts on soil physical properties and greenhouse gas emissions. Agronomy 3:313–339. https://doi.org/10.3390/agronomy3020313

Park J, Lee Y, Ryu C, Park YK (2014) Slow pyrolysis of rice straw: analysis of products properties, carbon and energy yields. Bioresour Technol 155:63–70. https://doi.org/10.1016/j.biortech.2013.12.084

Pessenda LCR, Gouveia SEM, Aravena R (2001) Radiocarbon dating of total soil organic matter and humin fraction and its comparison with ^{14}C ages of fossil charcoal. Radiocarbon 43:595–601

Pituello C, Francioso O, Simonetti G, Pisi A, Torreggiani A, Berti A, Morari F (2015) Characterization of chemical-physical, structural and morphological properties of biochars from biowastes produced at different temperatures. J Soils Sediments 15:792–804. https://doi.org/10.1007/s11368-014-0964-7

Shariff A, Aziz NSM, Abdullah N (2014) Slow pyrolysis of oil palm empty fruit bunches for biochar production and characterisation. J Phys Sci 25:97–112

Shi J, Xing D, Li J (2012) FTIR studies of the changes in wood chemistry from wood forming tissue under inclined treatment. Energy Proc 16:758–768. https://doi.org/10.1016/j.egypro.2012.01.122

Sohi S, Carter S, Shackley S (2010) Monitoring, verification, accounting and reporting. In: Shakely S, Sohi S (eds.) An assessment of the benefits and issues associated with the application of biochar to soil, UK Biochar Research Centre, Edinburgh, pp 69–74

Tan C, Yaxin Z, Hongtao W, Wenjing L, Zeyu Z, Yuancheng Z, Lulu R (2014) Influence of pyrolysis temperature on characteristics and heavy metal adsorptive performance of biochar derived from municipal sewage sludge. Bioresour Technol 164:47–54. https://doi.org/10.1016/j.biortech.2014.04.048

Wang Y, Yin R, Liu R (2014) Characterisation of biochar from fast pyrolysis and its effect on chemical properties of the tea garden soil. J Anal Appl Pyrol 110:375–381. https://doi.org/10.1016/j.jaap.2014.10.006

Wu W, Yang M, Feng Q, McGrouther K, Wang H, Lu H, Chen Y (2012) Chemical characterization of rice straw-derived biochar for soil amendment. Biomass Bioenergy 47:268–276. https://doi.org/10.1016/j.biombioe.2012.09.034

Yanik J, Kommayer C, Saglam M, Yuksel M (2007) Fast pyrolysis of agricultural waste: characterization of pyrolysis products. Fuel Process Technol 88:942–947. https://doi.org/10.1016/j.fuproc.2007.05.002

Ye L, Zhang J, Zhao J, Luo Z, Tu S, Yin Y (2015) Properties of biochar obtained from pyrolysis of bamboo shoot shell. J Anal Appl Pyrol 114:172–178. https://doi.org/10.1016/j.jaap.2015.05.016

Yin R, Liu R, Mei Y, Fei W, Sun X (2013) Characterization of bio-oil and bio-char obtained from sweet sorghum bagasse fast pyrolysis with fractional condensers. Fuel 112:96–104. https://doi.org/10.1016/j.fuel.2013.04.090

Yuan H, Lu T, Zhao D, Huang H, Noriyuki K, Chen Y (2013) Influence of temperature on product distribution and biochar properties by municipal sludge pyrolysis. J Mater Cycles Waste Manage 15:357–361. https://doi.org/10.1007/s10163-013-0126-9

Zhang A, Cui L, Pan G, Li L, Hussain Q, Zhang X, Zheng J, Crowley D (2010) Effect of biochar amendment on yield and methane and nitrous oxide emissions from a rice paddy from Tai Lake plain. China Agric Ecosystems Environ 139:469–475. https://doi.org/10.1016/j.agee.2010.09.003

Chapter 15
Parametric Evaluation of Leachate Generated from a Non-engineered Landfill Site and Its Contamination Potential of Surrounding Soil and Water Bodies

Rajiv Ganguly, Deepika Sharma, Anchal Sharma, Ashok Kumar Gupta and B. R. Gurjar

Abstract Open dumping of municipal solid waste causes environmental degradation including air, soil and groundwater pollution leading to adverse impact on public health. The present study provides the physico-chemical characterization of groundwater, leachate and surface water being affected by the percolation of leachate into aquifers in the study region Solan, Himachal Pradesh. Testing was carried out in two seasons (monsoon season and winter season) to study the effect of leachate contamination on the groundwater. The physico-chemical characterization of groundwater study observed the pH value of groundwater 7.41 in monsoon season and 8.2 in winter season that varied from slightly neutral to alkaline. The total dissolved solids were observed 242 mg/L in monsoon season and 250 mg/L in winter season. The value of sulfate was evaluated as 63 mg/L in monsoon season and 68 mg/L in winter season whereas nitrate, ammoniacal nitrogen, biological oxygen demand and chemical oxygen demand has been found

R. Ganguly (✉) · D. Sharma · A. Sharma · A. K. Gupta
Department of Civil Engineering, Jaypee University of Information Technology, Waknaghat, Solan 173234, Himachal Pradesh, India
e-mail: rajiv.ganguly@juit.ac.in

D. Sharma
e-mail: deepikasharmacivil89@gmail.com

A. Sharma
e-mail: anchalsharam881@gmail.com

A. K. Gupta
e-mail: ashok.gupta@juit.ac.in

B. R. Gurjar
Department of Civil Engineering, IIT Roorkee, Roorkee 247667, Uttarakhand, India
e-mail: bholafce@iitr.ernet.in

R. A. Agarwal et al. (eds.), *Pollutants from Energy Sources*,
Energy, Environment, and Sustainability,
https://doi.org/10.1007/978-981-13-3281-4_15

below the detection level. However, the biological oxygen demand and chemical oxygen demand of surface water was found 6.2 and 20 mg/L in monsoon season whereas 6.0 and 22 mg/L in winter season, respectively. The national foundation sanitation method was applied to determine the water quality index in Solan region. It revealed the poor quality of water due to the open dumping, and thus percolation of leachate into the groundwater.

Keywords Groundwater · Heavy metal · Leachate · Water quality index Soil contamination

15.1 Introduction

Rapid growth in urbanization and industrialization has led to severe environmental degradation including increased generation of solid waste (Puri et al. 2008; Sethi et al. 2013). In particular, solid waste management has always been a pertinent issue for developing countries (Shekdar 2009). This is primarily due to poor waste management practices including lack of authentic data and information to assess the existing management systems (Chang and Davila 2008; Hancs et al. 2008). The increased rate in the population of Indian cities is one of the major contributors to the generation of municipal solid waste. Further, the enhanced rate of migration of people from rural to the urban areas has led to overwhelming demographic growth in many cities through worldwide. The increased rate of production and consumption of synthetic products and services is generating a bulk quantity of solid waste in cities. Municipal solid wastes are hence produced from municipal services including dead animals waste, vegetable market wastes, municipal wastes, commercial wastes and institutional wastes (Sharma et al. 2018). The rapid growth of municipal solid waste depends upon the living standards of people and consumption pattern of goods by the residents. The population of India has also rapidly migrated from agricultural-based nation to the urbanization and industrialization. Urban areas in India generates about 48 million tonne of municipal solid waste annually whereas per capita national MSW generation ranges between 200 and 600 gm. The three mega cities in India including Greater Mumbai, Kolkata and Delhi having a population of more than 10 million, 53 cities have more than 1.0 million populations and 415 cities having population 100,000 (CPCB 2013). This has led to further increased growth of municipal solid waste (MSW) generated in urban areas. The population growth in India between 1911 and 2011 has been shown in Table 15.1.

The current scenario of municipal solid waste management in Indian cities is not very satisfactory. It is reported that municipal solid waste generated in India is 127,486 tonne per day and 47 million tonne per year as per the status of CPCB 2013. Out of the total solid waste generated in India, 89,334 tonne (70%) is collected, 15,881 tonne (12.50%) is being treated while 22,271 tonne (17.5%) is not being collected. Increasing industrialization and rising income levels lead to greater use of resources which further leads to the increased MSW generation and more

Table 15.1 Population growth in India between 1911 and 2011 (CPCB 2013)

Census year	Population	Average annual exponential rate (%)	Population growth rate compared with 1911 (%)
1911	252.0	0.56	5.76
1921	251.3	−0.03	5.42
1931	278.9	1.04	17.02
1941	318.6	1.33	33.67
1951	361.6	1.25	51.47
1961	439.2	1.96	84.25
1971	548.1	2.20	129.94
1981	683.3	2.22	186.64
1991	846.4	2.16	255.05
2001	1028.7	1.97	331.52
2011	1210.2	1.64	407.62

Table 15.2 Estimated waste generation in Himachal Pradesh (Sharma et al. 2018)

Year	Per capita waste generation	Urban population	Waste generated (tonne/day)
2011	0.413	736.33	304.3
2021	0.472	883.32	416.6
2031	0.538	1023.42	550.9
2041	0.614	1155.249	709.6

complex composition of MSW than earlier the generation of municipal solid waste in Himachal Pradesh was estimated to be 350 tonne per day in the year 2015 (Sharma et al. 2018). The estimated waste generation in the municipal solid waste in Himachal Pradesh has been shown in Table 15.2.

In low-income countries like India, the waste collected from the cities are often not segregated. The mixed form solid waste leads to generation of cocktail of different toxic chemicals producing leachate which often pass through the soil thereby contaminating the surrounding soil and groundwater sources and other potential environmental consequences (Mor et al. 2006; Kaushik and Sethi 2007a, b). The problem of environmental contamination has severely increased due to open dumping of the wastes in non-engineered landfill sites. Further, almost 90% of the solid waste generated from major cities and town in India is open dumped as it is a highly cost-effective method (Hazra and Goel 2009; Rana et al. 2015). It is estimated that 950 million tonne of municipal solid waste is generated on an annual basis because of various human activities including municipal, agricultural and industrial activities in India. Of the total waste generated, 350 million tonne of solid waste is organic waste. Inorganic waste accounts for 290 million tonne from industrial activities and 5 million tonne is a hazardous waste (Kumar and Alappat 2005). Further, the per capita generation of municipal solid waste varies within the range of 0.20–0.87 kg/capita/day with the significantly higher values in urban areas in comparison to rural areas (Hazra and Goel 2009; Rana et al. 2015).

Rainwater coming in contact with the municipal solid waste generally dissolves the organic fraction of the MSW. The resulting liquid effluent has a complex brown colour and is known as leachate (Mor et al. 2006; Bhalla et al. 2012). Leachate thus generated from the degradation of municipal solid waste in the open dumps can migrate to the aquifers, thereby polluting groundwater and soil in the periphery of the dumping ground rendering them unsuitable for any of the domestic or commercial use (Mor et al. 2006; Manaf et al. 2009; Pillai et al. 2014). Further, the closure of such disposal sites still has the potential to produce leachate for many years and can degrade the surrounding environment (Nagarajan et al. 2012; Ogundiran and Afolabi 2008).

The impact of leachate on contamination of groundwater has been reported in many studies indicating the presence of high concentrations of both organic and inorganic material cause pollution to environment due to percolation of leachate (Longe and Balogun 2010; Akinbile and Yusoff 2011; Parameswari et al. 2015). The various factors on which the composition of the leachate depends on landfill age, rainfall intensity as well as the amount of municipal solid waste and decomposition of waste (Shivasharanappa and Huggi 2011). To summarize, leachate is a significant source of environmental problems. Therefore, the physico-chemical characterization and assessment of heavy metal in leachate and its potential contamination of surrounding water bodies that are affected by leachate is of significant concern. The potential contamination of water sources by leachate is described by water quality index method reported in earlier studies (Swamee and Tyagi 2000). Aggregate index is the technique that has a tendency to decrease with the incremental of time due to the degradation of municipal solid waste whereas also increases when increased the distance from the respective dumpsite (Sharma et al. 2016; Swamee and Tyagi 2007). The contamination of the soil by leachate in principle generally alters the engineering properties of soil including its shear strength and CBR properties. This is because, with the decay in the organic fraction of the MSW, they react with the existing soil fraction leading to change in soil properties. This is particularly important if the dumpsite is to be reused for constructing purposes after the design period of dumpsite. In such conditions, the engineering properties are most predominant in determining the reusability of such dumpsites. The purpose of the present study is to analyze the physico-chemical characterization of leachate, groundwater, surface water and soil quality that is being affected by percolation of leachate into aquifers in non-engineered dumping sites. However, the toxicity level of the leachate on groundwater has been presented in single term known as an aggregate index.

15.2 Site Location

Solan region lies within the Universal Transverse Mercator coordinates of (700384.18, 3420901.86) in the zone of 43R. The waste generation rate is estimated in the range of 21–22 tonne per day (TPD) and the per capita waste generation is

Fig. 15.1 Location of the study area in Himachal Pradesh

0.42 kg per person per day in the study region (Sharma et al. 2018). The collection efficiency of the region was observed around 60% that is not satisfactory for the proper waste management system. The location of the study area has been shown in Fig. 15.1.

The MSW dumpsite in Solan city is located in Salogra and experiences about 18.5–20 tonne per day of waste. The collection efficiency of the waste in the study location is 60% with a high fraction of organic waste being dumped at the Salogra location. Along with the waste collected from different households, the vegetable vendors also dispose of rotten fruits and vegetables at the Salogra dumpsite leading to an increased fraction of organics in the waste. The dumpsite is an open dumpsite and is non-engineered landfill site.

15.3 Methodology

The section has been explained in the following sub-headings as follows:

15.3.1 Collection of Samples

The leachate samples were collected from the downstream section of the municipal solid waste dump site in Salogra in Solan region whereas the groundwater samples were collected from hand pumps near the periphery of the dumping site. All the samples were collected for two seasons, i.e. monsoon season and winter seasons to evaluate the seasonal variation on the quality of groundwater. The samples were collected in tight plastic bottles for the evaluation studies. The water and leachate samples were then transported to the laboratory and analysed for physico-chemical and heavy metal parameters within 2 days according to the standard procedures (Parameswari et al. 2015).

Experimental investigations were performed as per APHA 22nd Edition 2012 for analyses of pH, Turbidity, Total Dissolve Solid (TDS), Chloride, nitrate, sulfate, trace metals, bacteriological parameters, biological oxygen demand (BOD), and chemical oxygen demand (COD). The pH of the samples was also measured to site with the help of pH strip. The turbidity of sample solution can be measured by using Nephelometer. It is usually measured in Nephelometric turbidity units (NTU). The heavy metal content of water and leachate were determined using an atomic absorption spectrophotometer (AAS). The working principle of the AAS basically involves the utilization of free atoms (gas) that are generated from the atomizer absorbing the radiation generated at that particular frequency.

15.3.2 Aggregate Index Method

Aggregate index or water quality index method was applied to evaluate the quality of groundwater collected within the periphery of dumping site. The water quality index method utilized for determining the quality of the water was based on the method as proposed by National Sanitation Foundation (Swamee and Tyagi 2000, 2007) to evaluate the toxicity potential of leachate into the groundwater. In particular, the study includes how indices are calculated and how they are used in determining water quality index using National Sanitation Foundation work.

15.3.2.1 Water Quality Index (NSF Method)

The sub-index of different water quality variables (surface water and groundwater) has been determined by the National Sanitation Foundation method to evaluate the water quality index. The method including a selection of parameters and assigned weightage to each parameter based on its importance and the parameters including pH, turbidity, total dissolved solids, and biochemical oxygen demand was introduced. Thereafter, the data were recorded and then transfer to a weighting curve chart, where a numerical value of Q_i is obtained. The mathematical expression for national sanitation foundation (WQI) is given below:

$$\mathrm{WQI} = \sum_{i=1}^{n} Q_i W_i$$

Q_i ith water quality parameter for sub-index
W_i weight assigned with ith water quality parameter
n number of water quality parameters.

15.4 Results and Discussions

15.4.1 Leachate Analysis

Laboratory tests were performed for the analysis of leachate. For this purpose, different parameters were analysed like; pH, TDS, nitrate, sulfate, heavy metals, BOD, COD, and bacteriological analysis for leachate samples. The physico-chemical characteristics of leachate samples have been shown in Table 15.3.

The pH value observed for leachate sample was found 7.4 in monsoon season (September 2015) and 7.8 in the winter season (February 2015) whereas the concentration of TDS was observed high for both the monsoon season and winter season, i.e. 968 and 2000 mg/L respectively. The COD for leachate sample was observed 7150 and 7200 mg/L that clearly indicates the presence of higher amount of inorganic matter in the municipal solid waste. The BOD in leachate sample was also reported very high for both the seasons, i.e. 2300 and 2410 mg/L. The concentration of sulfate of leachate sample was observed 50 and 48 mg/L for both the seasons including monsoon season and winter season. These values have been found lesser than the values observed from earlier works as reported by Pillai et al. (2014) whereas the concentration of sodium (1400–8000 mg/L) and chloride (900–11,500 g/L) were reported higher for both the seasons. Apart from this, the

Table 15.3 Physico-chemical parameters of leachate samples

S. No.	Parameters	Results (September 2015)	Results (February 2016)
1.	Conductivity (μmhos/cm)	2960	2880
2.	pH	7.4	7.8
3.	TDS (mg/L)	1968	2000
4.	Sulfate (mg/L)	50	48
5.	Nitrate (mg/L)	27	28
6.	Ammoniacal nitrogen (mg/L)	Nil	5
7.	BOD at 27 °C 3 day (mg/L)	2300	2410
8.	COD (mg/L)	7150	7200

Table 15.4 Testing results of leachate samples for heavy metal

S. No.	Parameters	Values (mg/L) (September 2015)	Values (mg/L) (February 2016)
1.	Lead	0.0351	0.04
2.	Zinc	0.0838	0.078
3.	Chromium	BDL	BDL
4.	Nickel	0.0168	0.0189
5.	Iron	0.21	0.28

groundwater showed higher values of total dissolved solids ranged between 470–2990 mg/L during post-monsoon and 120–2800 mg/L during pre-monsoon, whereas chloride content ranged between 140–1500 mg/L during post-monsoon and 120–2800 mg/L during pre-monsoon. The BOD and COD of the groundwater were found nil for monsoon season and winter season, respectively. The concentration of parameters for leachate sample including calcium, magnesium, nitrate, and TDS were observed on the higher side than the prescribed limits. The study clearly indicated that most of the parameters have been found exceeding their permissible limits. Moreover, the results revelled were found greater than the earlier works as reported in the literature (Parameswari et al. 2015).

The heavy metal concentration of leachate samples has been listed in Table 15.4. The results revealed that the concentration of lead content was higher than permissible limits for the leachate sample, i.e. 0.0351 mg/L that may cause problems such as brain damage, kidney failure, etc. The concentration of zinc content in leachate has been found 0.0838, 0.078 mg/L for both the seasons. The concentration of Zn was found within the permissible limits (0.264 and 0.947 mg/L) of the World Health Organization for all samples whereas the concentration of chromium in leachate was found below the detection limit. The COD was also reported high 518.14 and 725.01 mg/L.

15.4.2 Groundwater and Surface Water Analysis

Laboratory tests were performed for determining the effect of decomposition of solid waste and percolation of on groundwater quality. For this purpose, different parameters were analysed like pH, total dissolved solids, nitrate, sulfate, heavy metals, BOD, and COD testing for surface water and groundwater. Table 15.5 shows testing of surface and groundwater samples for physico-chemical parameters and comparison with WHO standards.

The turbidity for surface water and groundwater was determined to be 7 and 40 NTU, respectively for samples collected during September 2015. However, it was determined to be 8 and 42 NTU for samples obtained in February 2016. This shows that turbidity of groundwater was significantly higher than surface water

Table 15.5 Physico-chemical analysis of surface water and groundwater samples

S. No	Parameters	Result (surface water) September 2015	Results (surface water) February 2016	Results (groundwater) September 2015	Results (groundwater) February 2016	Acceptable limits (WHO)	Permissible limits (WHO)
1.	Turbidity (NTU)	7	8	40	42	–	–
2.	EC (micro mhos/cm at 25 °C)	598	616	372	385	–	–
3.	pH	8.28	8	7.41	8.2	6.5–8.5	No relaxation
4.	TDS (mg/L)	389	400	242	250	500	2000
5.	Sulfate (mg/L)	18	20	63	68	200	400
6.	Nitrate (mg/L)	0.15	0.2	BDL	BDL	45	No relaxation
7.	Ammoniacal nitrogen (mg/L)	Nil	Nil	Nil	Nil	–	–
8.	BOD (mg/L)		6.0	Nil	Nil	–	30 (surface water)
9.	COD (mg/L)	20	22	Nil	Nil	–	250 (surface water)

Table 15.6 Heavy metal analysis of surface water and groundwater comparison with WHO standards

Parameters	Surface water (September 2015)	Groundwater (September 2015)	Surface water (February 2016)	Groundwater (February 2016)	Acceptable limits (WHO)	Permissible limits (WHO)
Lead (mg/L)	0.0241	0.0271	0.0271	0.025	0.01	No relaxation
Zinc (mg/L)	0.0137	0.0178	0.014	0.02	5	15
Chromium (mg/L)	BDL	BDL	BDL	BDL	0.05	No relaxation
Nickel (mg/L)	0.0056	0.0024	0.008	0.0028	0.02	No relaxation

sources for both the seasons but illustrates no marked difference for intra-source comparisons. pH values observed for the entire monitoring campaign were within 'near-neutral ranges', and hence were suitable for disposal purposes. Similarly, TDS and sulfate concentrations were well within the permissible ranges prescribed by WHO. No BOD and COD concentrations were reported for groundwater sources over the two monitoring seasons and the concentrations obtained for surface water sources were well within the permissible limits. These reported results were lesser than earlier values reported in the literature (Akinbile and Yusoff 2011). The results clearly indicate that some of the parameters show the amount of traceable pollution level but are below the World Health Organization (WHO) and the National Standard for Drinking water quality (NSDWQ) limits. The results of heavy metals for surface water and groundwater was shown in Table 15.6.

The major heavy metals obtained in the analysis of the collected samples revealed concentrations lead, zinc, chromium, and nickel. It was observed that the lead concentrations from both surface and groundwater exceeded the acceptable limits prescribed by WHO (Parameswari et al. 2015). Zinc and Nickel concentrations were well within or below the prescribed limits. Chromium concentrations were undetectable being less than the least count of the instrument. Biological examination of the collected samples was carried out and the analysis revealed that biological contamination was absent in both water samples.

15.4.3 Water Quality Index

Groundwater is highly susceptible to pollution by leachate. The degree of pollution depends on number of factors including the toxicity potential of leachate, the underlying soil strata which determines the hydraulic gradient of the permeability of

the leachate, the depth of water table and the direction of flow of groundwater. These conditions primarily determine the seepage of leachate and contamination of groundwater.

Water quality index is an effective approach for the prediction of water quality that is found helpful for the selection of allocated and effective treatment processes. In this context, it is depicted that the indices utilized in the aggregate indexing are based on the different types of water quality parameters depending upon the importance of each individual parameter and their comparison with the standards. The water quality indexing or aggregate indexing has been determined by National Sanitation Foundation (NSF) Method based on the different physico-chemical parameters utilized for the study purpose including pH, BOD, turbidity, and total solids.

Calculation of Sub-indices The sub-indices of different water quality parameters for surface water and groundwater were determined based on water quality index method named National Sanitation Foundation of weighting curve chart given by (NSF) as given in Tables 15.7 and 15.8. The gradation of water quality index was listed in Table 15.9. After the calculation of sub-indices of groundwater and surface water for both seasons (monsoon and winter) in September 2015 and February 2016, respectively, water quality index has been determined to analyze the quality of surface water and groundwater. The water quality was measured on the scale of 0–100 and the quality of water varies in the range of very bad to excellent.

The water quality index based on National sanitation foundation (NSF) of various sub-indices for different parameters of surface water and groundwater are shown in Tables 15.10 and 15.11, respectively

The weightage to different quality variables were given based on National Sanitation Foundation method (NSF) of water quality index. The product of

Table 15.7 Sub-indices of surface water quality variables (NSF)

S. No.	Parameters	Surface water (September 2015)	Sub-index (S)	Surface water (February 2016)	Sub-index (S)
1.	Turbidity	7	81	8	79
2.	EC (micro mhos/cm at 25 °C)	598	–	616	
3.	pH	8.28	83	8	87
4.	TDS (mg/L)	389	49	400	48
5.	Sulfate (mg/L)	18	–	20	–
6.	Nitrate (mg/L)	0.15	–	0.2	–
7.	Ammoniacal nitrogen (mg/L)	Nil	–	Nil	–
8.	BOD at 27 day (mg/L)	6.2	49	6.0	50
9.	COD (mg/L)	20	–	22	–

Table 15.8 Sub-indices of ground water quality variables (NSF)

Parameters	Ground water (September 2015)	Sub-index (S)	Ground water (February 2016)	Sub-index (S)
Turbidity (NTU)	40	44	42	42
EC (micro mhos/cm at 25 °C)	372	–	385	
pH	7.41	94	8.2	82
TDS (mg/L)	242	69	250	67
Sulfate (mg/L)	63	–	68	–
Nitrate (mg/L)	BDL	–	BDL	–
Ammoniacal nitrogen (mg/L)	Nil	–	Nil	–
BOD at 27 °C (mg/L) 3 day(mg/l)	Nil	0	Nil	0
COD (mg/L)	Nil	–	Nil	–

Table 15.9 Water quality index table (NSF)

S. No.	Range	Quality of water
1.	0–25	Very bad
2.	26–50	Bad
3.	51–70	Medium
4.	71–90	Good
5.	91–100	Excellent

Table 15.10 Water quality index of surface water quality variables (NSF)

Parameters	Sub-indices (September 2015) S_i	Weightage w_i	$S_i \times w_i$	Sub-indices (February 2016) S_i	Weightage w_i	$S_i \times w_i$
Turbidity (NTU)	81	0.25	20.25	79	0.25	19.75
pH	83	0.315	26.15	87	0.315	27.40
BOD (mg/L)	49	0.26	12.74	50	0.26	13
TDS (mg/L)	49	0.25	12.25	48	0.25	12

sub-index and weightage has been calculated and the summation of product and weight of these calculated sub-indices has been determined. The summation of surface water and weight of surface water in the year September 2015 was 71.39 and in the year February 2016, it was 72.15. The water quality lies in the range of 71–90 which indicated the good quality of water and the impact of leachate on surface water was not significant as yet. As in the case of groundwater quality,

Table 15.11 Water quality index of groundwater quality variables (NSF)

Parameters	Sub-indices (September 2015) S_i	Weightage w_i	$S_i \times w_i$	Sub-indices (February 2016) S_i	Weightage w_i	$S_i \times w_i$
Turbidity (NTU)	44	0.25	11.0	42	0.25	10.50
pH	94	0.315	29.61	82	0.315	25.83
BOD (mg/L)	0	0.26	0	0	0.26	0
TDS (mg/L)	69	0.25	17.25	67	0.25	16.75

quality index in the initial year was 57.86 and in the final year 2016, it was 53.08. This lies in the medium quality range 51–70 that indicated some minor contamination of groundwater, and if unchecked could deteriorate further due to seepage of leachate in the groundwater.

15.4.4 Soil Pollution

The physico-chemical and heavy metals analysis of soil samples in the vicinity of the dumpsite were carried out for possible contamination and are shown in Tables 15.12 and 15.13, respectively.

The observed value of pH for the soil sample was slightly acidic because organic acids are formed by the degradation of the organic matter. Apart from this, sodium, sulfate, chloride, and nitrate content were observed 760, 20.63, 960, and 103.55 mg/L. This higher concentration of parameters was mainly due to improper disposal of solid waste and percolation of leachate into soil causing adverse effects to the soil. These results were compared to those as reported in the text showing similar contamination levels (Ogundiran and Afolabi 2008; Akinbile and Yusoff 2011).

Table 15.12 Testing results of physico-chemical parameters for soil samples

S. No.	Parameters	Results (September 2015)	Results (February 2016)
1	pH	7.9	7.11
2	Conductivity (micro mhos/cm at 25 °C)	600	560
3	Sulfate (mg/kg)	345	325
4	Nitrate (mg/kg)	17	15
5	Ammoniacal nitrogen (mg/kg)	18	16

Table 15.13 Testing results of heavy metal parameters for soil samples

S. No.	Parameters	Heavy metals (mg/kg) (September 2015)	Heavy metals (mg/kg) (February 2016)
1	Iron	1.2	1.4
2	Nickel	0.428	0.440
3	Lead	2.908	3.0
4	Chromium	0.050	0.070
5	Zinc	1.850	1.860

From Table 15.13, it is observed that heavy metals in soil sample included iron, nickel, chromium, and zinc has been found 1.2, 0.426, 0.050, and 1.850 mg/kg in monsoon season and 1.4, 0.440, 0.070, and 1.860 mg/kg in winter season, respectively. The value for lead was found on the higher side it was 2.908 mg/kg in September 2015 and 3.0 mg/kg in February 2016. pH is a key factor which affects the leaching of the metals from upper soil profile to lower. If the pH is low, it will accelerate the migration of metal from upper to lower soil profile. In municipal solid waste dump sites, pH depends upon anaerobic decomposition of waste. More anaerobic decomposition means more acid will produce, it will decrease the pH and in acidic condition, metal will move from upper to lower soil profile.

15.5 Conclusions

Leachate causes soil and water contamination as it percolates through the soil strata. The present study reports the possible water and soil pollution due to leachate generated at an open dumpsite in Salogra (Solan District) in Himachal Pradesh from samples collected over two seasons. Parameters tested for leachate samples show very high concentrations of certain physico-chemical parameters leading to increased toxicity of the leachate generated. Heavy metals concentration was significantly in lesser concentrations. The water quality index assessment carried out shows that the surface water quality was good and thereby had not been affected by the leachate contamination but groundwater quality was classified as relatively medium suggesting some probable contamination. Further, there is a possibility of further contamination of groundwater due to the process of continued dumping of waste. Determination of soil characteristics showed that not much adverse effect has happened yet at the dumpsite but with continued dumping of waste at the site, possibility exists of increased contamination at the dumpsite. Hence, for the prevention of leachate percolation into the aquifer, the trend of open dumping should be restricted and properly engineered landfill facility should be made with liner and leachate collection system for the safe discharge of leachate.

Conflict of Interest On behalf of all authors, the corresponding author states that there is no conflict of interest.

References

Akinbile CO, Yusoff M (2011) Assessment of groundwater quality near a municipal landfill in Akure, Nigeria. Int Conf Environ Sci Technol 6:83–87

Bhalla G, Swamee PK, Kumar A, Bansal A (2012) Assessment of ground water quality near municipal solid waste landfill by an aggregate index method. Int J Environ Sci 2:1409–1503

Chang NB, Davila E (2008) Municipal solid waste characterization and management strategies for the Lower Rio Grande Valley, Texas. Waste Manag 28:776–794

CPCB (2013) Status report on municipal solid waste management. Retrieved from http://www.indiaenvironmentportal.org.in/content/374639/status-report-on-municipal-solid-wastemanagement

Hancs A, Novak P, Dvorak M, Habart J Svehla P (2008) Composition and parameters of household bio-waste in four seasons. Waste Manag 31:1450–1460

Hazra T, Goel S (2009) Solid waste management in Kolkata, India: practises and challenges. Waste Manag 29:470–478

Kaushik MK, Sethi S (2007a) Study on ground water contamination due to landfill leachate in India. In: Global conference of production and industrial engineering (CPIE-2007). Dr. B. R. Ambedkar NIT, Jalandhar, India

Kaushik MK, Sethi S (2007b) Solid waste management in Punjab—a study. In: International congress of environmental research (ICER-07). Govt. Geetanjali Girls P. G. College, Bhopal, Dept. of Higher Education, Govt. of M.P., India

Kumar D, Alappat BJ (2005) Evaluating leachate contamination potential of landfill sites using leachate pollution index. Clean Technol Environ Policy 7:190–197

Longe EO, Balogun MR (2010) Groundwater quality assessment near a municipal landfill, Lagos, Nigeria. J Appl Sci Eng Technol 2:39–44

Manaf LA, Samah MA, Zukki A (2009) Municipal solid waste management in Malaysia: practices and challenges. J Waste Manag 29:2902–2906

Mor S, Ravindra K, Dahiya RP, Chandra A (2006a) Leachate characterization and assessment of groundwater pollution near municipal solid waste disposal site. Environ Monit Assess 118:435–456

Mor S, Khaiwal R, Dahiya RP, Chandra A (2006) Leachate characterization and assessment of groundwater pollution near municipal solid waste landfill site. Environ Monit Assess 435–456

Nagarajan R, Thirulaisamy S, Lakshmanan E (2012) Impact of leachate on groundwater pollution due to non-engineered municipal solid waste landfill sites of Erode city, Tamil Nadu, India. Iran J Environ Health Sci Eng 9:1–12

Ogundiran OO, Afolabi TA (2008) Assessment of the physico-chemical parameters and heavy metal toxicity of leachate from municipal solid waste open dumpsite. Int J Environ Sci Technol 5:243–250

Parameswari K, Mudgal BV, Padmini TK (2015) Environment development and sustainability. https://doi.org/10.1007/s10668-015-9668-4

Pillai S, Peter AE, Sunil BM, Shrihari S (2014) Soil pollution near a municipal solid waste disposal site in India. In: International conference on biological, civil and environmental engineeringg (BCEE-2014), Dubai (UAE), 17–18 Mar 2014

Puri A, Kumar M, Johal E (2008) Solid waste management in Jalandhar city and its impact on community health. Indian J Occup Environ Med 12:76–81

Rana R, Ganguly G, Gupta AK (2015) An assessment of solid waste management system in Chandigarh city, India. Electron J Geotech Eng 20:1547–1572

Sethi S, Kothiyal NC, Nema AK, Kaushik MK (2013) Characterization of municipal solid waste in Jalandhar city, Punjab, India. J Hazard Toxic Radioactive Waste 17:97–106

Sharma A, Kaushik MK, Kumar A, Bansal A (2016) Assessment of ground water quality and feasibility of tire derived aggregates for use as a leachate drainage material. Electron J Geotech Eng 21:3113–3136

Sharma A, Ganguly R, Gupta AK (2018) Matrix method for evaluation of existing solid waste management system in Himachal Pradesh, India. J Mater Cycles Waste Manag. Available online at https://doi.org/10.1007/s10163-018-0703-z. (Article in Press)

Shekdar AV (2009) Sustainable solid waste management: an integrated approach for Asian countries. Waste Manag 29:1438–1460

Shivasharanappa SP, Huggi MS (2011) Assessment of ground water quality characteristics and water quality index of Bidar city and its industrial area, Karnataka state, India. Int J Environ Sci 2(2):965–976

Swamee PK, Tyagi A (2000) Describing water quality with an aggregate index. J Environ Eng 126:451–455

Swamee PK, Tyagi A (2007) Improved method for aggregation of water quality sub-indices. J Environ Eng 133:220–225

Part V
Coatings

Chapter 16
Sustainable Coating Design and Role of Liquid-Mediated Contact

R. K. Upadhyay and L. A. Kumaraswamidhas

Abstract Development of new technological innovations needs more reliable and cost-effective materials for design. However, their overall working performance did not depend on its intrinsic properties. Generally, it depends on various operating and environmental conditions such as load, sliding velocity, time, temperature, and humidity. In the present time, loss of material during sliding contact is a major concern for all industries operating under severe contact condition. Hence, the industrial practice has accelerated the application of tribological study. Coating design in tribology plays an important role to eliminate material degradation and resist contact hysteresis. In the current work, interstitial nitride (tungsten/tungsten nitride—W/W_2N) multilayer coatings were prepared by physical vapor deposition process, and their surface tribological behavior is investigated. Influence of liquid-mediated contact and surface adhesion phenomena with intrinsic mechanism between sliding pairs is also discussed. The scope of the work aims small to large scale automotive components for better tribological performance with high productivity.

Keywords Coating design · Tribology · Surfactants · Adhesion
Physical vapor-deposition · Sliding contact · Adhesion · Liquid-mediate contact

16.1 Introduction

Surface coating design has become an extremely well-established technology for improving component performance by resisting materials failure and chemical degradation. Coating technology is versatile that adds functional properties within the

R. K. Upadhyay (✉)
Indian Institute of Technology, Kanpur 208016, India
e-mail: ramku@iitk.ac.in; ramku.iitk@gmail.com

R. K. Upadhyay · L. A. Kumaraswamidhas
Indian Institute of Technology (ISM), Dhanbad, India

R. A. Agarwal et al. (eds.), *Pollutants from Energy Sources*,
Energy, Environment, and Sustainability,
https://doi.org/10.1007/978-981-13-3281-4_16

substrate material to perform the specific function without yield. With ever increasing physical, chemical, and mechanical properties of materials, coating enhances the reliability and overall operating life of the component (Kathrein et al. 2005; Dey and Deevi 2003). In order to provide efficient tribological properties in terms of low friction and wear, a suitable coating methodology must be selected. In recent times, several coating deposition methods and techniques were developed to overcome surface intrinsic/extrinsic problems (Upadhyay and Kumaraswamidhas 2014a). The superficial enhancement of material tribological properties with the aid of single/multilayer physical vapor deposition (PVD), chemical vapor deposition (CVD), thermal spraying, and electrochemical deposition coatings has now become extensively used in practical application. Addition of these coatings in the form of a thin and hard layer on metallic surfaces can provide desired mechanical, physical, and chemical properties. Among all the coatings deposition, PVD is more versatile due to its sputtering suitability on nonmetallic surfaces (Upadhyay and Kumaraswamidhas 2014a). While comparing other coatings of thin and hard film, the multilayer coating system has been demonstrated to be one of the superior technological advances in the field of coating tribology. The use of thin/thick hard multilayer coating offers extended lifetime and machining performance of any component due to its added mechanical properties such as fracture resistance, hardness, and controlled wear resistance. These mechanical properties can vary with the rate of increasing/decreasing coating/film thickness (Kathrein et al. 2005; Dey and Deevi 2003; Upadhyay and Kumaraswamidhas 2014a, 2015). In practical tribological application, numerous components are operating under the dry sliding contact, whose functionality needs to be controlled by applied coatings.

In order to smoothen the dry sliding contact, the coating/film hardness must be high enough to carry loads and properly combined with good adhesion, low plastic deformation, resistance to shock, and resistance to oxidation at relatively high temperatures (Upadhyay and Kumaraswamidhas 2015; McIntyre et al. 1990; Smith et al. 1998; Harris et al. 2001). In order to fulfill the desired requirements, a variety of coating methodology has been proposed to achieve better tribological behavior. Nanoscale multilayered coatings with a small number of thin layers on the substrate surface have been reported to be a promising deposition technique in dry machining. These nanoscale multilayer coatings are well known to inhibit crack propagation during applied load, minimize developed residual stresses, and provide high adhesion and high microhardness values to the deposited coating layers (Helmersson et al. 1987; Yashar and Sproul 1999; Basu et al. 2012; Khlifi et al. 2013; Niu et al. 2014). Multilayer structures can enhance surface properties such as hardness and resilience as compared to the single-layer homogeneous coatings. It combines the favorable properties of the target materials and supports other material on which it has to be deposited (Rahman et al. 2011; Sproul 1996; Upadhyay and Kumaraswamidhas 2016a; Meneve et al. 1997; Prabhu et al. 2014; Kulkarni et al. 2013). Low friction coefficient, chemical, and physical properties may realize by combining various physical and chemical properties of monolayer/single-layer analogues in a multilayer coating system (Bull and Jones 1996; Zheng and Ramalingam 1996; Zhang et al. 1998). Interstitial nitrides of transition elements and

carbides are extensively used in engineering sciences to provide high melting point and hardness, low friction and wear values, chemical inertness, respectively. These superficial properties can be easily realized by combining individual or multi-properties of the various single-layer/monolayers in a multilayer coating system.

From the above literature, it is clear that the material properties can be preciously tailored according to the specific need by applied coatings. However, selecting the target material is one of the critical assessments, which needs to be identified before the coating deposition (Kothari and Kale 2002; Upadhyay and Kumaraswamidhas 2016b). In the present study, novel high alloyed powdered metallurgical high-speed steel is developed and provided with tungsten/tungsten nitride (W/W_2N) multilayer coatings. The coating is deposited by PVD-unbalanced magnetron sputtering technique. The application of PVD coating ranges from the automotive industry to the mining industry. In automotive, various contact surfaces such as linings, bearings, piston ring, and cylinder walls can provide with PVD coatings for materials wear reduction. Also, for sustainable energy control, these components are provided with lubrication, which controls the heat dissipation. Drilling operation in mining industry generates excess temperature and results in tool/bit damage (Upadhyay and Kumaraswamidhas 2015). Application of PVD coatings in drilling bit enhances the tool life with a reduction in contact forces.

16.1.1 Prerequisite of Coating Design

Coating selection criteria are based on the base material properties, type of target material and method of deposition. Some of the basic prerequisites of coating selection are listed here as follows:

- Coating target material and base substrate material must suit each other.
- Coating target material must suit the selected counterpart for tribological study.
- Coating material must suit the specified running condition of a test.
- Coating thickness must suit the desired application.
- Coating adhesion between the substrate material and target material should be strong enough to resist delamination.

Suitability of coating and substrate material is defined in terms of better hardness, resistance to fracture, high coating adhesion, high ductility, and decreasing the amount of tensile stresses.

16.1.2 Type of Coatings

In tribology, coating technology is an effective and economical way to reduce friction and protect the substrate surface from wear out. However, selection of the

type of the material used for a given tribological application is still mysterious due to the involvement of many factors like substrate material property, counterparts, operating conditions, and machine parameters. Particularly, in the drilling operation, carbon-deposited coatings by chemical vapor deposition cannot sustain in extreme environmental conditions of high temperature and pressure. The thickness provided by the CVD coating is very less compared to the physical vapor deposition coating (Upadhyay and Kumaraswamidhas 2015). Under the influence of high pressure and increasing temperature, the bonding strength between the film and material becomes lower and results in coating spallation.

Different coating strategies have been proposed by the distinguished scientist to overcome surface problems, but there is no strict route to pick the modest one. Coating technology ranges from single layer to multilayer to gradient (Upadhyay and Kumaraswamidhas 2014b; Donnet and Erdemir 2004; Voevodin et al. 1998). They possess several advantages in the area of mechanical (hardness, toughness, stress, and adhesion behavior), physical (low friction, and diffusion barrier) and chemical (growth of metals) sciences. A different type of coating deposition with their characteristics has been illustrated in Fig. 16.1a–h. Depending on the application each coating has their advantages over others. Compare to monolayer/single-layer coatings, other coating techniques (Fig. 16.1b–h) require more investment, however, they provide improved physical, chemical, and mechanical properties to sustain contact hysteresis. The only demerit of these coatings is that if the thickness is increased beyond permissible limit coating surfaces tends to induce brittleness and results in spallation (Upadhyay and Kumaraswamidhas 2014a).

Single-Layer Coating

Single-layer coatings are the simplest one in design, see Fig. 16.1a. In most of the situations, coatings are deposited with single-layer structure such as chromium carbide (CrC), chromium nitride (CrN), titanium carbide (TiC), titanium nitride (TiN), titanium aluminum nitride (TiAlN), and diamond-like coating (DLC), etc. These coatings are not suitable where extremely low friction and wear resistance are of high interest. Hence, for better tribological performance different coating strategy should be adopted to strengthen the bonding between the films.

Sandwich Coating

In sandwich-type structures, different compositional arrangements deployed to achieve more than one property at a time (see Fig. 16.1b). In a simple machining process, the carbide–aluminum–nitride composition was used to gain high bonding strength, high operating temperature, and better wear resistance for stainless steel. Furthermore, nitride reduces the sticking of work material during the machining process.

Multicomponent Coating

Multi-component coatings are composed in the form of grains, particles, or fibers of two or more successive materials (see Fig. 16.1c). The multi-component coating with the addition of other constituents increases oxidation, hardness, and high operating temperature. Grains, basically involved with the surface boundary where

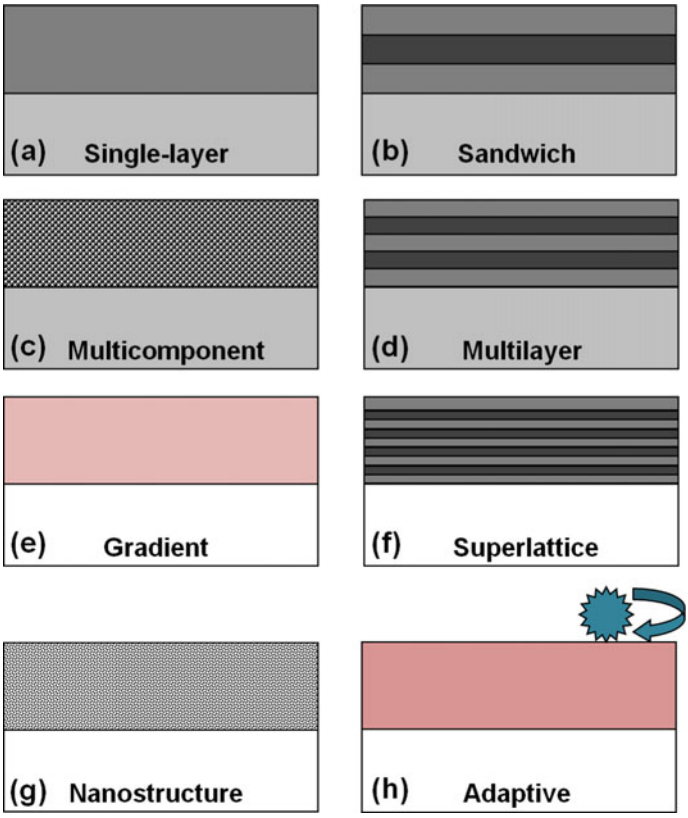

Fig. 16.1 Schematic representation of the different type of coatings available for the tribological process

the physiochemical process occurs and formation of a protective layer between consecutive material starts forming which further protect the surface from oxidation and high temperature.

Multilayer Coating

Multilayer coatings are periodically repeated structures of two or more materials, basically, successive layers of different composition (see Fig. 16.1d). The thickness of the coatings can vary from nanometers to few tenths of micrometers. These coatings possess higher toughness and hardness compared to other homogeneous material coatings. A thick layer of the multilayer structure can resist crack propagation by providing an interlayer, through which coating delamination should be neglected.

Gradient Coating

A graded structure improves the load carrying capacity of materials by changing the mechanical properties of softer materials with the addition of hard coatings over it

(see Fig. 16.1e). Gradient coating enables the material to distribute their load equally over a large area to reduce developed stresses in the coating–substrate interface. These coatings deposited onto the steel substrates by nitriding process using PVD technique. Coating deposition process largely affects the gradient coating structure by improving its adhesion properties and wear resistance. Gradient coatings act as a barrier to diminish failure mechanism by suppressing a sudden change in physiochemical and mechanical properties.

Superlattice Coating
Superlattice coatings are periodically repeated multilayer structures of titanium nitride/tungsten nitride and titanium nitride/chromium nitride (TiN/WN, and TiN/CrN) with a thickness in the range of 5–25 nm (see Fig. 16.1f). These coatings possess excellent hardness, as well as toughness, and thermal stability compared to monolayer analogues. They composed of a columnar structure extending throughout the coating. Superlattice coating with thin lamellae is used in cutting steels to improve their resistance against wear, corrosion, and oxidation process.

Nanostructure Coating
Nanostructure coatings composed of nanostructure films and nanocomposite films, the particle size of nanostructures were in the range of nanometric scale (see Fig. 16.1g). It is a nanoscale coating, composed of amorphous and crystalline phases. The crystal dislocation behavior controlled by the decreasing the size of the particles in the interface. The hardness, elastic modulus, and toughness increase with decreasing grain size according to the well known Hall–Petch relation (Hansen 2004). Nanocrystalline material coatings are best suited to the tribological application due to their high thermal expansion, low thermal conductivity, and better optical, magnetic, electronic properties.

Adaptive Coating
Adaptive coatings can change their behavior according to the processing parameters, temperature, load, and environment conditions (see Fig. 16.1h). Adaptive coating involves a deep knowledge of crystal structure, material's intrinsic properties, and relationship with their processing parameters. Oxide has better lubrication behavior at higher temperatures (>500 °C). Diamond-like carbon (DLC) and titanium carbide/diamond-like carbon (TiC/DLC) coatings provide self-regulation of surface mechanical properties (Bull and Jones 1996). At extreme load condition ($\sim$150 N) these coatings distributed the load on a larger surface area and resisted brittle fracture.

16.1.3 Coating Deposition Techniques

There are several deposition techniques, but only a few were selected to demonstrate tribological application due to restricted low adhesion strength and thickness (Mellor 2006). Excessive thickness induces poor adhesion and brittleness in the

Table 16.1 Various coating deposition techniques for industry

State	Deposition phases	Technique	Source
Surface treatment technology	Vapor/gas state	PVD	Plasma
		CVD	
	Solution state	Chemical deposition	Chemical reduction
		Electrochemical deposition	Electroless deposition
		Sol-Gel	Chemical conversion
	Molten state	Laser	Plasma
		Thermal spraying	
		Welding	

coating. Coating deposition process is divided into three basic groups, i.e., gaseous state, solution state, molten or semi-molten state (see Table 16.1). The common deposition methods are physical vapor deposition, chemical vapor deposition, thermal spraying, and electrochemical deposition. In recent times, many new deposition techniques are being developed to provide a wide range of coating selection that depends on the required application. Selection of the coating material for deposition is a time consuming, and an expensive approach. Furthermore, it allows the researchers a tough task to make their decision before proceed. Alternatively, it is difficult to test each proposed material for a particular tribological application. The most significant way to proceed is with a trial and error method by which a better one should be selected and proposed.

16.1.4 The Significance of Liquid-Mediate Contact

Liquid between contact surfaces plays an important role in tribology. The most dominant and widely recognized role of liquids surfactants in tribology is to control friction and wear by providing a lubricating mechanism. Surfactants have unique properties and characteristics that make them ideal for many lubrication based applications. Surfactants have both hydrophilic and hydrophobic nature that imparts partial affinity toward polar and nonpolar surfaces (see Fig. 16.2a, b) (Mittal 2008). The hydrophobic surfactant molecules consist of nonpolar moieties such as carbon–hydrogen units. The hydrophilic surfactant molecules contain ionic functional groups such as ammonium. Thus, surfactants are least partially soluble in polar liquids (water) as well as nonpolar liquid (hexane). Three main types of surfactants are ionic, nonionic, and zwitterionic. Zwitterionic surfactants have both anionic and cationic constituents. Ionic surfactants are cationic (positive charge) or anionic (negative charge) when dissolved in aqueous media from a neutral salt form.

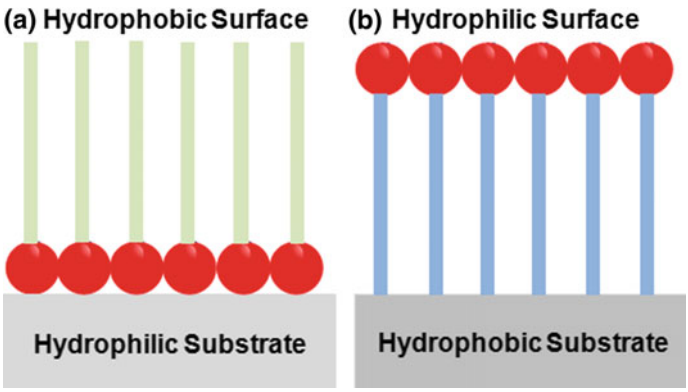

Fig. 16.2 Surfactant molecules represented by spheres and lines adsorbed at **a** hydrophilic substrate, and **b** hydrophobic substrate

Cationic surfactants are generally made of cetyl trimethyl ammonium bromide (C-TAB) salts. Nonionic surfactants generally consist of alcohols that have attached hydrocarbon chains. Anionic surfactant includes sulfate functional groups in salt forms such as sodium dodecyl sulfate. Nonionic surfactants do not equip with any charges, therefore, they are not found in salt forms. The addition of surfactant provides more balanced bonding in the interface, hence, reduces surface tension. Bare surfaces contain water molecules (hydrogen bonds) that are strongly attached to the nearby surfaces, which increases the surface tension and results in high friction coefficient. However, the addition of surfactant on the surface breaks the bonding of strong water molecule and provides low surface tension, friction coefficient, respectively. In tribology, when two solid surfaces are in relative contact, a thin monolayer of surfactant into interface act as a deformation barrier where the chemisorptions and physisorption process of surfactants influence the friction coefficient. With increases in surfactant film thickness, direct solid asperity contact diminishes and provides lower friction coefficient value (Davidson et al. 2006). However, the more thick film will provide a higher friction coefficient due to solvent viscosity and internal friction. As the film thickness increases, counterpart material required more amount of shearing force to pass the sliding surface. However, the increased drag force opposing the materials movement on account of increased internal friction force.

The adsorption of monolayer surfactants (see, Fig. 16.2a, b) causes hydrophilic substrates to change to hydrophobic surfaces (Mittal 2008). The process involved orientation of hydrophobic functional head groups toward the substrate. Similarly, monolayer adsorption on hydrophobic substrates changes them to hydrophilic substrates which makes it easier to retain polar lubricants molecules at the surface. During contact, the presence of both head and tail structure in surfactant influences the resultant friction coefficient. Surfactant molecules with the acidic head group are adsorbing onto metal surfaces via covalent or hydrogen bonding with low shear

strength. The tail group not only helps to dissolve oil into a medium but also it aligns perpendicular to the surface and interacts cohesively through Van der Waals force. This interaction produces a hydrocarbon layer while the head group is adsorbed on the base material. The chemistry of the tail group also influences the resultant friction.

Given the advantageous properties of the surface coating and liquid lubrication mechanism, the current work focuses on the tribological investigation of tungsten/tungsten nitride multilayer coating deposited by a physical vapor deposition technique. The application of prepared surfaces ranges from nano to microelectronics industry to automotive to the aerospace industry. Potential targeted devices or components are a storage device, semiconductor, interior/exterior decorative parts, piston, piston rings, injection system, and bearings.

16.2 Materials for Investigation and Adopted Methodology

16.2.1 Substrate Material

High alloyed powdered metallurgical high-speed steel was chosen as a base material due to high abrasive wear resistance and compressive strength. The substrate has a hardness value of 62 HRC with following chemical composition (C: 1.28 wt%, Cr: 4.2 wt%, Mo: 5 wt%, W: 6.4 wt%, and V: 3.1 wt%). Nitriding process results in a hard surface layer, which gives resistant to wear and erosion. However, sometimes this process induces brittleness and results in coating delamination due to exposure of substrate surface under mechanical or thermal shock. At this stage, the bonding between the coating and substrate material is weakened due to the mismatch in the elastic modulus (Upadhyay and Kumaraswamidhas 2015).

16.2.2 Coating Target and Material

A nitride is a compound of nitrogen where it has a formal oxidation state of −3 with a wide range of properties and applications (Greenwood and Earnshaw 1997). Nitrides are considered to be refractory materials with high lattice energy. These higher lattice energies are associated with a stronger attraction of N^{3-} toward the metallic cation. Transition metal nitrides are refractory, with high melting point and chemically stable. The nitrogen element forms compound with other elements and are of equal or lower electronegativity. The other factors which influence the formation of nitride are the size of respective atoms and the electronic bonding between atoms. The nitrides are divided into five general categories (Pierson 1996),

i.e., interstitial, covalent, intermediate, salt-like, and volatile nitrides. The present study focuses only on interstitial nitrides. Interstitial nitrides have a large variation in atom size and electronegativity. The strong metallic bonding between the atoms gives high electrical and thermal conductivity. Tungsten nitride (W_2N) is a nitride of tungsten and an inorganic compound. Tungsten nitride is a brown-colored hard and solid ceramic material that is electrically conductive and decomposes in water. Tungsten application ranges from microelectronics devices to hard metallic coatings.

16.2.3 Method of Deposition and Tribology Test

Physical vapor deposition (PVD-W/W_2N) films were fabricated under argon, nitrogen environment. The achieved film thickness was 2.70 μm (A/B = 0.3/0.6 μm). The following parameters such as coating temperature 300 °C, bias voltage −75 V, working pressure 2×10^{-1} Pa, and source to substrate distance 100 mm, nitrogen flow rate 60 sccm, the argon flow rate 90 sccm, cathode current 3 A, and power 4 kW were used for coating deposition process. The magnetron target dimensions are 600 × 125 mm (height and width). Pin-on-Disk tribometer has been used to determine friction and wear response of the prepared coatings. In tribometer, a vertical pin consists of alumina ball (Dia 6 mm) rotates against a substrate material (Dia 20 mm) at 5 N load and sliding speed of 9.41 cm/s. Alumina ball of hardness 66 HRC and purity over 92% is utilized as sliding counterpart. Before coating, deposition substrate material was mirror polished and the value of surface roughness was 2 μm. After tribology tests, coating microstructure and the presence of different phases were evaluated by scanning electron microscopy and X-ray diffraction technique.

16.2.4 Mechanical Investigation

Mechanical investigation of coatings was done by scratch and nanoindentation tests see Fig. 16.3a–c. The scratch adhesion tests were carried out by the scratch tester at a load range of 1–100 N. A diamond Rockwell indenter of the spherical tip (radius 200 μm) scratches the surface at a constant speed of 10 mm/min. The total length of scratch distance was 10 mm. At some point, due to poor load carrying capacity at the coating–substrate interface result in chipping or flaking of the coating. Normally, three parameters are measured by the integrated sensors first: residual penetration depths, second: normal and tangential loads, and third: acoustic emission intensity. The nanoindentation test measures the movement of a diamond probe in contact with a surface, where the depth of indentation was 2 μm. In order to make a load–displacement curve measurement, a continuously increasing load is applied, and the probe indents the coating surface. Force, displacement, and time

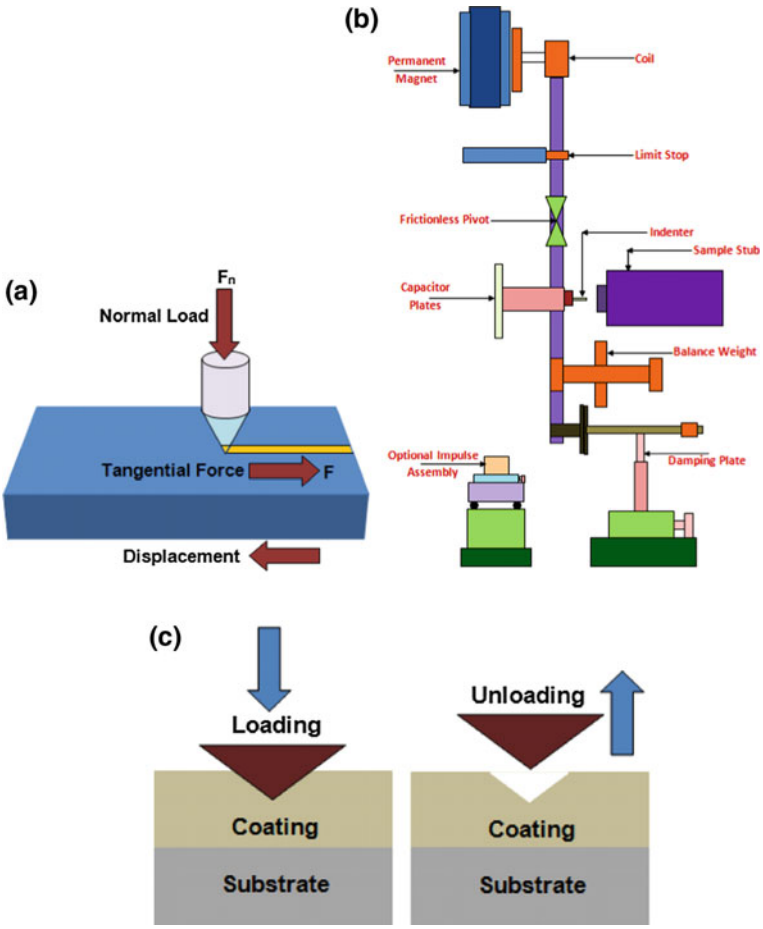

Fig. 16.3 Schematic representation of **a** scratch process, **b** nanoindentation and **c** loading and unloading process during nanoindentation measurement

are recorded throughout the test. It can be used with low load head (0.1–500 μN) or high load head (0.1–20 N). The loading, dwell, and unloading time of the indentation process were 20, 10, and 20 s, respectively. The mechanical properties of the substrate material, sliding ball, and coating material have been listed in Table 16.2.

16.2.5 Surfactant as Liquid-Mediated Contact

Surfactant wetting properties are very crucial due to its phenomenal advantages such as low friction and wear rate, lowering the heat generation, and provides

Table 16.2 Mechanical properties of materials under investigation

Materials mechanical properties	Base material	Counterpart material (Al_2O_3)	Target material
Hardness (HRC)	62	60	x
Density (g/cm^3)	7.98	x	19.25
Young's modulus (GPa)	230	x	411
Thermal conductivity (W/(m K))	2400	x	173
Electrical resistivity (Ω*m*10^{-9})	x	x	52.8
Ultimate compressive strength (MPa)	x	x	x
Tensile strength (MPa)	1000	190	1510

lubrication mechanism. Surfactants are compounds that reduce surface tension between two liquid or solid–liquid surfaces. It acts as a wetting agent, dispersant, and forming a homogeneous colloidal solution. In this work, four types of surfactants are used to conduct the test in an oil medium. Sodium dodecyl sulfate (SDS) is an organic compound with the formula $CH_3(CH_2)_{11}OSO_3Na$. It is an anionic surfactant attached to a sulfate group, giving the material the amphiphilic property that turns into soapiness behavior on to the surface. SDS is a highly effective surfactant and is used highly as dispersant and detergent. Sodium hexametaphosphate (SHMP) is a hexamer of composition $(NaPO_3)_6$ and an anionic surfactant. The preparation of SHMP includes melting followed by rapid cooling of monosodium orthophosphate. SHMP, particularly, under acidic conditions, hydrolyzes in aqueous solution. SHMP used as a dispersant agent to break down agglomerates. Cetyltrimethylammonium bromide (C-TAB) or Cetrimonium bromide ($(C_{16}H_{33})N(CH_3)_3Br$) is the components of the topical antiseptic cetrimide. C-TAB is a cationic surfactant and an effective antiseptic agent. As a surfactant, it forms micelles in aqueous solutions. At a temperature of 30 °C, it forms micelles with aggregation number 75–120. Zinc dialkyldithiophosphates (ZDDP), $Zn[(S_2P(OR)_2]_2$ feature zinc [Zn] attached to the anion of a dithiophosphoric acid, where nonionic compounds are not salts. ZDDP contains longer chain derivatives and has a property to dissolve in nonpolar solvents such as mineral and synthetic oils. In boundary lubrication condition, ZDDP is used as extreme pressure additives. Addition of ZDDP into the base oil significantly reduces surface tension and gives lower friction values.

16.2.6 Synthetic Base Oil

Synthetic polyalphaolefin 6 oil is used to prepare a suspension with different types of surfactants. The suspensions were prepared by suspending 10 ml of oil with 1 wt% surfactant using a 15 min ultrasonication process to break agglomerates.

The frequency and power during the ultrasonication process were fixed at 20 kHz and 100 W, respectively. Polyalphaolefin oil has the density of 0.826 g/cm^3 at 15 °C and kinematic viscosity of 30.5 cSt at 40 °C.

16.3 Microstructural, Mechanical, and Tribological Investigation

16.3.1 Surface Characterization

Chemical composition, microstructure, and presence of phases in the multilayer PVD-W/W_2N coatings are shown in Fig. 16.4a–d. The chemical element of tungsten and nitride were shown with their relative proportions of layer coating for the tested substrate. SEM cross-section micrographs of W/W_2N coating showed typical columnar morphology, developed within the films by a surface diffusion process and influenced by geometrical shadowing effects. The XRD intense peak at (111) can be ascribed as a polycrystalline cubic W_2N phase.

16.3.2 Scratch and Nanoindentation Test

Figure 16.5a, b represents acoustic emission with varying distance and normal force (F_n). As the normal force and sliding distance increases, the coating surface experiences some form of deflection, which could be assessed by the acoustic

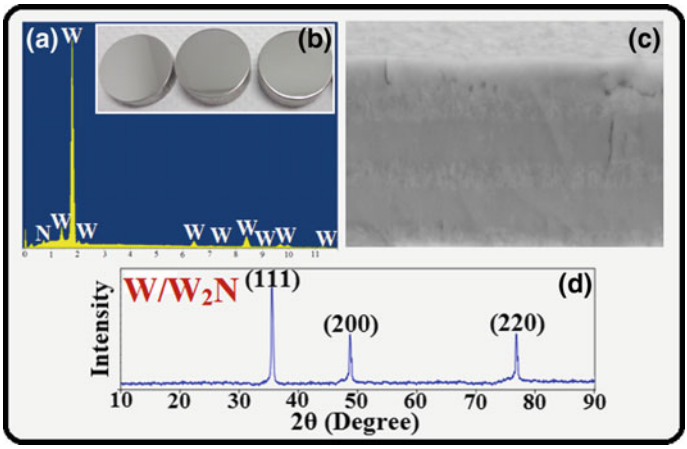

Fig. 16.4 **a** EDS element analysis of coated surfaces, **b** prepared samples for adhesion, friction and wear measurements, **c** cross-sectional micrograph of multilayer coating system, and **d** XRD pattern of W/W_2N coatings

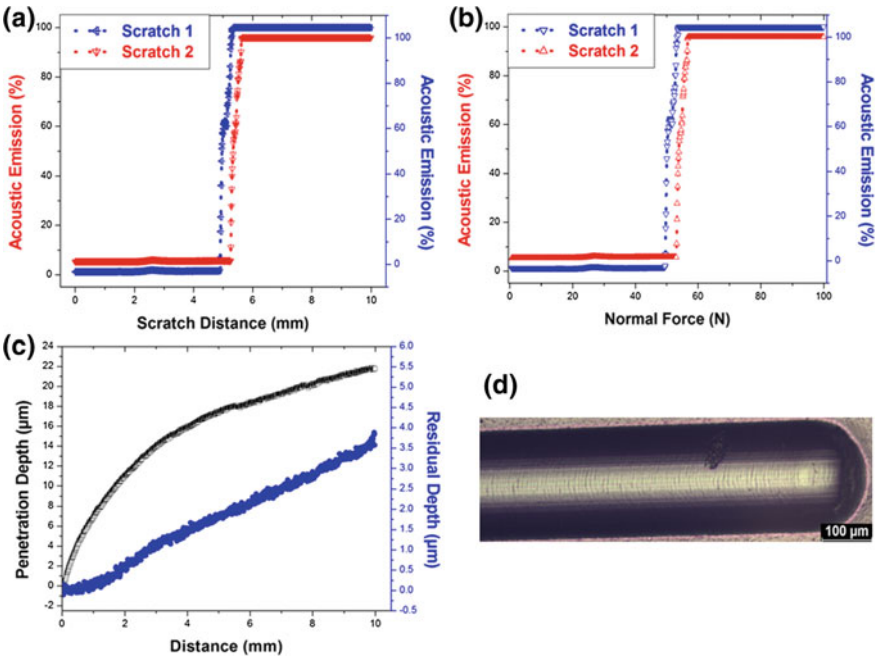

Fig. 16.5 **a** Scratch test measurement up to 10 mm distance and **b** up to a normal load of 100 N, **c** scratch penetration and residual depth during the test, post-scan measurement, respectively, and **d** scratched image of W/W_2N multilayer coating up to 100 N load

emission behavior. At this stage, the formation of crack initiates which progresses with a normal load and sliding distance. Linear behavior of acoustic emission signal signifies non-detachment of coatings due to sufficient bonding strength. Figure 16.5c shows the actual penetration depth and residual depth during the scratch, post-scan measurement, respectively. At low load regime, while indenter runs through a scratched track, surface provides a fracture indication without any marked transition. Figure 16.5d shows scratch made along with the surface of PVD coated substrate. A fish-type scratched mark is the indication of crack the initiation on the surface. The deposited coating up to 100 N loads does not result in any coating delamination/flake formation due to significant adhesion strength. Sometimes, more adverse or high-frequency peaks can frequently be obtained due to surface irregularities and substrate-coating material elastic modulus mismatch. This mismatch suddenly peels off the deposited coatings under the action of load.

Nanoindentation tests were performed to evaluate the hardness and Young's modulus of the deposited coating. The hardness and reduced elastic modulus of W/W_2N multilayer coatings were higher, and the values are associated with a pile-up, sink-in behavior (for lower hardened surfaces), respectively. Three parameters, i.e., indenter shape, thermal drift, and indentation creep affect the loading and unloading curves (see Fig. 16.6) (Pharr et al. 1992). The value of hardness and elastic modulus

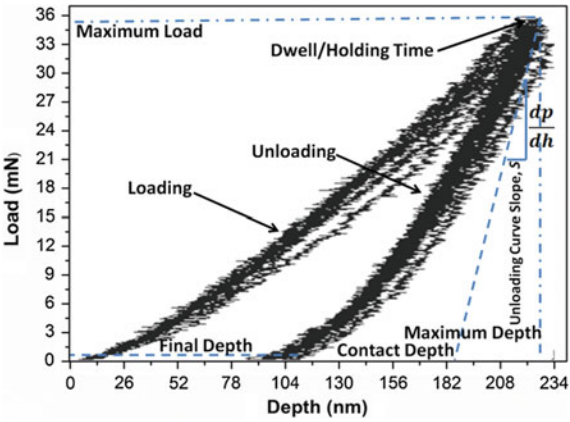

Fig. 16.6 Nanoindentation of multilayer W/W_2N coating

increases with the rate of increase in nitrogen partial pressure. However, increment beyond the specified limit induces brittleness into the sample, which deteriorates coating from the surface of the material. The observed value of hardness and Young's modulus were 31, 315 GPa, respectively. During high contact condition, the material should be capable of resisting plastic deformation. The permanent plastic deformation of the material can be controlled by the hardness of the film H and its elastic modulus E, where coating hardness must be higher and elastic modulus should keep low as much as possible. The ratio of hardness to elastic modulus is an important parameter to determine at what extent coating will deflect under applied load without yielding or surface resistance to plastic deformation. Enhancing the H/E ratio can provide a better perspective to tribological performance. In the present work, the observed H/E ratio of W/W_2N coating was 0.098. The value of H/E ratio is close to 0.1 which is a promising result for any tribological application.

16.3.3 Tribological Performance

Friction coefficient performance and sliding wear track of uncoated and coated substrate at room temperature condition are shown in Fig. 16.7. The rate of wear was calculated by considering the average cross-sectional area of the track wear at several locations of the test substrate with the help of profilometer. While sliding against alumina (Al_2O_3) balls in dry condition average friction coefficient and wear values of coated substrate was 0.25, 4×10^{-6} mm^3/N m, respectively. On the other hand, the uncoated substrate provides a higher friction coefficient and wear values. Thick, strong layers of material (refer inset image of before coating: black in appearance) adhere toward the sliding track of the substrate surface, which triggered the coefficient of friction (COF) value. For uncoated surfaces, the measured values of COF and wear rate were 0.32 and 6×10^{-6} mm^3/N m. Multilayer coatings with

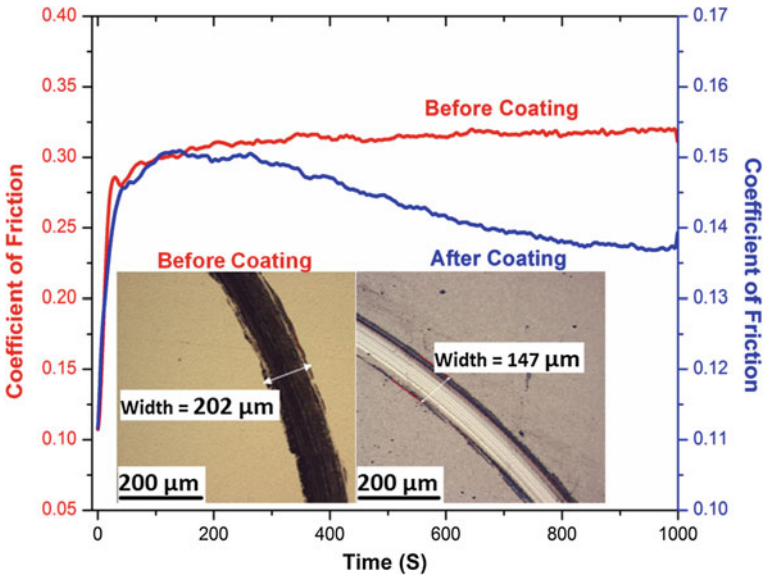

Fig. 16.7 Friction coefficient and wear track of uncoated and coated substrates

tungsten nitride formed a strong layer of oxide film over the wear track surface (see, wear track inset image of after W/W_2N coating). These protective oxide films are capable of reducing counterpart interference and subsequently reduces wear rate by restricting the material transfer. The formed oxides layer had higher stability compared to nitride bonding which acts as a barrier between the coating and sliding counterpart material. In the case of uncoated surfaces, the transferred material adheres from the substrate to the ball side because high hardened material shears the softer one at asperities junction and accumulates the material with its side. After some time a firm oxide layer formed throughout the track surface which acts as a diffusion barrier and lowered the friction and wear values at its minimum compared to the initial stage of sliding. These self-lubricious oxide films restrict the contact between ball and substrate which stands till the final stage of sliding.

Figure 16.8a, b represents average friction coefficient and wear rate of coated, uncoated substrates with/without surfactant, respectively. In most of the industrial practice, rotating or sliding equipment damages the contacting surface due to enormous pressure and load. For this purpose, a suitable homogeneous suspension is used to separate the surfaces from wearing out by providing a thin protective layer between the rotating/sliding contacts. PAO6 base oil alone provides higher COF values compared to surfactant immersed solution. The prepared solutions act as a coolant, which increases lubricity and furthermore dissipated heat from the contacting surfaces. Addition of engine oil additive ZDDP to the PAO6 base oil reduces COF value to some extent. It is also considered that ZDDP amorphous polyphosphate tribo-film is presumed to dominate the surface properties.

The outermost layer of the surface is surrounded by a sulfide film, which is better served to control friction properties. Friction values of C-TAB and SHMP are relatively higher than ZDDP due to flake formation and accumulation between the contact zone. Whereas, ZDDP consume on the empty surface pockets and provide lubrication mechanism. A cationic surfactant C-TAB can be used as a stabilizer in aqueous media to prevent agglomeration and yield highly stable suspension solution for the suspended particles (Bicker and Sisman 2010). On the other hand, SDS outperforms among all with the least achievable friction coefficient value due to its soapiness behavior at the substrate surface. Addition of SDS creates a slipping phenomenon rather than sticking at the surface, which further decreases wear rate and friction coefficient. The wear rate in the presence of surfactants reduced dramatically from its initial values of uncoated surface. Figure 16.8c shows the SEM microstructure of coated substrate in the presence of liquid mediates contact after sliding tests. SEM microstructure of ZDDP indicates largely covered smooth surfaces with few dark patches. SHMP, C-TAB, and SDS are composed of regular morphology, uniform crystalline state, and spherical microstructure respectively. Small solid particles of C-TAB on the substrate surfaces showed a significant in-homogeneity.

16.3.4 Mechanism Between Contacting Pairs

Friction and wear phenomena at interfaces are very complex due to involved uncertainty such as test parameters, deposition condition material suitability, counterpart challenges, and many more. After several attempts of continuous sliding/rubbing, some of the abrasive particles trapped inside the contact zone, these tiny particles itself gain a charge and starts exchanging the electrons at interfaces. The interaction between atoms or molecules (at the nanoscale) mainly caused by Van der Waals attraction (Dzyaloshinskii et al. 1961) and it increases with a decrease in distance between two contacting surfaces, see Fig. 16.9. During the material transfer process, the electrons are the main charge carrier that is transferred from one to another and triggering contact adhesion between the frictional pairs. High sliding velocity damages the surface in an excess and causes diffusion by plastic deformation. After surface diffusion, atoms rearranged themselves and hindered the charge phenomena by separation. At the initial stage of sliding, both surfaces are smooth enough to surpass each other without any significant damage. However, as time progresses, continuous sliding between both surfaces causes the material to flow. In such case, high roughness parametric surfaces transfer more asperities compared to the lower ones because the contact area is increasing with the shearing process for rough surfaces under the action of sliding.

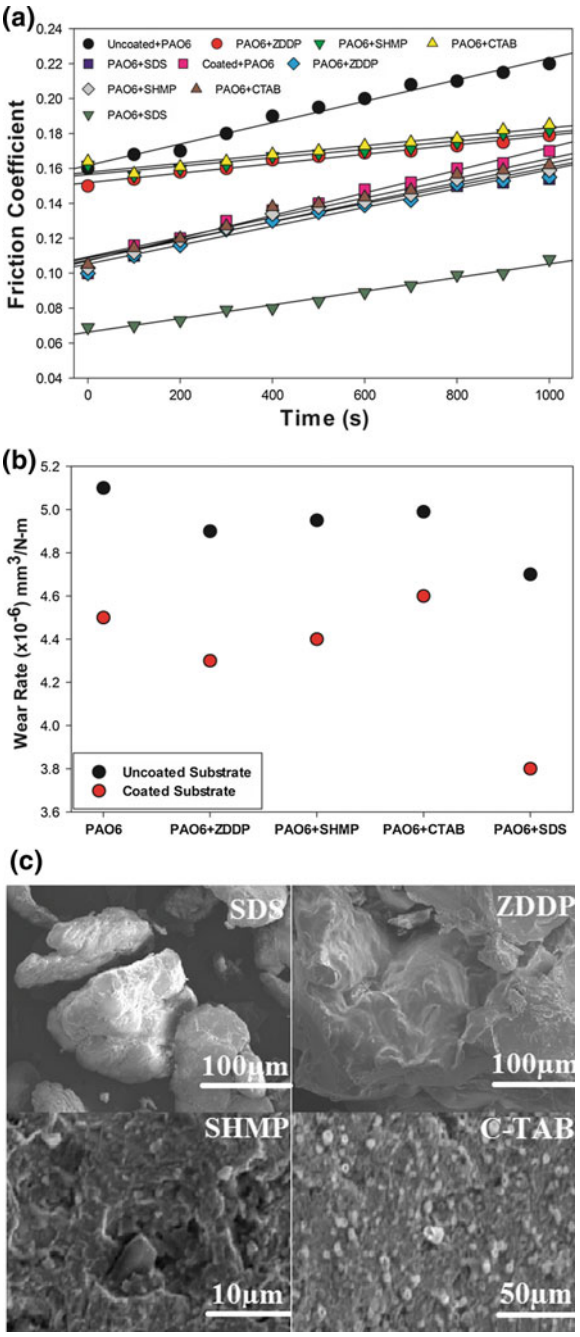

Fig. 16.8 **a** Friction coefficient, **b** wear performance of uncoated and W/W_2N coated surfaces, and **c** SEM microstructure of coating surfaces under the influence of surfactant

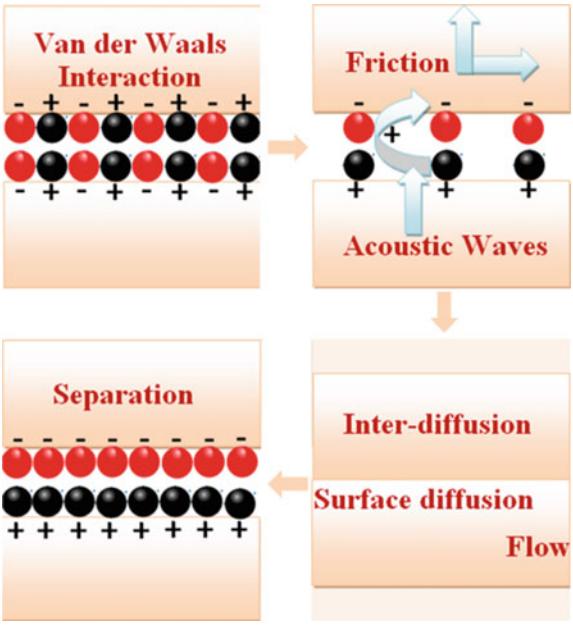

Fig. 16.9 Van der Waals attraction and repulsion between two surfaces

16.4 Economy Aspect of Automotive Sector

In the automotive industry, every year enormous economy loss results from maintenance cost, downtime, surface fatigue, and incorrect lubrication, see Fig. 16.10. The downtime refers to the machinery or a component which is not performing its assigned tasks due to the sudden failure or scheduled maintenance. At this stage, the non-functionality of the machine or a component is considered to be idle. Among all factors, the consumptions of suitable maintenance strategy itself require half of the total investment. Hence, scheduled maintenance is required to

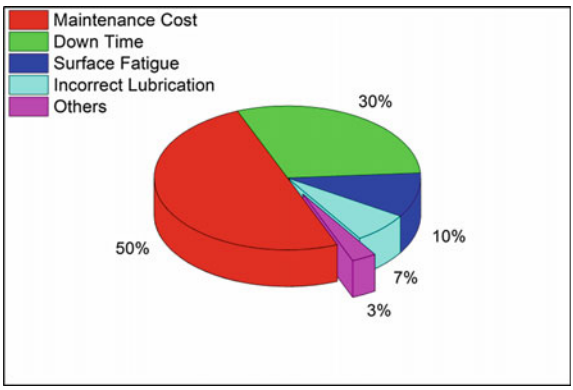

Fig. 16.10 Sources of various economy losses in the automotive industry

overcome future failure occurrence. Moreover, industry should adopt a proactive or predictive maintenance strategy with the application of nondestructive testing to avoid unnecessary investment. Downtime is related to the idle time, where the specified function is stopped due to the failure of an instrument/component or machinery. Production or operational cost increases with an increase in downtime. The cumulative effect of maintenance cost and downtime in the automotive industry is extended from 70–80%. Another failure results from surface fatigue and incorrect lubrication mechanism. In severe contact condition, surface forms pits and crack which is progresses with time and result in complete failure. Other failure costs are associated with the material selection, design considerations, and improper mounting. Therefore, incorporating suitable tribological practices such as coating, lubrication, maintenance strategy reduces overall economy consumption and provides efficient functioning to the components.

16.5 Summary

The main reason behind the loss of energy in industry and day to day life is due to the involved friction, directly or indirectly, which further decreases a significant amount of nation's Gross Domestic Product (GDP) every year. Thousands of components and machine are removed by the companies every year due to an excessive rate of wear. Therefore, in the viewpoint of total energy and cost saving it is realized to raise the issue regarding minimization of friction and wear through applied surface coatings. Surface engineering, through surface coatings, is one of the most effective solutions for any tribological problems. It adds various properties (residual compressive stresses, increased hardness, and minimum surface roughness) at the surface interface and extending the life of the component. In coating technology, materials surface is playing a key role because the surface itself governs all the coating properties. If the base material surface properties and the coating target material are not supported by each another, the coating will deflect under high load and pressure, which can result in delamination.

In the present work, friction, wear, and adhesion measurement of the multilayer coating system were investigated. Results confirm that as the crack growth progresses, the acoustic emission signals reached its maximum value due to deflecting of the coating under the action of normal load, as it increased from low to high values. However, there is no coating delamination/failure occurred under an applied load. During pin-on-disk test, friction coefficient values of uncoated substrates were higher due to abrupt contact. However, in the presence of a surfactant, significant reductions in friction coefficient, and wear rate have been achieved. Multilayer coatings of tungsten have provided much lower tribological values due to building up protective film over the surface. The detailed investigation indicates that the deposited coating increases the adhesion strength by protecting against wear.

References

Basu A, Majumdar JD, Manna I (2012) Structure and properties of CrxN coating. Surf Eng 28 (3):199–204

Bicker M, Sisman I (2010) Controlled synthesis of copper nano/microstructures using ascorbic acid in aqueous CTAB solution. Powder Technol 198:279–284

Bull SJ, Jones AM (1996) Multilayer coatings for improved performance. Surf Coat Technol 78:173–184

Davidson JE, Hinchley SL, Harris SG, Parkin A, Parsons S, Tasker PA (2006) Molecular dynamics simulations to aid the rational design of organic friction modifiers. J Mol Graph Modell 25(4):495–506

Dey SP, Deevi SC (2003) Single layer and multilayer wear resistant coatings of (Ti, Al)N: a review. Mater Sci Eng A 342:58–79

Donnet C, Erdemir A (2004) Historical developments and new trends in tribological and solid lubricant coatings. Surf Coat Technol 180–181:76–84

Dzyaloshinskii IE, Lifshitz EM, Pitaevskii LP (1961) General theory of van der waals' forces. Sov Phys Usp 4(2):153

Greenwood N, Earnshaw A (1997) Chemistry of the elements, 1st edn. Butterworth-Heinemann, U.K.

Hansen N (2004) Hall-Petch relation and boundary strengthening. Scripta Mater 51:801–806

Harris SG, Doyle ED, Vlasveld AC, Dolder PJ (2001) Dry cutting performance of partially filtered arc deposited titanium aluminium nitride coatings with various metal nitride base coatings. Surf Coat Technol 146–147:305–311

Helmersson U, Todorova S, Barnett SA, Sundgren JE, Markert LC, Greene JE (1987) Growth of single-crystal TiN/VN strained-layer superlattices with extremely high mechanical hardness. J Appl Phys 6:481–484

Kathrein M, Michotte C, Penoy M, Polcik P, Mitterer C (2005) Multifunctional multi-component PVD coatings for cutting tools. Surf Coat Technol 200:1867–1871

Khlifi K, Ben C, Larbi A (2013) Investigation of adhesion of PVD coatings using various approaches. Surf Eng 29(7):555–560

Kothari DC, Kale AN (2002) Recent trends in surface engineering using cathodic arc technique. Surf Coat Technol 158–159:174–179

Kulkarni AP, Joshi GG, Sargade G (2013) Performance of PVD AlTiCrN coating during machining of austenitic stainless steel. Surf Eng 29(5):402–407

McIntyre D, Greene JE, Hakansson G, Sundgren JE, Mu¨nz WD (1990) Oxidation of metastable single-phase polycrystalline $Ti_{0.5}Al_{0.5}N$ films: kinetics and mechanisms. J Appl Phys 67: 1542–1543

Mellor BG (2006) Surface coatings for protection against wear. CRC Press, Cambridge, England

Meneve J, Vercammen K, Dekempeneer E, Smeets J (1997) Thin tribological coatings: magic or design. Surf Coat Technol 94–95:476–482

Mittal KL (2008) Surfactants in tribology, 1st edn. CRC Press, Boca Raton

Niu J, Ji Y, Wu J, Yu Z (2014) Improvement of properties of TiN coating by optimising microstructural design. Surf Eng 30(1):36–40

Pharr GM, Oliver WC, Brotzen FR (1992) On the generality of the relationship among contact stiffness, contact area, and elastic modulus during indentation. J Mater Res 7:613–617

Pierson HO (1996) Handbook of refractory carbides and nitrides, 1st edn. Noyes Publications, USA

Prabhu TR, Varma VK, Vedantam S (2014) Tribological and mechanical behavior of multilayer Cu/SiC þ Gr hybrid composites for brake friction material applications. Wear 317:201–212

Rahman A, Jayaganthan R, Prakash S, Chawla V, Chandra R (2011) Cyclic high temperature oxidation behaviour of sputtered Cr/Al multilayer coatings on superalloy. Surf Eng 27(5): 393–401

Smith IJ, Mu¨nz WD, Donohue LA, Petrov I, Greene JE (1998) Improved Ti_1–xAlxN PVD coatings for dry high speed cutting operations. Surf Eng 14(1):37–42

Sproul WD (1996) Reactive sputter deposition of polycrystalline nitride and oxide superlattice coatings. Surf Coat Technol 86–87:170–176

Upadhyay RK, Kumaraswamidhas LA (2014a) Surface modification by multilayered W/W_2N coating. Surf Eng 30:475–482

Upadhyay RK, Kumaraswamidhas LA (2014b) Tungsten/tungsten nitride performance at elevated temperature. Mater High Temp 31:102–108

Upadhyay RK, Kumaraswamidhas LA (2015) Investigation of monolayer-multilayer PVD coating. Surf Eng 31:124–133

Upadhyay RK, Kumaraswamidhas LA (2016a) Friction and wear response of nitride coating deposited through PVD magnetron sputtering. Tribol Mater Surf Interfaces 10:196–205

Upadhyay RK, Kumaraswamidhas LA (2016b) Multilayer nitride coating performance optimized by an artificial neural network approach. Ciência Tecnologia dos Mater 28:47–54

Voevodin AA, Bultman J, Zabinski JS (1998) Investigation into three-dimensional laser processing of tribological coatings. Surf Coat Technol 107:12–19

Yashar PC, Sproul WD (1999) Nanometer scale multilayered hard coatings. Vacuum 55:179–190

Zhang W, Xue Q, Zhang X (1998) The influence of brighteners on the friction and wear of electrodeposited multilayer films. Wear 214:74–78

Zheng L, Ramalingam S (1996) Multi-layer and composite structures for advanced coating. Surf Coat Technol 81:52–71